Final Report: Geochemistry of Natural Gases from Tight-Gas-Sand Fields in the Rocky Mountains

07122-09.FINAL

Authors

Nicholas B. Harris, TingWei Ko, Colorado School of Mines
R. Paul Philp, University of Oklahoma
Michael D. Lewan, U.S. Geological Survey
Chris J. Ballentine, Zheng Zhou, University of Manchester
Donald L. Hall, Fluid Inclusion Technologies, Inc.

Project Title: APPLICATION OF NATURAL GAS COMPOSITION TO MODELING COMMUNICATION WITHIN AND FILLING OF LARGE TIGHT-GAS-SAND RESERVOIRS, ROCKY MOUNTAINS

Subcontract # 07122-09

December 20, 2013

Nicholas B. Harris, Principal Investigator
Department of Geology and Geological Engineering,
Colorado School of Mines, Golden, CO 80401

LEGAL NOTICE

This report was prepared by *Colorado School of Mines* as an account of work sponsored by the Research Partnership to Secure Energy for America, RPSEA. Neither RPSEA, members of RPSEA, the National Energy Technology Laboratory, the U.S. Department of Energy, nor any person acting on behalf of any of the entities:

a. MAKES ANY WARRANTY OR REPRESENTATION, EXPRESS OR IMPLIED WITH RESPECT TO ACCURACY, COMPLETENESS, OR USEFULNESS OF THE INFORMATION CONTAINED IN THIS DOCUMENT, OR THAT THE USE OF ANY INFORMATION, APPARATUS, METHOD, OR PROCESS DISCLOSED IN THIS DOCUMENT MAY NOT INFRINGE PRIVATELY OWNED RIGHTS, OR

b. ASSUMES ANY LIABILITY WITH RESPECT TO THE USE OF, OR FOR ANY AND ALL DAMAGES RESULTING FROM THE USE OF, ANY INFORMATION, APPARATUS, METHOD, OR PROCESS DISCLOSED IN THIS DOCUMENT.

THIS IS A FINAL REPORT. THE DATA, CALCULATIONS, INFORMATION, CONCLUSIONS, AND/OR RECOMMENDATIONS REPORTED HEREIN ARE THE PROPERTY OF THE U.S. DEPARTMENT OF ENERGY.

REFERENCE TO TRADE NAMES OR SPECIFIC COMMERCIAL PRODUCTS, COMMODITIES, OR SERVICES IN THIS REPORT DOES NOT REPRESENT OR CONSTIITUTE AND ENDORSEMENT, RECOMMENDATION, OR FAVORING BY RPSEA OR ITS CONTRACTORS OF THE SPECIFIC COMMERCIAL PRODUCT, COMMODITY, OR SERVICE.

ABSTRACT

Tight-gas-sand reservoirs in the Rocky Mountains, western United States, represent a major natural gas resource. Major fields brought into production in the past 15 years, located in Colorado, Wyoming and Utah, represent more than 100 TCF of recoverable gas reserves. Despite the significance of these reserves, gas compositions in these fields are largely undocumented, and controls on gas composition are poorly understood. This study reports a large data set of gas compositions from three major tight-gas-sand reservoirs: Jonah Field, in the Greater Green River Basin, southwestern Wyoming; the Mamm Creek – Rulison – Parachute – Grand Valley complex of fields in the Piceance Basin, western Colorado; and Greater Natural Buttes Field, Uinta Basin, northeastern Utah. Data gathered included: fractions of hydrocarbon species and CO_2 in production gas and mud samples; compound-specific carbon and hydrogen isotopes in production gas and mud gas samples; noble gas isotopes in production gas samples; fluid inclusion compositions from formations (Jonah Field and the Piceance Basin fields); gas compositions generated from source rocks during hydrous pyrolysis experiments.

Natural gas compositions are influenced by several variables: (1) the composition of the organic matter in the formation from which the gas is sourced; (2) the thermal maturity at which the gas is generated from the source rock; (3) the gas generation process, specifically whether gas is generated through primary cracking of kerogen, from secondary cracking of oil to gas, or from secondary cracking of wet gas to dry gas; (4) fractionation during gas migration from source to reservoir; (5) leakage from the reservoir; (6) bacterial alteration (oxidation) of gases. The premise of this research is that by collecting large data sets analyzed for multiple components of natural gas, the specific processes involved in generation and preservation of the gases can be identified and described.

Production gas samples from the Jonah, Greater Natural Buttes and the Piceance Basin fields exhibit a significant geographic and vertical range of compositions within each field, but the overall range of compositions was similar in all three fields. Compositions generally range from pure methane to 35% C2+ fraction, with a small number of wetter gas samples. The carbon isotopic composition of methane ranged from -25 to -45‰; in general, the carbon isotopic compositions of wetter gases were more positive (heavier) and exhibited less variation. The CO_2 content of gases ranged from 0 to 10%.

Production gas compositions from the three fields are distinguishable by:

1) Carbon isotopic composition of CO_2, relatively heavy at Greater Natural Buttes (close to the expected value of CO_2 associated with decomposition of carbonate); lighter for the Piceance fields and significantly lighter at Jonah Field.
2) Hydrogen isotopic composition of the C_{2+} gases is lighter by 25 to 40‰ for the Jonah gases in comparison to the Piceance and Greater Natural Buttes gases.
3) Greater Natural Buttes gases can be distinguished by a smaller ratio of *i*-C_4 to *n*-C_4.
4) Piceance gases have heavier $\delta^{13}C_{C3}$ at a given $\delta^{13}C_{C2}$ than Greater Natural Buttes and Jonah gases.
5) Noble gas parameters, including $1/^{22}Ne$ and $1/^{36}Ar$ and $^{3}He/^{4}He$.

Mud gases exhibit distinct vertical variation, and the patterns differ between the two fields where abundant data were gathered. Jonah gases are distinguished by gas compositions that become wetter and isotopically lighter with depth, with a wide range of bulk gas and isotopic compositions at a given depth. Piceance gases are distinguished by gases that become dryer and isotopically heavier with depth, although a shift to much lighter values is suggested for the deepest samples. Isolated Piceance mud gases consist of pure methane and are isotopically extremely heavy.

The Piceance and Greater Natural Buttes Fields are associated with coal-rich formations that likely contributed significant volumes of gas, whereas no such formations are present in the Jonah area; but despite this difference, the overall compositions of gases are very similar. This result is consistent with hydrous pyrolysis experiments on both coaly and marine sources that demonstrate similar gases are generated from both types of source rocks.

Processes that have influenced the composition of gases includes (1) mixing of gases produced by primary cracking with gases from the secondary cracking of oil; however there is no evidence of gases produced by secondary cracking of wet gas to dry gas; (2) gases produced by primary cracking from similar source rocks at varying thermal maturity; (3) gas compositions altered by bacterial oxidation of hydrocarbon gases, yielding gases that are dry, isotopically heavy and contain isotopically light CO_2. This effect is pervasive in the upper part of the gas column at Jonah Field and locally significant in stratigraphically distinct levels in a few of the Piceance wells.

The striking stratigraphic variability in gas compositions and the variation in gas compositions at particular depths suggest complex migration pathways, probably through fracture systems and localized channeling of migrating gases through relatively permeable beds. Gas compositions cannot be attributed to the pervasive vertical diffusion of gases or to rapid migration through overpressured-induced fractures.

THIS PAGE INTENTIONALLY LEFT BLANK

TABLE OF CONTENTS

		Page no.
1	INTRODUCTION	1
1.1	Significance of Tight-Gas-Sand Reservoirs in the United States and Key Unknowns	1
1.2	Models for Gas Migration in Tight-Gas-Sand Reservoirs	2
1.3	Research Methodology and Background	3
1.4	Study Sites	4
1.5	Key Research Personnel	5
1.6	Organization of the Report	6
1.7	References	6
	Figures for Chapter 1	8
2	SUMMARY OF THE GAS FIELDS	10
2.1	Mamm Creek – Rulison – Parachute – Grand Valley fields, Piceance Basin, Colorado	10
2.1.1	Stratigraphy and reservoirs	10
2.1.2	Reservoir quality	11
2.1.3	Source rocks	11
2.1.4	Burial history and thermal maturity	12
2.1.5	Gas distribution	12
2.2	Greater Natural Buttes Field, Uinta Basin, Utah	13
2.2.1	Stratigraphy and reservoirs	13

2.2.2 Structural geology 14
2.2.3 Source rocks 14
2.2.4 Burial history and thermal maturity 14
2.2.5 Reservoir quality 15
2.2.6 Gas distribution 15

2.3 Jonah Field, Greater Green River Basin, Wyoming 15

2.3.1 Stratigraphy and reservoirs 15
2.3.2 Structure and trapping 16
2.3.3 Source rocks 17
2.3.4 Burial history and thermal maturity 17
2.3.5 Reservoir quality 18
2.3.6 Hydrocarbon distribution 18

2.4 References for Chapter 2 19

Figures for Chapter 2 23

3 SAMPLING AND ANALYTICAL METHODS 32

3.1 Gas Sampling 32

3.2 Fluid Inclusion Sampling 32

3.3 Gas Analysis 33

3.4 Fluid Inclusion Analysis 33

3.5 References for Chapter 3 33

4	PICEANCE BASIN RESULTS AND INTERPRETATION	34
4.1	Data Set	34
4.2	Production Gases	34
4.2.1	Bulk gas composition	34
4.2.2	Carbon and hydrogen isotopic composition	35
	Carbon isotopes	35
	Hydrogen isotopes	36
4.2.3	Integrated bulk compositions and isotopes	37
4.2.4	Noble gases	38
4.3	Mud gases	39
4.3.1	Bulk gas compositions	39
4.3.2	Carbon and hydrogen isotopic composition	40
	Carbon isotopes	40
	Hydrogen isotopes	41
4.4	Fluid Inclusion Analysis	41
4.4.1	Mamm Creek (14-22 Friport well)	41
4.4.2	Rulison (2 Clough well)	42
4.4.3	Parachute (ARCO GV 53-34 well)	42
4.4.4	Grand Valley (Mobil MV-23-27 well)	42
4.4.5	Grand Valley (Federal MV-12-3 well)	43
4.5	Interpretation	43
4.5.1	Regional variability in production gas composition	43
4.5.2	Thermal maturity of source rocks	44

4.5.3 Sources of gas 44
4.5.4 Evidence of secondary cracking 45
4.5.5 Evidence for bacterial oxidation of gases 46

4.6 References for Chapter 4 47

Table 4.1. Average compositions of Piceance Basin production gases 49

Table 4.2. Average Compositions of Piceance Basin Mud Gas Samples 50

Figures for Chapter 4 51

5 JONAH FIELD RESULTS AND INTERPRETATION 78

5.1 Data set 78

5.2 Production gases 78

5.2.1 Bulk gas compositions 78
5.2.2 Carbon and hydrogen isotopic composition 79
Carbon isotopes 79
Hydrogen isotopes 80
5.2.3 Integrated bulk compositions and isotopes 81
5.2.4 Noble gases 82

5.3 Mud Gases 82

5.3.1 Bulk gas compositions 82
5.3.2 Carbon and hydrogen isotopic composition 84
Carbon isotopes 84
Hydrogen isotopes 84
5.3.3 Integrated bulk compositions and isotopes 84

5.4 Fluid inclusion analysis 85

5.4.1 Yellow Point 5-13 well 85
5.4.2 Stud Horse Butte 14-17 well 86

5.4.3 Stud Horse Butte 10-26 well 86
5.4.4 Stud Horse Butte 3-28 well 87
5.4.5 SAG Unit 5-17 well 88
5.4.6 Jonah Federal 4-8 88

5.5 Interpretation 89

5.5.1 Variability in production and mud gas composition 89
5.5.2 Thermal maturity of source rocks 91
5.5.3 Controls on gas composition: hydrocarbon source and/or secondary alteration 91
5.5.4 Evidence of Secondary Cracking 93
5.5.5 Migration Pathways 94
5.5.6 Compartmentalization within the Gas Column 95

5.6 References 96

Table 5.1. Summary of compositions of Jonah production gases. 98

Table 5.2. Average Compositions of Jonah Field Mud Gas Samples 99

Figures for Chapter 5 100

6 GREATER NATURAL BUTTES FIELD 140

6.1 Data set 140

6.2 Production gases 140

6.2.1 Bulk gas compositions 140
6.2.2 Carbon and hydrogen isotopic composition 141

Carbon isotopes 141
Hydrogen isotopes 142

6.2.3 Integrated bulk compositions and isotopes 142
6.2.4 Noble gases 143

6.3 Mud gases 144

6.3.1 Bulk gas compositions 144
6.3.2 Carbon and hydrogen isotopic composition 145

Carbon isotopes 145
Hydrogen isotopes 146

6.3.3 Integrated bulk compositions and isotopes 146

6.4 Interpretation 147

6.4.1 Variability in production and mud gas composition 147
6.4.2 Thermal maturity of source rocks 147
6.4.3 Control on gas composition by source or secondary alteration 148
6.4.4 Evidence of secondary cracking 149
6.4.5 Internal seals (compartmentalization) within gas column and migration 150

6.5 References 150

Table 1. Summary of Greater Natural Buttes production gas compositions 152

Table 2. Summary of Greater Natural Buttes mud gas compositions 153

Figures for Chapter 6 154

7 COMPARISON BETWEEN PICEANCE BASIN FIELDS, JONAH FIELD AND GREATER NATURAL BUTTES FIELD 187

7.1 Similarities in gas composition between the Piceance Basin fields, Greater Natural Buttes Field and Jonah Field 187

7.2 Contrasts in composition between the Piceance Basin fields, Greater Natural Buttes Field and Jonah Field 187

7.2.1 Butane composition 187

7.2.2 Carbon isotopic composition of CO_2 188
7.2.3 D-H composition 188
7.2.4 Noble gas composition 188
7.3 Interpretation 189

7.3.1 Interpretation of hydrogen isotope data 189
7.3.2 Carbon isotopic composition of CO_2 191
7.4.3 Noble gas data 192

7.4 References 192

Table 7.1 Average δD compositions of gas species 194

Figures for Chapter 7 195

8 HYDROUS PYROLYSIS EXPERIMENTS ON ROCKY MOUNTAIN SOURCE ROCKS 204

8.1 Research Objectives 204

8.2 Research Summary 205

8.3 References 206

Figures for Chapter 8 207

9 SUMMARY AND CONCLUSIONS 212

10 ACKNOWLEDGEMENTS 214

APPENDIX 1 - GAS ANALYSES 215

Piceance Basin fields production gases 215

Jonah Field production gases 218

Greater Natural Buttes Field production gases 221

Piceance Basin fields mud gases **224**

Jonah Field mud gases **230**

Greater Natural Buttes Field mud gases **241**

Noble gas data, Piceance fields, Jonah Field, Greater Natural Buttes Field **244**

Noble gas ratios, Piceance fields, Jonah Field, Greater Natural Buttes Field **248**

1 INTRODUCTION

1.1 Significance of Tight-Gas-Sand Reservoirs in the United States and Key Unknowns

The tight-gas-sand reservoirs of the Rocky Mountains represent one of the most significant gas resources in the United States. Major fields brought into production in the past 15 years comprise more than 100 TCF of producible gas reserve. These fields include: Pinedale Field (44 TCF), Wamsutter Field (30-50 TCF) and Jonah Field (14 TCF) in the Greater Green River Basin, Wyoming; the Mamm Creek – Rulison – Parachute – Grand Valley cluster of fields (>8 TCF) in the Piceance Basin, Colorado; and the Greater Natural Buttes Field (5 TCF) in the Uinta Basin, Utah.

The processes by which gas fills these reservoirs is largely unknown, although it is likely that the reservoirs fill from the bottom up, in contrast to conventional reservoirs that fill from the top seal downwards. This behavior of the tight-gas-sand reservoirs arises from their extremely low permeabilities and the absence of a well-defined top seal. The extent to which these reservoirs are compartmentalized is also unknown. If this system is dynamic, in other words gas is actively migrating, the concentration of gas at any point in the system is given by the relationship:

Mass flux = concentration * velocity

At steady state, the mass flux of gas is constant in a vertical transect through the reservoir. Concentration is therefore inversely related to migration velocity: in parts of the reservoir where gas migrates quickly, the concentration is low, and where it migrates slowly the concentration is high. The sections of a gas column with high gas saturations are those parts of the rock column with low permeabilities and slow migration velocities.

Because the filling processes and reservoir compartmentalization are unknown, our predictive capabilities in exploiting tight-gas-sand reserves are limited in several areas:

- We cannot effectively predict the top of gas and the top of producible gas from one field to another without actual well test data. Because of the complications in interpreting water saturations, well logs can be ineffective, especially near the top of gas.
- We cannot effectively predict gas pressures without well test data.
- We cannot predict gas composition without well test data.
- Our capability for predicting reservoir compartmentalization is very limited.

Furthermore, estimates of undiscovered natural gas resources in the Rocky Mountains depend on the model we assume for the tight-gas-sand accumulations. We refer here to the

controversy over the basin-centered gas model, which is essentially this: are tight-gas fields simply "sweet-spots" in a continuous accumulation, or are these fields conventionally-trapped accumulations in very low-permeability rock? If there is a continuous accumulation of gas at deep levels in the Rocky Mountain basins, then gas resources in the Rockies are very large indeed. But if the producing fields are conventionally trapped, then estimates of ultimate gas resources must be much lower.

1.2 Models for Gas Migration in Tight-Gas-Sand Reservoirs

There are at least three possible models for gas migration within tight-gas-sand reservoirs:

1. One model is that gas fills the reservoirs by hydraulic fracturing (Cumella and Scheevel 2008). In essence, gas fills the deepest reservoir compartments, increasing pressure until it exceeds the fracture strength of the top seals of those compartments. The seals of the deep compartments then rupture, allowing gas to fill the overlying compartments. Seal of each compartment ruptures in sequence upward as they fill with gas when their fracture strength is exceeded. This process continues until gas reaches its present-day distribution.

2. A second model is that the reservoirs fill by upward diffusion, with horizontally distributed shales behaving as a series of semi-permeable membranes that retard the vertical flow of gas. The driving force for gas migration is pressure.

3. A third model is that the reservoir fill by gas channeled vertically along faults or fractures, traveling upward until pressures decrease to a point that it is easier to migrate laterally into adjacent reservoir sandstones than it is to force open fractures to allow the passage of gas.

Each of these models should leave a distinctive record in the gas composition. Consider the second model, which is vertical diffusion through a series of semi-permeable seals. This process should lead to considerable fractionation of gas species with methane enrichment in shallower horizons; this is, in essence, gas chromatography on a large scale. It should also be expressed in terms of ^{13}C and D-H isotopes, with lighter compositions in shallower horizons as ^{12}C and hydrogen diffuse more rapidly through seals than ^{13}C and deuterium and possibly small atomic-radii gases such as helium in preference to larger molecules such as the hydrocarbon gases and CO_2. Alternatively, if gas fills the reservoirs through successive natural hydraulic fracturing and rapid filling of successive compartments (model 1), the fractionation should be much less pronounced. Finally, if gas is channeled along faults and fractures, then migrates laterally, we should see non-systematic vertical differences in composition as wells contact reservoir beds with varying connection to permeability pathways. There may also be fractionation laterally away from the channels.

1.3 Research Methodology and Background

This research project applied the analysis of natural gas compositions to constrain models for how these reservoirs fill and for the extent of lateral communication and compartmentalization. This included: 1) bulk hydrocarbon gases (methane, ethane, etc. and CO_2); 2) the ^{13}C and D-H isotopic composition of compound-specific gases, i.e. of methane, ethane propane, etc.; 3) the radiogenic noble gases such as Ar and Ne. Bulk hydrocarbon gas composition has been studied in the tight-gas-sand reservoirs, although published data are limited, and compound-specific isotopes have been analyzed to a very limited degree. Radiogenic noble gases have not been tested.

The combination of data on bulk hydrocarbon composition and ^{13}C compound-specific carbon isotopes has been used for a number of years to examine and interpret the processes of gas generation, migration, filling and leaking from conventional reservoirs. This approach was initially pioneered by Martin Schoell (Schoell 1983), employing: 1) concentration of C_{2+} gases; 2) $\delta^{13}C$ of methane; 3) δD of methane; and 4) the $\delta^{13}C$ of ethane. Schoell (1983) demonstrated applications of this approach to case-studies of the Gulf of California, the south German Molasse basin, the Vienna basin and the north Italian Po basin. Several empirical, experimental and theoretical studies have followed. Prinzhofer and Huc (1995) proposed a procedure to distinguish gas generated from primary cracking of kerogen from gas generated by secondary cracking of oil by plotting $\delta^{13}C_2$- $\delta^{13}C_3$ versus C_2/C_3 and to distinguish a trend in gas composition related to thermal maturity of the source from mixing of gas from two sources from the leakage of gas through a reservoir cap rock by diffusion by plotting $\delta^{13}C_1 - \delta^{13}C_2$ versus C_1/C_2.

Rooney et al. (1995) developed one of the first theoretical models relating carbon isotope ratios of natural gases to the temperature at which gas was generated from kerogen. They noted that different source rocks require different models, more specifically that Type III kerogen generates gas with a greater difference between $\delta^{13}C_1$ and $\delta^{13}C_2$ than Type II kerogen. This point is significant, namely that it is important to know not only the thermal maturity at which possible source rocks generate gas, but the type and composition of organic matter in those source rocks. Tang et al. (2000) expanded on Rooney's theoretical work with a kinetic model using a set of first-order gas generation reactions, which can be used to predict the isotopic composition of methane, the methane yield and the rate of methane generation. These authors stress the importance of calibrating these models (equations) with laboratory data from specific study areas; in other words, it is necessary to develop kinetic data specific to individual source rocks and basins. The impact of migration processes on gas composition has barely been addressed in experimental or theoretical studies. One exception is an experimental study by Zhang and Krooss (2001), which tested the fractionation of carbon isotopes in methane by diffusion through shale and detected substantial depletion of ^{13}C as a result of the diffusion process.

A very different body of research has focused on the application of noble gas content in natural gas and the isotopic compositions of the noble gases. Gases of interest here include He, Ne and Ar. Ballentine and others (e.g. Ballentine and O'Nions, 1994) have shown that natural gas

accumulations include noble gas contributions from the atmosphere, crust and mantle. Because the noble gases are inert and conservative, they act as tracers for sources of gas components and can be used to quantify the contributions from these different sources. Ballentine and Lollar (2002) studied gas compositions in the Panhandle-Hugoton gas field, applying nitrogen isotopes and the radiogenic noble gases, and concluded that (1) nitrogen was sourced in part from the devolatilization of low grade metamorphic rocks and in part from denitrification of organic matter in shales, and (2) there was a substantial interaction between eastward-flowing groundwater and an already-emplaced gas pool. The metamorphics-derived nitrogen, as well as magmatic-derived He, were stripped from the migrating groundwater as it flowed under and interacted with the gas pool.

The full set of these gases has rarely been applied to natural gas fields (Ballentine and Lollar's (2002) study is a rare example and never to the Rocky Mountain tight-gas reservoirs.

Researchers cited above have noted the critical importance of understanding the composition of gases yielded by specific source rocks. This is critical in the Rocky Mountain basins, where both formations rich in coaly Type III organic matter (e.g. the Mesa Verde in the Piceance Basin) and formations enriched in algal-derived marine Type II organic matter probably yield gas. Both the kinetic and composition of gases will differ in these source rocks. Experimental techniques are now developed that can provide constraints on the composition of gas entering the reservoirs. The most appropriate technique is hydrous pyrolysis (see Kotarba and Lewan, 2013), which yields realistic hydrocarbon products and volumes at reasonable thermal maturities. Gases evolved during hydrous pyrolysis (Henry and Lewan 1999, Lewan and Henry 1999) can be analyzed and compared to gases present in reservoirs.

1.4 Study Sites

Three large tight-gas-sand fields or groups of fields were chosen for study: Jonah Field, Greater Green River Basin, Wyoming; the Mamm Creek – Rulison – Parachute – Grand Valley complex of fields in the Piceance Basin, Colorado; Greater Natural Buttes Field, Uinta Basin, Wyoming (Figure 1.1). These fields share some important similarities:

- All three fields are developed in Upper Cretaceous sandstone reservoirs.
- The reservoir section in all fields is overlain by higher permeability Lower Tertiary sandstones.
- All three fields are overpressured, with a top of overpressure near the top of the reservoir section.
- The reservoirs are primarily vertically and laterally isolated fluvial sandstone bodies, although more laterally continuous reservoir sandstones do exist in some fields, particularly Jonah Field.

- All three fields are underlain by marine shales that can function as source rocks, the Mancos Shale in the Piceance fields and at Greater Natural Buttes Field and the Baxter and Mowry Shales at Jonah Field.

Some important differences exist between the fields:

- Most significantly, coal is potentially a major source rock for gas in the Piceance Basin fields. Type III source rocks are considered to be less important at Jonah Field and may be less significant at Greater Natural Buttes Field.

- Jonah Field has clear structural fault boundaries, with reservoir sandstones dipping downdip from a structural culmination between two faults. Wells are less productive in a down-dip direction. The Piceance Basin fields and Greater Natural Buttes Field lack clear structural definition, although locally structural features play a role in gas distribution.

1.5 Key Research Personnel

Dr. Nicholas Harris, Department of Geology and Geological Engineering, Colorado School of Mines and Department of Earth and Atmospheric Sciences, University of Alberta. Dr. Harris served as project leader. He led the gas sampling, coordinated efforts with sponsoring companies and led the interpretation. He also served as advisor to M.Sc. student TingWei Ko at the Colorado School of Mines, who carried out hydrous pyrolysis experiments.

Dr. Michael Lewan, U.S. Geological Survey, Lakewood, Colorado. Dr. Lewan guided the CSM M.Sc. student who carried carried out the hydrous pyrolysis experiments at the U.S. Geological Survey.

Prof. R. Paul Philp, School of Geology and Geophysics, University of Oklahoma, Norman, Oklahoma. Prof. Philp carried out the bulk gas and compound-specific carbon and hydrogen gas geochemical analyses.

Prof. Chris Ballentine, School of Earth, Atmospheric and Environmental Sciences, University of Manchester, England (now at University of Oxford). Prof. Ballentine analyzed and interpreted the trace / noble gas compositions.

Ms. Tingwei Ko, Colorado School of Mines (now at University of Texas). Ms. Ko carried out hydrous pyrolysis experiments at the U.S. Geological Survey on potential source rocks for gases in the tight gas sand fields. Her experimental study was supervised by Dr. Michael Lewan.

Dr. Zheng Zhou, University of Manchester (now at Lancaster University), England. Dr. Zhou worked with Prof. Ballentine on the analysis and interpretation of noble gases.

Dr. Don Hall, Fluid Inclusion Technologies, Tulsa, OK. Dr. Hall managed the analysis of fluid inclusion samples from the Piceance Basin fields and from Jonah Field and was responsible for their interpretation.

1.6 Organization of the Report

This report is organized into the following major sections:

1) Introduction
2) Sampling and analytical methods
3) Review of the geology of Jonah, Greater Natural Buttes and the Piceance Basin fields
4) Piceance Basin results and interpretation
5) Jonah Field results and interpretation
6) Greater Natural Buttes results interpretation
7) Comparison of data between the fields
8) Summary
9) Appendix 1: Data tables (in this report and as separate Excel files)
10) Appendix 2: Detailed reports on fluid inclusion analyses from Jonah and Piceance Basin fields (as separate PDF files)
11) Appendix 3: TingWei Ko M.Sc. thesis on hydrous pyrolysis experiments on three potential gas sources in the Rocky Mountain tight gas sand fields (as a separate PDF file)

1.7 References

Ballentine, C. J., & O'nions, R. K. (1994). The use of natural He, Ne and Ar isotopes to study hydrocarbon-related fluid provenance, migration and mass balance in sedimentary basins. *Geological Society, London, Special Publications*, *78*(1), 347-361.

Ballentine, C. J., & Sherwood Lollar, B. (2002). Regional groundwater focusing of nitrogen and noble gases into the Hugoton-Panhandle giant gas field, USA. *Geochimica et Cosmochimica Acta*, *66*(14), 2483-2497.

Cumella, S. P., & Scheevel, J. (2008). The influence of stratigraphy and rock mechanics on Mesaverde gas distribution, Piceance Basin, Colorado, in S. P. Cumella, K. W. Shanley, and W. K. Camp, eds., Understanding, exploring, and developing tight-gas sands— 2005 Vail Hedberg Conference: AAPG Hedberg Series, no. 3, p. 137 – 155.

Henry, A. A. & Lewan, M. D. (1999). Comparison of kinetic-model predictions of deep gas generation. USGS Open-File Report: 99-32, 25 pp.

Kotarba, M. J., & Lewan, M. D. (2013). Sources of natural gases in Middle Cambrian reservoirs in Polish and Lithuanian Baltic Basin as determined by stable isotopes and hydrous pyrolysis of Lower Palaeozoic source rocks. *Chemical Geology*.

Lewan, M. D. & Henry, A. A. (1999). Gas-oil ratios for source rocks containing Type-I, -II, -IIS, and -III kerogens as determined by hydrous pyrolysis.USGS Open-File Report: 99-327, 9 pp.

Prinzhofer, A. A., & Huc, A. Y. (1995). Genetic and post-genetic molecular and isotopic fractionations in natural gases. *Chemical Geology*, *126*(3), 281-290.

Rooney, M. A., Claypool, G. E., & Chung, H.M. (1995). Modeling thermogenic gas generation using carbon isotope ratios of natural gas hydrocarbons. *Chemical Geology*, *126*(3), 219-232.

Schoell, M. (1983). Genetic characterization of natural gases. *AAPG bulletin*,*67*(12), 2225-2238.

Tang, Y., Perry, J. K., Jenden, P. D., & Schoell, M. (2000). Mathematical modeling of stable carbon isotope ratios in natural gases. *Geochimica et Cosmochimica Acta*, *64*(15), 2673-2687.

Zhang, T., & Krooss, B. M. (2001). Experimental investigation on the carbon isotope fractionation of methane during gas migration by diffusion through sedimentary rocks at elevated temperature and pressure. *Geochimica et Cosmochimica Acta*, *65*(16), 2723-2742.

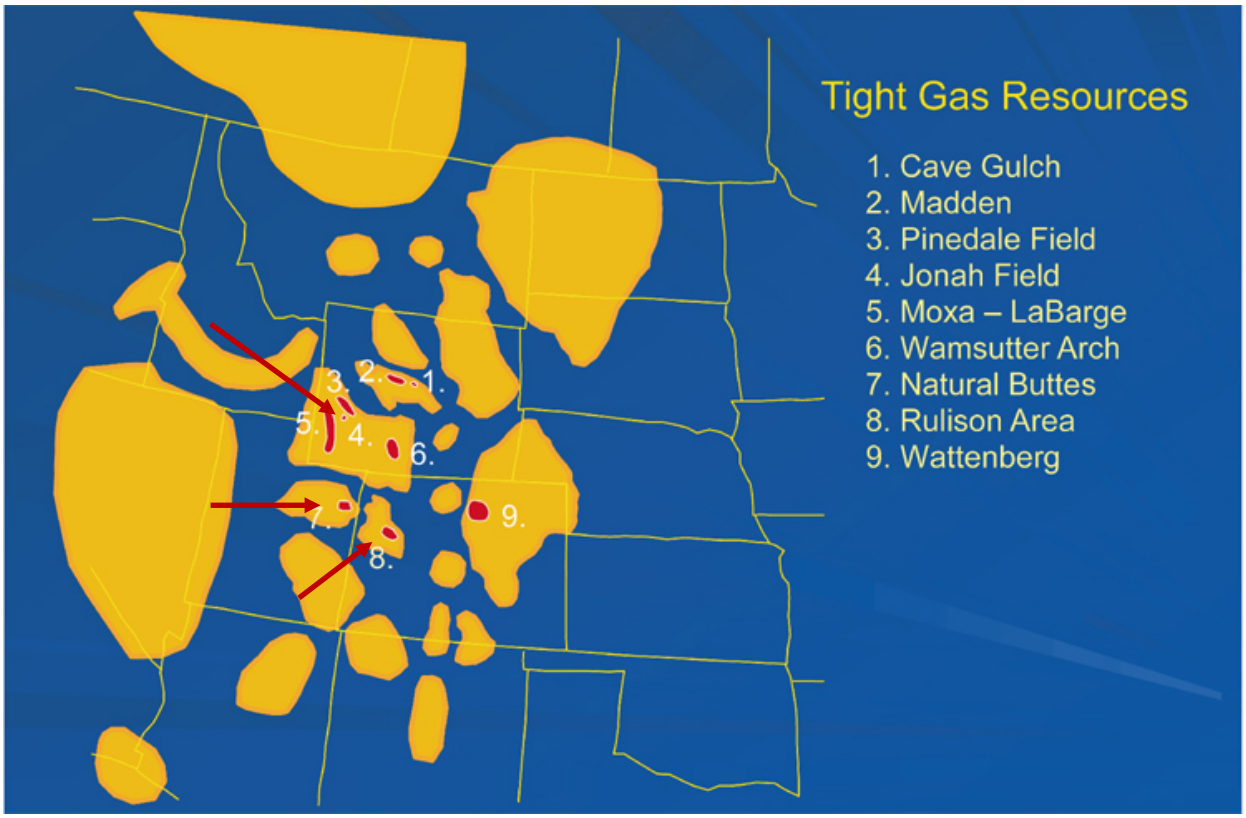

Figure 1.1. Map of sedimentary basins in the Rocky Mountains, showing location of sedimentary basins (yellow) and tight gas sand fields (red arrows). Fields in this study are indicated by arrows.

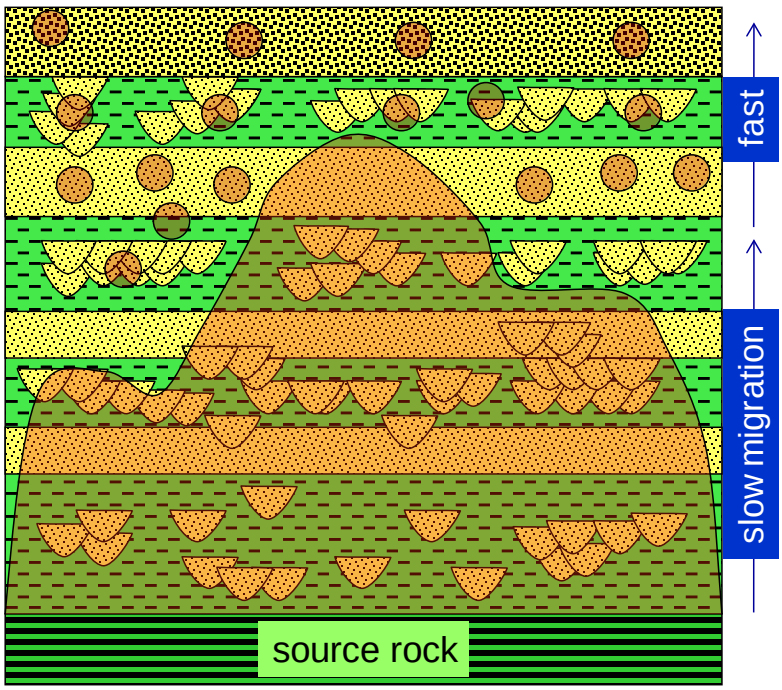

Figure 1.2. Model for steady state migration of oil through a tight-gas-sand reservoir.

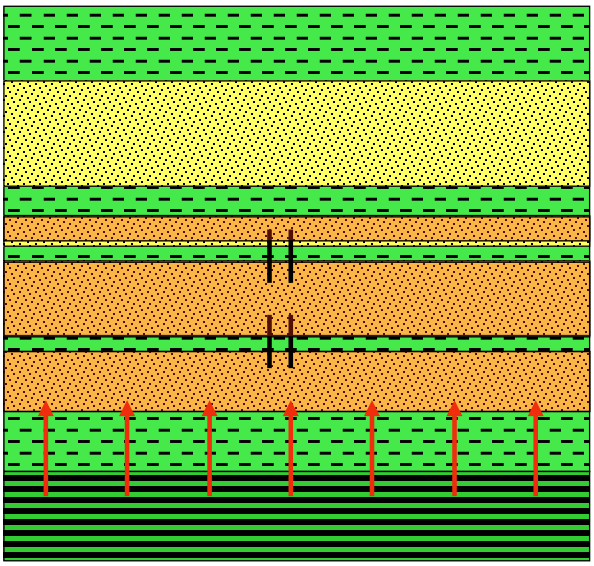

Model 1 - Self-fracturing (after Cumella and Scheeval, 2008):

The reservoir fills from bottom to top by the successive fill – seal rupture of successive reservoir compartments.

Top-of-gas depends on: (1) differences in fracture strength of intermediate seals; (2) differences in geometry and distribution of lowermost reservoirs.

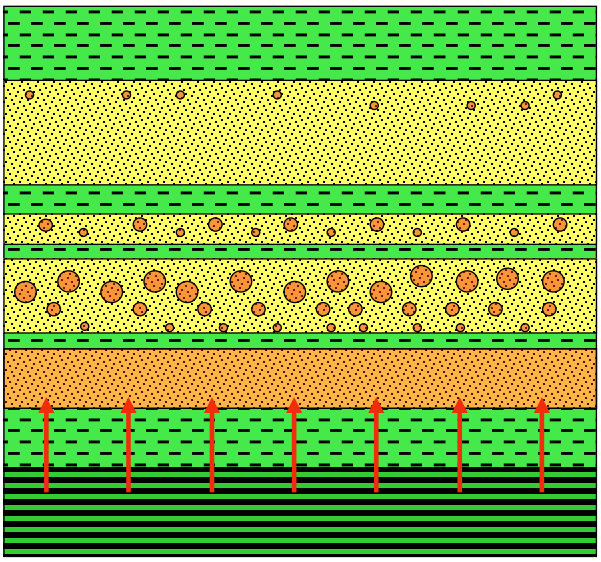

Model 2 - Diffusion:

Reservoir compartments fill by gas diffusion across intermediate seals (semi-permeable membrane).

Diffusion is driven by pressure differences and concentration gradients.

Top-of-gas controlled by: (1) unevenly distributed gas inputs into lowermost reservoir; (2) initial differences in gas distribution; (3) diffusion / permeability pathways.

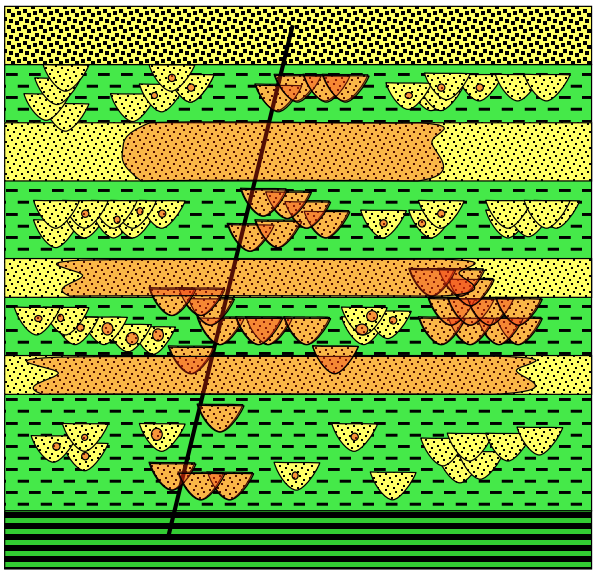

Model 3 – Migration fairways

Gas migrates vertically along fracture- / fault-controlled permeability pathways.

Gas migrates laterally by flow along continuous reservoir pathways or by diffusion across side-seals.

Figure 1.3. Models for gas migration in large tight-gas-sand reservoirs.

2 SUMMARY OF THE GAS FIELDS

2.1 Mamm Creek – Rulison – Parachute – Grand Valley fields, Piceance Basin, Colorado

The Mamm Creek – Rulison – Parachute – Grand Valley fields form a cluster of gas fields in the eastern Piceance Basin (Figure 2.1), more or less following the Colorado River and Interstate 70, from approximately 11 miles east of Rifle to 10 miles northwest of Parachute. The easternmost field is Mamm Creek, which lies approximately 6 miles from the eastern margin of the basin, defined by the Grand Hogback. Mamm Creek Field is located in the structurally deepest part of the Piceance Basin (Cumella and Ostby, 2003); from here to the west, stratigraphic levels become progressively shallower, and as a result, producing horizons are shallowest at the Grand Valley field northwest of the town of Parachute (Figure 2.2, courtesy of Larry Moyer).

2.1.1 Stratigraphy and reservoirs

The Mesaverde Group is the primary gas reservoir in the Piceance Basin (Figure 2.3). This is an Upper Cretaceous fluvial to shallow marine sequence deposited on the western margin of the Cretaceous Western Interior Seaway (Cumella and Ostby, 2003) that forms a westward tapering wedge (Cumella and Scheeval, 2008). Sediments were largely shed from the Sevier orogenic belt to the west. The Mesaverde is overlain by the Wasatch Formation, a relatively coarse clastic unit. It is underlain by the Mancos Shale, a mudstone-dominated sequence.

Gas production is largely from the Williams Fork Formation of the Mesaverde Group. This formation contains sandstones deposited in the channels of meandering fluvial systems, largely encased in floodplain mudstones and siltstones. The Cameo Coal zone occurs at the base of the Williams Fork, immediately overlying the Rollins Sandstone. The Cameo Zone is a thick sequence of interbedded sandstone, mudstone and coal, with an aggregate thickness of coal of approximately 90 feet (Hettinger and Kirschbaum, 2002).

The Williams Fork reservoir bodies are notably discontinuous, a primary reason for the dense well spacing that has been applied to development of these reservoirs. Pranter et al. (2007, 2009) have carried out detailed measurements of sandstone body geometries and described single story channel sands with a range of thicknesses from 4 to 30 feet and range of apparent widths from 44 to 1700 feet. Multistory channel sandstone bodies range in thickness from 5 to 47 feet and in apparent width from 53 to 2790 feet. In a subsurface study, Cumella and Ostby (2003) documented similarly discontinuous sandstones at well spacings of several hundred feet.

The Williams Fork Formation is underlain by the Iles Formation of the Mesaverde Group. Regressive sandstones within the Iles Formation include the Corcoran, Cozette and Rollins Members; these are substantially more continuous than the fluvial sandstones shallower in the section. Some production is derived from these units.

2.1.2 Reservoir quality

The Mesaverde sandstones are characterized by low porosities and permeabilities. Cumella and Ostby (2003) cited porosity values ranging from 6 to 12% and permeabilities from 0.1 to 2 µD (=0.0001 to 0.02 mD). In a more recent study, Stroker et al. (2013) characterized the porosity, permeability and mineralogy of 32 Mesaverde samples from the MWX-1 well and a second well from the Mamm Creek – Rulison – Parachute – Grand Valley complex of fields. These samples averaged 7.56% porosity and 62 µD permeability.

2.1.3 Source rocks

Two stratigraphic intervals are considered the primary source rocks for Piceance Basin gas reservoirs. These are the Cameo Coal section at the base of the Williams Fork Formation and the Mancos Shale (Nuccio and Roberts 2003, Yurewicz et al., 2003). The Cameo Coal zone generally contains 20 to 50 feet of net coal, locally up to 90 feet of coal (Yurewicz et al., 2003; Hettinger and Kirschbaum, 2002); this is considered to be Type III, gas-prone organic matter. Thinner coal zones are locally present in the Iles Formation and discontinuously dispersed in the Williams Fork above the Cameo Zone. In a basin modeling study, Yurewicz et al (2003) modeled the coals with an average TOC of 65% and an average HI of 225 mgHC/gC.

The Mancos Shale, which underlies the Mesaverde section, contains some organic-rich intervals. In their basin modeling study, Yurewicz et al (2003) modeled the Mancos Shale as a source rock 1000 feet thick, with an average total organic carbon (TOC) content of 1.25% and an initial hydrogen index (HI) of 150 mgHC/gC. In a later study of the Mancos Shale from the western Piceance Basin, Anderson and Harris (2006) identified one 70 foot thick, organic carbon-rich zone; in this zone, TOC values average 2.23% and HI values ranged from 343 to 457, indicating a concentration of oil-prone organic matter.

2.1.4 Burial history and thermal maturity

Burial history models from the Piceance Basin by Nuccio and Roberts (2003) typically show relatively slow subsidence from the late Paleozoic until approximately the beginning of the Cenomanian age (Figure 2.4). At this time, subsidence accelerated markedly and continued to remain high until approximately 20 Ma when formations reached their maximum burial depth. Regional uplift has occurred from 10 Ma to present. Subsidence models by Yurewicz et al. (2003) are similar. Estimates of the timing of maximum burial and the amount of uplift and erosion both carry significant uncertainty. Nuccio and Roberts (2003) estimated 5000 feet of uplift and erosion at the MWX-1 well at Rulison Field. Yurewicz et al. (2003) applied thermal maturity data, including apatite fission track analysis, and estimated that the amount of section removed could have been between 1800 and 5000 feet.

As a result of the deep burial occurring just prior to 20 Ma, thermal maturities are relatively high for their present-day burial depth in the area of the Mamm Creek– Rulison – Parachute – Grand Valley fields (Nuccio and Roberts, 2003). Modeled maturities at the base of the Mesaverde / top of Mancos section range from approximately 1.0 to 1.9% Ro. According to this model , hydrocarbon production began from 20 to 50 Ma. Yurewicz et al. (2003) modeled the Exxon No. Love Ranch well, approximately 30 miles north of the fields included in this study. Their results were broadly similar to that of Nuccio and Roberts (2003), with a modeled maturity of approximately 1.4% Ro at the level of the Cameo Coal Zone. Yurewicz et al. (2003) suggested that wells in the southern part of Piceance Basin increase in maturity more rapidly with depth than wells in the northern part of the basin, the former including the fields studied here. They attribute this to the presence of volcanics and igneous intrusions in the southern Piceance Basin.

2.1.5 Gas distribution

Gas saturation is continuous from a level within the Williams Fork Member down at least to the top of the Mancos Shale. From a regional perspective, the top of continuous gas cross-cuts stratigraphy. It is stratigraphically highest in the area of the Parachute and Rulison Fields and cuts downsection both to the east and west. In eastern Mamm Creek Field, the top of gas is approximately 500 feet above the top of the Cameo Coal, in Rulison Field it is 1800 feet above the Cameo, and in the Grand Valley Field, it is 1200 feet above the Cameo (from Cumella and Scheeval, 2008; their Figure 3). Cumella and Ostby (2003) suggest that the top of gas is at least locally controlled by the position of the Upper Williams Fork Shale Marker, a locally transgressive intervals that forms a relatively continuous shale. In the region of the Mamm

Creek – Rulison – Parachute – Grand Valley fields, the top of continuous gas is close to the base of this sequence (Cumella and Scheeval, 2008). Farther to the west and to the east, the top of gas may be determined by the invasion of percolating ground water.

2.2 Greater Natural Buttes Field, Uinta Basin, Utah

Greater Natural Buttes Field is a gas field in the northeastern part of the Uinta Basin, northeastern Utah, just west of the Douglas Creek Arch that separates the Uinta and Piceance Basins (Figure 2.1). At the location of Greater Natural Buttes, the depth to basement is approximately 15,000 to 20,000 feet. From here, the basin dips northwestward to a point in central Duschene County, Utah, where the depth to basement exceeds 30,000 feet. The basin is highly asymmetric, with steepest dips southward into the basin from the fault-bounded Uinta Mountain front.

2.2.1 Stratigraphy and Reservoirs

Commercial gas accumulations are found in the Mesaverde Group (Upper Cretaceous) and Wasatch Formation (Paleocene to Lower Eocene) (Cuzella and Stancel, 2006).

In the Greater Natural Buttes area, the Mesaverde Group is subdivided by Deo et al. (2013) into four units, which are from oldest to youngest: Blackhawk Formation, Castlegate Sandstone Formation, the Neslen Formation, and the Tuscher and Ferrer Formations (undifferentiated in the area of Greater Natural Buttes (Figure 2.5). The Mesaverde is a largely clastic sequence consisting of sandstones, siltstones and mudstones, deposited in settings ranging from deltaic to alluvial plain. The Mesaverde overlies and in part interfingers with the Mancos Shale, such that the Castlegate is overlain by the Buck Tongue shale unit within the Mancos. Cuzella and Stancell (2006) note that the Blackhawk Formation includes the shallow marine Desert, Grassy and Kenilworth Members.

Two intervals within this sequence are coaly: the Neslen Formation and the Blackhawk Formation, with net coal thicknesses of up to 29 and 80 feet, respectively.

Reservoirs in the Mesaverde are clearly discontinuous (Deo et al., 2013), often at a scale of 1000 feet separation. Wasatch reservoir sandstones are described as ‘lenticular’ (Stancel et al., 2008), suggesting these reservoir elements are discontinuous as well.

2.2.2 Structural Geology

Greater Natural Buttes is located in an area of relatively gentle northwest dip (Stancel et al., 2008). The field is bisected by a major northwest-trending fault at basement level (Figure 2.6). Cuzella and Stancel (2006) and Stancel et al. (2008) describe a zone of relatively intense fracturing in the central part of the field, with an orientation parallel to that of the basement fault.

2.2.3 Source Rocks

Potential source rocks for the Greater Natural Buttes gas accumulation include coals in the Blackhawk and Neslen Formations. Stratigraphic details, including thickness of coaly sections, are summarized in Johnson and Roberts (2003).

Two deeper formations are recognized as potential source rocks. Intervals within the Mancos Shale have sufficient organic matter to be considered both oil and gas source rocks (Anderson and Harris, 2006; Kirschbaum, 2003). As discussed in section 2.1, the nearest published information on the Mancos identified an 80 foot thick zone with an average of 2.25% TOC with relatively oil-prone kerogen (Anderson and Harris, 2006).

Greater Natural Buttes Field is located near the southern limit of Mowry deposition, so this formation may also have been a source of hydrocarbon(Kirschbaum, 2003);. Kirschbaum (2003) reported that the TOC content of 8 Mowry samples ranged from 1.6to 2.4%, containing a mixture of Type II and Type III organic matter. Ko (2010) reported on the analysis of 31 Mowry Shale samples from the Rock Springs uplift in southwestern Wyoming; these averaged 2.4%, with a range of HI values from 86 to 234, suggesting a mixture of Type II and Type III kerogen.

2.2.4 Burial History and Thermal maturity

Subsidence curves for wells near the Greater Natural Buttes Field are similar to those for the Piceance Basin, namely steady and relatively slow subsidence from 300 to 90 Ma, more rapid subsidence from 90 to 20 Ma, and uplift from 10 Ma to present (Figure 2.7; burial history model for the Conoco 22-1 Federal well, Nuccio and Roberts, 2003).

Models published by Nuccio and Roberts (2003) and Stancel et al. (2008) suggest a wide range of thermal maturity levels across the Greater Natural Butte Field, a result of the large east-to-

west distance across the field – 36 miles – in a region where burial depths increase from east to west. Stancel et al. (2008; their Figure 20) indicate that maturities at the eastern edge of the Greater Natural Field were approximately 0.7% Ro at Lower Mesaverde level, increasing to 1.6% Ro at the western edge of the field.

2.2.5 Reservoir Quality

Deo et al. (2013) cite porosities of 0.43 to 8.64% and permeabilities of 0.1 to 31 µD in the Mesaverde reservoirs. Nelson and Hoffman (2009) report an average porosity of 8.75% and average permeability 95 µD for the Wasatch Formation. Authigenic clays including kaolinite and chlorite and cements including quartz, feldspar, carbonate, halite and anhydrite were largely responsible for the low porosities (Shade and Hansen, 1992, Pitman et al., 1986).

2.2.6 Gas Distribution

Greater Natural Buttes is described by Schmoker et al. (1996) as a 'continuous gas accumulation', lacking distinct gas-water contacts. The top of gas is generally within the Wasatch Formation, but in detail, Stancel et al. (2008) show that the top of gas saturation cuts up and down section within this reservoir. In addition, sections of Wasatch that are gas-saturated downdip may be water-wet updip (Stancel et al., 2008; their figures 22 and 25).

2.3 Jonah Field, Greater Green River Basin, Wyoming

Jonah Field is a major gas field in the Hoback subbasin in the northern part of the Greater Green River Basin (Figure 2.8), southwestern Wyoming, located just south of the larger Pinedale Field and approximately 30 miles southwest of the Wind River Thrust fault (Montgomery and Robinson, 1997; Dubois et al., 2004), the major basement-penetrating thrust fault that marks the southwestern margin of the Wind River mountain range.

2.3.1 Stratigraphy and Reservoirs

Jonah Field reserves are primarily found in sandstones of the Upper Cretaceous Lance Formation (Figure 2.9). The Lance is a thick sequence of interbedded sandstones, siltstones and muddy sandstones, deposited in a fluvial and floodplain setting (Chapin et al., 2009). It ranges in thickness from 2000 feet in the southwestern corner of Jonah Field to 3000 feet downdip to the northeast. It was deposited by river systems that flowed from north-northwest to south-

southeast. Sediments were sourced from the Sevier orogenic highlands to the west, but uplift of the Wind River Range, which was contemporaneous with deposition of the Lance, strongly influenced depositional trends (Hanson et al., 2004). Sandstone reservoir bodies within the Lance consist of isolated channel sequences up to 20 feet thick and amalgamated channel sequences up to 50 feet thick, deposited by meandering rivers (Dubois et al., 2004). Sand bodies locally occur up to 100 feet thick, which are interpreted as deposited by braided river systems. Net sandstone within the Lance increases downdip from 800 to 1000 feet in the updip part of the Jonah structure to more than 1500 feet in downdip parts of the field (Cluff and Cluff, 2004a).

The Mesaverde Group underlies the Lance Formation. At Jonah Field, it is divided four formations, which in ascending order are: Blair Formation (dominantly sandstone; Rock Springs Formation (siltstone and mudstone with minor sandstone); Ericson Sandstone (dominantly sandstone with minor siltstone or mudstone); and Upper Mesaverde (dominantly siltstone and mudstone) (Dubois et al., 2004). The Rock Springs and Upper Mesaverde are interpreted as fluvial and floodplain deposits. The Blair Formation is interpreted as a delta front deposit (Rohler, 1988) and is therefore transitional to the underlying marine Baxter Shale.

The Lance Formation is overlain by the Unnamed Tertiary unit. Like the Lance, the Unnamed Tertiary unit consists of discontinuous fluvial sandstone bodies encased in overbank siltstone and mudstone (Dubois et al., 2004) and ranges in thickness from 600 to 1000 feet. The Unnamed Unit is in turn overlain by the Fort Union and Wasatch Formations.

2.3.2 Structure and Trapping

Unlike other fields in this study, there is a clear structural component to the gas accumulation at Jonah Field. The field is wedge-shaped, bounded on the south and west by steeply dipping faults (Figure 2.10) (Dubois et al., 2004; Hanson and Vega, 2004). The structural culmination is in the southwest corner of the field where these faults intersect, where the top of the Lance is at an elevation of 400 below MSL. Downdip to the northeast, the depth to the top of the Lance reaches 1600 feet below MSL in the syncline separating Jonah Field from the Pinedale Field. The present configuration of the southern bounding fault is down to the south (Dubois et al., 2004), but relative thicknesses vary across the fault for different stratigraphic intervals, suggesting a complex structural history; Hanson et al. (2004) interpret as a predominantly left lateral strike-slip fault. The Jonah structure is subdivided by a number of north to northeast trending internal faults that exhibit complex offsets (Dubois et al., 2004).

One important manifestation of the Jonah structure is variation in formation pressure. Within the Jonah structure, the top of overpressure is reached near the base of the Fort Union Formation, whereas outside the structure, overpressure is reached within or near the top of the Lower Lance section (Cluff and Cluff, 2004b). Cluff and Cluff (2004b) interpret the overpressured cell at Jonah Field to be the remnant of regional overpressure, now largely bled off following Late Tertiary uplift and erosion.

2.3.3 Source Rocks

Source rocks for the Jonah accumulation may have included coaly intervals in the Upper and Lower Mesaverde sections, particularly the latter (Figure 2.9) (Coskey, 2004). The Baxter and Hilliard Shale intervals are time-equivalent to the Mancos Shale of the Piceance and Uinta Basins; however data from the Green River Basin indicate relatively low TOC values (≤ 1.39%; Law, 1984), and Coskey (2004) suggested that there was no evidence to link any of the Jonah Field hydrocarbons to these formations. The underlying Mowry Shale must also be considered a potential source rock, given TOC values from the Rock Springs uplift to the south of Jonah Field that averaged 2.4% (Ko, 2010).

Hanson et al. (2004) concluded that the Jonah gases originated from the secondary cracking of oil. Dubois et al. (2004) suggested that the two viable sources were marine shales underlying the reservoir, either the Baxter / Hilliard section or the deeper Mowry Shale.

2.3.4 Burial History and Thermal maturity

Burial history models for Jonah Field show a period of rapid subsidence from 90 to 50 Ma (Coskey, 2004). This was followed by a period of very little subsidence from 50 to 5 Ma and then uplift and erosion from 5 Ma to present.

Within the Jonah structure, thermal maturities within the Lance section range from 0.7 to 0.9% Ro, interpreted to be too low for significant gas generation (Coskey, 2004). Maturities in the Mesaverde section range from 0.9 to 1.3% Ro. These results from Coskey (2004) suggest that either (1) gas was generated from deeper than the Mesaverde (ie. Baxter/Hilliard or Mowry), (2) gas was generated from the Lance or Mesaverde where these formations were buried more deeply and then migrated laterally to fill the Jonah structure, or (3) significant volumes of gas were generated from rocks at lower maturity than Coskey (2004) considered viable. Coskey

(2004) suggested that the Ericson Sandstone of the Mesaverde Group could have served as a pathway for lateral migration.

The burial history with rapid burial to 50 Ma implies that source rocks generated much of the hydrocarbon charge beginning at 55 to 50 Ma and that the rate of hydrocarbon generation decreased significant after 50 Ma, when the rate of burial decreased substantially (Coskey, 2004).

2.3.5 Reservoir Quality

Sandstones in the Lance Formation are generally characterized by low porosity and permeability. The average porosity of 255 core samples was 7.7% with a maximum of 12.9% (Cluff and Cluff, 2004a). Approximately 30% of the samples had porosities greater than 9%. The average permeability determined in this laboratory analysis was 145 µD (0.145 mD), but this may include samples with microfractures. Well test data cited by Eberhard and Mullen (2001) indicate that the effective permeability to gas in most reservoir bodies was on the order of a few tens of microdarcies.

2.3.6 Hydrocarbon Distribution

Dubois et al. (2004) noted that Jonah Field gases are relatively wet and that the liquid content increases downsection by a factor of nearly 4 times, from approximately 12 to 45 bbls liquid/mmcf gas from the top of the Lance to 2500 meters below the top.

2.4 References

Anderson, D. S., & Harris, N. B. (2006). Integrated Sequence Stratigraphic and Geochemical Resource Characterization of the Lower Mancos Shale, Uinta Basin, Utah. *Utah Geological Survey, Open File Report*, *483*.

Chapin, M. A., Govert, A., & Ugueto, G. (2009). Examining Detailed Facies and Rock Property Variation in Upper Cretaceous, Tight Gas Reservoirs, Pinedale Field, Wyoming. AAPG Search and Discovery Article #20077, 10 pp.

Cluff, S. G., & Cluff, R. M. (2004). Petrophysics of the Lance sandstone reservoirs in Jonah field, Sublette County, Wyoming. In Jonah Field: Case Study of a Giant Tight-Gas Fluvial Reservoir, J. W. Robinson and K. W. Shanley, eds.: AAPG Studies in Geology 52 and Rocky Mountain Association of Geologists 2004 Guidebook, 215-241.

Cluff, R. M., & Cluff, S. G. (2004b). The Origin of Jonah Field, Northern Green River Basin, Wyoming. In Jonah Field: Case Study of a Giant Tight-Gas Fluvial Reservoir, J. W. Robinson and K. W. Shanley, eds.: AAPG Studies in Geology 52 and Rocky Mountain Association of Geologists 2004 Guidebook, 127-145.

Coskey, R. J. (2004). Burial-history modeling of the Jonah field area: An unusual and possibly unique gas accumulation in the Green River Basin, Wyoming. In Jonah Field: Case Study of a Giant Tight-Gas Fluvial Reservoir, J. W. Robinson and K. W. Shanley, eds.: AAPG Studies in Geology 52 and Rocky Mountain Association of Geologists 2004 Guidebook, 93-125.

Cumella, S., & Ostby, D. B. (2003). Geology of the basin-centered gas accumulation: Rocky Mountain Association of Geologists. *Piceance Basin Guidebook, p. 171-193*.

Cumella, S. P., & Scheevel, J. (2008). The influence of stratigraphy and rock mechanics on Mesaverde gas distribution, Piceance Basin, Colorado, in S. P. Cumella, K. W. Shanley, and W. K. Camp, eds., Understanding, exploring, and developing tight-gas sands— 2005 Vail Hedberg Conference: AAPG Hedberg Series, no. 3, p. 137 – 155.

Cuzella, J. J., & Stancel, S. G. (2006). Greater Natural Buttes Field, Uinta Basin, Utah. *The Mountain Geologist*, Vol. 43, No. 3 (July 2006), p 213-218.

Deo, M.D., Sorkhabi, R., McLennan, J., Bhide R., Zhao, N., Sonntag, R., Evans, J., Morgan, C., Carney, S., & LaPointe, P. (2013). Gas Production Forecasting From Tight Gas Reservoirs: Integrating Natural Fracture Networks and Hydraulic Fractures, RPSEA, 07122-44 Final Report.

DuBois, D. P., Wynne, P. J., Smagala, T. M., Johnson, J. L., Engler, K. D., & McBride, B. C. (2004). Geology of Jonah field, Sublette County, Wyoming. In Jonah Field: Case Study of a Giant Tight-Gas Fluvial Reservoir, J. W. Robinson and K. W. Shanley, eds.: AAPG Studies in Geology 52 and Rocky Mountain Association of Geologists 2004 Guidebook, p. 37-59.

Eberhard, M., & Mullen, M. (2001). The effect of stimulation methodologies on production in the Jonah field. Rocky Mountain Petroleum Technology Conference, Society of Petroleum Engineers, Keystone, 21– 23 May 2001, SPE paper 71048, 9 pp.

Hanson, W. B., Vega, V., & Cox, D. (2004). Structural geology, seismic imaging, and genesis of the giant Jonah gas field, Wyoming, USA. *In* J. W. Robinson and K. W. Shanley, eds., Jonah Field: Case Study of a Giant Tight-Gas Fluvial Reservoir: AAPG Studies in Geology 52, chapter 6, p. 61-92.

Hettinger, R. D., & Kirschbaum, M. A. (2002). *Stratigraphy of the Upper Cretaceous Mancos Shale (upper part) and Mesaverde Group in the southern part of the Uinta and Piceance basins, Utah and Colorado*. US Geological Survey, GEOLOGIC INVESTIGATIONS SERIES I–2764, 21 pp.

Johnson, R. C., & Roberts, S. B. (2003). The Mesaverde total petroleum system, Uinta-Piceance Province, Utah and Colorado. *Petroleum systems and geologic assessment of oil and gas in the Uinta-Piceance province, Utah and Colorado: US Geological Survey Digital Data Series DDS-69-B*, 63 pp.

Kirschbaum, M. A. (2003). Geologic assessment of undiscovered oil and gas resources of the Mancos/Mowry Total Petroleum System, Uinta-Piceance Province, Utah and Colorado. *Petroleum Systems and Geologic Assessment of Oil and Gas in the Uinta-Piceance Province, Utah and Colorado. US Geological Survey Digital Data Series DDS-69-B*, 29 pp.

Ko, T. (2010). Characterization of Gas Generated by Sequential Hydrous Pyrolysis of Potential Gas-Prone Source Rocks for Tight-Gas Reservoirs in the Rocky Mountain Area: M.Sc. thesis, Colorado School of Mines.

Montgomery, S. L., & Robinson, J. W. (1997). Jonah Field, Sublette County, Wyoming; gas production from overpressured Upper Cretaceous Lance sandstones of the Green River basin. *AAPG bulletin*, *81*(7), 1049-1062.

Nuccio, V. F., & Roberts, L. N. (2003). Thermal maturity and oil and gas generation history of petroleum systems in the Uinta-Piceance Province, Utah and Colorado. *Petroleum Systems and Geologic Assessment of Oil and Gas in the Uinta–Piceance Province, Utah and Colorado: United States Geological Survey, Digital Data Series DDS-69-B*, Chapter 4, 35 pp.

Osmond, J.C. (1992). Greater Natural Buttes gas field, Uintah County, Utah. In: Fouch, T.D., Nuccio, V.F., and Chidsey, T.C. (eds.), Hydrocarbon and Mineral Resources of the Uinta Basin, Utah and Colorado. Utah Geological Association Guidebook 20, p. 143- 163.

Pitman, J.K., Anders, D.E., Fouch, T.D., & Nichols, D.J., (1986). Hydrocarbon potential of nonmarine Upper Cretaceous and Lower Tertiary rocks, eastern Uinta basin, Utah, *in* Spencer, C.W., and Mast, R.F., eds., Geology of tight gas reservoirs: American Association of Petroleum Geologists Studies in Geology 24, p. 235–252.

Pranter, M. J., Ellison, A. I., Cole, R. D., & Patterson, P. E. (2007). Analysis and modeling of intermediate-scale reservoir heterogeneity based on a fluvial point-bar outcrop analog, Williams Fork Formation, Piceance Basin, Colorado. *AAPG bulletin*, *91*(7), 1025-1051.

Pranter, M. J., Cole, R. D., Panjaitan, H., & Sommer, N. K. (2009). Sandstone-body dimensions in a lower coastal-plain depositional setting: lower Williams Fork Formation, Coal Canyon, Piceance Basin, Colorado. *AAPG Bulletin*, *93*(10), 1379-1401.

Rohler, H.W., (1988). Submarine slumps in delta-front sandstones of the Upper Cretaceous Blair Formation, Rock Springs Uplift, Wyoming. U.S. Geological Survey Bulletin 1699, 11 pp.

Schmoker, J.W., T.D. Fouch, and R.R. Carpentier, 1996, Gas in the Uinta Basin, Utah – resources in continuous accumulations: The Mountain Geologist, v. 33, n. 4, p. 95-104.

Shade, M.E., & Hansen, D.K.T., (1992). Drilled sidewall cores aid in interpretation of the Tertiary Wasatch Formation, Natural Buttes Field, Utah, in Fouch, T.D., Nuccio, V.F., and Chidsey, T.C., Jr., eds., Hydrocarbon and Mineral Resources of the Uinta Basin: Utah Geological Association Guidebook 20, p. 193–218.

Stroker, T. M., Harris, N. B., Elliott, W. C., & Wampler, M. J. (2013). Diagenesis of a tight gas sand reservoir: Upper Cretaceous Mesaverde Group, Piceance Basin, Colorado. *Marine and Petroleum Geology*, *40*, 48-68.

Yurewicz, D. A., Bohacs, K. M., Yeakel, J. D., & Kronmueller, K. (2003). Source rock analysis and hydrocarbon generation, Mesaverde Group and Mancos Shale, northern Piceance Basin, Colorado.

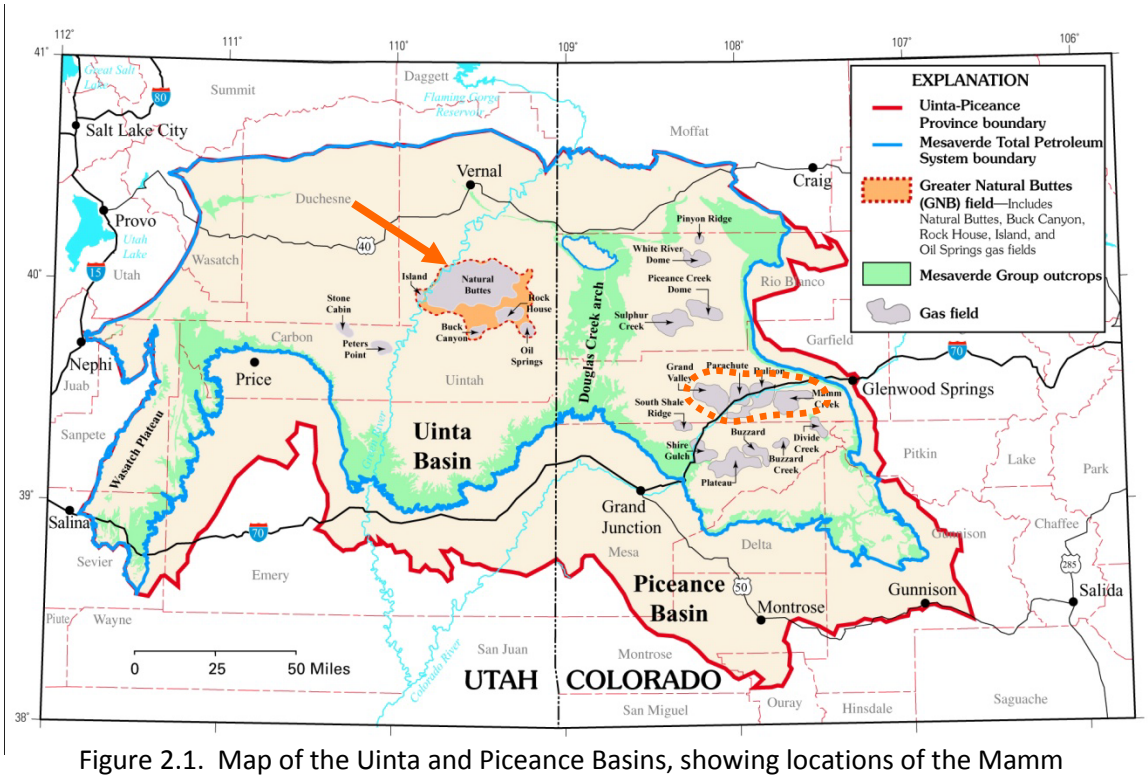

Figure 2.1. Map of the Uinta and Piceance Basins, showing locations of the Mamm Creek-Rulison-Parachute-Grand Valley complex of fields in the Piceance Basin (orange outline) and the Greater Natural Buttes Field in the Uinta Basin (orange arrow). Modified from Johnson and Roberts (2003).

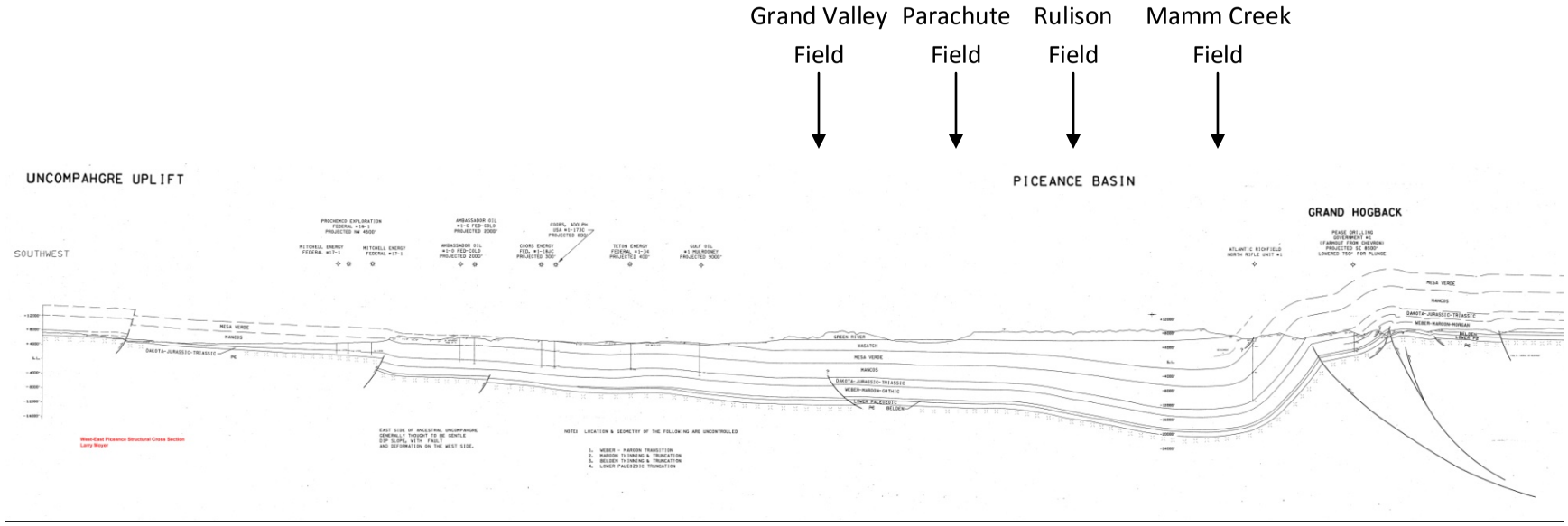

Figure 2.2. East – west cross-section through the Piceance Basin. Courtesy of Larry Moyer.

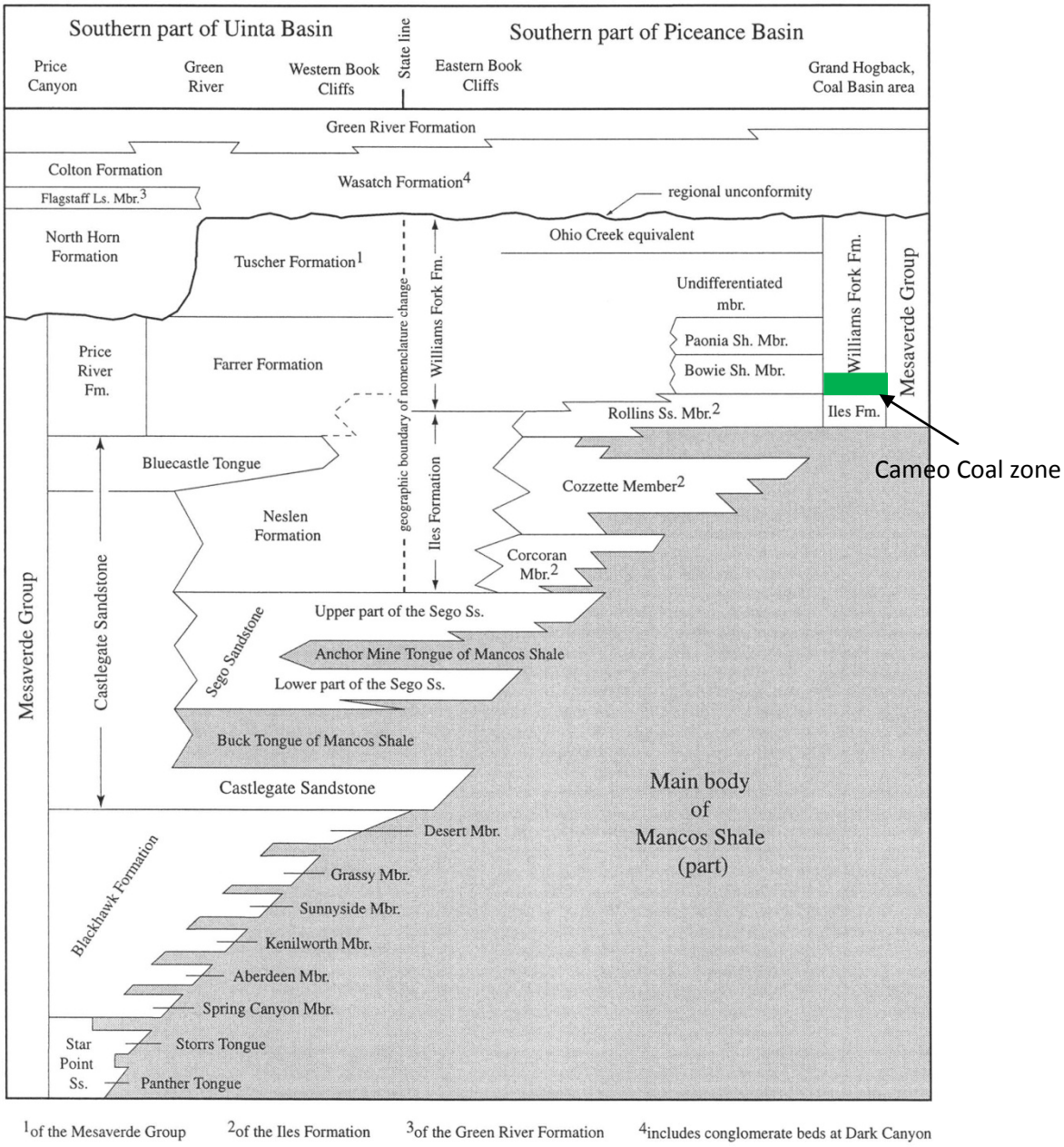

Figure 2.3. Stratigraphy of the southern Piceance and southern Uinta Basins, modified from Hettinger and Kirschbaum (2002).

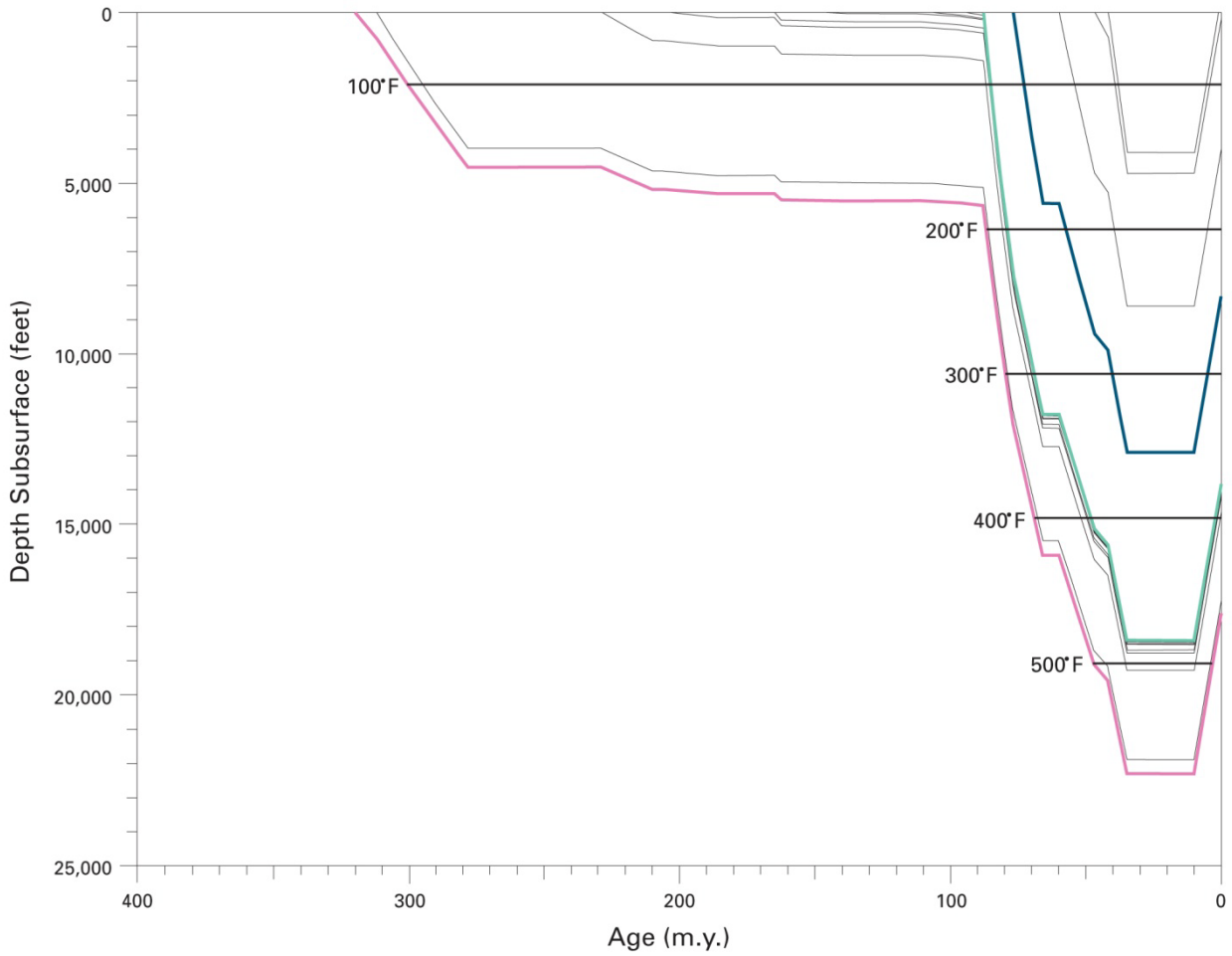

Figure 14. Burial curve representing area around the CER Corp., MWX-1 well. Data used to construct the curve are presented in table 1. Location shown in figure 1. Red curve represents base of Permian Phosphoria Formation or other potential Pennsylvanian-Permian source rocks. Green curve represents base of Mancos Shale. Blue curve represents base of Mesaverde Group/top of Mancos Shale. All but a few hundred feet of Tertiary rocks has been eroded.

Figure 2.4. Burial history diagram for the MWX-1 well, Rulison Field, Piceance Basin. From Nuccio and Roberts (2003).

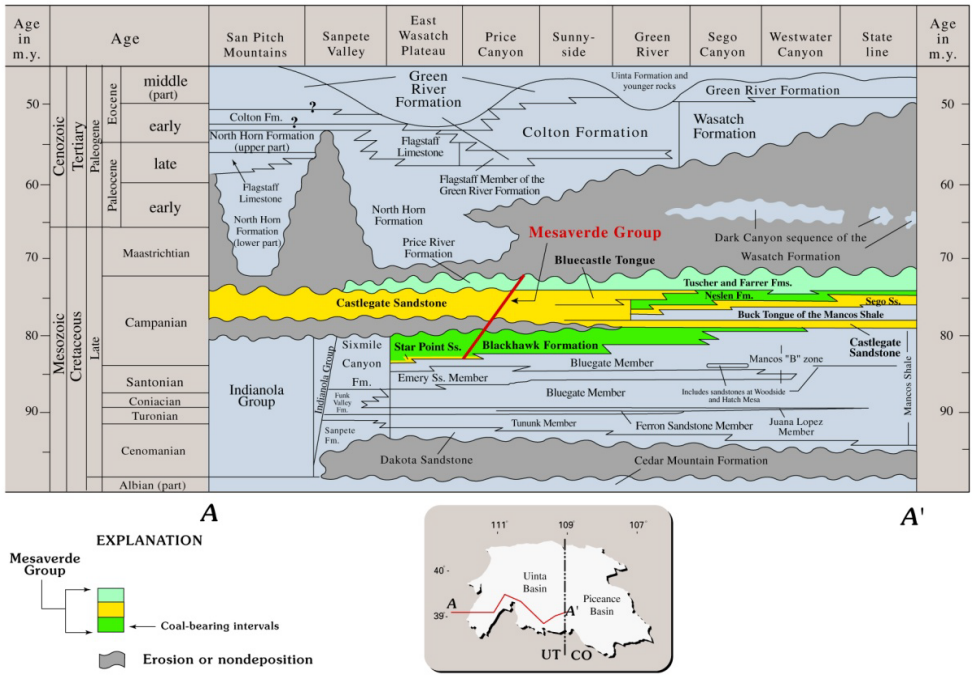

Figure 2.5. Chronostratigraphic chart of the Uinta Basin. From Johnson and Roberts, 2003.

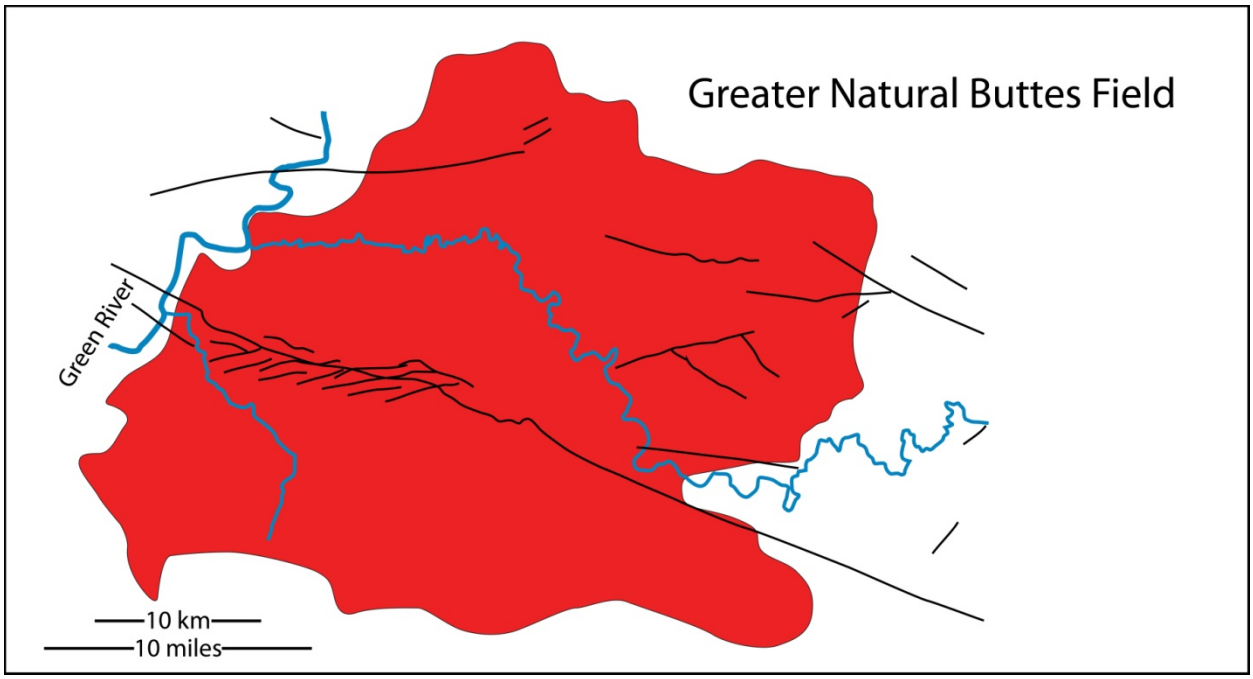

Figure 2.6. Outline of the Greater Natural Buttes Field, showing major structures. Map courtesy of Anadarko Petroleum.

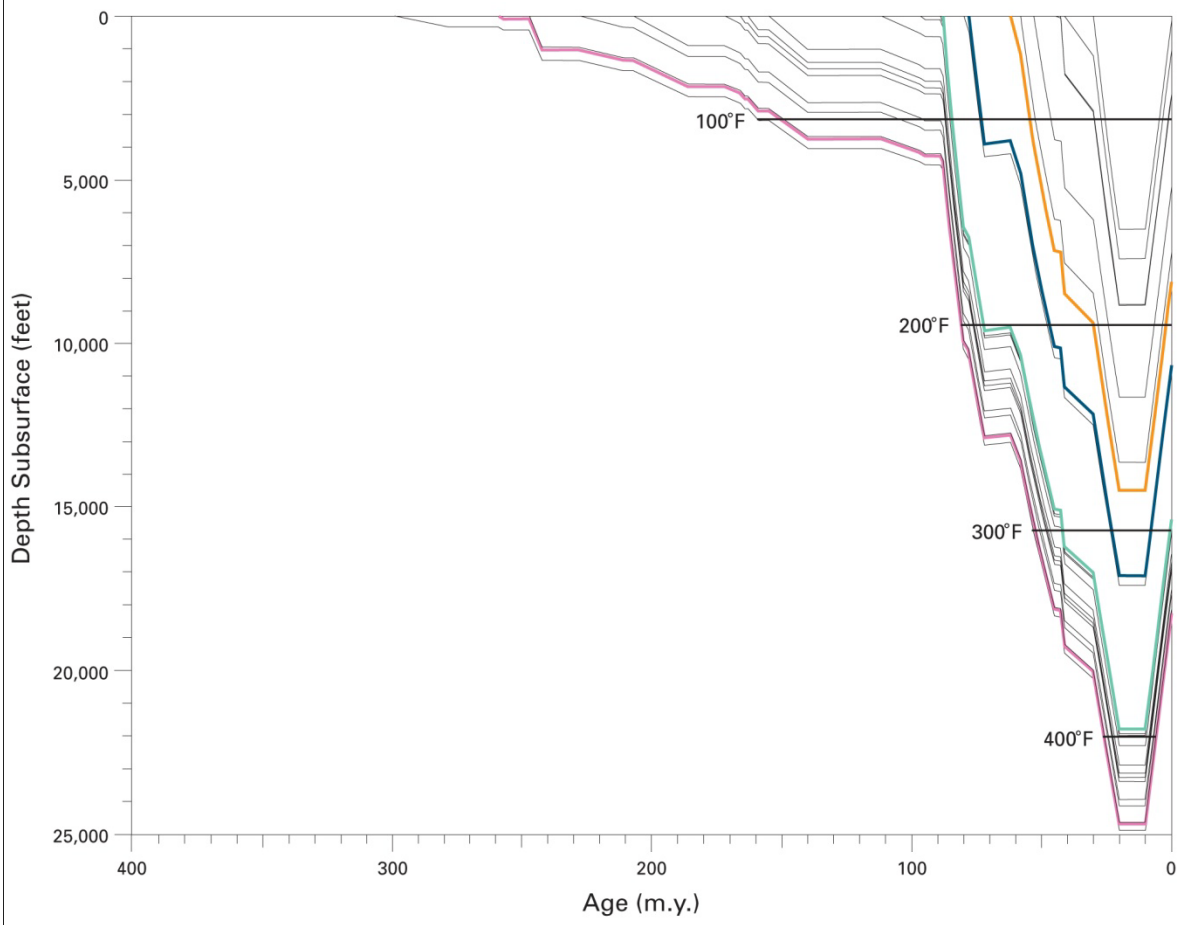

Figure 7. Burial curve representing area around the Conoco, 22-1 Federal well. Data used to construct the curve are presented in table 1. Location shown in figure 1. Red curve represents base of Permian Phosphoria Formation or other potential Pennsylvanian-Permian source rocks. Green curve represents base of Mancos Shale. Blue curve represents base of Mesaverde Group/top of Mancos Shale. Orange curve represents lower part of Green River Formation.

Figure 2.7. Burial history diagram for the Conoco 22-1 Federal well, eastern Uinta Basin. From Nuccio and Roberts (2003).

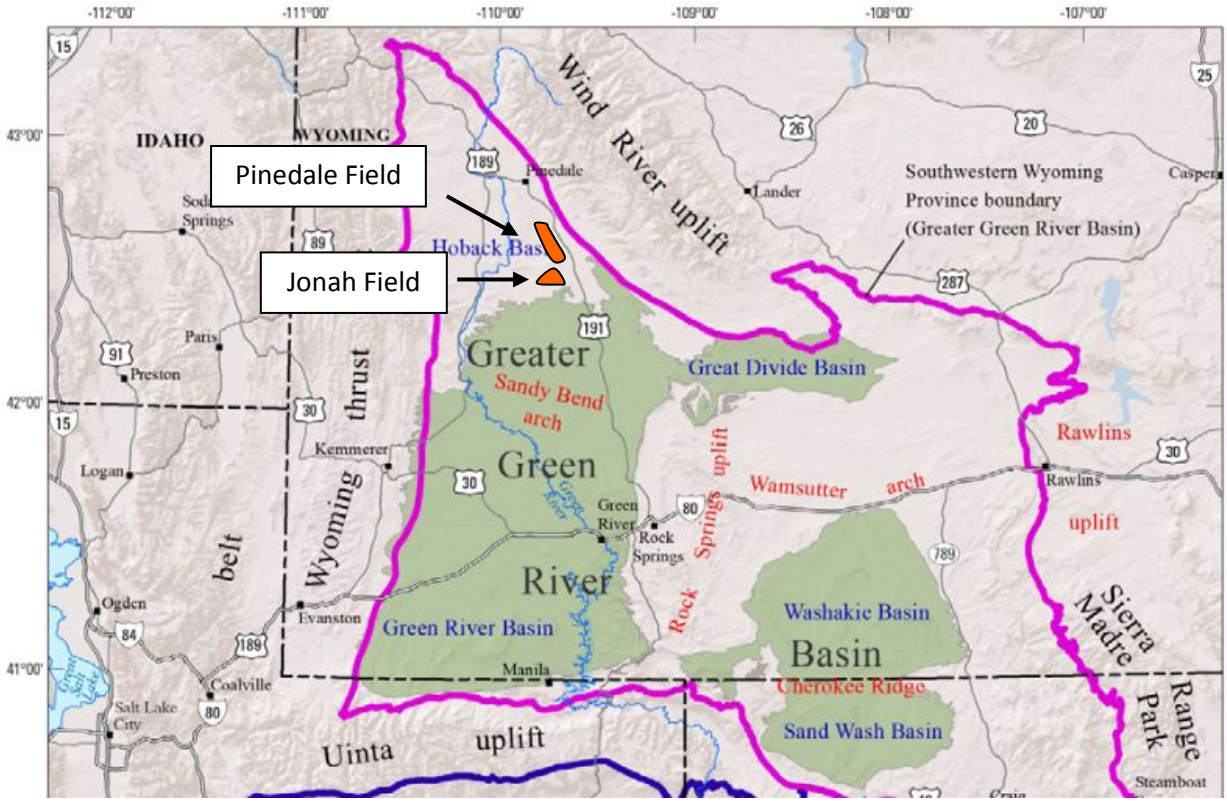

Figure 2.8. Map of the Greater Green River Basin, showing location of Jonah and Pinedale Fields.

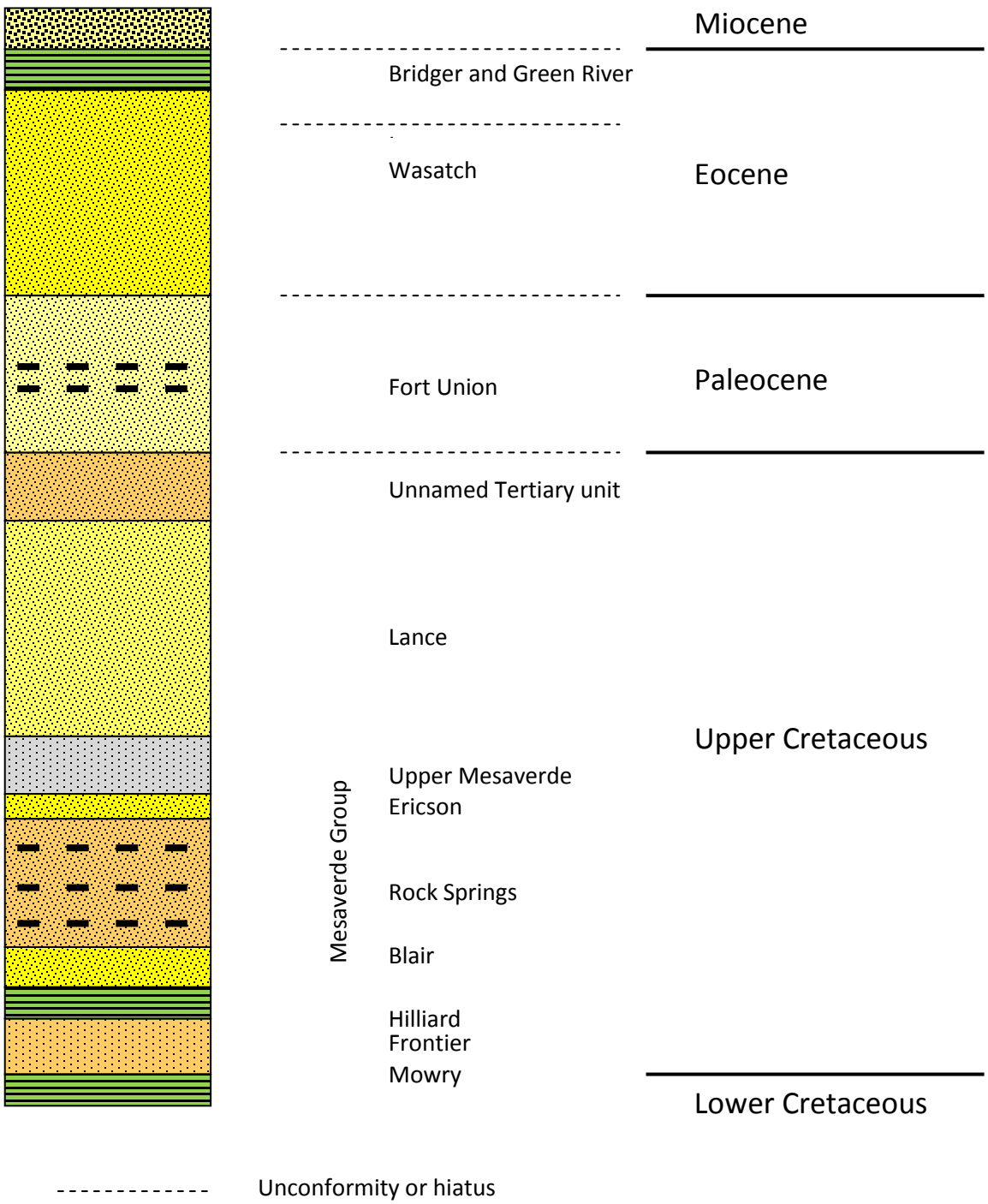

Figure 2.9. Stratigraphic column for the Cretaceous through Tertiary section in the vicinity of Jonah Field. Based on Coskey (2004) and Dubois et al. (2004).

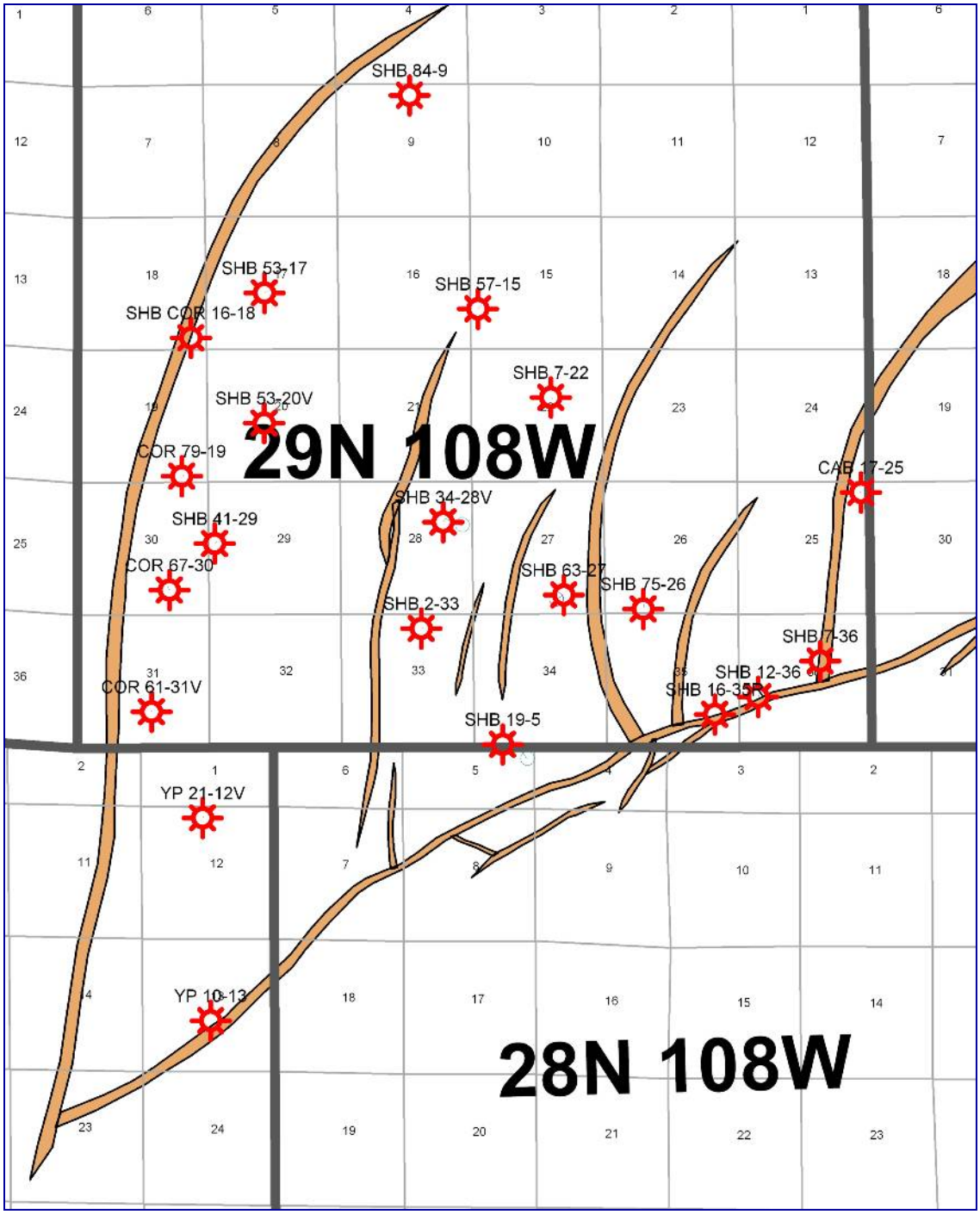

Figure 2.10. Map of the Jonah field, showing location of major faults. The high point of the structure is located at the southwest corner of the structure. Map provided by Encana.

3 SAMPLING AND ANALYTICAL METHODS

3.1 Gas Sampling

Production gas samples were taken from well heads. Isotubes® were attached to valves on the well head with a sampling manifold. The well head valve was opened and gas was allowed to flow through the isotube for 30 seconds to 1 minute. The isotube was released from sampling manifold and end caps placed on the isotubes. Well head pressure was recorded. Isotubes were shipped the University of Oklahoma for analysis.

Mud gas samples were taken from the mud gas line. Isotubes in a mud gas sampling manifold was placed in line with the mud gas system, either directly in front of the Payson or in front of the mud pit. Mud gas readings were monitored, and samples were taken when mud gas readings reached values of 4 or 5 times background values. Gas kicks were correlated with drilling connections, such that connection gas kicks were not sampled. Sample spacing was generally 100 to 200 feet. Mud gas concentrations were recorded for background gas and gas kicks. Circulation times were also recorded. Isotubes were shipped the University of Oklahoma for analysis.

Noble gas samples were taken from well heads. Sampling lines were attached to valves on the well head. Gas flowed through the sampling lines and through a 60 cm-long refrigerator-grade copper tube that was held in a stainless steel bracket. Gas was allow to flow through the tube for 3 to 5 minutes, depending on well head pressure. The downstream end of the tube was clamped, forming a cold weld. The upstream end was then clamped and sealed, and the tube was disconnected from the well head. Sampling tubes, clamped and sealed in their brackets, were shipped to University of Manchester for analysis.

3.2 Fluid Inclusion Sampling

Fluid inclusion analysis was performed on cuttings samples from the Mamm Creek – Rulison – Parachute – Grand Valley area in the Piceance Basin and on samples from Jonah Field, Greater Green River Basin. Samples from the Piceance Basin were taken from the U.S. Geological Survey sample collection in Lakewood, Colorado, focusing on sandstones in the section. Samples from Jonah Field were provided by Encana.

3.3 Gas analysis

Gas compositions and carbon ($\delta^{13}C$) and hydrogen (δD) isotope analyses were conducted at the University of Oklahoma, Organic Geochemistry Laboratories. Gas compositional analyses were determined from the m/z 44 chromatogram generated during the GCIRMS (gas chromatography – isotope ratio mass spectroscopy) analysis. The isotopic composition of the individual compounds in the gas samples was measured by gas chromatography–isotope ratio mass spectrometry using a Varian 3400 gas chromatograph coupled through a combustion reactor with a Finnigan MAT 252 isotope ratio mass spectrometer. The GC was equipped with a Pora-Plot-Q#CP7551column (SN9220868; length 27.5m; internal diameter 0.3mm; film thickness 20um). Temperature program: 40°C, hold for 12min., 15°C per min to 220°C, hold for 15min.; flow rate=1ml/min.; injector temperature 240°C; split ratio 1 to 15. For carbon isotope determination the oxidation reactor was set at a temperature of 1030°C and for HD determination the Pyrocell was set at 1420°C.

Noble gas isotope concentrations were measured at the University of Manchester for He, Ne, Ar, Kr and Xe as described by Macintosh and Ballentine (2012). Briefly, most of the active gases were removed by reaction with a Ti sponge at 900°C followed by exposure of gases to a SAES NP10 Ti/Al/Zr 'getter' at 350°C. from aliquots of gas. Ar, Kr and Xe were removed in a high temperature cryogenic trap, followed by removal of Ne in a low temperature trap, leaving a gas consisting solely of He. Analyses were carried out on a MAP 215 mass spectrometer, sequentially analyzing He, Ne, Ar, Kr and Xe. Mass spectrometer linearity and reproducibility of noble gas isotope rations was confirmed by replicate analysis of an air standard.

3.4 Fluid Inclusion Analysis

See appendices for details on analysis of the fluid inclusion samples.

3.5 References

Mackintosh, S. J., & Ballentine, C. J. (2012). Using $^{3}He/^{4}He$ isotope ratios to identify the source of deep reservoir contributions to shallow fluids and soil gas. *Chemical Geology*, *304*, 142-150.

4 PICEANCE BASIN RESULTS AND INTERPRETATION

4.1 Data Set

The dataset from the Piceance Basin includes:

- Production gas samples (47) from Grand Valley, Parachute, Rulison, and the eastern part of Mamm Creek fields, analyzed for bulk gas composition and C/H isotopes (Figure 4.1).
- Mud gas samples from 13 wells from Grand Valley, Parachute, Rulison, and eastern Mamm Creek fields, analyzed for bulk composition and C/H isotopes (Figure 4.2).
- Production gas samples (29) from Grand Valley, Parachute and Rulison, analyzed for noble gas composition (Figure 4.3).
- Fluid inclusion samples (cuttings) from five wells in Grand Valley, Parachute, Rulison, and Mamm Creek fields (Figure 4.4).

4.2 Production Gases

4.2.1 Bulk Gas Compositions

The compositions of production gases are summarized in Table 4.1.

In the Rulison, Parachute and Grand Valley fields, production gases averaged 10 to 11% C_{2+} component, with 87% methane, 6 to 8% ethane, 2.5 to 4% propane, 2% butane and 1% pentane. The average CO_2 content in the three fields ranged from 3 to 5%. Gas compositions were notably wetter in the Mamm Creek field. The Mamm Creek gas had an average C_{2+} content of 25%, with 75% methane, 13% ethane, 7% propane, 6% butane and 1% pentane. CO_2 was not measured in these samples.

The distribution of gas wetness is shown in Figure 4.5. Wet gases are clearly concentrated in the Mamm Creek area. There is otherwise little obvious spatial pattern to gas wetness, except for possibly a concentration of the driest gases along the central axis of the Rulison – Parachute – Grand Valley trend.

C_2/C_3 is another measure of gas wetness, with low values typical of wet gases. The distribution of C_2/C_3 values is shown in Figure 4.6. Mamm Creek gases are characterized by low ratios,

consistent with the gas wetness data. Gases from Rulison, Parachute and Grand Valley are characterized by a wide range of C_2/C_3 ratios with no obvious spatial pattern.

4.2.2 Carbon and Hydrogen Isotopic Composition

Carbon isotopes

The average carbon isotopic composition varied significant in the methane fraction (Table 4.1). The Mamm Creek gases averaged $\delta^{13}C_{C1}$ of -39.06‰, more negative than the other fields. Parachute methane compositions were also relatively negative (-38.12‰), while the Rulison and Grand Valley methane compositions were more positive (-36.11‰ and -34.03‰, respectively). A map of $\delta^{13}C_{C1}$ (Figure 4.7) shows no obvious spatial pattern, except that relatively negative values predominate at Mamm Creek: relatively positive values are present in all fields.

The carbonate isotopic composition of the ethanes are all quite similar (-25.97 to -26.82‰), as are the propanes (-24.08 to -24.18‰). The butane and pentane compositions are similar, with the *iso*-butane and *iso*-pentane compositions systematically heavier than the *n*-butane and *n*-pentane by 0.6 to 1.0‰. The pentanes had slightly more positive $\delta^{13}C$ values than the other fields by 1.0 to 1.5‰.

Chung plots (Chung et al., 1988) are used to examine the isotopic composition of hydrocarbon gas species, excluding the *iso* forms of C_4 and C_5, on a sample by sample basis. Gases generated from a single source rock at uniform maturity should have a linear trend on this plot, with the slope of the line becoming flatter with increasing thermal maturity (Tang, 2000).

Most of the Mamm Creek gas samples (Figure 4.8) define a similar, nearly linear trend of increasingly negative $\delta^{13}C$ values with decreasing carbon number. N-pentane samples have $\delta^{13}C$ values of approximately -23‰, while methane samples have $\delta^{13}C$ values of approximately -40‰. Two samples in this data set are distinctive, with much more positive (heavier) $\delta^{13}C_{C1}$: the BBC 12D-24-692 well, with $\delta^{13}C_{C1}$ of -30.7‰ and the JOLLEY FED 21A-28-691 Jolley Federal 21A-28-691 well, with a $\delta^{13}C_{C1}$ of -34.7‰; the total range in $\delta^{13}C_{C1}$ is 10.6‰.

Rulison samples (Figure 4.9) display more variability and fundamentally different patterns as compared to the Mamm Creek samples. A number of the samples show a trend of increasing $\delta^{13}C$ from the pentane to butane and / or propane fractions, instead of the normal trend to more negative $\delta^{13}C$ compositions. These samples are Rulison wells: Z, GG, Y, RR, U, V, X and HH. These wells are located primarily in the northwest part of the field. Three wells (H, X, W)

had anomalously positive $\delta^{13}C_{C1}$. An 7.7‰ range in $\delta^{13}C_{C1}$ range is present in the methane fraction, with the most positive wells recorded in wells X and W.

Parachute field samples (4.10) display trends similar to the Rulison data, with a few samples (wells I, M, O, P, OO and NN) showing a positive trend in $\delta^{13}C$ compositions from pentane to butane and/or propane. An 11‰ range in $\delta^{13}C_{C1}$ is present in the methane fraction, with the most positive values recorded in wells M and O.

Three Grand Valley wells (4.11) display a positive trend in $\delta^{13}C$ compositions from pentane to butane and/or propane: F, KK and LL. Grand Valley wells display the widest (12.3‰) range of methane compositions.

Wells with anomalous Chung plots (increasing $\delta^{13}C$ from pentane to butane and / or propane) are identified in Figure 4.12.

The carbon isotopic composition of CO_2 exhibits significant variation in the Piceance Basin fields (Table 4.1, Figure 4.13). The $\delta^{13}C_{CO2}$ is most positive in the Mamm Creek samples, averaging -3.60‰, and generally becomes increasingly negative westward, averaging -6.59‰ at Rulison, 7.75‰ at Parachute and 8.01‰ at Grand Valley. Two points are exceptional and noteworthy; these are wells 'AA' and 'U' along the eastern margin of Rulison Field. Gases from these two wells contained the most negative $\delta^{13}C_{CO2}$ in the entire Piceance dataset, -12.1 and -12.8‰ respectively.

<u>Hydrogen isotopes</u>

The average hydrogen isotopic composition of production gases (Table 4.1) also varied significantly in the methane fraction, similar to the carbon isotopic data. The δD_{C1} at Mamm Creek averaged -188.6‰, compared to -171.4‰ at Rulison, -168.7‰ at Parachute and -166.7‰ at Grand Valley. Hydrogen isotopic compositions exhibit a similar but more subtle variation in the C^{2+} fractions.

The hydrogen isotopic composition of the gases is investigated with a set of $\delta^{13}C$ – δD cross-plots, one for each gas species (Figures 4.14 to 4.20).

Mamm Creek samples are distinguished by δD_{C1} and δD_{C2} values that are overall more negative than the other fields, although there is some overlap with Rulison data. This distinction is much more subtle in the C_3 and *n*-C_4 data and is not apparent in the DH *i*-C_4, *i*-C_5 and *n*-C_5, data, where the data for the four gas fields almost completely overlap.

4.2.3 Integrated bulk compositions and isotopes

More details are apparent in cross-plots that are commonly used to interpret the origin of natural gases.

Figure 4.21, a Bernard plot (Bernard et al., 1977), is primarily used to distinguish biogenic from thermogenic gases. This plot examines the carbon isotopic composition of methane combined with the proportion of methane to ethane and propane. Thermogenic gases have distinctively more positive (heavier) isotopic compositions than biogenic gases and typically a higher proportion of ethane and propane, although with increasing thermal maturity, the ratio $C_1/(C_2+C_3)$ increases and $\delta^{13}C_{C1}$ becomes more positive. In this cross-plot, there is an overall similarity in the composition of gases from all four Piceance fields, but Mamm Creek gases are displaced to lower $C_1/(C_2+C_3)$ (ie. wetter compositions). Most of the Mamm Creek samples have more negative $\delta^{13}C_{C1}$ than most of the Grand Valley and Rulison samples, but similar in composition to Parachute samples.

Figure 4.22 is one of a series of cross-plots devised by Schoell (1983) to examine the origin and maturity of gases. This plot utilizes the isotopic compositions of methane and ethane. In this cross-plot, gases from Mamm Creek and Parachute have slightly more negative $\delta^{13}C_{C1}$, but ethane compositions are similar in all four gas fields.

Figure 4.23 is another in the series of Schoell's (1983) cross-plots. This utilizes the wetness (C_{2-4})/C_{1-4}) and the $\delta^{13}C_{C1}$ and is similar to the Barnard plot (Figure 4.21). Mamm Creek samples are distinguished by higher wetness; the other three fields effectively overlap in composition. Mamm Creek samples have a slightly more negative $\delta^{13}C_{C1}$, but this isotopic composition overlaps the range of samples from Parachute.

Figure 4.24, after Lorant et al. (1998) examines the ratio of C_2 to C_3 and the difference in carbon isotopic composition between these species, in order to distinguish gases derived by primary cracking of kerogen from those derived by various kinds of secondary cracking. In this cross-plot, Mamm Creek gases are distinguished from the Rulison, Grand Valley and most of the Parachute gases by lower ratio of C_2/C_3 (ie. a higher concentration of the wetter gases) and slightly increased difference between $\delta^{13}C_{C2}$ and $\delta^{13}C_{C3}$. All but one of the Rulison gases are tightly clustered on this plot. Grand Valley gases exhibit a large range of C_2/C_3, while the Parachute gases exhibit a small range of C_2/C_3 but a relatively large range (3‰) range in ($\delta^{13}C_{C2}$ - $\delta^{13}C_{C3}$). One Parachute well ('L') has a composition on this cross – plot that is identical to the Mamm Creek gases; this well is from the south side of Parachute Field.

Figure 4.25 examines $\ln(C_1/C_2)$ versus $\ln(C_2/C_3)$ (after Prinzhofer and Huc, 1995) to distinguish the effects of secondary cracking from primary cracking. In this cross-plot, the overall set of data describes a linear trend from low values of $\ln(C_1/C_2)$ and $\ln(C_2/C_3)$ to high values of these ratios. The Mamm Creek gases are distinguished by high values of both ratios. Most of the Rulison, Parachute and Grand Valley have relatively low ratios. One Rulison sample (well 'HH') and two Grand Valley samples (wells 'S' and 'KK') have distinctively higher ratios, similar to the driest samples in the Mamm Creek data set.

Figure 4.26 examines $\ln(C_1/C_2)$ versus the difference in carbon isotopic composition between these species. This plot, after Prinzhoffer and Huc (1995), attempts to identify leakage from reservoirs, maturity of source rocks and mixing of thermogenic and biogenic gas. Mamm Creek gases are distinguished from the other fields by lower $\ln(C_1/C_2)$ and, on average, slightly greater differences between $\delta^{13}C_{C1}$ and $\delta^{13}C_{C2}$, although the range in $\delta^{13}C_{C1}$ - $\delta^{13}C_{C2}$ is substantial (~10‰).

4.2.4 Noble Gases

Noble gases serve to distinguish contributions from three primary sources: mantle, crust and atmosphere and to identify fractionation processes.

Crustal contributions to natural gas are dominated by ^{4}He and therefore crustal-derived gas is characterized by low ratios of ^{3}He/^{4}He. Samples from Rulison, Parachute and Grand Valley fields have identical ^{3}He/^{4}He (Figure 4.27). Samples largely overlap in 1/^{4}He, although average values increase slightly from east to west, from Rulison to Grand Valley.

Low concentrations of ^{22}Ne and 36Ar are indicative of gases derived from the atmosphere, which typically enter natural gases through meteoric water. Samples exhibit a wide range of values on a plot of 1/^{22}Ne versus 1/^{36}Ar (Figure 4.28). All but one of the Parachute samples have elevated 1/^{22}Ne. Samples from Rulison and Grand Valley have values ranging from low to high values. Two pairs of samples from Rulison display very different values. The geographic distribution of 1/^{22}Ne values is shown in Figure 4.29. Samples from Rulison generally low, except for samples on the west side of the field. Parachute samples are elevated, with one exception on the north side of the field. Grand Valley samples display a range of values.

4.3 Mud Gases

Mud gas analyses come primarily from four wells at Rulison Field, two wells at Parachute Field and one well at Grand Valley Field. These data are supplemented by additional mud gas analyses from these fields and from Mamm Creek Field. Our ability to collect a detailed profile at Mamm Creek was hampered by the common practice of adding lime to the drilling mud to control pH; this generates CO_2, contaminating the mud gas. Gas analyses with CO_2 concentrations greater than mole fraction greater than 10% were discounted as having been contaminated by the addition of lime.

4.3.1 Bulk gas compositions

Gas compositions from mud gas samples are summarized in Table 4.2.

Bulk gas compositions from mud gas samples are similar to those determined from production gas samples but are systematically shifted to slightly drier compositions. Thus, for example, gas wetness in Mamm Creek samples was 0.25 as determined from production gas samples but was 0.18 as determined from mud gas samples. At Rulison, the production gases had an average wetness of 0.11 compared to an average wetness of 0.09 in the mud gas samples. There is little difference between production gas and mud gas analyses in the Grand Valley data set.

Similarly, differences emerge between production gas and mud gas analyses in ratios of bulk gases, specifically the ratios C_1/C_2 and C_2/C_3. These ratios are substantially higher in the mud gas samples, except in the Grand Valley data set where similar ratios are calculated.

Trends between fields in mud gas data are generally similar to those observed in production gas data. Specifically Mamm Creek samples are substantially wetter on average than those from the other fields. Parachute samples have the lowest wetness, averaging 93% methane.

Gas wetness-depth profiles for Rulison, Parachute, Grand Valley wells are shown in Figures 4.30, 4.31 and 4.32. Successful samples were too sparse in the Mamm Creek wells to provide meaningful profiles.

Bulk gas compositions exhibit considerable scatter with increasing depth. However there is a subtle trend of decreasing wetness with depth, exemplified by wells K and R at Parachute Field and well FF at Rulison and a plot of consolidated data from wells K, R and D, referenced in depth to the top of the Mesaverde (Figure 4.33). Samples above the Cameo Coal generally

have wetness values in the range of 0.1 to 0.2, but with scattered samples of pure methane. Samples below Cameo level commonly have wetness values of 0.05 or less.

4.3.2 Carbon and Hydrogen Isotopic Composition

<u>Carbon isotopes</u>

Carbon isotopic compositions of gas species from mud gas samples are summarized in Table 4.2. Compositions are generally similar to production gas samples with two notable exceptions:

- The $\delta^{13}C_{C1}$ in mud gas samples from Parachute and Grand Valley fields is more negative than production gas samples by an average of 4.4 and 6.6‰.

- The $\delta^{13}C_{CO2}$ in mud gas samples in all fields is more positive than production gas samples by an average 5 to 11‰. The mud gas sample set excludes all samples with mole fraction of CO_2 greater than 0.12, in order to exclude samples that might contain CO_2 generated from reaction in the drilling mud resulting from the addition of lime. Moreover, since most limestone has isotopic composition close to 0‰, it is likely that any contribution to the CO_2 in mud gas would tend to increase the $\delta^{13}C_{CO2}$; in other words, the true CO_2 composition in mud gas could be even more negative.

Parachute mud gas samples have distinctly more negative (lighter) $\delta^{13}C_{C1}$ values than the other fields and slightly more positive $\delta^{13}C_{i\text{-}C5}$ values than either Rulison or Parachute samples (Table 4.2). Rulison mud gas samples have distinctly more positive $\delta^{13}C_{C1}$ values and slightly more negative $\delta^{13}C_{C2}$ values than the other fields. Average carbon isotope compositions are otherwise quite similar among the fields.

Depth profiles could only be developed for methane, as the carbon isotope data were too sparse to develop meaningful profiles for the heavier gases. Profiles from Parachute and Grand Valley fields (Figure 4.34), show gradual increase in $\delta^{13}C_{C1}$ composition from the top of the Williams Fork down to the top of the Cameo Coal from approximately -45 to -35‰ and a profile of consolidated data from wells D, K and R is shown in Figure 4.35. Below the Cameo, $\delta^{13}C_{C1}$ decreases 6 to as much as 19‰. Extremely negative values were recorded in well R of -52.2 and -56.6‰.

The Rulison $\delta^{13}C_{C1}$ profiles (Figure 4.36) display quite different features. The carbon isotopic composition of methane is highly variable in the Williams Fork section, with values as negative

as -49.9‰ in well BB and -46.7‰ in well FF and as positive as -11.5‰ in well BB and -13.5‰ in well FF. The profiles in wells BB and FF are strikingly similar, such that the anomalies appear to occur at the same stratigraphic levels. The $\delta^{13}C_{C1}$ of samples below the top Cameo horizon are more consistent; they appear to show a decrease of approximately 6‰ in $\delta^{13}C_{C1}$ from values of approximately -FF‰ in wells BB and PP and -34.1‰ in well BB.

Hydrogen isotopes

Hydrogen isotopes of methane (δD_{C1}) are systematically more negative in the mud gas samples than in the production gas samples at Mamm Creek, Rulison and Grand Valley by 15.2 to 22.5‰. The δD_{C1} of mud gas samples at Parachute average only 2.8‰ more negative than the production gas samples. A similar difference also exists between mud gas and production gas samples in the heavier gases. Profiles are shown in Figures 4.37 and 4.38.

4.4 Fluid Inclusion Analysis

Cuttings samples from five wells in the study area were analyzed by Fluid Inclusion Technologies Inc., including two wells from Grand Valley and one each from Parachute, Rulison and Mamm Creek. Well locations are shown in Figure X.4. The complete reports from Fluid Inclusions Technology Inc. are provided in the Appendix. A summary of the results is provided here.

Mamm Creek (14-22 Friport; API # 05-045-06410)

Formation tops reported in this well are the Mesaverde at 3525 feet and the Mancos at 8148.

Hydrocarbon anomalies range from dry gas to oil-like responses. Dry gas to wet gas is noted at 5010-5580 ft. Wet gas to gas-condensate is documented at 5590-5690 ft and below 7270 ft. The most significant interval consists of gas-condensate spectra at 5710-7220 ft. A thin section from this particular zone (5740 ft) reveals common, blue fluorescent, upper-moderate gravity gas-condensate inclusions in sand grains. High petroleum inclusion abundance suggests the presence of an oil column or paleo-column of oil at 5740 ft.

Other thin sections include 5670 ft and 6870 ft. Both contain rare, blue-fluorescent, upper-moderate gravity gas-condensate to light oil inclusions.

No proximity to pay or sulfur species anomalies are identified.

4.4.2 Rulison (2 Clough; API # 05-045-06178)

Formation tops reported in this well are the Mesaverde at 4170 feet and the Cozzette-Corcoran at 8457 feet.

Dry gas responses are noted through most of the analyzed section with minor wet gas at 5480 ft, 6410 ft, 7250 ft and 8375 ft. No proximity to pay or sulfur species are identified.

Thin sections were prepared from three depths. Rare white fluorescent, moderate gravity and rare, blue fluorescent, upper-moderate to high gravity petroleum inclusions were noted at 5480 in sand grains and 7230 in carbonate cement, respectively. No liquid petroleum inclusions are observed in the third thin section at 8375 ft. Rock types include a variety of shales and sands, some of which are carbonate rich.

Parachute (ARCO GV 53-34; API # 05-045-06650)

Formation tops reported in this well are Fort Union at 1958 feet, Mesaverde at 3917 feet, Cameo Coal at 6715 feet and Rollins at 7272 feet.

The analyzed interval consists of dry gas to wet gas responses with a single sample at 4510 ft displaying a gas-condensate spectrum. Methane responses appear to be slightly higher below 5140 ft. Proximity to gas indications are recorded at 4540 ft and 7140-7280 ft. Trace amounts of probable thermal-derived sulfur species are identified at 7370 ft.

Thin sections were prepared from four depths (4540 ft, 5200, 6830 ft and 7370 ft). The shallower three reveal rare, blue fluorescent, upper-moderate to high gravity gas-condensate or light oil inclusions. Rare, white-fluorescent, unknown gravity light oil inclusions are identified in carbonate cement at 7370 ft.

Grand Valley (Mobil MV-23-27; API # 05-045-06539)

Formation tops reported in this well are Fort Union (2585 feet), Mesaverde (4050 feet), Cameo (6545 feet), Rollins (7145 feet), Cozzette (7412 feet), Corcoran (7653 feet), and Sego (7900 feet).

The interval above 5390 ft consists of largely dry gas responses with minor wet gas at 4300 ft and 4680 ft. The section below 6100 ft contains wet gas responses and is the most significant

zone of the well. Proximity to gas indications are documented at the basal section below 7040 ft. A sample at 6910 ft displays possible thermal-derived sulfur species.

Thin sections were prepared from three depths. A single sample from 6310 ft contains several, blue fluorescent, upper-moderate to high gravity gas-condensate inclusions in sand grains. No liquid petroleum inclusions are documented at 6910 ft or 7520 ft.

Grand Valley (Federal MV-12-3; API # 05-045-06522)

Formation tops reported in this well are Fort Union (2245 feet), Lance (3600 feet), Cameo Coal (6140 feet), Rollins (6620 feet), Cozzette (6888 feet) and Corcoran (7128 feet).

Dry gas anomalies are recorded at 4010-5030 ft, dry gas to wet gas responses are noted at 5100-6020 ft and wet gas to gas condensate is identified at 6230-7320 ft. The latter section appears to be the most significant. No proximity to pay or sulfur species are documented.

Thin sections were prepared from three depths. Rare occurrences of blue-fluorescent, upper-moderate gravity light oil or condensate inclusions are identified at 7020 ft. No liquid petroleum inclusions are observed at 5100ft or 6380 ft.

4.5 INTERPRETATION

4.5.1 Regional variability in production gas composition

The Mamm Creek gases are notably wetter than gases from any of the other three fields. This is evident in comparing the average composition from the four fields, which have a wetness of 0.25 at Mamm Creek (range from 0.21 to 0.32) and 0.10 to 0.11 in Rulison, Parachute and Grand Valley samples (range from 0.00 to 0.22). There is thus virtually no overlap in compositions.

This difference in the composition of produced gases is paralleled by:

(1) A difference in the composition mud gases, which average 0.18 at Mamm Creek and 0.05 to 0.10 in Rulison, Parachute and Grand Valley.

(2) Fluid inclusion results, which strongly indicate the presence of a paleo-oil column at Mamm Creek but only gas at Rulison, Parachute and Grand Valley.

These results are consistent with findings by Ellis et al. (2010). They described a striking increase in gas wetness from the western part of Mamm Creek field to the eastern part and reported values from eastern Mamm Creek very similar to those reported here.

The geographic variability represented by these gas compositions suggests either (1) a difference in source rocks generating gas for these accumulations, and / or (2) different thermal maturities of the same source rock(s) generating gas for these accumulations.

4.5.2 Thermal maturity of source rocks

The carbon isotopic composition of gases (C_1, C_2 and C_3) can be used to infer the thermal maturity of the gas sources at the time of generation (Figures 4.39 and 4.40). These data suggest the gases were generated at maturities of 1.5% R_o to as much as 2.0% R_o. This analysis suggests no significant differences between the fields in the thermal maturity at which these gases were generated.

The thermal maturities estimated from gas compositions are consistent with results of basin modeling in the Mamm Creek area (Ellis et al., 2010), which estimated maturities generally in the range of 1.4 to 2.0 at Cameo level, with a measured maturity of approximately 1.6% R_o at Cameo level in the MWX-1 well at Rulison (Nelson, 2003), and with unpublished maturity data from well files at the U.S. Geological Survey (Figure 4.4).

If thermal maturities are approximately 1.5% R_o at Cameo level, then deeper potential source rocks, specifically the Mancos Shale, already generated oil and are now likely to be generating gas through secondary cracking of oil (Nuccio and Roberts, 2003). Nuccio and Roberts (2003) estimate significant oil and gas generation began at 55 Ma and peaked at 52 Ma in the deepest part of the Piceance Basin, along the structural trough at approximately the location of Rulison and Mamm Creek fields.

4.5.3 Sources of Gas

The relatively similar, high thermal maturities indicated by vitrinite reflectance studies and gas compositions suggest that the differences in hydrocarbon compositions, evident in comparing Mamm Creek to the other gas fields and in evidence for the paleo-oil column, do not result from maturity differences within the basin. An alternative interpretation is that the Mamm

Creek gases include a component generated from a more oil-prone source rock than the other fields; the likely candidate here is the Mancos Shale. Maturity modeling (Nuccio and Roberts, 2003) indicates that the wet components migrated into the reservoir approximately 50 Ma.

The production gas plot of $\ln(C_1/C_2)$ versus $\ln(C_2/C_3)$ (Figure 4.25) describes a linear trend with Mamm Creek gases plotting at low values of $\ln(C_1/C_2)$ and $\ln(C_2/C_3)$ and the Rulison and Grand Valley samples plotting at higher values. The Mamm Creek data, in particular, form a very strong linear trend. This can be interpreted as the product of mixing of two components, one a wet gas that is enriched in the Mamm Creek samples and one a dry gas that is enriched in the Rulison and Grand Valley samples. The driest samples are from wells HH (Rulison) and S and KK (Grand Valley), all with a wetness of 0.08; these may represent a near-endmember contribution from a single source. The wettest Mamm Creek sample has a wetness of 0.31, which would represent the maximum contribution of the oil-prone source rock.

The absence of a wet signature in the Rulison, Parachute and Grand Valley gases, despite similarly high thermal maturities even at Cameo level, suggest that the control on gas wetness was the lack of a migration pathway for oil from the Mancos or deeper source rocks into shallower reservoirs. Migration of oil and wet gas in the Mamm Creek field may be associated with the presence of the Gibson Gulch graben (Cumella and Scheeval, 2008).

4.5.4 Evidence of Secondary Cracking

Mud gas data from three wells at Parachute and Grand Valley provide evidence for a contribution of gases derived from secondary cracking of oil to gas. The evidence is (1) a trend toward decreasing wetness below Cameo level in these wells, such that gases at the base of the well have compositions very close to pure methane (Figure 4.33); and (2) isotopic compositions of methane in these wells display a reversal (Figure 4.35; isotopic compositions become more positive with increasing depth down to Cameo level, then become more negative below Cameo level. Two samples had $\delta^{13}C_{C1}$ more negative than -50‰. Rulison gases also show a trend toward dry compositions and relatively negative in $\delta^{13}C_{C1}$ in deep parts of the wells.

Gas compositions that are dry and isotopically light could be interpreted as indicative of bacterial methanogenesis. However these samples are relatively deep and high temperature, and it is unreasonable to expect that the contribution from methanogenic bacteria would increase with depth. The more reasonable interpretation is that these samples are derived from secondary cracking of oil, which produces dry, isotopically very negative gases.

The presence of a secondary cracking signature in the Parachute, Grand Valley and Rulison wells may result from the fact that oil apparently did not migrate into these fields. If large amounts of oil were retained in the Mancos, it would then be available for secondary cracking. The greater mobility of gas (higher buoyancy, smaller molecules) would enable gas to migrate into shallower reservoirs than oil could.

4.5.5 Evidence for Bacterial Oxidation of Gases

Selected mud gas samples from two wells are distinguished by bulk compositions that are pure methane and carbon isotopic values that are extremely positive (-28.5 to -11.5‰). These samples are bracketed in depth by samples much wetter (wetness = 0.08 to 0.14) and isotopically negative (generally -36 to -43‰).

Methanogenesis produces gases of pure methane, but these gases are isotopically extremely negative, with $\delta^{13}C_{C1}$ at least -55‰). Diffusion of gases through a seal could also produce gases enriched in methane, but this ought to be accompanied by fractionation of carbon isotopes, also yielding gases that are isotopically more negative, not more positive.

We propose that these gases result from the bacterial oxidation of a wetter precursor. Methanotrophic bacteria preferentially consume the wetter gases because this is energetically favorable; they also preferentially consume compounds with isotopically light carbon because of energy considerations. The residual gases from this reaction are enriched in pure methane that is isotopically more positive, with CO_2 derived from the reaction that is isotopically negative.

This model is supported by two additional lines of evidence: the isotopic composition of CO_2 in production gases and mud gas samples and noble compositions. The carbon isotopic composition of CO_2 in production gas samples is distinctly anomalous in Rulison, Parachute and Grand Valley fields, ranging between an average of -6.59‰ at Rulison to -8.01‰ at Grand Valley, substantially lighter than at Mamm Creek. The average isotopic composition of CO_2 in mud gas samples is even lighter, averaging -10.9, 13.4, 18.0 and 13.7‰ in Mamm Creek, Rulison, Parachute and Grand Valley samples, respectively. Samples from well PA 544-36 in Parachute Field have $\delta^{13}C_{CO2}$ values ranging from -14-4 to -25.7‰. These data are consistent with the bacterial alteration of Rulison, Parachute and Grand Valley gases in the upper part of the Williams Fork section.

4.6 References

Bernard, B.B., Brooks, J.M., Sackett, W.M. (1977). A geochemical model for characterization of hydrocarbon gas sources in marine sediments. In Offshore Technology Conference, May 1977. OTC 2934, pp. 435–438.

Chung, H.M., Gormly, J.R., & Squires, R.M. (1988). Origin of gaseous hydrocarbons in subsurface environments: theoretical considerations of carbon isotope distribution. Chemical Geology 71, 97–103.

Cumella, S. P., & Scheevel, J. (2008). The influence of stratigraphy and rock mechanics on Mesaverde gas distribution, Piceance Basin, Colorado, in S. P. Cumella, K. W. Shanley, and W. K. Camp, eds., Understanding, exploring, and developing tight-gas sands— 2005 Vail Hedberg Conference: AAPG Hedberg Series, no. 3, p. 137 – 155.

Ellis, G.S., Lillis, P.G., Cumella, S.P., Dewane, T.J. (2010). Kinetic isotope fractionation modeling of natural gas geochemistry in the Mamm Creek Field, Piceance Basin, Colorado: AAPG Annual Meeting, poster presentation.

Lorant, F., Prinzhofer, A., Behar, F., & Huc, A. Y. (1998). Carbon isotopic and molecular constraints on the formation and the expulsion of thermogenic hydrocarbon gases. *Chemical Geology*, *147*(3-4), 249-264.

Nelson, P. H. (2003). A Review of the Multiwell Experiment, Williams Fork and Iles Formations, Garfield County, Colorado. *USGS Uinta-Piceance Assessment Team, Comp., Petroleum systems and geologic assessment of oil and gas in the Uinta-Piceance Province, Utah and Colorado*. *Petroleum Systems and Geologic Assessment of Oil and Gas in the Uinta–Piceance Province, Utah and Colorado: United States Geological Survey, Digital Data Series DDS-69-B*, Chapter 15, 24 pp.

Nuccio, V. F., & Roberts, L. N. (2003). Thermal maturity and oil and gas generation history of petroleum systems in the Uinta-Piceance Province, Utah and Colorado. *Petroleum Systems and Geologic Assessment of Oil and Gas in the Uinta–Piceance Province, Utah and Colorado: United States Geological Survey, Digital Data Series DDS-69-B*, Chapter 4, 35 pp.

Prinzhofer, A. A., & Huc, A. Y. (1995). Genetic and post-genetic molecular and isotopic fractionations in natural gases. *Chemical Geology*, *126*(3), 281-290.

Schoell, M. (1983). Genetic characterization of natural gases. *AAPG bulletin*,*67*(12), 2225-2238.

Tang, Y., Perry, J.K., Jenden, P.D., & Schoell, M. (2000). Mathematical modeling of stable carbon isotope ratios in natural gases. Geochimica et Cosmochimica Acta 64, 2673–2687.

Table 4.1. Average compositions of Piceance Basin production gases.

Average composition	Mamm Creek	Rulison	Parachute	Grand Valley
C1 (fraction)	0.75	0.87	0.87	0.88
C2 (fraction)	0.13	0.08	0.065	0.073
C3 (fraction)	0.07	0.04	0.031	0.026
i-C4 (fraction)	0.03	0.01	0.011	0.01
n-C4 (fraction)	0.03	0.01	0.011	0.01
i-C5 (fraction)	0.01	0.01	0.01	< 0.01
CO_2 (fraction)	NA	0.03	0.05	0.048
Wetness	0.25	0.11	0.10	0.10
$\delta^{13}C_{C1}$ (‰)	--39.06	-36.11	-38.11	-34.02
$\delta^{13}C_{C2}$ (‰)	-26.82	-26.53	-25.97	-26.13
$\delta^{13}C_{C3}$ (‰)	-24.08	-24.27	-24.4	-24.18
$\delta^{13}C_{i\text{-}C4}$ (‰)	-24.35	-24.76	-24.8	-24.05
$\delta^{13}C_{n\text{-}C4}$ (‰)	-23.35	-23.68	-23.9	-23.34
$\delta^{13}C_{i\text{-}C5}$ (‰)	-23.36	-24.83	-24.51	-24.39
$\delta^{13}C_{n\text{-}C5}$ (‰)	-22.78	-24.13	-23.77	-23.66
$\delta^{13}C_{CO2}$ (‰)	-3.60	-6.59	-7.75	-8.01
δD_{C1} (‰)	-188.6	-171.4	-168.7	-166.8
δD_{C2} (‰)	-136.8	-130.2	-130.5	-128.4
δD_{C3} (‰)	-125.1	-121.7	-122.0	-121.4
$\delta D_{i\text{-}C4}$ (‰)	-118.8	-115.6	-116.3	-114.8
$\delta D_{n\text{-}C4}$ (‰)	-121.05	-115.3	-115.2	-114.8
$\delta D_{i\text{-}C5}$ (‰)	-105.1	-101.8	-102.3	-100.5
$\delta D_{n\text{-}C5}$ (‰)	-118.0	-115.0	-111.6	-112.5

Table 4.2. Average Compositions of Piceance Basin Mud Gas Samples

Average composition	Mamm Creek	Rulison	Parachute	Grand Valley
C1 (fraction)	0.78	0.90	0.93	0.88
C2 (fraction)	0.06	0.08	0.05	0.07
C3 (fraction)	0.03	0.02	0.02	0.02
i-C4 (fraction)	0.01	0.002	0.004	0.005
n-C4 (fraction)	0.02	0.002	0.003	0.003
i-C5 (fraction)	0.02	0.001	0.001	0.001
CO_2 (fraction) *	0.05	0.03	0.04	0.03
Wetness	0.18	0.09	0.05	0.10
$\delta^{13}C_{C1}$ (‰)	-39.38	-37.73	-42.50	-40.65
$\delta^{13}C_{C2}$ (‰)	-25.90	-27.39	-26.88	-26.62
$\delta^{13}C_{C3}$ (‰)	-22.33	-24.53	-24.42	-23.91
$\delta^{13}C_{i\text{-}C4}$ (‰)	-24.80	-25.15	-24.09	-25.41
$\delta^{13}C_{n\text{-}C4}$ (‰)	-22.90	-23.43	-23.31	-24.37
$\delta^{13}C_{i\text{-}C5}$ (‰)		-25.25	-24.75	-25.47
$\delta^{13}C_{n\text{-}C5}$ (‰)		-23.79	-23.77	-23.85
$\delta^{13}C_{CO2}$ (‰) *	-10.93	-13.39	-18.01	-13.74
δD_{C1} (‰)	-204.1	-186.6	-171.5	-189.3
δD_{C2} (‰)	-174.0	-147.6	-141.1	-142.7
δD_{C3} (‰)		-144.9	-130.9	-137
$\delta D_{i\text{-}C4}$ (‰)		-120.8	-113.7	
$\delta D_{n\text{-}C4}$ (‰)		-107.3	-109.7	
$\delta D_{i\text{-}C5}$ (‰)				
$\delta D_{n\text{-}C5}$ (‰)				

- Possible contamination by generation of CO_2 by addition of lime to drilling mud.

W 108° 15' 59"

W 107° 28' 10"

N 39° 43' 35"

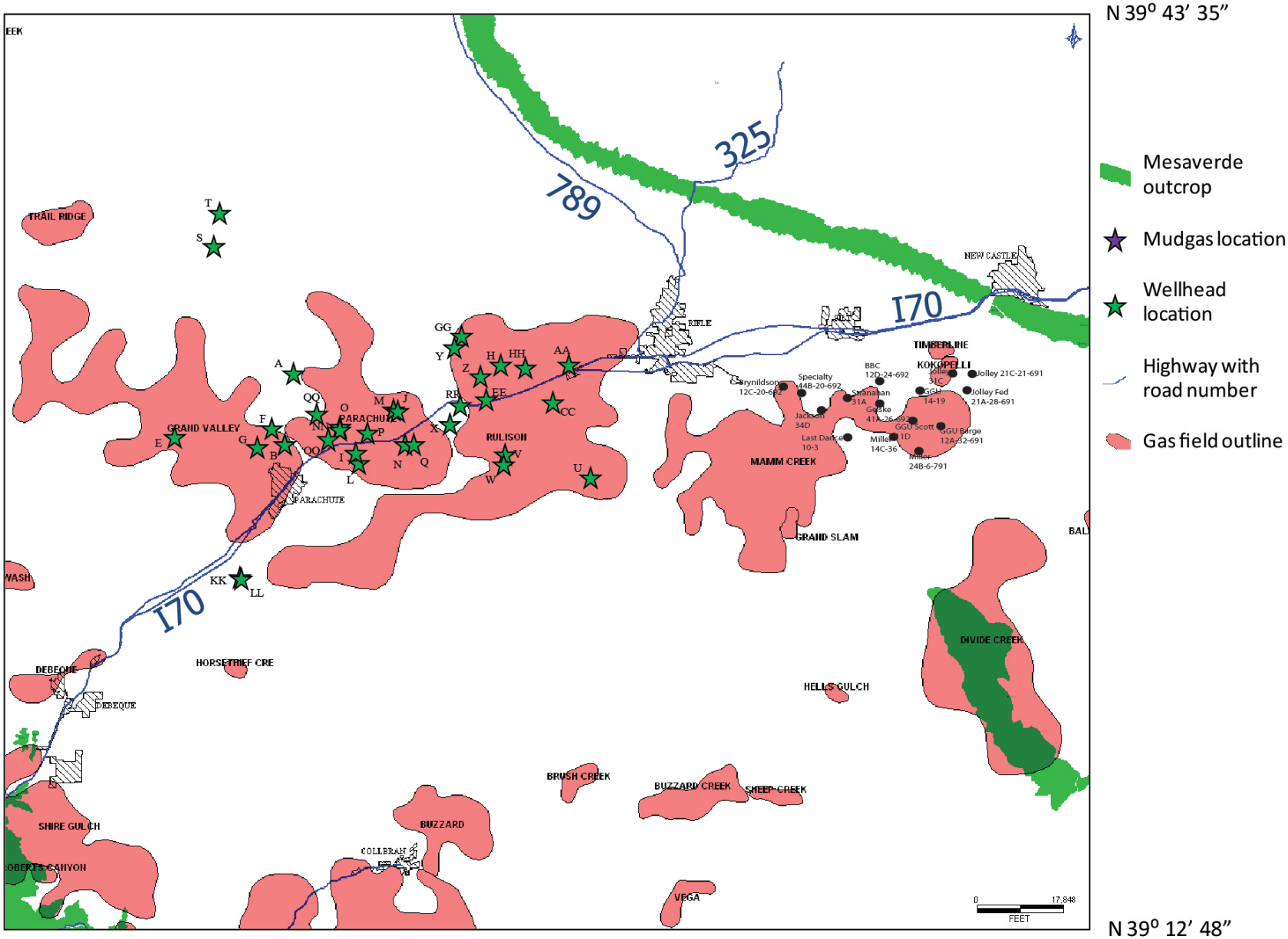

N 39° 12' 48"

Figure 4.1 Map of the Mamm Creek – Rulison – Parachute – Grand Valley fields, showing the locations of production gas samples.

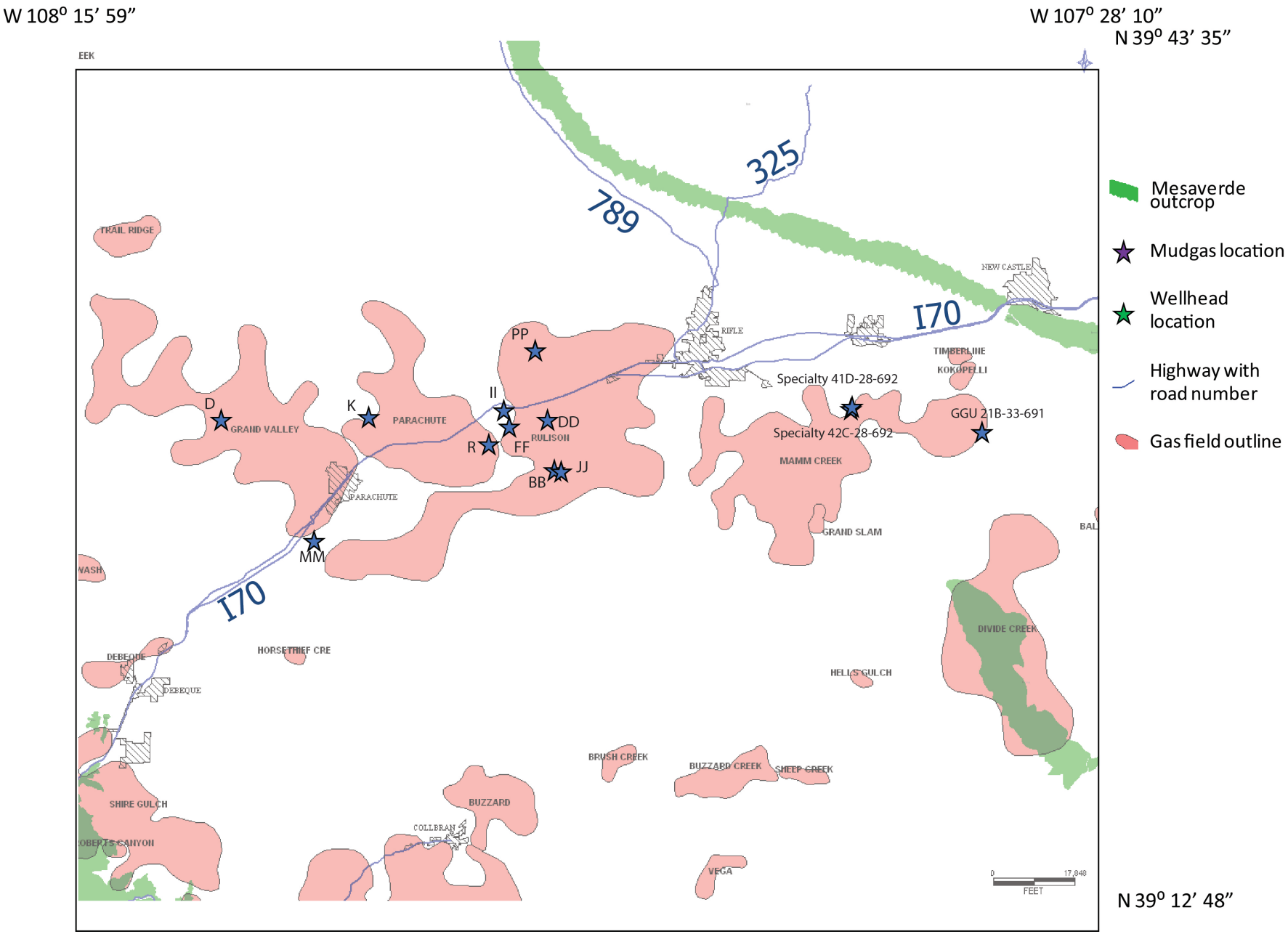

Figure 4.2 Map of the Mamm Creek – Rulison – Parachute – Grand Valley fields, showing the locations of mud gas samples.

W 108° 15' 59"

W 107° 28' 10"
N 39° 43' 35"

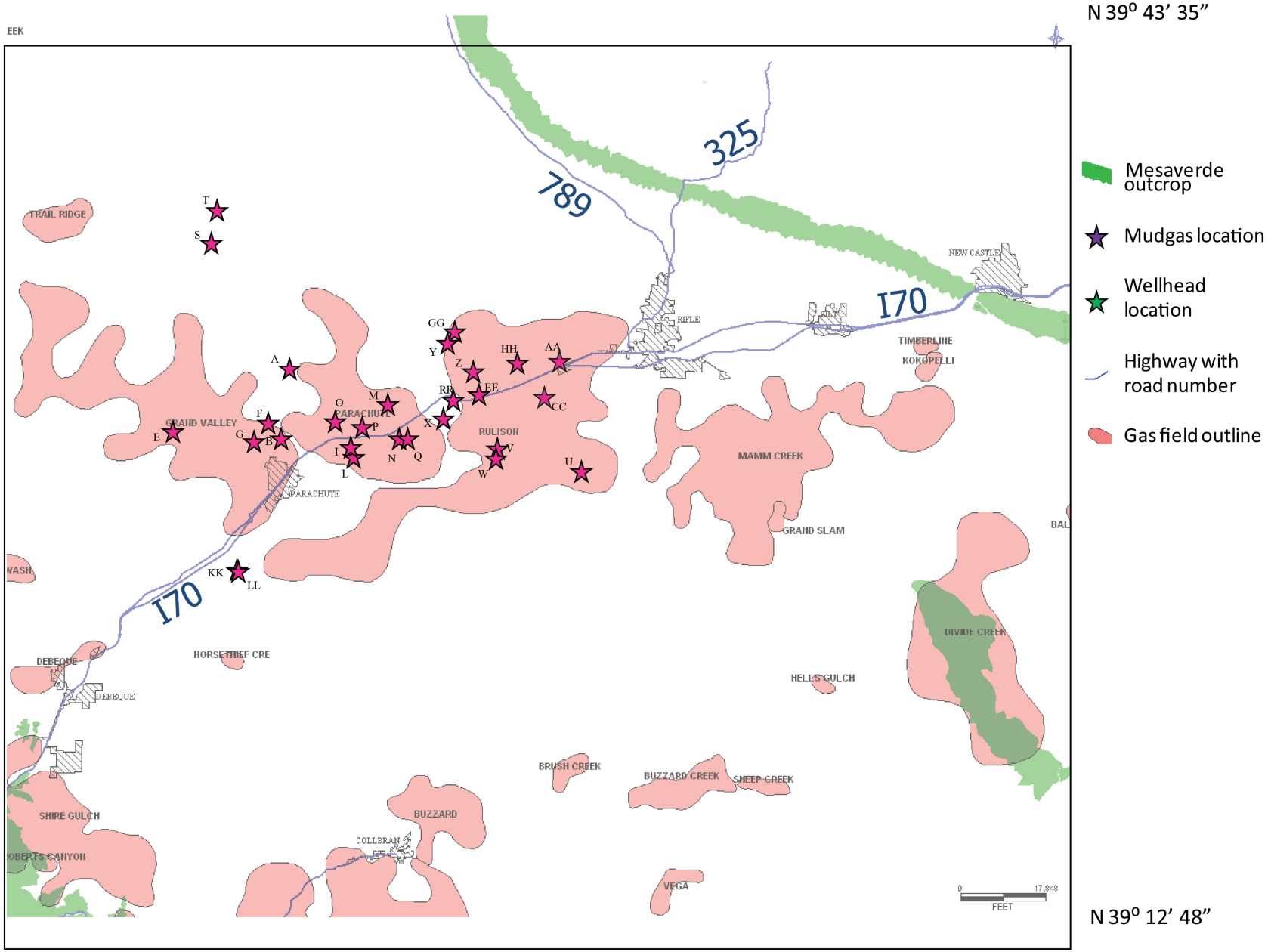

Figure 4.3 Map of the Mamm Creek – Rulison – Parachute – Grand Valley fields, showing the locations of production gas samples for noble gas analysis.

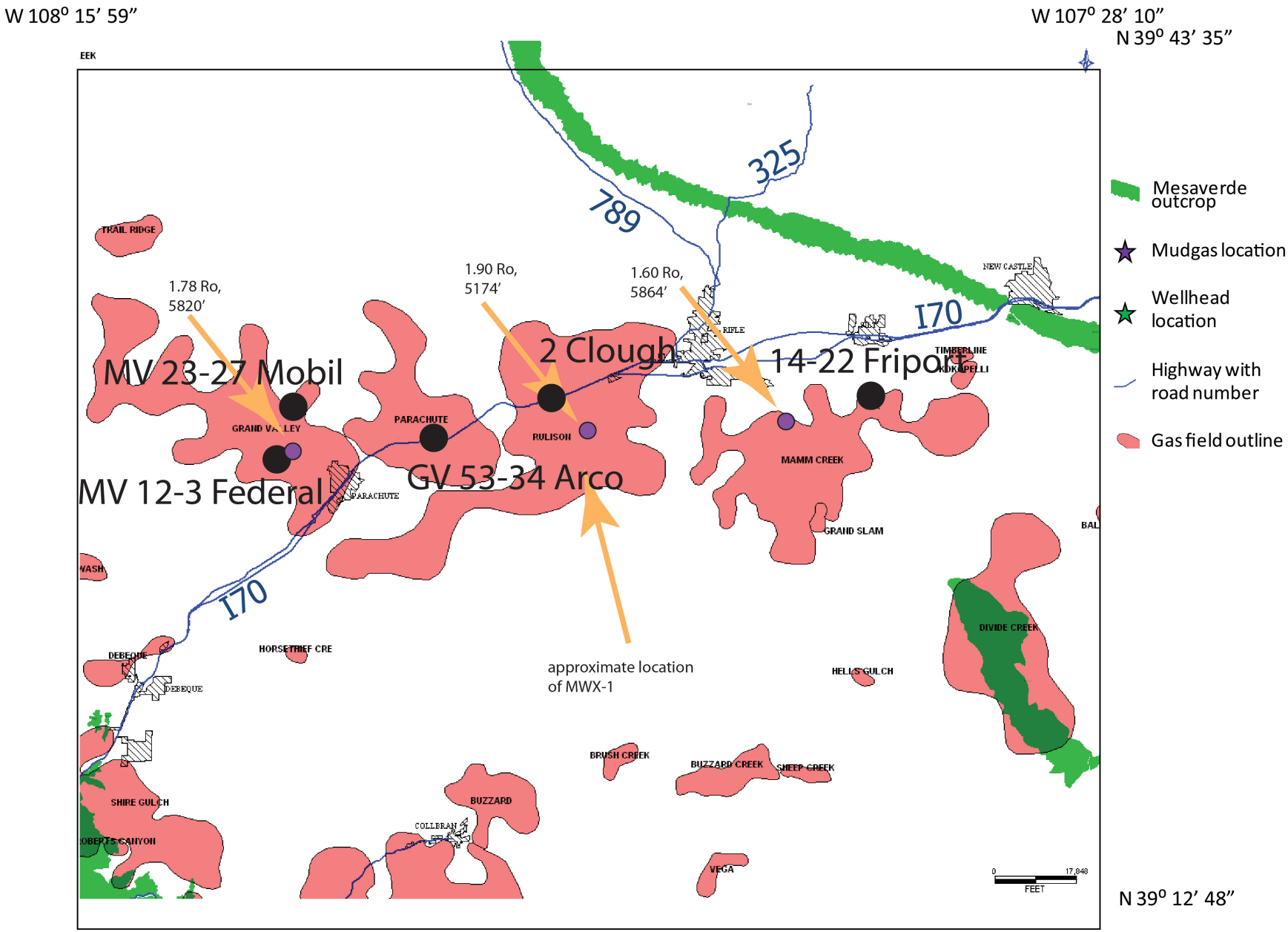

Figure 4.4 Map of the Mamm Creek – Rulison – Parachute – Grand Valley fields, showing the locations of fluid inclusion samples and vitrinite reflectance data.

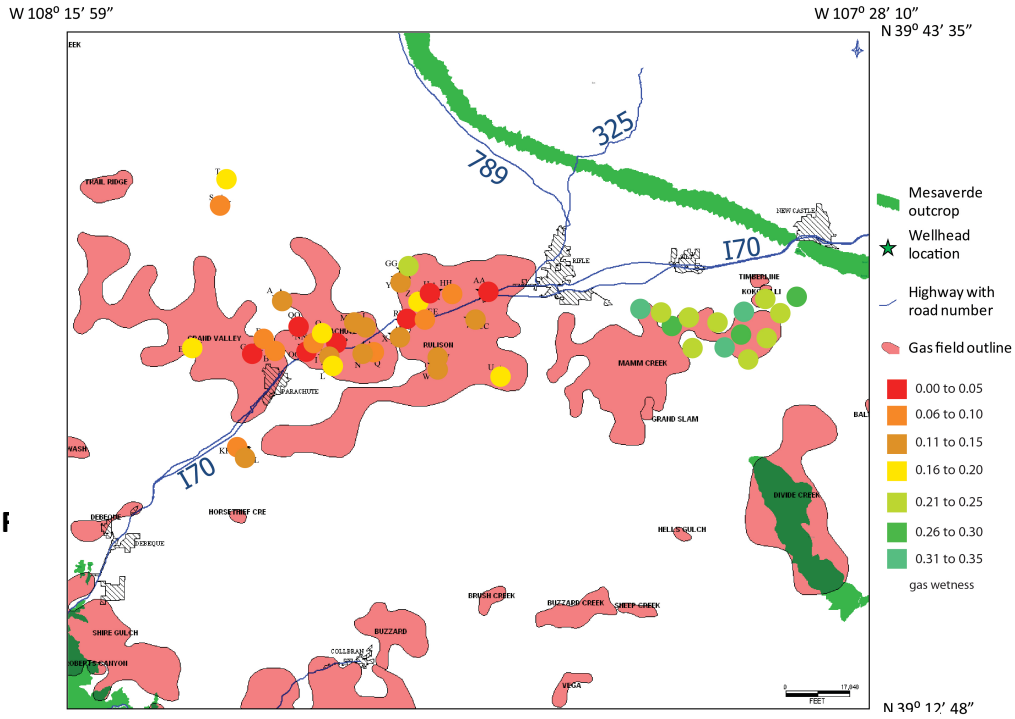

Figure 4.5. Gas wetness in production gas samples from Mamm Creek, Rulison, Parachute and Grand Valley fields.

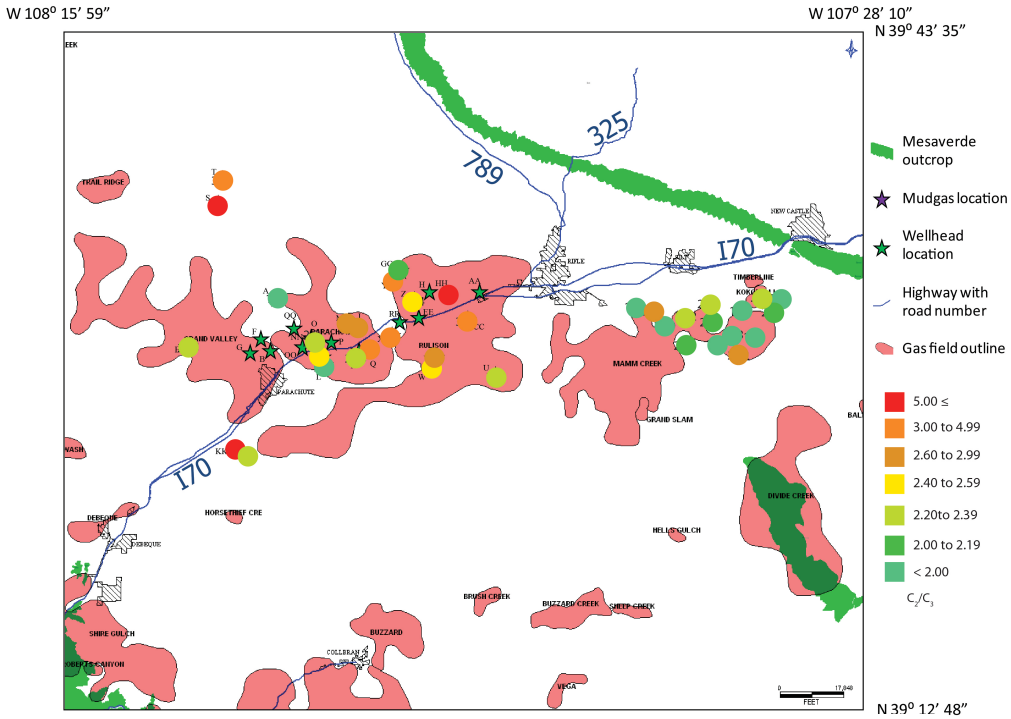

Figure 4.6. C_2/C_3 ratios in production gas samples from Mamm Creek, Rulison, Parachute and Grand Valley fields.

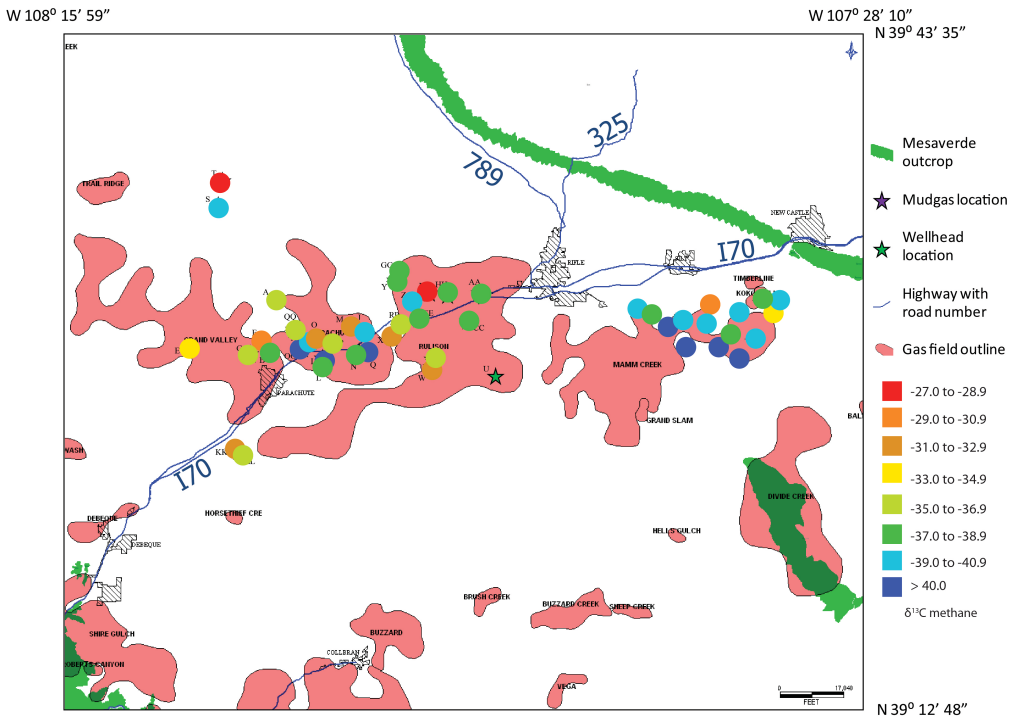

Figure 4.7. Carbon isotopic composition of C1 ($\delta^{13}C_{C1}$) in production gas samples from Mamm Creek, Rulison, Parachute and Grand Valley fields.

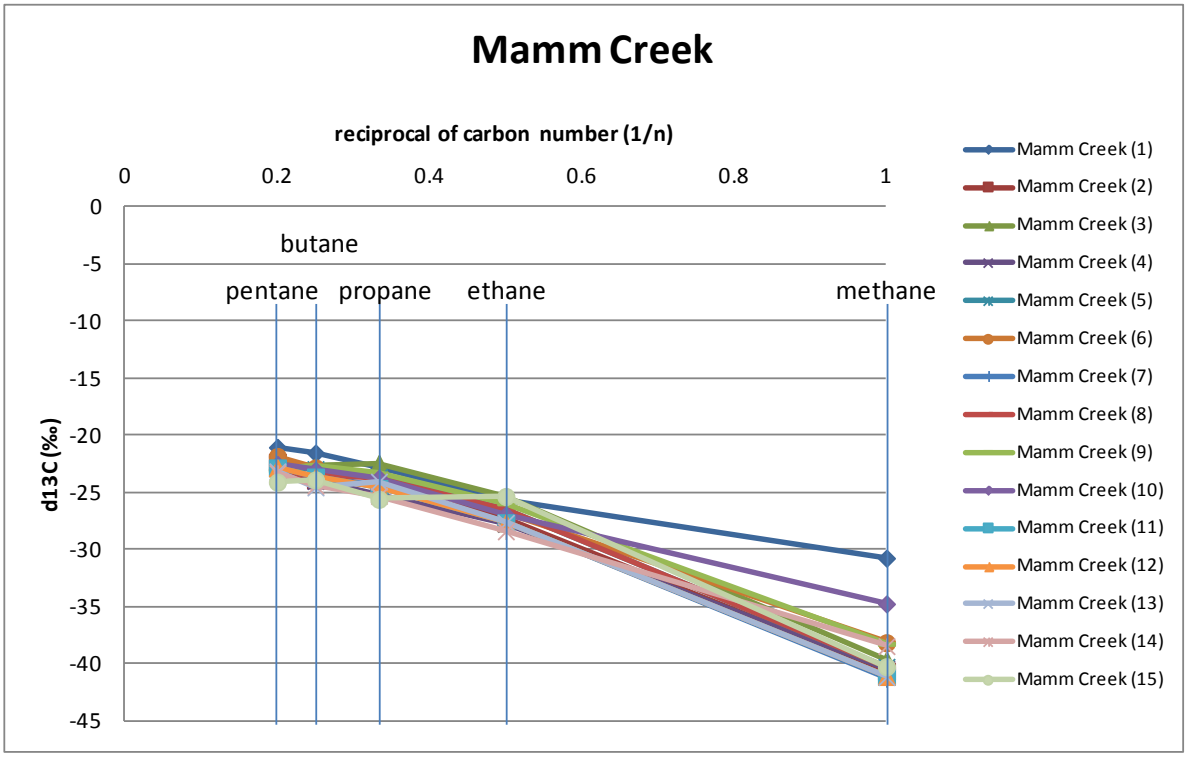

Figure 4.8. Chung plot showing carbon isotopic composition of gases from Mamm Creek field.

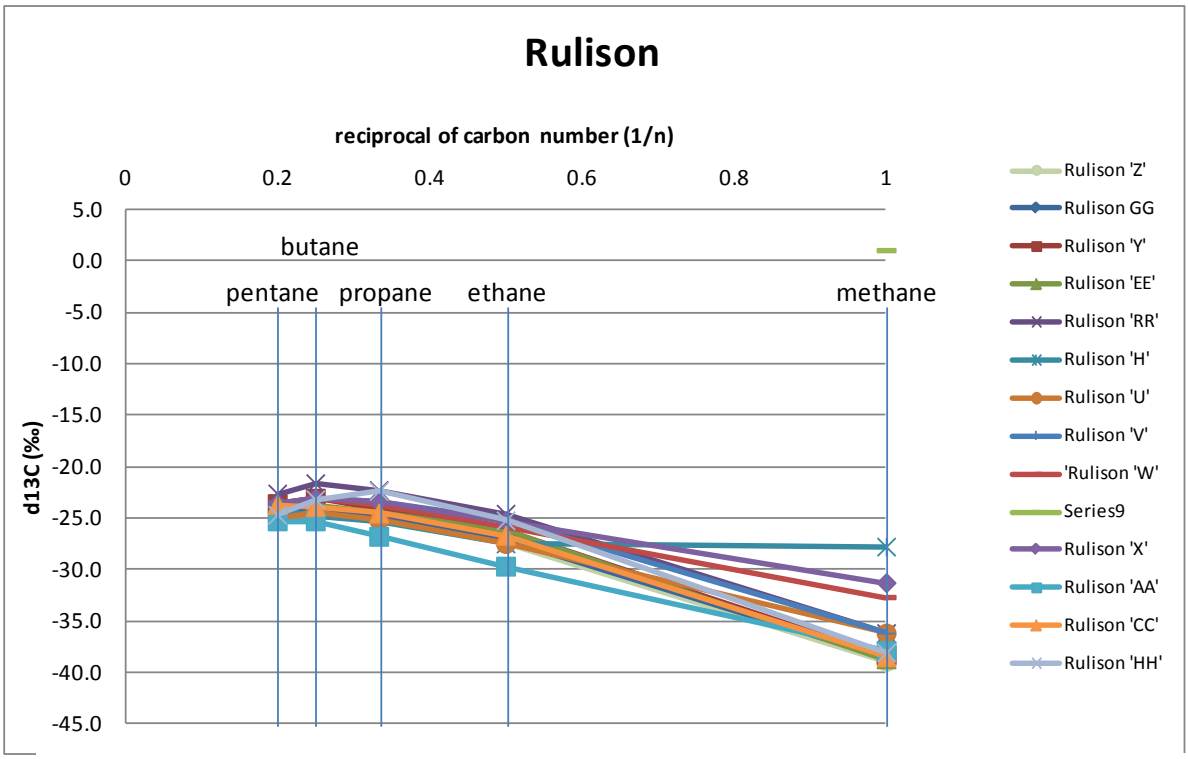

Figure 4.9. Chung plot showing carbon isotopic composition of gases from Rulison field.

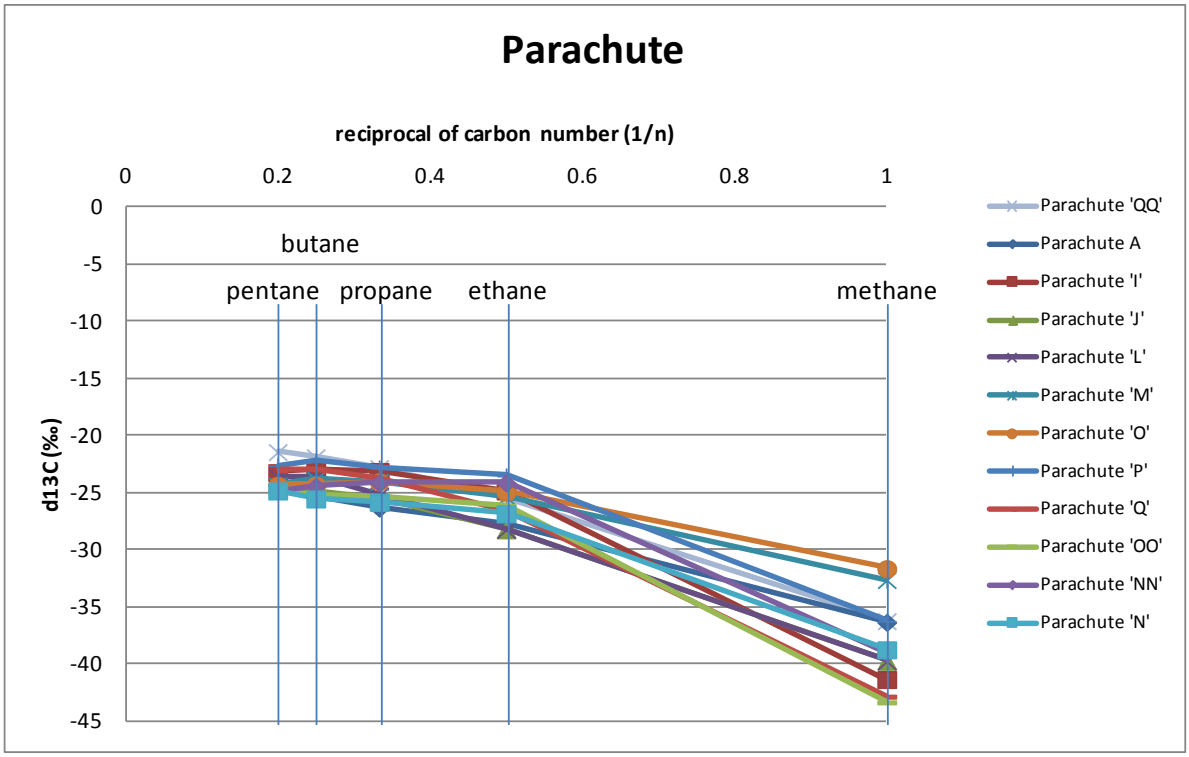

Figure 4.10. Chung plot showing carbon isotopic composition of gases from Parachute field.

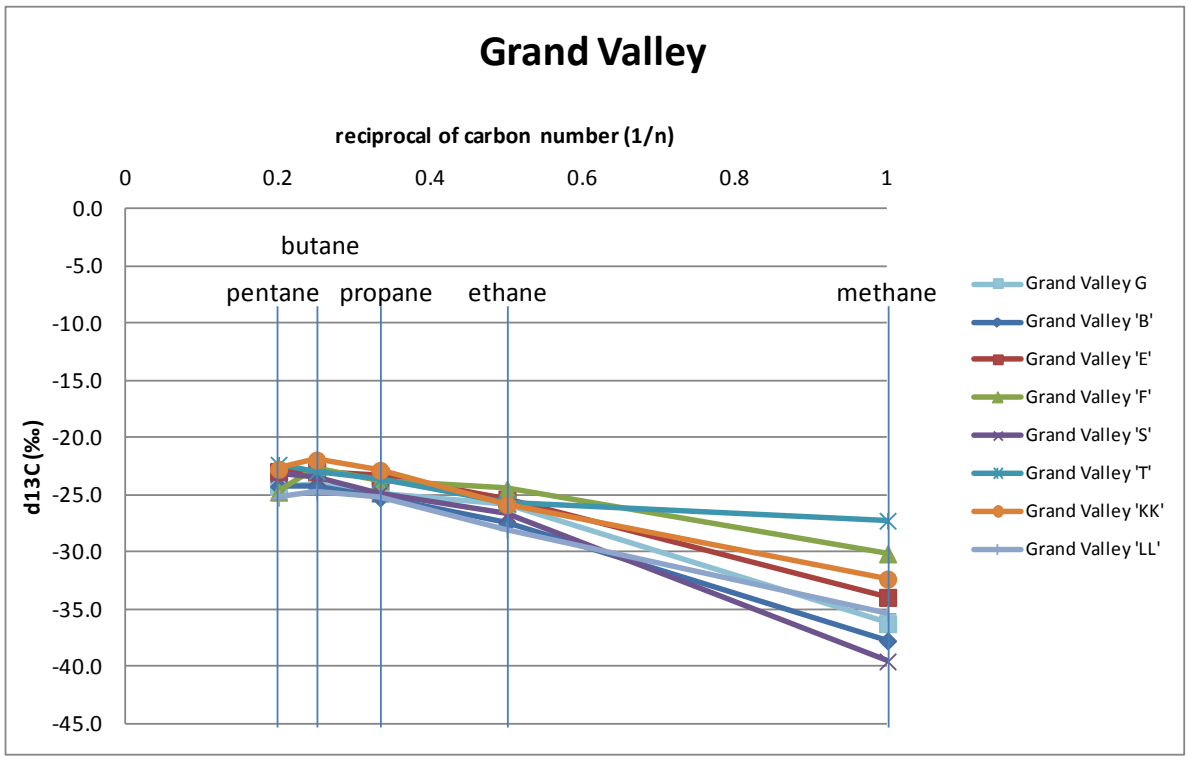

Figure 4.11. Chung plot showing carbon isotopic composition of gases from Grand Valley field.

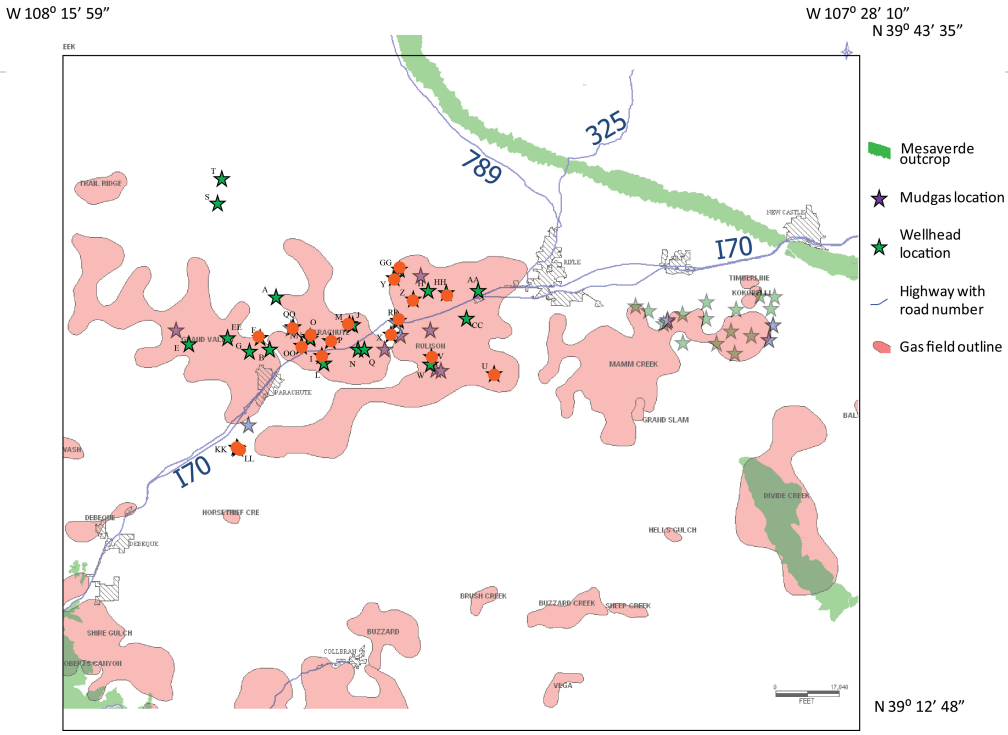

Figure 4.12. Wells with anomalous Chung plots (orange stars), showing increasing $\delta^{13}C$ from pentane to butane and / or propane in production gas wells from Mamm Creek, Rulison, Parachute and Grand Valley fields.

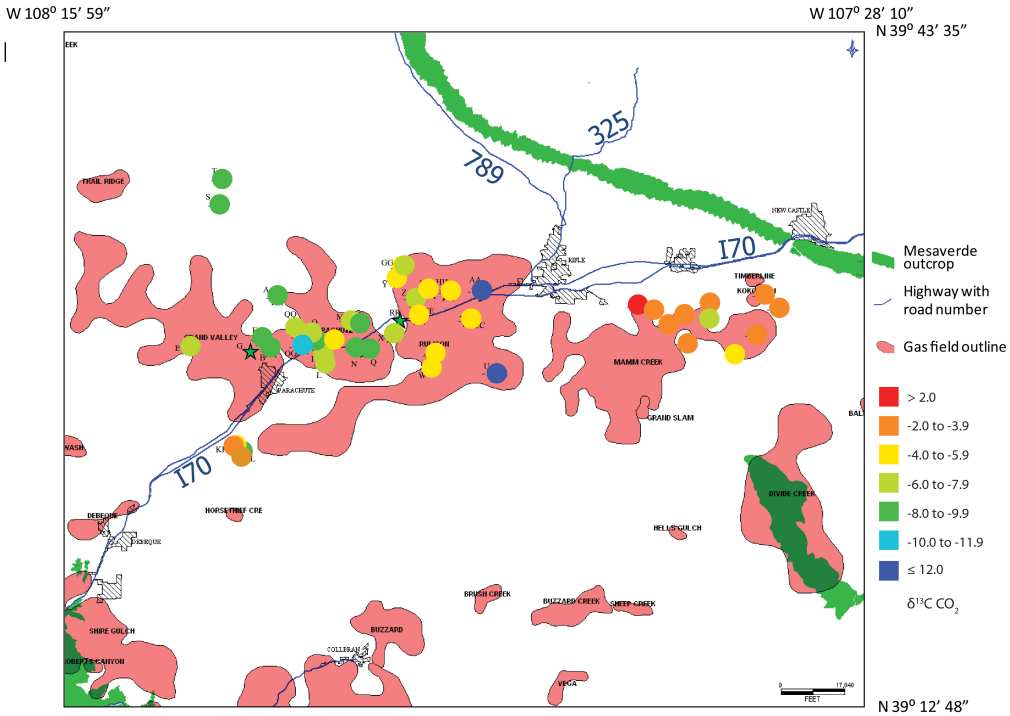

Figure 4.13. Carbon isotopic composition of CO_2 ($\delta^{13}C_{CO2}$) in production gas wells from Mamm Creek, Rulison, Parachute and Grand Valley fields.

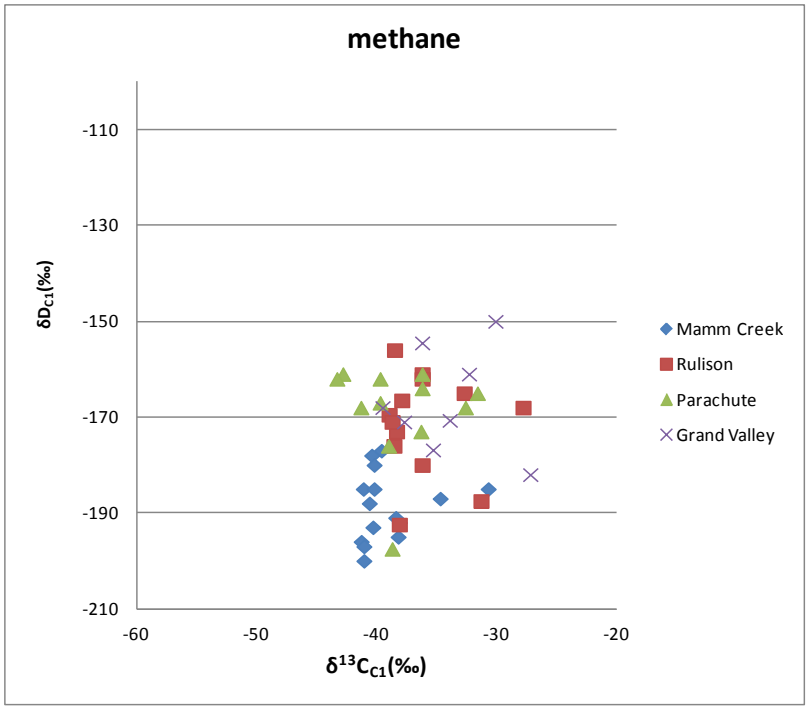

Figure 4.14. Carbon and hydrogen isotopic composition of methane in production gas samples from Mamm Creek, Rulison, Parachute and Grand Valley fields.

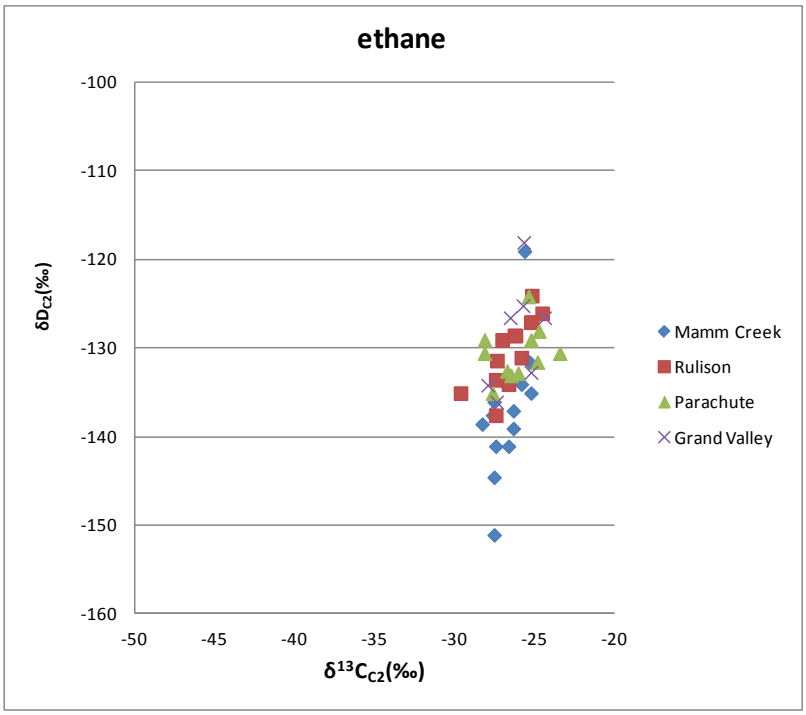

Figure 4.15. Carbon and hydrogen isotopic composition of ethane in production gas samples from Mamm Creek, Rulison, Parachute and Grand Valley fields.

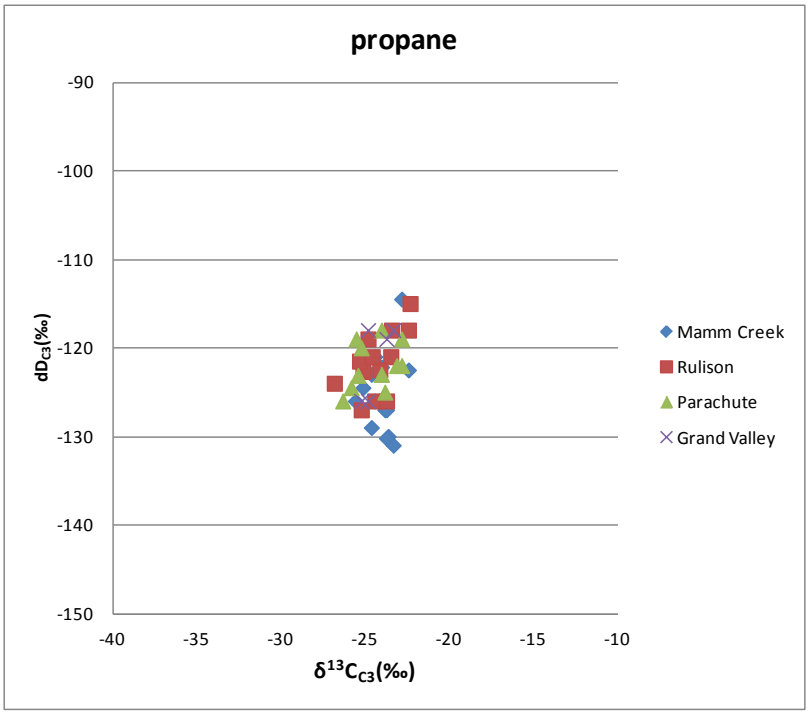

Figure 4.16. Carbon and hydrogen isotopic composition of propane in production gas samples from Mamm Creek, Rulison, Parachute and Grand Valley fields.

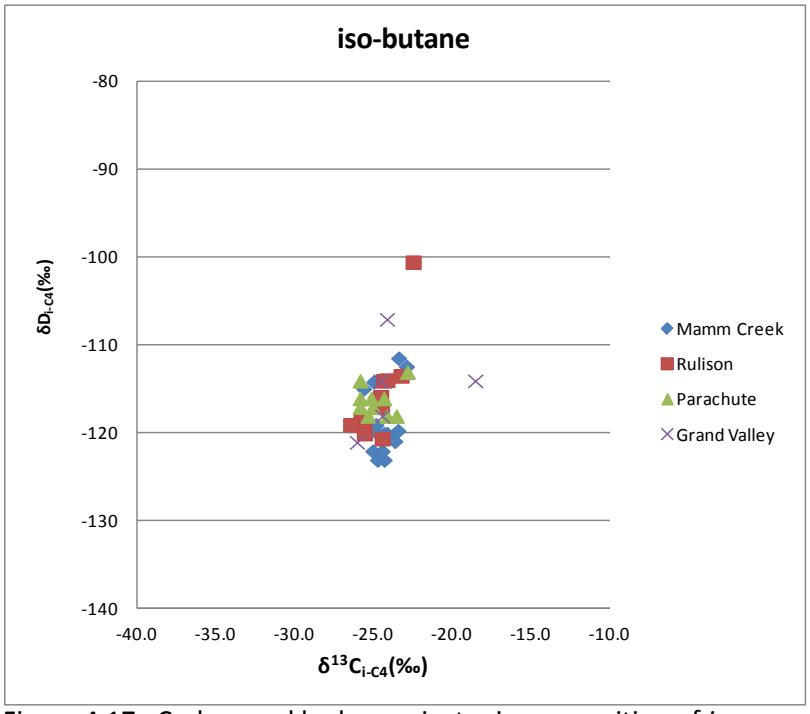

Figure 4.17. Carbon and hydrogen isotopic composition of *iso*-butane in production gas samples from Mamm Creek, Rulison, Parachute and Grand Valley fields.

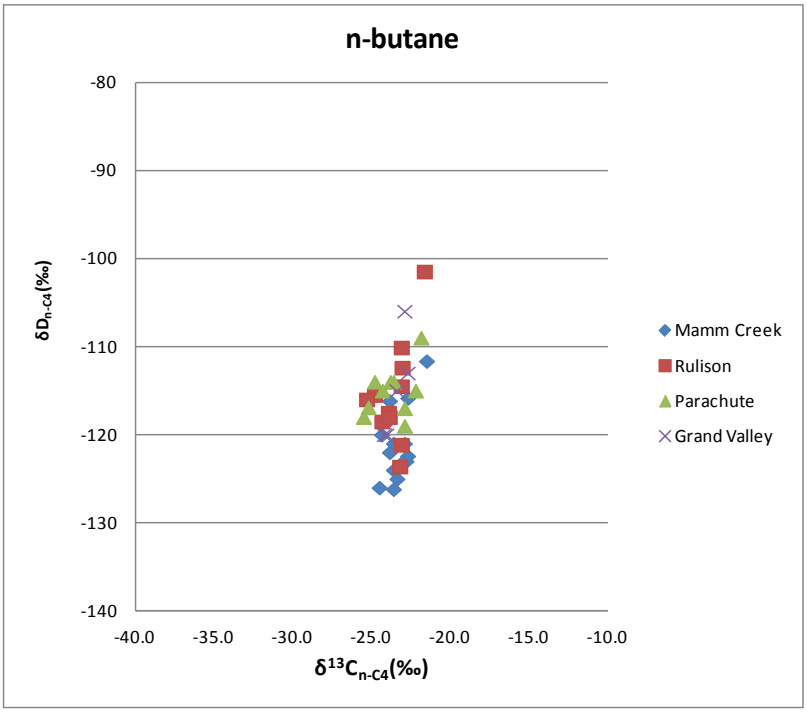

Figure 4.18. Carbon and hydrogen isotopic composition of *n*-butane in production gas samples from Mamm Creek, Rulison, Parachute and Grand Valley fields.

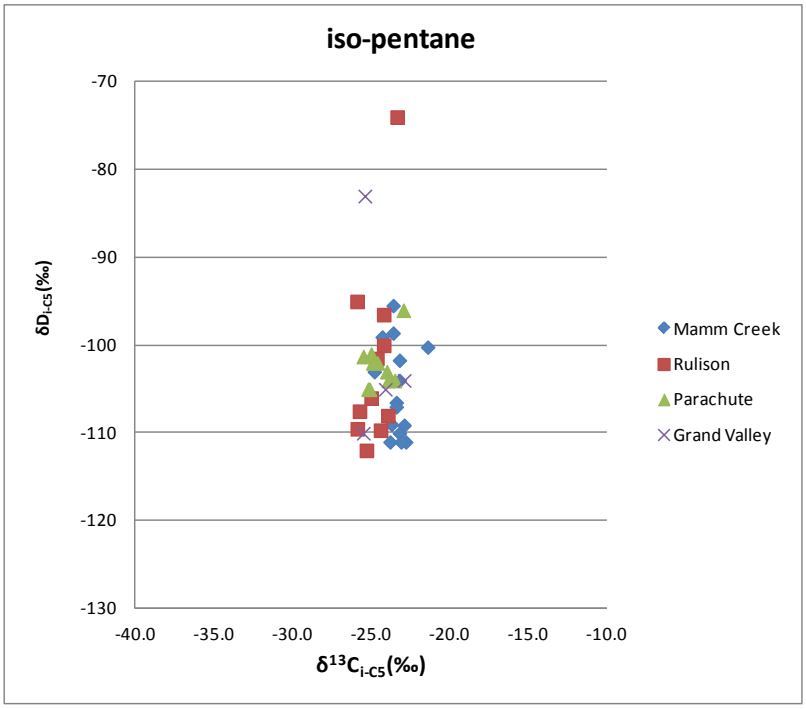

Figure 4.19. Carbon and hydrogen isotopic composition of *iso*-pentane in production gas samples from Mamm Creek, Rulison, Parachute and Grand Valley fields.

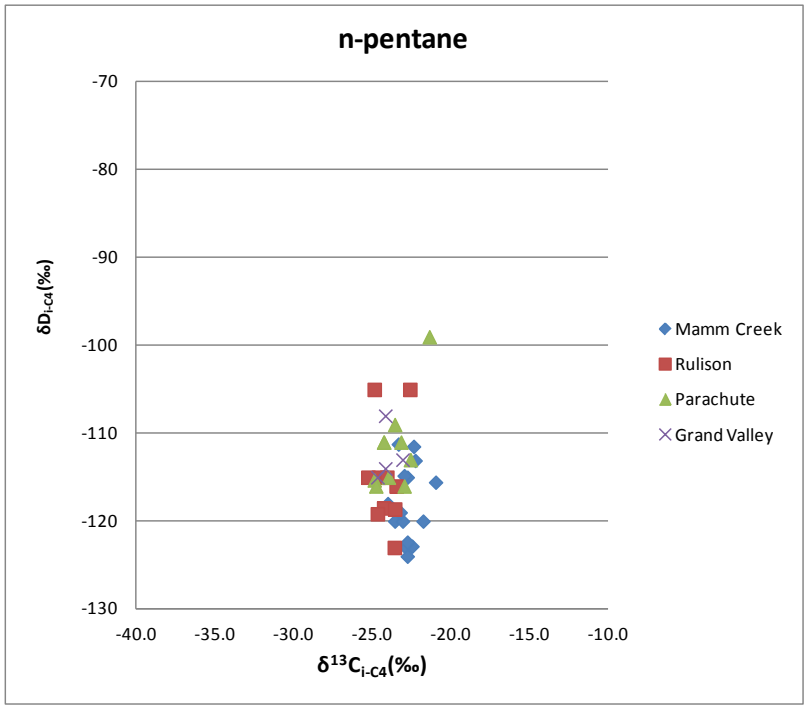

Figure 4.20. Carbon and hydrogen isotopic composition of *n*-pentane in production gas samples from Mamm Creek, Rulison, Parachute and Grand Valley fields.

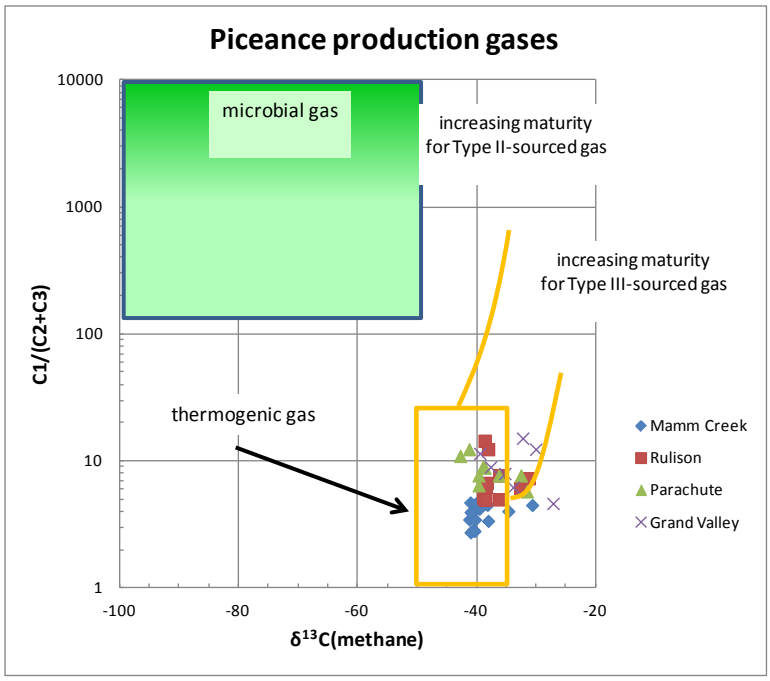

Figure 4.21. Carbon isotopic composition of methane versus the ratio of C_1 to C_2+C_3. Mamm Creek gases have slightly lower $\delta^{13}C_{C1}$ and lower ratios of $C_1/(C_2+C_3)$ in comparison to the other fields. Gases fall within the field for thermogenic gases

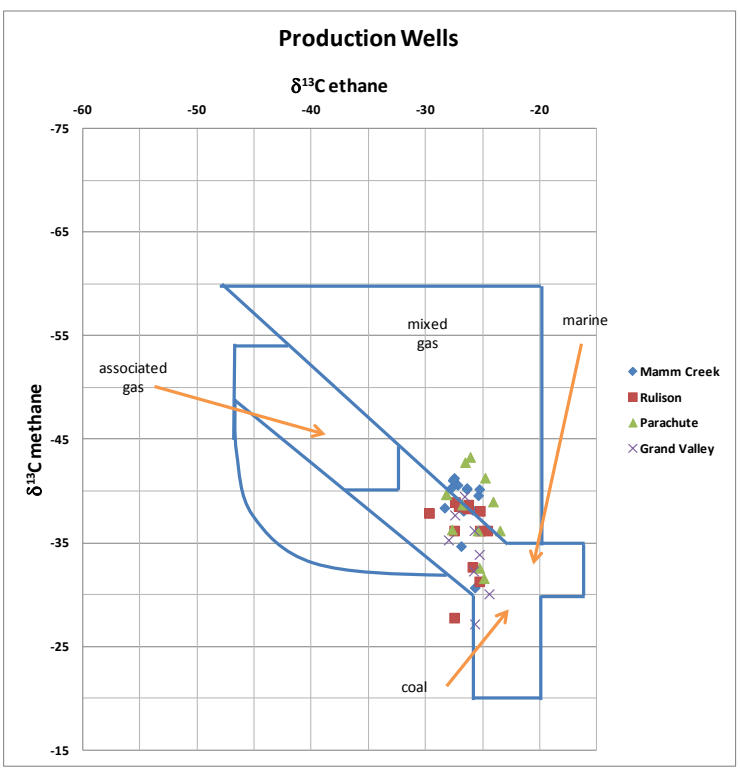

Figure 4.22. Carbon isotopic composition of methane versus ethane, after Schoell (1983). Gas compositions are similar in all four fields.

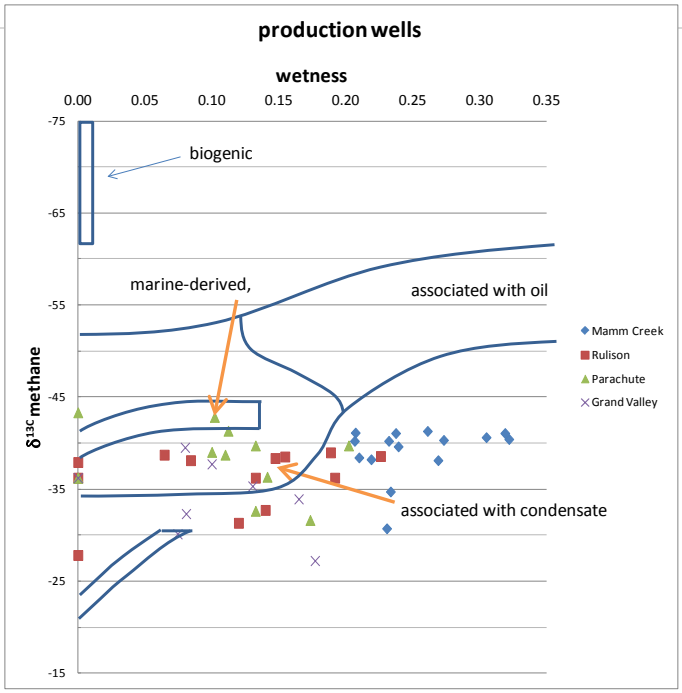

Figure 4.23. Carbon isotopic composition of $\delta^{13}C_{C1}$ versus ethane (after Schoell, 1983). This plot is similar to the Bernard plot (Figure X.21). Mamm Creek gases are distinguished by higher wetness and slightly higher average $\delta^{13}C_{C1}$. The compositions of gases from the other three fields are similar.

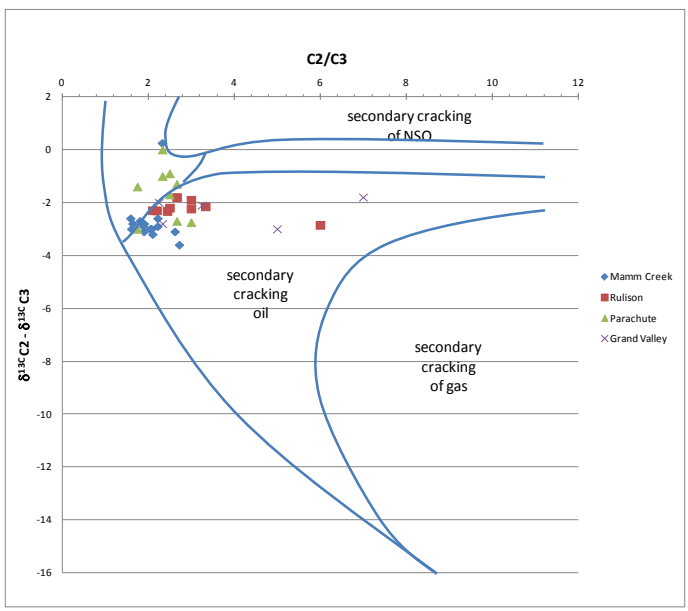

Figure 4.24. Ratio C_2/C3 versus the difference in carbon isotopic composition between C_2 and C_2 (after Lorant et al., 1998). This plot distinguishes gases derived from primary cracking from those derived from secondary cracking. This plot suggests that some gases from Parachute, Rulison and Grand Valley contain a proportion of gas derived from secondary cracking of oil.

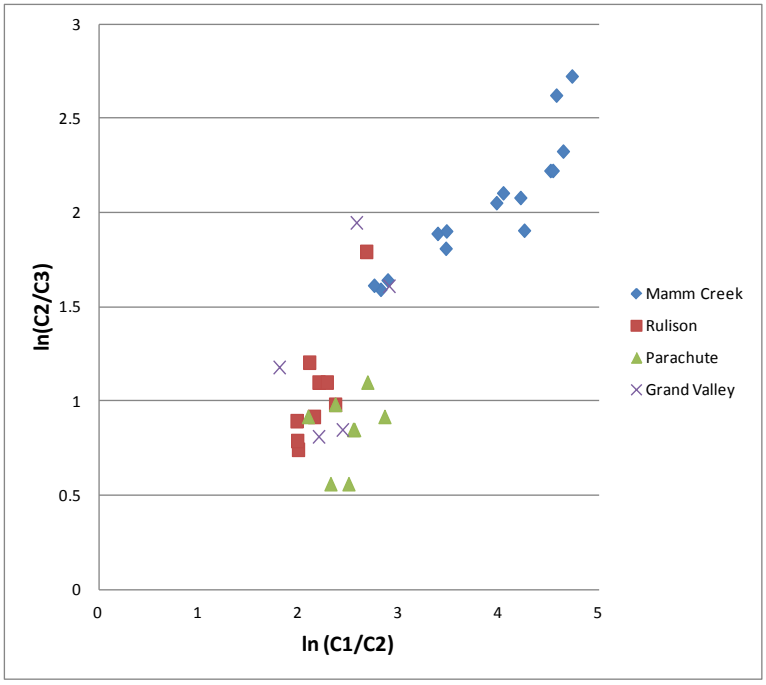

Figure 4.25. Ratio of $\ln(C_1/C_2)$ versus $\ln(C_2/C_3)$ after Prinzhofer and Huc (1995) can be used to distinguish the effects of secondary cracking from primary cracking, where increasing $\ln(C_2/C_3)$ in the absence of increasing $\ln(C_1/C_2)$ can indicate secondary cracking.

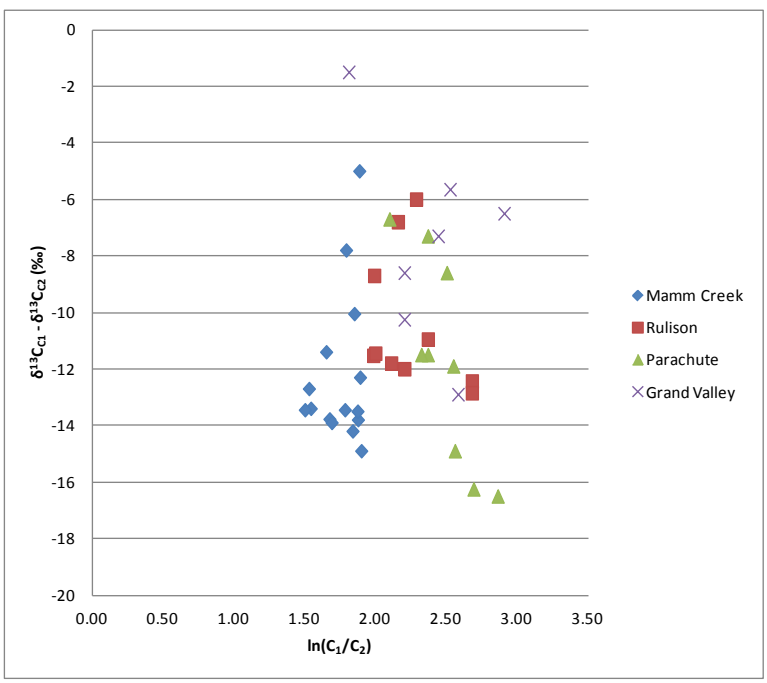

Figure 4.26. Ratio of $\Delta\delta^{13}C_{C1\text{-}C2}$ versus $\ln(C_1/C_2)$ after Prinzhofer and Huc (1995) is used to differentiate maturation trends from leakage. Diagonal trends indicate maturation effects. Mamm Creek gases have lower ln(C1/C2) ratios than other fields, but $\Delta\delta^{13}C_{C1\text{-}C2}$ values are generally similar.

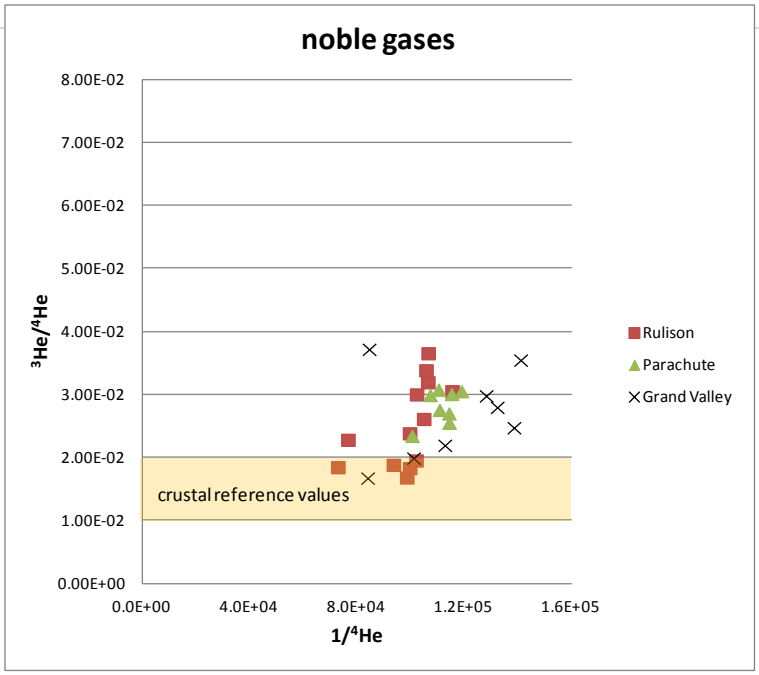

Figure 4.27. $^3He/^4He$ ratios are indicative of contributions of gas from crustal or other sources. Gas compositions from Rulison, Parachute and Grand Valley fields have similar

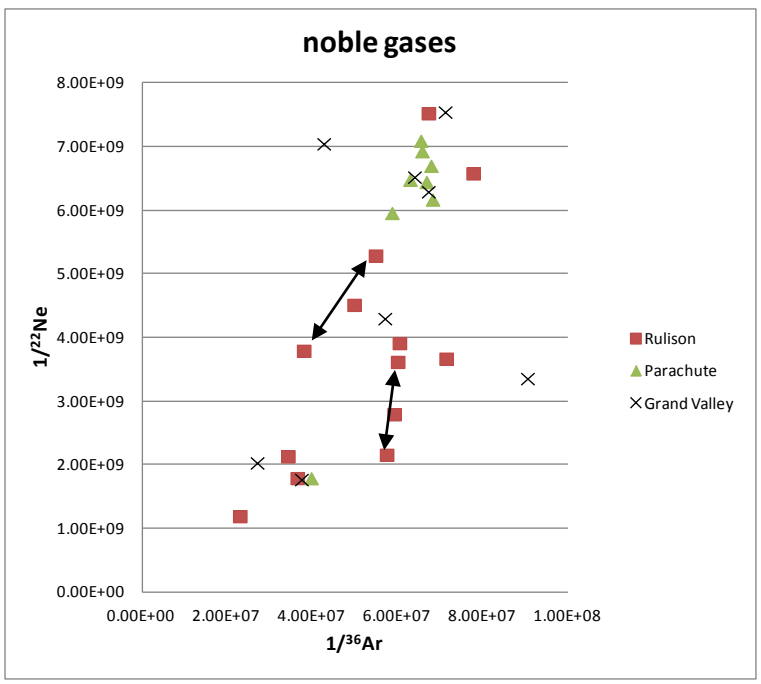

Figure 4.28. ^{22}Ne and ^{36}Ar concentrations are indicative of contributions of gas from atmospheric sources, typically through degassing from meteoric water. Gases from Parachute generally have a strong meteoric water signature; gases from Rulison and Grand Valley display a range of compositions. Arrows highlight two pairs of samples from closely spaced wells.

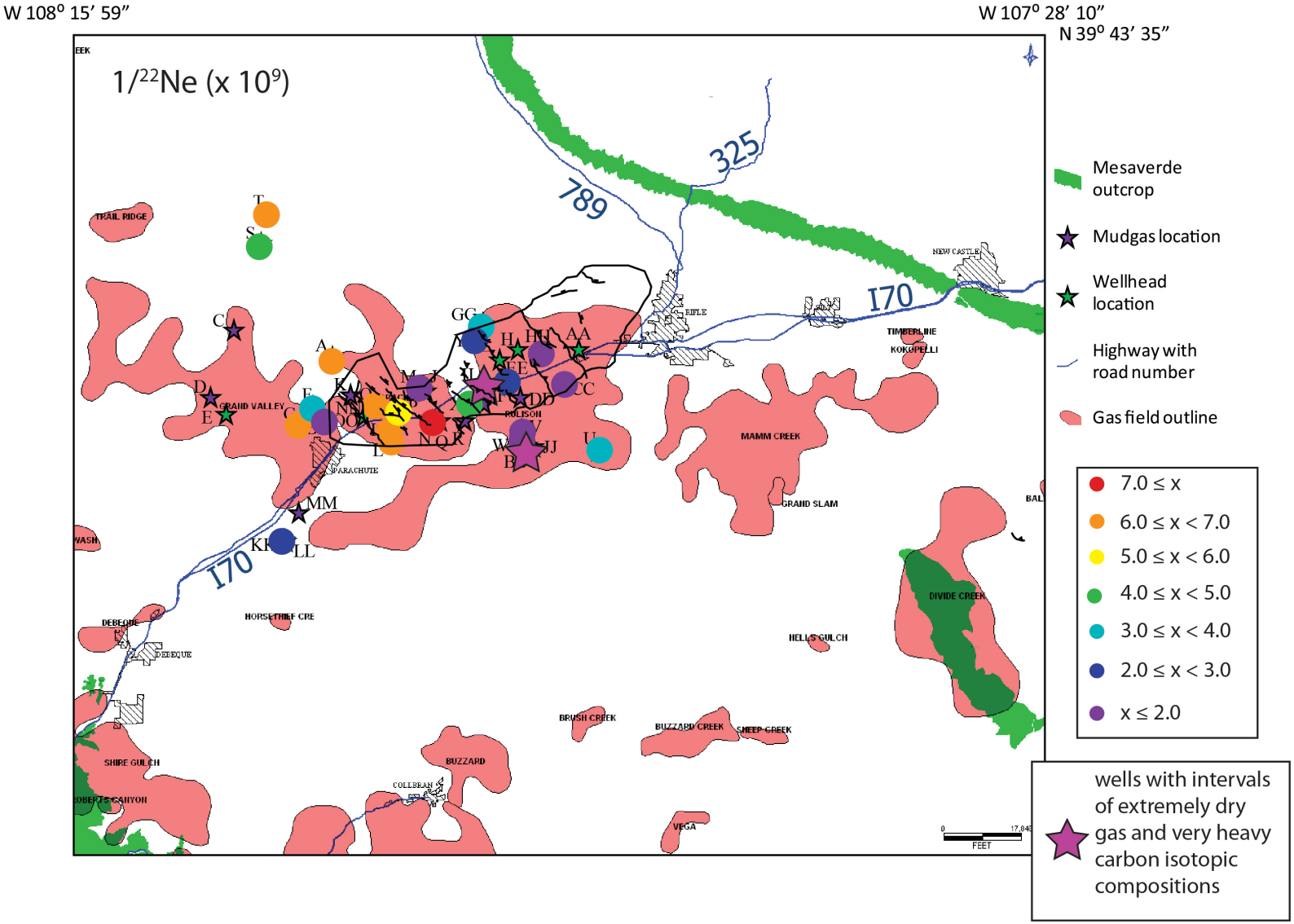

Figure 4.29. ^{22}He and ^{36}Ar concentrations are indicative of contributions of gas from atmospheric sources, typically through degassing from meteoric water. Gases from Parachute generally have a strong meteoric water signature; gases from Rulison and Grand Valley display a range of compositions. Arrows highlight two pairs of samples from closely spaced wells.

Grand Valley

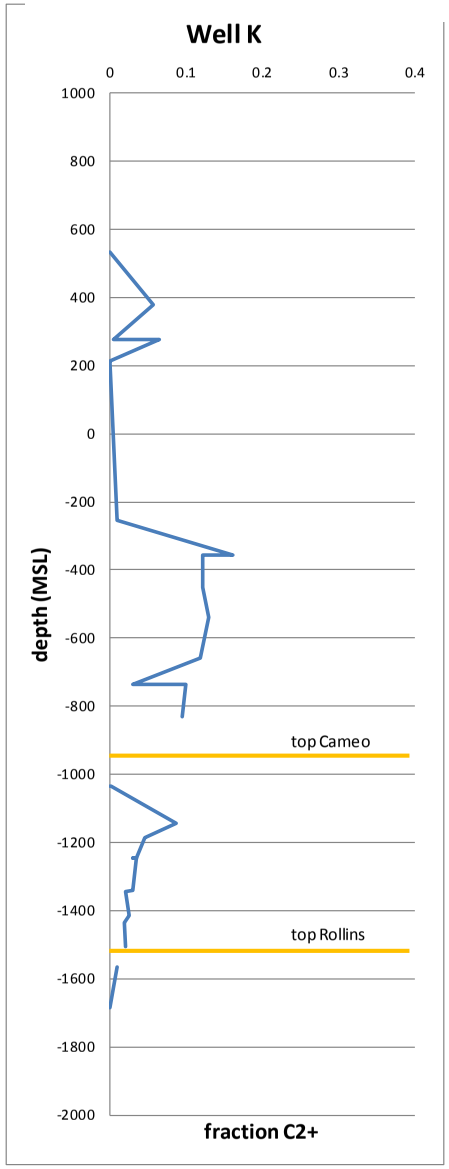

Parachute

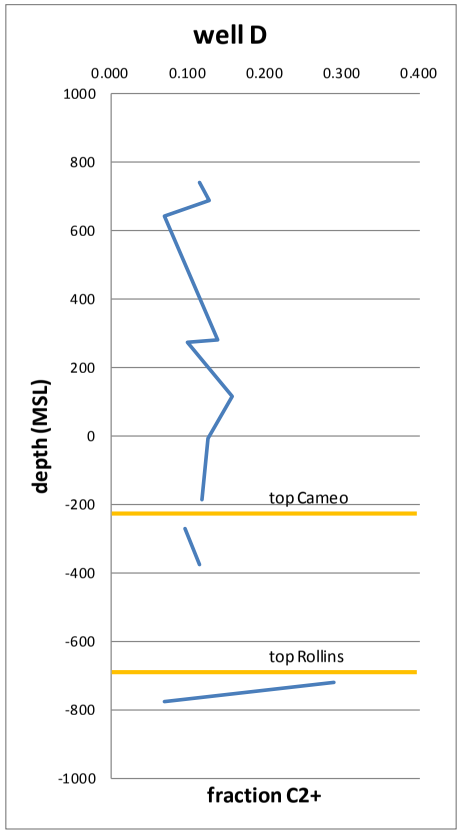

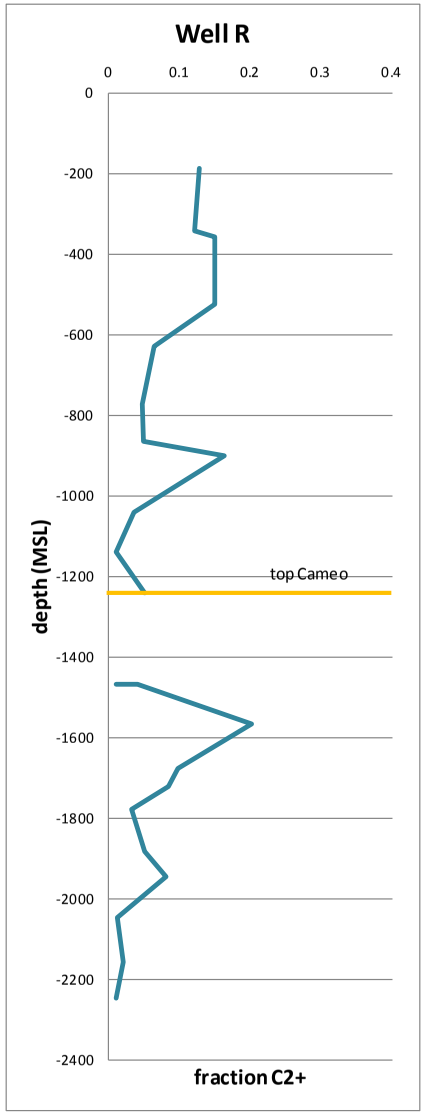

Figure 4.30. Gas wetness profiles in three wells from Parachute and Grand Valley Fields. Yellow lines indicate the tops of the Cameo Coal and Rollins sandstone.

Rulison

south

north

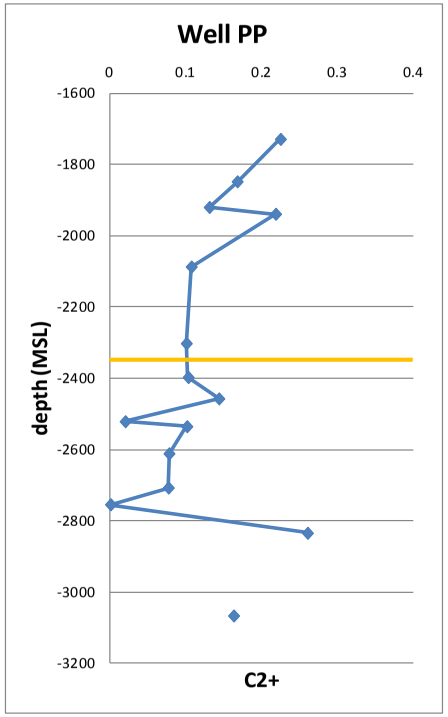

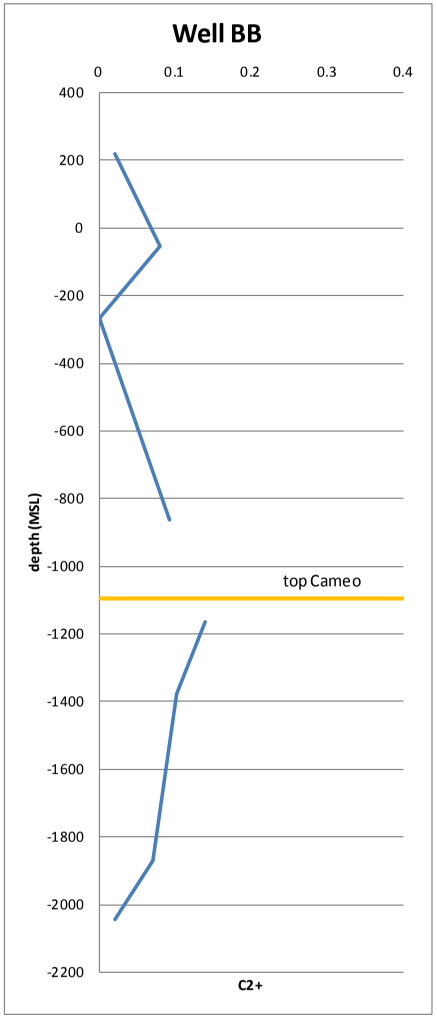

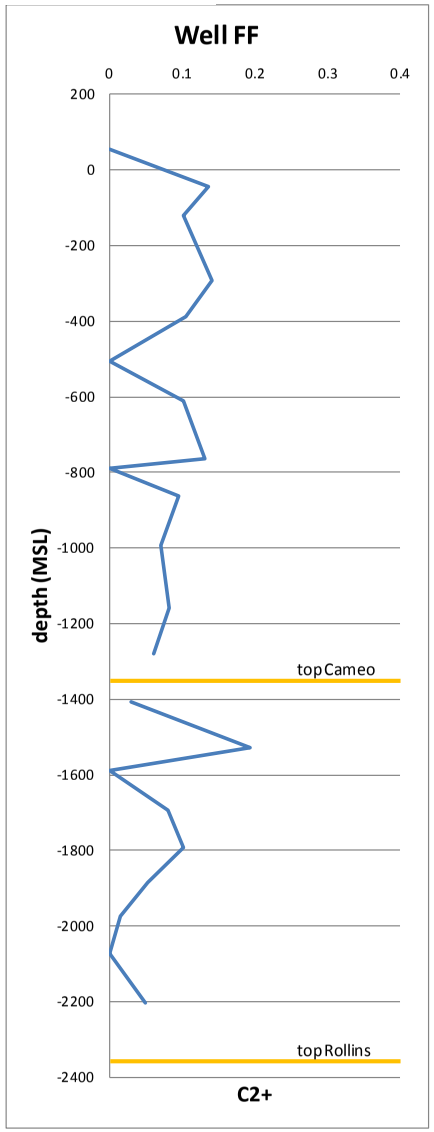

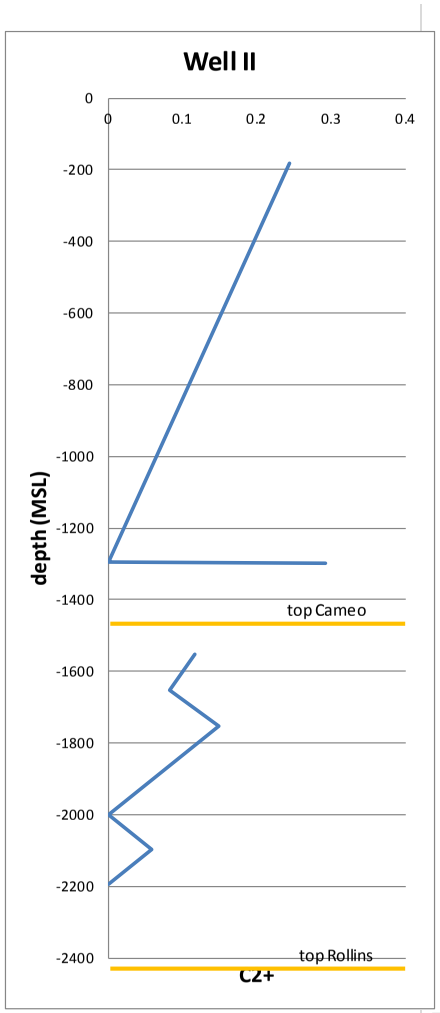

Figure 4.31. Gas wetness profiles in four wells from Rulison Field. Yellow lines indicate the tops of the Cameo Coal and Rollins sandstone.

Rulison

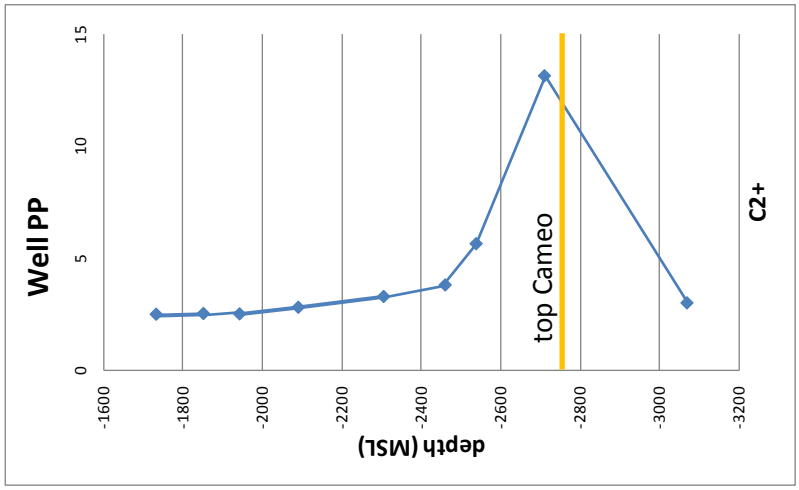

Figure 4.32. Gas wetness profile, well PP at Rulison Field.

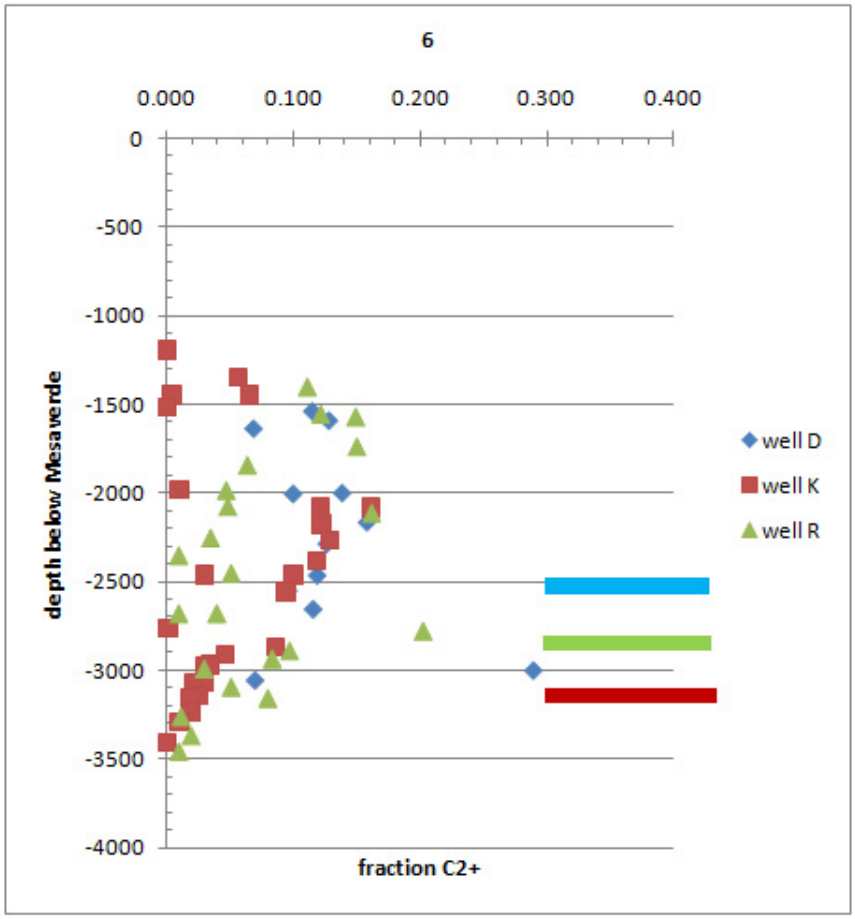

Figure 4.33. Gas wetness in wells from Grand Valley and Parachute fields. Depths are referenced to the top of the Mesaverde.

Grand Valley

Parachute

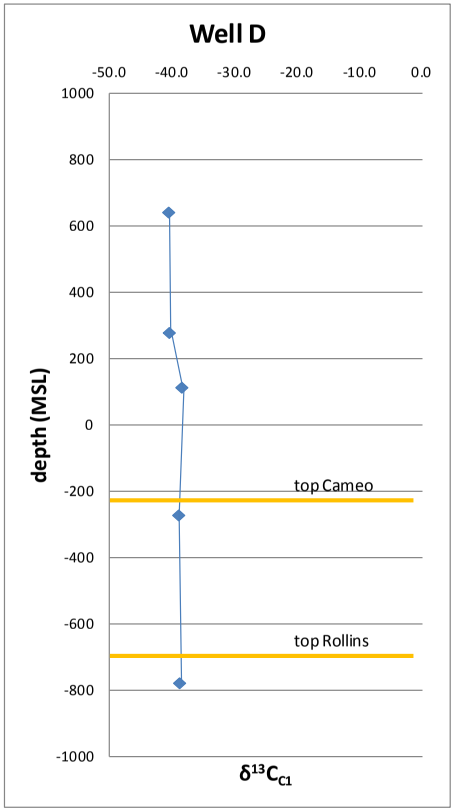

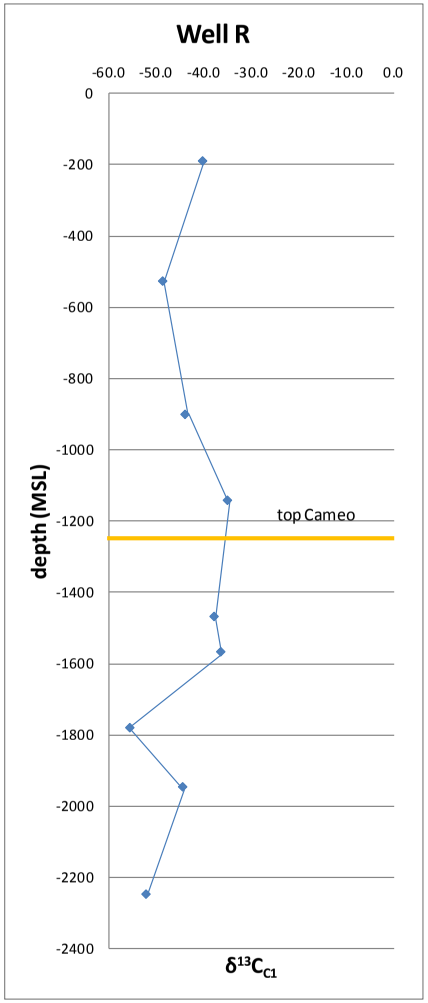

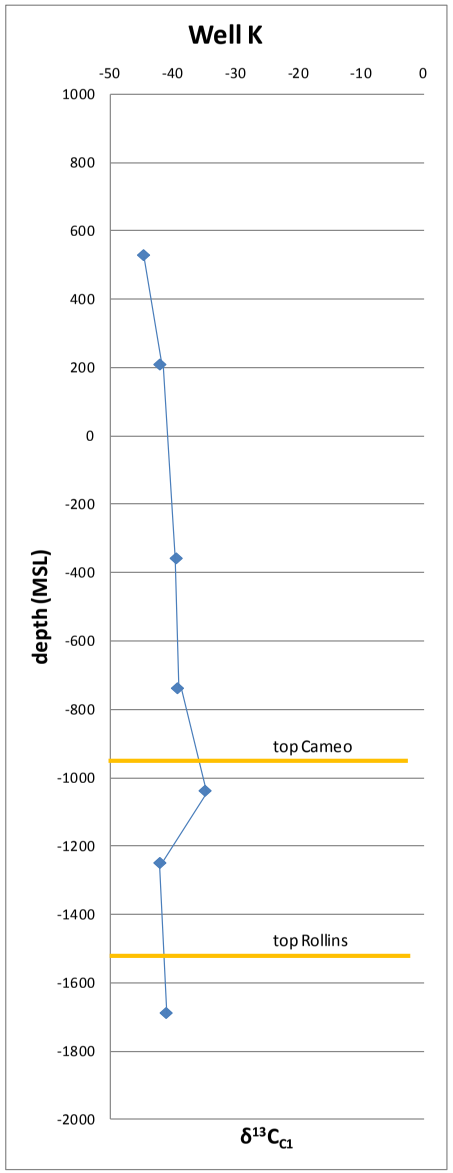

Figure 4.34. Carbon isotopic composition of methane in profiles in three wells from Parachute and Grand Valley Field. Yellow lines indicate the tops of the Cameo Coal and Rollins sandstone.

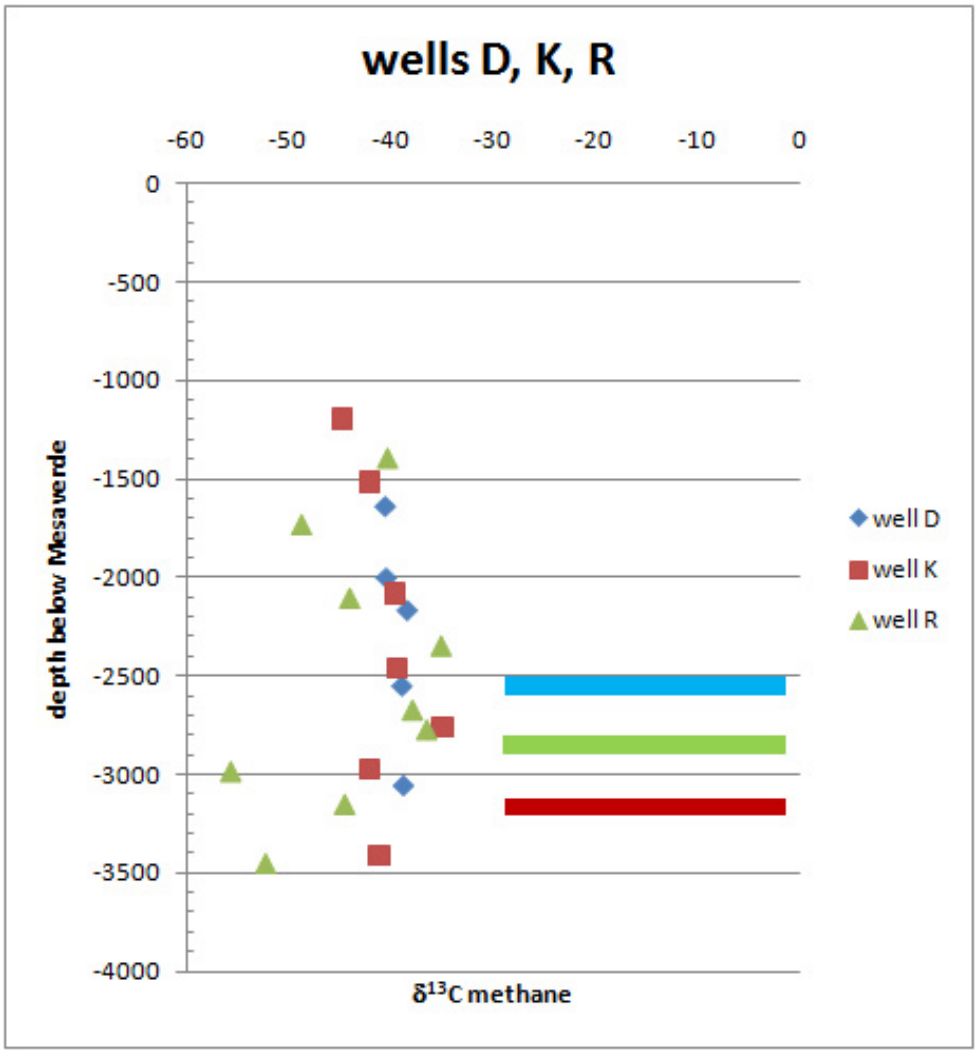

Figure 4.35. Carbon isotopic composition of methane in wells from Grand Valley and Parachute fields. Depths are referenced to the top of the Mesaverde.

Rulison

south

north

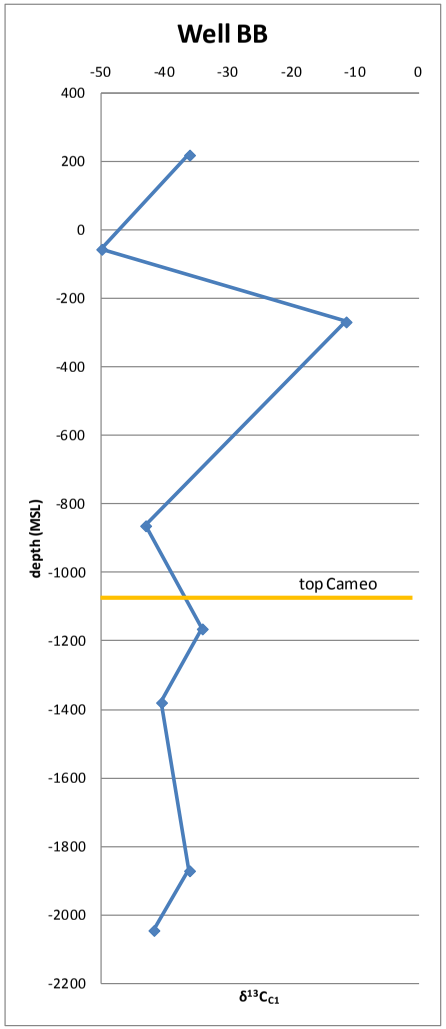

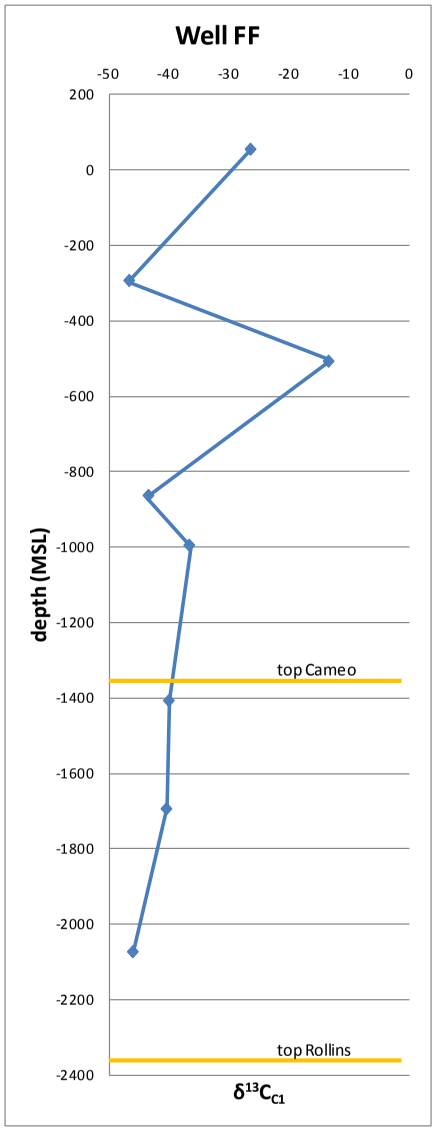

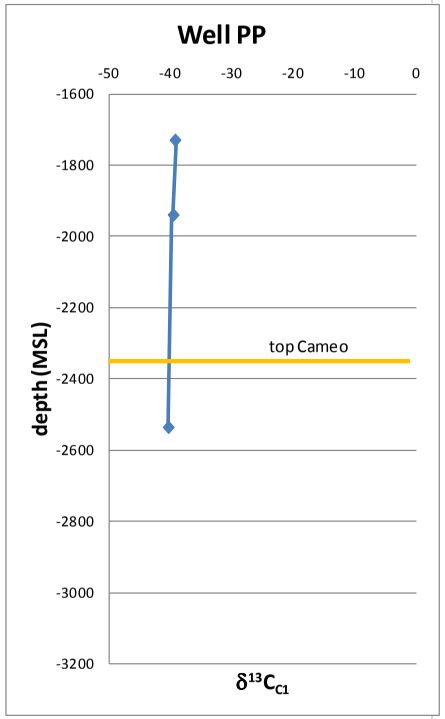

Figure 4.36. Carbon isotopic composition of methane in profiles in three wells from Rulison Field. Yellow lines indicate the tops of the Cameo Coal and Rollins sandstone.

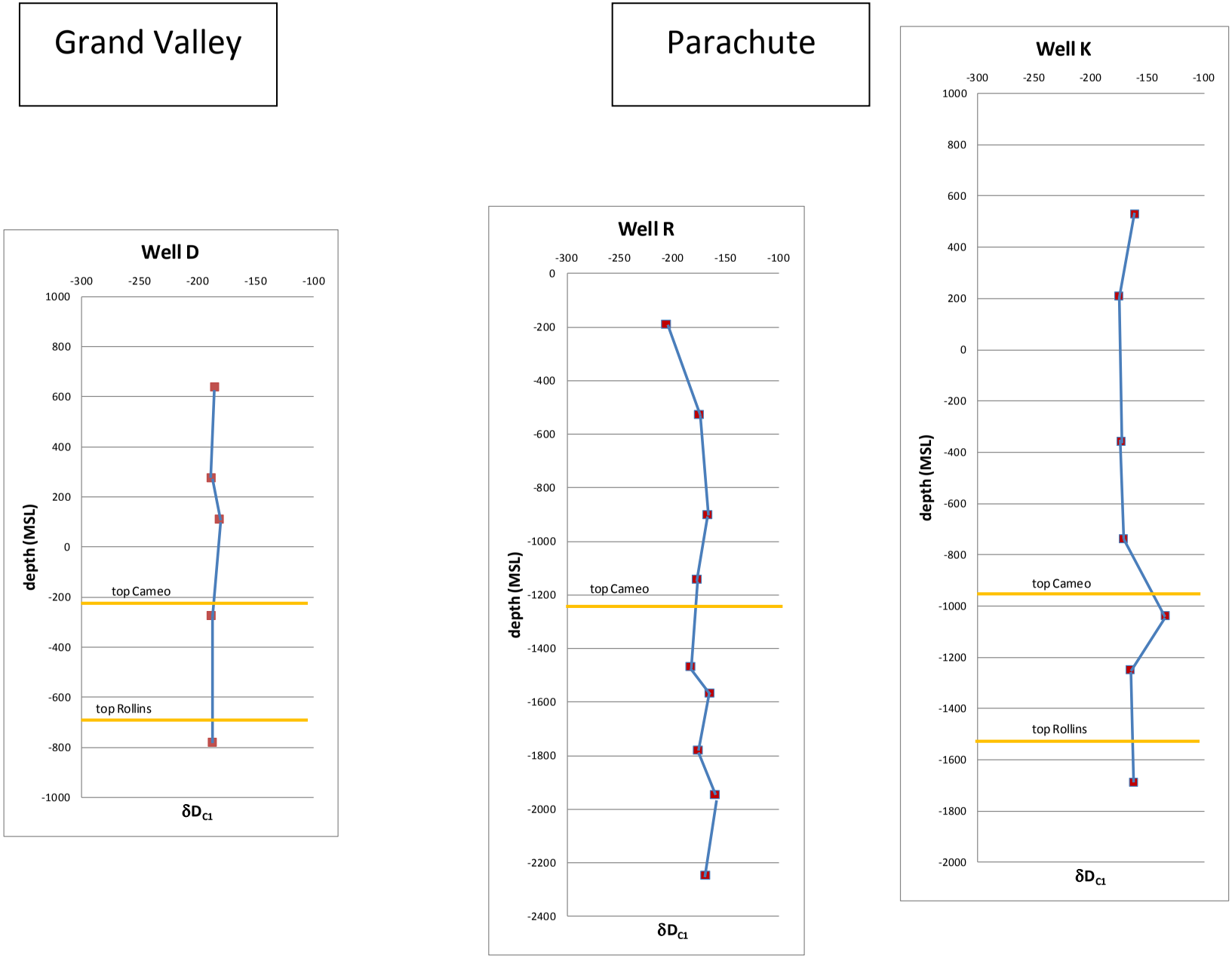

Figure 4.37. Hydrogen isotopic composition of methane in profiles in three wells from Parachute and Grand Valley Field. Yellow lines indicate the tops of the Cameo Coal and Rollins sandstone.

Rulison

south

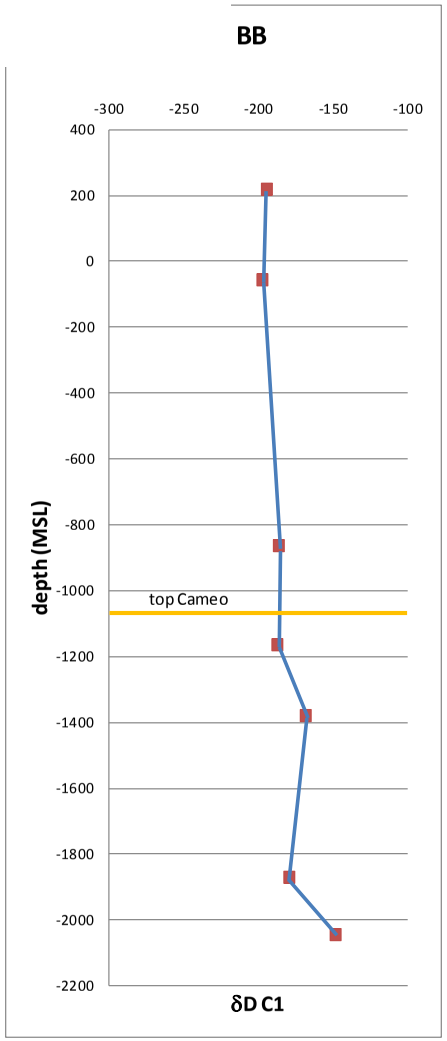

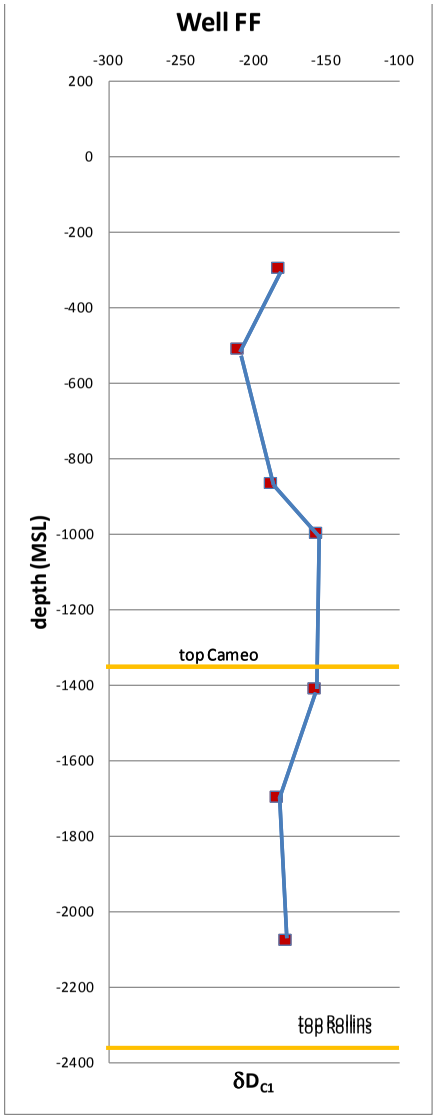

north

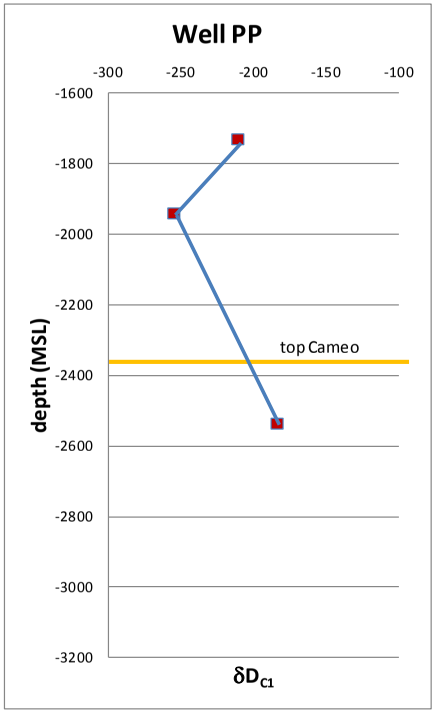

Figure 4.38. Hydrogen isotopic composition of methane in profiles in three wells from Rulison Field. Yellow lines indicate the tops of the Cameo Coal and Rollins sandstone.

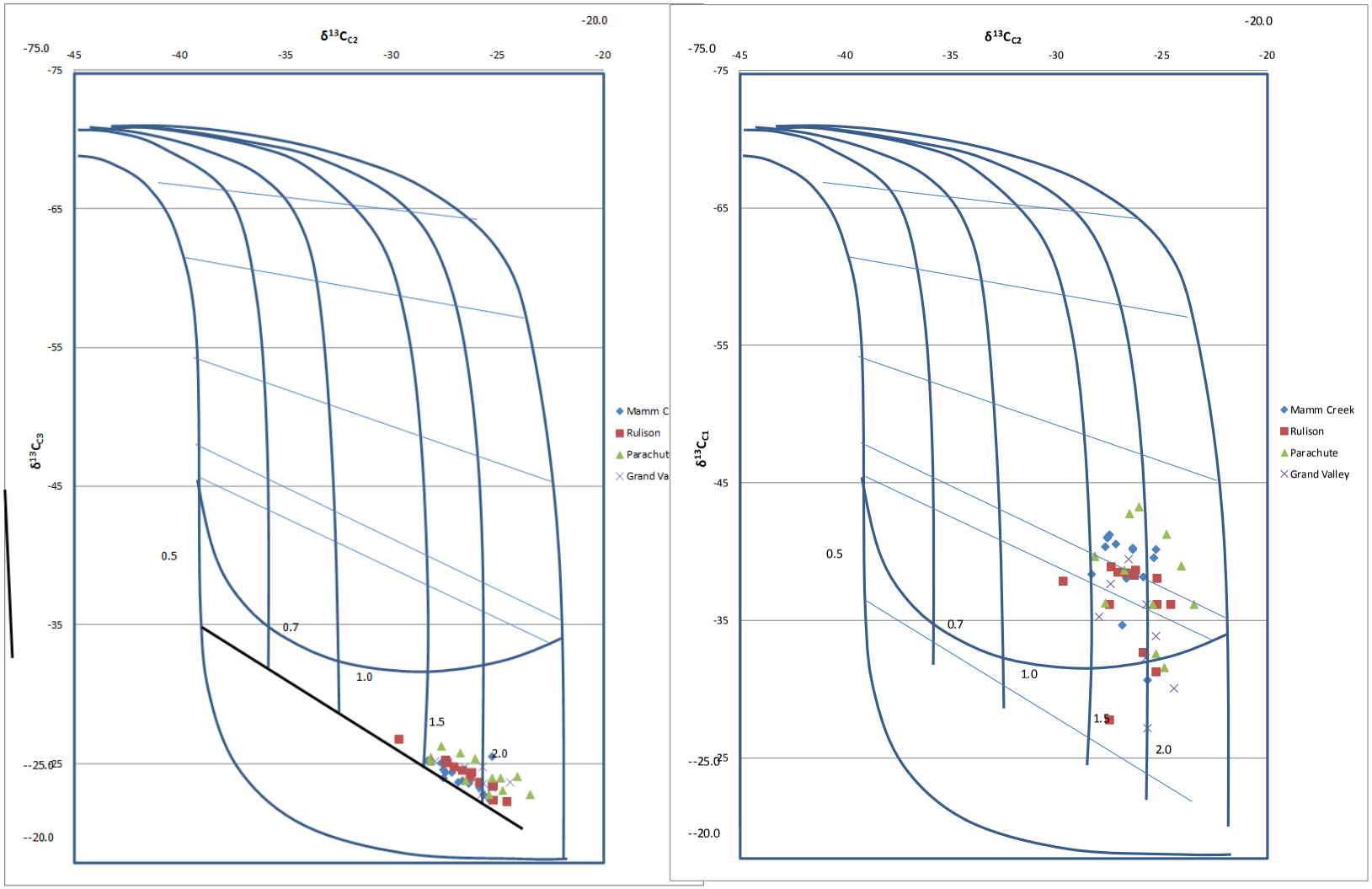

Figure X.39. $\delta^{13}C_{C2}$ versus $\delta^{13}C_{C3}$ (left) and $\delta^{13}C_{C1}$ (right). Compositions are consistent with generation from a source rock at maturities of 1.5% to greater than 2.0% R_o.

5 JONAH FIELD RESULTS AND INTERPRETATION

5.1 Data Set

The dataset from Jonah Field includes:

- Production gas samples (30) from the Jonah Field area, including 4 samples from wells from the periphery of the main Jonah structure, analyzed for bulk composition and C/H isotopes (Figure 5.1).
- Mud gas samples (261) from 19 wells from Jonah Field, analyzed for bulk composition and C/H isotopes (Figure 5.2).
- Production gas samples (14) from Jonah Field, analyzed for noble gas composition (Figure 5.3).
- Fluid inclusion samples (cuttings) from 6 wells in (Figure 5.4).

5.2 Production Gases

5.2.1 Bulk Gas Compositions

The compositions of production gases are summarized in Table 5.1.

The Jonah field production gas samples averaged 17% C_{2+} component (wetness), with 82% methane, 9% ethane, 5% propane, 3% butane and 3% pentane. The average CO_2 content was 2%.

The distribution of gas wetness is shown in Figure 5.5. Within the spatial resolution of our sampling, it is not possible to identify a pattern in gas wetness. Closely spaced wells can have very different compositions. For example SHB 16-18 and SHB 53-17, which are approximately 0.6 miles apart, have a gas wetness of 0.14 and 0.38, respectively. Three of the four wells that produce from normally pressured Lance, the SOL 7-36, Scarlett 11-24 and Yellow Point 4-24, are relatively wet (0.29, 0.23 and 0.32, respectively). The fourth well, JP 11-18, produces a drier gas at 0.18.

C_2/C_3 is another common measure of gas wetness, with low values typical of wet gases. The distribution of C_2/C_3 values is shown in Figure 5.6. Unlike gas wetness, most samples vary

within a narrow range, from 1.80 to 2.25, and C_2/C_3 ratios do not correlate with gas wetness. These data suggest that higher ratios (drier compositions) are concentrated along the western boundary fault and locally the southern boundary fault. However compositions are variable at a small scale, and there are individual wells with lower ratios (wetter compositions) near the western boundary fault.

The CO_2 content of production gases is generally low, in most cases less than or equal to a mole fraction of 0.01 (Figure 5.7). Two exceptional wells are located within overpressured Lance reservoir adjacent to the western border fault of the Jonah structure: SHB 53-17 and Corona 79-19, which contained mole fractions 0.05 and 0.07 CO_2, respectively.

5.2.2 Carbon and Hydrogen Isotopic Composition

<u>Carbon isotopes</u>

The average carbon isotopic composition varied significant in the methane fraction (Table 5.1). The values of $\delta^{13}C_{C1}$ range from -44.0 to -27.7‰. The distribution of $\delta^{13}C_{C1}$ presents no obvious geographic pattern (Figure 5.8). Nearby wells often have quite different methane isotopic compositions, for example SHB 75-26 and SHB 63-27, with of $\delta^{13}C_{C1}$ of -42.4‰ and -27.7‰, respectively. There is a tendency for the most isotopically positive (heavy) values are localized near major faults, but other wells very near faults may have isotopically quite negative (light) values.

The carbon isotopic composition of ethanes exhibits a much smaller range of values (-24.2 to -29.8‰) (Figure 5.9), as does the composition of the propanes (-22.6 to -27.8‰) (Table 5.1). Variability in the butane and pentane compositions is similar, with the iso-butane and iso-pentane compositions systematically heavier than the n-butane and n-pentane by 0.1 to 0.8‰ (Table 5.1).

Chung plots (Chung et al., 1988) show a considerable variability (Figure 5.10). As noted above, there is a wide range in $\delta^{13}C_{C1}$ with compositions well distributed between -44.0 and -27.7‰, without any clustering that suggests the presence of distinct families. The range in $\delta^{13}C$ decreases with the heavier gases but is still significant, approximately 5‰ in the butanes and pentanes. In the ethane to pentane range, there is a variety of slopes represented in the data, with some samples showing a distinct decrease in $\delta^{13}C$ from n-pentane to ethane and other samples showing little change in $\delta^{13}C$. Spatial variation in the $\delta^{13}C$ difference between C_5 to C_2 and from C_5 to C_3 is shown in Figures 5.11 and 5.12, respectively. While there is great variability at several scales in these diagrams, in general, samples from normally pressured Lance wells

outside the main Jonah structure show a substantially larger decrease in $\delta^{13}C_{C5}$ to $\delta^{13}C_{C3}$ and to $\delta^{13}C_{C2}$ (C_2 and C_3 are isotopically much lighter than C_5) than most wells within the Jonah structure, particularly along the western boundary fault.

The carbon isotopic composition of CO_2 exhibits significant variation at Jonah Fields (Table 5.1, Figure 5.13), averaging -11.4‰ but ranging from as negative as -17.2‰ to as positive as -7.1‰. The $\delta^{13}C_{CO2}$ is most positive in two normally pressured Lance wells outside the main Jonah structure, the Yellow Point 2-24 well (-7.1‰) and the Scarlett 11-34 well (-7.4‰). Within the Jonah structure (overpressured Lance reservoir), values as positive as -8.1 and -8.8‰ are found in the central and eastern parts of the field. The most negative values are found primarily along the western bounding fault of the Jonah structure, where values as light as -17.2‰ occur.

Hydrogen isotopes

The average hydrogen isotopic composition of production gases (Table 5.1) also varied significantly in the methane fraction, similar to the carbon isotopic data. The δD_{C1} at Jonah averaged -195.4‰, and ranged from -147 to 244‰. Ranges of δD were substantial for the heavier gases as well, including C_3 (from -82 to -226‰), *i*-C_4 (-149.5 to -289‰), *n*-C_4 (-144 to -180‰). Ranges of δD for the pentanes was smaller, although we had many fewer analyses of these (*i*-C_5 from -145 to -147‰) and *n*-C_5 (from -156 to --173‰).

The hydrogen isotopic composition of the gases is investigated with a set of $\delta^{13}C$ – δD cross-plots, one for each gas species (Figures 5.14 to 5.20). These plots distinguish between normally pressured Lance from outside of the Jonah structure (red squares) from overpressured Lance within the Jonah structure (blue diamonds). The methane data show that samples exhibit a wide range of $\delta^{13}C$ but a very limited range of δD. Normally pressured Lance samples are slightly depleted in D (lower δD) than the overpressured samples. Ethane samples are all tightly clustered with respect to hydrogen and carbon isotopes. Propane samples exhibit very small range with respect to carbon isotopes hydrogen isotopes in the overpressured Lance samples, but a remarkably wide range in the normally pressured Lance samples (δD = -199 to -135‰). Both *i*-C_4 and *n*-C_4 samples from overpressured Lance reservoir similarly exhibit very narrow ranges in $\delta^{13}C$ and δD, but a wide range of values in δD for normally pressured Lance reservoir. The *i*-C_5 and *n*-C_5 components exhibit similar ranges for the overpressured and normally pressured Lance reservoirs.

5.2.3 Integrated bulk compositions and isotopes

More details are apparent in cross-plots that are commonly used to interpret the origin of natural gases.

Figure 5.21, a Bernard plot (Bernard, 1977), is primarily used to distinguish biogenic from thermogenic gases. This plot examines the carbon isotopic composition of methane combined with the proportion of methane to ethane and propane. Thermogenic gases have distinctively more positive (heavier) isotopic compositions than biogenic gases and typically a higher proportion of ethane and propane, although with increasing thermal maturity, the ratio $C_1/(C_2+C_3)$ increases and $\delta^{13}C_{C1}$ becomes more positive. In this cross-plot, gas samples generally fall within the range of thermogenic gases, although some samples have $\delta^{13}C_{C1}$ values between -35.0 and -27.7‰ that are more positive (heavier) than the normal upper limit for methane isotopic compositions. Overpressured Lance gases are not differentiated from normally pressured Lance gases in this cross-plot.

Figure 5.22 is one of a series of cross-plots devised by Schoell (1983) to examine the origin and maturity of gases. This plot utilizes the isotopic compositions of methane and ethane. Gas compositions fall within the field of marine-source thermogenic gas, trending toward mixed gas. Overpressured Lance gases are not distinguished from normally pressured Lance gases in this cross-plot.

Figure 5.23 is another in the series of Schoell's (1983) cross-plots. This utilizes the wetness (C_{2-4})/C_{1-4}) and the $\delta^{13}C_{C1}$ and is similar to the Barnard plot (Figure X.21). Many samples fall outside the normal range of thermogenic or associated gases in this cross-plot, with isotopic compositions that are more positive (heavier) than would be expected for gases with this degree of wetness. In other words, gases with wetness values in the range of 0.15 to 0.4 typically have isotopically more negative (lighter) compositions than many of the Jonah gases.

Figure 5.24, after Lorant et al. (1998) examines the ratio of C_2 to C_3 and the difference in carbon isotopic composition between these species, in order to distinguish gases derived by primary cracking of kerogen from those derived by various kinds of secondary cracking. In this cross-plot, sample compositions are tightly clustered and lie in the field for thermogenic gases derived by primary cracking.

Figure 5.25 examines $\ln(C_1/C_2)$ versus $\ln(C_2/C_3)$ (after Prinzhofer and Huc, 1995) to distinguish the effects of secondary cracking from primary cracking; the criterion for secondary cracking is increased $\ln(C_2/C_3)$ in the absence of increased $\ln(C_1/C_2)$. In this cross-plot, most of the data

describe a very tight cluster, particularly with respect to $\ln(C_2/C_3)$. Samples from normally pressured Lance reservoirs do not notably differ from those from overpressured Lance reservoirs.

Figure 5.26 examines $\ln(C_1/C_2)$ versus the difference in carbon isotopic composition between these species. This plot, after Prinzhoffer and Huc (1995), attempts to identify leakage from reservoirs, maturity of source rocks and mixing of thermogenic and biogenic gas. Jonah Field gases display a considerable range in $\Delta\delta^{13}C_{C1-C2}$ (~14‰). There is no systematic variation with respect to $\ln(C_1/C_2)$, nor are normally pressured Lance samples clearly distinguished from overpressured Lance samples.

5.2.4 Noble Gases

Noble gases serve to distinguish contributions from three primary sources: mantle, crust and atmosphere and to identify fractionation processes.

Crustal contributions to natural gas are dominated by ^{4}He and therefore crustal-derived gas is characterized by low ratios of ^{3}He/^{4}He, all tightly clustered within the range of crustal sources of He (Figure 5.27). Samples also cluster relatively tightly in 1/^{4}He.

Low concentrations of ^{22}Ne and 36Ar are indicative of gases derived from the atmosphere, which typically enter natural gases through meteoric water. Samples from Jonah Field typically have low values of 1/^{22}Ne (Figure 5.28 and 5.29), indicating degassing from meteoric water.

5.3 Mud Gases

Mud gas analyses come from 19 wells at Jonah Field, with sample profiles that include from 2 to 39 samples. Five samples were deleted from the dataset presented here because of high CO_2 contents, assumed to be the result of adding lime to the drilling mud. All remaining samples contained no more than 14% CO_2 and generally substantially less than that.

5.3.1 Bulk gas compositions

Gas compositions from mud gas samples are summarized in Table 5.2.

Bulk gas compositions from mud gas samples are very similar to those determined from production gas samples. The methane fraction in mud gas averaged 0.84, as compared to 0.82 in production samples. Gas wetness in mud gas samples averaged 0.15, compared to 0.17 in

production samples. Excluding 5 samples with highly anomalous CO_2 content, the CO_2 fraction in mud gas samples averaged 0.03, compared to 0.02 in the production samples.

A systematic difference between production gas and mud gas data only existed with the C_1/C_2 ratio, which was higher in the mud gas data than in the production gas data (18.34 versus 9.97). C_2/C_3 ratios were similar in mud gas and production gas data.

Bulk gas compositions show a weak trend of increasing wetness with depth (Figure 5.30). With four exceptions, gas samples taken from shallow depths (8000 to 10000 feet) have a maximum wetness of 0.19. Deeper samples tend to be wetter, and gas samples taken between 11,000 and 13,000 feet have a maximum wetness of 0.37. There are extremely dry samples from the complete range of depths, however. Location within the field do not discriminate compositional trends. Samples taken from the vicinity of the southern boundary fault of the Jonah structure have wetness values similar to other wells in the field.

C_2/C_3 ratios show a subtle decrease with depth (Figure 5.30), consistent with the increase in gas wetness.

When individual wells are plotted, consistent relationships to stratigraphy emerge. Figure 5.31 shows gas wetness versus depth for 6 wells with the densest sample coverage. Wetness values are intermediate in the Mesaverde sandstone, the basal unit sampled in most of the wells. Wetness increases upward into overlying sandstone units, which may be the Wardell, Jonah or Lower Lance sandstones, to values of 0.25 to 0.35. Wetness values then decrease upward to quite dry values of 0.0 to 0.1, typically in the Middle Lance. Values then increase again upward toward the contact with the Unnamed unit.

C_2/C_3 ratios also display consistent patterns with respect to stratigraphy (Figure 5.32). Ratios generally peak at 2.5 to 3.0 within the Lance and decrease upward to the contact with the Unnamed unit. A secondary peak is present near the upper contact of the Mesaverde sandstone.

CO_2 profiles are shown in Figure 5.33, which excludes five data points with highly anomalous CO_2 content, assumed to be the result of lime added to drilling mud. The remaining data show spikes to high values just above the Mesaverde (Wardell, Yellowpoint) and a smaller peak in the Lower Lance.

5.3.2 Carbon and Hydrogen Isotopic Composition

Carbon isotopes

Carbon isotopic compositions of gas species from mud gas samples are summarized in Table 5.2.

The $\delta^{13}C$ of mud gases are generally similar to the production gases, except that mud gases average -2.3‰ more negative than the average of the production gases. Other than that, mud gases average 1‰ or less heavier than the production gases.

The $\delta^{13}C_{C1}$ profiles generally show subtle upward increases (Figure 5.34), typically -42 to -45‰ in the Mesaverde section, increasing to approximately -35‰ in the Upper Lance. Two wells, the 113-10 and 60-22, show significant local variation in the Yellowpoint, Jonah and lowermost Lance section (Figure 5.35). The $\delta^{13}C_{C2}$ profiles also show an upward increase, from approximately -29‰ to -23‰ from the Mesaverde to the top of the Lance section (Figure 5.36).

While there is generally considerable scatter in $\delta^{13}C_{C1}$ at a particular depth, on the order of 10 to 15‰, one set of wells shows much more coherent behavior (Figure 5.37). Both $\delta^{13}C_{C1}$ and $\delta^{13}C_{C2}$ in this set of 5 wells from the southern part of Jonah field show a systematic decrease in carbon isotopic composition and tight clustering of data around a trend line.

Hydrogen isotopes

The hydrogen isotopic compositions from mud gas samples are summarized in Table 5.2.

The δD of mud gases are systematically more negative (lighter) than production gases by 11 to 32‰. The difference is least for the *n*-C4 gases and greatest for the *i*-C4 gases.

The δD_{C1} reaches a maximum of -190 to -200‰ in Mesaverde sandstone, decreases to -205 to -215‰ in the middle Lance, then increases upward toward the contact with the Unnamed unit (Figure 5.38).

5.3.3 Integrated Bulk Compositions and Isotopes

The cross-plot of C_2/C_3 versus $\delta^{13}C_{C2}$- $\delta^{13}C_{C3}$ can indicate primary cracking versus different types of secondary cracking, where low values are typical of primary cracking and elevated values indicate secondary cracking from oil.

Unlike the production gases which largely lie within the primary cracking field, a considerable number of mud gas data points fall within the secondary cracking field. Samples which exhibit characteristics of secondary cracking are shown by arrows in Figure 5.39. These samples do not appear to be randomly distributed but rather are concentrated in specific wells. Of the six wells for which extensive sample suites were taken, two (113-10 and 60-22) have a large number of samples with the characteristics of secondary cracking (Figure 5.40). The other four wells do not.

5.4 Fluid Inclusion Analysis

Cuttings samples from six wells in the study area were analyzed by Fluid Inclusion Technologies Inc. Well locations are shown in Figure 5.4. The complete reports from Fluid Inclusions Technology Inc. are provided in the Appendix. A summary of the results is provided here.

5.4.1 Yellow Point 5-13; API # 49-035-21873

Formation tops reported in this well are the Fort Union at 5750 feet, Lance – Upper 8978, Lance – Middle at 8978, Jonah at 9236, Yellowpoint at 9577, Wardell at 9910, and Mesaverde at 10340.

FIS data range from dry gas to oil-like spectra, and most of the analyzed section is considered anomalous on a global intensity scale. The analyzed interval, overall, is dominated by wet gas and wet gas to gas-condensate responses. Stronger methane responses occur below 8500 ft. The most significant anomalies are documented at 6910-7150 ft (mostly gas-condensate to oil), 8760-9060 ft (mainly wet gas to gas-condensate) and 9320-9760 ft (dry gas to wet gas).

Thin sections were prepared from five depths. A thin section from 7810 ft reveals rare, blue-fluorescent, upper-moderate gravity petroleum inclusions in fractured detrital quartz grain. No visible petroleum inclusions are identified at 7090 ft, 8880 ft, 9420 ft and 10520 ft. Moderate to abundant gas-prone kerogen and live (fluorescent) stain are recorded in shale. Rock types include shale, coal and sandstone in variable proportion.

Proximal Pay Indications: Samples displaying anomalous acetic acid are recorded at 7780-7810 ft and 8460-8600 ft. These may be sensing nearby oil or condensate charge.

Potential Seals: Possible seals are identified at 6910 ft, 7180 ft, 7750 ft, 8480 ft, 8760 ft, 9320 ft, 10080 ft and 10460 ft.

Evidence for Bacterial or Thermal Alteration: None documented.

Other: Nothing of note.

5.4.2 Stud Horse Butte 14-17; API # 49-035-22755

Formation tops are reported as follows: top of Middle Lance at 10117 feet, top of Jonah at 10304 feet, top of Yellowpoint at 10730 feet, top of Wardell at 11124 feet.

Petroleum Indications Type and Quality: FIS data consist of dry gas responses throughout, with minor wet gas noted at 8150-8270 ft, 10970-11090 ft, intermittently at 7640-8030 ft, 8368-8540 ft and below 11238 ft. The most significant anomalies are recorded toward the deeper section at 10970-11090 ft (wet gas) and 11296-11373 ft (dry gas to wet gas).

Thin sections were prepared from five depths (see Table: II). A thin section from 11498 ft reveals rare, blue-fluorescent, upper-moderate gravity oil inclusions in fractured detrital quartz. No visible petroleum inclusions are identified at 7640 ft 8240 ft, 9230 ft or 11030 ft. Thin sections are comprised of sandstone and shale. Moderate amounts of gas-prone kerogen are identified in shale throughout. Moderate amounts of live (fluorescent) stain are documented in thin sections from 7640-9230 ft.

Proximal Pay Indications: None identified.

Potential Seals: Possible seals are interpreted at 7340 ft, 7760 ft, 8210 ft, 8360 ft, 9050 ft, 9860 ft, 10970 ft and 11300 ft.

Evidence for Bacterial or Thermal Alteration: None detected.

Other: Nothing of note.

5.4.3 Stud Horse Butte 10-26: API # 49-035-22512

Formation tops reported in this well are Lance – Upper at 8839, Lance – Middle 10430, Jonah at 10708 feet, Yellow Point 10992, and Wardell at 11784 feet.

Petroleum Indications, Type and Quality: FIS data consist of dry gas to wet gas responses throughout, with wet gas more common below 8830 ft. The most significant responses occur at 11590-11740 ft.

Thin sections were prepared from five depths (see Table: II). Rare, white to blue-fluorescent, upper-moderate gravity petroleum inclusions are noted in fractured detrital quartz grains at 8560 ft, 10060 ft, 10750 ft and 11620 ft. Rare, yellow-fluorescent, moderate gravity petroleum inclusions are identified at 9340 ft and 10060 ft. Rock types consist of sandstone and shale. Shale contains moderate gas-prone kerogen and rare live (fluorescent) petroleum stain.

Proximal Pay Indications: None documented.

Potential Seals: Possible seals are identified at 8450 ft, 8830 ft, 9190 ft, 9520 ft, 9760 ft, 10030 ft, 10360 ft, 10630 ft, 11290 ft and 11590ft.

Evidence for Bacterial or Thermal Alteration: Minor concentrations of sulfur species of probable thermal origin are noted at 9880 ft, 10630 ft, 10750 ft and 11350 ft. These compounds suggest thermochemical sulfate reduction at temperatures in excess of 140°C.

Other: Nothing of note.

5.4.4 Stud Horse Butte 3-28: API #49-035-21716

Formation tops reported in this well are Fort Union at 4100, Lance at 8410, Jonah at 10100 feet, Yellow Point at 10460, Wardell at 10725 feet and Mesaverde at 11200.

Petroleum Indications Type and Quality: FIS data display extensive dry gas anomalies throughout the well, with exceptions at 10980-11280 ft (dry gas to wet gas) and below 11280 ft (wet gas to gas-condensate). The most significant responses occur within this deepest Interval. Thin zones of wet gas are recorded sporadically above 8610 ft as well.

Thin sections were prepared from five depths (see Table: II). Rare, white/blue-fluorescent_ Upper-moderate gravity petroleum inclusions are identified at 9720 ft, 10500 ft and 11433 ft in fractured detrital quartz grains. No visible petroleum inclusions are observed at 7680 ft and 8610 ft. Rock types consist of sandstone, shale and minor carbonate. Shale contains moderate amounts of gas-prone kerogen throughout and moderate live stain is identified in several samples.

Proximal Pay Indications: Anomalous concentrations of acetic acid (with or without Benzene) are identified above 7890 ft. In general, samples containing acetic acid anomalies suggest the nearby presence of reservoired liquid petroleum (oil or condensate).

Potential Seals: Possible seals are identified at 7680 ft, 8280 ft, 8700 ft, 9690 ft, 10980 ft and 11160 ft.

Evidence for Bacterial or Thermal Alteration: Nothing documented.

Other: Nothing of note.

5.4.5 SAG Unit 5-17; API # 49-035-23319

Formation tops reported in this well are Yellow Point (11800 feet), Wardell (12496 feet), Mesaverde (13150 feet), Ericson (14390 feet).

Petroleum Indications Type and Quality: The dominant response throughout the analyzed section is dry gas to wet gas. Several zones of stronger hydrocarbon responses are noted, as follows.

FIS data from the intervals 8330 ft, 8600-8690 ft, 8870-9170 ft and 9500 ft consist of wet gas to gas condensate responses. Thin sections from 8330 ft and 9500 ft consist of sandstone with rare to several occurrences of yellow and white fluorescent, moderate and upper moderate gravity liquid petroleum inclusions in fractured detrital quartz grains.

The intervals at 11510 ft, 13340-13370 ft, 14120 ft and 14300-14520 ft consist of wet gas to gas condensate responses. Thin sections from 11510 ft, 11718 ft, 12030 ft and 13340 ft consist predominantly of sandstones and shales with rare, white and blue fluorescent, moderate to upper-moderate gravity liquid petroleum inclusions in fractured detrital quartz grains. Thin sections from 12030 ft, 14120 ft and 14480 ft are dominated by lost circulation material. Shale and/or coal hosted gas prone kerogen is observed throughout. Some coal may represent a mud additive.

Proximal Pay Indications: Anomalous concentrations of acetic acid (with or without Benzene) are identified at 12240 ft, 12440 ft and 14513-14520 ft. In general, samples containing acetic acid anomalies suggest the nearby presence of reservoired liquid petroleum (oil or condensate).

Potential Seals: Possible seals are identified at 8200 ft, 9500 ft, 10100 ft, 11400 ft, 13300 ft and 14350 ft.

Evidence for Bacterial or Thermal Alteration: Sulfur species of probable thermal origin are noted intermittently at 8210-9500 ft. These compounds generally indicate thermo-chemical sulfate reduction at temperatures above 140°C.

Other: Nothing noted.

5.4.6 Jonah Federal 4-8; API # 49-035-21322

No formation tops are provided in the WOGC records. The nearby Jonah Federal 37-8 well provided the following formation tops: top of Unnamed at 7742 ft, top of Lance at 8414, top of Jonah at 9814 ft, top of Yellowpoint at 10064 ft, top of Wardell at 10404 ft.

Petroleum Indications Type and Quality: Anomalous concentrations of hydrocarbons are identified throughout the wellbore, with spectra generally dominated by dry gas to wet gas. The shallower sections of the well are generally richer in heavier hydrocarbons with the intervals 7030 ft to 8570 ft characterized by wet gas to oil responses with the richest gas condensate to oil intervals noted at 7330-7570 ft, 7780-7880 ft, 7990-8060 ft and 8160-8220 ft. Spectra are somewhat methane depleted, which can indicate the presence of source rock. This is confirmed petrographically, as the section contains coal (possibly an additive). A thin section from 7180 ft consists of mixed carbonate, sandstone, coal and shale with rare occurrences of yellow fluorescent, moderate gravity liquid petroleum inclusions in sandstone.
A thin section from 8170ft consists of coal, shale and sandstone with rare, blue fluorescent, upper moderate gravity inclusions in sandstone. Other thin sections from 7480 ft, 7810 ft and 8040 ft contain no visible liquid petroleum inclusions. Coal may represent a mud additive.

FIS data from the interval below 8550 ft record higher methane response, and indicate dry gas with occasional wet gas spectra. Thin sections from this interval (8760 ft, 9240 ft, 9550 and 10090 ft) consist of carbonate rich shales and minor sands with no visible liquid petroleum inclusions.

Proximal Pay Indications: None identified.

Potential Seals: Possible seals are identified at 7300 ft, 7780 ft, 8020 ft, 8180 ft, 8550 ft, 9200 ft, 9400 ft, 9500 ft and 9900 ft.

Evidence for Bacterial or Thermal Alteration: Sulfur species of possible thermal origin are identified at 7930 ft, 8250 ft, 8480 ft, 8620 ft and 9720 ft. In this case, thermochemical sulfate reduction at temperatures in excess of 140°C is suggested.

Other: Nothing noted.

5.5 Interpretation

5.5.1 Variability in production and mud gas composition

Much of Jonah Field produces gas that ranges in wetness between 0.10 and 0.20 (Figure 5.5). Wells near the western boundary fault of the Jonah structure exhibit more variability: two wells, the Corona 79-19 and SHB 53-20, produced gas that is nearly pure methane, and one well, the SHB 53-17, produced the wettest gas from within the Jonah structure. Two wells in relatively down-dip positions, the SHB 7-22 and Cabrito 7-25, produced gas that was slightly wetter than the majority of gases from within the Jonah structure.

Four wells from normally pressured Lance reservoirs outside the main Jonah structure were also sampled; three of these produced gases wetter than almost all of the samples of overpressured reservoirs within the Jonah structure.

C_2/C_3 ratios, also measure of gas wetness, display a similar pattern. A core area of the field has ratios between 1.8 and 2.2 (Figure 5.6). Production wells near the western boundary fault display a wide range of values, from very wet compositions with ratios less than 1.5 to dry compositions with ratios between 2.2 and 4.4.

The CO_2 content of gases is another significant measure of gas composition. The CO_2 content of Jonah gases is typically low (Figure 5.7), with almost all wells producing gas with a mole fraction of less than 0.02. Two wells along the western boundary fault produce gases relatively enriched in CO_2. The Corona 79-19 and SHB 53-17 produced gas with 0.07 and 0.05 mole fraction of CO_2.

While data from individual wells indicates that gases become systematically drier with length of time of production (Dean Dubois, personal communication, November 2014), this effect is not evident in our data set (Figure 5.41). Production gas compositions do suggest a small effect of production time on the carbon isotopic composition of ethane and propane (Figure 5.42), which on average become 2 to 3‰ heavier with increasing time since production started. There is no parallel effect on δD compositions.

Neither gas wetness nor the carbon isotopic compositions of gases are related to maximum production rates of gas or condensate in wells or to the volume of water produced.

This work demonstrates that there is substantial variation in mud gas composition. In general, gas compositions become wetter with depth, but there is substantial stratigraphic variability to bulk gas compositions.

Vertical variability in mud gas composition suggests that differences in the composition of production gases could reflect differing production rates from different parts of the stratigraphic section. In other words, relatively dry gases in most of the field could result from the bulk of production from the middle Lance section, whereas the relatively wet gas compositions produced near the western boundary fault could result from greater production from deeper in the section.

5.5.2 Thermal maturity of source rocks

The carbon isotopic composition of gases (C_1, C_2 and C_3) can be used to infer the thermal maturity of the gas sources at the time of generation (Figures 5.43).

The thermal maturities estimated from the carbon isotopic composition of production gas suggest a range of maturities at which gas was generated, from a vitrinite reflectance of 1.5 to 2.5%. Because the data form a nearly linear trend of $\delta^{13}C_{C2}$ versus $\delta^{13}C_{C3}$, the isotopic composition of either C_2 or C_3 can be used as a proxy for thermal maturity, where the more positive (heavier) compositions indicate higher thermal maturity. The map of $\delta^{13}C_{C2}$ (Figure 5.9) shows no clear spatial pattern, with gases of relatively negative compositions occurring near gases of relatively positive composition.

Maturities estimated from the carbon isotopic composition of mud gas samples (Figure 5.44) define a similar trend and can also be interpreted to indicate thermal maturities. The range of maturities predicted is greater, from 1.2% R_o to as much as 2.5% R_o.

5.5.3 Controls on gas composition: hydrocarbon source and/or secondary alteration

We first summarize some key observations about gas compositions at Jonah Field:

1) Production gases exhibit a significant range in $\delta^{13}C_{C1}$, from -42.4 to -27.7‰. Compositions as positive as -27.7‰ are uncommon in natural gas and suggest that an unusual process has produced this methane. Moreover, the $\delta^{13}C_{C1}$ show no clear relationship to $\delta^{13}C_{C2}$, suggesting that the processes controlling ethane composition were not the same as those controlling methane composition.

2) Every production gas sample in which $\delta^{13}C_{CO2}$ was measured had compositions less than -4‰. The isotopically heaviest CO_2 was -8.1‰, while the isotopically lightest carbon was -17.2‰. A group of wells adjacent to the western boundary fault had systematically lighter carbon than other wells in the field, ranging from -14.2 to -17.2‰.

3) Compositions are particularly methane-rich in the shallow part of the section and become wetter with depth.

4) Methane and ethane are isotopically heavy in the shallow part of the section and become isotopically lighter with increasing depth.

There are two viable explanations for these patterns in the gas data.

A) Gases were substantially affected by bacterial oxidation (Figure 5.45), particularly in shallow parts of the field where meteoric water is more likely to penetrate. This model explains two observations about the mud gas data: Bacterial oxidation particularly affects the wetter gases, leaving a residual gas that is enriched in methane (Kinnaman et al., 2007). It also more strongly fractionates the lighter gases, leaving a residual gas that is enriched in ^{13}C, in other words isotopically heavy (Kinnaman et al., 2007). While bacterial oxidation was once thought to be a low temperature phenomenon, it has now been demonstrated in gas reservoirs at depths to 2350 meters (Katz et al., 2002), and methanotrophic bacteria have been shown to live at depths of 3.3 km in South African gold mines (Trimarco et al., 2006).

   One product of bacterial oxidation of gas is isotopically negative (light) carbon in CO_2. CO_2 generated through the decomposition of carbonate minerals will inherit the isotopic signature of the carbonate. Because most carbonate formed as depositional carbonate in equilibrium with sea water, most CO_2 generated from carbonate minerals has a $\delta^{13}C_{CO2}$ between 0 and -4‰. The isotopically light carbon characterizing the CO_2 at Jonah Field is not consistent with the breakdown of carbonate minerals but instead indicates an organic source, including derivation from hydrocarbons through bacterial oxidation.

   This distribution of $\delta^{13}C_{CO2}$ in production gas samples suggests that bacterial oxidation of gas was a pervasive phenomenon at Jonah Field and that it was particularly strongly felt near the northwestern margin of the field.

B) An alternative explanation is that shallower gases are sourced from coaly source rocks and deeper gases from marine source rocks (Figure 5.46). Typically coaly source rocks generate gases that are isotopically more positive (heavier) and more methane-rich than marine source rocks. Coskey (2004) noted that the Upper and Lower Mesaverde units contain sufficient Type III organic matter to be considered potential source rocks and that the deeper Hilliard and Mowry Shales are also potential source rocks.

   Coalbed gas can generate considerable CO_2, and that CO_2 can have a large range of isotopic compositions, from $\delta^{13}C$ as light as -27‰ to as heavy as +18‰ (Rice, 1993). In an experimental hydrous pyrolysis study of source rocks in the Rocky Mountains,

Ko (2010) found that the Cameo Coal (Piceance Basin) yielded isotopically much lighter CO_2 than either the Mowry or Baxter (Hilliard) Shales. The Cameo, which can serve as an analog for coaly intervals in the Mesaverde, yielded gases ranging from $\delta^{13}C$ values of CO_2 of 26.28‰ to -24.95‰. The Mowry and Baxter Shales yield CO2 in the range of -7.25 ‰ to -5.97 ‰ and -1.65 ‰ to 1.62, respectively.

The noble gas data (Figure 5.28) provide qualified support for the bacterial oxidation model. The noble gas data indicate a strong level of meteoric water interaction in all of the Jonah production wells, to a larger extent and more consistently than in the other two areas (Piceance Basin and Greater Natural Buttes) sampled for this project. Influx of meteoric water into upper levels of the Jonah gas column would provide bacteria and oxygen for the oxidation reactions. However, while gases have both low ratios of $1/^{22}Ne$ and light $\delta^{13}C_{CO2}$ in the field, there is no correlation between these two parameters in the Jonah data set. In other words, the samples with the lightest $^{13}C_{CO2}$ do not have the lowest $1/^{22}Ne$ ratios.

A third model should be mentioned, although we think this does not provide a satisfactory explanation for Jonah Field. It would require that shallow gases were generated by relatively high maturity source rocks while deeper gases were generated by lower maturity source rocks. The high maturity gases would have to have bypassed the low maturity gases during vertical migration. Presumably this would happen by high maturity gases migrating vertically through faults, then laterally into shallow reservoir sandstones. However this model requires a peculiar migration system and does not explain the anomalously negative (light) $\delta^{13}C_{CO2}$ values measured in production gases; we do not favor this model.

5.5.4 Evidence of Secondary Cracking

The production gas data do not provide evidence of secondary cracking as a source of gas (Figure 5.24). Gas compositions have relatively low C_2/C_3 ratios, indicating the relative abundance of wetter gases, and relatively small differences between $\delta^{13}C_{C2}$ and $\delta^{13}C_{C3}$. Following Lorant et al (1995), production gases were dominantly produced by primary cracking from kerogen.

Many of mud gas data clearly show evidence of secondary cracking (Figure 5.29). Whereas the production gases had only one sample (3% of the samples) with C_2/C_3 in excess of 2.25, 43% of the mud gas samples had C_2/C_3 in excess of 2.25, and an additional 10% of the samples had no measureable C_3, making it impossible to calculate this ratio. In the production gas samples only

two samples (6%) had ($\delta^{13}C_{C2}$ - $\delta^{13}C_{C3}$) less than -2‰, whereas in the mud gas samples 38% of the samples had ($\delta^{13}C_{C2}$ - $\delta^{13}C_{C3}$) less than -2‰.

The fact that the production gas samples contained a much smaller proportion of samples with a signature of secondary cracking suggests that either:

- the intervals sampled in the mud gas data set with a composition reflecting secondary cracking contributed very little to the overall production of the well, or

- production from intervals with secondary cracking depleted quickly, with the longer term flow from intervals primarily sourced by primary cracking of kerogen.

These two models imply very different reservoir permeability for the two types of producing intervals. If the former model is correct, periodic sampling of production gases should yield relatively similar compositions. Small contributions of the secondary-cracked gas would presumably come from lower relative permeability intervals. Because these intervals flow gas at lower rates, production would dominantly come from the higher permeability intervals charged with primary-cracked gas.

If the latter model is correct, the intervals producing primarily secondary-cracked gas had higher permeability that the rest of the section. This model suggests that if we periodically sampled a well after production, we should see gas composition changing from high to low C_2/C_3 and from large negative differences in ($\delta^{13}C_{C2}$ - $\delta^{13}C_{C3}$) to small differences.

The second model appears to be more likely and could be explained by late gas derived from secondary cracking preferentially migrating into the highest permeability parts of the reservoir section.

5.5.5 Migration Pathways

The fluid inclusion data suggest that migration through the Jonah system was not uniform. Two wells near the crest of the Jonah structure at the intersection of the western and southern boundary faults, the Yellowpoint 5-13 well within the Jonah structure and the Jonah Federal 4-8 well just south of the southern boundary fault, contain strong indications of condensate or oil in shallow parts of the section. The JF 4-8 well had indications of condensate and oil in the Fort Union and Unnamed units and dry gas with occasional wet gas indications in the Lance and below. The YP-5-13 well had gas condensate to oil indications within the Fort Union, wet gas top gas-condensate within the Unnamed and only dry gas and wet gas in deeper intervals.

The downdip SAG 5-17 well also had multiple indications of wet gas to gas-condensate responses in the fluid inclusion data in shallow parts of the section (probably Unnamed and/or Lance, but these formation tops are not reported in this well). This well is located immediately adjacent to one of the major faults bisected the Jonah structure.

The other three wells for which we developed fluid inclusion data had indications of condensate and oil deep in the section, if at all. The Stud Horse Butte 14-17 showed wet gas responses only below the top of the Yellow Point and no indications of condensate or oil. The Stud Horse Butte 10-26 had wet gas throughout and no indications of condensate or oil. The Stud Horse Butte 3-28 had dry gas indications throughout, wet gas within the Wardell and wet gas to gas-condensate only within the Mesaverde.

These data indicate that some faults were major pathways for liquid hydrocarbon migration. These are represented by data from the YP 5-13, JF 4-8 and SAG 5-17. The other wells, however, were also located near faults and do not have indications of shallow liquid hydrocarbons, suggesting that the simple presence of faults is not sufficient to assure migration of hydrocarbons from deep sources. Some faults are conduits, while others are not; and it is likely that the same fault will be open and sealing in different sections.

5.5.6 Compartmentalization within the Gas Column

Every well for which we have developed detailed mud gas profiles exhibits stratigraphic intervals where compositions change abruptly and reversals, particularly with regard to gas wetness and C_2/C_3 ratios (Figures 5.31 and 5.32). These changes occur in every stratigraphic unit: the Lance, Jonah, Yellowpoint, Wardell and Mesaverde. One trend that appears to be consistent in all wells with detailed data sets is a sharp increase in the C_2/C_3 ratio (gas becomes drier) at approximately 1100 feet above the top of the Mesaverde. Depending on which well is considered, this may be within the Middle Lance, Jonah or Yellowpoint sections. Isotopic changes in gases vary more smoothly and show features that may be correlatable between wells, for example, the profile of $\delta^{13}C_{C2}$ in the SHB 113-10 and the SHB 60-22 wells.

We infer a number of characteristics about the reservoir and migration pathways based on these observations:

- There are a number of intermediate seals within the reservoir section that effectively serve to compartmentalize the reservoir. Without such intermediate seals, gas compositions would vary more gradationally.

- The multiple reversals in gas composition cannot be modeled solely as the product of processes operating vertically, with migration from below, possibly modified by oxidation from above. The combination of one or two processes working vertically should either produce unidirectional trends (properties changing in one direction – for example gases becoming drier upward) or single reversals (for example gases becoming drier, then wetter upward).

- The multiple reversals with sharp boundaries imply that lateral migration along preferential pathways must be significant in the Jonah reservoir. The migration could be migration of hydrocarbons from deeper source rocks OR meteoric water migrating downward and then laterally along fluid pathways.

With the exception of one set of wells in the southern part of Jonah Field (Figure 5.37), gas compositions are dissimilar at the same depth or stratigraphic level. The similar compositions in this one particular group of wells suggests a common migration system, possibly through the major south bounding fault of the Jonah structure and the central north-trending fault that splays off from it. Otherwise, migration routes and seals apparently varied on a small scale within the field.

5.6 References

Bernard, B., Brooks, J.M., & Sackett, W.M. (1977). A geochemical model for characterization of hydrocarbon gas sources. Ninth Annual Offshore Technology Conference, OTC 2934, p. 435-438.

Chung, H.M., Gormly, J.R., & Squires, R.M. (1988). Origin of gaseous hydrocarbons in subsurface environments. Theoretical considerations of carbon isotope distribution, in M. Schoell (Guest Editor), Origins of Methane in the Earth: Chemical Geology, v. 71, p. 97-103.

Katz, B.J., Narimanov, A., & Huseinzadeh, R. (2002). Significance of microbial processes in gases of the South Caspian basin. Marine and Petroleum Geology, v. 19, p. 783-796.

Kinnaman, F.S., Valentine, D.L., & Tyler, S.C. (2007). Carbon and hydrogen isotope fractionation associated with the aerobic microbial oxidation of methane, ethane, propane and butane. Geochimica et Cosmochimica Acta, v. 71, p. 271-283.

Kotelnikova, S. (2002). Microbial production and oxidation of methane in

deep subsurface. Earth-Science Reviews, v. 58, p. 367–395.

Lorant, F., Prinzhofer, A., Behar, F., & A. Y. Huc (1998). Carbon isotopic and molecular constraints on the formation and the expulsion of thermogenic hydrocarbon gases: Chemical Geology, v. 147, p. 249–264.

Trimarco, E., Balkwill, D., Davidson, M., & Onstott, T. C. (2006). In Situ Enrichment of a Diverse Community of Bacteria from a 4–5 km Deep Fault Zone in South Africa. Geomicrobiology Journal, v. 23, p. 463–473.

Rice, D.D. (1993). Composition and Origins of Coalbed Gas. In eds., Ben E. Law and D.D. Rice, AAPG Studies in Geology #38, p. 159-184.

Schoell, M. (1983). Genetic characterization of natural gases: AAPG Bulletin, v. 67, p. 2225-2238.

Tang, Y., Perry, J. K., Jenden, P. D., & Schoell, M. (2000). Mathematical modeling of stable carbon isotope ratios in natural gases. *Geochimica et Cosmochimica Acta*, *64*(15), 2673-2687.

Table 5.1. Summary of compositions of Jonah production gases.

	minimum	average	maximum
C1 (fraction)	0.59	0.82	0.94
C2 (fraction)	0.00	0.09	0.14
C3 (fraction)	0.01	0.05	0.10
i-C4 (fraction)	0.01	0.02	0.05
n-C4 (fraction)	< 0.01	0.02	0.06
i-C5 (fraction)	<0.01	0.01	0.03
n-C5	< 0.01	0.02	0.08
CO_2 (fraction)	< 0.01	0.02	0.07
Wetness	0.00	0.17	0.38
$\delta^{13}C_{C1}$ (‰)	-44.0	-36.76	-27.7
$\delta^{13}C_{C2}$ (‰)	-29.8	-26.37	-24.2
$\delta^{13}C_{C3}$ (‰)	-27.8	-25.20	-22.6
$\delta^{13}C_{i\text{-}C4}$ (‰)	-27.0	-24.37	-21.2
$\delta^{13}C_{n\text{-}C4}$ (‰)	-26.5	-24.52	-22.0
$\delta^{13}C_{i\text{-}C5}$ (‰)	-25.5	-24.07	-20.5
$\delta^{13}C_{n\text{-}C5}$ (‰)	-26.2	-23.93	-20.4
$\delta^{13}C_{CO2}$ (‰)	-17.2	-11.41	-7.1
δD_{C1} (‰)	-190	-178.73	-172
δD_{C2} (‰)	-162.5	-156.01	-149
δD_{C3} (‰)	-199	-159.09	-135
$\delta D_{i\text{-}C4}$ (‰)	-152.5	-142.85	-120
$\delta D_{n\text{-}C4}$ (‰)	-160.5	-151.63	-135
$\delta D_{i\text{-}C5}$ (‰)	-138	-127.88	-105.6
$\delta D_{n\text{-}C5}$ (‰)	-154	-145.08	-124.5

Table 5.2. Average Compositions of Jonah Field Mud Gas Samples

	Minimum	Average	Maximum
C1 (fraction)	0.58	0.84	1.00
C2 (fraction)	0.00	0.08	0.17
C3 (fraction)	0.00	0.04	0.14
i-C4 (fraction)	0.00	0.014	0.061
n-C4 (fraction)	0.00	0.00013	0.054
i-C4 (fraction)	0.00	0.008	0.040
n-C4 (fraction	0.00	0.006	0.049
CO_2 (fraction) *	0.002	0.033	0.15
Wetness	0.00	0.15	0.42
$\delta^{13}C_{C1}$ (‰)	-52.4	-39.06	-4.4
$\delta^{13}C_{C2}$ (‰)	-30.1	-25.88	-17.3
$\delta^{13}C_{C3}$ (‰)	-28.1	-24.19	-19.8
$\delta^{13}C_{i\text{-}C4}$ (‰)	-27.2	-23.26	-18.9
$\delta^{13}C_{n\text{-}C4}$ (‰)	-26.5	-23.24	-18.0
$\delta^{13}C_{i\text{-}C5}$ (‰)	-28.2	-23.78	-19.2
$\delta^{13}C_{n\text{-}C5}$ (‰)	-26.0	-23.31	-19.2
$\delta^{13}C_{CO2}$ (‰) *	-23.7	-11.46	13.3
δD_{C1} (‰)	-244	-195.4	-147
δD_{C2} (‰)	-226	-168	-82
δD_{C3} (‰)	-215	-187.2	-158
$\delta D_{i\text{-}C4}$ (‰)	-289	-174.2	-149.5
$\delta D_{n\text{-}C4}$ (‰)	-180	-163.2	-144
$\delta D_{i\text{-}C5}$ (‰)	-147	-146	-145
$\delta D_{n\text{-}C5}$ (‰)	-173	-161.7	-156

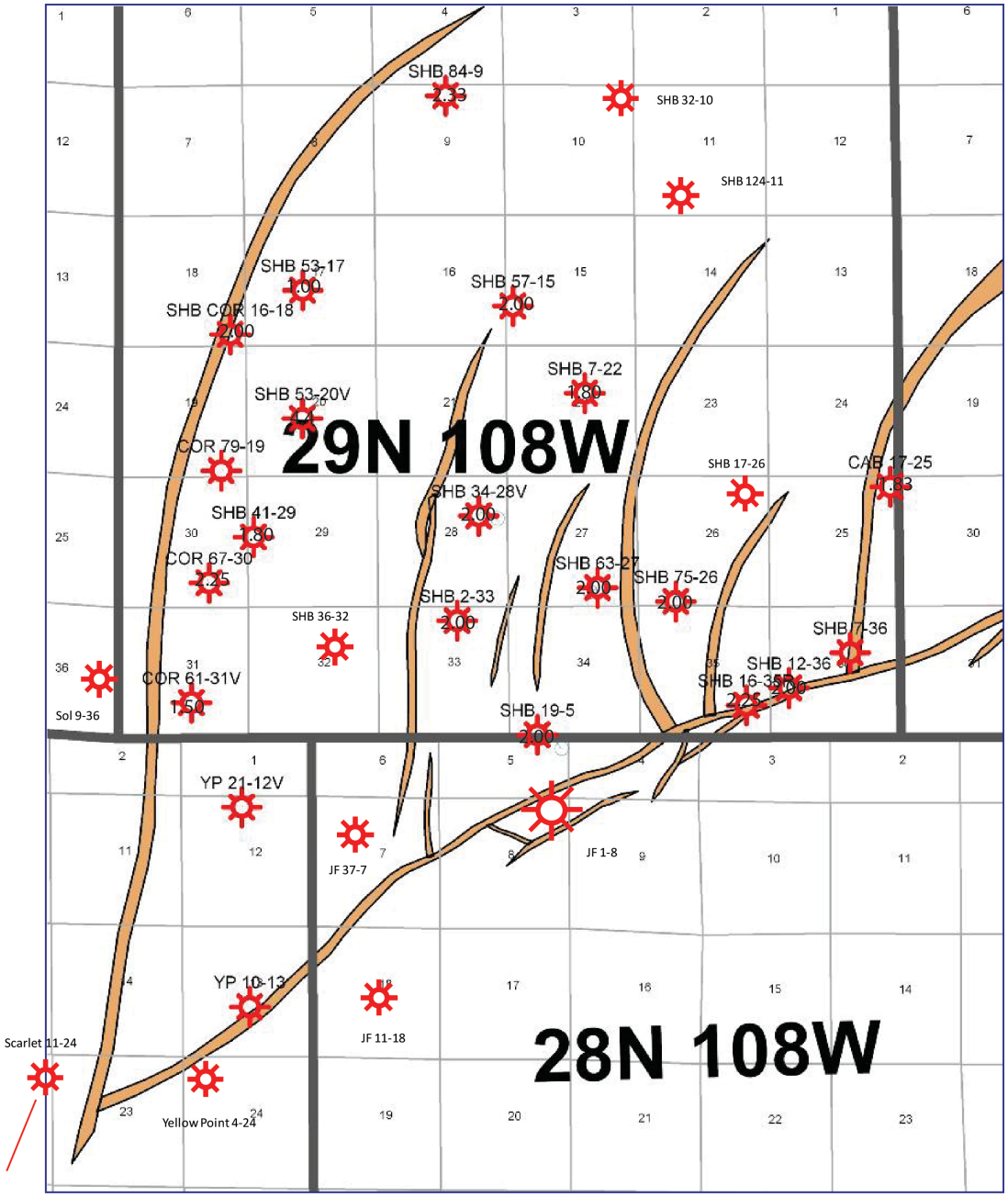

Figure 5.1. Map of the Jonah field, showing the locations of production gas samples.

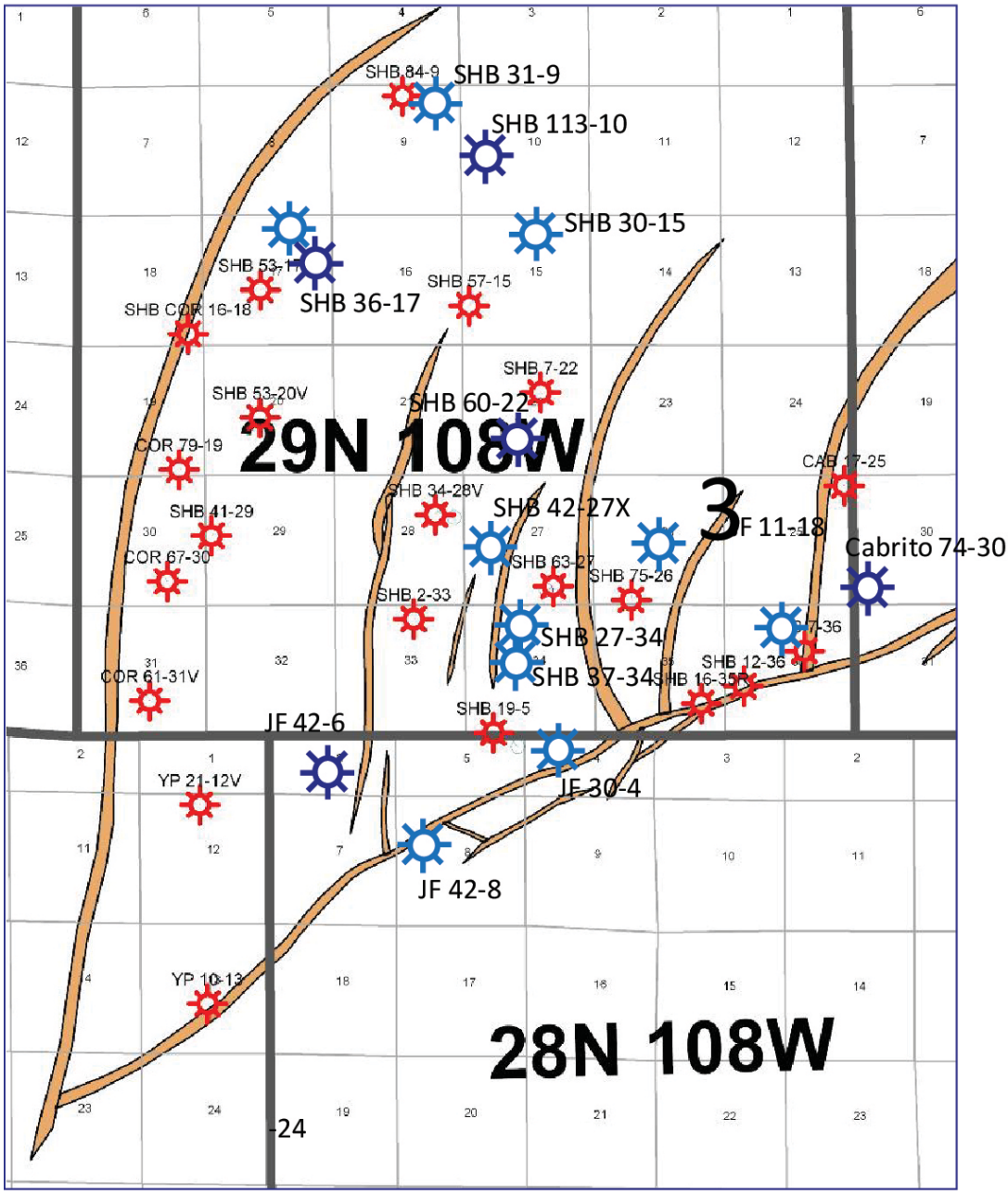

Figure 5.2. Map of Jonah field, showing the locations of mud gas samples (blue symbols).

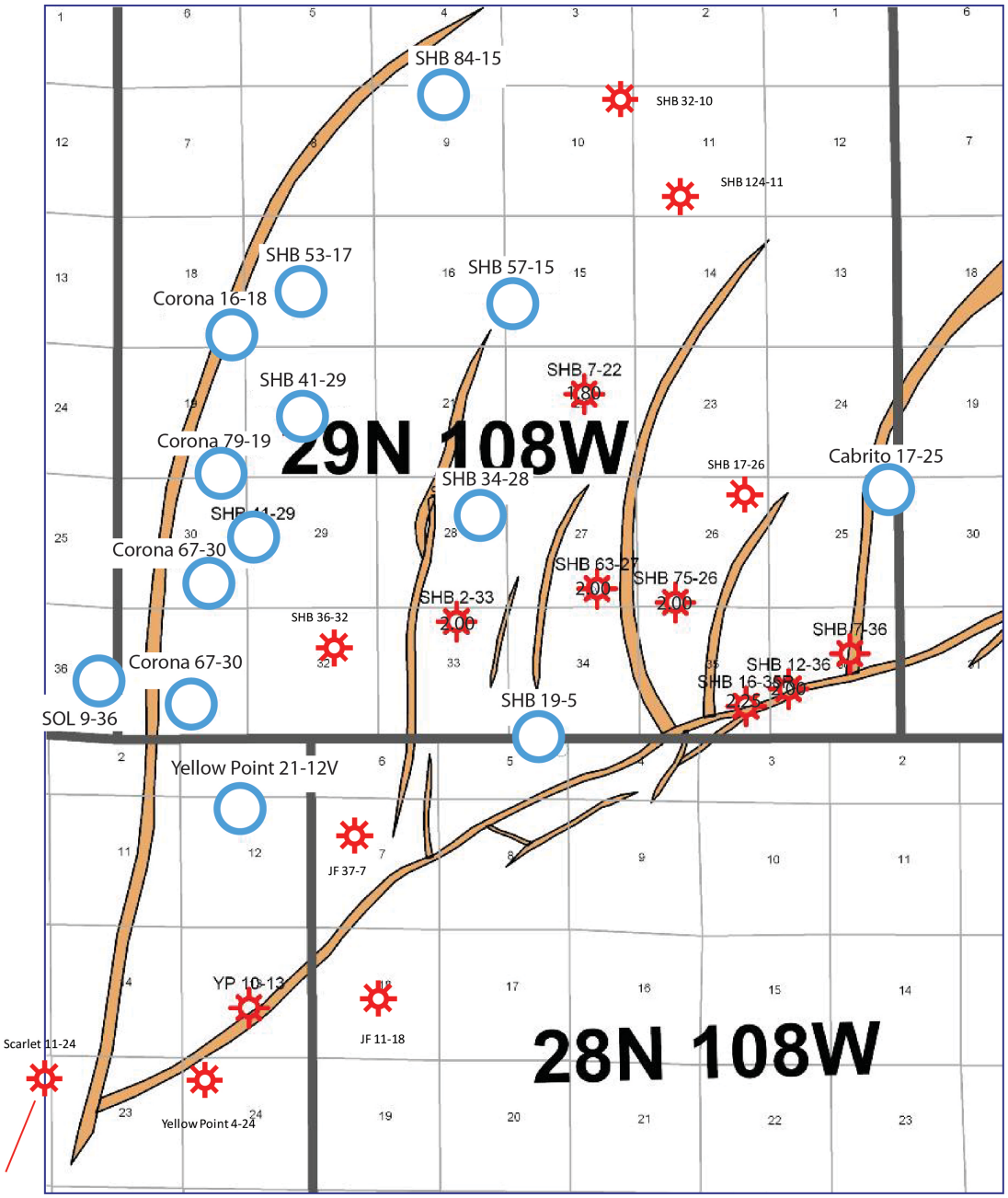

Figure 5.3. Map of Jonah Fields, showing the locations of production gas samples for noble gas analysis (open blue circles).

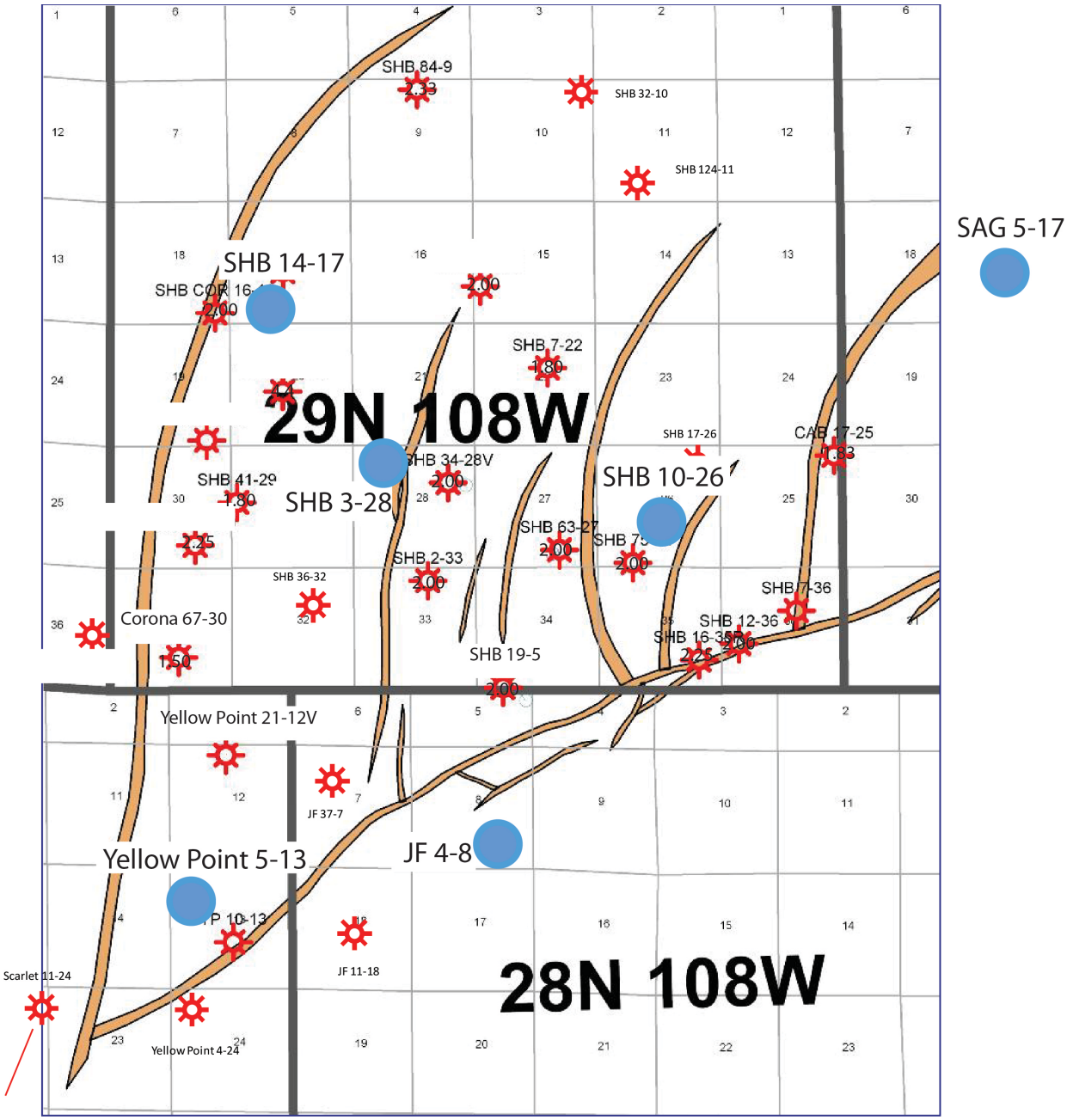

Figure 5.4. Map of Jonah Field, showing the locations of fluid inclusion samples (solid blue circles).

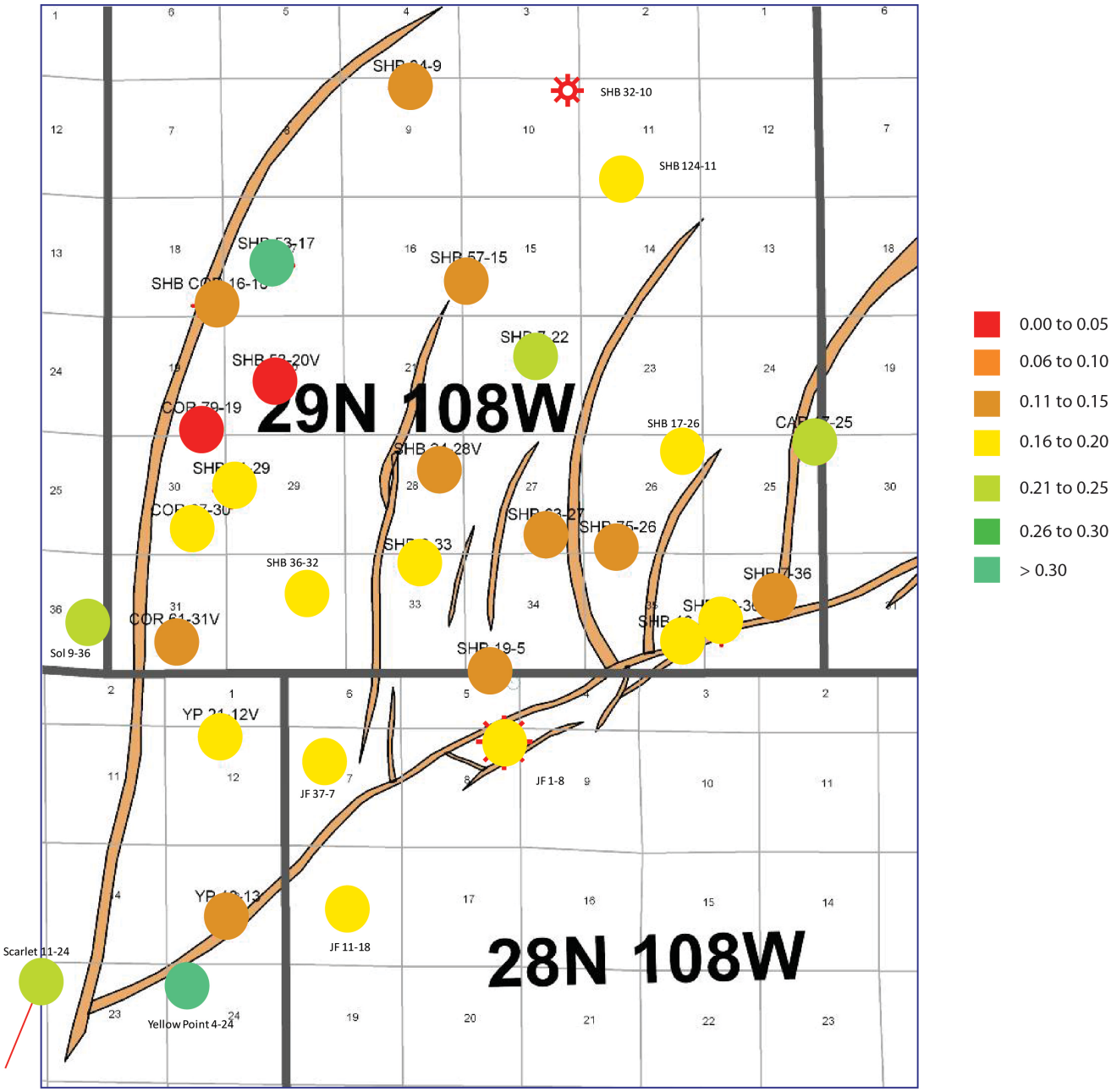

Figure 5.5. Map of gas wetness in Jonah Field.

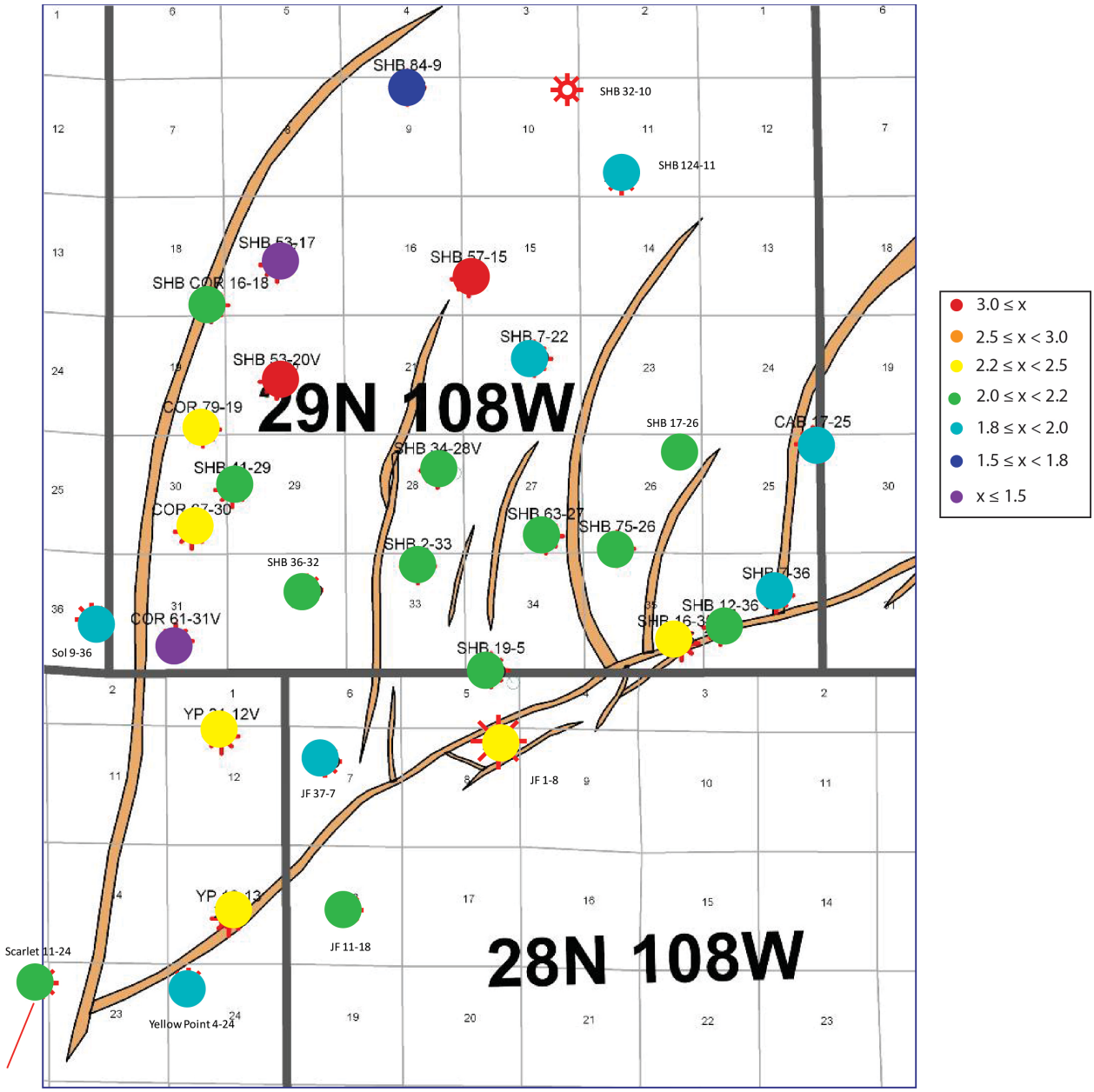

Figure 5.6. C_2/C_3 ratios in production gas samples from Jonah Field.

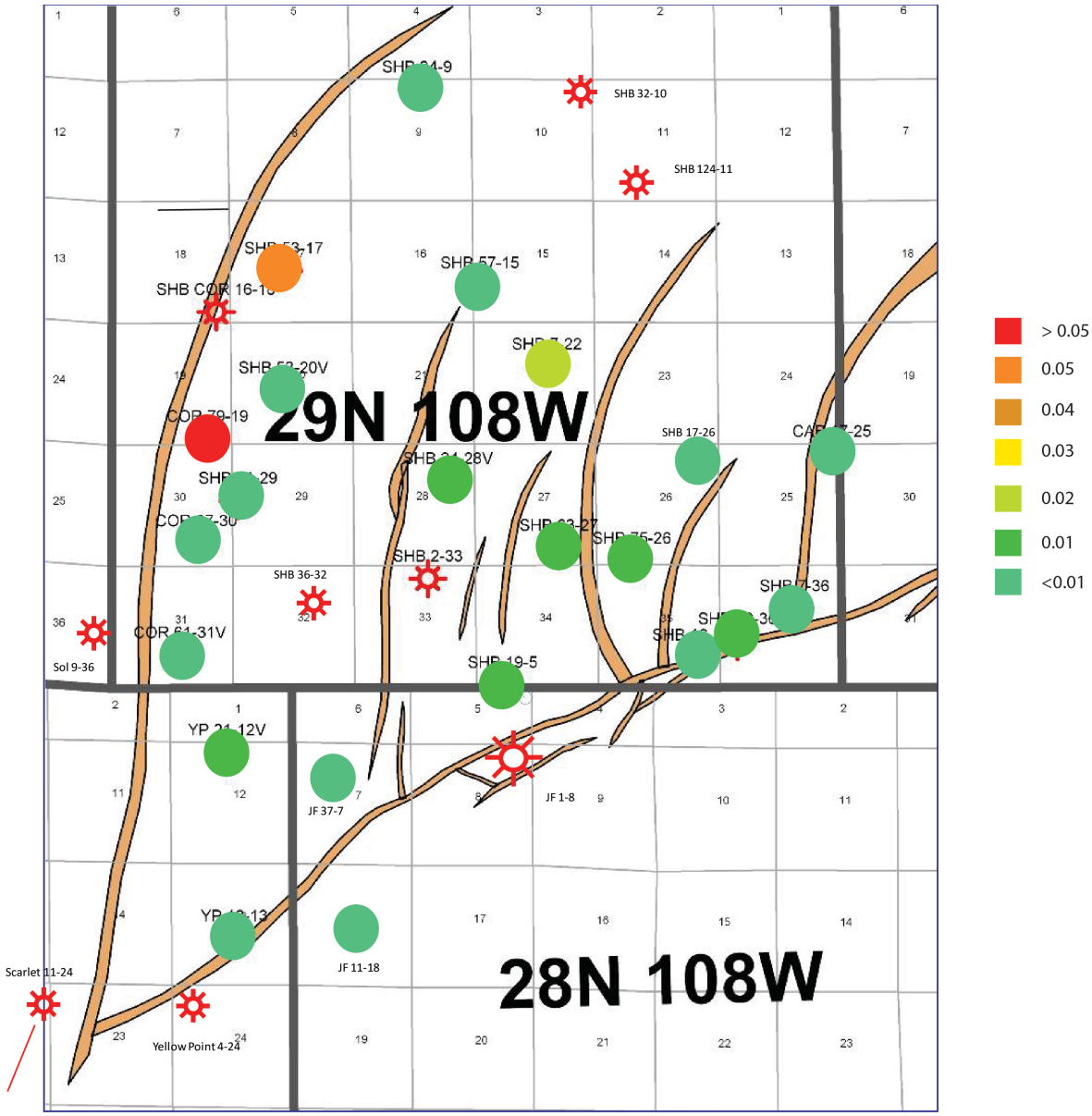

Figure 5.7. Mole fraction CO_2 in production gas samples from Jonah Field.

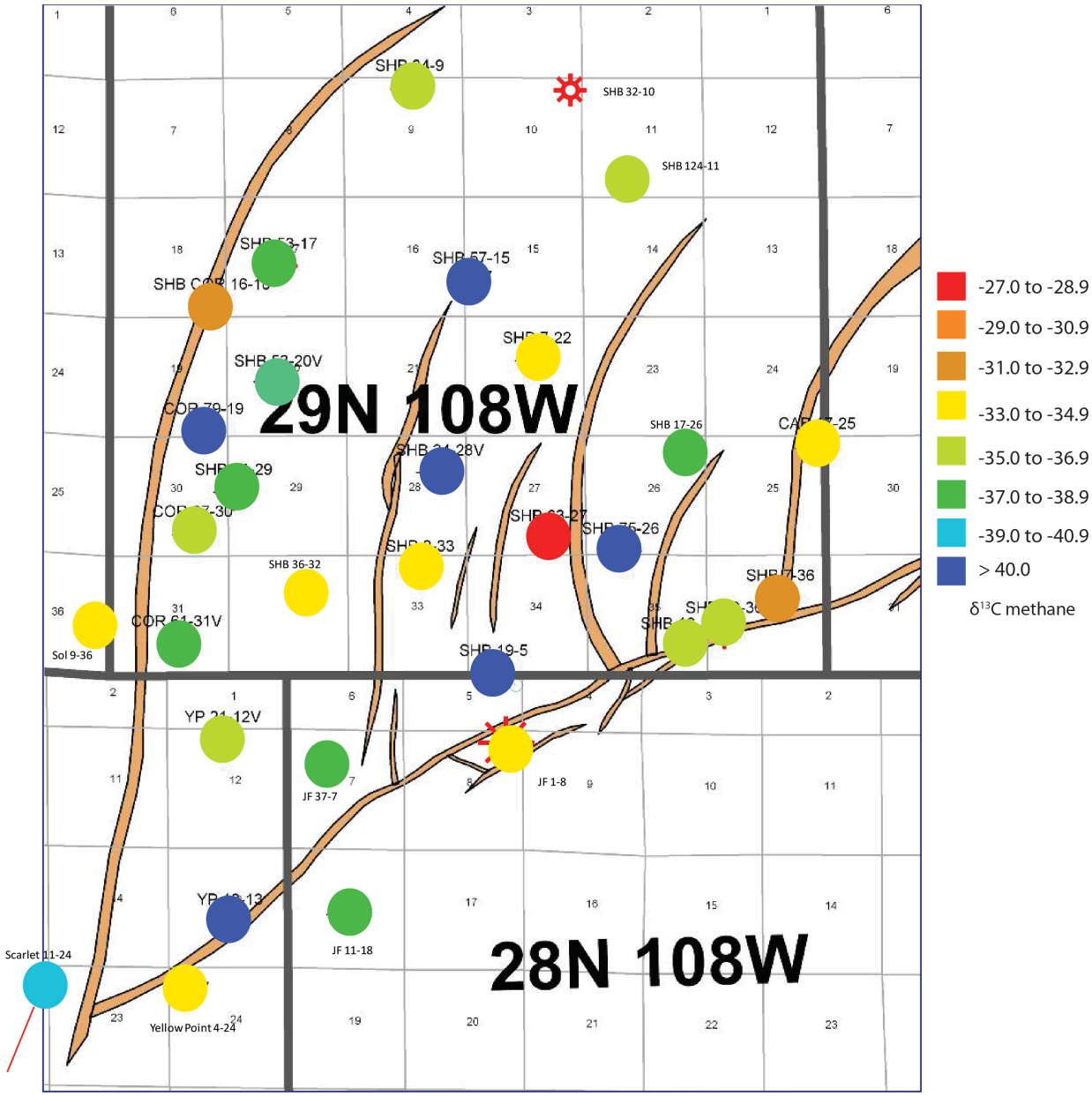

Figure 5.8. Carbon isotopic composition of C_1 ($\delta^{13}C_{C1}$) in production gas samples from Jonah Field.

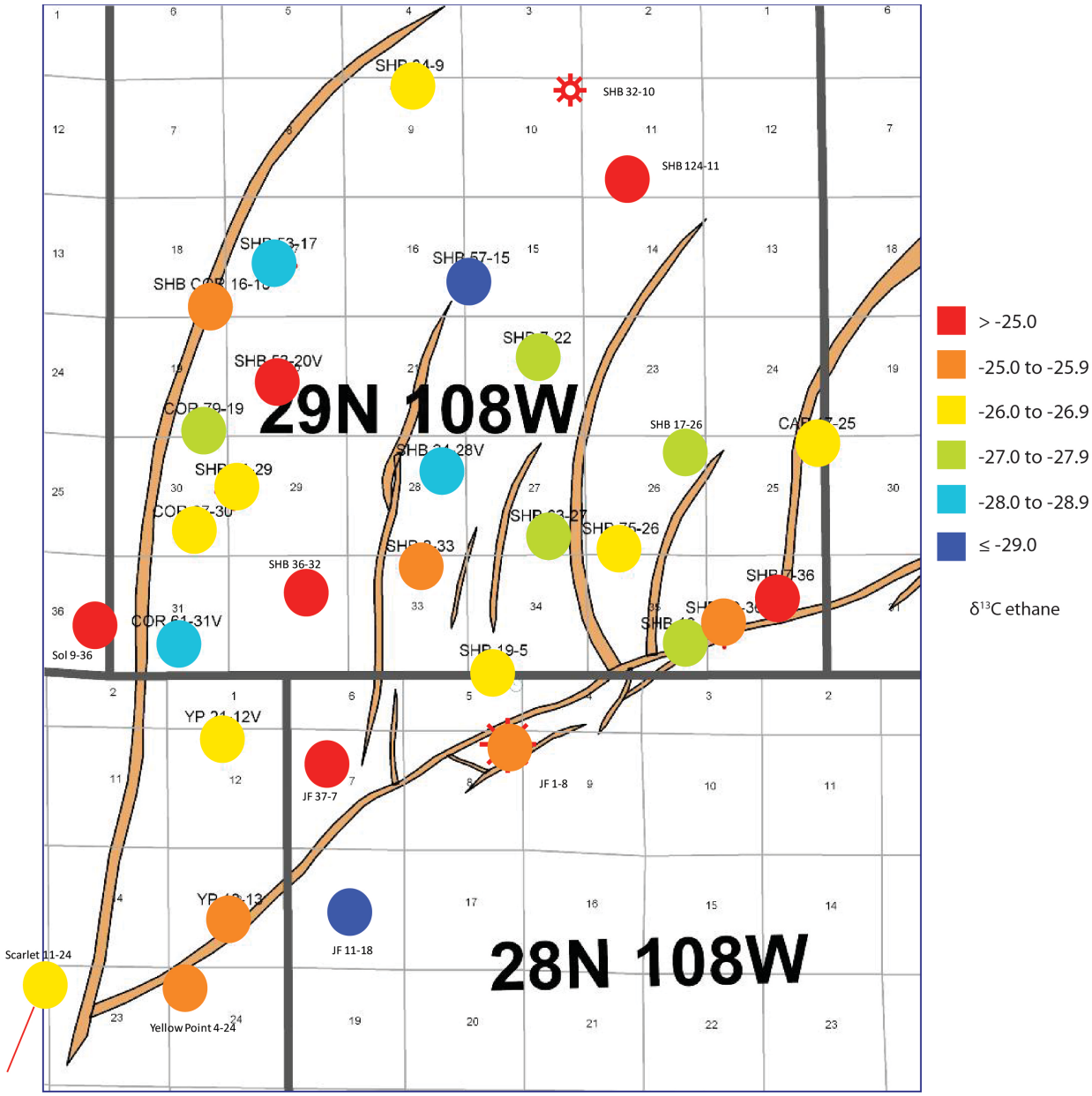

Figure 5.9. Carbon isotopic composition of C_2 ($\delta^{13}C_{C2}$) in production gas samples from Jonah Field.

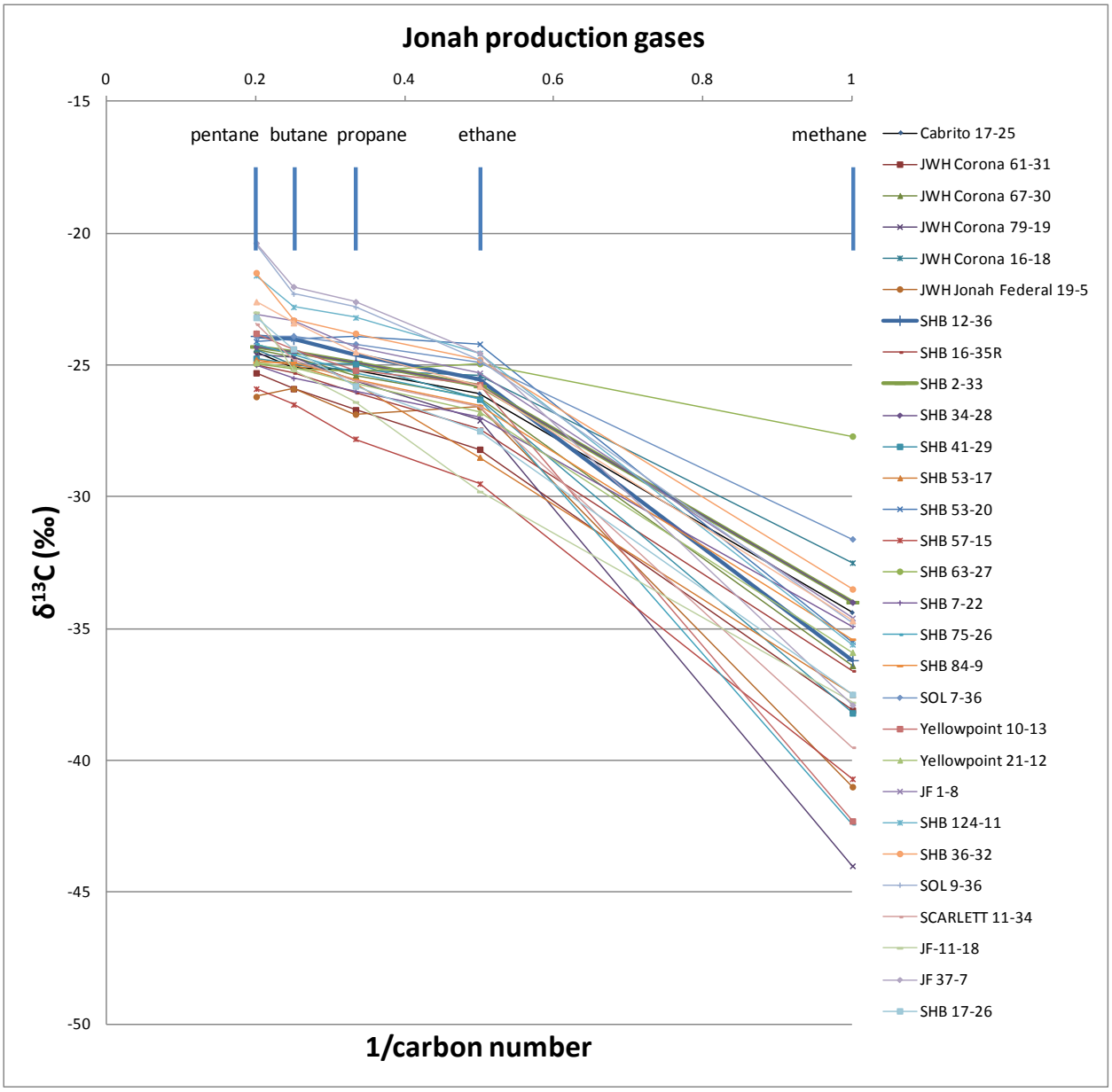

Figure 5.10. Chung plot showing carbon isotopic composition of gases from Jonah Field.

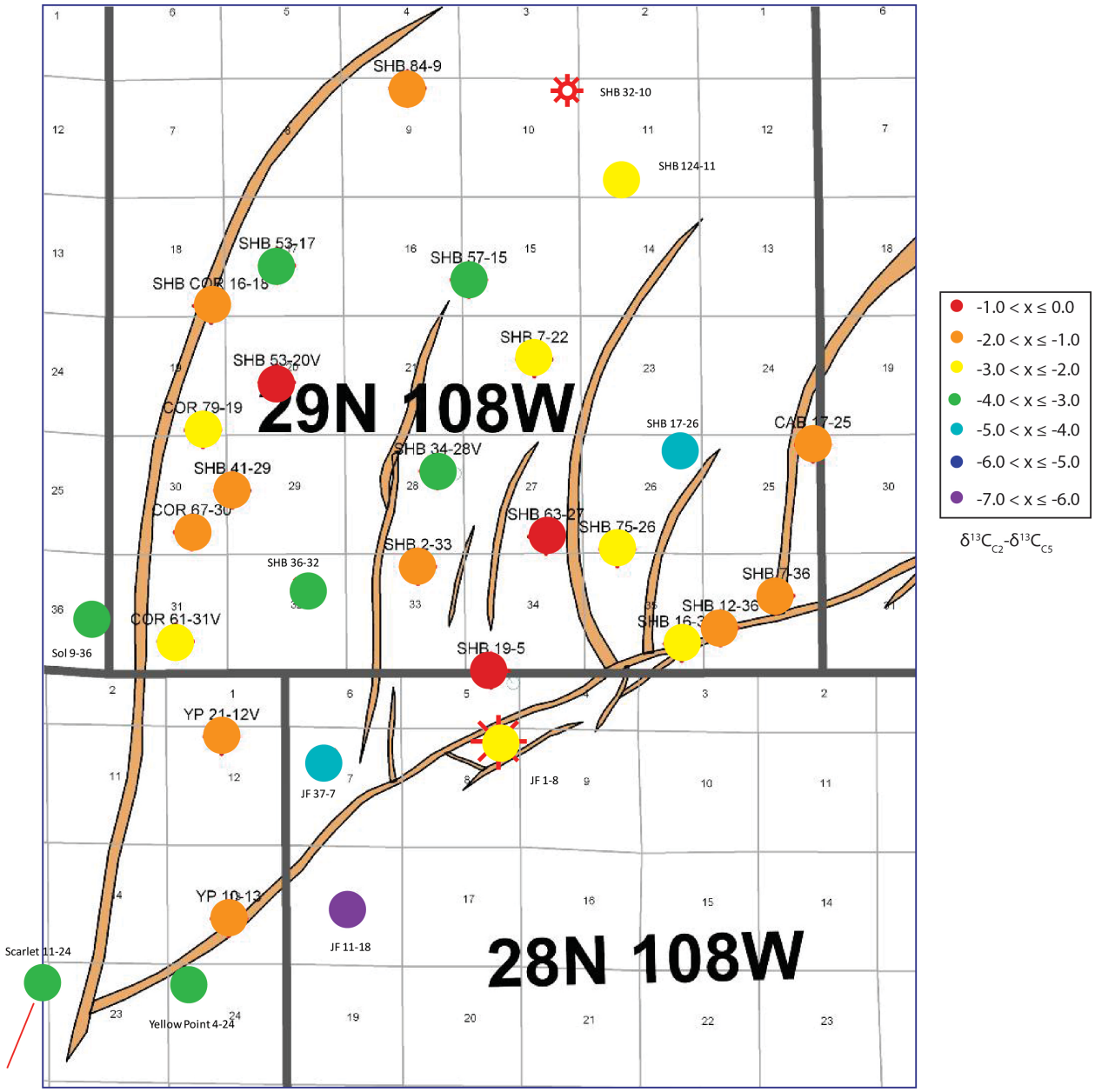

Figure 5.11. Difference in $\delta^{13}C$ between ethane and n-pentane.

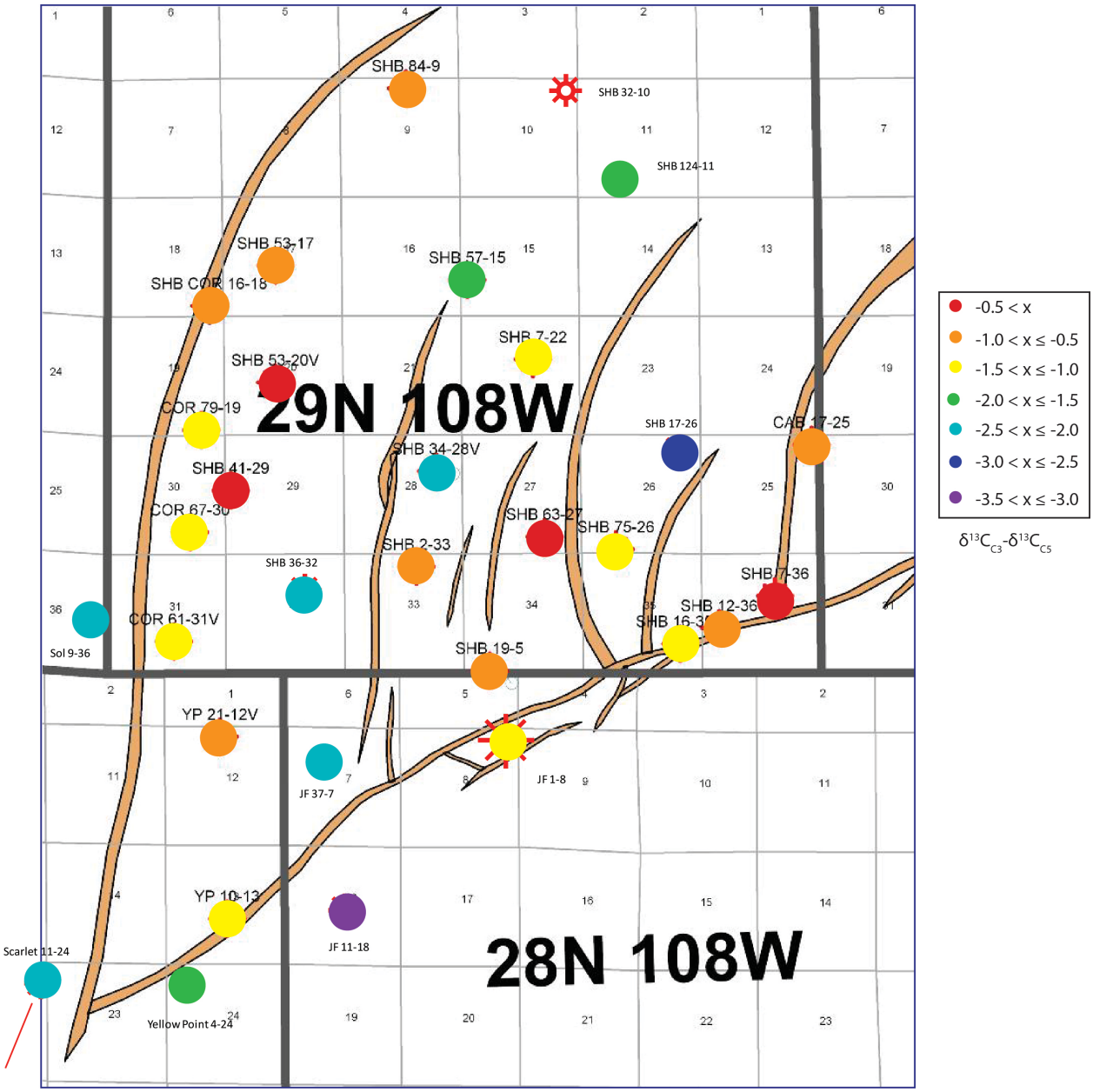

Figure 5.12. Difference in $\delta^{13}C$ between propane and n-pentane.

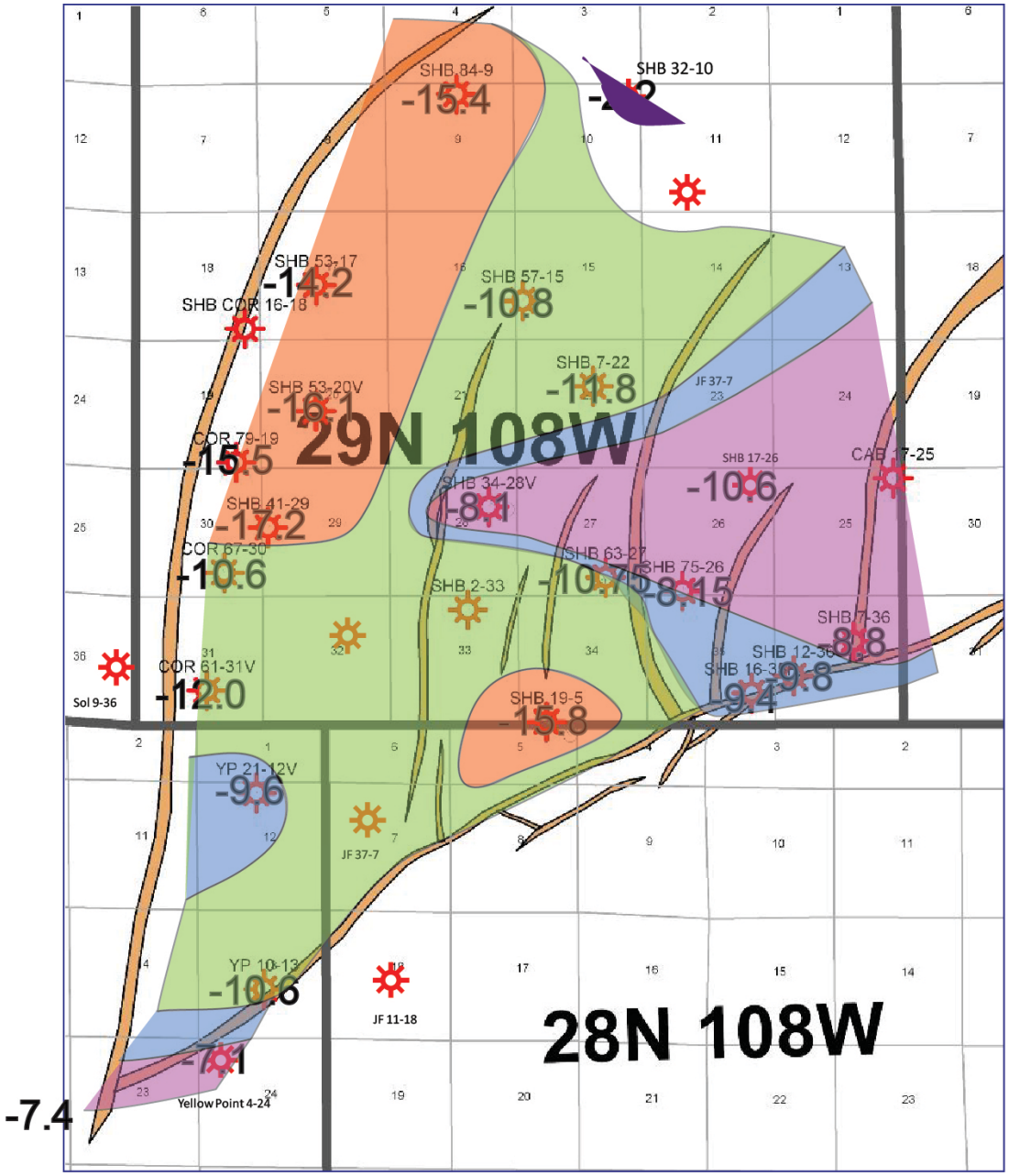

Figure 5.13. Carbon isotopic composition of CO_2 in Jonah Field production gas samples.

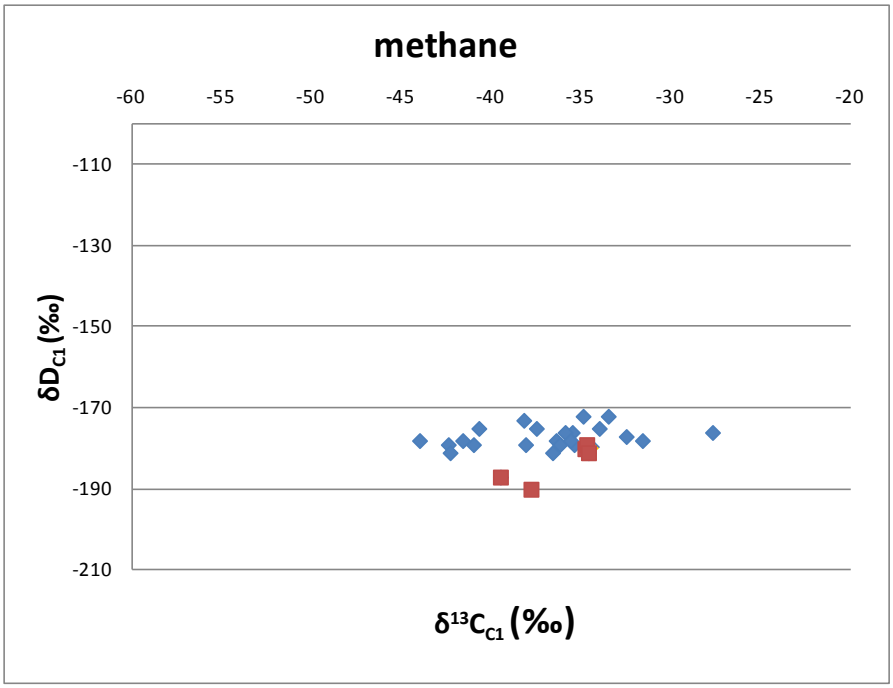

Figure 5.14. Carbon and hydrogen isotopic composition of methane in production gas samples from Jonah Field. Normally pressured or transitional pressure wells are in red symbols.

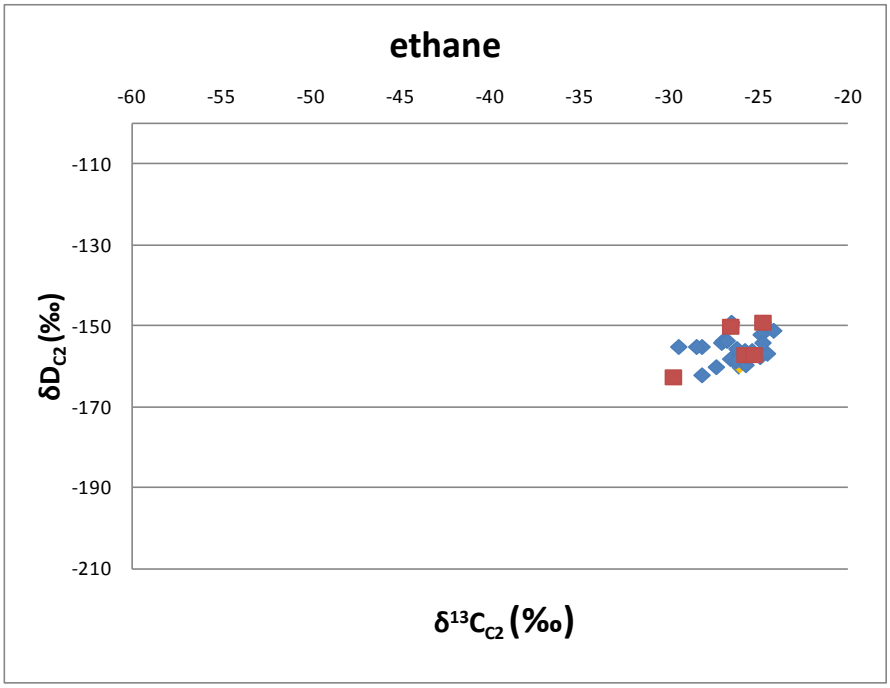

Figure 5.15. Carbon and hydrogen isotopic composition of ethane in production gas samples from Jonah Field. Normally pressured or transitional pressure wells are in red symbols.

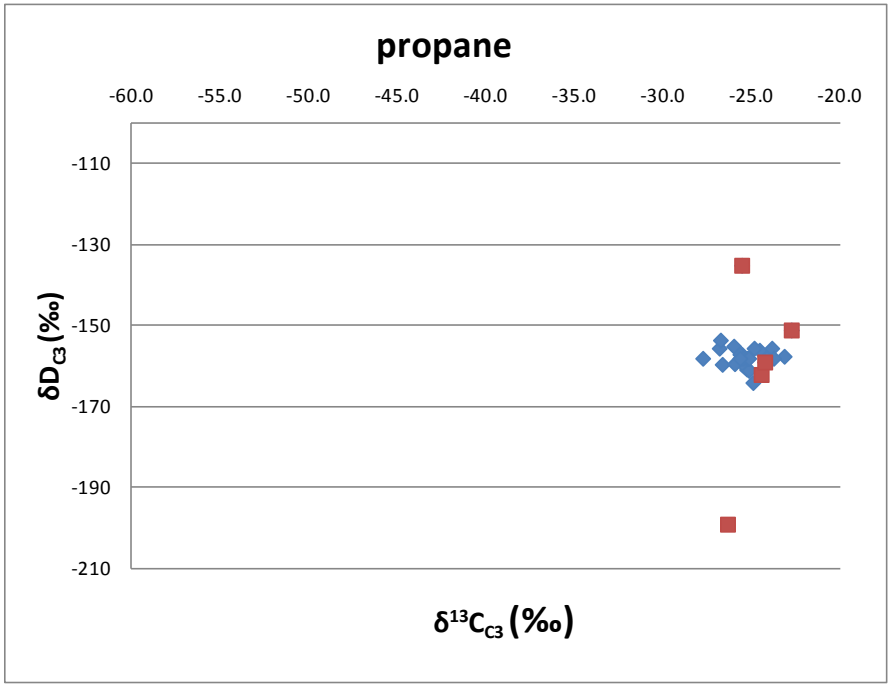

Figure 5.16. Carbon and hydrogen isotopic composition of propane in production gas samples from Jonah Field. Normally pressured or transitional pressure wells are in red symbols.

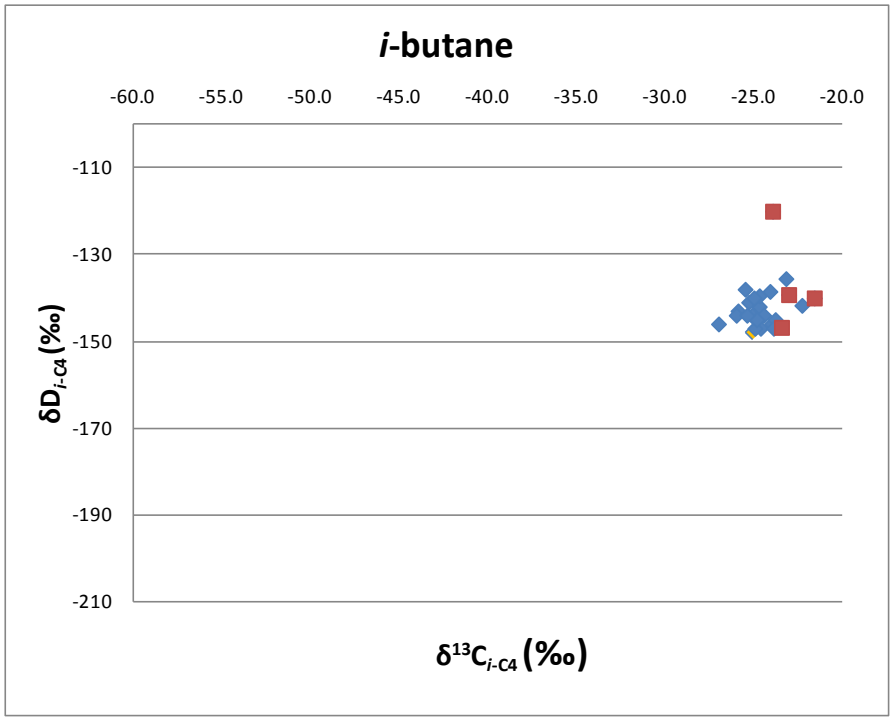

Figure 5.17. Carbon and hydrogen isotopic composition of *iso*-butane in production gas samples from Jonah Field. Normally pressured or transitional pressure wells are in red symbols.

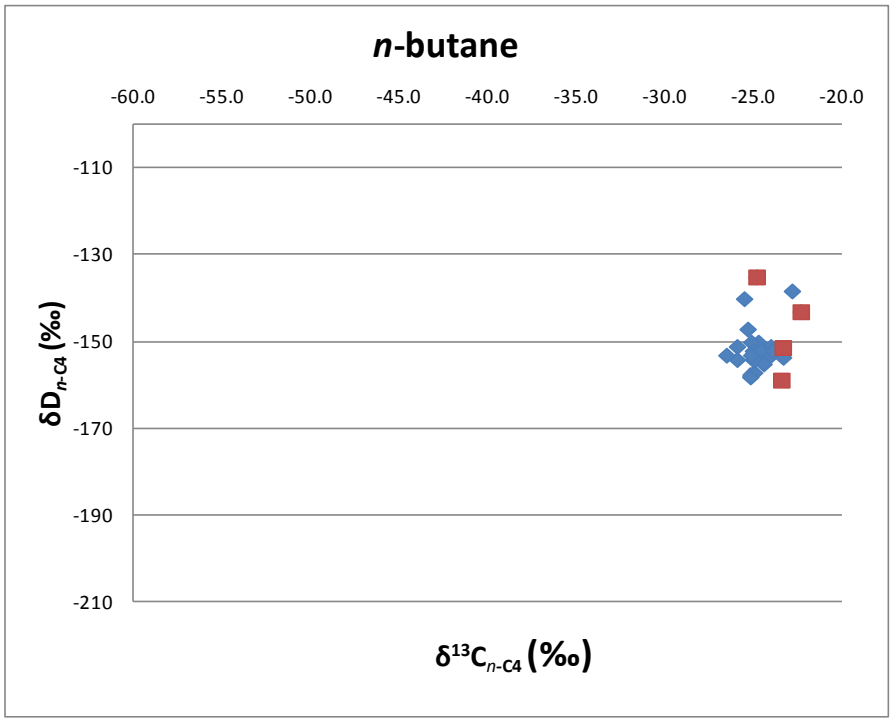

Figure 5.18. Carbon and hydrogen isotopic composition of *n*-butane in production gas samples from Jonah Field. Normally pressured or transitional pressure wells are in red symbols.

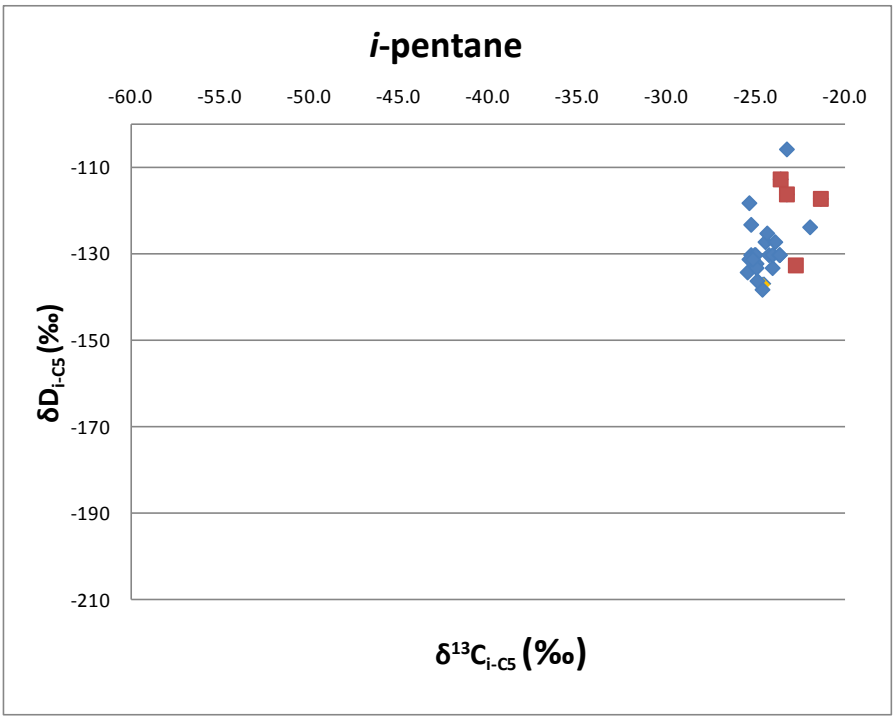

Figure 5.19. Carbon and hydrogen isotopic composition of *i*-pentane in production gas samples from Jonah Field. Normally pressured or transitional pressure wells are in red symbols.

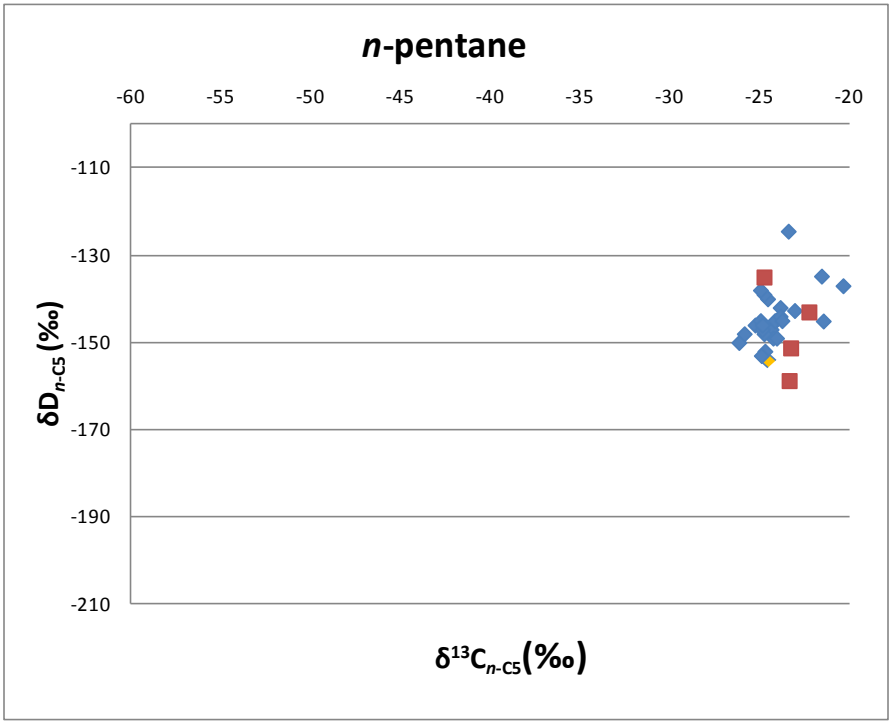

Figure 5.20. Carbon and hydrogen isotopic composition of *n*-pentane in production gas samples from Jonah Field. Normally pressured or transitional pressure wells are in red symbols.

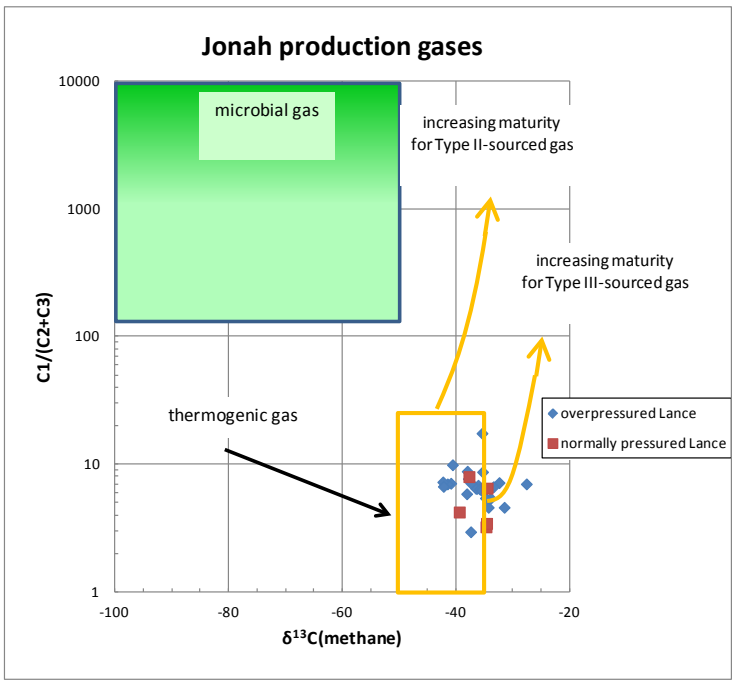

Figure 5.21. Carbon isotopic composition of methane versus the ratio of C_1 to C_2+C_3. Gases largely fall within the region for thermogenic gases.

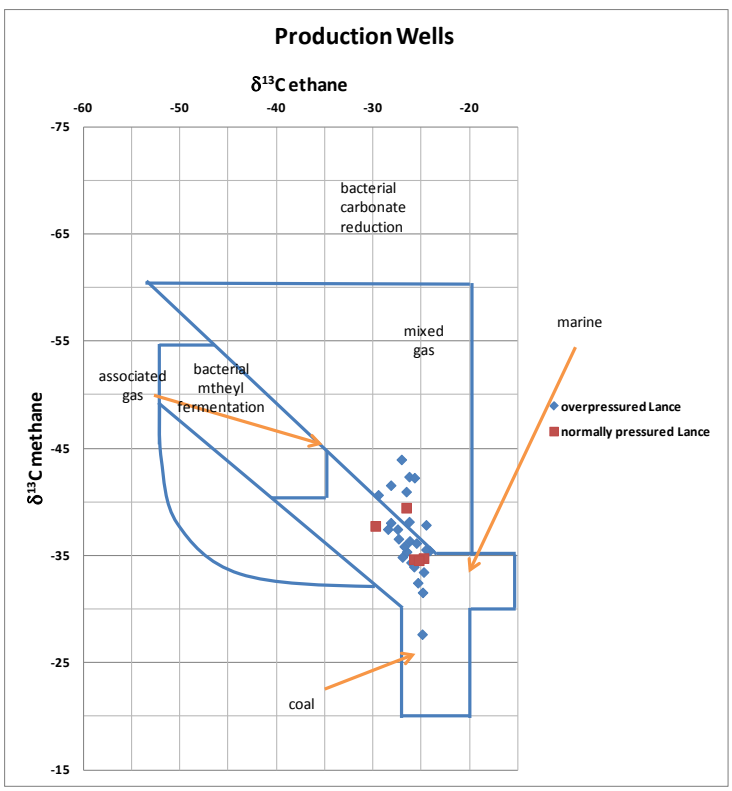

Figure 5.22. Carbon isotopic composition of methane versus ethane, after Schoell (1983). Gas compositions largely fall within the range of gases generated through primary cracking of marine kerogen. In this case, gases plotting with relatively high $\delta^{13}C_{C1}$ are not the product of mixing with biogenic gases.

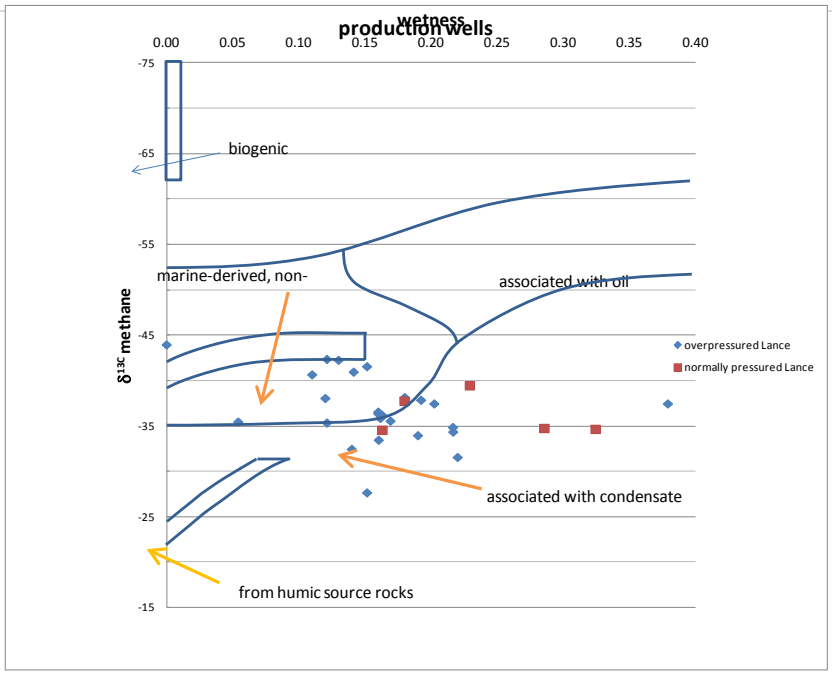

Figure 5.23. Carbon isotopic composition of $\delta^{13}C_{C1}$ versus ethane (after Schoell, 1983). This plot is similar to the Bernard plot (Figure X.21). Many of the samples have anomalously positive (heavy) methane carbon isotopic compositions.

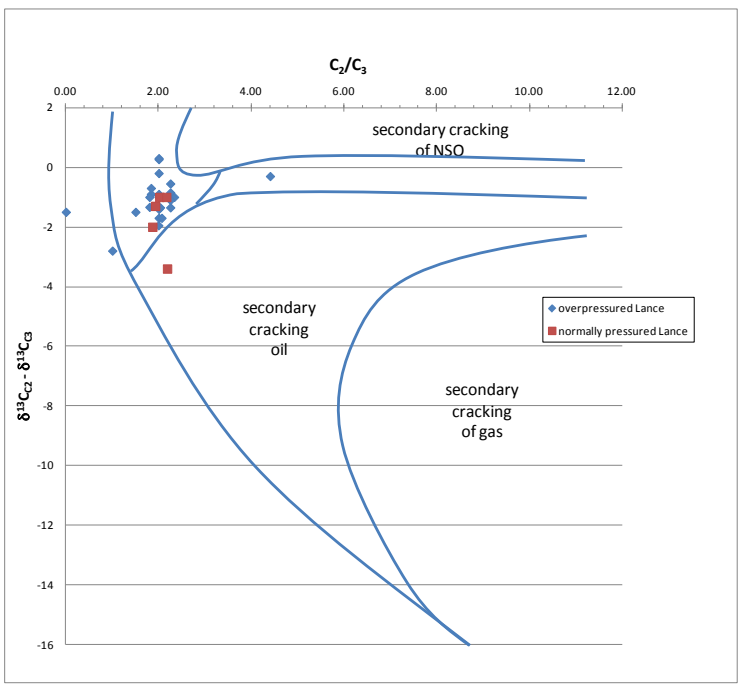

Figure 5.24. Ratio C_2/C3 versus the difference in carbon isotopic composition between C_2 and C_2 (after Lorant et al., 1998). This plot distinguishes gases derived from primary cracking from those derived from secondary cracking. This plot suggests that production gases are largely derived from primary cracking of kerogen.

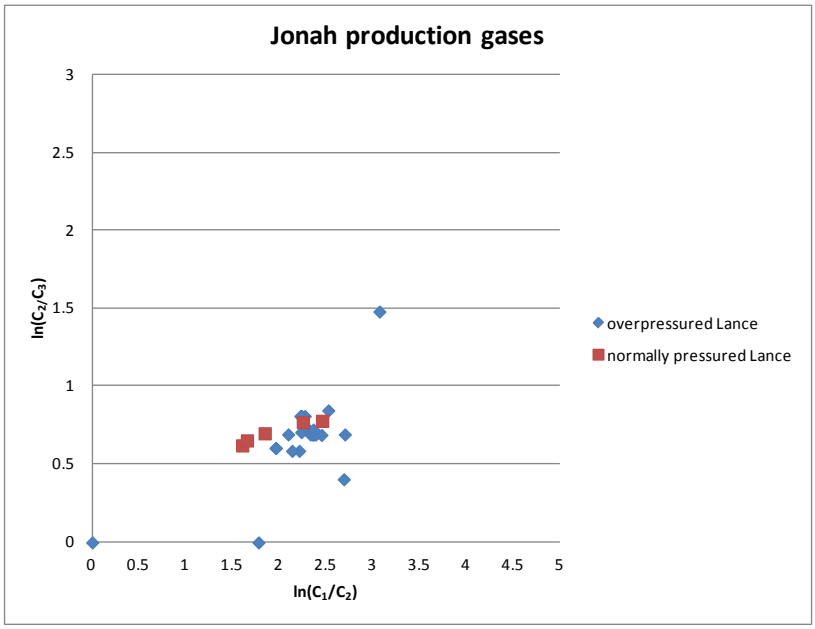

Figure 5.25. Ratio of $\ln(C_1/C_2)$ versus $\ln(C_2/C_3)$ after Prinzhofer and Huc (1995) can be used to distinguish the effects of secondary cracking from primary cracking, where increasing $\ln(C_2/C_3)$ in the absence of increasing $\ln(C_1/C_2)$ can indicate secondary cracking. Production gas data show no evidence of secondary cracking

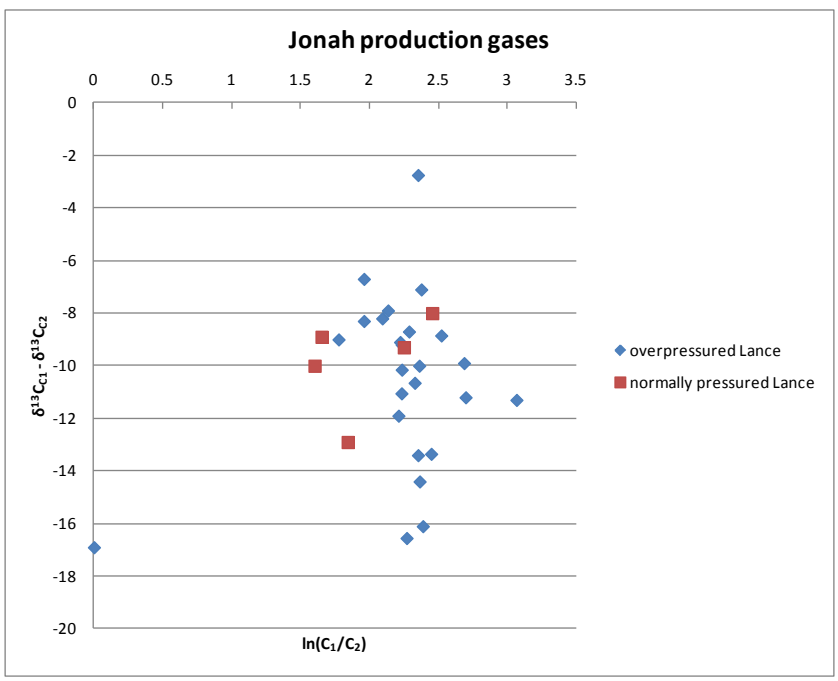

Figure 5.26. Ratio of $\Delta\delta^{13}C_{C1\text{-}C2}$ versus $\ln(C_1/C_2)$ after Prinzhofer and Huc (1995) is used to differentiate maturation trends from leakage. Diagonal trends indicate maturation effects. Gases from both the overpressured Lance reservoirs and normally pressured Lance show similar wide ranges of composition. It is not possible to distinguish leakage or maturation effects in this cross-plot.

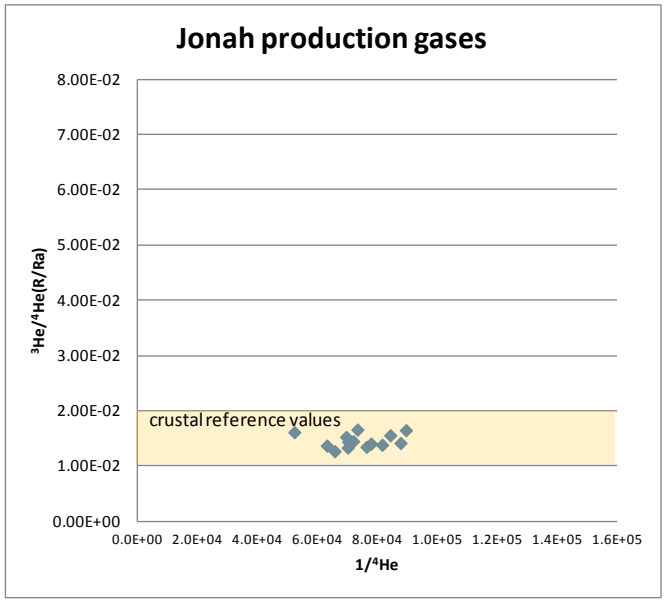

Figure 5.27. $^{3}He/^{4}He$ ratios are indicative of contributions of gas from crustal or other sources. Gas compositions from Jonah Field are tightly clustered in the field for crustal-sourced He.

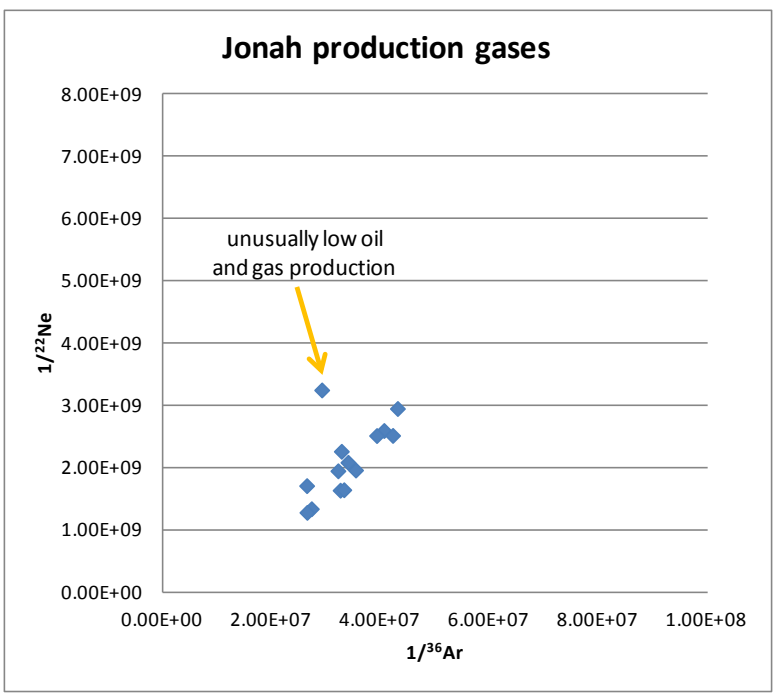

Figure 5.28. ^{22}Ne and ^{36}Ar concentrations are indicative of contributions of gas from atmospheric sources, typically through degassing from meteoric water. Gases from Jonah Field have low values for $1/^{22}Ne$ and $1/^{36}Ar$ and describe a linear trend, indicating a significant but variable contribution from meteoric water. One sample that falls off the linear trend is from the least productive well in the data set.

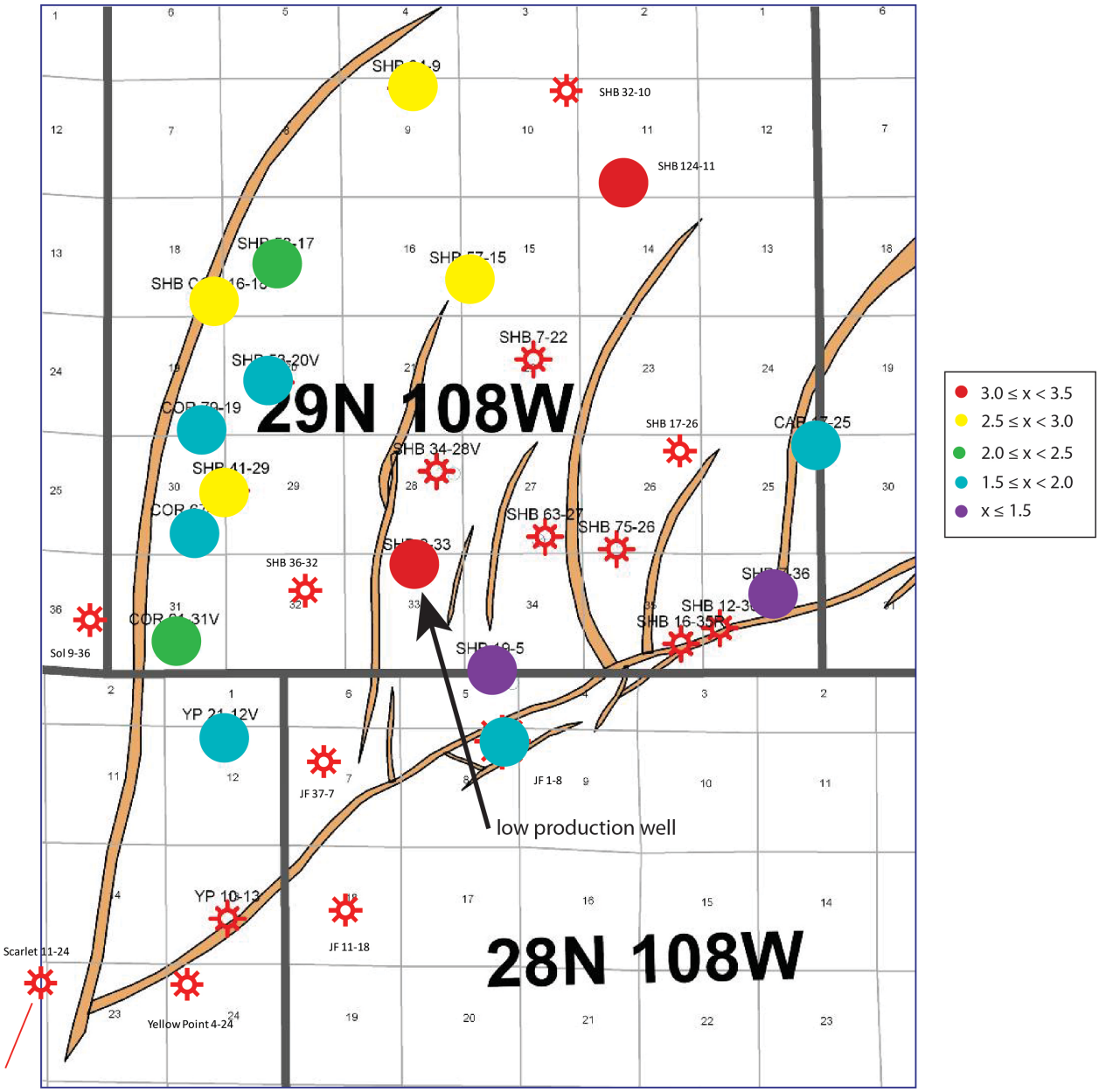

Figure 5.29. Map of Jonah Field, showing $1/^{22}Ne$ ratios. Low values of this ratio are indicative of meteoric sources of noble gases. Jonah Field samples are generally characterized by low values, with extreme values located on or near the southern boundary fault for the Jonah structure.

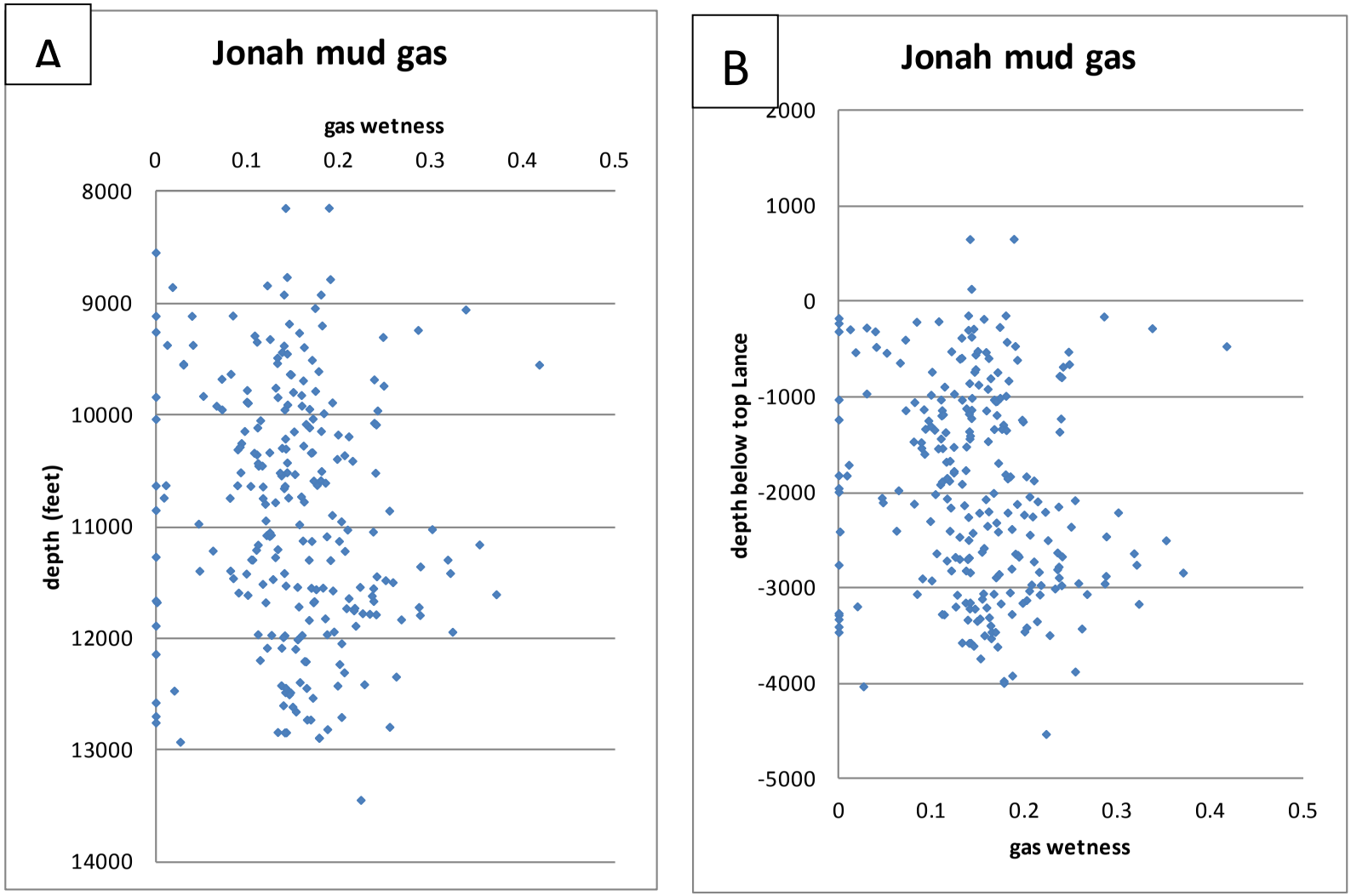

Figure 5.30. Mud gas data from Jonah Field, showing (A) gas wetness versus depth and (B) gas wetness versus depth below top Lance.

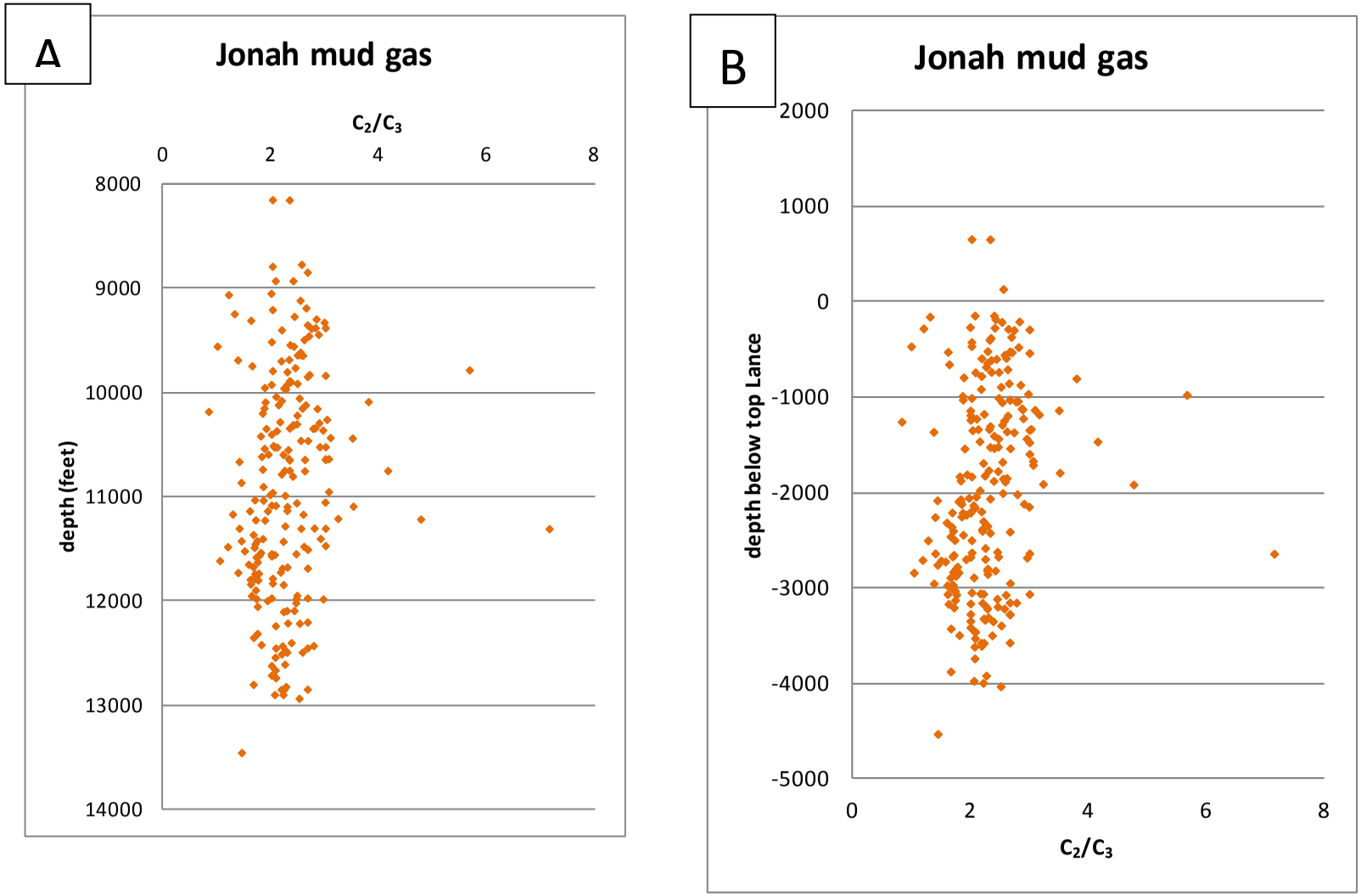

Figure 5.30. Mud gas data from Jonah Field, showing (A) C_2/C_3 ratio versus depth and (B) C_2/C_3 ratio versus depth below top Lance.

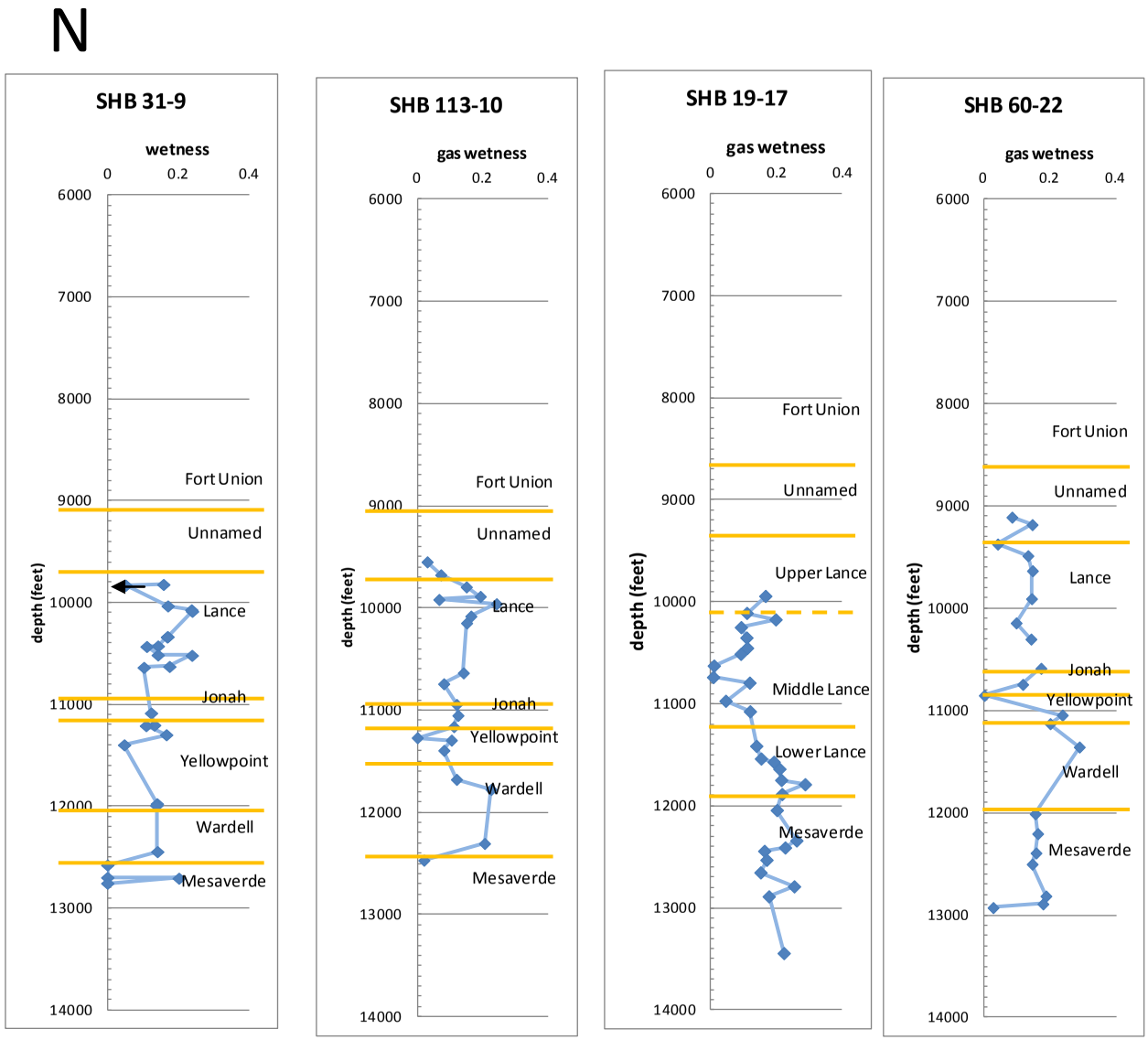

Figure 5.31. Gas wetness in mudgas profiles from 5 wells at Jonah Field. The JF 42-8 well in just south of the southern boundary fault to the Jonah structure, in a transition zone between overpressured Lance reservoirs within the Jonah structure and normally pressure Lance reservoirs outside the Jonah structure.

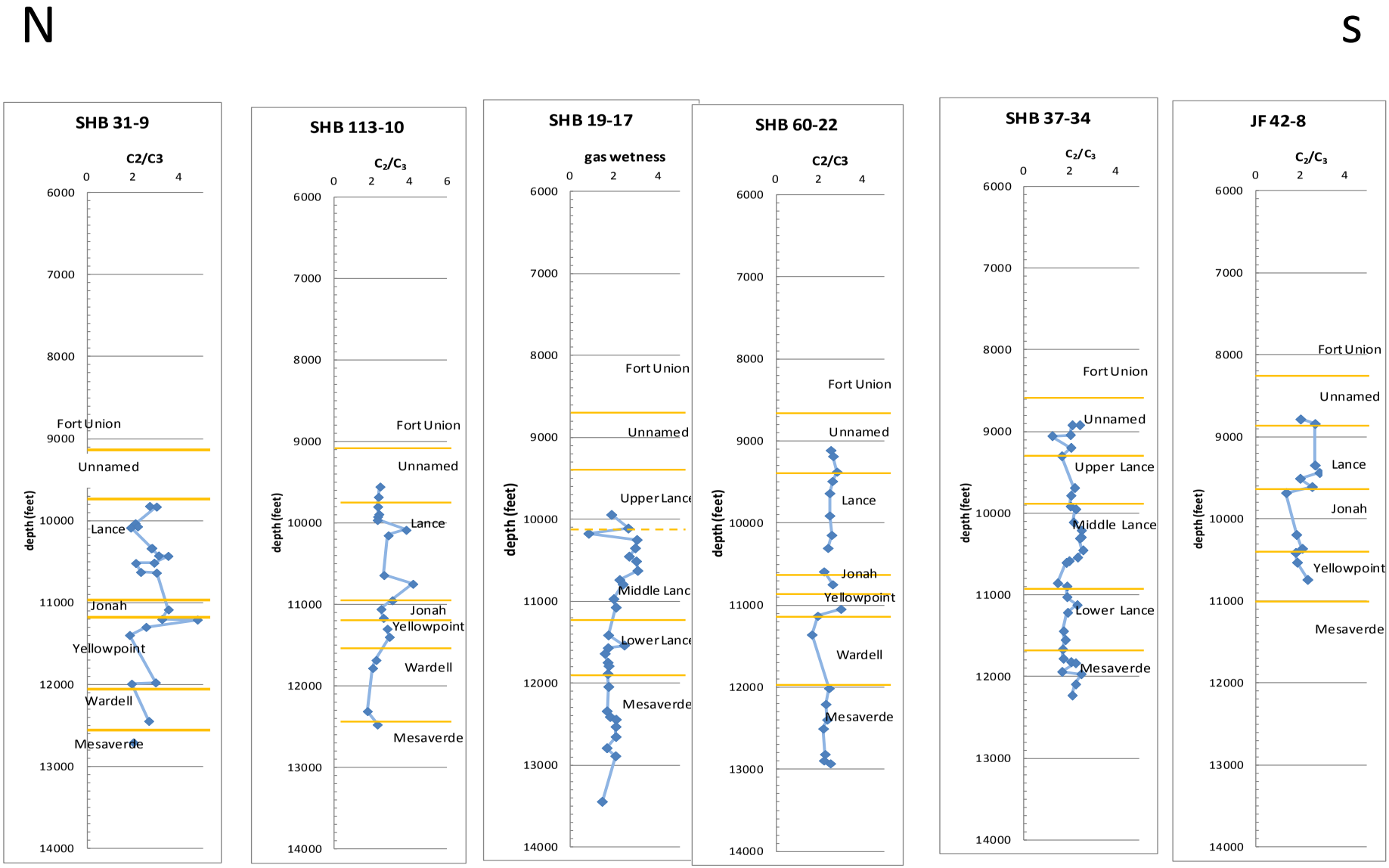

Figure 5.32. Gas wetness profiles in three wells from Parachute and Grand Valley Fields. Yellow lines indicate the tops of the Cameo Coal and Rollins sandstone.

N S

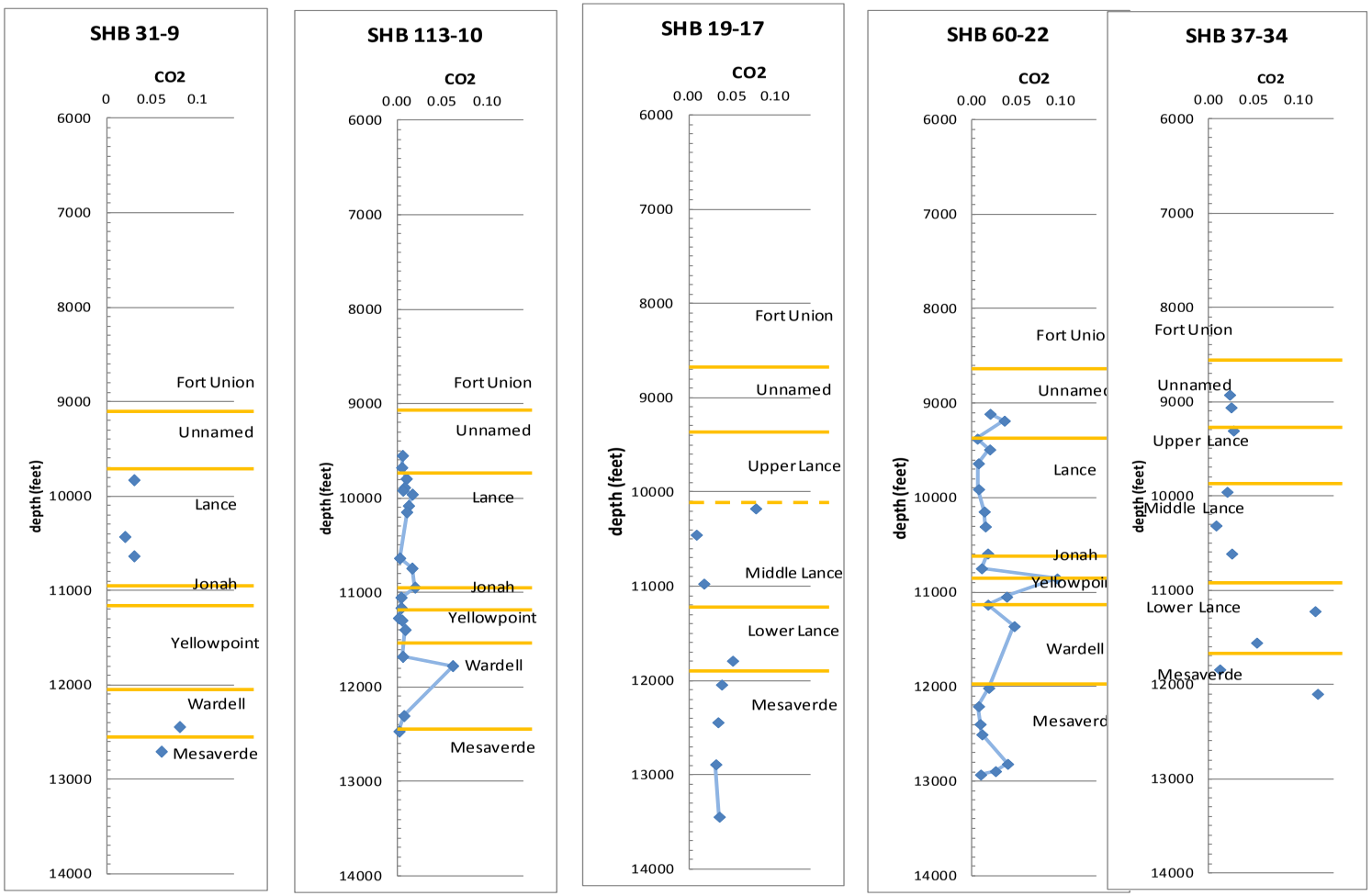

Figure X.33. CO_2 content in five wells from Jonah Field. Yellow lines indicate the tops of the Cameo Coal and Rollins sandstone.

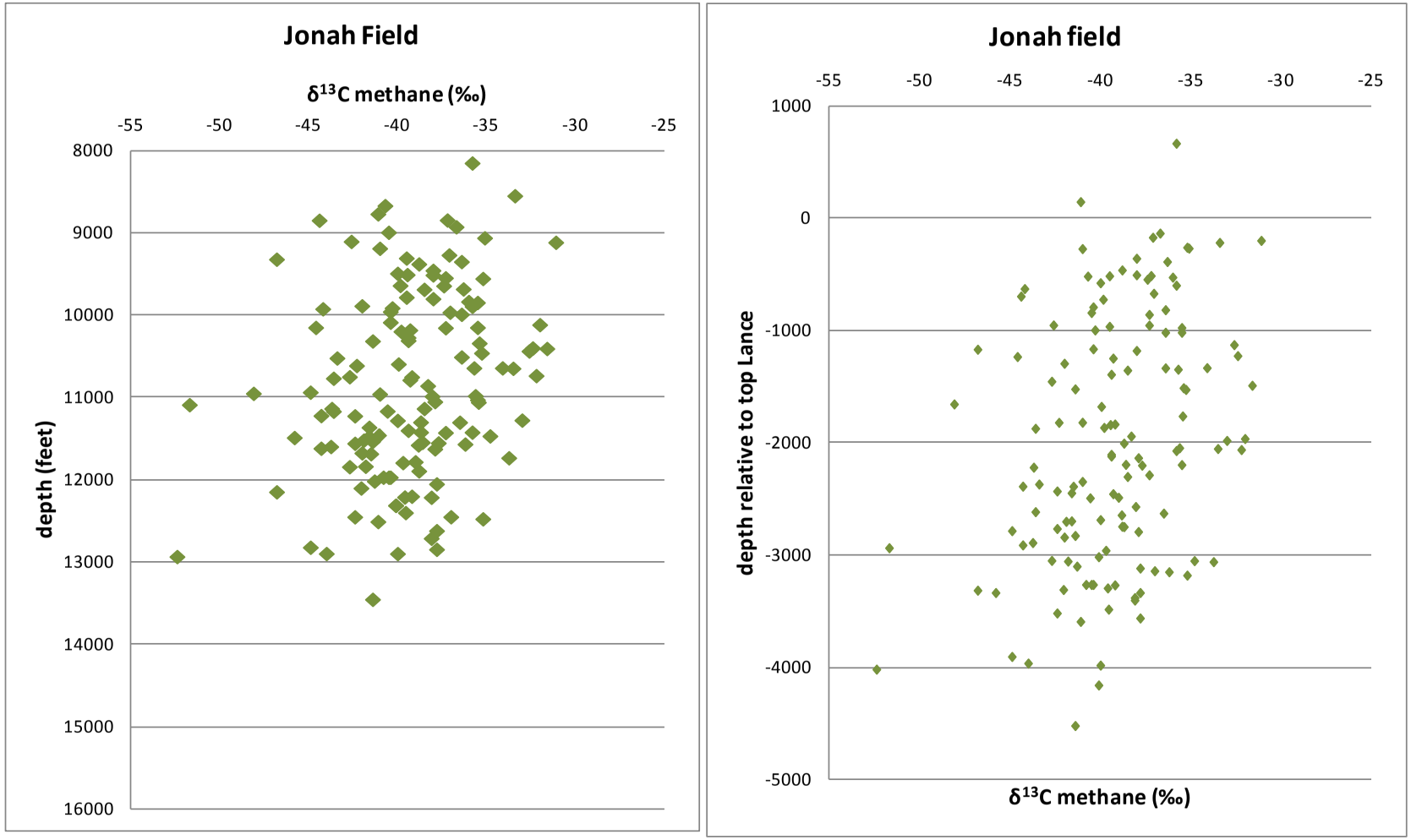

Figure 5.34. Mud gas data from Jonah Field, showing (A) $\delta^{13}C_{C1}$ versus depth and (B) $\delta^{13}C_{C1}$ versus depth below top Lance.

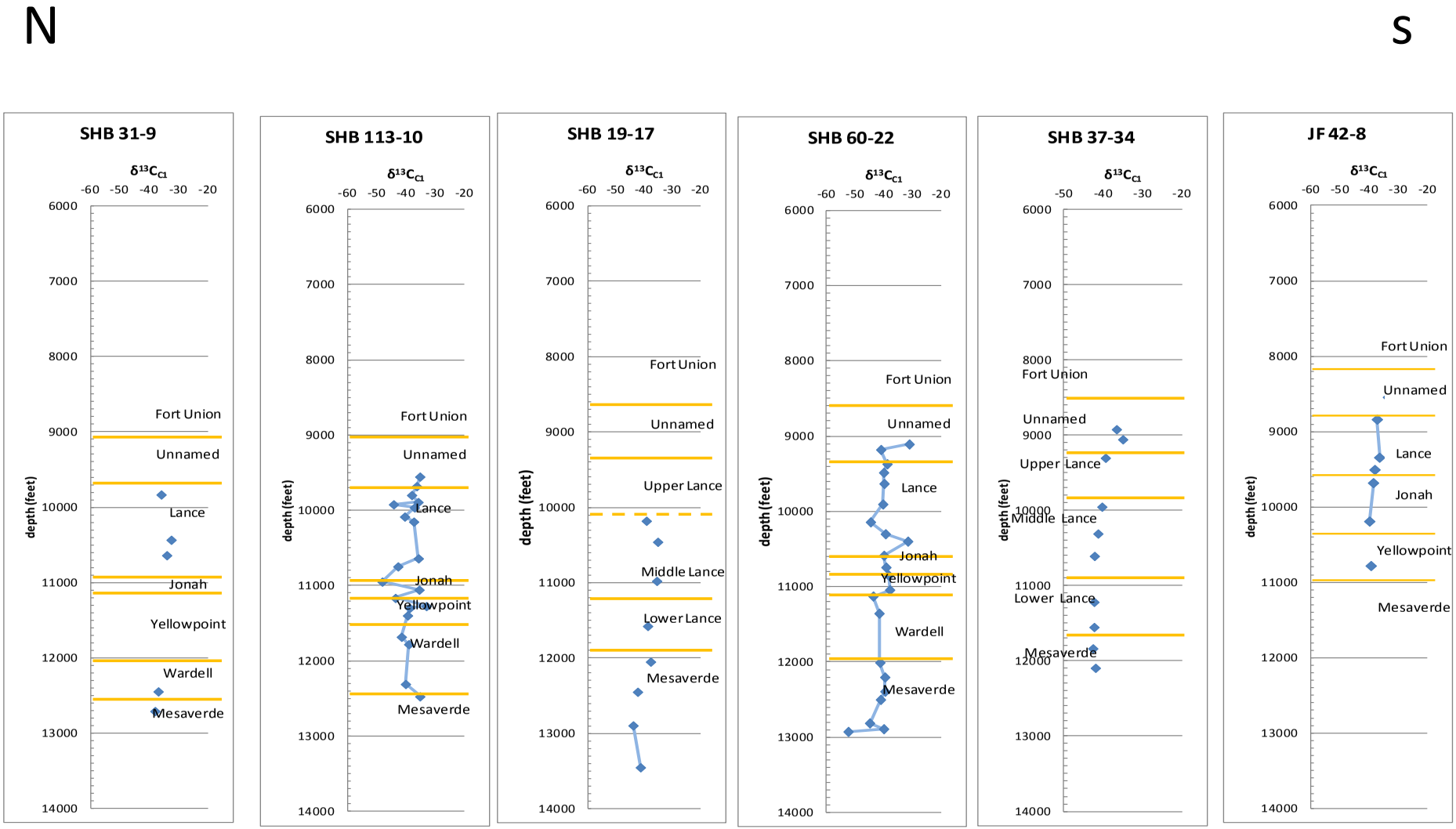

Figure X.35. Carbon isotopic composition of methane in profiles in six wells from Jonah Field. Yellow lines indicate formation tops.

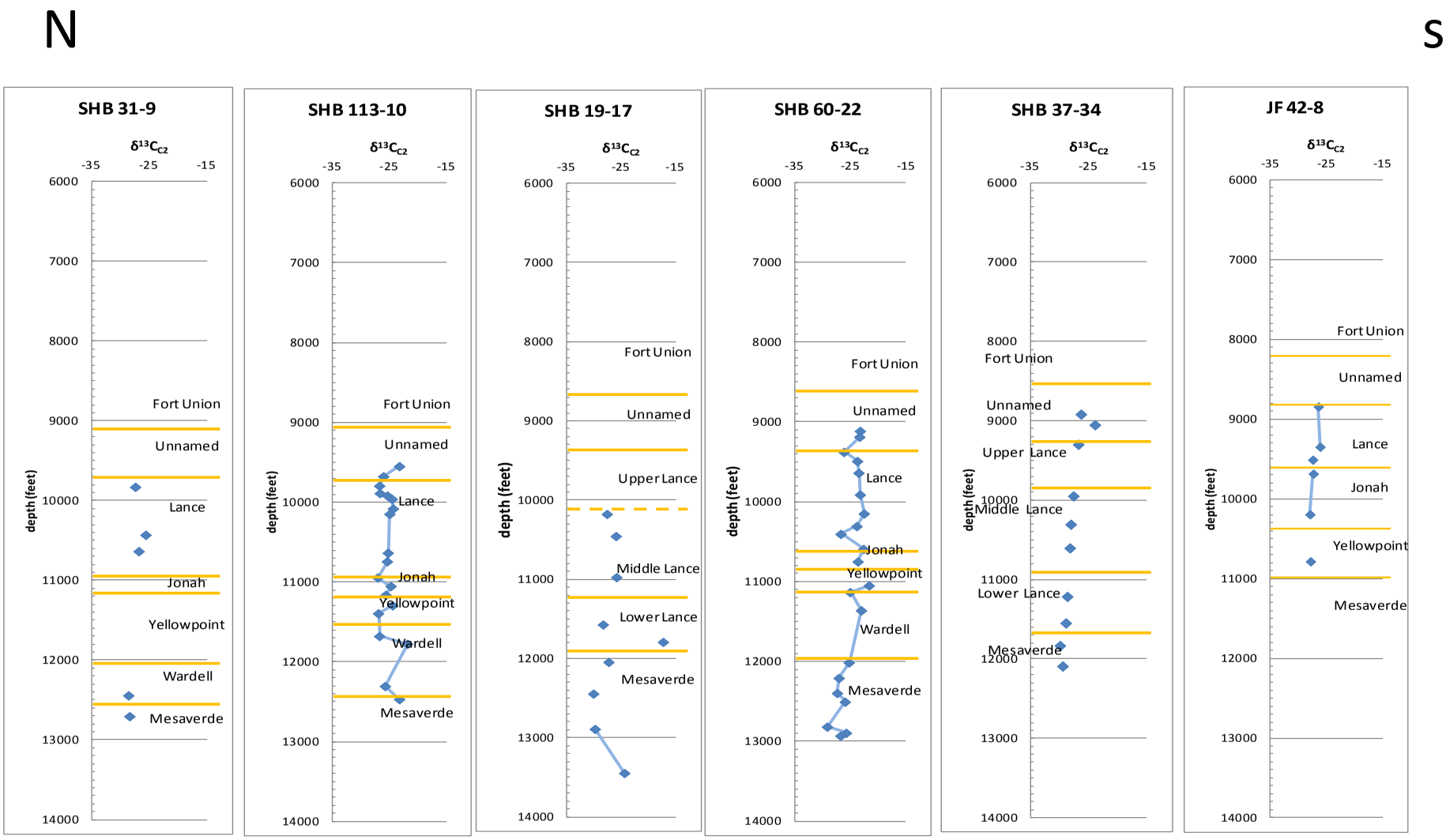

Figure 5.36. Carbon isotopic composition of ethane in profiles in six wells from Jonah Field. Yellow lines indicate formation tops.

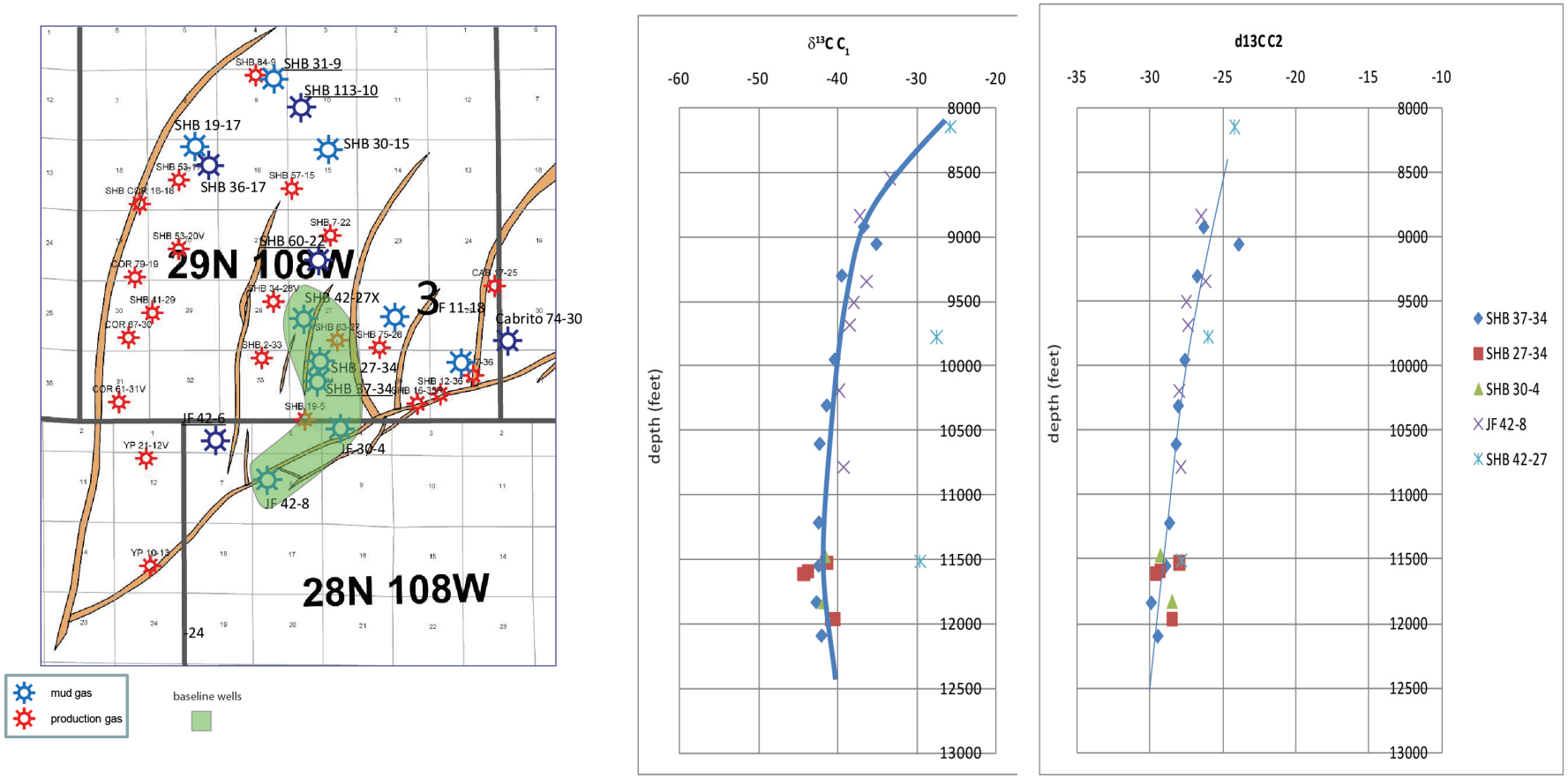

Figure 5.37. Coherent pattern of decreasing $\delta^{13}C_{C1}$ and $\delta^{13}C_{C2}$ in wells from the southern part of Jonah Field.

N S

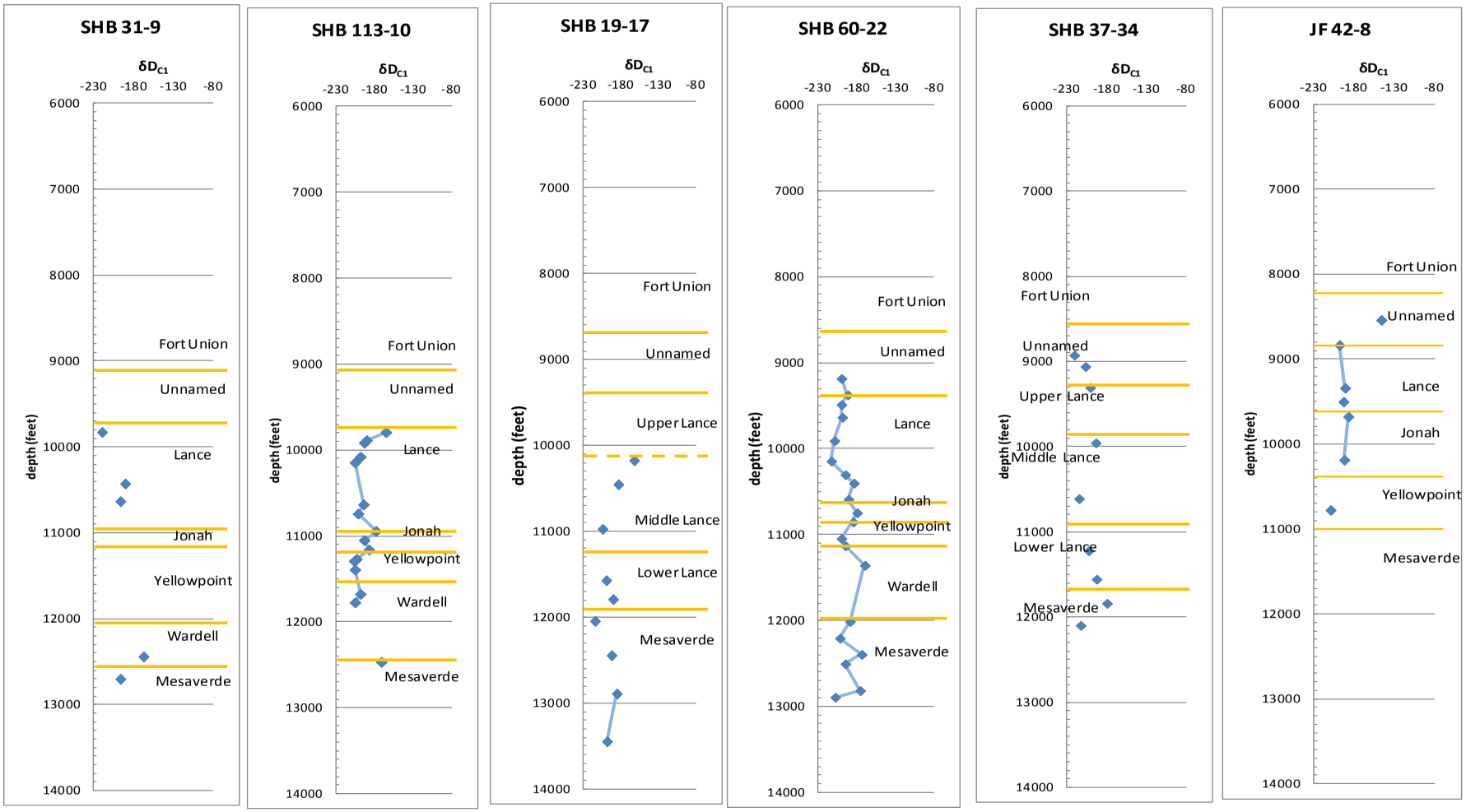

Figure 5.38. Hydrogen isotopic composition of methane in profiles in six wells from Jonah Field. Yellow lines indicate formation tops.

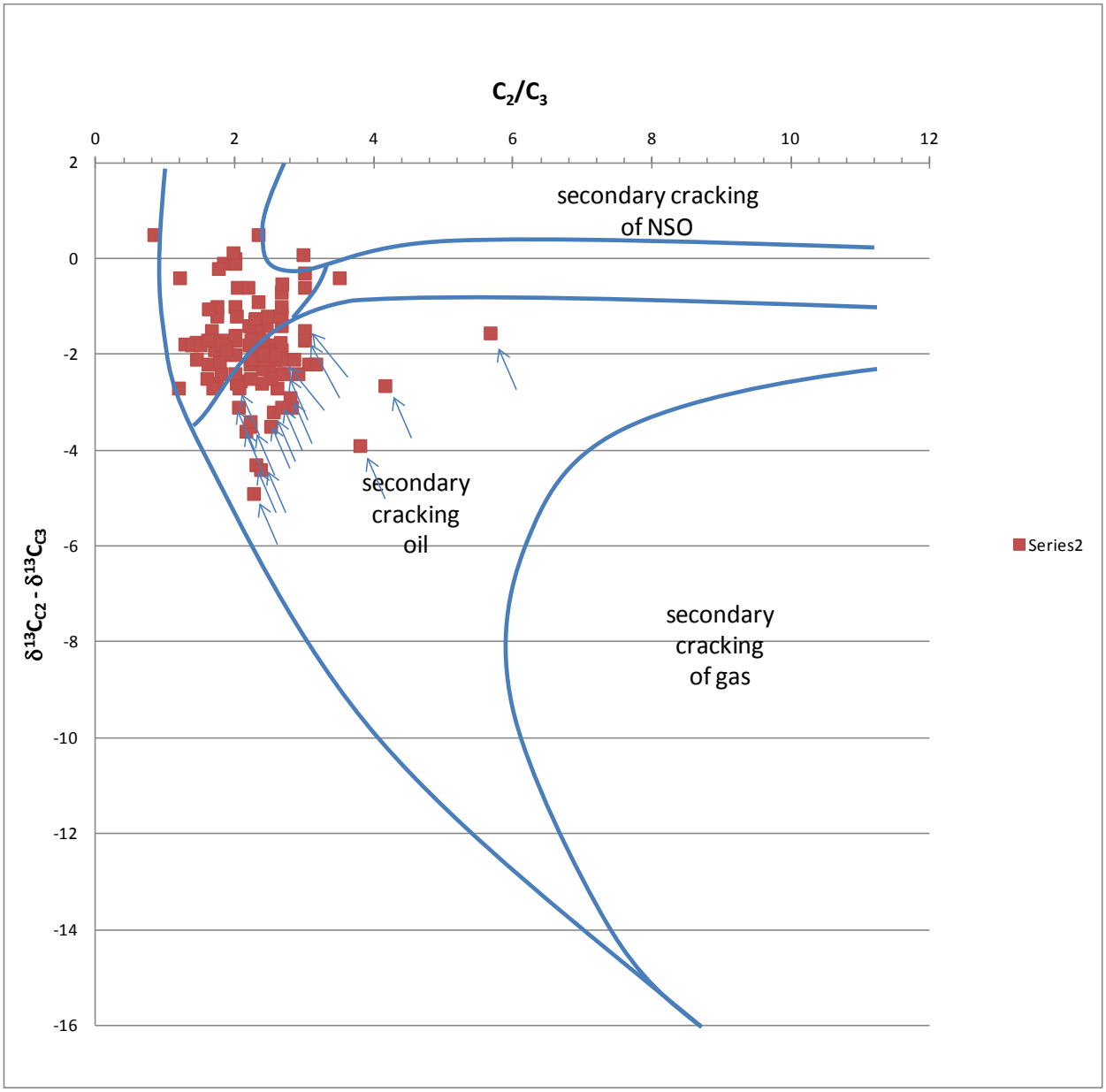

Figure 5.39. Cross-plot of C_2/C_3 versus $\delta^{13}C_{C2}$- $\delta^{13}C_{C3}$ in mud gas data. Data points plotting with elevated C_2/C_3 and $\delta^{13}C_{C2}$- $\delta^{13}C_{C3}$ are indicative of secondary cracking of oil. Arrows indicate points located in Figure X.36.

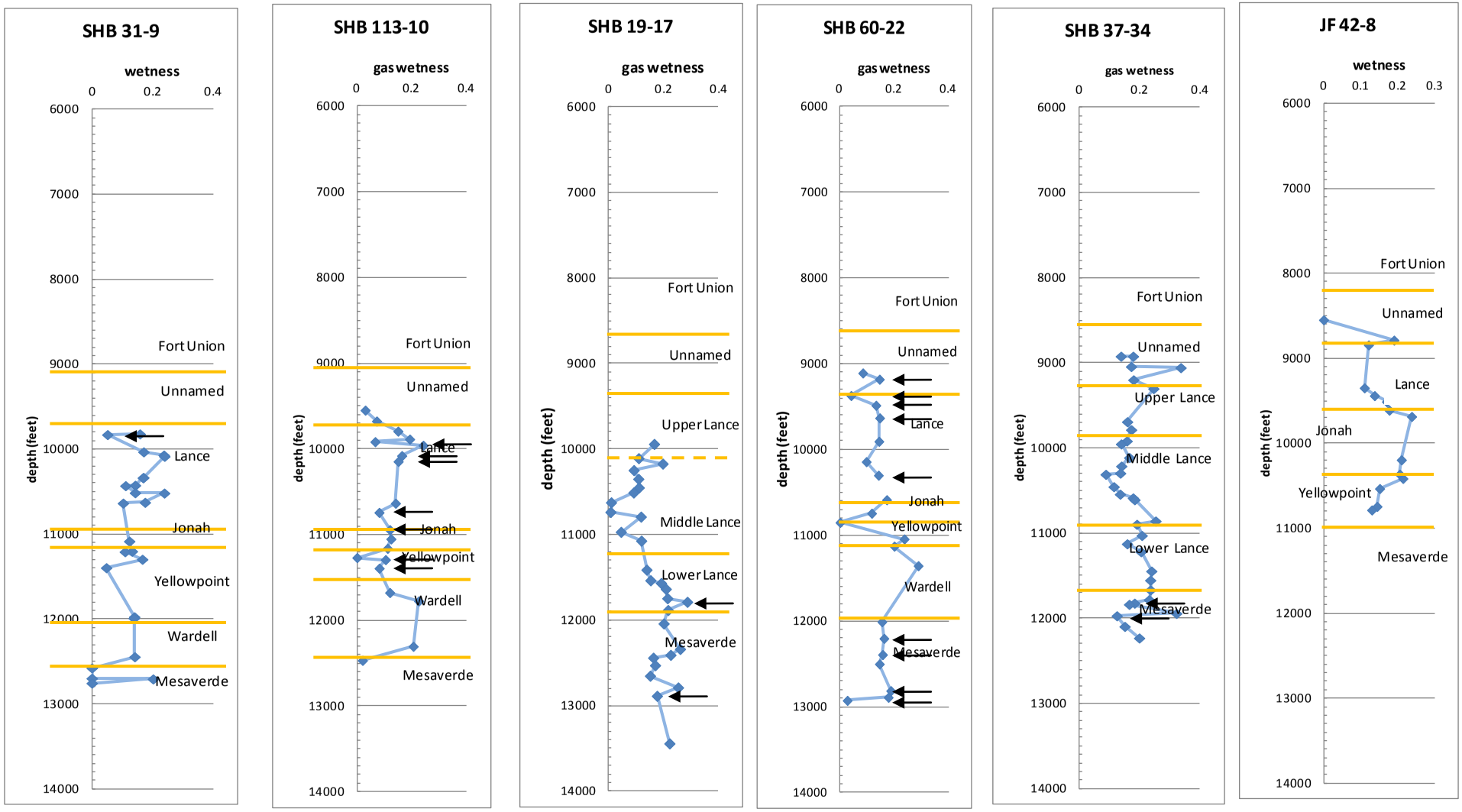

Figure 5.40. Gas wetness profiles in six wells from Jonah Field. Yellow lines indicate formation tops. Arrows indicate points with possible secondary cracking (from Figure X.35)

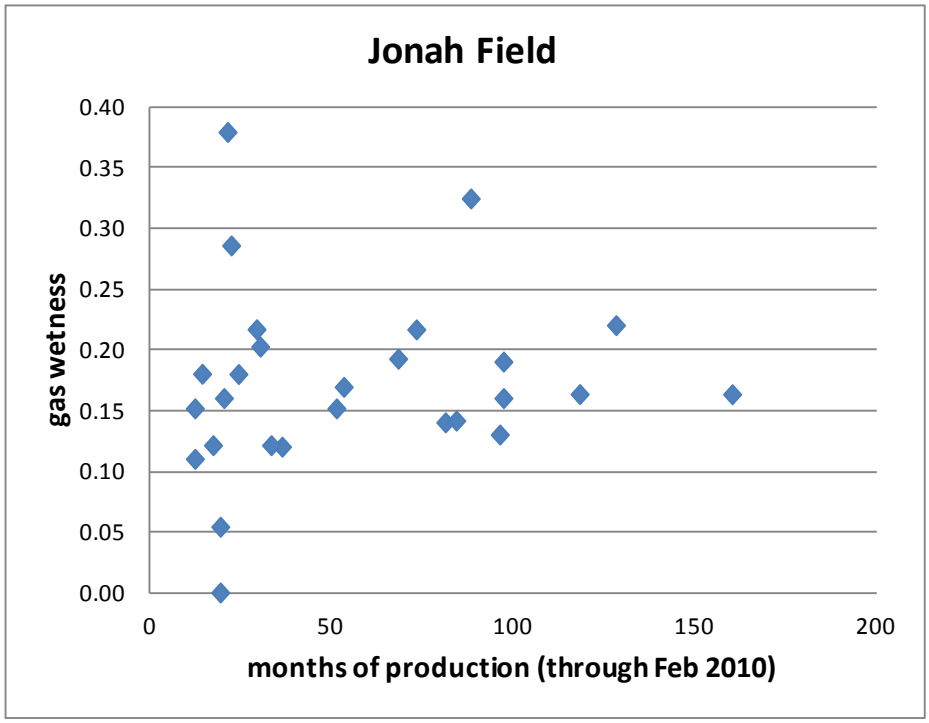

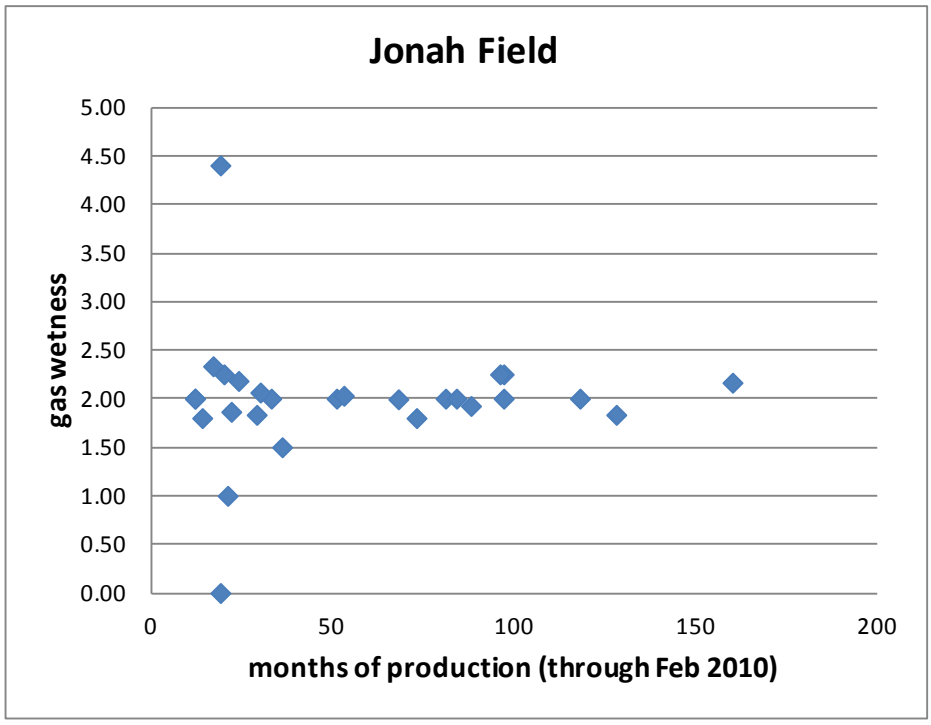

Figure 5.41. Cross-plot of time since start of production versus gas wetness (top) and C_2/C_3 ratio. Gases do not appear to become drier with length of production.

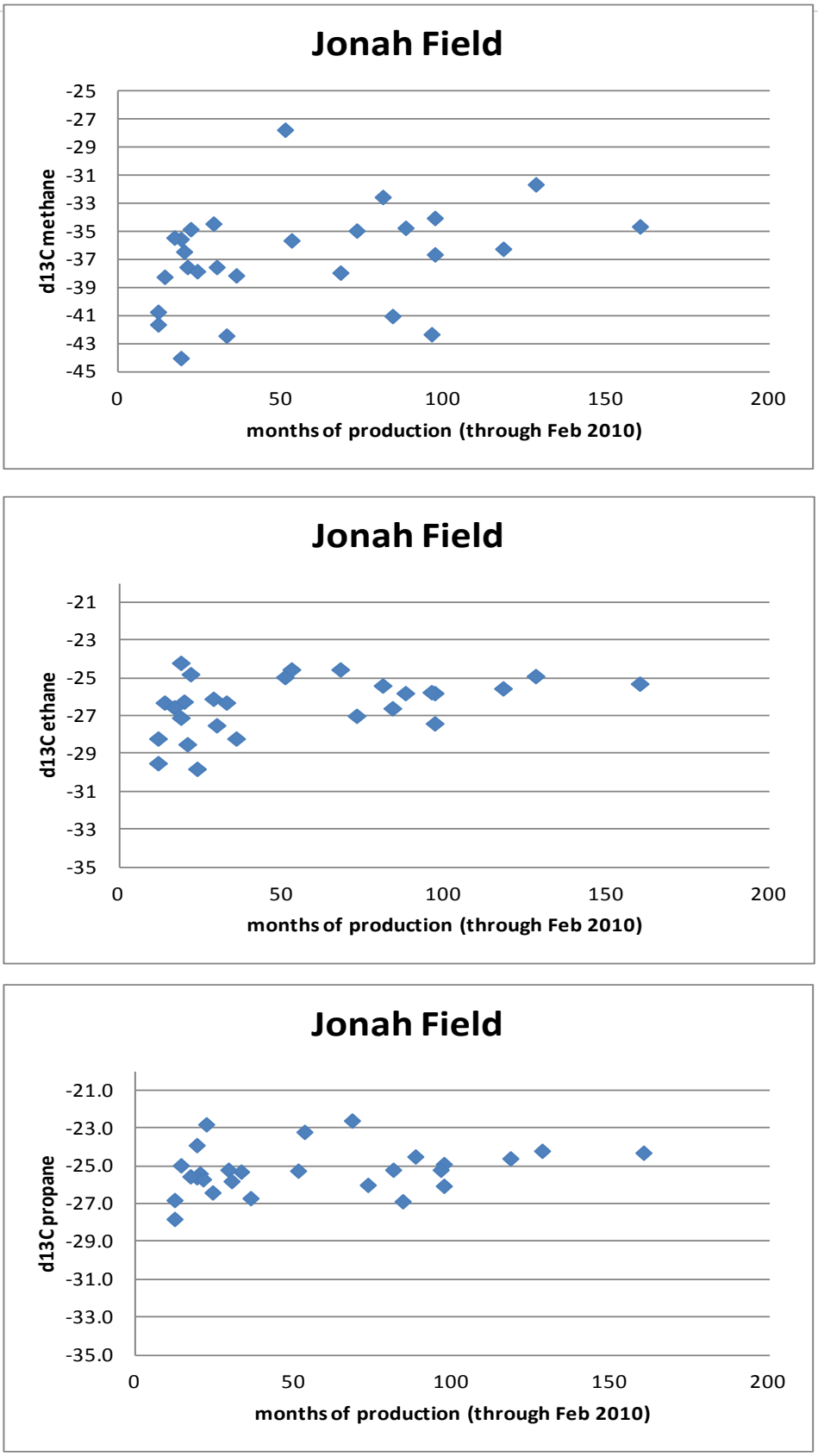

Figure 5.42. Cross-plot of time since start of production versus carbon isotopic composition of methane (top), ethane (middle) and propane (bottom). Ethane and propane compositions become heavier by approximately 2-3‰ with increasing time of production; there is little or no discernible effect in methane.

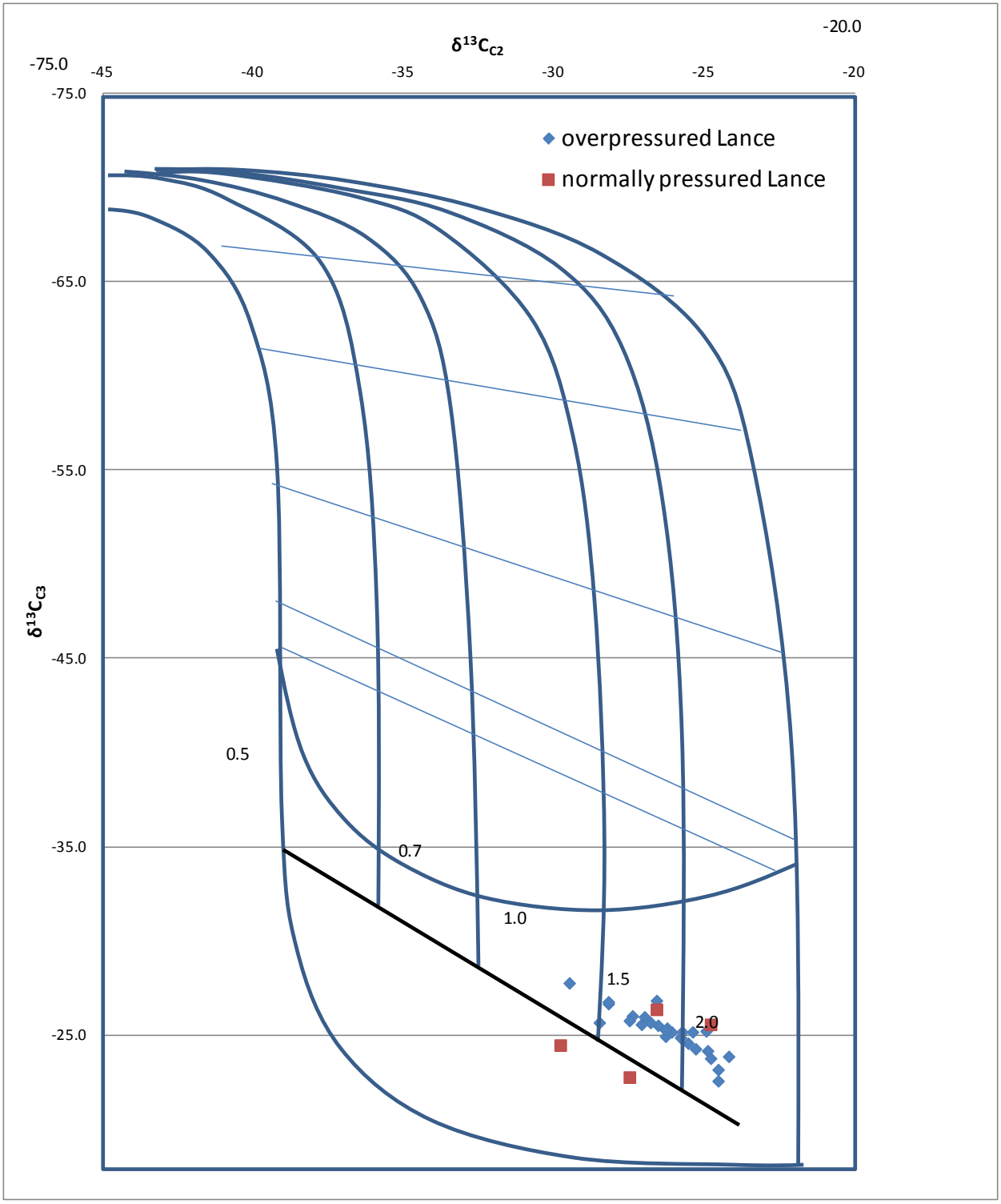

Figure 5.43. Cross-plot of $\delta^{13}C_{C2}$ versus $\delta^{13}C_{C3}$ for production gases. The composition of gases from overpressured Lance reservoirs describe a generally linear trend, indicating a range of thermal maturities over which gases were generated, from 1.5 to 2.5% R_o. Gases from normally pressured Lance reservoirs fall to higher or lower $\delta^{13}C_{C3}$, suggesting that other processes have affected these gases.

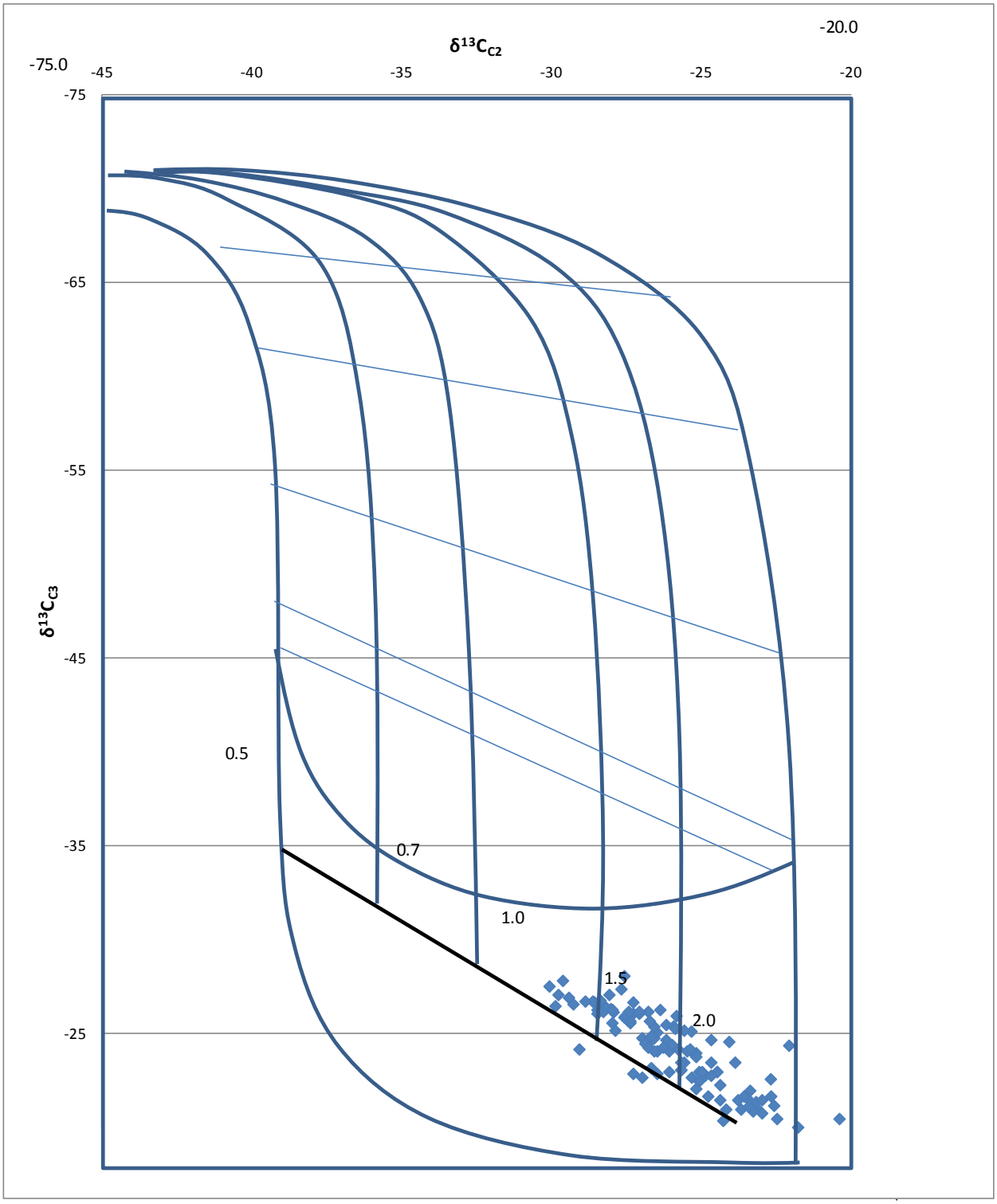

Figure 5.44. Cross-plot of $\delta^{13}C_{C2}$ versus $\delta^{13}C_{C3}$ for mud gas samples. Mud gas data fall along the same trend as production gas data, although a larger range of thermal maturities is indicated.

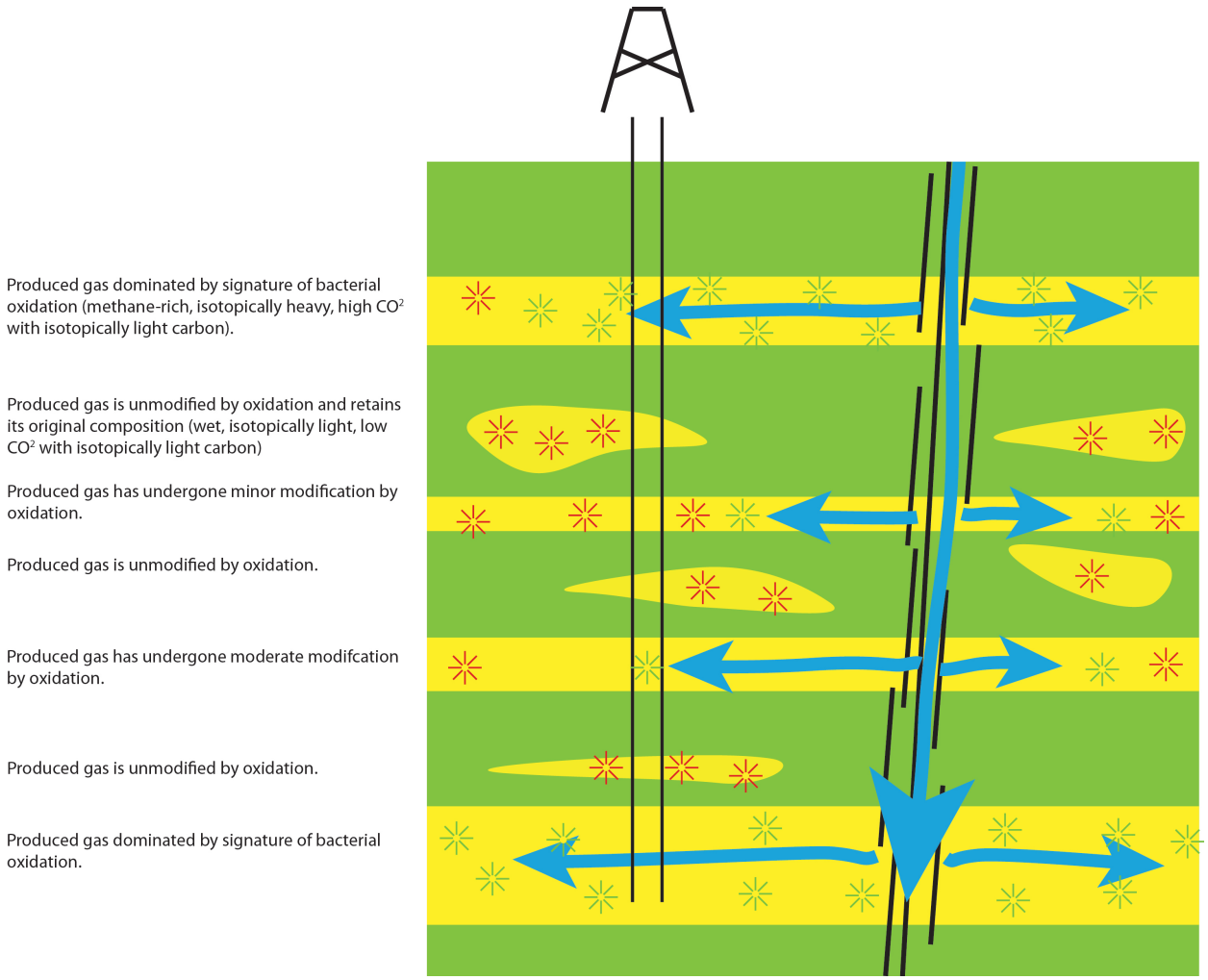

Figure 5.45. Model A for gas compositions at Jonah Field. Gas has one primary source that generates a relatively wet, isotopically light gas. This gas is locally modified by bacterial oxidation in continuous sandstones with access to infiltrating deep meteoric water, resulting in gases that are (1) drier, (2) isotopically heavier, and (3) have CO_2 with an isotopically light signature.

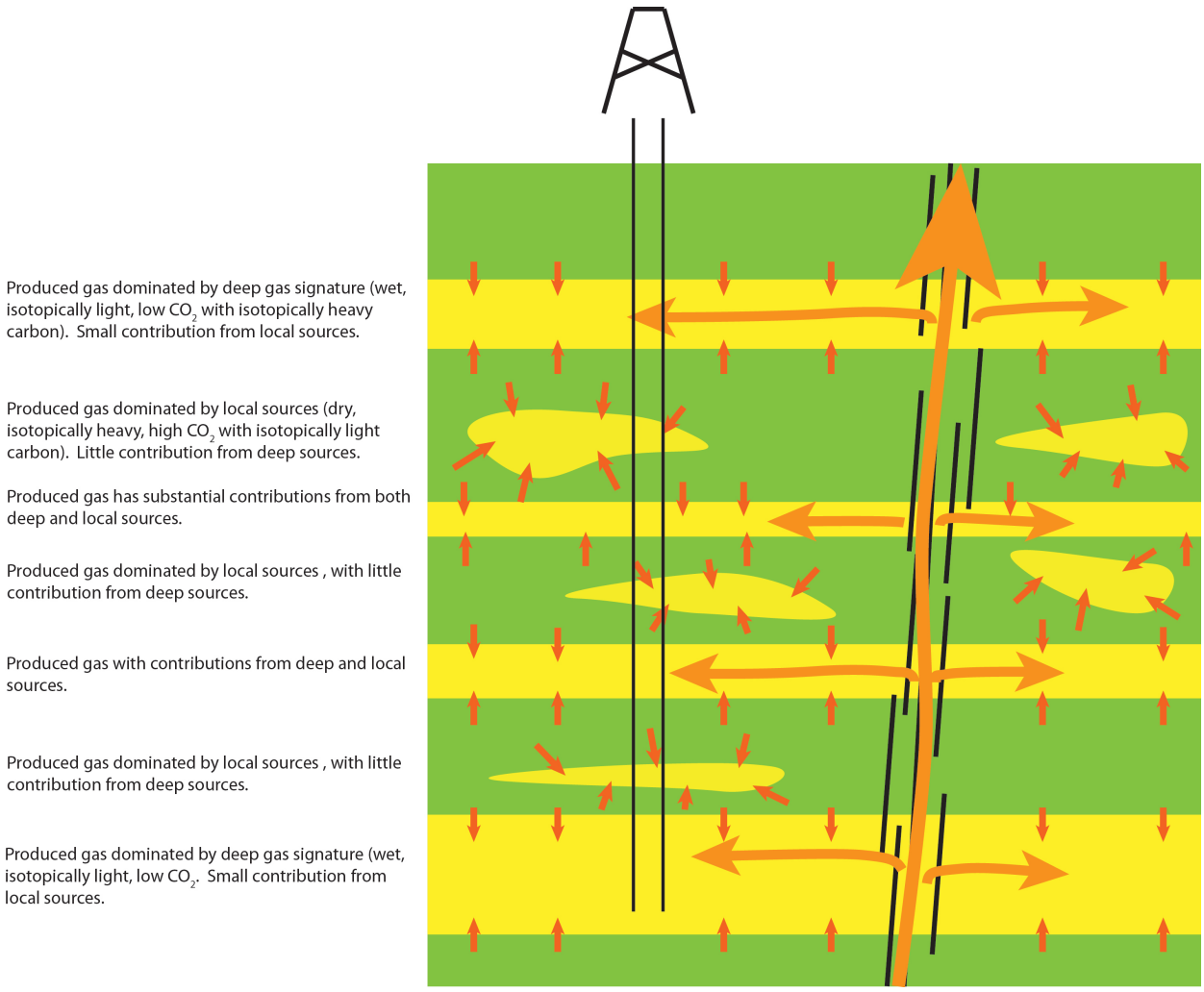

Figure 5.46. Model 1 for controls on gas composition at Jonah Field. Gas has two sources:

1) a local source within or near the reservoir column with a Type III signature (methane-rich, isotopically heavy C_1 and C_2, relatively high CO_2 fraction that is isotopically light);

2) a deep source with a Type II signature (relatively wet, istopically light C1 and C2, lower CO2 fraction that is isotopically heavy, possibly incorporating some gas derived from secondary cracking.

In this model, the deep-sourced gases will migrate upward along faults and fracture systems and laterally from the faults into laterally continuous reservoir sandstones. Locally source gas is restricted to discontinuous reservoir bodies with short, direct migration pathway from surrounding mudstones.

6 GREATER NATURAL BUTTES FIELD

6.1 Data Set

The dataset from Greater Natural Buttes Field (GNB) includes:

- Production gas samples (33) from the GNB Field area, analyzed for bulk composition and C/H isotopes (Figure 6.1).
- Mud gas samples (46) from 19 wells from GNB Field, analyzed for bulk composition and C/H isotopes (Figure 6.1).
- Production gas samples (17) from GNB Field, analyzed for noble gas composition (Figure 6.2).

6.2 Production Gases

6.2.1 Bulk Gas Compositions

The compositions of production gases are summarized in Table 6.1.

The GNB field production gas samples averaged 15% C_{2+} component (wetness), with 85% methane, 7% ethane, 4% propane, 2% butane and 1% pentane. The CO_2 content was not measured.

The distribution of gas wetness is shown in Figure 6.3. Within the resolution of our sampling, it is not possible to discern any clear spatial pattern in gas wetness. Three wells with very dry compositions are clustered in the west central part of the field, and the wettest gases measured in our data set are found at least a few kms to the north or south of the main WNW-ESE trending fault through the field. Wells along the main fault can have a considerable range in compositions, from as low as 0.01 to as high as 0.19.

C_2/C_3 is another common measure of gas wetness, with low values typical of wet gases. The distribution of C_2/C_3 values is shown in Figure 6.4. Most samples varied from 1.26 to 2.93; this ratio correlated very poorly with gas wetness. As with the gas wetness data, there is no clear spatial pattern to the distribution of C_2/C_3 values.

6.2.2 Carbon and Hydrogen Isotopic Composition

Carbon isotopes

The average carbon isotopic composition of methane ranged from -39.6 to -27.6‰ (Table 6.1). There is no clear geographic pattern to the distribution of values, although relatively positive (heavy) values occur in the central, southern and eastern parts of the field (Figure 6.5). The $\delta^{13}C_{C1}$ of nearby wells vary by as much as 6‰.

The carbon isotopic composition of ethanes exhibits a slightly smaller range of values (-21.1 to -29.8‰) (Figure 6.6), as does the composition of the propanes (-21.5 to -27.4‰) (Table 6.1). Variability in the butane and pentane compositions is similar. *Iso*-butane and *iso*-pentane compositions are essentially identical to the corresponding n-butane and n-pentane values (Table 6.1).

Chung plots (Chung et al., 1988) show substantial variation in the absolute values of the carbon isotopes and in the shapes of the curves (Figures 6.7 and 6.8). We identified 9 groups of gas samples. Two groups of samples (groups 1 and 2) show reversals in the slope of the Chung plots from C2 to *n*-C_4 and/or *n*-C_5. These are generally located along or near the major WNE-ESE fault structure that bisects Greater Natural Buttes field (Figure 6.9).

Five groups (3-7) (Figures 6.7 and 6.8) have nearly parallel curves on Chung plots, distinguished only by differences in isotopic composition for each compound. Group 3 has the most positive (heaviest) compositions ($\delta^{13}C_{C1}$ = -32.0‰, $\delta^{13}C_{n\text{-}C5}$= -22.9‰), while Group 7 has the most negative (lightest) compositions ($\delta^{13}C_{C1}$ = -39.0‰, $\delta^{13}C_{n\text{-}C5}$= -26.5‰). These groups typically show a profile that flattens somewhat in the C_2 to C_5 range. There appears to be no systematic geographic distribution for these groups (Figure 6.10).

Groups 8 and 9 (Figures 6.7 and 6.8) are distinguished by steeper slopes on the Chung plot than Groups 3 to 7. Group 8 shows very little flattening between C_2 and C_5, while Group 9 shows more flattening in this range. These groups are widely distributed across the Greater Natural Buttes Field (Figure 6.11).

The carbon isotopic composition of CO_2 exhibits significant variation at Greater Natural Buttes Field (Table 6.1, Figure 6.12), averaging -5.6‰ but ranging from as negative as -17.7‰ to as positive as -1.6‰. The very negative (light) value from the Love 1121-7N well on the southern edge of the field was a substantial outlier; the next most negative CO_2 value was -7.7‰, recorded in the Love 1121-2M well.

Hydrogen isotopes

The average hydrogen isotopic composition of production gases (Table 6.1) exhibited a smaller range of values than in other fields. The δD_{C1} at Jonah averaged -168.9‰, and ranged from -158 to -183‰. Ranges of δD for the heavier gases -119 to -164‰ for C2, -109 to -143‰ for C3, -95 to -119‰ for *i*-C_4, --96 to -132‰ for *n*-C_4, -74 to -109‰ for *i*-C_5 and -92 to -127‰ for *n*-C_5.

The hydrogen isotopic composition of the gases is investigated with a set of $\delta^{13}C$ – δD cross-plots, one for each gas species (Figures 6.13). The methane data show that samples exhibit a wide range of $\delta^{13}C$ but a very limited range of δD. Other gas species exhibit tightly clustered values with respect to both $\delta^{13}C$ and δD. For most gas species, $\delta^{13}C$ shows no significant correlation to δD. *n*-C_4 is an exception, exhibiting a correlation of 0.68 between $\delta^{13}C$ and δD (figure 6.13E); *i*-C_4, *i*-C_5 and *n*-C_5 exhibit weak correlations of approximately 0.50 (Figures 6.13 D, F and G).

6.2.3 Integrated bulk compositions and isotopes

More details are apparent in cross-plots that are commonly used to interpret the origin of natural gases.

Figure 6.14, a Bernard plot (Bernard, 1977), is primarily used to distinguish biogenic from thermogenic gases. This plot examines the carbon isotopic composition of methane combined with the proportion of methane to ethane and propane. Thermogenic gases have distinctively more positive (heavier) isotopic compositions than biogenic gases and typically a higher proportion of ethane and propane, although with increasing thermal maturity, the ratio $C_1/(C_2+C_3)$ increases and $\delta^{13}C_{C1}$ becomes more positive. In this cross-plot, Greater Natural Buttes gas samples generally fall within the range of thermogenic gases for $C_1/(C_2+C_3)$ ratios. although a large fraction of the samples have $\delta^{13}C_{C1}$ values between -35.0 and -27.6‰, more positive (heavier) than Bernard considered to be the upper limit for methane isotopic compositions.

Figure 6.15 is one of a series of cross-plots devised by Schoell (1983) to examine the origin and maturity of gases. This plot utilizes the isotopic compositions of methane and ethane. Most samples fall within the field of marine-source thermogenic gas. Three samples lie within the range for coal-sourced gas.

Figure 6.16 is another of Schoell's (1983) cross-plots. This utilizes the wetness (C_{2-4})/C_{1-4}) and the $\delta^{13}C_{C1}$ and is similar to the Barnard plot (Figure 6.14). Many samples fall outside the normal range of thermogenic or associated gases in this cross-plot, with isotopic compositions that are more positive (heavier) than would be expected for gases with this degree of wetness. In other words, gases with wetness values in the range of 0.12 to 0.25 typically have isotopically more negative (lighter) compositions than many of the Greater Natural Buttes gases.

Figure 6.17, after Lorant et al. (1998) examines the ratio of C_2 to C_3 and the difference in carbon isotopic composition between these species, in order to distinguish gases derived by primary cracking of kerogen from those derived by various kinds of secondary cracking. Lorant et al. (1998) found that secondary cracking is generally indicated by a difference of more than 1 to 3‰ between C_2 and C_3. In this cross-plot, sample compositions are tightly clustered and lie in the field for thermogenic gases derived by primary cracking.

Figure 6.18 examines $\ln(C_1/C_2)$ versus $\ln(C_2/C_3)$ (after Prinzhofer and Huc, 1995) to distinguish the effects of secondary cracking from primary cracking; the criterion for secondary cracking is increased $\ln(C_2/C_3)$ in the absence of increased $\ln(C_1/C_2)$. In this cross-plot, most of the data describe a very tight cluster, particularly with respect to $\ln(C_2/C_3)$.

Figure 6.19 examines $\ln(C_1/C_2)$ versus the difference in carbon isotopic composition between these species. This plot, after Prinzhoffer and Huc (1995), attempts to identify leakage from reservoirs, maturity of source rocks and mixing of thermogenic and biogenic gas. Leaked gases are identified by a range of ($\delta^{13}{}_{C1}$- $\delta^{13}C_{C2}$), while maturity trends are identified by increased $\ln(C_1/C_2)$ concurrently with increased ($\delta^{13}{}_{C1}$- $\delta^{13}C_{C2}$). In the Greater Natural buttes data set, most samples are tightly clustered with a limited range of $\ln(C_1/C_2)$ and ($\delta^{13}{}_{C1}$- $\delta^{13}C_{C2}$). Two samples (NBU 1022-11F and NBU 176, both near the complex WNW-ESE fault structure that bisects Greater Natural Buttes Field) have similar $\ln(C_1/C_2)$ but small ($\delta^{13}{}_{C1}$- $\delta^{13}C_{C2}$) and one sample (621-05E) has a typical ($\delta^{13}{}_{C1}$- $\delta^{13}C_{C2}$) but unusually large $\ln(C_1/C_2)$.

6.2.4 Noble Gases

Noble gases serve to distinguish contributions from three primary sources: mantle, crust and atmosphere and to identify fractionation processes.

Crustal contributions to natural gas are dominated by ^{4}He and therefore crustal-derived gas is characterized by low ratios of ^{3}He/^{4}He. Samples from Greater Natural Buttes Field generally exceed the typical range of crustal sources of He (Figure 6.20). Samples also cluster relatively tightly in 1/^{4}He. Three of the samples with the highest ^{3}He/^{4}He ratios are located at the center

of the field along the major WNEW-ESE fault (Figure 6.22); these samples also exhibit roll-over in $\delta^{13}C$ of C_3, C_4 and C_5.

High concentrations of ^{22}Ne and ^{36}Ar are indicative of gases derived from the atmosphere, which typically enter natural gases through meteoric water; thus low ratios of $1/^{22}Ne$ and $1/^{36}Ar$ reflect contributions from meteoric water. Samples from Greater Natural Buttes Field exhibit a wide range values of $1/^{22}Ne$ (Figure 6.21 and 6.23), indicating degassing from meteoric water. Samples exhibiting low $1/^{22}Ne$ ratios are widely and non-systematically distributed across the field.

6.3 Mud Gases

Mud gas analyses come from 2 wells at Greater Natural Buttes Field, the NBU 921 2703 (16 samples) and STATE 1021-32 O (29 samples); the latter includes samples from a sidetrack well.

6.3.1 Bulk gas compositions

Gas compositions from mud gas samples are summarized in Table 6.2.

Bulk gas compositions from mud gas samples are similar to those determined from production gas samples. The methane fraction in mud gas averaged 0.89, as compared to 0.85 in production samples. Gas wetness in mud gas samples averaged 0.11, compared to 0.15 in production samples. The CO_2 fraction was not analyzed.

Production gas and mud gas data differed in the C_1/C_2 ratio, which was higher in the production gas data than in the mud gas data (18.19 versus 10.85). C_2/C_3 ratios were similar in mud gas and production gas data.

The State 1021-32O well shows a clear pattern of decreasing wetness with depth (Figure 6.24). Samples in the range of 3500 to 7000 feet, which is within the Wasatch section, have gas wetness values of 0.24 to 0.34. Samples become drier below this depth in the Mesaverde, and the three deepest samples between 8331 and 8991 feet are all pure methane. Samples from the NBU 921-27D3AS well are almost entirely within the Mesaverde Formation and with the exception of two samples, have relatively dry compositions (≤7% C_{2+} gases).

In the State 1021-32O well, C_2/C_3 ratios show a small increase in the same interval in which gas wetness decreases substantially (Figure 6.25). Our C_2/C_3 data are too sparse to reach a conclusion about the NBU 921-27D3AS well.

6.3.2 Carbon and Hydrogen Isotopic Composition

<u>Carbon isotopes</u>

Carbon isotopic compositions of gas species from mud gas samples are summarized in Table 6.2.

The $\delta^{13}C$ of mud gases are very similar to the production gases. The $\delta^{13}C_{C1}$ of mud gas averaged 1.6‰ more negative (heavier) than the production gas . Other than that, the average of mud gas species was within 1‰ of the production gases.

The $\delta^{13}C_{C1}$ profiles are quite different in the two wells (Figure 6.26). The NBU 921-27D3AS well varies within a fairly narrow range, at a minimum of -40.4‰ approximately 600 feet above the top Mesaverde contact, increasing to a maximum of -34.8‰ approximately 2000 feet below the contact, then decreasing to -39.7‰. In the State 1021-32O well, compositions were relatively positive (heavy) within the Wasatch section, ranging from -35.5 to -29.0‰. Below the top of the Mesaverde, compositions were extremely variable, ranging from -48 to -31‰ over very short stratigraphic distances.

We applied Chung plots to the mud gas data. In the NBU 921 27O3 AS well, three distinct groups are defined, based on the Chung plots, which largely coincide with depth ranges (Figure 6.27). The shallow group is characterized by very negative (light) $\delta^{13}C_{C1}$ values (-38.8 to -40.4‰) and nearly flat profiles from C_2 to C_5. The intermediate depth group has less negative $\delta^{13}C_{C1}$ values (-34.8 to -37.3 ‰) and isotopic reversal from C_2 to C_5. The deep group has a diverse range of isotopic compositions but typically no reversal and relatively positive (heavy) $\delta^{13}C_{C5}$ values (-16.7 to -25.7‰).

Samples from the State 1021-32O well divide into five groups based on Chung plots (Figure 6.28). One of these has a distinctive behavior in the heavier gases, with isotopically lighter propane and butane than ethane and pentane ('kinked reversal') (Figure 6.28A). Two of the three samples from this group are the shallowest two samples in the well (Figure 6.29), from above the Wasatch section. Two groups exhibits distinct reversal, with lighter pentane or butane than ethane or propane; these two groups are distinguished by relatively light $\delta^{13}C_{C1}$ methane (Figure 6.28B) and relatively heavy methane (Figure 6.28C). These two groups come from the Wasatch Formation and the upper part of the Mesaverde section.. These samples are clustered at the base of the Wasatch and top of the Mesaverde units (Figure 6.29). The fourth group is characterized by relatively flat profiles in the C_2 to C_5 range between -25 and -30‰ and light methane between -44 and -48‰ (Figure 6.28D). These samples are restricted to the

lower part of the Mesaverde section (Figure 6.29) at depths where gases transition downward to much drier compositions. The fifth group is characterized by normal Chung plots without reversal, with continuously increasing $\delta^{13}C$ from methane to pentane and a wide range of $\delta^{13}C_{C1}$ from -30 to -46‰ (Figure 6.28E). These gases are primarily found in the Wasatch and upper part of the Mesaverde (Figure 6.29), where compositions are relatively wet.

Hydrogen isotopes

The hydrogen isotopic compositions from mud gas samples are summarized in Table 6.2.

The δD of mud gases are systematically more negative (lighter) than production gases by 9 to 17‰, except for *n*-C4 and *n*-C5, where the compositions are almost identical.

The δD_{C1} data are quite different in the two wells for which we have mud gas profiles (Figure 6.30). In the State 1021-32O well, δD_{C1} values are relatively positive in the Wasatch section, reaching values as positive (heavy) as -160‰. Values begin to decrease systematically at the Wasatch-Mesaverde contact (6880 feet), declining to -218‰ at 8587 feet. The downward transition to lighter H/D ratios coincides with increased dryness in the mud gas samples. The deepest sample in this well at 8921 feet suggests an increase in δD_{C1} to -170‰.

The NBU 921-27D3AS does not show the sharp decrease in δD_{C1} at the Mesaverde contact, with values between -183 and -156‰ in the Mesaverde section.

6.3.3 Integrated Bulk Compositions and Isotopes

The cross-plot of C_2/C_3 versus $\delta^{13}C_{C2}$- $\delta^{13}C_{C3}$ can indicate primary cracking versus different types of secondary cracking, where low values are typical of primary cracking and elevated values indicate secondary cracking from oil.

The mud gas data from both wells fall primarily within the primary cracking field (Figure 6.31). A few points, mostly from the State 1021-32O well, fall slightly across the boundary into the secondary cracking field.

6.4 Interpretation

6.4.1 Variability in production and mud gas composition

Much of production gas from Greater Natural Buttes Field ranges in wetness between 0.10 and 0.20 (Table 6.1, Figure 6.3). A few wells produce wetter gases, between 0.20 and 0.30. Only three wells produce drier gas, with wetness values that are less than 0.05; two of these are located on the main WNE-ESE fault system that bisects the Greater Natural Buttes field.

C_2/C_3 ratios in production wells, also measure of gas wetness, ranges between 1.26 and 2.93 (Figure 6.4). The correlation between gas wetness and C2/C3 ratios is low (-0.43), suggesting that these parameters are vary independently.

Both wells analyzed for mud gas compositions also exhibit considerable variability in composition. One well (State 1021-32O) had gas wetness values ranging from 0.34 to 0.00; the second (NBU 921-27D3AS) from 0.26 to 0.00 (Figure 6.24). In the former well, there was an apparent trend of decreasing gas wetness with depth; in the latter, there was no obvious trend. Stratigraphic variability in C_2/C_3 ratios was also evident (Figure 6.25).

Differences in bulk gas composition can result from varying input from different source rocks, varying maturity of one source rock, different cracking processes (primary cracking of kerogen, secondary cracking of oil, secondary cracking of wet gas), or migration effects.

6.4.2 Thermal maturity of source rocks

The carbon isotopic composition of gases (C_1, C_2 and C_3) can be used to infer the thermal maturity of the gas sources at the time of generation (Figures 6.32, 6.33, 6.34).

The thermal maturities estimated from the carbon isotopic composition of production gas suggest a range of maturities at which gas was generated, from a vitrinite reflectance of 1.5 to 2.5%. Because the data form a nearly linear trend of $\delta^{13}C_{C2}$ versus $\delta^{13}C_{C3}$, the isotopic composition of either C_2 or C_3 can be as a proxy for thermal maturity, where the more positive (heavier) compositions indicate higher thermal maturity. The map of $\delta^{13}C_{C2}$ shows no clear spatial pattern, with gases of relatively negative compositions occurring near gases of relatively positive composition, suggesting that the central fault system provides no significant pathway for the piping of deep, more mature gases to shallow reservoirs.

Maturities estimated from the carbon isotopic composition of mud gas samples (Figure 6.33 and 6.34) define a similar trend and can also be interpreted to indicate thermal maturities. The range of maturities predicted is greater, from 1.2% R_o to as much as 3.0% R_o. A somewhat larger range of maturities is indicated for the State 1021-32O well than for the NBU 921 2703 well. When mud gas compositions for the State 1021-32O well are distinguished by formation, the data suggest that the Wasatch gases were generated at higher thermal maturities than the Mesaverde gases; in other words, the shallow formation contains the more mature gases.

6.4.3 Control on gas composition by source or secondary alteration

We first summarize some key observations about gas compositions at Greater Natural Buttes Field:

5) Compositions for all parameters (wetness, carbon or hydrogen isotopes, noble gases) show no systematic spatial distribution, with the exception that gases showing partial reversal on Chung plots (generally taken to indicate a contribution from secondary cracking of oil) are clustered near the major northwest-southeast trending fault through the field.

6) Production gases exhibit a significant range in $\delta^{13}C_{C1}$, from -39.6 to -27.7‰. $\delta^{13}C_{C1}$ is moderately correlated with $\delta^{13}C_{C2}$ (correlation coefficient of 0.61) suggesting that similar processes controlled these gas species.

7) The isotopic composition of CO_2 was not notably light, with the exception of one sample with a composition of -17.7‰. Five samples out of 23 had isotopic compositions between 0 and -4‰ and the remainder had compositions between -4 and -8‰. There was no systematic geographic distribution to $\delta^{13}C_{CO2}$ values.

8) In one well, mud gas compositions become systematically dryer below the Wasatch section, coinciding with generally decreased (lighter) $\delta^{13}C_{C1}$ and δD_{C1}. The $\delta^{13}C$ is generally lighter (more negative) in the Mesaverde than in the Wasatch, suggesting that gases in the Mesaverde could have been generated at lower maturity than gases in the overlying Wasatch Formation. Wasatch gases are also more commonly characterized by partial reversal on Chung plots, consistent with a contribution from secondary cracking.

9) A number of wells indicate contributions from deep sources of gas, based on noble gas compositions. Similarly noble gas data from a number of wells suggest some level of degassing of meteoric water.

These observations suggest that there are two sources of gas that mix to varying degrees at Greater Natural Buttes:

a) A relatively dry, isotopically light gas without reversal. This gas is typical of the deeper Mesaverde section in the State 1021-32O well.

b) A relatively wet, isotopically heavier gas that exhibits partial isotopic reversal; this gas is evident of the Wasatch section in the State 1021-32O well and production wells near the large NW-trending structure that bisects the Greater Natural Buttes Field.

The wet Wasatch gases are relatively mature, indicated both by the relatively heavy isotopic composition of the $\delta^{13}C_{C2}$ and $\delta^{13}C_{C3}$ and by rollover in the Chung plots. The dry Mesaverde gases are relatively immature; the fact that they are dry suggests that they have a coaly Type III source. The mature wet gases could themselves be formed by either secondary cracking of oil and / or by mixing from sources.

With one exception, gases from Greater Natural Buttes Field show little evidence of substantial bacterial oxidation. In other data sets, this type of alteration is indicated by isotopically heavy methane, isotopically light CO_2, very dry gas compositions and noble gas compositions with low $1/^{22}Ne$. While a few production gases contain methane with relatively heavy ^{13}C (three samples heavier than -30‰), few samples contain CO_2 with notably light ^{13}C. This suggests that the heavy ^{13}C was probably source controlled rather than affected by later alteration, particularly since samples with heavy ^{13}C do not have low $1/^{22}Ne$.

6.4.4 Evidence of Secondary Cracking

Neither the production gas nor mud gas data provide evidence of secondary cracking of wet gas to dry gas. Gas compositions have relatively low C_2/C_3 ratios, indicating the relative abundance of wetter gases, and relatively small differences between $\delta^{13}C_{C2}$ and $\delta^{13}C_{C3}$. In addition, decreasing $\delta^{13}C_{C2}$ associated with very dry gases (called “rollover”) is now being used to interpret secondary cracking of wet gas to dry gas (Zumberge et al., 2012; Burruss and Laughrey, 2010). These interpretations require that ethane compositions be isotopically lighter than methane; that does not occur in our samples (Figure 6.35).

While the well-defined partial isotopic reversals in our data cannot be interpreted as resulting from the cracking of wet gas to dry gas, we suggest that they can be interpreted to result from

the cracking of oil to wet gas. Such an interpretation would be consistent with the high maturities inferred from the isotopic composition of the ethane.

6.4.5 Internal Seals (Compartmentalization) within the Gas Column and Migration

The higher maturity gas, regardless of its origin (mixed or derived from secondary cracking of oil), formed at a deeper level than the dry gas. It then migrated upward and then laterally into the Wasatch and upper Mesaverde reservoir in some locations, including the State 1021-32O well. The fact that this gas is not found in the lower part of the Mesaverde reservoir (eg. in the deeper part of the State 1021-32S section) could be because (a) the Wasatch and Upper Mesaverde had higher effective permeability, allow the lateral migration of hydrocarbons, (b) the deeper part of the Mesaverde already had gas in the pore system that could not be displaced by the later generated wet gas, or (c) relative permeability effects prevented the migration of wet gas into the deeper Mesaverde section.

The spatial variability in the composition of production gas suggests that migration varied on a local scale, specifically vertical pathways allowed the deeper gas to migrate upward and fill shallow reservoirs in places, but that this did not occur pervasively. These pathways were probably fracture systems.

Similarly, two wells sampled for mud gases exhibit quite different vertical trends: one showing decreased wetness and lighter carbon and hydrogen isotopic composition of methane with depth, while the other does not. The overall range of compositions exhibited by mud gases is similar to that of production gases.

6.5 References

Bernard, B., Brooks, J.M., & Sackett, W.M. (1977). A geochemical model for characterization of hydrocarbon gas sources. Ninth Annual Offshore Technology Conference, OTC 2934, p. 435-438.

Burruss, R. C., and Laughrey, C. D. (2010). Carbon and hydrogen isotopic reversals in deep basin gas: Evidence for limits to the stability of hydrocarbons. *Organic Geochemistry*, *41*(12), 1285-1296.

Chung, H.M., Gormly, J.R., & Squires, R.M. (1988). Origin of gaseous hydrocarbons in subsurface environments. Theoretical considerations of carbon isotope distribution, in M. Schoell (Guest Editor), Origins of Methane in the Earth: Chemical Geology, v. 71, p. 97-103.

Cuzella, J. J., & Stancel, S. G. (2006). Greater Natural Buttes Field, Uinta Basin, Utah: 2006 Rocky Mountain Natural Gas Geology and Resource Conference, 6 pp.

Lorant, F., Prinzhofer, A., Behar, F., & A. Y. Huc (1998). Carbon isotopic and molecular constraints on the formation and the expulsion of thermogenic hydrocarbon gases: Chemical Geology, v. 147, p. 249–264.

Rice, D.D. (1993). Composition and Origins of Coalbed Gas. In eds., Ben E. Law and D.D. Rice, AAPG Studies in Geology #38, p. 159-184.

Schoell, M. (1983). Genetic characterization of natural gases: AAPG Bulletin, v. 67, p. 2225-2238.

Tang, Y., Perry, J. K., Jenden, P. D., & Schoell, M. (2000). Mathematical modeling of stable carbon isotope ratios in natural gases. *Geochimica et Cosmochimica Acta*, *64*(15), 2673-2687.

Zumberge, J., Ferworn, K., & Brown, S. (2012). Isotopic reversal ('rollover') in shale gases produced from the Mississippian Barnett and Fayetteville formations. *Marine and Petroleum Geology*, *31*(1), 43-52.

Table 6.1. Summary of compositions of Greater Natural Buttes production gases.

	minimum	average	maximum
C1 (fraction)	0.75	0.85	1.00
C2 (fraction)	0.00	0.073	0.122
C3 (fraction)	0.00	0.040	0.079
i-C4 (fraction)	0.00	0.010	0.019
n-C4 (fraction)	0.00	0.014	0.031
i-C5 (fraction)	0.00	0.006	0.013
n-C5 (fraction)	0.00	0.006	0.015
CO_2 (fraction)	not analyzed	not analyzed	not analyzed
Wetness	0.00	0.150	0.251
$\delta^{13}C_{C1}$ (‰)	-39.6	-35.2	-27.6
$\delta^{13}C_{C2}$ (‰)	-28.7	-25.9	-21.1
$\delta^{13}C_{C3}$ (‰)	-27.4	-24.7	-21.5
$\delta^{13}C_{i\text{-}C4}$ (‰)	-27.4	-24.8	-21.5
$\delta^{13}C_{n\text{-}C4}$ (‰)	-28.1	-24.5	-21.0
$\delta^{13}C_{i\text{-}C5}$ (‰)	-27.2	-24.4	-20.4
$\delta^{13}C_{n\text{-}C5}$ (‰)	-27.0	-24.1	-20.8
$\delta^{13}C_{CO2}$ (‰)	-17.2	-5.6	-1.6
δD_{C1} (‰)	-183	-168.9	-158
δD_{C2} (‰)	-164	-138.5	-119
δD_{C3} (‰)	-143	-128.0	-109
$\delta D_{i\text{-}C4}$ (‰)	-119	-109.5	-95
$\delta D_{n\text{-}C4}$ (‰)	-131.9	-117.5	-96
$\delta D_{i\text{-}C5}$ (‰)	-109	-95.0	-74
$\delta D_{n\text{-}C5}$ (‰)	-127	-114.4	-92

Table 6.2. Average Compositions of Greater Natural Buttes Field Mud Gas Samples

	Minimum	Average	Maximum
C1 (fraction)	0.65	0.89	1.00
C2 (fraction)	0.00	0.06	0.15
C3 (fraction)	0.00	0.03	0.10
i-C4 (fraction)	0.00	0.007	0.031
n-C4 (fraction)	0.00	0.007	0.033
i-C4 (fraction)	0.00	0.003	0.015
n-C4 (fraction	0.00	0.002	0.013
CO_2 (fraction)	NA	NA	NA
Wetness	0.00	0.11	0.34
$\delta^{13}C_{C1}$ (‰)	-48.4	-36.79	-29.2
$\delta^{13}C_{C2}$ (‰)	-30.6	-25.76	-18.5
$\delta^{13}C_{C3}$ (‰)	-28.7	-24.08	-14.5
$\delta^{13}C_{i\text{-}C4}$ (‰)	-28.0	-23.76	-16.9
$\delta^{13}C_{n\text{-}C4}$ (‰)	-28.4	-23.72	-15.1
$\delta^{13}C_{i\text{-}C5}$ (‰)	-26.8	-23.88	-17.5
$\delta^{13}C_{n\text{-}C5}$ (‰)	-26.9	-23.92	-16.7
$\delta^{13}C_{CO2}$ (‰) *	-13.4	-9.34	-2.7
δD_{C1} (‰)	-218	-179.0	-153
δD_{C2} (‰)	-274	-149.4	-123
δD_{C3} (‰)	-204	-144.7	-122
$\delta D_{i\text{-}C4}$ (‰)	-131	-119.2	-109
$\delta D_{n\text{-}C4}$ (‰)	-147	-120.0	-99
$\delta D_{i\text{-}C5}$ (‰)	-118	-106.2	-86
$\delta D_{n\text{-}C5}$ (‰)	-141	-115.2	-88

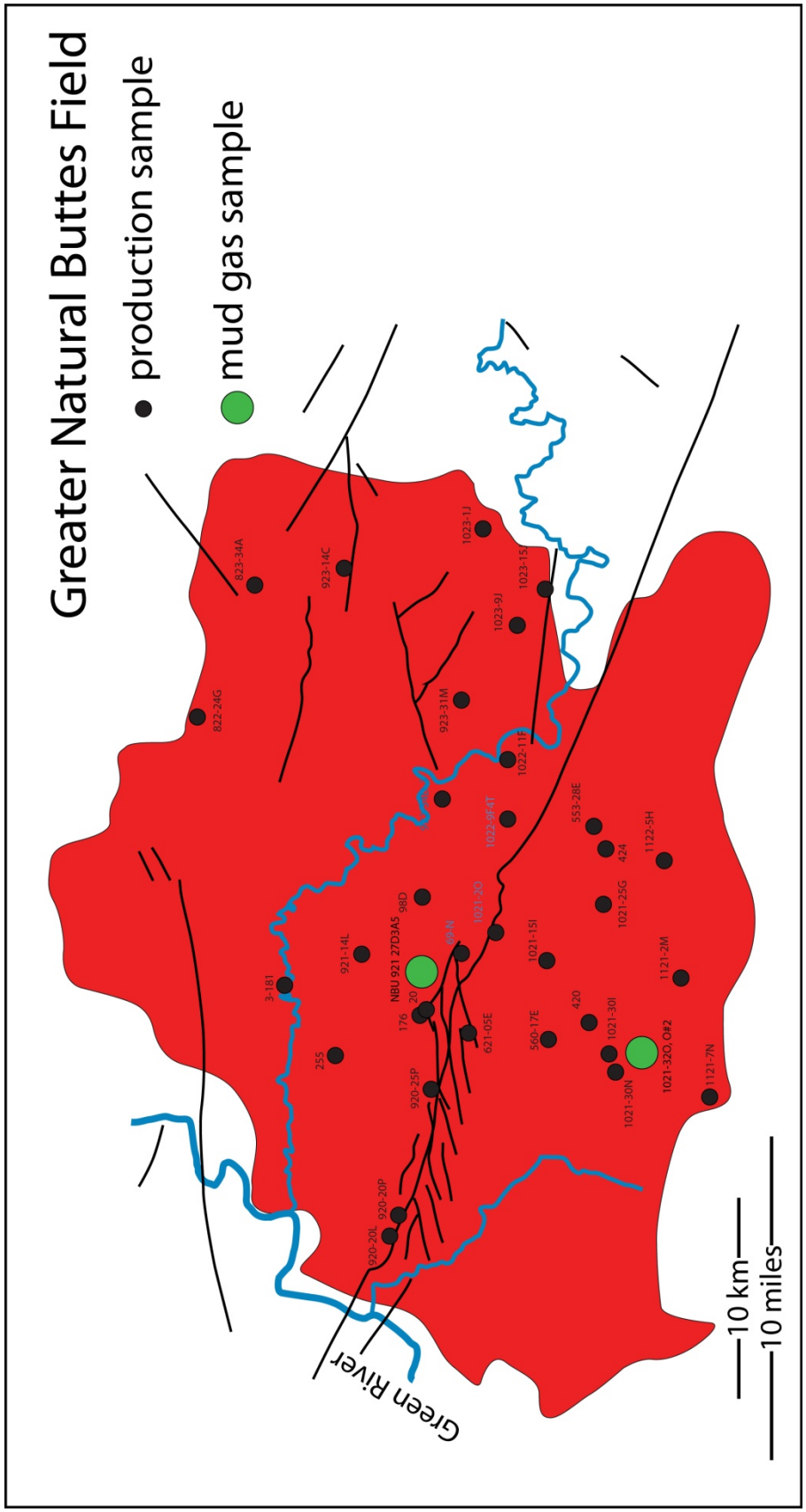

Figure 6.1. Map of Greater Natural Buttes Field, showing the locations of production gas samples and two wells sampled for mud gas profiles.

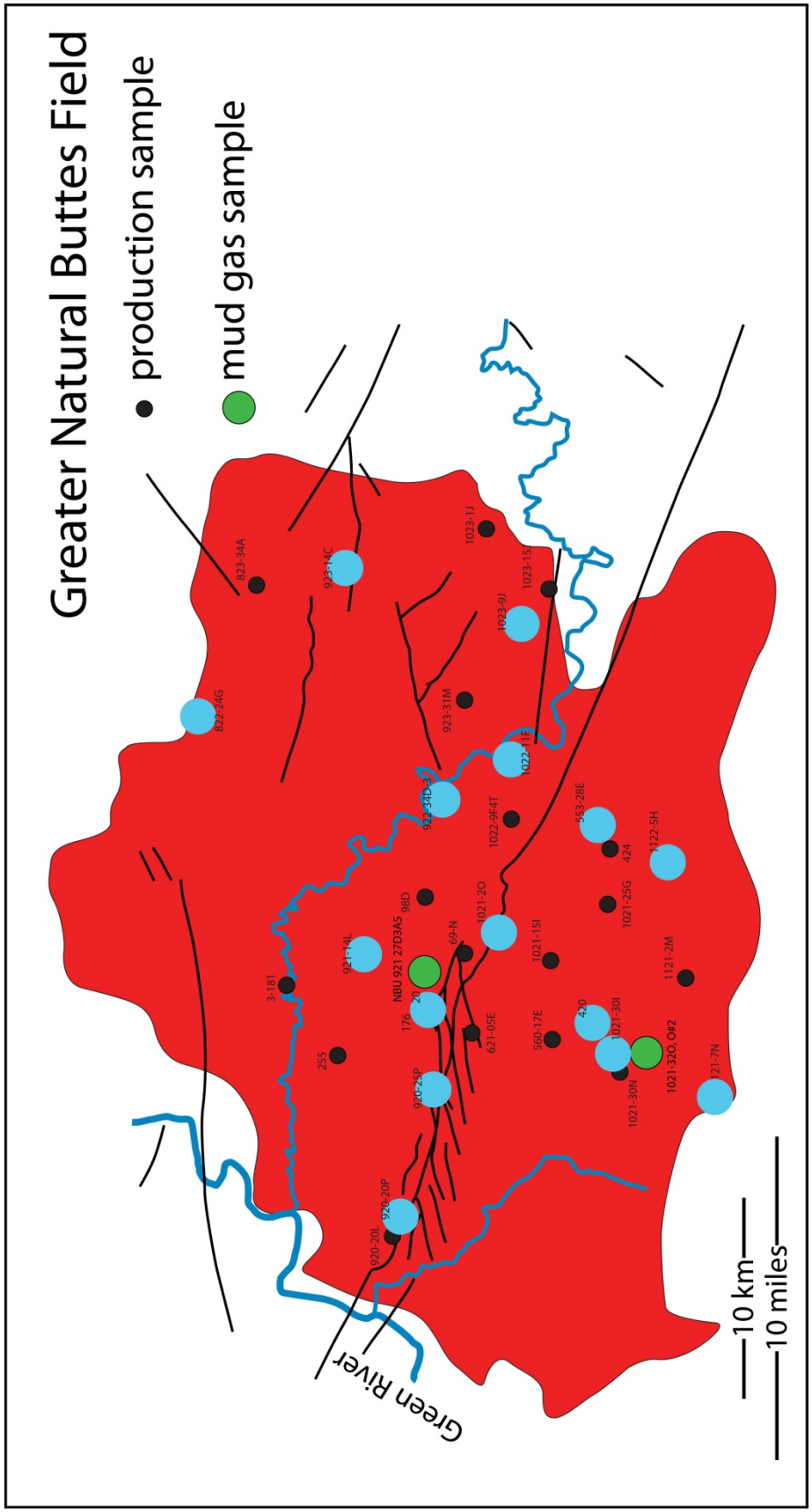

Figure 6.2. Map of Greater Natural Buttes Field, showing the locations of production gas samples for noble gas analysis.

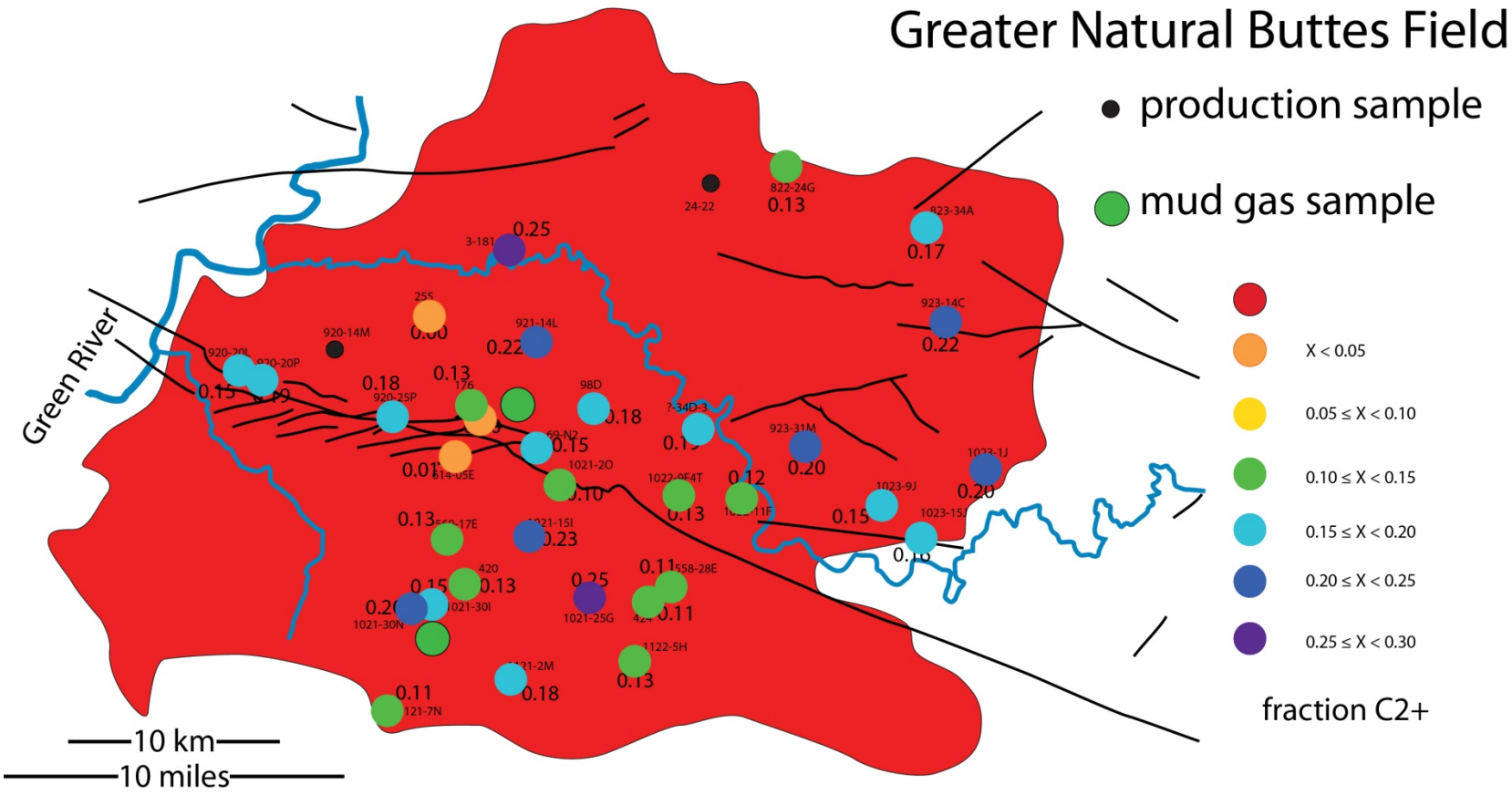

Figure 6.3. Map of gas wetness in production wells at Greater Natural Buttes Field.

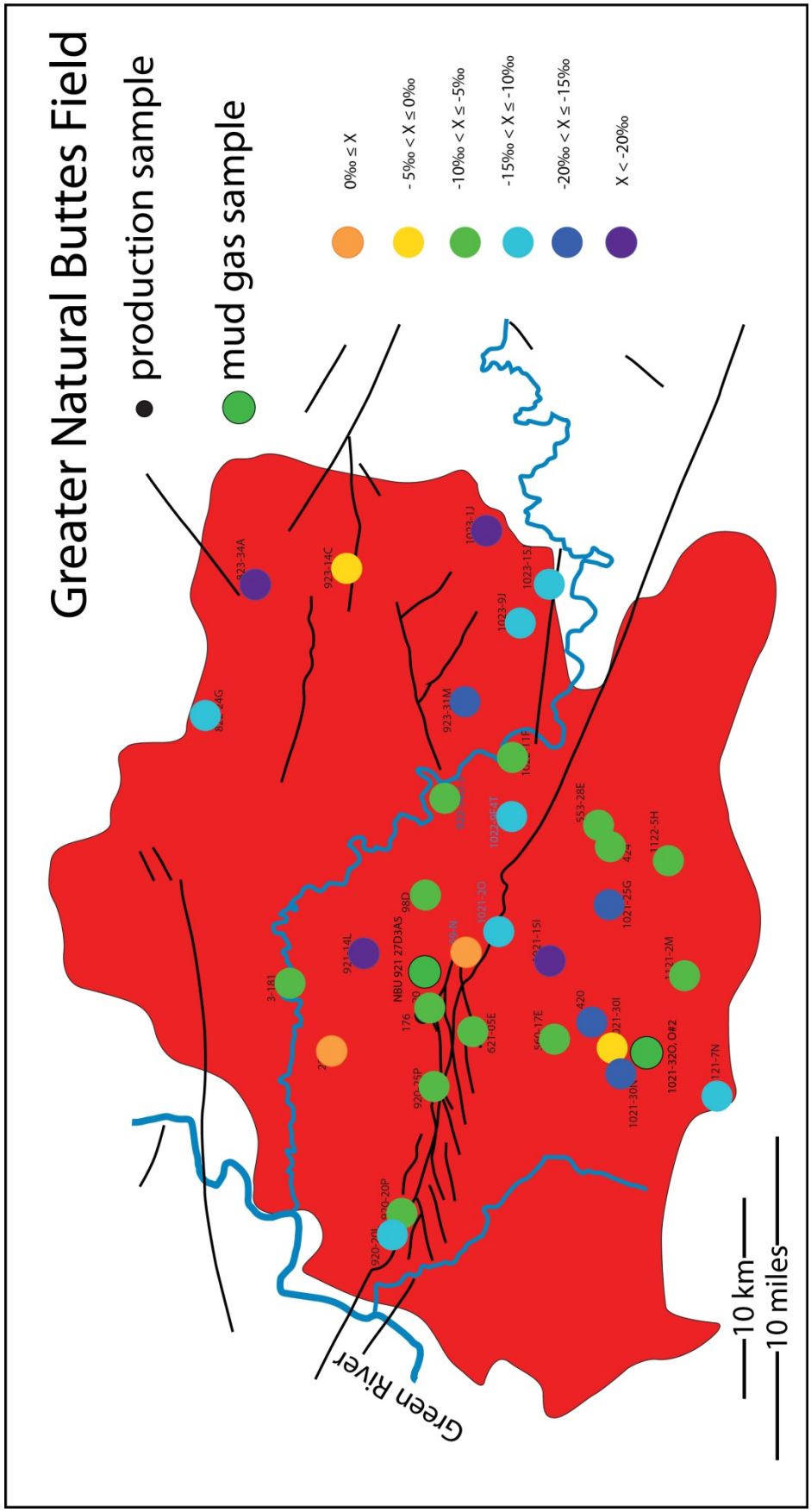

Figure 6.4. Map of C_2/C_3 ratios in production wells at Greater Natural Buttes Field.

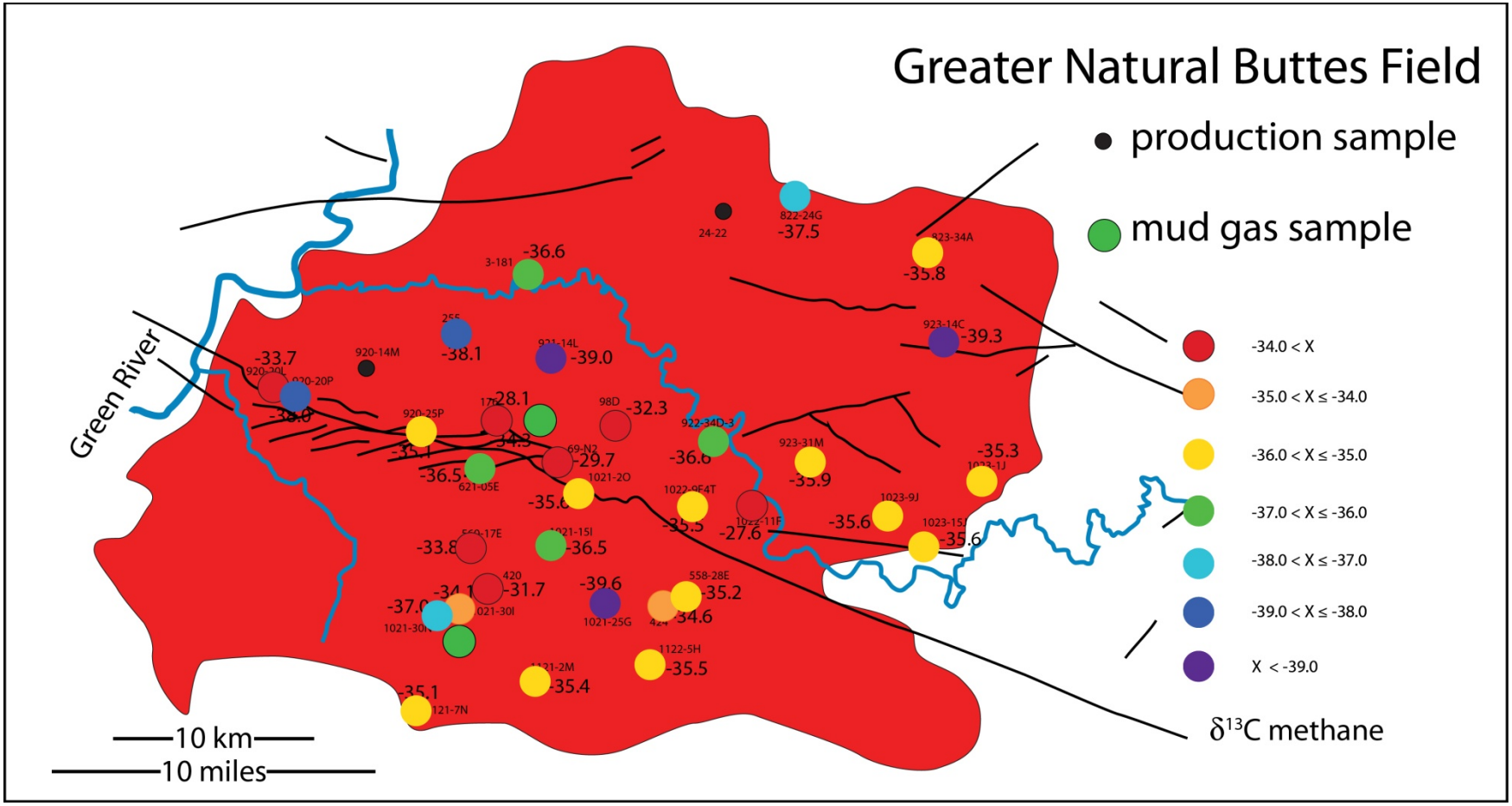

Figure .65. Carbon isotopic composition of C_1 ($\delta^{13}C_{C1}$) in production gas samples from Greater Natural Buttes Field.

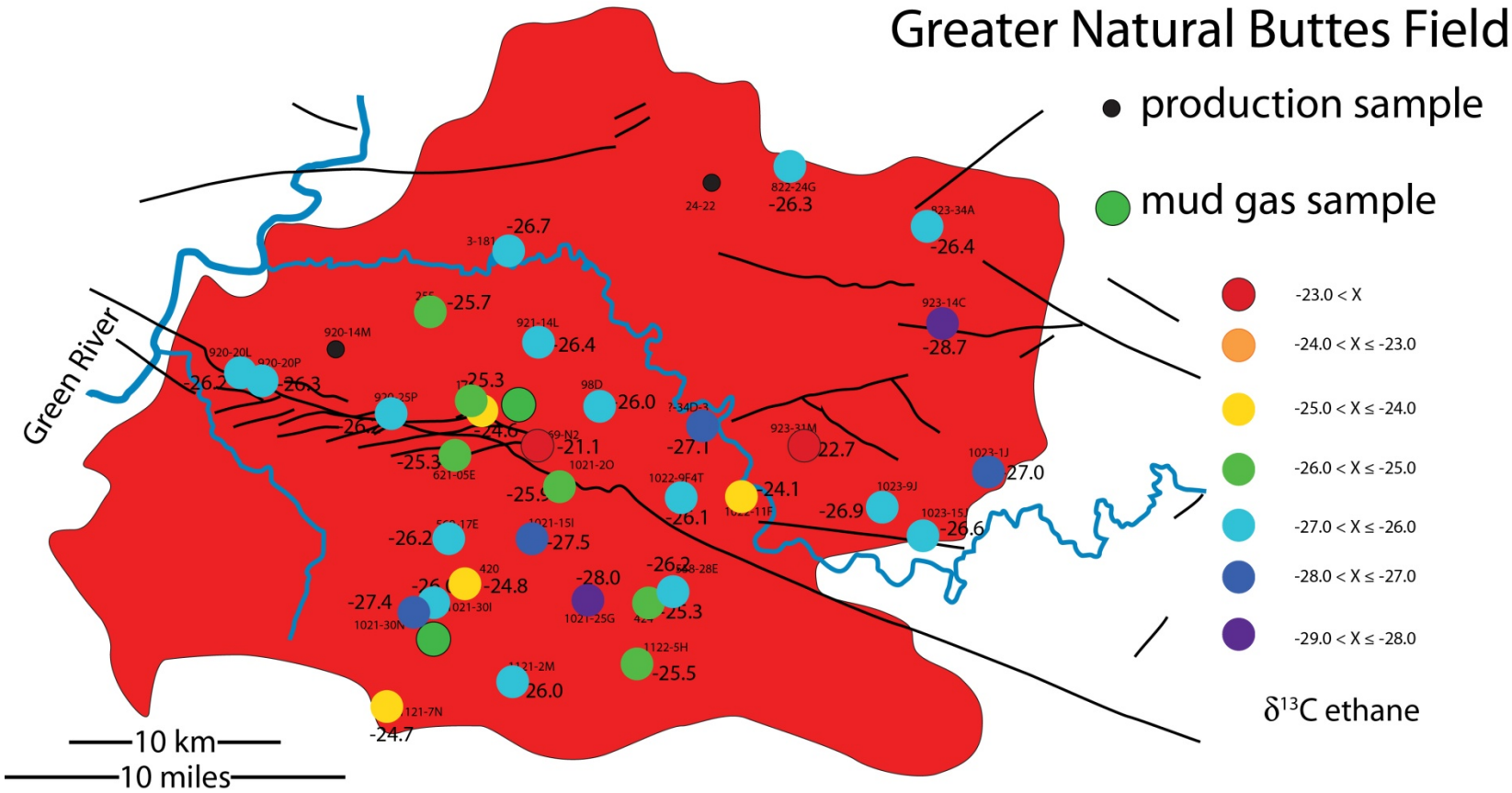

Figure 6.6. Carbon isotopic composition of C_2 ($\delta^{13}C_{C2}$) in production gas samples from Greater Natural Buttes Field.

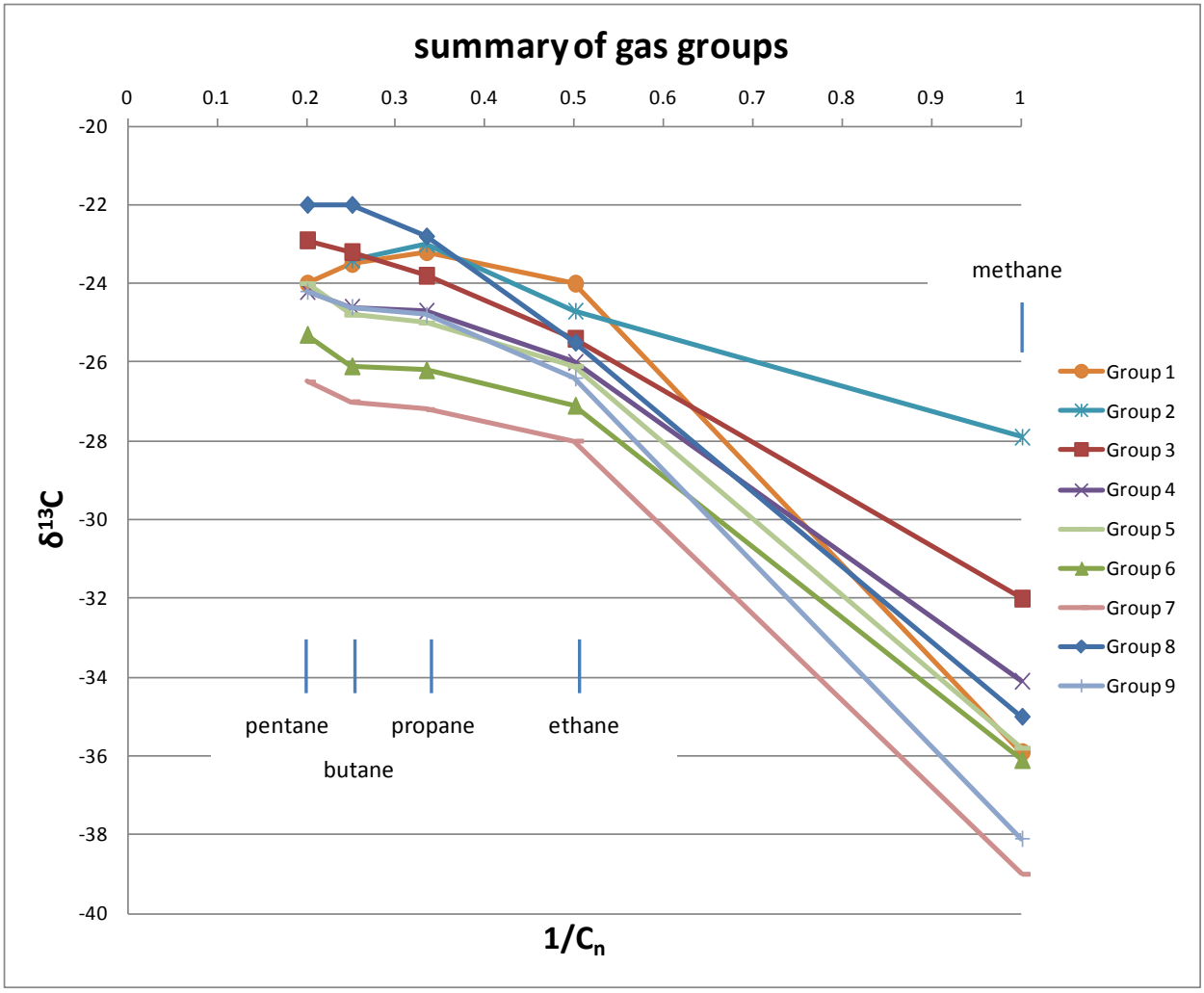

Figure 6.7. Summary of production gas groups, based on Chung plots. Individual groups are shown in the following figure.

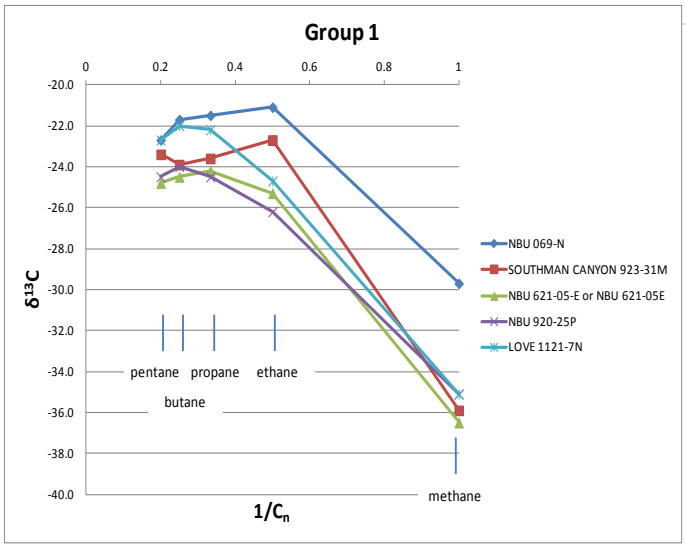

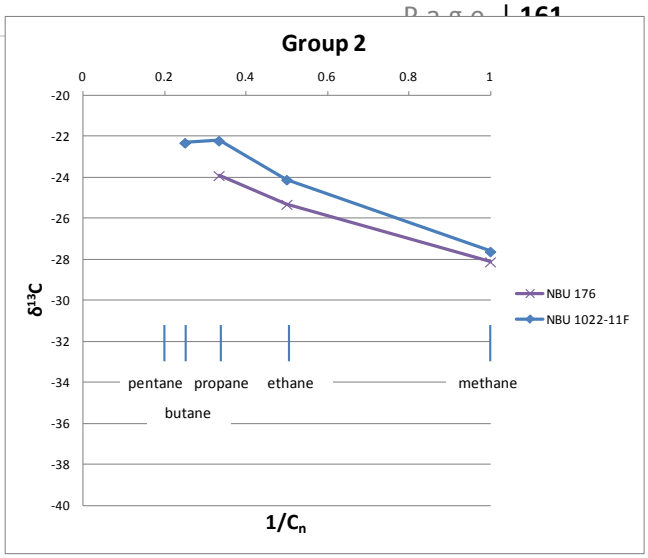

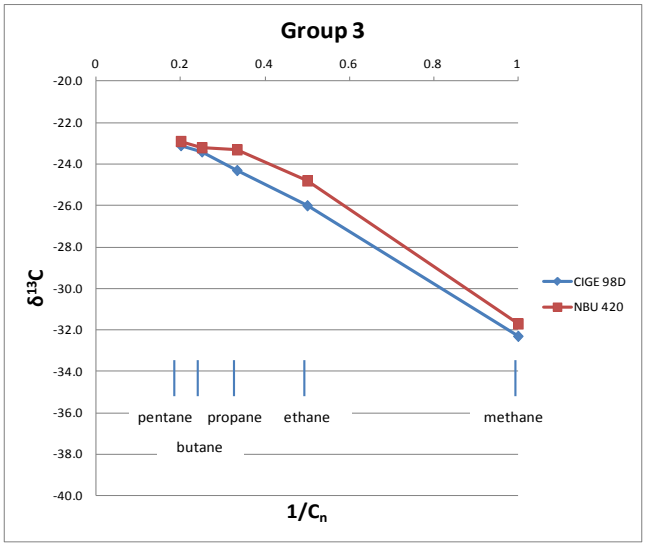

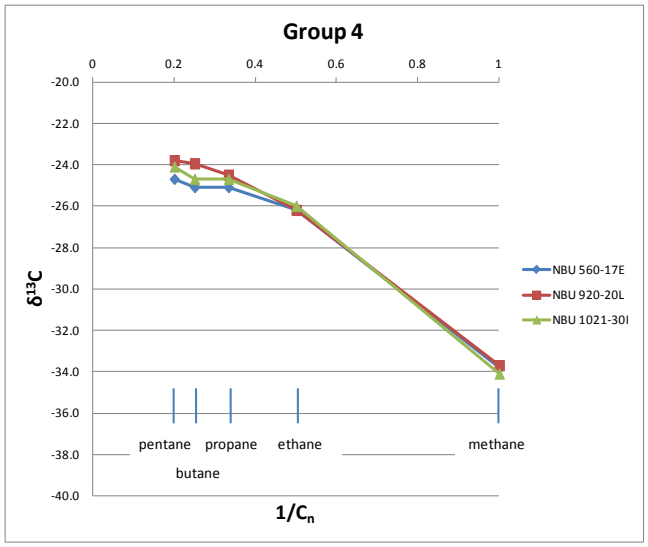

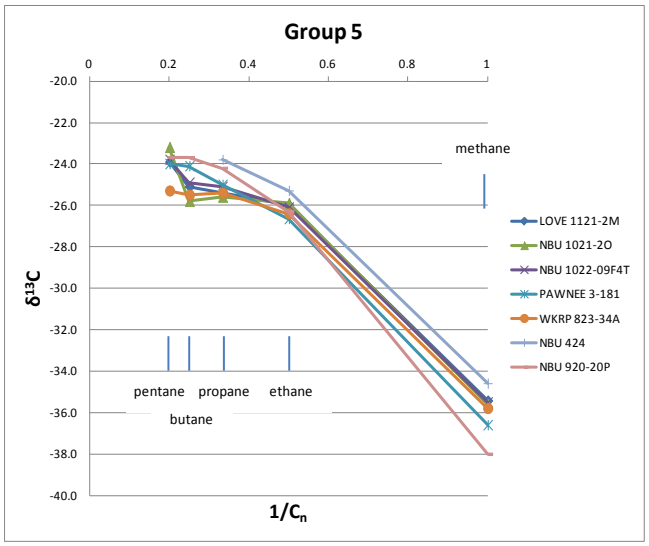

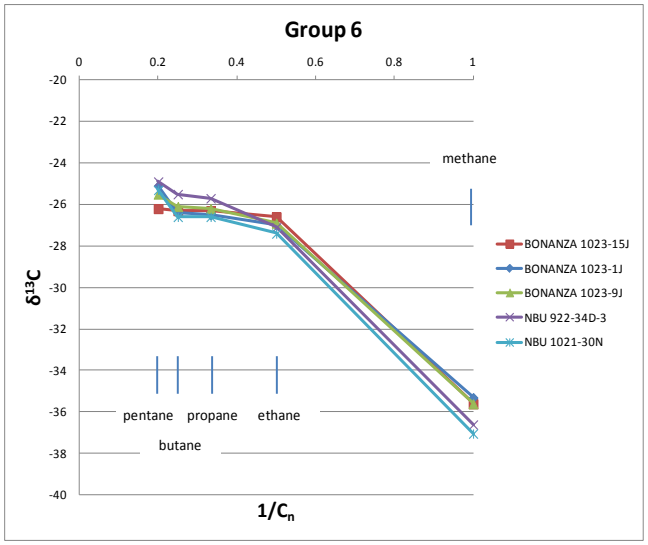

Figure 6.8a-f. Chung plots showing carbon isotopic composition of gases from Greater Natural Buttes Field. Each group represents a set of wells with similar gas isotopic characteristics.

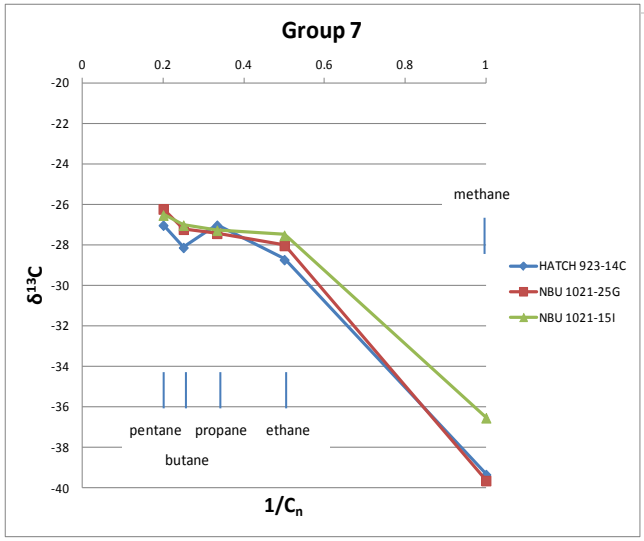

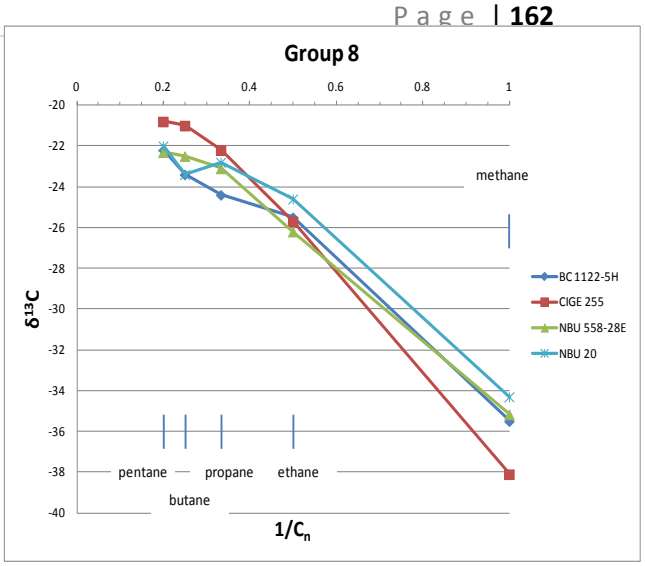

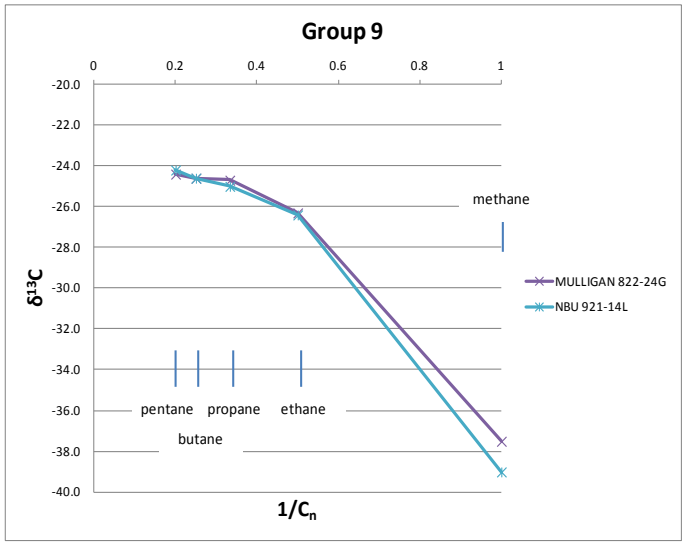

Figure 6.8g-i. Chung plots showing carbon isotopic composition of gases from Greater Natural Buttes Field. Each group represents a set of wells with similar gas isotopic characteristics.

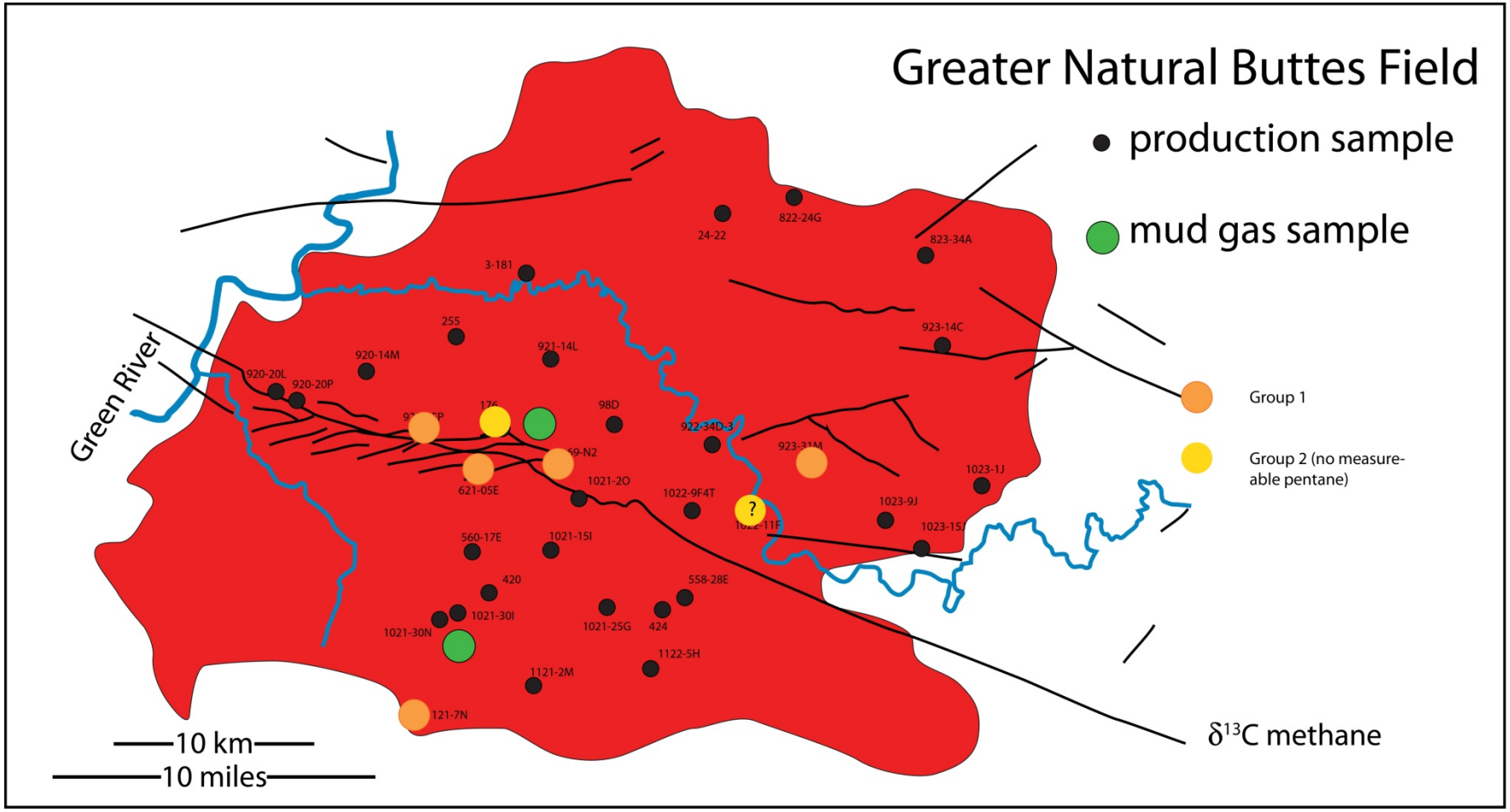

Figure 6.9. Location of samples with reversals on Chung plots (for example, $\delta^{13}C_{C5} < \delta^{13}C_{C4}$) in composition of C3, C4 and/or C5). Groups refer to families of gas compositions shown in Figure 6.8.

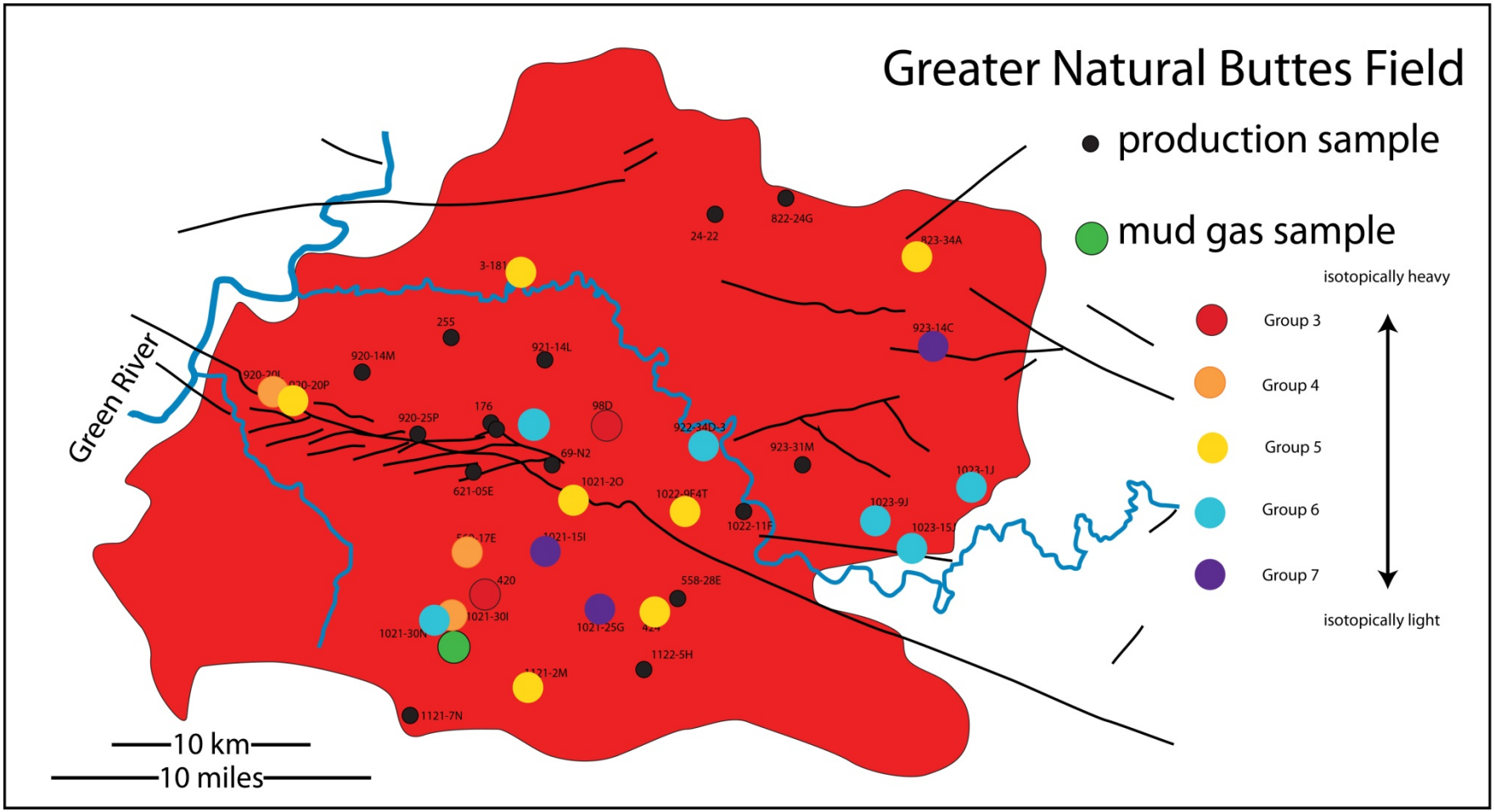

Figure 6.10. Location of wells with normal (unreversed) Chung plots, shown from isotopically heavy (red, orange) to intermediate (yellow) to isotopically light (blue, purple). Groups refer to families of gas samples with similar isotopic composition, shown in Figure 6.8.

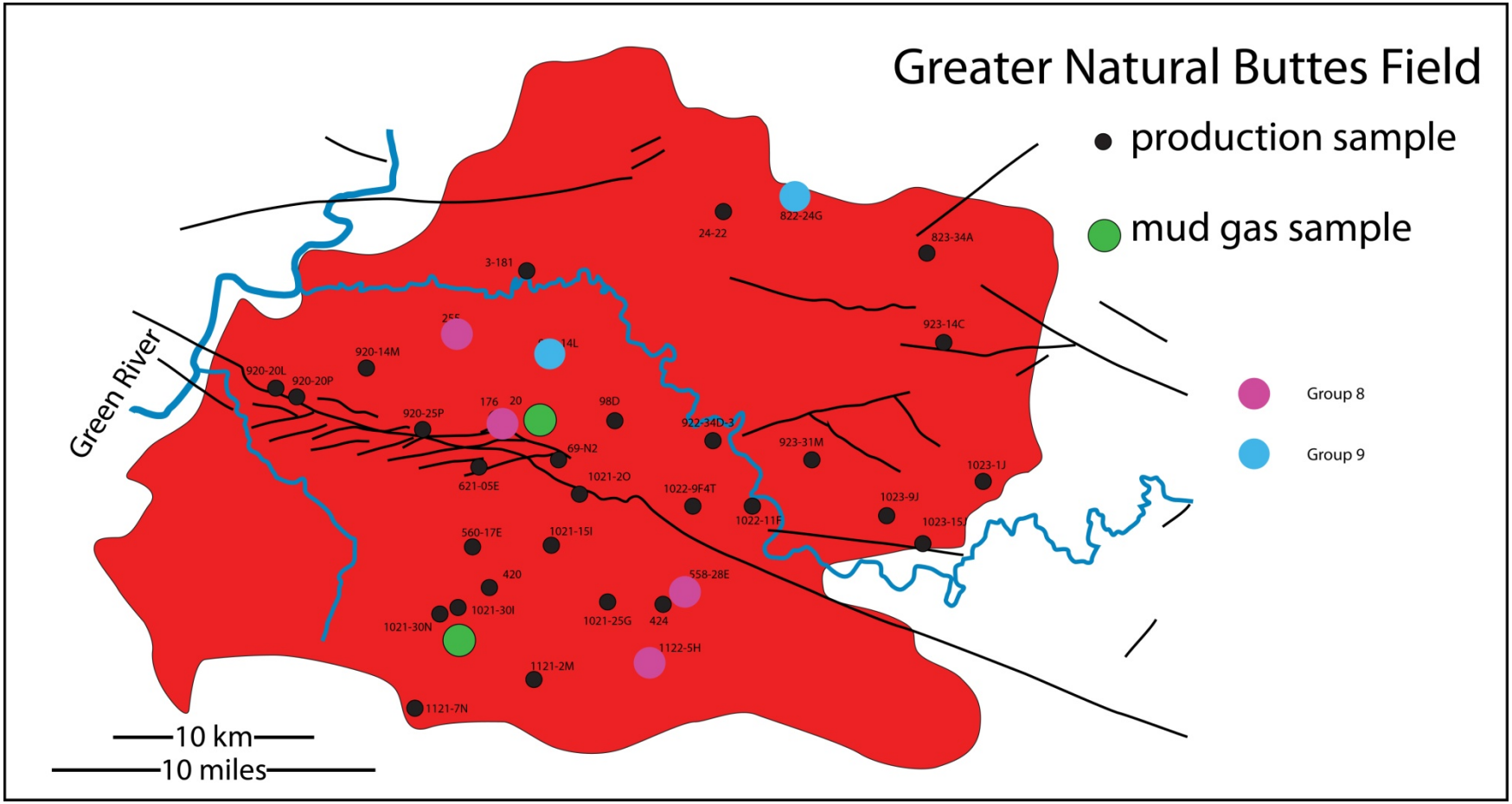

Figure 6.11. Location of wells with anomalously steep unreversed slopes on Chung plots (Groups 8 and 9). Groups refer to families of isotopically similar gases, shown in Figure 6.8.

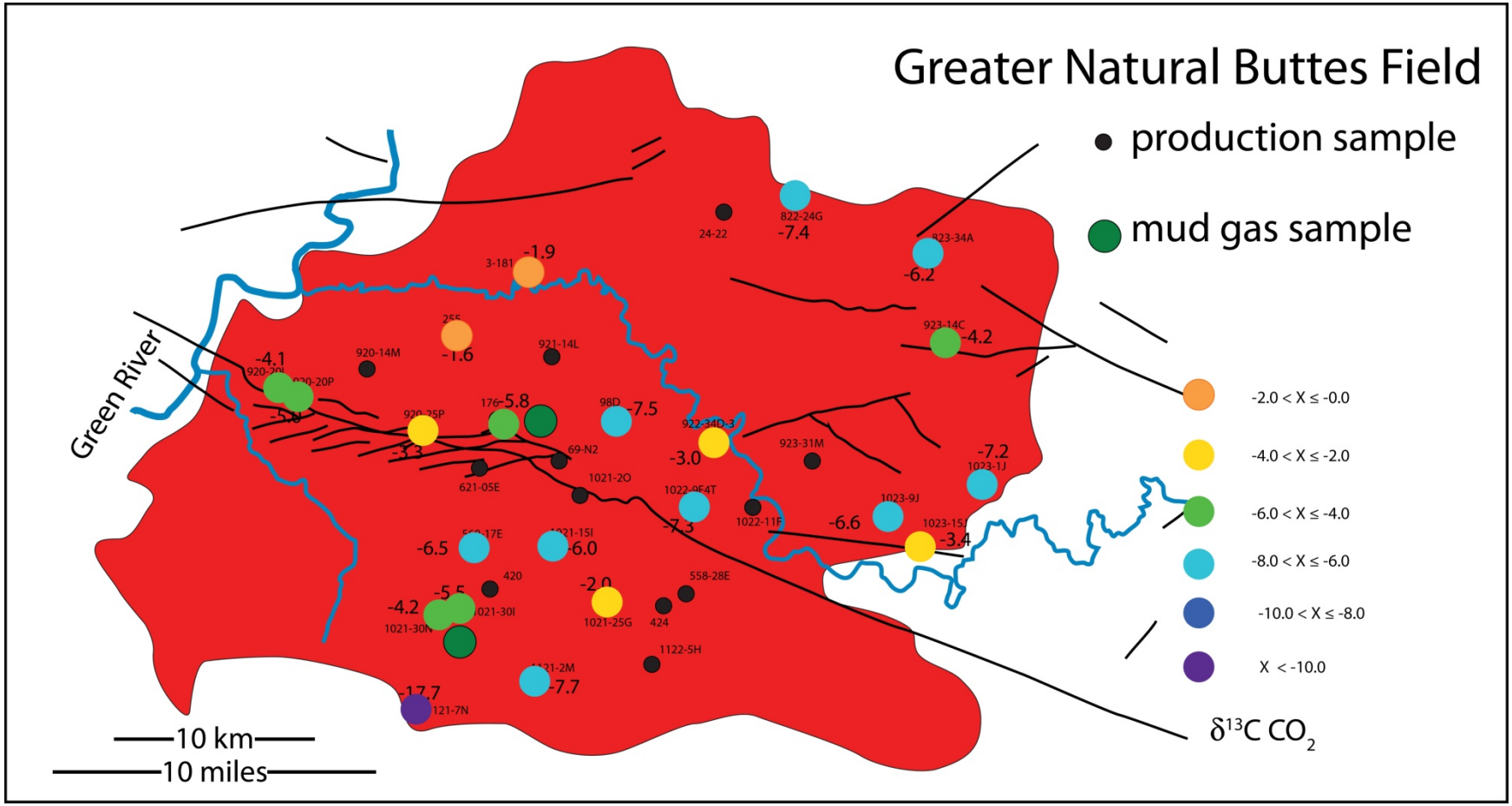

Figure 6.12. Carbon isotopic composition of CO_2 in Greater Natural Buttes production gas samples..

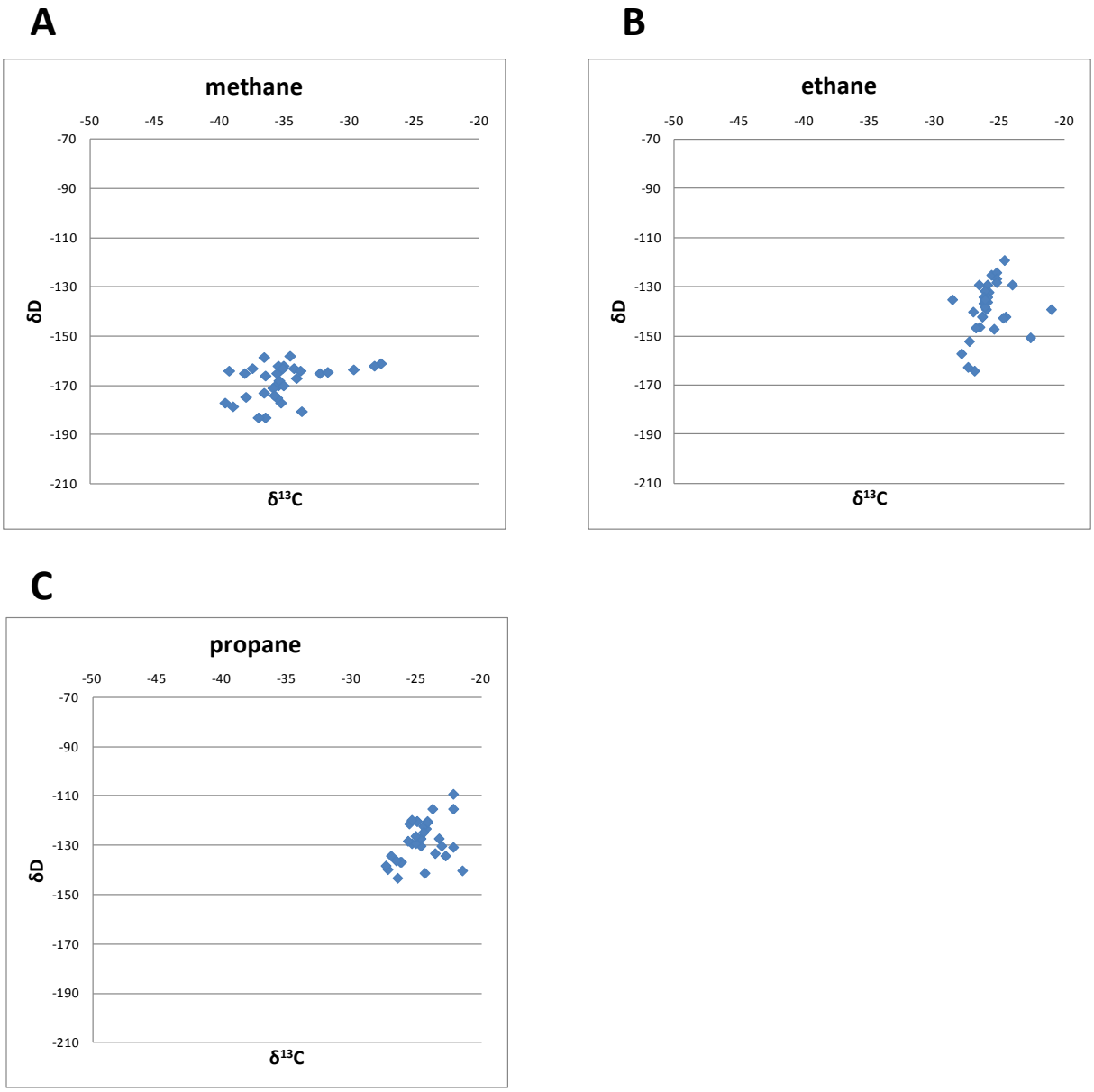

Figure 6.13A-G. Carbon and hydrogen isotopic composition of hydrocarbon gases from Greater Natural Buttes Field.

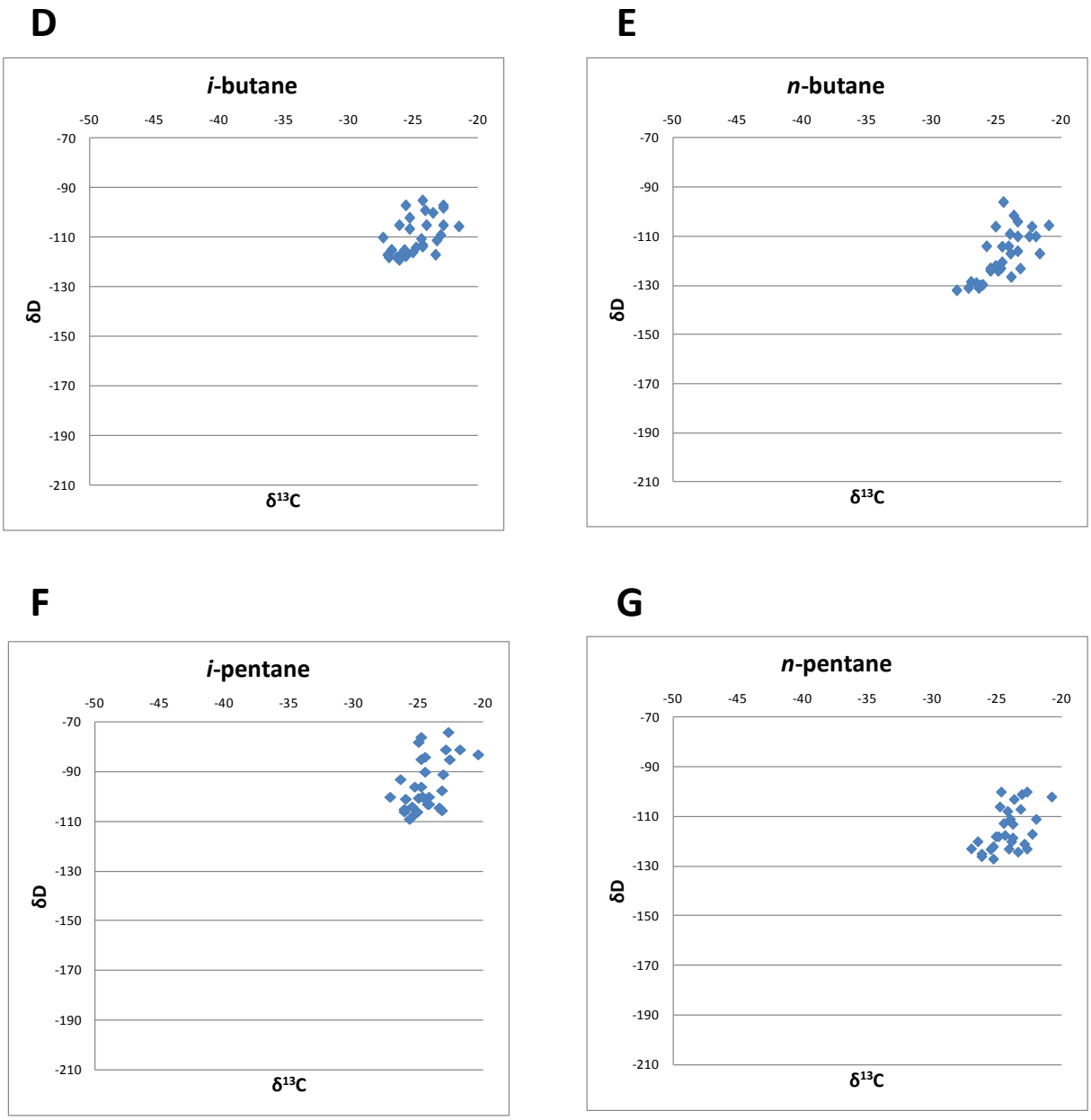

Figure 6.13A-G. Carbon and hydrogen isotopic composition of hydrocarbon gases from Greater Natural Buttes Field.

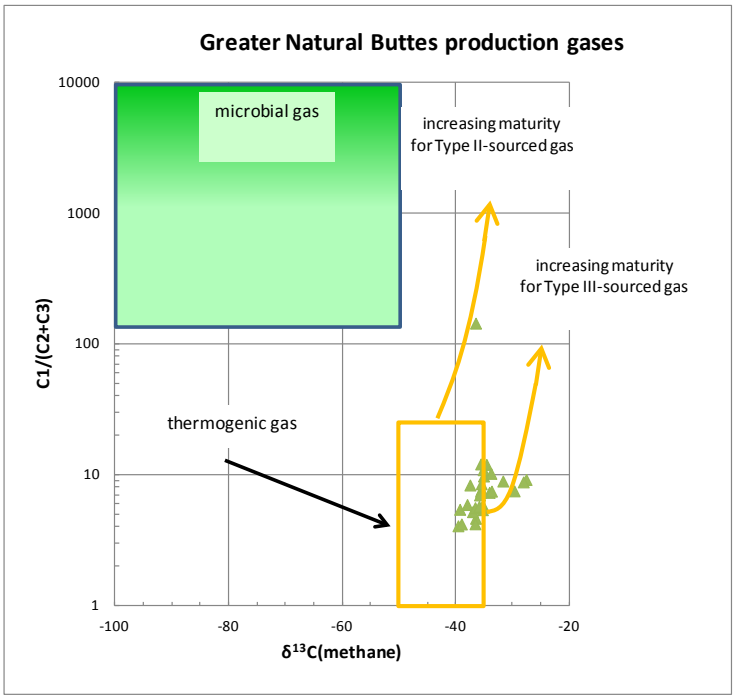

Figure 6.14. Carbon isotopic composition of methane versus the ratio of C_1 to C_2+C_3. Gases largely fall within the region for thermogenic gases.

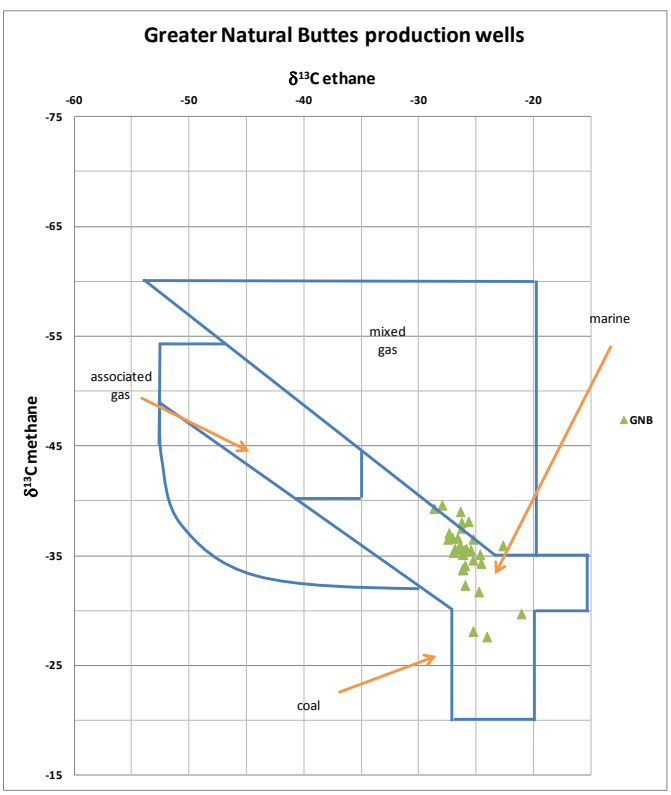

Figure 6.15. Carbon isotopic composition of methane versus ethane, after Schoell (1983). Gas compositions largely fall within the range of gases generated through primary cracking of marine kerogen. In this case, gases plotting with relatively high $\delta^{13}C_{C1}$ are not the product of mixing with biogenic gases.

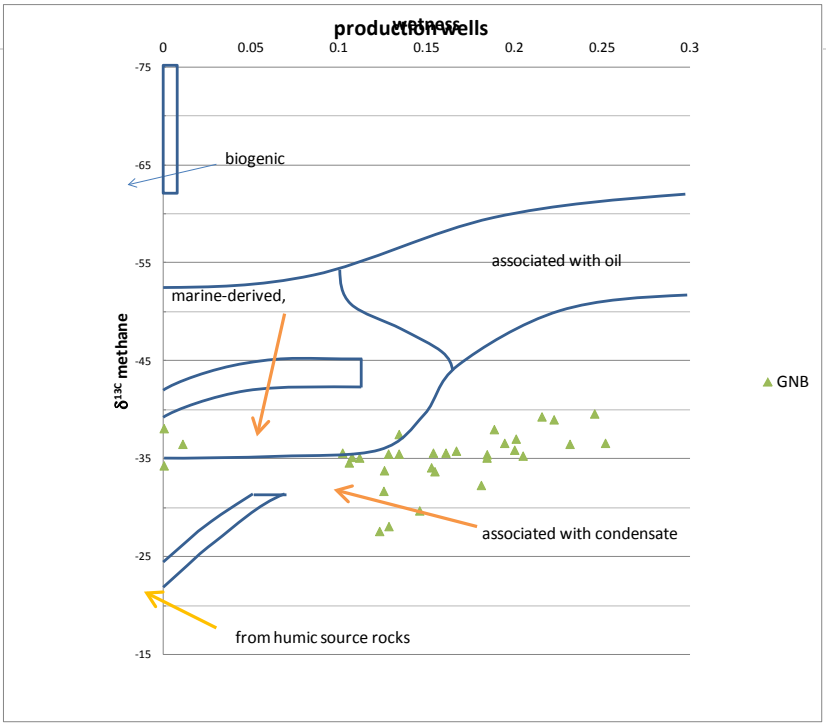

Figure 6.16. Carbon isotopic composition of $\delta^{13}C_{C1}$ versus ethane (after Schoell, 1983). This plot is similar to the Bernard plot (Figure X.21). Many of the samples have anomalously positive (heavy) methane carbon isotopic compositions.

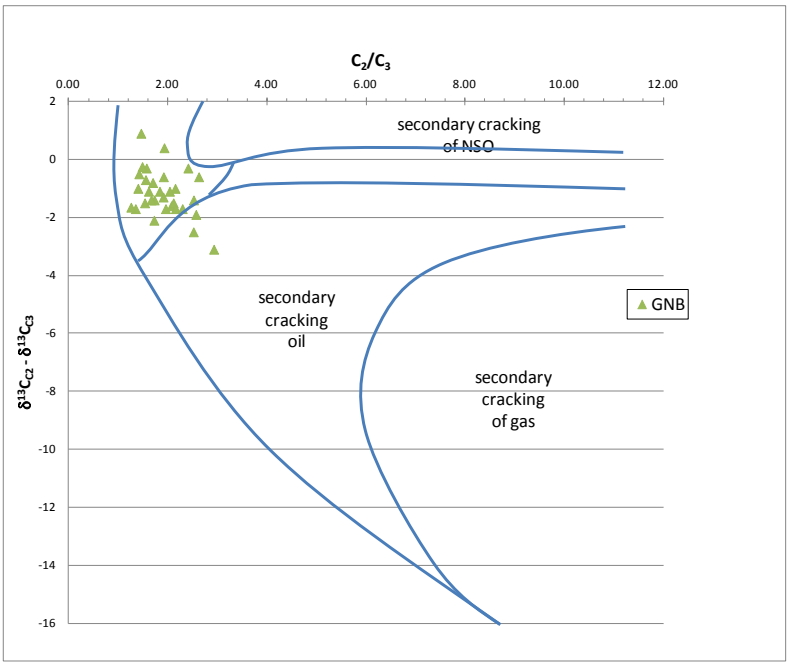

Figure 6.17. Ratio C_2/C3 versus the difference in carbon isotopic composition between C_2 and C_2 (after Lorant et al., 1998). This plot distinguishes gases derived from primary cracking from those derived from secondary cracking. This plot suggests that production gases are largely derived from primary cracking of kerogen.

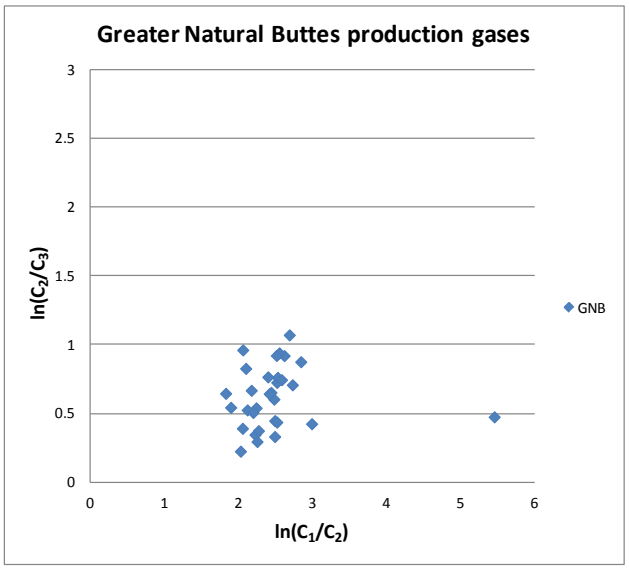

Figure 6.18. Ratio of $\ln(C_1/C_2)$ versus $\ln(C_2/C_3)$ after Prinzhofer and Huc (1995) can be used to distinguish the effects of secondary cracking from primary cracking, where increasing $\ln(C_2/C_3)$ in the absence of increasing $\ln(C_1/C_2)$ can indicate secondary cracking. Production gas data show no evidence of secondary cracking

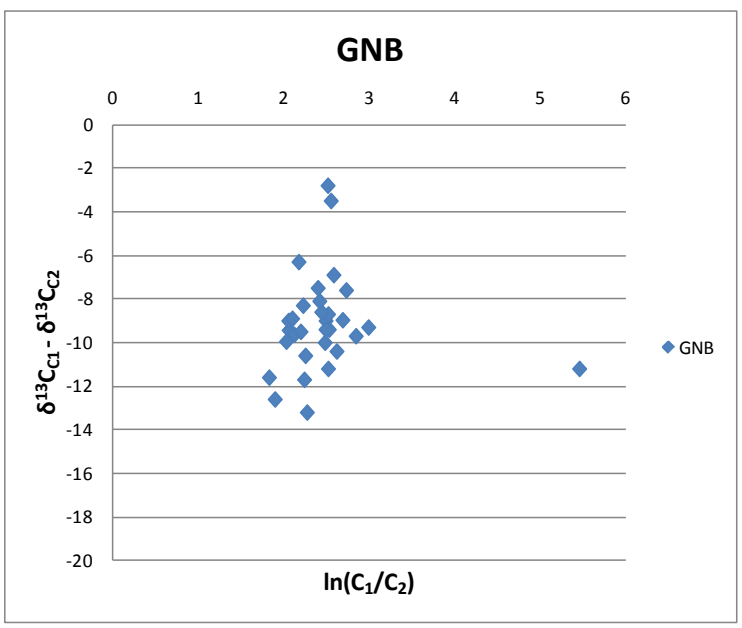

Figure 6.19. Ratio of $\Delta\delta^{13}C_{C1\text{-}C2}$ versus $\ln(C_1/C_2)$ after Prinzhofer and Huc (1995) is used to differentiate maturation trends from leakage. Diagonal trends indicate maturation effects. Gases from both the overpressured Lance reservoirs and normally pressured Lance show similar wide ranges of composition. It is not possible to distinguish leakage or maturation effects in this cross-plot.

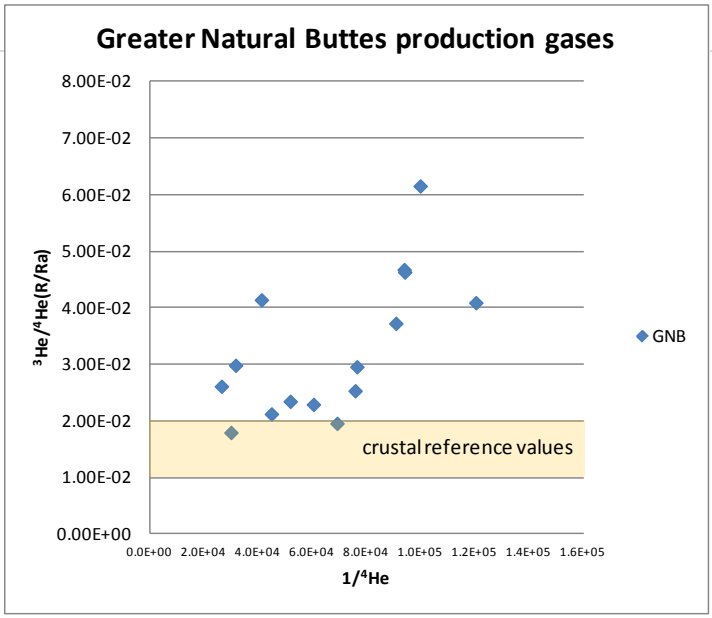

Figure 6.20. $^3He/^4He$ ratios are indicative of contributions of gas from crustal or other sources. Gas compositions from Jonah Field are tightly clustered in the field for crustal-sourced He.

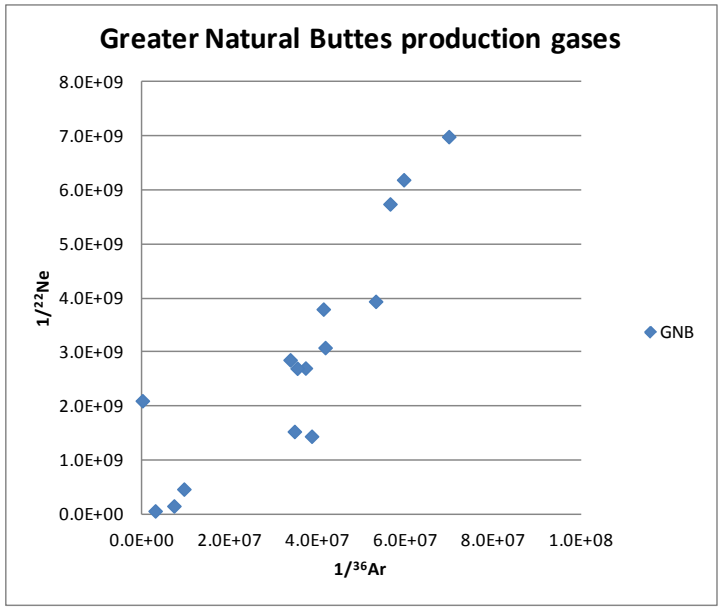

Figure 6.21. ^{22}Ne and ^{36}Ar concentrations are indicative of contributions of gas from atmospheric sources, typically through degassing from meteoric water. Gases from Jonah Field have low values for $1/^{22}Ne$ and $1/^{36}Ar$ and describe a linear trend, indicating a significant but variable contribution from meteoric water. One sample that falls off the linear trend is from the least productive well in the data set.

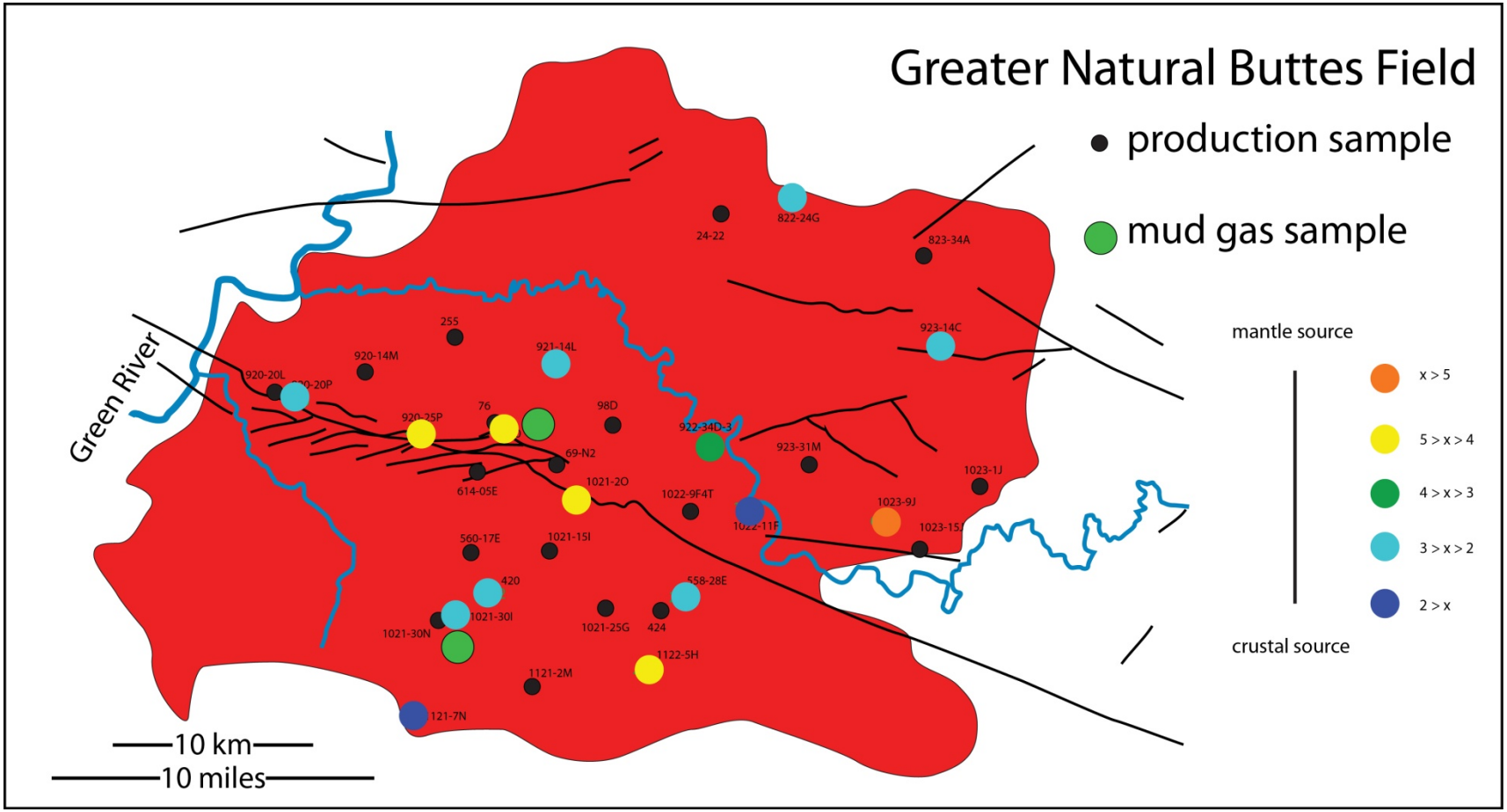

Figure 6.22. 3He/4He ratios in Greater Natural Buttes production gas samples.. High values (orange, yellow) indicate contributions from mantle sources.

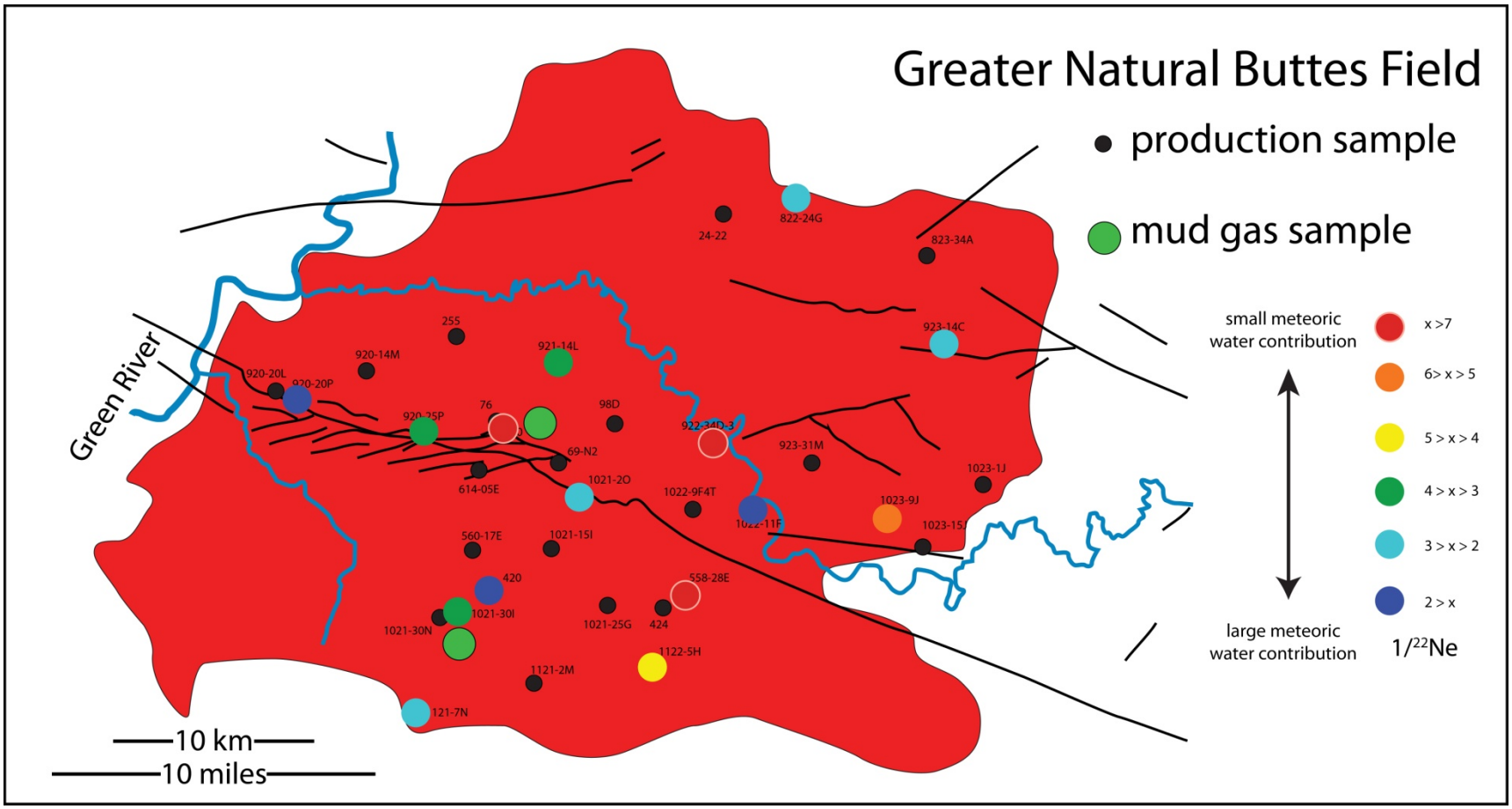

Figure 6.23. $1/^{22}Ne$ concentration in Greater Natural Buttes production gas samples. Low values are indicative of a contribution from meteoric water.

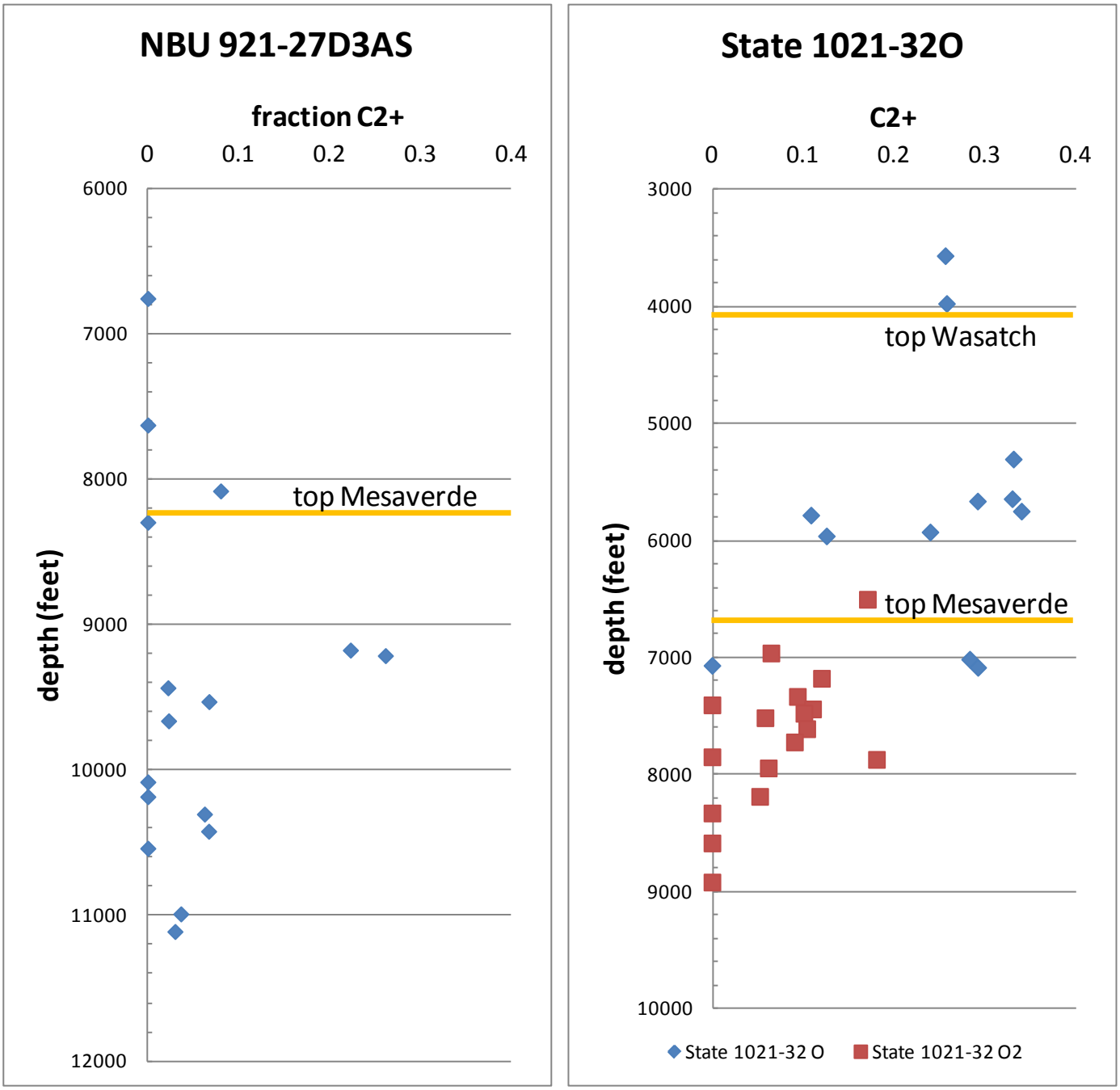

Figure 6.24. Gas wetness for two mud gas profiles at Greater Natural Buttes Field.

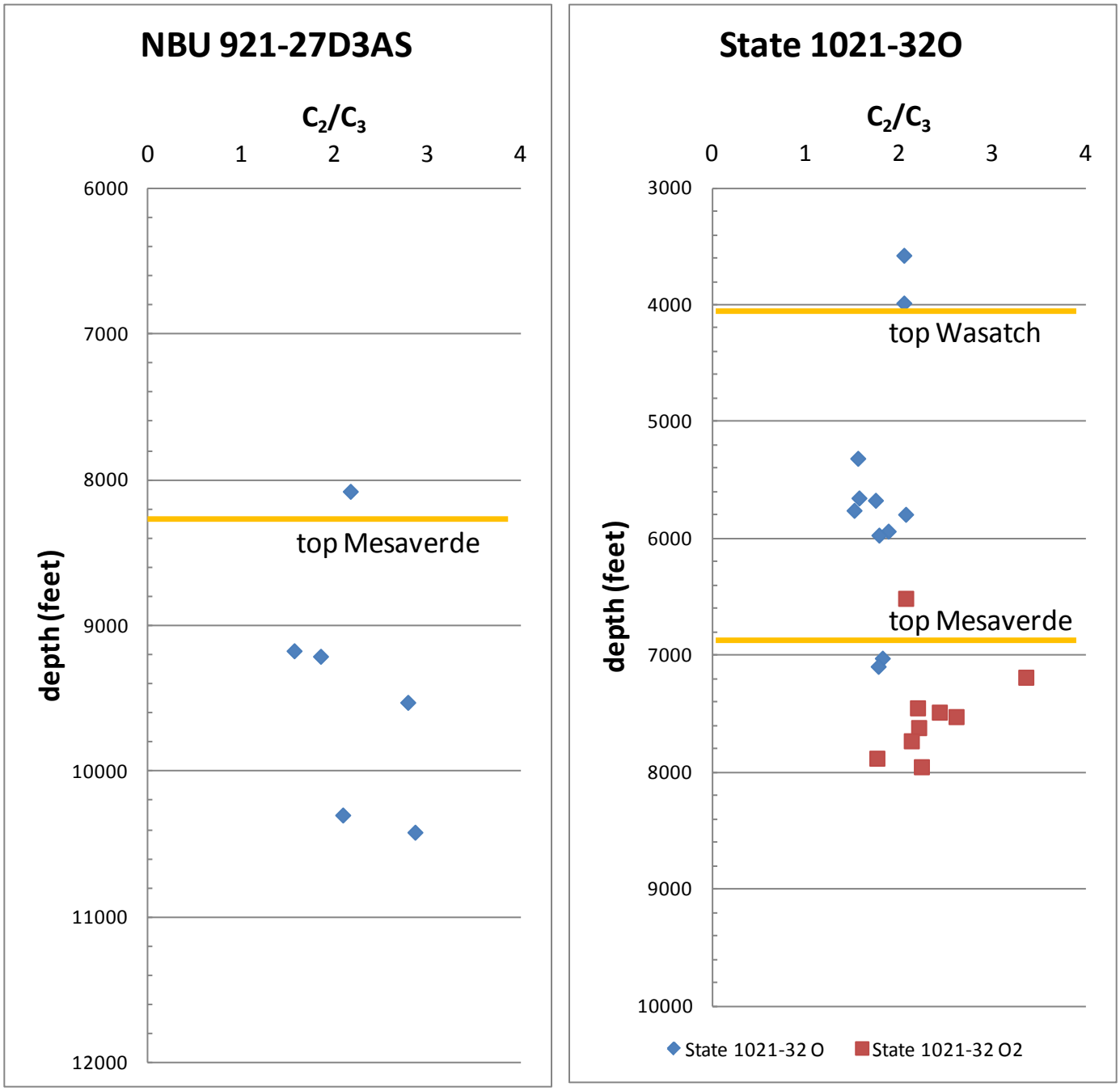

Figure 6.25. C_2/C_3 ratios for two mud gas profiles at Greater Natural Buttes Field.

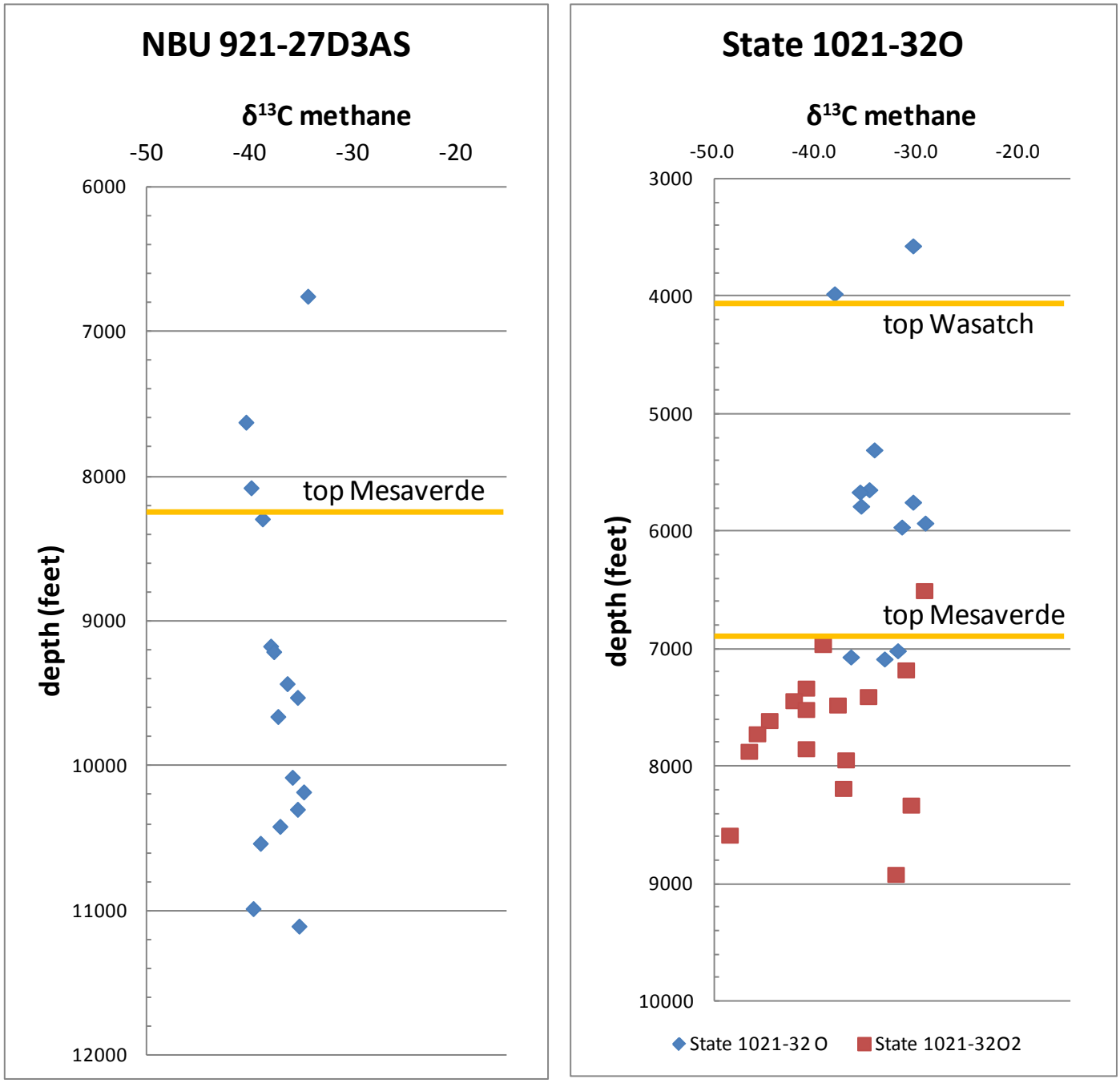

Figure 6.26. $\delta^{13}C_{C1}$ for two mud gas profiles at Greater Natural Buttes Field.

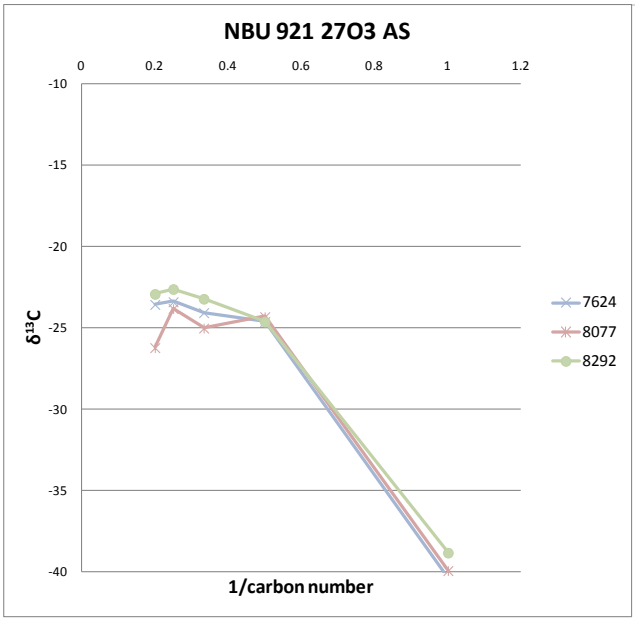

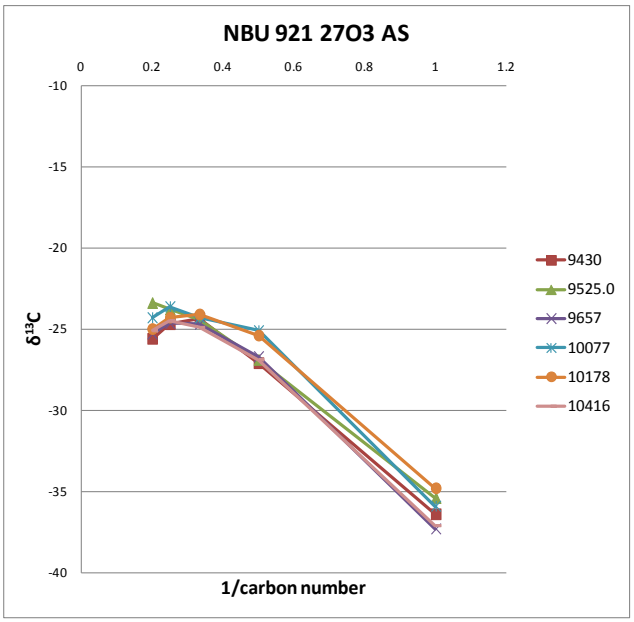

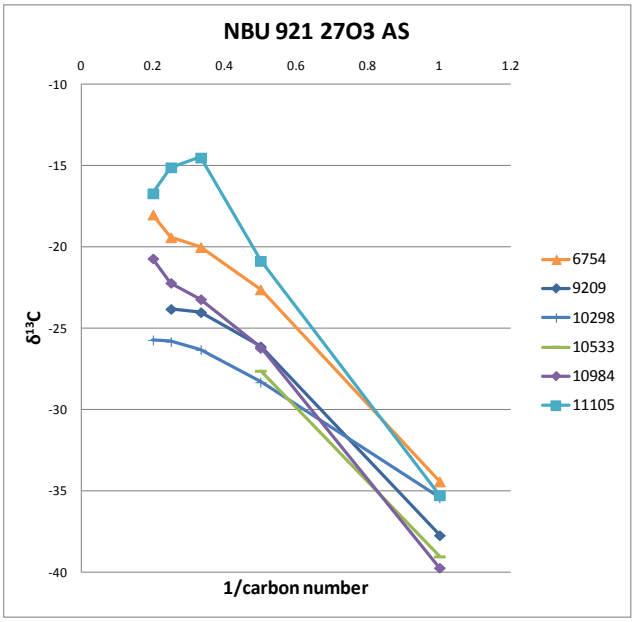

Figure 6.27. Chung plots for mud gas samples from the NBU 921 27O3 well at Greater Natural Buttes. Samples define three groups. Group 1 (upper): nearly identical $\delta^{13}C$ compositions for the heavier gases (~ -24‰) and compositions of -38 to -41‰ for C_1; Group 2 (middle): nearly identical $\delta^{13}C$ compositions for the heavier gases (~ -24‰) and compositions of -35 to -37‰ for C_1; and Group 3 (lower): normal Chung plots with increasingly heavy carbon isotopic compositions from C_1 to C_5 and a wide range of compositions, with C5 ranging from -26 to -17‰.

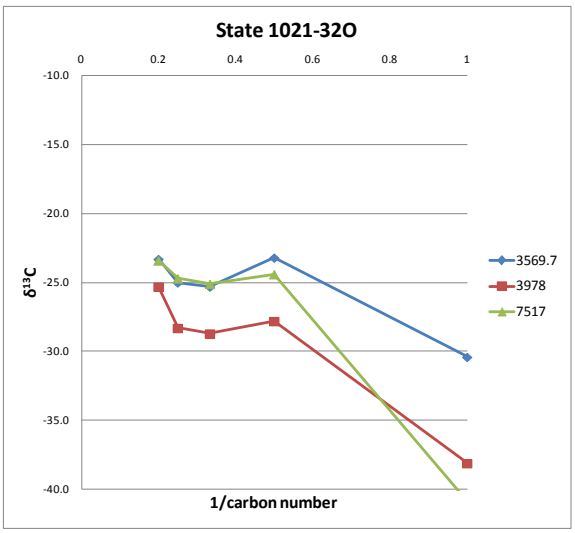

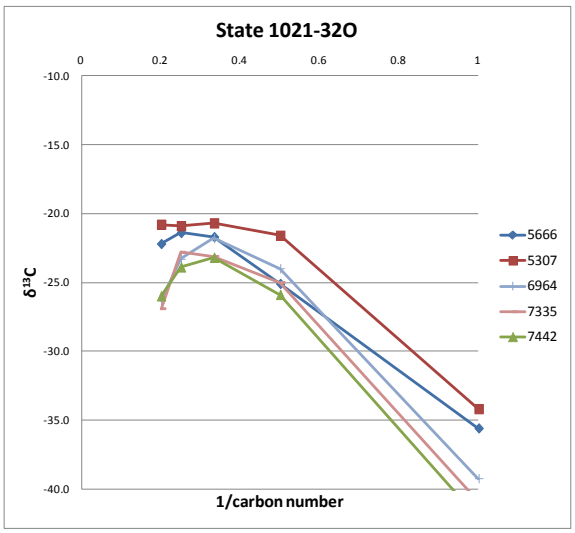

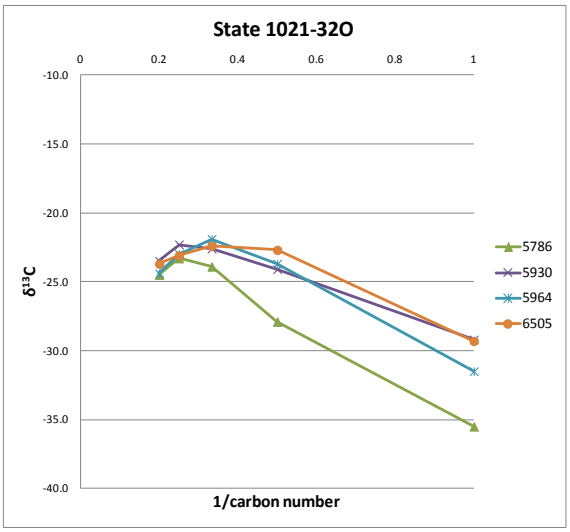

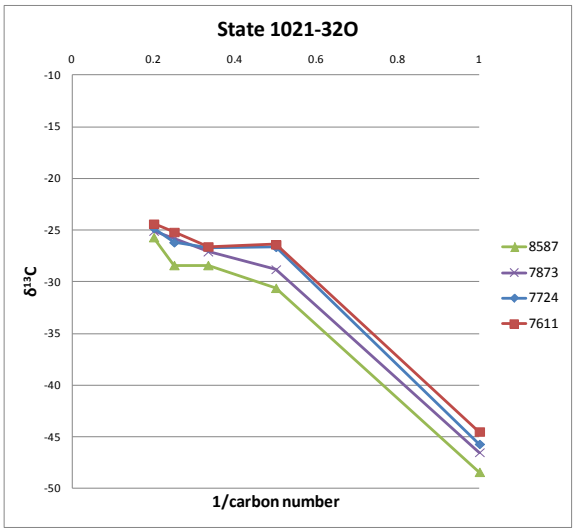

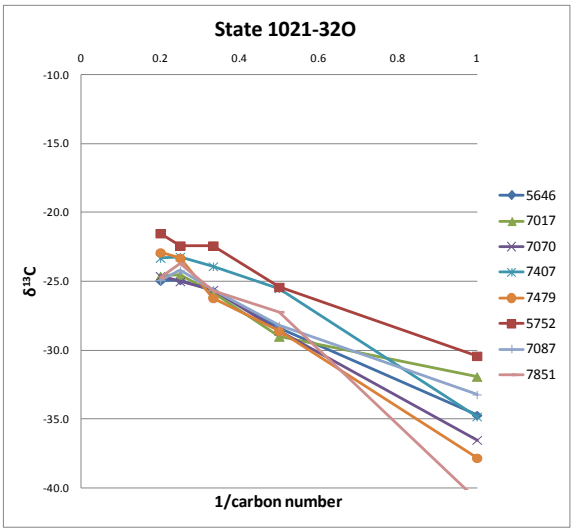

Figure 6.28. Groups of mud gas samples from the State 1021-32O well, based on similar Chung plots.

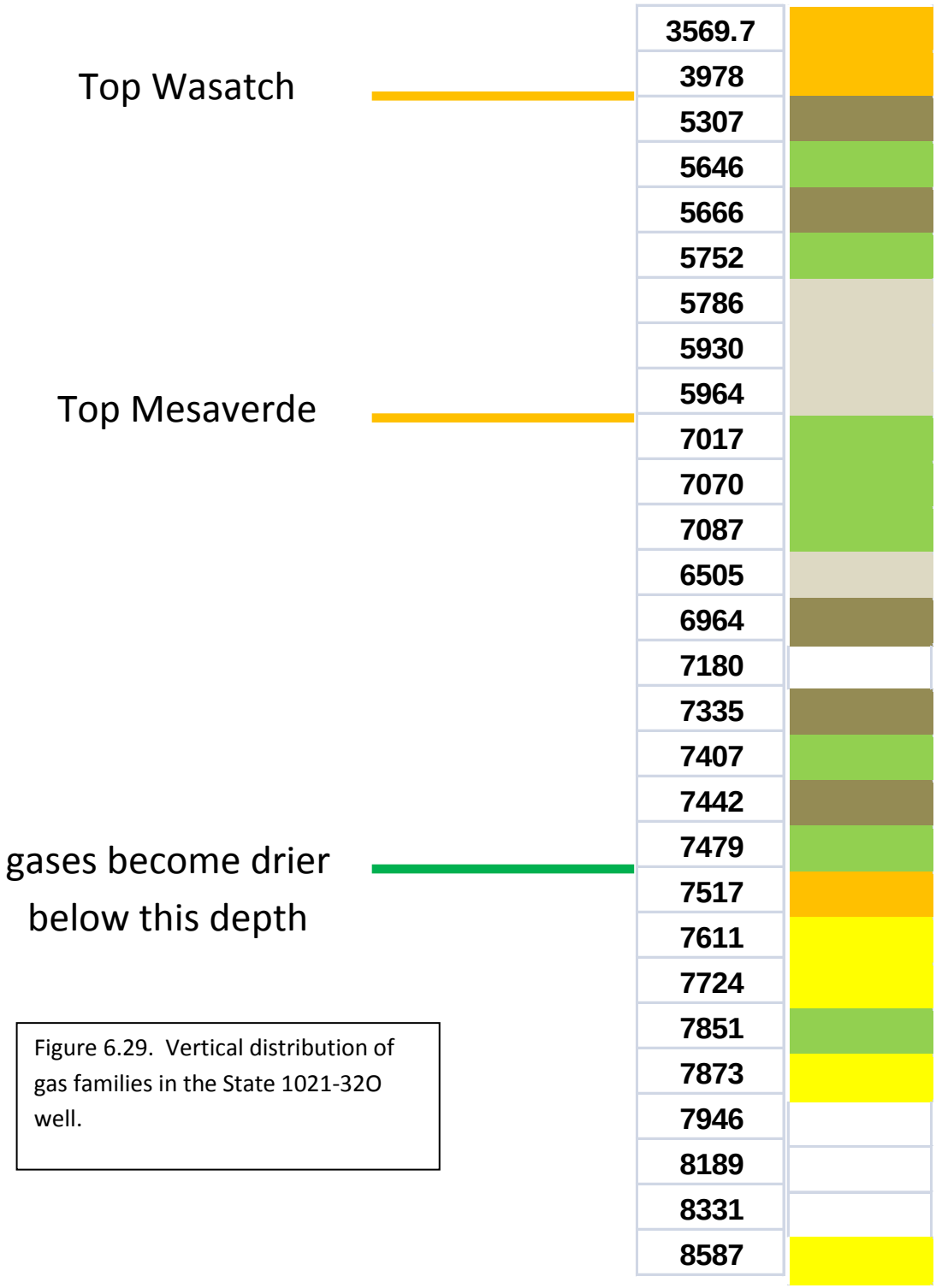

Figure 6.29. Vertical distribution of gas families in the State 1021-32O well.

	rollover, light methane
	rollover, heavier methane
	kinked rollover
	flat in C2+
	no rollover

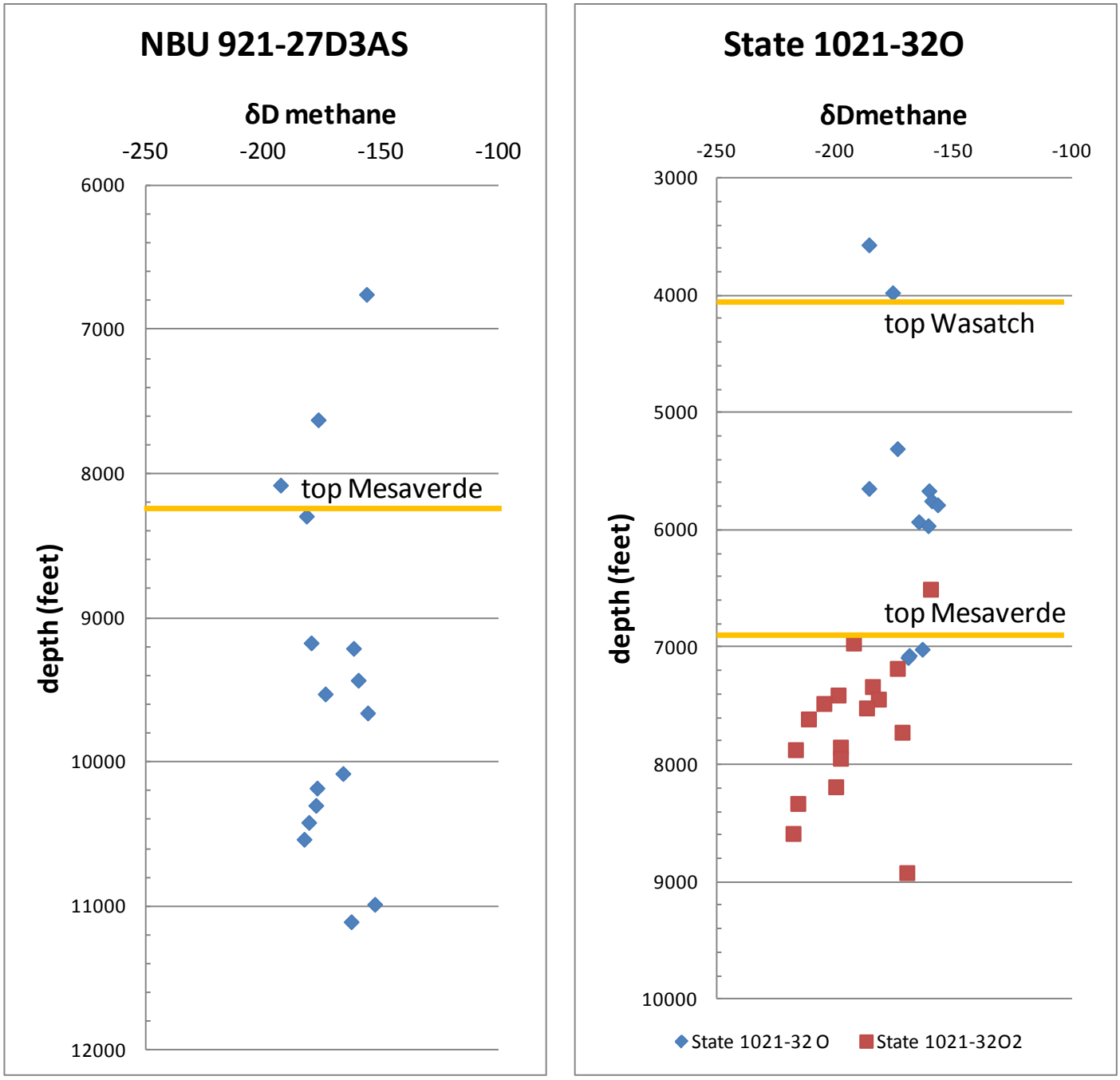

Figure 6.30. δD_{C1} for two mud gas profiles at Greater Natural Buttes Field.

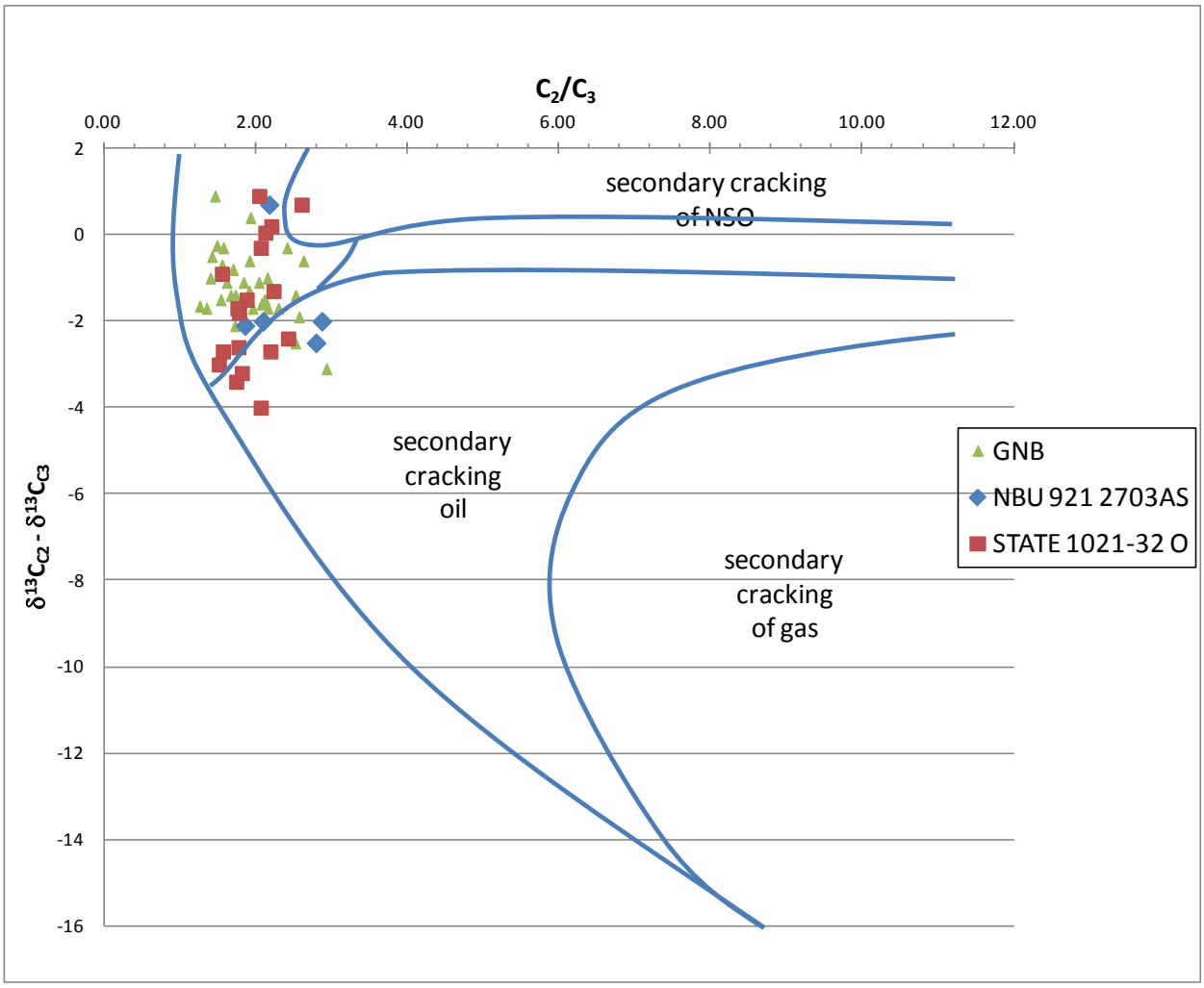

Figure 6. 31. Cross-plot of C_2/C_3 versus $\delta^{13}C_{C2}$- $\delta^{13}C_{C3}$ in mud gas data. Data points plotting with elevated C_2/C_3 and $\delta^{13}C_{C2}$- $\delta^{13}C_{C3}$ are indicative of secondary cracking of oil. Arrows indicate points located in Figure X.36.

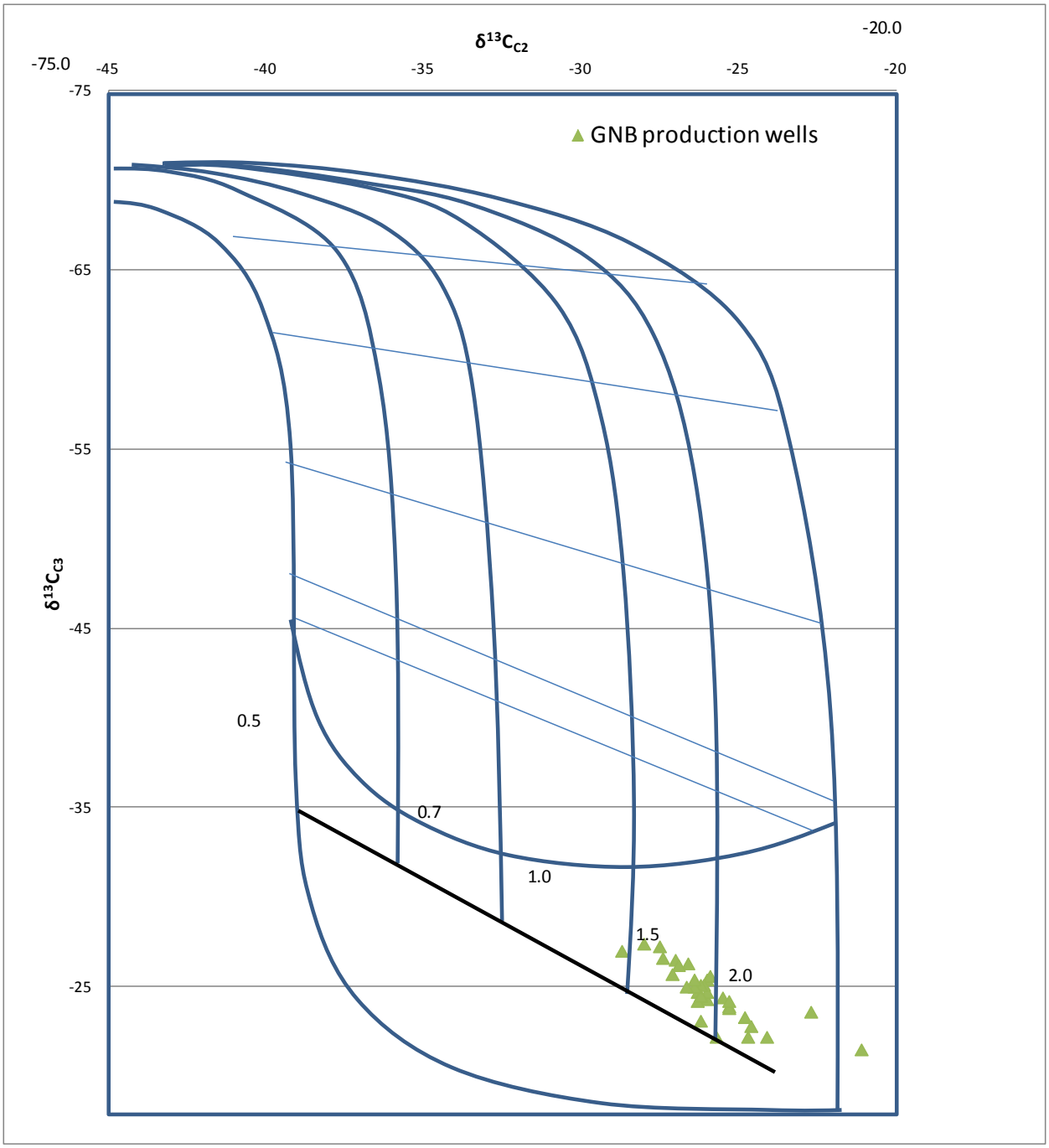

Figure 6.32. Cross-plot of $\delta^{13}C_{C2}$ versus $\delta^{13}C_{C3}$ for production gases. The composition of gases from Greater Natural Buttes production wells describes a generally linear trend, indicating a range of thermal maturities over which gases were generated, from 1.4 to ~3.0% R_o.

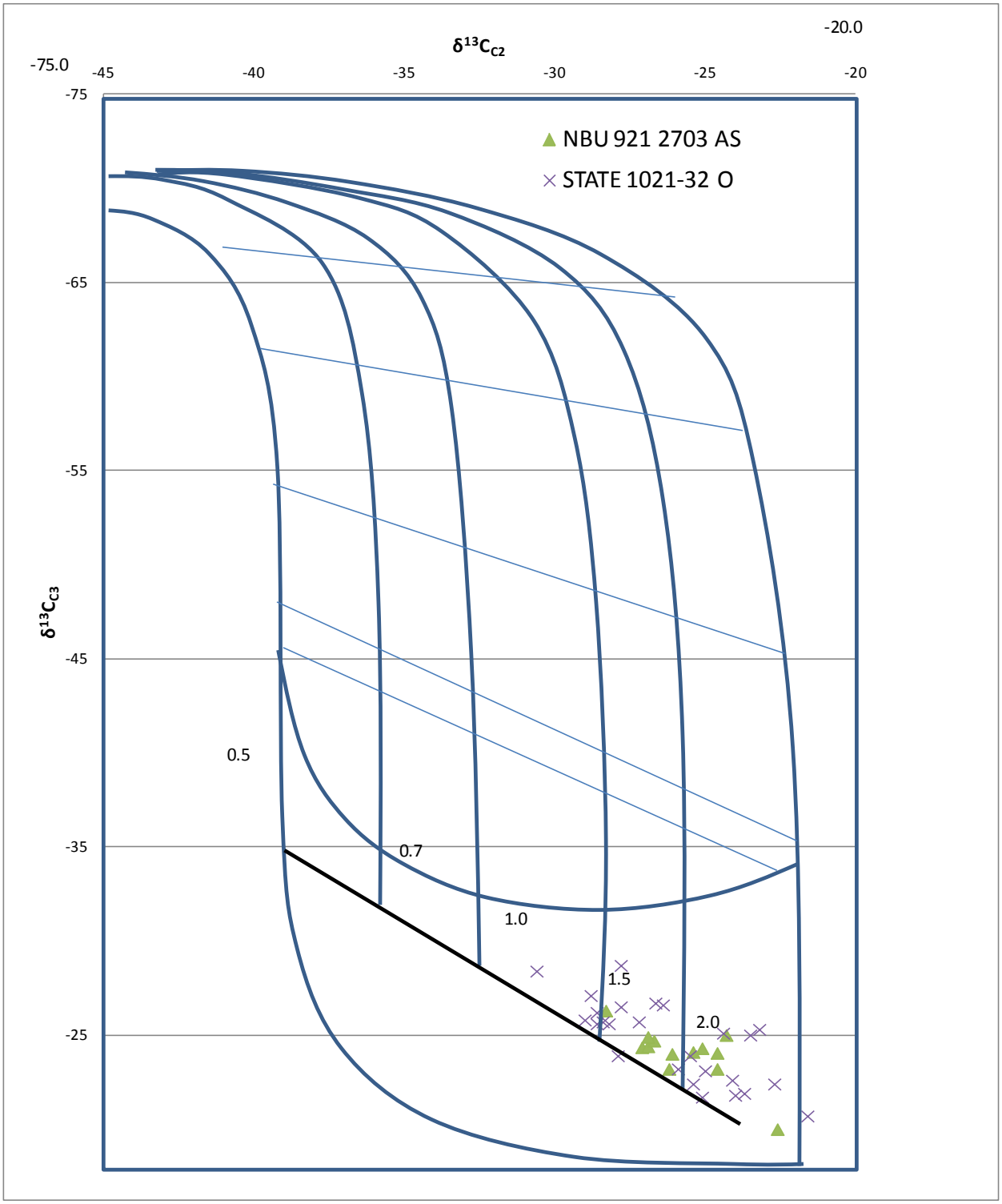

Figure 6.33. Cross-plot of $\delta^{13}C_{C2}$ versus $\delta^{13}C_{C3}$ for mud gas samples. Mud gas data fall along the same trend as production gas data. A wider range of thermal maturities is indicated for gases from the State 1021-32O well.

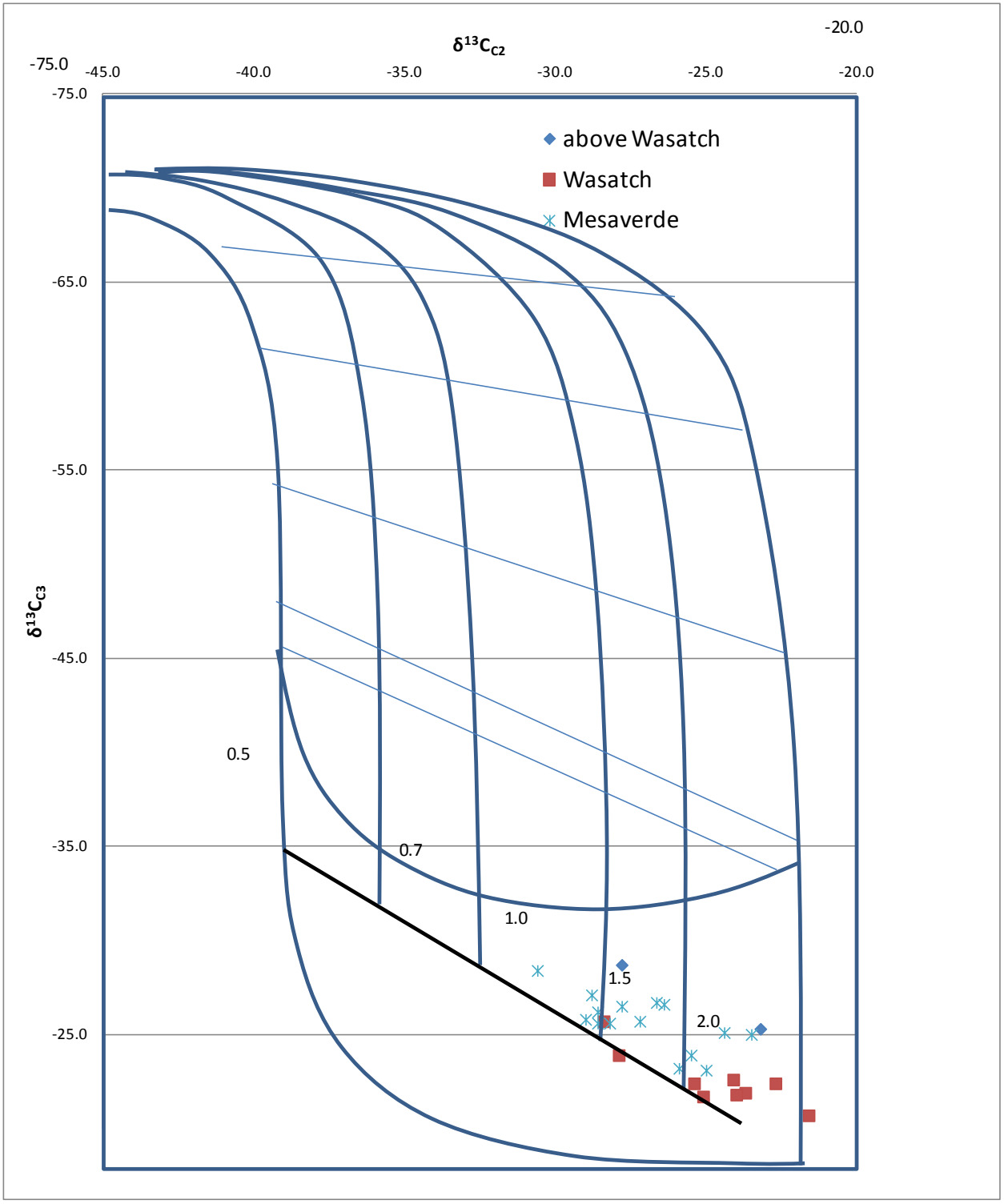

Figure 6.34. Cross-plot of $\delta^{13}C_{C2}$ versus $\delta^{13}C_{C3}$ for mud gas samples from the State 1021-32O well. Wasatch gases generally appear to cluster at more positive (heavier) values for $\delta^{13}C_{C2}$ and $\delta^{13}C_{C3}$ than Mesaverde gases, suggesting that they were generated at higher maturity.

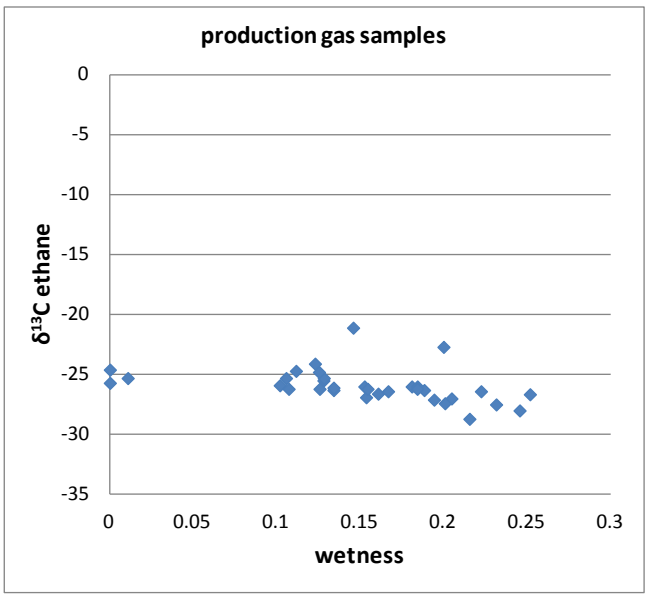

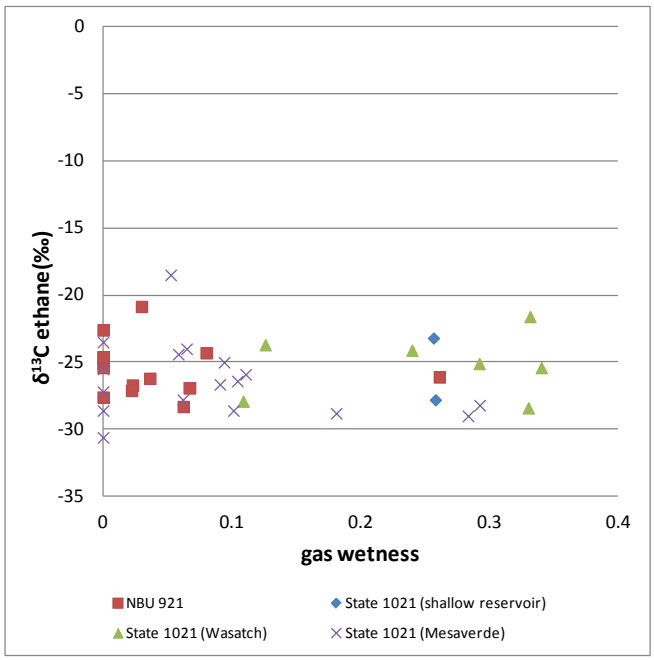

Figure 6.35. Wetness versus the carbon isotopic composition of ethane in production gas samples (upper) and mud gas samples (lower). A normal trend is increasing $\delta^{13}C_{C2}$ with decreasing gas wetness; a reversal of this trend ('rollover') has been interpreted by Zumberge et al (2012) as indicating secondary cracking of wet gas to dry gas.

7 Comparison between Piceance Basin fields, Jonah Field and Greater Natural Buttes Field

7.1 Similarities in gas composition between the Piceance Basin fields, Greater Natural Buttes Field and Jonah Field

On several standard cross-plots, the composition of both production gases and mud gases from the Piceance Basin fields, Greater Natural Buttes Field and Jonah Field are strikingly similar. These include:

- Gas wetness versus the carbon isotopic composition of methane (Figure 7.1; after Schoell, 1983).
- $\delta^{13}C$ methane versus $\delta^{13}C$ ethane (Figure 7.2; after Schoell, 1983).
- Ratio of C_2/C_3 versus the difference in carbon isotopic composition between C_2 and C_3 (Figure7.3; after Lorant et al., 1998).

7.2 Contrasts in composition between the Piceance Basin fields, Greater Natural Buttes Field and Jonah Field

While bulk hydrocarbon gas compositions are generally similar among the fields, certain differences exist and are summarized here.

7.2.1 Butane composition

Gases from Greater Natural Buttes field can be distinguished from Jonah and the Piceance Basin fields a lower ratio of *i*-C4 to *n*-C4, recognized by a lower slope on a cross-plot of these two variables (Figure 7.4).

Other bulk composition variables are not effective at discriminating between samples from the different fields.

7.2.2 Carbon isotopic composition of CO_2

The carbon isotopic composition of CO_2 for the entire data set encompasses a wide range of values, from as heavy (positive) as -1.6‰ to as light (negative) as -17.7‰. Within this range, the different fields can be generally differentiated (Figure 7.5). The Greater Natural Buttes gases are the heaviest in terms of $\delta^{13}C_{CO2}$, averaging -5.6‰, although there is a single isotopically extremely light CO2 analysis. The Piceance gases are slightly lighter in terms of $\delta^{13}C_{CO2}$, averaging -6.4‰. Jonah Field samples are much lighter, averaging -11.4‰.

7.2.3 D-H composition

Production gases from Jonah Field can be distinguished from the Piceance and Greater Natural Buttes Fields by significantly lighter (more negative) δD values (Figures 7.6 to 7.8). This is most evident for the C_{3+} gases, where Jonah gases are uniformly lighter by approximately 25 to 40‰. The difference between the fields is less for C_2, and the fields are not readily distinguishable by the δD of methane.

7.2.4 Noble gas composition

The Piceance Basin fields, Greater Natural Buttes Field and Jonah Field are differentiated by several noble gas parameters.

- The Piceance and Greater Natural Buttes samples are distinguished by higher ratios of $^{3}He/^{4}He$ (Figure 7.9). Jonah values are restricted to a range essentially that of crustal radiogenic $^{3}He/^{4}He$ values.

- The Piceance are distinguished by a wide range of $^{20}Ne/^{22}Ne$and $^{21}Ne/^{22}Ne$ ratios. The Greater Natural Buttes samples are characterized by invariant $^{20}Ne/^{22}Ne$ but a wide range of $^{21}Ne/^{22}Ne$ ratios. Jonah data are characterized by relatively invariant $^{20}Ne/^{22}Ne$ and $^{21}Ne/^{22}Ne$ ratios.

- The Piceance and Greater Natural Buttes data are characterized by $1/^{22}Ne$ and $1/^{36}Ar$ ratios that vary significantly and collinearly. Jonah data are very restricted and generally occupy the low end of the trend formed by the Piceance and Greater Natural Buttes data.

7.3 Interpretation

Substantial difference between the gas fields exist in terms of (1) hydrogen isotopic composition of the C2+ gases, (2) carbon isotopic composition of CO_2 and (3) a number of noble gas parameters.

7.3.1 Interpretation of hydrogen isotope data

The difference in δD for the C2+ hydrocarbon fraction is significant; δD values of Jonah Field gases are more negative than those from the Piceance Basin or Greater Natural Buttes Field by 24 to 40‰. This difference could have at least four different origins:

- The gases could have been sourced from kerogen with different hydrogen-deuterium compositions; the gases cracked from the kerogen would have inherited this difference.
- The gases could have been cracked at different thermal maturities, producing gases of different isotopic composition.
- The gases could have equilibrated with formation water of different composition.
- The gases are fractionated during secondary cracking of wet gas to dry gas.

Thermal maturity is an unlikely explanation for the difference in hydrogen-deuterium composition. Differing thermal maturity would have also had a demonstrable effect on $\delta^{13}C$ of the hydrocarbon gases (Schoell, 1983), and no such difference is evident in our data set. That this is an effect of fractionation during secondary cracking seems unlikely as well, given that carbon isotopic compositions do not differ between the fields.

Jonah Field differs from the other fields in Type III source rocks (terrestrial or coaly organic matter) are largely lacking from the sedimentary section (Hanson 2004, and Dubois et al., 2004), although Coskey (2004) considers that terrestrial organic matter in the Mesaverde section may have generated some gas. Coals probably contributed to gas generation in the Piceance Basin fields (particularly the Cameo Coal section; Yurewicz et al., 2003) and in the Greater Natural Buttes Field (Blackhawk and Neslen Formations; Johnson and Roberts, 2003).

An investigation by Schimmelmann et al. (2004) compiled D-H ratios in oils generated from both marine and non-marine source rocks. Their Figure 2, which also draws on earlier studies by Yeh and Epstein (1981) and Peters et al. (1986), shows a systematic negative shift in δD of 15

to 30‰ from marine to non-marine oils, in other words the non-marine oils are isotopically lighter than the marine oils, although there is a substantial range in δD values for non-marine oils that Schimmelmann et al. (2004) relate to variability in the meteoric water taken up by plants that later become coalified. We are not aware of hydrogen isotope studies of organic matter in Rocky Mountain source rocks, but we note that the Piceance and Greater Natural Buttes gases – which should reflect greater input from terrestrial source rocks – are isotopically heavier, not lighter than the Jonah gases. Based on this information, a model based source rock control of δD does not appear viable, but because we lack information of the hydrogen isotopic composition of source rocks in the Rocky Mountains, control by source rock composition cannot ruled out.

The third model relies on hydrogen exchange with formation water. Presumably exchange of hydrogen with water that is relatively depleted in deuterium (very negative δD) would shift the composition of the associated gas to more negative values. A comparison of water geochemistry suggests that formation waters at Jonah Field are very different from formation waters at Greater Natural Buttes and in the Piceance fields, the former more dilute by a factor of at least 10 (Figure 7.11). Hydrogen isotope data are only published for Uinta Basin formation waters (Zhang et al., 2009). But we can begin the analysis from an assumption that salinity in the formation waters reflects degree of evaporation. In that case, formation waters that are saline should have δD values that are relatively heavy, because evaporation concentrates deuterium in the non-evaporated fraction. Therefore the Jonah waters should be isotopically lighter with respect to hydrogen-deuterium than the Greater Natural Buttes and Piceance basin waters. Gases equilibrating with the formation waters should be isotopically lighter in Jonah Field, which is in fact consistent with our data.

We note that methane compositions are not differentiated with respect to hydrogen-deuterium, while the wetter gases are. If the isotopic exchange model applies to gases from these fields, it would imply that methane does not exchange at the same rate as the wetter gases.

This model is problematic in that exchange rates between natural gases are generally considered to be extremely slow, too slow to be effective even at geologic time scales (Sessions et al, 2004; A. Schimmelmann, personal communication 2013). However, based on data reported in Sessions et al., 2004) and a geothermal gradient for the Jonah area of 1.7°F/100 feet (from Finn, 2005), the half life for an exchange reaction between methane and water should be approximately 4 million years, assuming present day temperatures. Given that temperatures would have been higher prior to late Tertiary uplift and erosion, it is possible that the exchange reaction could have proceeded more quickly.

7.3.2 Carbon isotopic composition of CO_2

There are three primary sources of CO_2 gas in natural gas: CO_2 generated from cracking of kerogen; CO_2 derived from the breakdown of carbonate minerals under thermal stress; or oxidation reactions that react reduced carbon (either kerogen or hydrocarbons) to form CO_2. CO_2 formed by the thermal breakdown of carbonate minerals is similar to the carbon isotope composition of the carbon; in the case of the Rocky Mountain source rocks, that should produce a range of $\delta^{13}C$ values between 0 and -4‰. CO_2 derived from cracking of kerogen and CO_2 from oxidation of hydrocarbons should both be isotopically much lighter, because the carbon is derived from organic carbon that is isotopically light.

Gases from the Piceance fields, Greater Natural Buttes Field and Jonah Field exhibit a 16‰ range in $\delta^{13}C_{CO2}$. CO_2 in gases from Greater Natural Buttes Field is isotopically relatively heavy, ranging from approximately -2 to -8‰. The CO_2 in these gases are therefore dominated by a marine carbonate source. CO_2 in gases from the Piceance fields is intermediate in composition, ranging from approximately -4 to -13‰, indicating a variable but locally significant contribution from an organic source. CO_2 in gases from Jonah Field is isotopically light, ranging from approximately -8 to -18‰, indicating the most substantial contribution from an organic source.

Terrestrial organic matter (coaly material) can be a prolific source of CO_2 (Zhang et al., 2008; Ko, 2010). Ko's (2010) hydrous pyrolysis experiments confirmed that CO_2 generated during thermal maturation were most depleted in ^{13}C (very negative $\delta^{13}C_{CO2}$) from the Cameo Coal, less depleted in ^{13}C from the Mancos Shale and least depleted in ^{13}C from the Baxter Shale. This variation is a function of increasing contribution of carbon from marine carbonate in experiments on the two shale formations.

If CO_2 generation from coal were source of the isotopically light carbon in the natural gases, the most substantial contribution would be expected in the fields with the most mature coal in the stratigraphic section: the Piceance fields with the mature Cameo Coal, and the Greater Natural Buttes Field. Jonah Field should have the least contribution from coaly source rocks. This would imply that CO_2 from Jonah should be isotopically heavy compared to gases from the Piceance fields and from Greater Natural Buttes.

We therefore conclude that CO_2 from Jonah Field has been generated by oxidation of reduced carbon; the largest pool of reduced carbon is the natural gas.

7.4.3 Noble gas data

Noble gases function effectively as geochemical tracers because of their non-reactive nature. Multiple parameters in this data set effectively differentiate Jonah Field from the other data sets, including contributions of mantle He and input of atmospheric-derived Ne and Ar. These parameters are consistent with pervasive interaction of the Jonah gas column with deeply penetrating meteoric-derived subsurface water. The composition of gases from other fields indicates much more localized influences of meteoric water. These data are consistent with present day formation water compositions, which are fresher at Jonah Field and much more saline in the Piceance Basin fields and at Greater Natural Buttes Field (Figure

7.4 References

Ballentine, C. J., & Burnard, P. G. (2002). Production, release and transport of noble gases in the continental crust. *Reviews in mineralogy and geochemistry*,*47*(1), 481-538.

Coskey, R. J. (2004). Burial-history modeling of the Jonah field area: An unusual and possibly unique gas accumulation in the Green River Basin, Wyoming. In Jonah Field: Case Study of a Giant Tight-Gas Fluvial Reservoir, J. W. Robinson and K. W. Shanley, eds.: AAPG Studies in Geology 52 and Rocky Mountain Association of Geologists 2004 Guidebook, 93-125.

Dunai, Tibor J., and Donald Porcelli. "Storage and transport of noble gases in the subcontinental lithosphere." *Reviews in mineralogy and geochemistry* 47.1 (2002): 371-409.

DuBois, D. P., Wynne, P. J., Smagala, T. M., Johnson, J. L., Engler, K. D., & McBride, B. C. (2004). Geology of Jonah field, Sublette County, Wyoming. In Jonah Field: Case Study of a Giant Tight-Gas Fluvial Reservoir, J. W. Robinson and K. W. Shanley, eds.: AAPG Studies in Geology 52 and Rocky Mountain Association of Geologists 2004 Guidebook, p. 37-59.

Finn, T. M. (2005). Geothermal Gradient Map of the Southwestern Wyoming Province, Southwestern Wyoming, Northwestern Colorado, and Northeastern Utah. Petroleum Systems and Geologic Assessment of Oil and Gas in the Southwestern Wyoming Province, Wyoming, Colorado, and Utah. Denver. *US Geological Survey*, Digital Data Series DDS–69–D, Chapter 16, 11 pp.

Hanson, W. B., Vega, V., & Cox, D. (2004). Structural geology, seismic imaging, and genesis of the giant Jonah gas field, Wyoming, USA. *In* J. W. Robinson and K. W. Shanley, eds., Jonah Field: Case Study of a Giant Tight-Gas Fluvial Reservoir: AAPG Studies in Geology 52, chapter 6, p. 61-92.

Johnson, R. C., & Roberts, S. B. (2003). The Mesaverde total petroleum system, Uinta-Piceance Province, Utah and Colorado. *Petroleum systems and geologic assessment of oil and gas in the Uinta-Piceance province, Utah and Colorado: US Geological Survey Digital Data Series DDS-69-B*, 63 pp.

Ko, T. (2010). Characterization of Gas Generated by Sequential Hydrous Pyrolysis of Potential Gas-Prone Source Rocks for Tight-Gas Reservoirs in the Rocky Mountain Area: M.Sc. thesis, Colorado School of Mines.

Lorant, F., Prinzhofer, A., Behar, F., & A. Y. Huc (1998). Carbon isotopic and molecular constraints on the formation and the expulsion of thermogenic hydrocarbon gases: Chemical Geology, v. 147, p. 249–264.

Mamyrin, B.A.; Anufriev, G.S.; Kamenskii, I.L.; Tolstikhin, I.N. (1970). Determination of the isotopic composition of atmospheric helium. Geochem. Int. (Engl. Transl.) 7: 498-505(Jan).

Schimmelmann, A., Sessions, A. L., Boreham, C. J., Edwards, D. S., Logan, G. A., & Summons, R. E. (2004). D/H ratios in terrestrially sourced petroleum systems. *Organic Geochemistry*, *35*(10), 1169-1195.

Schoell, M. (1983). Genetic characterization of natural gases. *AAPG bulletin*, *67* (12), 2225-2238.

Yurewicz, D. A., Bohacs, K. M., Yeakel, J. D., & Kronmueller, K. (2003). Source rock analysis and hydrocarbon generation, Mesaverde Group and Mancos Shale, northern Piceance Basin, Colorado.

Zhang, E., Hill, R. J., Katz, B. J., & Tang, Y. (2008). Modeling of gas generation from the Cameo coal zone in the Piceance Basin, Colorado. *AAPG bulletin*,*92*(8), 1077-1106.

Zhang, Y., Gable, C. W., Zyvoloski, G. A., & Walter, L. M. (2009). Hydrogeochemistry and gas compositions of the Uinta Basin: A regional-scale overview. *AAPG bulletin*, *93*(8), 1087-1118.

Table 7.1 Average δD compositions of gas species

	Piceance fields	Greater Natural Buttes	Jonah
δD C_1	-175	-169	-179
δD C_2	-132	-138	-156
δD C_3	-123	-128	-159
δD *i*-C_4	-117	-109	-143
δD *n*-C_4	-117	-118	-152
δD *i*-C_5	-103	-95	-128
δD *n*-C_5	-115	-104	-145

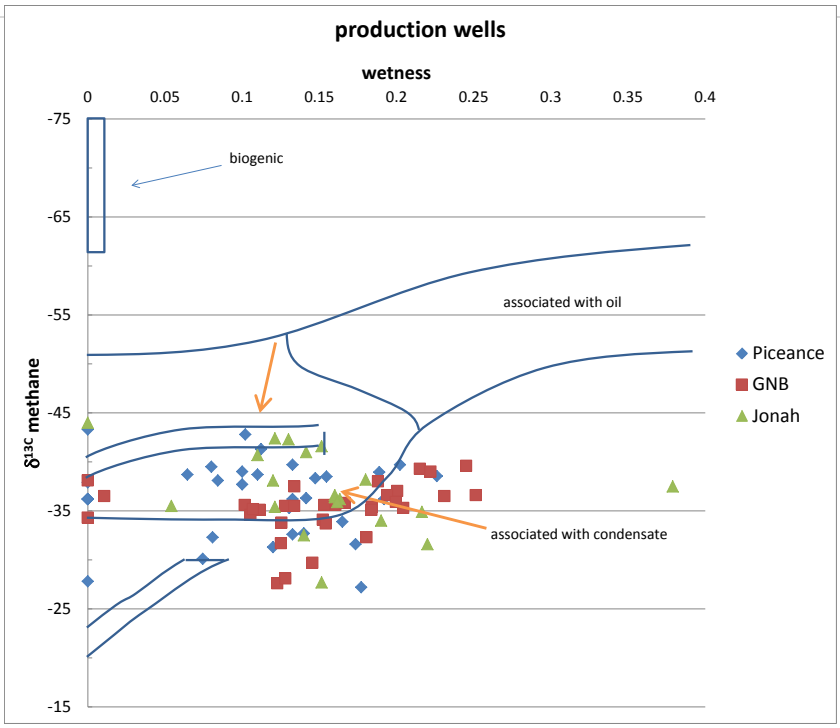

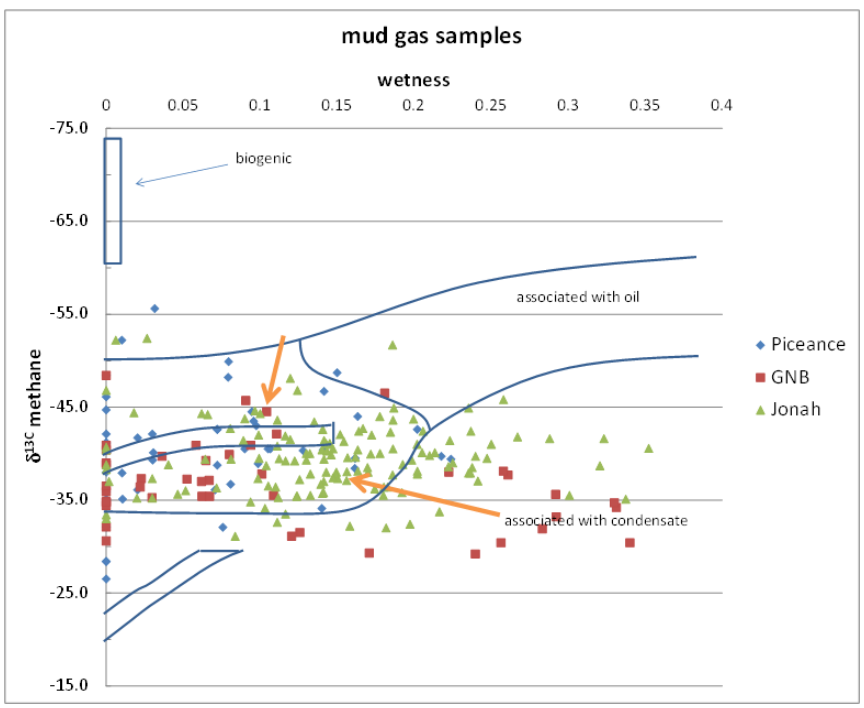

Figure 7.1. Production and mud gas wetness and methane isotopic composition for Piceance Basin, Greater Natural Buttes and Jonah fields. Compositions from the three areas are similar, despite Jonah Field probably lacking significant gas generation from coals. Gases from the Piceance Basin and Greater Natural Buttes do not have notably isotopically heavier gases than Jonah, although such compositions are generally taken to indicate input from Type III source rocks. Plot after Schoell (1983).

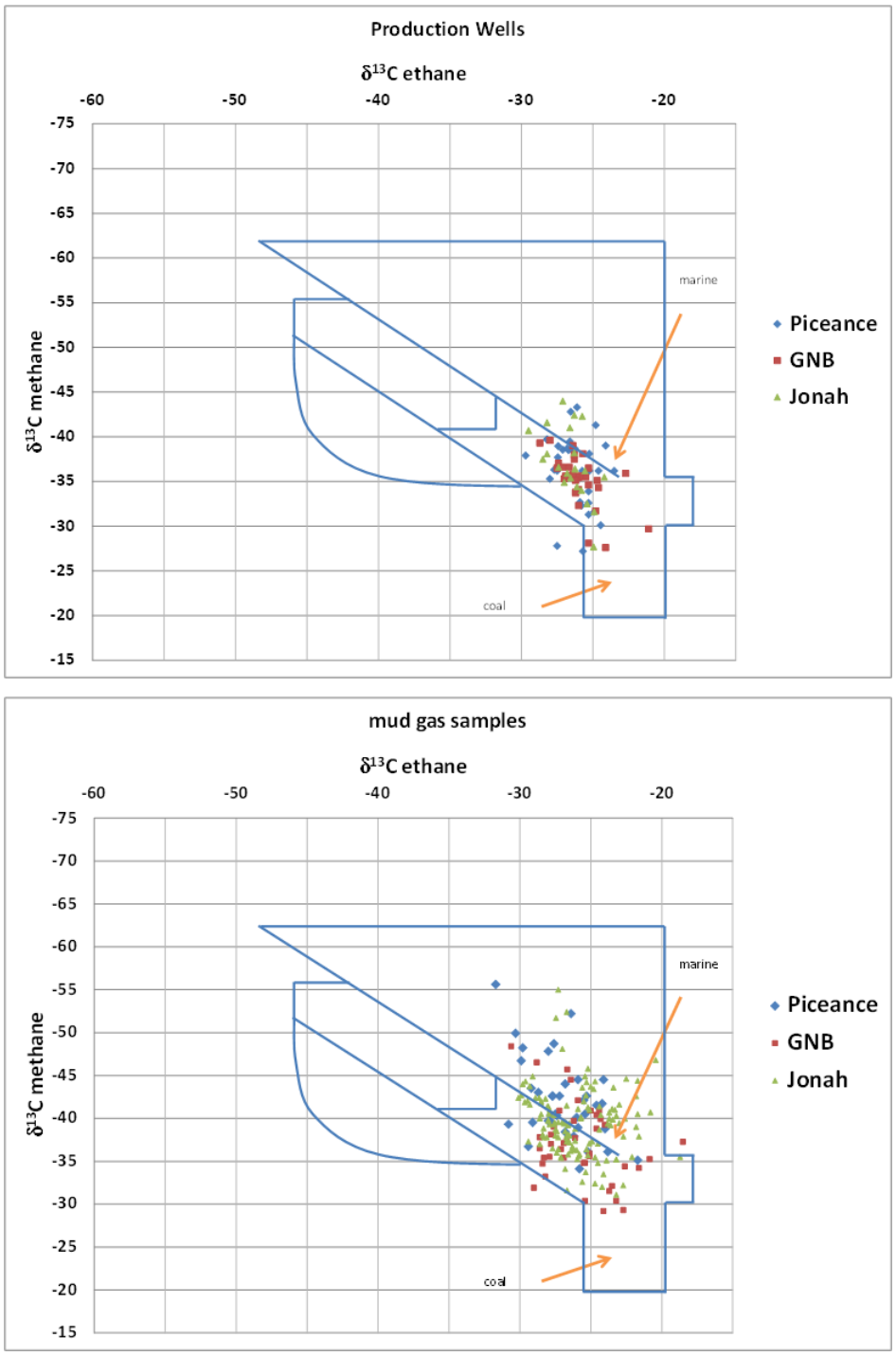

Figure 7.2. Production (top) and mud gas (bottom) carbon isotope compositions for Piceance Basin, Greater Natural Buttes and Jonah fields. Compositions from all three areas are very similar, despite Jonah Field probably lacking significant gas generation from coals. Gases from the Piceance Basin and Greater Natural Buttes do not have notably isotopically heavier gases than Jonah, although such compositions are generally taken to indicate input from Type III source rocks. Diagram after Schoell (1983).

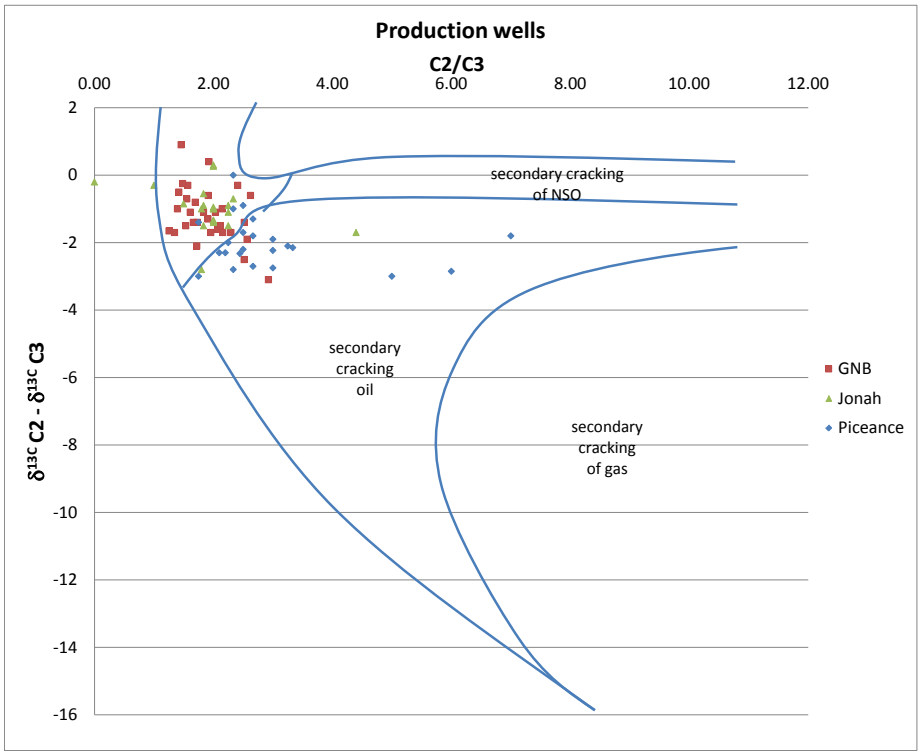

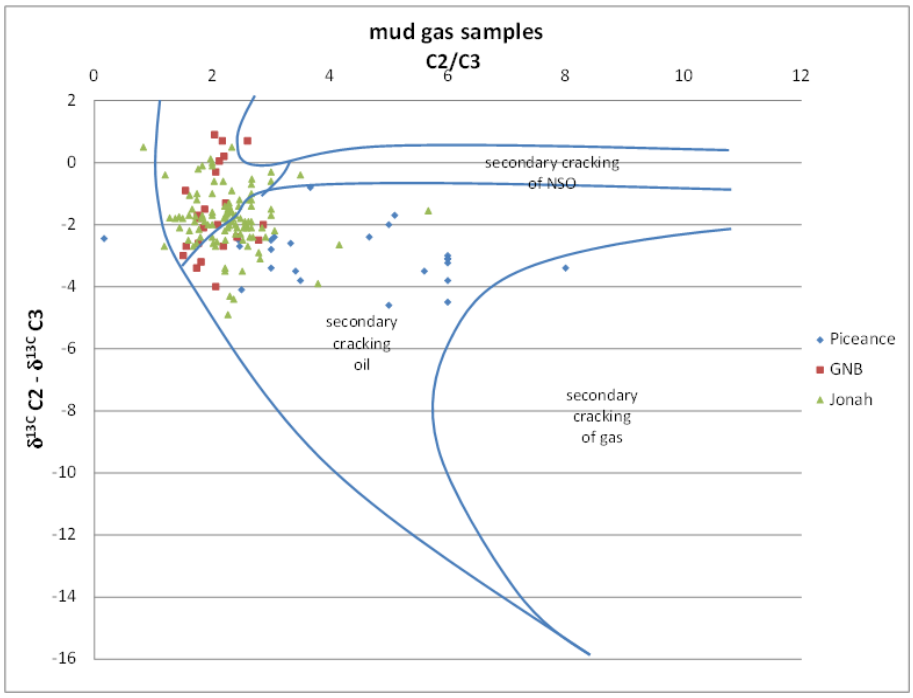

Figure 7.3. Production (top) and mud gas (bottom) ethane and propane compositions for Piceance Basin, Greater Natural Buttes and Jonah fields. Compositions from all three areas are similar, although some secondary cracking of oil to gas is suggested for Piceance gases and possible some Jonah gases. Diagram after Lorant et al. (1998).

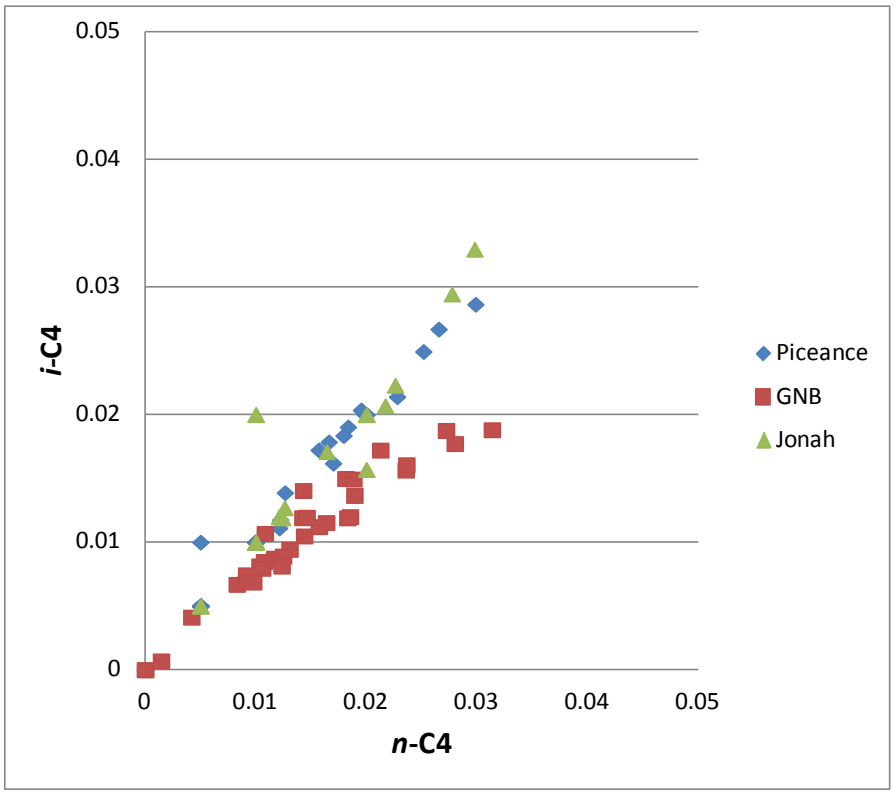

Figure 7.4. Production gas samples from Greater Natural Buttes Field are characterized by lower ratios of i-C4 / n-C4 than samples from the Piceance fields and Jonah Field

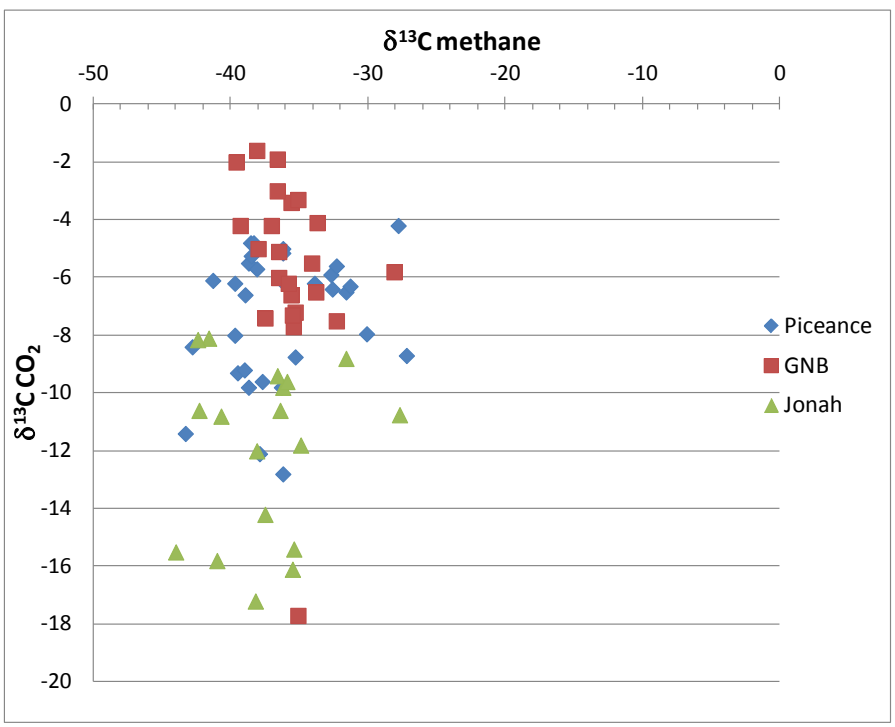

Figure 7.5. Production gas samples from Jonah Field are characterized by lower $\delta^{13}C_{CO2}$ than sample from the Piceance fields and from Greater Natural Buttes Field. GNB samples have the isotopically heaviest gases.

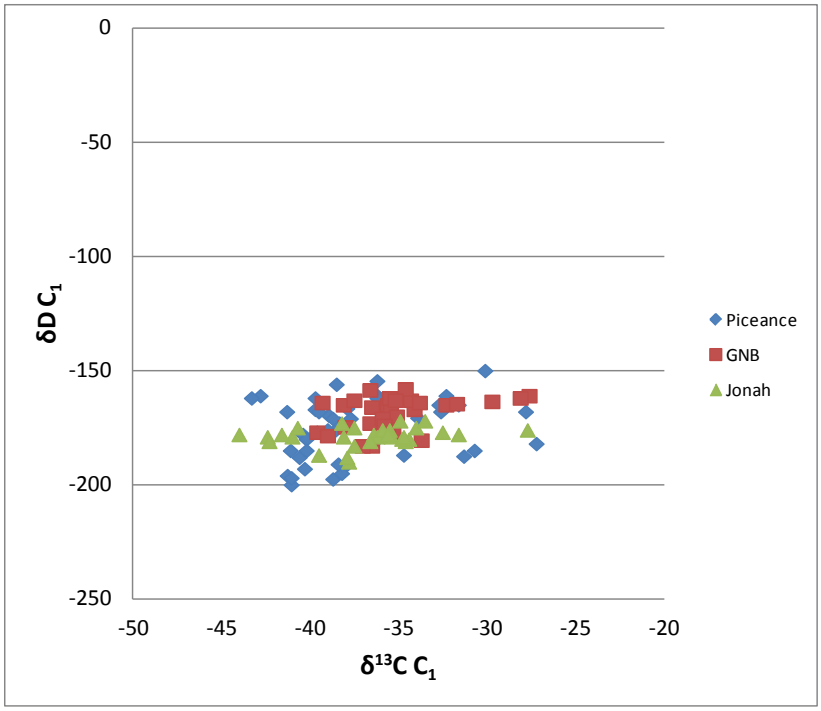

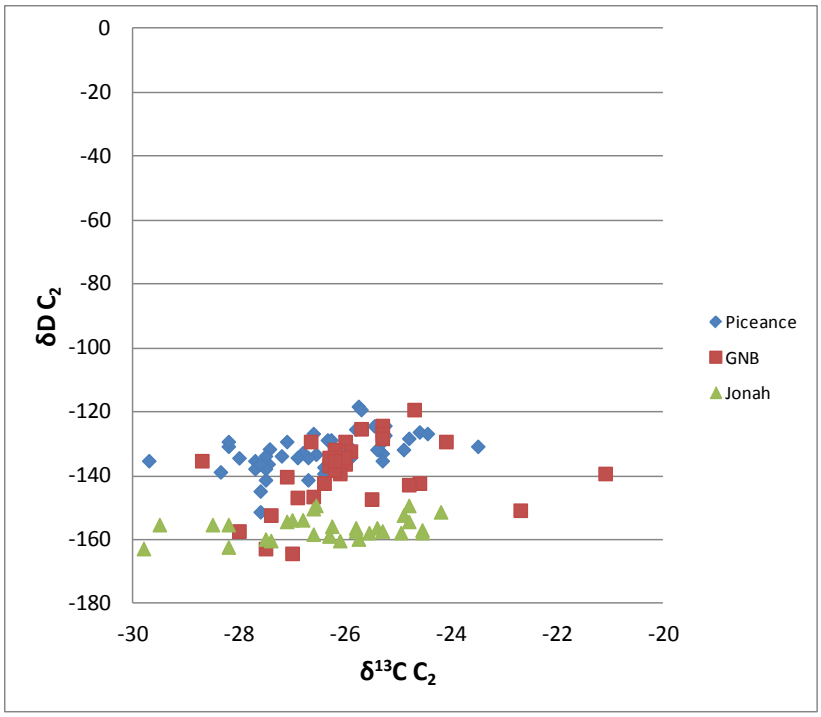

Figure 7.6. δD of methane (top) and ethane (bottom). Ethanes from Jonah field are distinguished by δD values that are more negative by approximately 25‰ compared to ethanes from the Piceance fields and Greater Natural Buttes Field. Methanes are not distinguishable by δD.

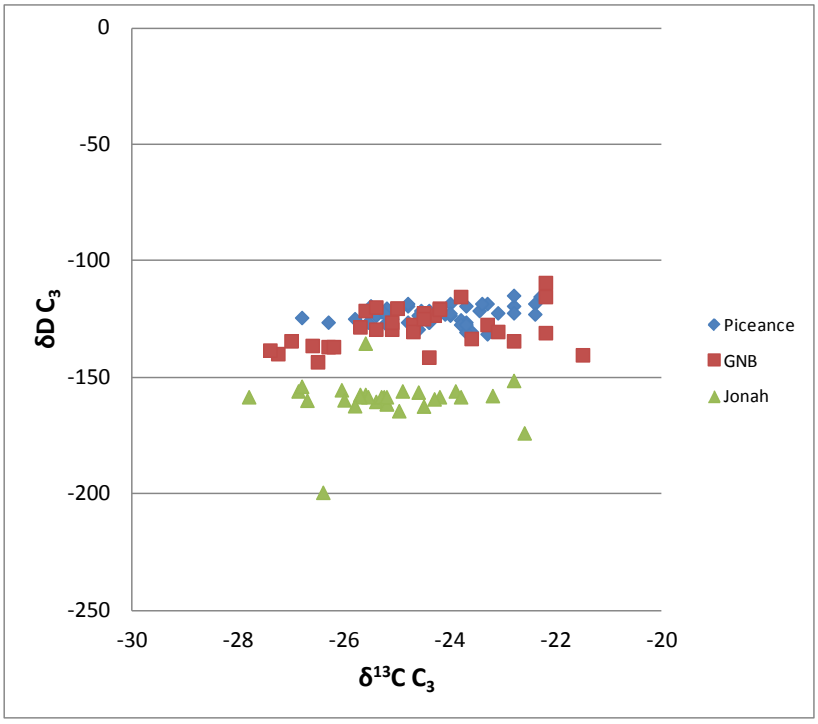

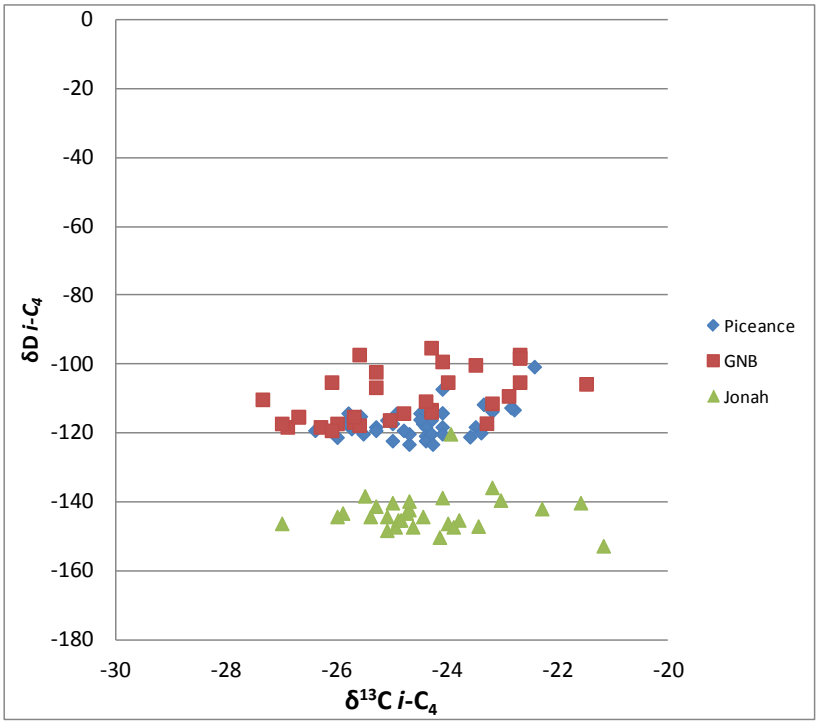

Figure 7.7 δD of propane (top) and iso-butane (bottom). These gas species from Jonah field are distinguished by δD values that are more negative by approximately 25 to 30‰ compared to the same gases from the Piceance fields and Greater Natural Buttes Field.

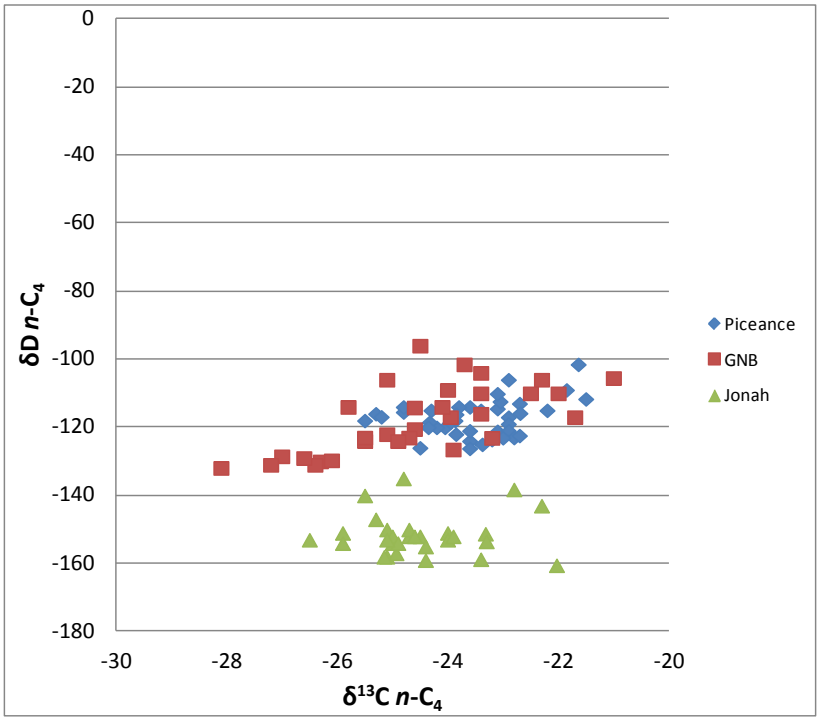

Figure 7.8 δD of iso-pentane (bottom). Jonah field gases are distinguished by δD values that are more negative by approximately 35‰ for this species compared to the same gases from the Piceance fields and Greater Natural Buttes Field.

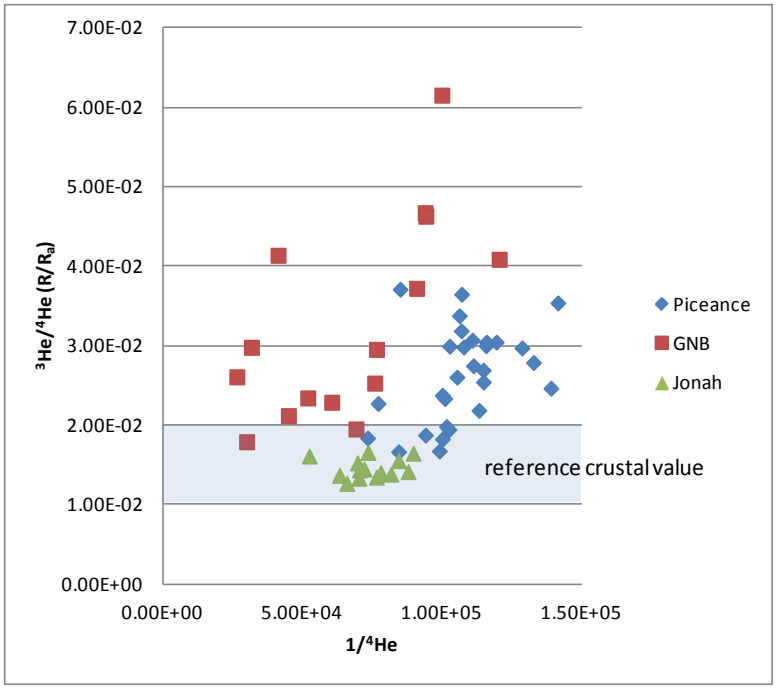

Figure 7.8 Measured $^3He/^4He$ ratios R_a, are normalized to the air value $R_a=1.4x10^{-6}$ (Mamyrin et al., 1970) and range between $0.013R_a$ and $0.062R_a$. The average crust end member have $^3He/^4He$ ration between 0.01 to 0.02Ra (shown in yellow range) (Ballentine and Burnard, 2002; Dunai and Porcelli, 2002). All our samples show strong crustal signature. $^3He/^4He$ in samples from Jonah field seems to be crustal radiogenic only. But samples from both Piceance and Greater Natural Buttes have higher $^3He/^4He$ ratios than average crust values. This could be due to a small mantle addition, fractionation of ^3He from ^4He on release or reflect a fractionation process.

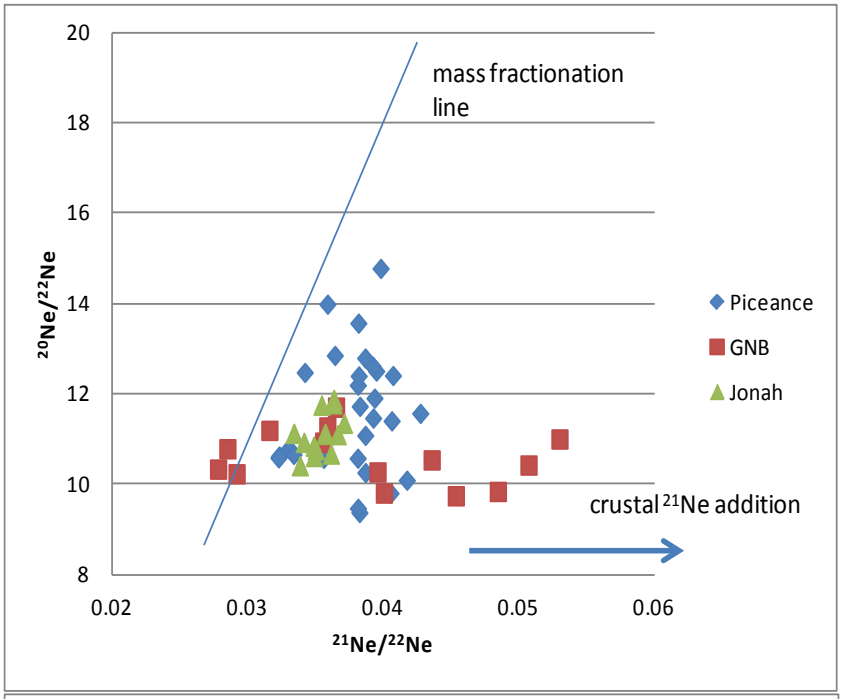

Figure 7.9 In the absence of mantle He, samples Ne isotopic ratios still show significant deviation from atmospheric values. $^{20}Ne/^{22}Ne$ ratios vary between 9.4 and 14.8. $^{21}Ne/^{22}Ne$ ratios vary between 0.028 and 0.053. High $^{21}Ne/^{22}Ne$ ratios can be explained by variable crustal radiogenic 21Ne (21Ne*) addition to air Ne, High $^{20}Ne/^{22}Ne$ ratios can only be accounted for by a mass fractionating process. Jonah field shows less fractionation and smaller addition of crustal ^{21}Ne than the other fields.

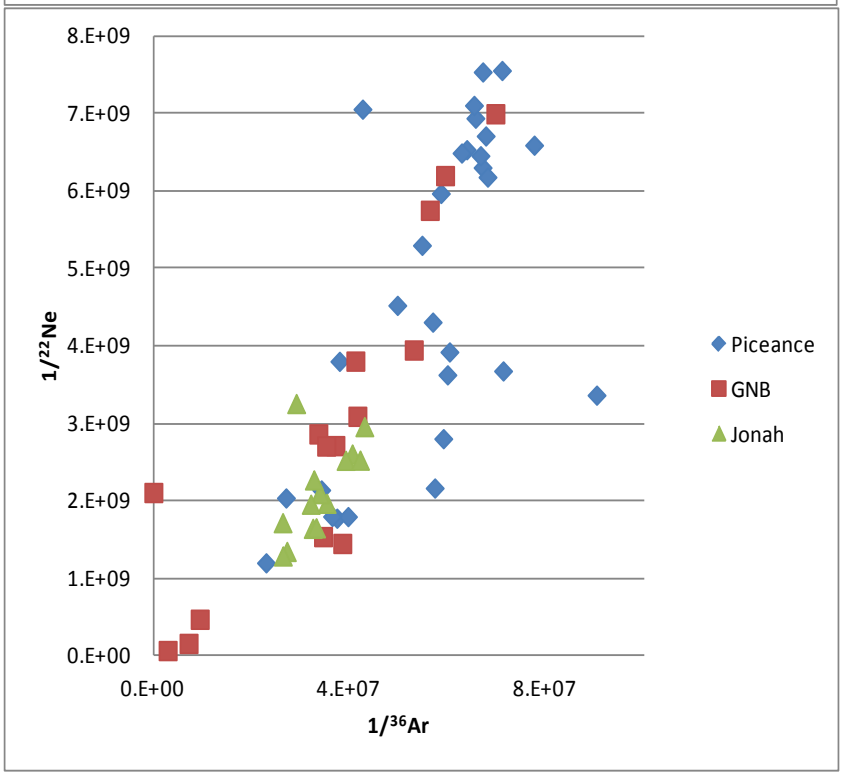

Figure 7.10 ^{36}Ar and ^{22}Ne are both derived from the atmosphere and enter natural through contact with meteoric water. $1/^{36}Ar$ and $1/^{22}Ne$ ratios are highly variable in the Piceance and Greater Natural Buttes data set indicate a wide range of interaction with meteoric water; the Jonah data are very consistent and indicate generally significant interaction with meteoric water.

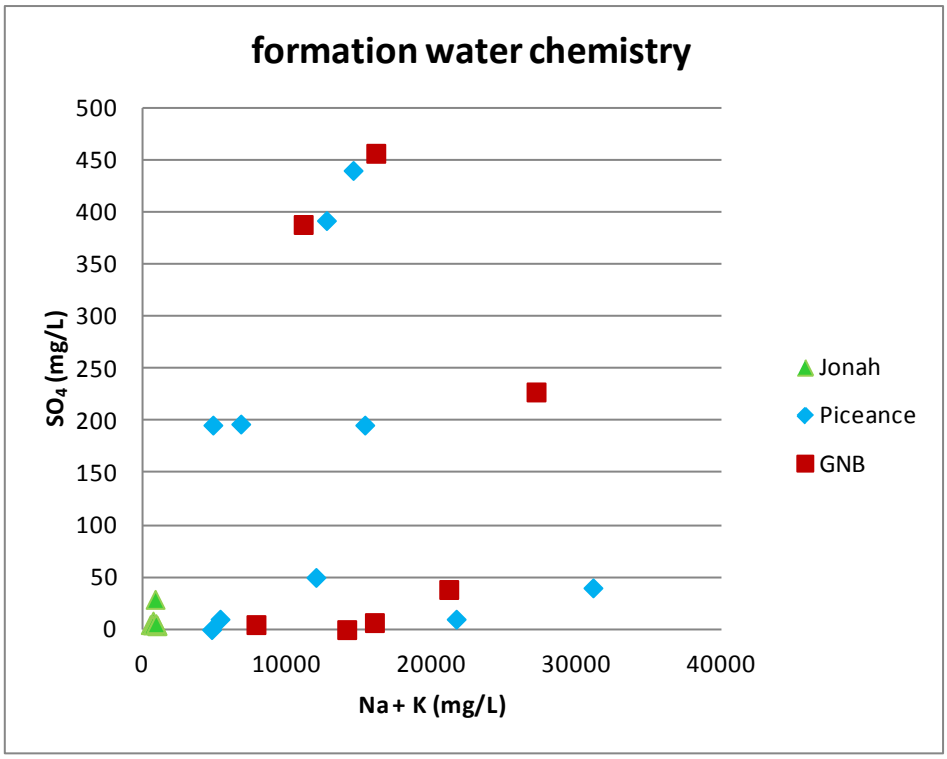

Figure 7.11. Formation water chemistry data from Jonah, Greater Natural Buttes and the Piceance Basin fields. Jonah waters are substantially more dilute than waters from the other fields. Piceance data from Zhang et al (2009). Jonah data from the Wyoming Oil and Gas Commission (downloaded Dec 18, 2013). Piceance data from S. Cumella (personal communication 2013).

8 HYDROUS PYROLYSIS EXPERIMENTS ON ROCKY MOUNTAIN SOURCE ROCKS

8.1 Research Objectives

In order to understand volumes and the bulk and isotopic compositions of gas generated from source rocks in the Piceance Basin and Jonah Field, SRA analysis (Weatherford Source Rock Analyzer®) and hydrous pyrolysis experiments were carried out on four possible source formations. In the Rocky Mountain basins, formations containing Type II marine, Type III terrestrial kerogen, or a mixture, are considered to be significant sources of gas by Coskey (2004) and Yurewicz et al. (2003). Those studies suggested primary source rocks in the Piceance Basin as the Cameo Coal, Mesaverde Group (Type III kerogen), and the Mancos Shale (Type II kerogen), and in the Jonah Field area, carbonaceous shales and coals of the Lance Formation and Mesaverde Group (Type III kerogen) and the Mowry and Hilliard Shale (Type II kerogen) (Coskey, 2004; Yurewicz et al., 2003).

Experiments on candidate source rocks in the Piceance and Green River Basin were used to develop relationships between the gas volumes, the bulk and isotopic composition of gases from these source rocks and the thermal maturity, and to understand:

1. Whether there is a maturity effect on the isotopic compositions of gases. If so, what is the relationship between the maturity and isotopic composition of gas evolved from different kerogens?

> Previous studies (Schoell, 1983; Chung et al., 1988; Schoell, 1988; Jenden et al., 1988; Jenden et al., 1993; Prinzhofer and Huc, 1995; Prinzhofer and Pernaton, 1997) all identified a strong relationship between the thermal maturity and the isotopic compositions of gases, especially with gases generated from kerogen early in primary cracking. However, recent studies of hydrous pyrolysis gases from Menilite Shale in Poland by Kotarba et al. (2009) indicates that thermal maturity has only subtle effects on the isotopic signatures of gases. Whether or not the level of thermal maturity affects the isotopic compositions of gases is the most critical question addressed in this study.
>
> A related question is whether, at a given maturity level, different types of kerogen produce gases of different isotopic composition? If both maturity and kerogen types affect the isotopic compositions of gases, which one has a greater impact on variations of stable isotopes in natural gases?

2. Gas generated from coals has CO2 and N2 as the main non-hydrocarbon gases. Does the composition of non-hydrocarbon gases provide information about source rocks?

> Sapropelic and humic organic matter generates different amounts and proportions of non-hydrocarbon gases. Comparison between laboratory-produced non-hydrocarbon

gases and field-collected non-hydrocarbon gases may help indirectly interpret the source rocks.

8.2 Research Summary

Sequential hydrous pyrolysis experiments were conducted on immature samples of the Cameo coal zone, Mowry, Mancos, and Baxter/Hilliard Shales to characterize their generated gases and evaluate their potential as sources for gas accumulations in the Greater Green River Basin and Piceance Basin. The experiments were conducted sequentially for 72 h at 300, 330, and 360°C, equivalent to measured vitrinite reflectance values of 1.0, 1.3, and 1.6 %Ro, respectively. After each 72 h experiment, the generated gas and expelled oil were removed from the reactor. Gases generated from each sequential experiment were analyzed for molecular composition and stable carbon and hydrogen isotopes.

All source rocks generated significant hydrocarbon and non-hydrocarbon gases (N_2, H_2S, H_2, and CO_2). Cumulative yields of methane to butane increased with increasing thermal maturation (Figures 8.1 and 8.2). On a per gram of total-organic-carbon (TOC) basis, the methane yield from the Cameo coal at 360°C exceeded that at 300°C by almost eightfold. The cumulative methane yields on a TOC basis, from highest to lowest, are Cameo coal, Baxter/Hilliard, Mowry, and Mancos Shales. Cumulative gas wetness from both Mancos and Mowry Shales was high.

With increasing thermal maturity, $\delta^{13}C$ of methane from all four source rocks became lighter, consistent with conventional models. Isotopic compositions of methane from the different source rocks were not significantly different (Figure 8.3). Ethane and propane generated from the Cameo Coal were isotopically heavier than from other source rocks.

The Baxter/Hillard Shale generated the greatest amount of H_2, H_2S, and CO_2, on a TOC basis, whereas Cameo coal generated the least (Figure 8.4). The relatively positive $\delta^{13}C$ values for CO_2 from the Mancos Shale and Baxter Shale suggests it was sourced from thermal decomposition of carbonate minerals in the original rock samples (Figure 8.5. More negative $\delta^{13}C$ values for CO_2 from the Cameo coal indicate that gas is from an organic source, while intermediate $\delta^{13}C$ of CO_2 from the Mowry Shale indicates contributions from both organic and inorganic sources or merely from the inorganic source.

Gases generated from laboratory experiments are isotopically lighter than gas sampled from the Jonah and Piceance Basin fields. Two explanations are proposed: 1) Migration effects from the source to the reservoir and escaping gas from reservoirs may significantly alter final gas compositions; 2) Gases from experiments only reach primary cracking stage of gas generation, whereas field gas may represent gas from secondary cracking of oils deeper in the basins.

8.3 References

Chung, H.M., Gormly, J.R., & Squires, R.M. (1988). Origin of gaseous hydrocarbons in subsurface environments: theoretical considerations of carbon isotope distribution. Chemical Geology 71, 97–103.

Coskey, R. J. (2004). Burial-history modeling of the Jonah field area: An unusual and possibly unique gas accumulation in the Green River Basin, Wyoming. In Jonah Field: Case Study of a Giant Tight-Gas Fluvial Reservoir, J. W. Robinson and K. W. Shanley, eds.: AAPG Studies in Geology 52 and Rocky Mountain Association of Geologists 2004 Guidebook, 93-125.

Jenden, P. D., Newell, K. D., Kaplan, I. R., & Watney, W. L. (1988). Composition and stable-isotope geochemistry of natural gases from Kansas, Midcontinent, USA. *Chemical geology*, *71*(1), 117-147.

Jenden, P. D., Drazan, D. J., & Kaplan, I. R. (1993). Mixing of thermogenic natural gases in northern Appalachian Basin. *AAPG Bulletin*, *77*(6), 980-998.

Kotarba, M. J., Curtis, J. B., & Lewan, M. D. (2009). Comparison of natural gases accumulated in Oligocene strata with hydrous pyrolysis gases from Menilite Shales of the Polish Outer Carpathians. *Organic Geochemistry*, *40*(7), 769-783.

Prinzhofer, A. A., & Huc, A. Y. (1995). Genetic and post-genetic molecular and isotopic fractionations in natural gases. *Chemical Geology*, *126*(3), 281-290.

Prinzhofer, A., & Pernaton, E. (1997). Isotopically light methane in natural gas: bacterial imprint or diffusive fractionation?. *Chemical Geology*, *142*(3), 193-200.

Schoell, M. (1983). Genetic characterization of natural gases. *AAPG bulletin*, *67*(12), 2225-2238.

Schoell, M. (1988). Multiple origins of methane in the earth. *Chemical Geology*,*71*(1), 1-10.

Yurewicz, D. A., Bohacs, K. M., Yeakel, J. D., & Kronmueller, K. (2003). Source rock analysis and hydrocarbon generation, Mesaverde Group and Mancos Shale, northern Piceance Basin, Colorado.

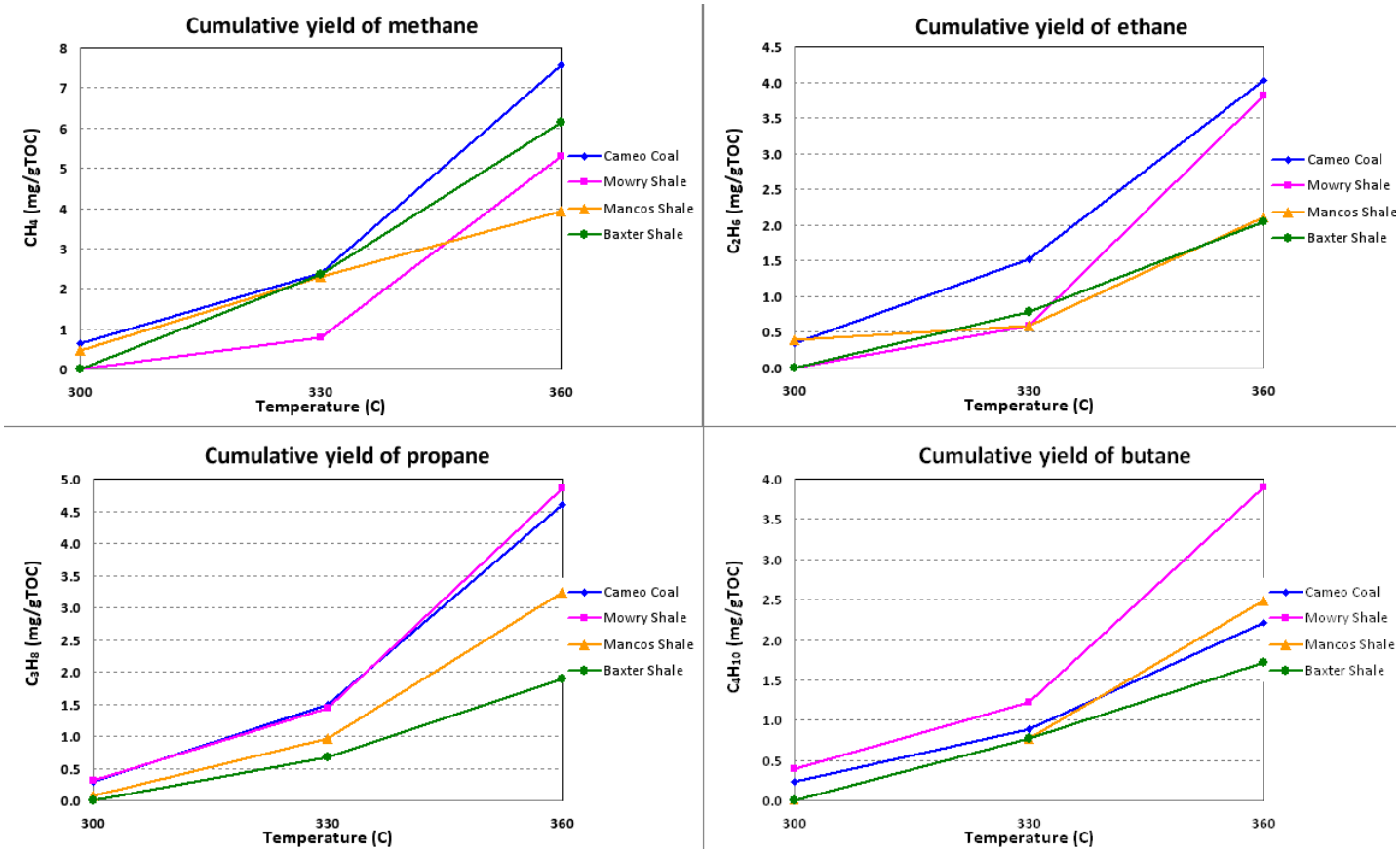

Figure 8.1. Cumulative yields of hydrocarbon gases of methane, ethane, propane, and butane from the four different source rocks- Cameo Coal (blue), Mowry Shale (pink), Mancos Shale (orange), and the Baxter Shale (green), on a per gram of TOC basis.

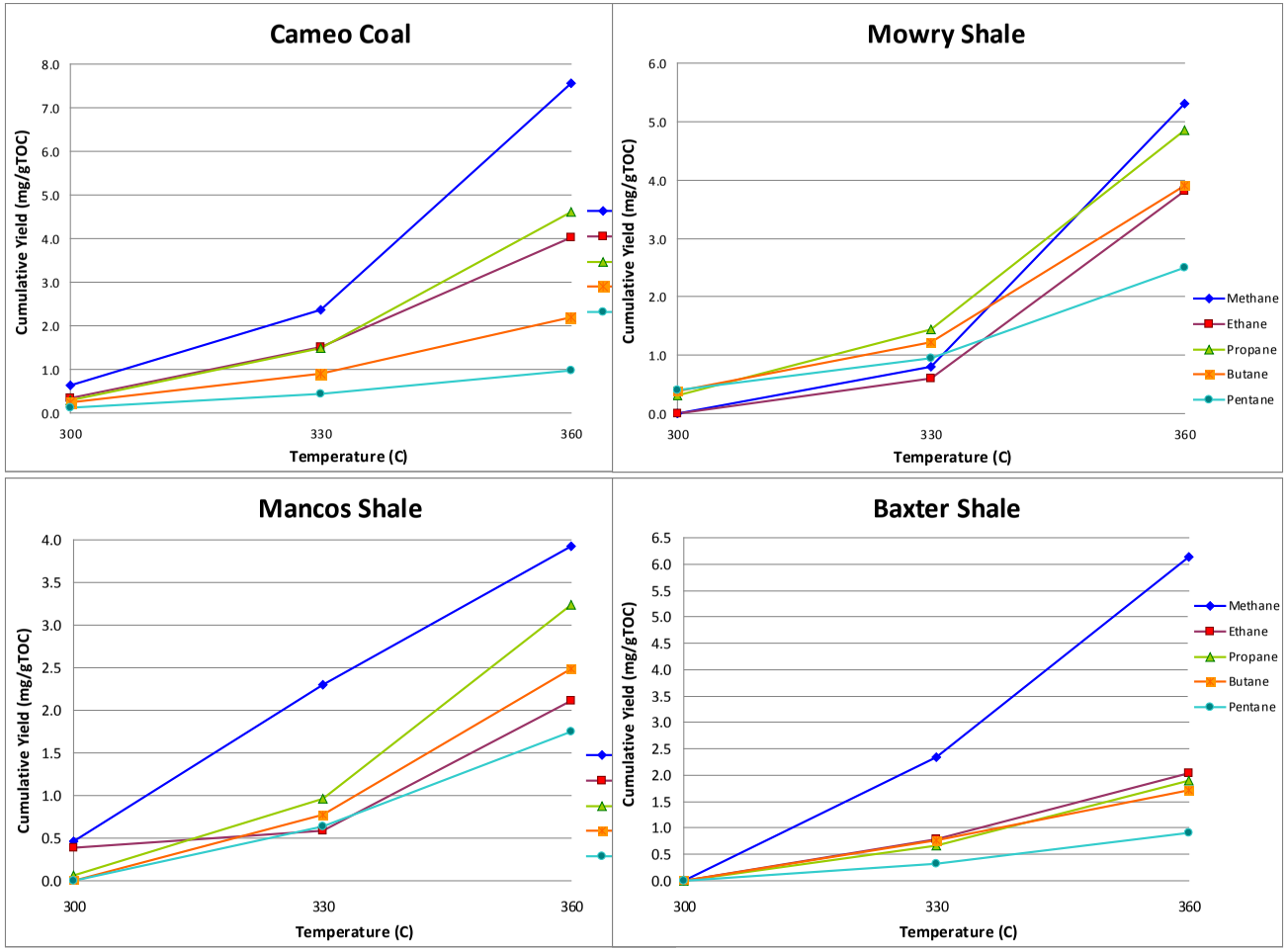

Figure 8.2. Cumulative yields of hydrocarbon gases of methane, ethane, propane, and butane in Cameo Coal, Mowry, Mancos, and Baxter Shale, on a per gram of TOC basis. Gas: C_1 (blue), C_2 (red), C_3 (green), C_4 (orange), and C_5 (light blue).

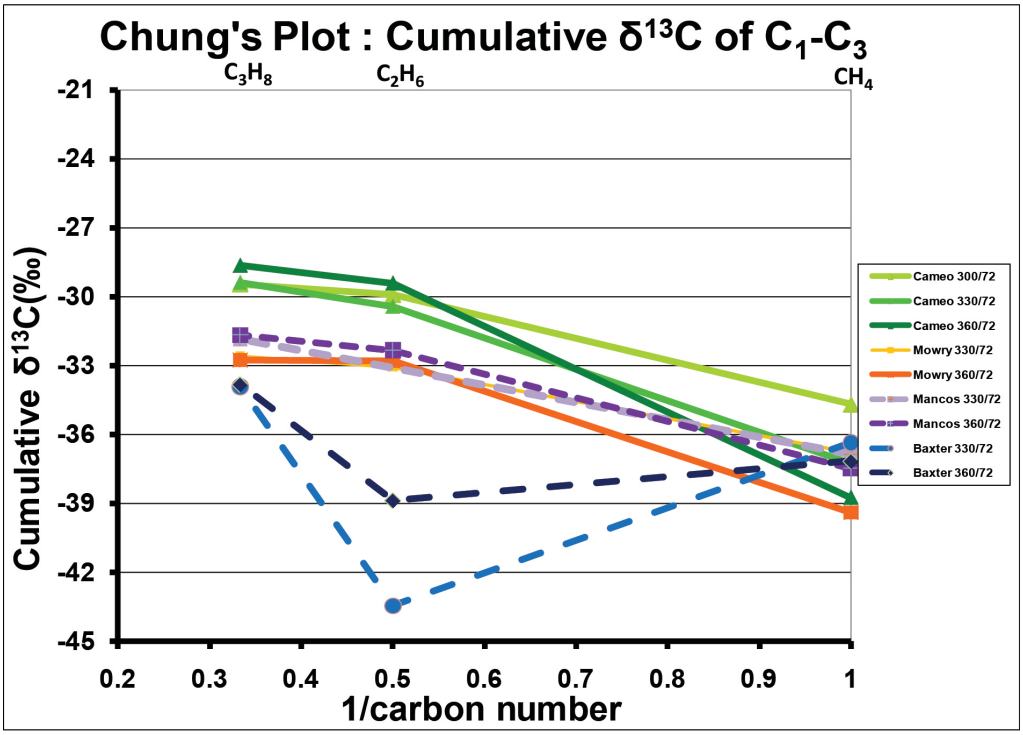

Figure 8.3 The cumulative $\delta^{13}C$ of methane, ethane, and propane generated from hydrous pyrolysis experiments versus the reciprocal of their carbon number. Cameo Coal (green), Mowry Shale (orange), Mancos Shale (purple), and Baxter Shale (blue).

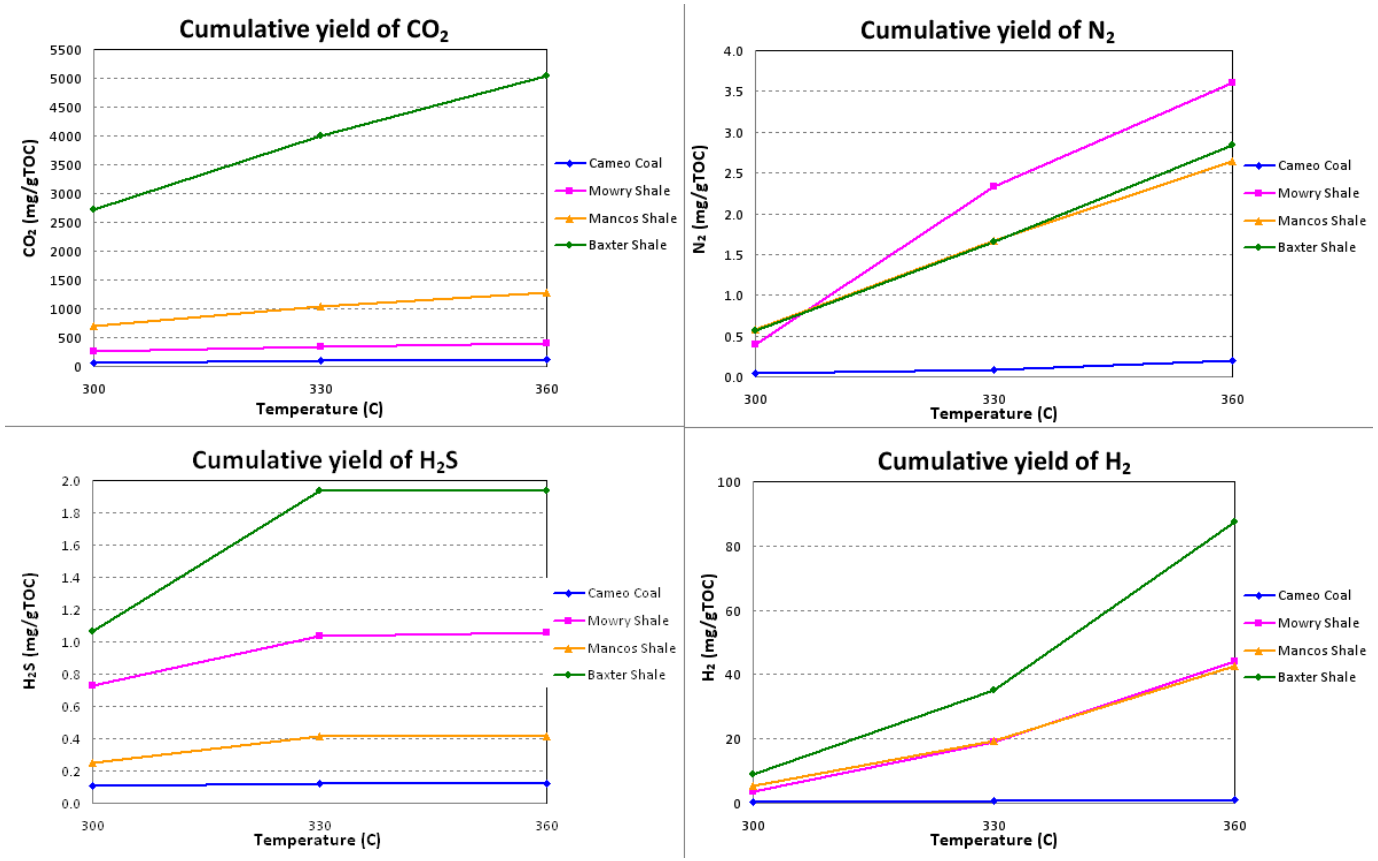

Figure 8.4. Cumulative yields of non-hydrocarbon gases (CO2, H2S, H2, and N2) in sequential hydrous pyrolysis experiments from Cameo Coal (blue), Mowry Shale (pink), Mancos shale (orange), and Baxter Shale (green).

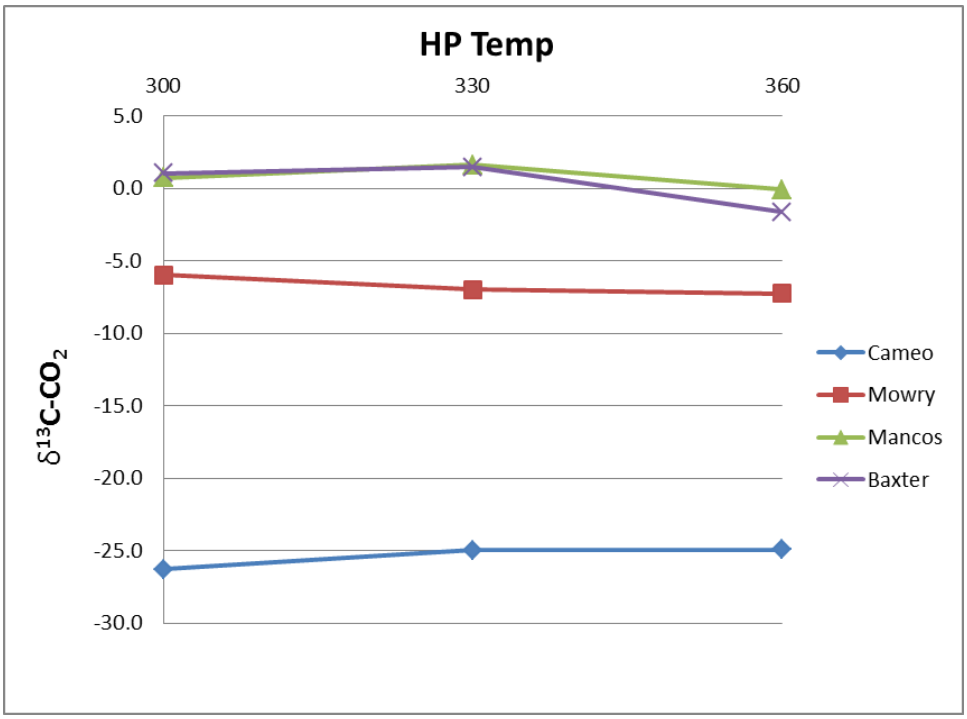

Figure 8.5. The $\delta^{13}C$ values of the carbon dioxide generated in the 300 °C, 330 °C and 360 °C experiments from four source rocks- Cameo Coal, Mowry Shale, Mancos Shale, and Baxter Shale.

9 SUMMARY AND CONCLUSIONS

1) This study of gas compositions in three major Rocky Mountain tight-gas-sand reservoirs has document a high degree of variability in gas compositions within gas fields. Gases vary in composition geographically within fields – in other words, different wells within the same field produce gases of differing composition – and they vary stratigraphically, with gases of different composition produced from different parts of the gas column, in some cases between samples spaced short vertical distances in a single well.

2) Production gases composition vary within the following ranges (as mole fractions):

Methane	0.59 to 1.00 (average = 0.83)
Ethane	0.00 to 0.15 (average = 0.08)
Propane	0.00 to 0.10 (average = 0.04)
iso-butane	0.00 to 0.21 (average = 0.014)
n-butane	0.00 to 0.22 (average = 0.015)
iso-pentane	0.00 to 0.10 (average = 0.008)
n-pentane	0.00 to 0.21 (average = 0.009)
wetness	0.00 to 0.38 (average = 0.16)
CO_2	0.00 to 0.15 (average = 0.02)

3) The two areas from which we have the most data, Jonah Field and the Piceance Basin fields (Mamm Creek, Rulison, Parachute, Grand Valley) exhibit different vertical trends in gas composition. Jonah Field is characterized by compositions that are relatively dry at the top of the gas column, with carbon isotopic compositions that are relatively heavy. Jonah gases become wetter and isotopically lighter with increasing depth.

The Piceance gases are relatively wet at the top of the gas column, with carbon isotopic compositions that are relatively light. Gases become drier with depth and isotopically heavy, although there is a suggestion in the data that gases become isotopically very light in the deepest samples.

Two Greater Natural Buttes wells do not exhibit systematic trends in composition.

4) The three areas sampled in this study can be distinguished by the following parameters:

- δD of the C2+ gases: lighter by 25 to 40‰ at Jonah Field in comparison to Greater Natural Buttes and the Piceance fields.

- $\delta^{13}C$ of CO_2: isotopically light at Jonah, intermediate in the Piceance fields and isotopically heaviest at Greater Natural Buttes.

- Several noble gas parameters, including $^{3}He/^{4}He$ (low at Jonah, higher in the other data sets), $1/^{22}Ne$ and $1/^{36}Ar$ (low at Jonah, higher and variable in the other data sets), $^{20}Ne/^{22}Ne$ and $^{21}Ne/^{22}Ne$ (low at Jonah, higher and variable in the other data sets).

- *i*-C_4/*n*-C_4: lower at Greater Natural Buttes, higher in the other fields.

5) The high degree of spatial variability in data sets from all three areas indicates that simple gas migration models do not apply. A model in which gases are fed into the bottom of the gas column and diffuse upward does not explain the trends in the data. Specifically, a diffusion model predicts that gases should become dryer and isotopically lighter upward. While gases become dryer upward at Jonah, they become isotopically heavier, and while gases in the Piceance fields become isotopically lighter upward, they also become wetter.

The variability also precludes a model of gas migration through naturally occurring systems of hydraulic fractures. If that model applied to gas migration on a large scale within these fields, gas compositions would be relatively consistent vertically. However our data show systematic vertical trends.

6) There is strong evidence for pervasive interaction with dilute formation water in the Jonah gases, probably in the upper part of the gas column, specifically: (1) isotopically light CO_2 (as light as -18‰), (2) low ratios of $1/^{22}Ne$ and $1/^{36}Ar$, (3) the coincidence of dry and isotopically heavy carbon in the absence of significant coaly source rocks. These patterns can be explained by bacterial oxidation of wet gases, leaving residual hydrocarbon gases that are isotopically heavy and methane-rich, plus CO_2 that is isotopically light.

Data from the Piceance fields suggests that local reaction with formation water and bacterial oxidation may have taken place, supported by isolated mud gas samples of pure methane with extremely positive (heavy carbon isotopes) composition, spatially coinciding with production wells with low $1/^{22}Ne$ and $1/^{36}Ar$.

7) Clear evidence for multiple source rocks exists in the Piceance data set, where wet gases are documented in the vicinity of Mamm Creek Field, compared to much drier compositions in the nearby Rulison, Parachute and Grand Valley Fields. This pattern has been interpreted by others as reflecting input from a deeper shale source rock, in addition to input from the shallower Cameo Coal. Our data, including fluid inclusion data that indicate the presence of a paleo-oil-water contact, are consistent with that interpretation.

8) Gas compositions indicate that some gases were derived from the secondary cracking of oil to gas; however there is no evidence of cracking of wet gases to drier gases.

10 ACKNOWLEDGEMENTS

This study was funded by RPSEA, whose support was critical. Additional funding was provided by the following companies: ExxonMobil, ConocoPhillips, Marathon Oil Company, BP, Newfield, Williams Production Company and Anadarko. We greatly appreciate their financial support.

We thank the following for cooperation and assistance with field sampling: at Jonah Field: Ira Pasternack and Dean Dubois (Encana); at Greater Natural Buttes Field: Steve Stancel (Anadarko); at Mamm Creek: Steve Sunnenberg (Bill Barrett Corporation). Field personnel from all three companies provided logistical support through extensive field trips, and Encana provided housing and food during sampling at Jonah Field.

The following field assistants helped with the sampling: TingWei Ko, Sheven Poole, Mike Halsema and Jaron Lucero.

We also owe a debt of gratitude to Steve Cumella and Dag Nummedal, who provided insights into the geology of these basins.

Appendix 1

Production gas data, Piceance Basin - bulk gas composition

Area	Field	Well	fraction C1	fraction C2	fraction C3	fraction i-C4	fraction n-C4	fraction i-C5	fraction n-C5	fraction CO2	wetness
Piceance	Grand Valley	G	1.00	0.00							0.00
Piceance	Grand Valley	B	0.90	0.10							0.10
Piceance	Grand Valley	E	0.81	0.09	0.04	0.01	0.01	0.01	<0.01	0.03	0.16
Piceance	Grand Valley	F	0.87	0.07	< 0.01	< 0.01	< 0.01	< 0.01	< 0.01	0.06	0.07
Piceance	Grand Valley	S	0.92	0.07	0.01	< 0.01	< 0.01	< 0.01	< 0.01	< 0.01	0.08
Piceance	Grand Valley	T	0.79	0.13	0.04	< 0.01	< 0.01	< 0.01	< 0.01	0.04	0.18
Piceance	Grand Valley	KK	0.91	0.05	0.01	0.01	0.01	<0.01	<0.01	0.03	0.08
Piceance	Grand Valley	LL	0.80	0.07	0.03	0.01	0.01	<0.01	<0.01	0.08	0.13
Piceance	Mamm Creek	**BBC 12D-24-692**	0.78	0.12	0.05	0.02	0.02	0.01	0.01		0.23
Piceance	Mamm Creek	**BRYNILDSON 12C-20-692**	0.69	0.15	0.09	0.02	0.03	0.01	0.01		0.31
Piceance	Mamm Creek	**GEISKE 41A-26-692**	0.76	0.12	0.06	0.02	0.02	0.01	0.01		0.24
Piceance	Mamm Creek	**GGU 14-19**	0.68	0.15	0.09	0.03	0.03	0.01	0.01		0.32
Piceance	Mamm Creek	**GGU BARGE 12A-32-691**	0.77	0.12	0.06	0.02	0.02	0.01	0.01		0.23
Piceance	Mamm Creek	**GGU SCOTT 11D**	0.73	0.14	0.07	0.02	0.02	0.01	0.01		0.27
Piceance	Mamm Creek	**JACKSON 34D**	0.74	0.14	0.07	0.02	0.02	0.01	0.01		0.26
Piceance	Mamm Creek	**JOLLEY 21C-21-691**	0.73	0.13	0.07	0.02	0.02	0.01	0.01		0.27
Piceance	Mamm Creek	**JOLLEY 31C**	0.78	0.12	0.05	0.02	0.02	0.01	0.01		0.22
Piceance	Mamm Creek	**JOLLEY FED 21A-28-691**	0.77	0.13	0.06	0.02	0.02	0.01	0.00		0.23
Piceance	Mamm Creek	**LAST DANCE 10-3**	0.76	0.13	0.06	0.02	0.02	0.01	0.00		0.24
Piceance	Mamm Creek	**MILLER 01C-36**	0.68	0.15	0.09	0.03	0.03	0.01	0.01		0.32
Piceance	Mamm Creek	**MILLER 24B-6-791**	0.79	0.12	0.05	0.01	0.01	0.01	0.01		0.21
Piceance	Mamm Creek	**SPECIALTY 44B-20-692**	0.79	0.13	0.05	0.01	0.01	0.01	0.01		0.21
Piceance	Mamm Creek	**STRANAHAN 31A**	0.79	0.12	0.05	0.01	0.01	0.01	0.00		0.21
Piceance	Parachute	QQ	1.00	0.00							0.00
Piceance	Parachute	A	0.85	0.07	0.04	0.01	0.01	0.01	<0.01	0.02	0.14
Piceance	Parachute	I	0.87	0.05	0.02	0.01	0.01	0.01	0.01	0.04	0.11
Piceance	Parachute	J	0.85	0.08	0.03	0.01	0.01	<0.01	<0.01	0.02	0.13
Piceance	Parachute	L	0.71	0.07	0.04	0.02	0.02	0.02	0.01	0.10	0.20
Piceance	Parachute	M	0.85	0.08	0.03	0.01	0.01	<0.01	<0.01	0.02	0.13
Piceance	Parachute	O	0.81	0.10	0.04	0.01	0.01	0.01	<0.01	0.03	0.17
Piceance	Parachute	P	0.85	<0.01	<0.01	<0.01	<0.01	<0.01	<0.01	0.15	0.00
Piceance	Parachute	Q	0.88	0.06	0.02	0.01	0.01	<0.01	<0.01	0.02	0.10
Piceance	Parachute	OO	1.00	< 0.01	< 0.01	< 0.01	< 0.01	< 0.01	< 0.01	< 0.01	0.00
Piceance	Parachute	NN	0.90	0.07	0.03	< 0.01	< 0.01	< 0.01	< 0.01	< 0.01	0.10
Piceance	Parachute	N	0.89	0.07	0.03	0.01	< 0.01	< 0.01	< 0.01	< 0.01	0.11
Piceance	Rulison	Z	0.80	0.11	0.05	0.01	0.01	0.01	<0.01	0.02	0.19
Piceance	Rulison	GG	0.77	0.11	0.05	0.02	0.02	0.02	0.01	0.03	0.23
Piceance	Rulison	Y	0.81	0.09	0.03	0.01	0.01	<0.01	<0.01	0.04	0.15
Piceance	Rulison	EE	0.94	0.06							0.06
Piceance	Rulison	RR	1.00	0.00							0.00
Piceance	Rulison	H	0.96	<0.01	< 0.01	< 0.01	< 0.01	< 0.01	< 0.01	0.03	0.00
Piceance	Rulison	U	0.80	0.11	0.05	0.01	0.01	0.01	<0.01	0.01	0.19
Piceance	Rulison	V	0.85	0.08	0.03	0.01	0.01	< 0.01	< 0.01	0.02	0.13
Piceance	Rulison	W	0.86	0.10	0.04	< 0.01	< 0.01	< 0.01	< 0.01	< 0.01	0.14
Piceance	Rulison	X	0.88	0.09	0.03	< 0.01	< 0.01	< 0.01	< 0.01	< 0.01	0.12
Piceance	Rulison	AA	1.00	< 0.01	< 0.01	< 0.01	< 0.01	< 0.01	< 0.01	< 0.01	0.00
Piceance	Rulison	CC	0.82	0.10	0.03	0.01	0.01	<0.01	<0.01	0.04	0.15
Piceance	Rulison	HH	0.87	0.06	0.01	<0.01	<0.01	0.01	<0.01	0.05	0.08

Note: See figure 4.1 for well locations.

Production gas data, Piceance Basin - carbon isotope composition

Area	Field	Well	13C C1	13C C2	13C C3	13C i-C4	13C n-C4	13C i-C5	13C n-C5	13C CO2
Piceance	Grand Valley	G	-36.2	-25.8	-24.8	-24.1	-24.1	-25.4	-24.2	
Piceance	Grand Valley	B	-37.7	-27.5	-25.2	-26.0	-24.2	-25.5	-24.2	-9.6
Piceance	Grand Valley	E	-33.9	-25.3	-23.3	-24.5	-22.9	-24.1	-22.9	-6.2
Piceance	Grand Valley	F	-30.1	-24.5	-23.7	-18.5	-22.7	-22.9	-24.7	-8.0
Piceance	Grand Valley	S	-39.5	-26.6	-24.8	-24.4	-23.4	-24.1	-23.1	-9.3
Piceance	Grand Valley	T	-27.2	-25.7	-23.6	-24.3	-22.9	-23.6	-22.3	-8.7
Piceance	Grand Valley	KK	-32.3	-25.8	-22.8	-24.5	-21.9	-23.6	-22.7	-5.6
Piceance	Grand Valley	LL	-35.3	-28.0	-25.2	-26.1	-24.7	-25.9	-25.2	-8.8
Piceance	Mamm Creek	BBC 12D-24-692	-30.7	-25.7	-22.8	-22.9	-21.5	-21.4	-21.0	-2.5
Piceance	Mamm Creek	BRYNILDSON 12C-20-692	-40.6	-27.2	-24.4	-24.9	-23.8	-23.6	-22.3	-1.8
Piceance	Mamm Creek	GEISKE 41A-26-692	-39.6	-25.4	-22.4	-23.4	-22.7	-23.6	-22.4	-7.4
Piceance	Mamm Creek	GGU 14-19	-40.4	-27.7	-25.1	-25.6	-24.0	-24.3	-23.4	
Piceance	Mamm Creek	GGU BARGE 12A-32-691	-40.2	-26.4	-23.6	-24.3	-22.9	-23.2	-22.8	-3.4
Piceance	Mamm Creek	GGU SCOTT 11D	-38.1	-26.7	-23.8	-24.4	-22.8	-23.2	-21.8	
Piceance	Mamm Creek	JACKSON 34D	-41.3	-27.5	-24.4	-25.0	-23.6	-23.8	-22.9	-2.5
Piceance	Mamm Creek	JOLLEY 21C-21-691	-40.3	-26.4	-23.7	-24.3	-23.4	-22.8	-23.6	
Piceance	Mamm Creek	JOLLEY 31C	-38.2	-25.9	-23.3	-23.4	-22.7	-23.2	-23.0	-3.8
Piceance	Mamm Creek	JOLLEY FED 21A-28-691	-34.7	-26.9	-23.7	-23.6	-23.0	-22.9	-22.5	-3.6
Piceance	Mamm Creek	LAST DANCE 10-3	-41.1	-27.6	-24.6	-24.7	-23.6	-23.4	-22.8	-3.6
Piceance	Mamm Creek	MILLER 01C-36	-41.1	-27.6	-24.6	-24.7	-23.6	-23.4	-22.8	
Piceance	Mamm Creek	MILLER 24B-6-791	-41.1	-27.6	-24.0	-24.1	-24.5	-23.1	-23.1	-4.4
Piceance	Mamm Creek	SPECIALTY 44B-20-692	-38.4	-28.4	-25.3	-25.3	-24.4	-23.7	-23.3	-3.8
Piceance	Mamm Creek	STRANAHAN 31A	-40.2	-25.3	-25.6	-24.8	-23.9	-24.8	-24.1	-2.8
Piceance	Parachute	QQ	-36.2	-25.5	-22.8	-22.8	-21.9	-23.0	-21.4	-6.2
Piceance	Parachute	A	-36.3	-27.7	-26.3	-25.3	-25.4	-24.4	-24.3	-9.8
Piceance	Parachute	I	-41.3	-24.8	-23.1	-24.3	-22.9	-24.0	-23.2	-6.1
Piceance	Parachute	J	-39.7	-28.2	-25.5	-25.8	-24.8	-25.2	-24.0	-8.0
Piceance	Parachute	L	-39.7	-28.2	-25.2	-25.0	-23.6	-24.6	-23.6	-6.2
Piceance	Parachute	M	-32.6	-25.3	-24.0	-25.1	-23.8	-25.0	-24.3	-6.4
Piceance	Parachute	O	-31.6	-24.9	-24.0	-25.8	-24.3	-24.9	-24.3	-6.5
Piceance	Parachute	P	-36.2	-23.5	-22.8	-23.5	-22.2	-23.5	-22.6	-5.0
Piceance	Parachute	Q	-42.8	-26.6	-23.8	-24.1	-22.9	-23.9	-23.0	-8.4
Piceance	Parachute	OO	-43.3	-26.1	-25.4	-25.8	-25.2	-25.5	-24.9	-11.4
Piceance	Parachute	NN	-39.0	-24.1	-24.1	-24.8	-24.4	-25.1	-24.8	-9.2
Piceance	Parachute	N	-38.7	-26.8	-25.8	-25.3	-25.5	-25.1	-24.8	-9.8
Piceance	Rulison	Z	-39.0	-27.4	-25.1	-25.7	-24.3	-25.7	-24.6	-6.6
Piceance	Rulison	GG	-38.6	-27.1	-24.8	-25.5	-23.9	-25.9	-24.3	-4.8
Piceance	Rulison	Y	-38.3	-26.3	-24.1	-24.5	-23.1	-23.9	-23.6	-4.8
Piceance	Rulison	EE	-38.7	-26.3	-24.4	-24.3	-23.9	-24.6	-23.5	-5.5
Piceance	Rulison	RR	-36.2	-24.6	-22.3	-22.4	-21.6	-23.3	-22.6	
Piceance	Rulison	H	-27.8	-27.5	-25.3	-25.6	-24.8	-25.0	-24.1	-4.2
Piceance	Rulison	U	-36.2	-27.5	-25.2	-26.4	-24.5	-25.8	-25.1	-12.8
Piceance	Rulison	V	-36.2	-25.3	-23.5	-24.5	-23.1	-24.2	-24.9	-5.2
Piceance	Rulison	W	-32.7	-25.9	-23.7	-24.4	-23.1	-24.4	-23.6	-5.9
Piceance	Rulison	X	-31.3	-25.3	-23.4	-24.1	-23.1	-24.2	-23.6	-6.3
Piceance	Rulison	AA	-37.9	-29.7	-26.8	-26.4	-25.3	-25.9	-25.3	-12.1
Piceance	Rulison	CC	-38.5	-26.7	-24.6	-24.9	-23.9	-24.4	-23.7	-5.3
Piceance	Rulison	HH	-38.1	-25.3	-22.4	-23.2	-23.2	-25.3	-24.7	-5.7

Note: See figure 4.1 for well locations.

Production gas data, Piceance Basin - hydrogen isotope composition

Area	Field	Well	dD C1	dD C2	dD C3	dD i-C4	dD n-C4	dD i-C5	dD n-C5
Piceance	Grand Valley	G	-155	-118	-126	-107	-120	-83	-108
Piceance	Grand Valley	B	-171	-136	-126	-121	-120	-110	-114
Piceance	Grand Valley	E	-171	-133	-118	-114	-106		
Piceance	Grand Valley	F	-150	-127	-119	-114	-113	-104	-115
Piceance	Grand Valley	S	-168	-127	-118	-118	-115	-105	-113
Piceance	Grand Valley	T	-182						
Piceance	Grand Valley	KK	-161	-125					
Piceance	Grand Valley	LL	-177	-134					
Piceance	Mamm Creek	BBC 12D-24-692	**-185**	**-119**	**-115**	**-112**	**-112**	**-100**	**-116**
Piceance	Mamm Creek	BRYNILDSON 12C-20-692	**-188**	**-134**	**-121**	**-114**	**-116**	**-99**	**-113**
Piceance	Mamm Creek	GEISKE 41A-26-692	**-177**	**-132**	**-123**	**-111**	**-116**	**-95**	**-111**
Piceance	Mamm Creek	GGU 14-19	**-178**	**-138**	**-125**	**-115**	**-118**	**-99**	**-111**
Piceance	Mamm Creek	GGU BARGE 12A-32-691	**-180**	**-139**	**-130**	**-120**	**-121**	**-104**	**-115**
Piceance	Mamm Creek	GGU SCOTT 11D	**-192**	**-141**	**-127**	**-122**	**-123**	**-110**	**-120**
Piceance	Mamm Creek	JACKSON 34D	**-196**	**-141**	**-126**	**-122**	**-124**	**-111**	**-123**
Piceance	Mamm Creek	JOLLEY 21C-21-691	**-193**	**-137**	**-130**	**-123**	**-125**	**-111**	**-120**
Piceance	Mamm Creek	JOLLEY 31C	**-195**	**-134**	**-131**	**-120**	**-122**	**-102**	**-115**
Piceance	Mamm Creek	JOLLEY FED 21A-28-691	**-187**	**-134**	**-127**	**-121**	**-123**	**-109**	**-123**
Piceance	Mamm Creek	LAST DANCE 10-3	**-200**	**-151**	**-129**	**-123**	**-126**	**-107**	**-122**
Piceance	Mamm Creek	MILLER 01C-36	**-197**	**-145**	**-123**	**-120**	**-121**	**-107**	**-124**
Piceance	Mamm Creek	MILLER 24B-6-791	**-185**	**-136**	**-122**	**-120**	**-126**	**-111**	**-120**
Piceance	Mamm Creek	SPECIALTY 44B-20-692	**-191**	**-139**	**-122**	**-119**	**-120**	**-109**	**-119**
Piceance	Mamm Creek	STRANAHAN 31A	**-185**	**-135**	**-126**	**-119**	**-122**	**-103**	**-118**
Piceance	Parachute	QQ	-161	-124	-119	-113	-109	-96	-99
Piceance	Parachute	A	-173	-135	-126				
Piceance	Parachute	I	-168	-128	-122	-116	-117	-103	-111
Piceance	Parachute	J	-162	-131	-119	-116	-114	-105	-115
Piceance	Parachute	L	-167	-129	-120	-117	-114	-102	-109
Piceance	Parachute	M	-168	-129	-118	-116	-114	-101	-111
Piceance	Parachute	O	-165	-132	-123	-117	-115	-102	-111
Piceance	Parachute	P	-164	-131	-122	-118	-115	-104	-113
Piceance	Parachute	Q	-161	-133	-125	-118	-119	-104	-116
Piceance	Parachute	OO	-162	-133	-123	-114	-117	-101	-115
Piceance	Parachute	NN	-176						
Piceance	Parachute	N	-198	-133	-125	-118	-118	-105	-116
Piceance	Rulison	Z	-170	-131	-123	-119	-119	-108	-115
Piceance	Rulison	GG	-176	-129	-119	-120	-118	-110	-119
Piceance	Rulison	Y	-173	-129	-123	-117	-115	-108	-123
Piceance	Rulison	EE	-171	-129	-126	-114	-118	-102	-116
Piceance	Rulison	RR	-161	-126	-115	-101	-102	-74	-105
Piceance	Rulison	H	-168	-134	-122	-119	-116	-106	-115
Piceance	Rulison	U	-180	-138	-127				
Piceance	Rulison	V	-162	-127	-121	-116	-112	-97	-105
Piceance	Rulison	W	-165	-131	-126	-121	-121	-110	-119
Piceance	Rulison	X	-188	-127	-118	-114	-110	-100	
Piceance	Rulison	AA	-167	-135	-124	-119	-116	-95	-115
Piceance	Rulison	CC	-156	-134	-121				
Piceance	Rulison	HH	-192	-124	-118	-113	-124	-112	-119

Note: See figure 4.1 for well locations.

Production gas data, Jonah Field - bulk gas composition

Area	Well	fraction C1	fraction C2	fraction C3	fraction i-C4	fraction n-C4	fraction i-C5	fraction n-C5	fraction CO2	wetness
Jonah	Cabrito 17-25	0.78	0.11	0.06	0.02	0.02	0.01	< 0.01	< 0.01	0.22
Jonah	JWH Corona 61-31	0.88	0.06	0.04	0.01	0.01	< 0.01	< 0.01	< 0.01	0.12
Jonah	JWH Corona 67-30	0.84	0.09	0.04	0.01	0.01	0.01	< 0.01	< 0.01	0.16
Jonah	JWH Corona 79-19	0.93	0						0.07	0.00
Jonah	JWH Corona 16-18	0.86	0.08	0.04	0.01	0.01	< 0.01	< 0.01		0.14
Jonah	JWH Jonah Federal 19-5	0.85	0.08	0.04	0.01	0.01	< 0.01	< 0.01	0.01	0.14
Jonah	SHB 12-36	0.82	0.08	0.04	0.02	0.02	< 0.01	< 0.01	0.01	0.16
Jonah	SHB 16-35R	0.84	0.09	0.04	0.01	0.01	0.01	< 0.01	< 0.01	0.16
Jonah	SHB 2-33	0.81	0.10	0.05	0.02	0.01	0.01	< 0.01		0.19
Jonah	SHB 34-28	0.84	0.08	0.04	0.01	0.01	0.01	< 0.01	0.01	0.15
Jonah	SHB 41-29	0.82	0.09	0.05	0.02	0.01	0.01	< 0.01	< 0.01	0.18
Jonah	SHB 53-17	0.59	0.10	0.10	0.05	0.06	0.03	0.02	0.05	0.38
Jonah	SHB 53-20	0.94	0.04	0.01	< 0.01	< 0.01	< 0.01	< 0.01	< 0.01	0.05
Jonah	SHB 57-15	0.89	0.06	0.03	0.01	0.01	< 0.01	< 0.01	< 0.01	0.11
Jonah	SHB 63-27	0.84	0.08	0.04	0.01	0.01	0.01	< 0.01	0.01	0.15
Jonah	SHB 7-22	0.76	0.09	0.05	0.02	0.02	0.02	0.01	0.02	0.22
Jonah	SHB 75-26	0.87	0.08	0.04	< 0.01	< 0.01	< 0.01	< 0.01	0.01	0.12
Jonah	SHB 84-9	0.87	0.07	0.03	0.01	0.01	< 0.01	< 0.01	< 0.01	0.12
Jonah	SOL 7-36	0.78	0.11	0.06	0.02	0.02	0.01	< 0.01	< 0.01	0.22
Jonah	Yellowpoint 10-13	0.87	0.09	0.04	< 0.01	< 0.01	< 0.01	< 0.01	< 0.01	0.13
Jonah	Yellowpoint 21-12	0.83	0.09	0.04	0.01	0.01	0.01	< 0.01	0.01	0.16
Jonah	SHB 124-11	0.83	0.09	0.04	0.01	0.01	0.01	0.00		0.17
Jonah	SHB 36-32	0.84	0.09	0.04	0.01	0.01	0.01	0.00		0.16
Jonah	JF 37-7	0.80	0.07	0.03	0.03	0.03	0.02	0.01	<0.1	0.19
Jonah	SHB 17-26	0.79	0.07	0.04	0.03	0.03	0.02	0.02	<0.1	0.20
Jonah	SOL 9-36	0.71	0.14	0.08	0.02	0.02	0.01	0.01		0.29
Jonah	SCARLETT 11-34	0.77	0.12	0.06	0.02	0.02	0.01	0.01		0.23
Jonah	JF-11-18	0.82	0.07	0.03	0.03	0.02	0.01	0.01	<0.1	0.18
Jonah	Yellowpoint 4-24	0.72	0.138	0.0717	0.0207	0.0217	0.0103	0.0831		0.32
Jonah	JF 1-8	0.84	0.09	0.04	0.01	0.01	0.01	0.00		0.16

Note: See Figure5.1 for well locations

Production gas data, Jonah Field - carbon isotope composition

Area	Well	13C C1	13C C2	13C C3	13C i-C4	13C n-C4	13C i-C5	13C n-C5	13C CO2
Jonah	Cabrito 17-25	-34.4	-26.1	-25.2	-25.1	-25.1	-24.6	-24.5	
Jonah	JWH Corona 61-31	-38.1	-28.2	-26.7	-25.9	-25.9	-25.3	-25.3	-12
Jonah	JWH Corona 67-30	-36.4	-26.25	-25.4	-24.8	-24.7	-24.5	-24.4	-10.6
Jonah	JWH Corona 79-19	-44	-27.1	-25.6	-24.7	-24.7	-24.4	-24.6	-15.5
Jonah	JWH Corona 16-18	-32.5	-25.4	-25.2	-24.9	-25.0	-25.1	-24.4	
Jonah	JWH Jonah Federal 19-5	-41	-26.6	-26.9	-27.0	-25.9	-25.5	-26.2	-15.8
Jonah	SHB 12-36	-36.2	-25.55	-24.6	-24.1	-24.0	-24.0	-23.9	-9.8
Jonah	SHB 16-35R	-36.6	-27.4	-26.1	-25.3	-25.3	-25.1	-25	-9.4
Jonah	SHB 2-33	-34.0	-25.8	-24.9	-24.7	-24.5	-24.3	-24.3	
Jonah	SHB 34-28	-41.6	-28.2	-26.8	-25.0	-25.1	-25.3	-24.8	-8.1
Jonah	SHB 41-29	-38.2	-26.3	-25.0	-24.6	-24.9	-24.7	-24.75	-17.2
Jonah	SHB 53-17	-37.5	-28.5	-25.7	-25.1	-25.0	-25.0	-24.8	-14.2
Jonah	SHB 53-20	-35.5	-24.2	-23.9	-24.0	-24.0	-24.1	-24.1	-16.1
Jonah	SHB 57-15	-40.7	-29.5	-27.8	-26.0	-26.5	-25.4	-25.9	-10.8
Jonah	SHB 63-27	-27.7	-24.95	-25.3	-25.0	-25.2	-25.0	-24.95	-10.75
Jonah	SHB 7-22	-34.9	-27.0	-26.0	-25.5	-25.5	-25.4	-25	-11.8
Jonah	SHB 75-26	-42.4	-26.3	-25.3	-24.5	-24.6	-24.1	-24.2	-8.15
Jonah	SHB 84-9	-35.4	-26.55	-25.6	-24.9	-24.9	-25.0	-24.9	-15.4
Jonah	SOL 7-36	-31.6	-24.9	-24.2	-23.8	-23.9	-23.7	-23.9	-8.8
Jonah	Yellowpoint 10-13	-42.3	-25.75	-25.2	-23.9	-24.4	-23.7	-23.8	-10.6
Jonah	Yellowpoint 21-12	-35.9	-26.8	-25.7	-25.4	-25.1	-25.2	-24.9	-9.6
Jonah	SHB 124-11	-35.6	-24.6	-23.2	-23.2	-22.8	-23.3	-21.6	
Jonah	SHB 36-32	-33.5	-24.8	-23.8	-22.3	-23.3	-22.0	-21.5	
Jonah	JF 37-7	-37.9	-24.6	-22.6	-21.2	-22.0	-20.5	-20.4	
Jonah	SHB 17-26	-37.5	-27.5	-25.8	-24.2	-24.4	-23.3	-23.2	-10.6
Jonah	SOL 9-36	-34.8	-24.8	-22.8	-21.6	-22.3	-21.4	-20.4	
Jonah	SCARLETT 11-34	-39.5	-26.6	-25.6	-24.0	-24.8	-23.7	-23.5	-7.4
Jonah	JF-11-18	-37.8	-29.8	-26.4	-24.3	-25.2	-22.5	-23.0	
Jonah	Yellowpoint 4-24	-34.7	-25.8	-24.5	-23.5	-23.4	-22.8	-22.6	-7.1
Jonah	JF 1-8	-34.6	-25.3	-24.3	-23.0	-23.3	-23.3	-23.1	

Note: See Figure5.1 for well locations

Production gas data, Jonah Field - hydrogen isotope composition

Area	Well	dD C1	dD C2	dD C3	dD i-C4	dD n-C4	dD i-C5	dD n-C5
Jonah	Cabrito 17-25	-180	-160	-161	-148	-158	-137	-154
Jonah	JWH Corona 61-31	-179	-162	-160	-143	-151	-130	-146
Jonah	JWH Corona 67-30	-178	-156	-160	-143	-152	-127	-146
Jonah	JWH Corona 79-19	-178	-154	-157	-142	-150	-125	-140
Jonah	JWH Corona 16-18	-177	-156	-161	-145	-154	-130	-147
Jonah	JWH Jonah Federal 19-5	-179	-158	-156	-146	-154	-134	-150
Jonah	SHB 12-36	-179	-158	-156	-139	-151	-127	-142
Jonah	SHB 16-35R	-181	-160	-155	-141	-147	-130	-145
Jonah	SHB 2-33	-175	-156	-156	-140	-152	-130	-149
Jonah	SHB 34-28	-178	-155	-154	-140	-150	-123	-139
Jonah	SHB 41-29	-173	-159	-164	-147	-157	-138	-152
Jonah	SHB 53-17	-175	-155	-157	-144	-152	-132	-148
Jonah	SHB 53-20	-176	-151	-156	-146	-153	-133	-149
Jonah	SHB 57-15	-175	-155	-158	-144	-153	-131	-148
Jonah	SHB 63-27	-176	-158	-158	-147	-158	-136	-153
Jonah	SHB 7-22	-172	-154	-159	-138	-140	-118	-138
Jonah	SHB 75-26	-179	-159	-158	-144	-152	-130	-145
Jonah	SHB 84-9	-179	-149	-158	-145	-154	-133	-147
Jonah	SOL 7-36	-178	-152	-158	-145	-152	-130	-144
Jonah	Yellowpoint 10-13	-181	-160	-158	-147	-155	-130	-145
Jonah	Yellowpoint 21-12	-176	-154	-158	-144	-153	-131	-146
Jonah	SHB 124-11	-178	-157	-158	-136	-138	-106	-135
Jonah	SHB 36-32	-172	-154	-158	-142	-153	-124	-145
Jonah	JF 37-7	-188	-158	-174	-153	-161	-132	
Jonah	SHB 17-26	-183	-160	-162	-150	-159	-135	-154
Jonah	SOL 9-36	-180	-149	-151	-140	-143	-117	-137
Jonah	SCARLETT 11-34	-187	-150	-135	-120	-135	-113	-125
Jonah	JF-11-18	-190	-163	-199				
Jonah	Yellowpoint 4-24	-179	-157	-162	-147	-159	-132	-152
Jonah	JF 1-8	-181	-157	-159	-139	-151	-116	-143

Production gas data, Greater Natural Buttes Field - bulk gas composition

field							bulk gas composition				
				C1	**C2**	**C3**	**I-C4**	**N-C4**	**I-C5**	**N-C5**	wetness
GNB	**BC 1122-5H**			0.872	0.074	0.040	0.004	0.004	0.003	0.002	0.13
GNB	**BONANZA 1023-15J**			0.840	0.070	0.045	0.012	0.018	0.008	0.008	0.16
GNB	**BONANZA 1023-1J**			0.796	0.087	0.061	0.016	0.024	0.009	0.008	0.20
GNB	**BONANZA 1023-9J**			0.847	0.069	0.044	0.012	0.016	0.006	0.006	0.15
GNB	**CIGE 255**			1.000	0.000	0.000	0.000	0.000	0.000	0.000	0.00
GNB	**CIGE 98D**			0.819	0.094	0.048	0.014	0.014	0.006	0.004	0.18
GNB	**HATCH 923-14C**			0.785	0.083	0.062	0.019	0.027	0.013	0.012	0.22
GNB	**LOVE 1121-2M**			0.816	0.105	0.040	0.012	0.014	0.007	0.006	0.18
GNB	**LOVE 1121-7N**			0.889	0.065	0.026	0.007	0.008	0.003	0.002	0.11
GNB	**MULLIGAN 822-24G**			0.866	0.070	0.034	0.009	0.012	0.005	0.004	0.13
GNB	**NBU 1021-15I**			0.769	0.099	0.067	0.018	0.028	0.010	0.009	0.23
GNB	**NBU 1021-25G**			0.755	0.122	0.064	0.017	0.021	0.011	0.010	0.25
GNB	**NBU 1021-2O**			0.898	0.053	0.022	0.007	0.009	0.005	0.006	0.10
GNB	**NBU 1021-30I**			0.848	0.076	0.040	0.010	0.014	0.006	0.005	0.15
GNB	**NBU 1021-30N**			0.800	0.097	0.057	0.015	0.018	0.008	0.006	0.20
GNB	**NBU 1022-09F4T**			0.866	0.070	0.032	0.009	0.012	0.006	0.005	0.13
GNB	**NBU 1022-11F**			0.877	0.069	0.027	0.008	0.010	0.005	0.004	0.12
GNB	**NBU 176**			0.872	0.071	0.028	0.008	0.011	0.005	0.004	0.13
GNB	**NBU 20**			1.000	0.000	0.000	0.000	0.000	0.000	0.000	0.00
GNB	**NBU 420**			0.875	0.067	0.032	0.008	0.011	0.005	0.004	0.13
GNB	**NBU 424**			0.895	0.045	0.030	0.008	0.012	0.005	0.005	0.11
GNB	**NBU 553-28E**			0.893	0.061	0.021	0.007	0.009	0.005	0.004	0.11
GNB	**NBU 560-17E**			0.875	0.058	0.028	0.007	0.010	0.008	0.015	0.13
GNB	**NBU 920-20L**			0.846	0.078	0.036	0.011	0.016	0.007	0.006	0.15
GNB	**NBU 920-20P**			0.812	0.087	0.051	0.015	0.019	0.009	0.007	0.19
GNB	**NBU 920-25P**			0.816	0.101	0.044	0.012	0.015	0.007	0.006	0.18
GNB	**NBU 921-14L**			0.778	0.118	0.068	0.011	0.011	0.008	0.007	0.22
GNB	**NBU 922-34D-3**			0.806	0.090	0.054	0.014	0.019	0.009	0.008	0.19
GNB	**PAWNEE 3-181**			0.749	0.099	0.079	0.019	0.031	0.012	0.011	0.25
GNB	**SOUTHMAN CANYON 923-31M**			0.800	0.083	0.057	0.016	0.024	0.011	0.009	0.20
GNB	**WKRP 823-34A**			0.834	0.070	0.050	0.012	0.019	0.008	0.008	0.17

Production gas data, Greater Natural Buttes Field - carbon isotope composition

		C1	C2	C3	I-C4	N-C4	I-C5	N-C5	CO2
GNB	BC 1122-5H	-35.5	-25.5	-24.4	-24	-23.4	-22.6	-22.2	
GNB	BONANZA 1023-15J	-35.6	-26.6	-26.3	-26.9	-26.3	-26.1	-26.2	-3.4
GNB	BONANZA 1023-1J	-35.3	-27	-26.5	-26.7	-26.4	-25.3	-25.1	-7.2
GNB	BONANZA 1023-9J	-35.6	-26.9	-26.2	-26.7	-26.1	-26	-25.5	-6.6
GNB	CIGE 255	-38.1	-25.7	-22.2	-21.5	-21.0	-20.4	-20.8	-1.6
GNB	CIGE 98D	-32.3	-26.0	-24.3	-23.5	-23.4	-22.9	-23.1	-7.5
GNB	HATCH 923-14C	-39.3	-28.7	-27	-25.7	-28.1	-27.2	-27	-4.2
GNB	LOVE 1121-2M	-35.4	-26	-25.4	-24.8	-25.1	-24.2	-23.9	-7.7
GNB	LOVE 1121-7N	-35.1	-24.7	-22.2	-22.7	-22	-21.8	-22.7	-17.7
GNB	MULLIGAN 822-24G	-37.5	-26.3	-24.7	-25.6	-24.6	-25.0	-24.4	-7.4
GNB	NBU 1021-15I	-36.5	-27.5	-27.3	-27.4	-27	-26.4	-26.5	-6
GNB	NBU 1021-25G	-39.6	-28.0	-27.4	-27.0	-27.2	-26.1	-26.2	-2.0
GNB	NBU 1021-2O	-35.6	-25.9	-25.6	-26.1	-25.8	-24.5	-23.2	
GNB	NBU 1021-30I	-34.1	-26.0	-24.7	-24.3	-24.7	-24.3	-24.1	-5.5
GNB	NBU 1021-30N	-37.0	-27.4	-26.6	-26.3	-26.6	-25.3	-25.3	-4.2
GNB	NBU 1022-09F4T	-35.5	-26.1	-25.1	-24.3	-24.9	-24.2	-23.8	-7.3
GNB	NBU 1022-11F	-27.6	-24.1	-22.2	-22.7	-22.3	-22.7		
GNB	NBU 176	-28.1	-25.3	-23.9					-5.8
GNB	NBU 20	-34.3	-24.6	-22.8	-24.3	-23.4	-24.5	-22.0	
GNB	NBU 420	-31.7	-24.8	-23.3	-23.2	-23.2	-23.4	-22.9	
GNB	NBU 424	-34.6	-25.3	-23.8					
GNB	NBU 553-28E	-35.2	-26.2	-23.1	-22.7	-22.5	-23.1	-22.3	
GNB	NBU 560-17E	-33.8	-26.2	-25.1	-25.6	-25.1	-24.8	-24.7	-6.5
GNB	NBU 920-20L	-33.7	-26.2	-24.5	-25.1	-24.0	-24.5	-23.8	-4.1
GNB	NBU 920-20P	-38	-26.3	-24.2	-25.3	-23.7	-24.8	-23.7	-5
GNB	NBU 920-25P	-35.1	-26.2	-24.5	-25.3	-24	-25.1	-24.5	-3.3
GNB	NBU 921-14L	-39.0	-26.4	-25.0	-24.4	-24.6	-24.8	-24.2	
GNB	NBU 922-34D-3	-36.6	-27.1	-25.7	-26	-25.5	-25.5	-24.9	-3
GNB	PAWNEE 3-181	-36.6	-26.7	-25.0	-25.7	-24.1	-24.7	-24.0	-1.9
GNB	SOUTHMAN CANYON 923-31M	-35.9	-22.7	-23.6	-23.3	-23.9	-23.2	-23.4	
GNB	WKRP 823-34A	-35.8	-26.4	-25.4	-26.1	-25.5	-25.7	-25.3	-6.2

Production gas data, Greater Natural Buttes, Field - hydrogen isotope composition

		C1	C2	C3	I-C4	N-C4	I-C5	N-C5
GNB	BC 1122-5H	-170	-147	-141	-105	-116	-85	
GNB	BONANZA 1023-15J	-170	-146	-137	-118	-130	-106	-126
GNB	BONANZA 1023-1J	-177	-164	-143	-115	-131	-96	-118
GNB	BONANZA 1023-9J	-165	-147	-137	-115	-130	-101	-123
GNB	CIGE 255	-165	-125	-131	-106	-106	-83	-102
GNB	CIGE 98D	-165	-129	-123	-100	-110	-81	-101
GNB	HATCH 923-14C	-164	-135	-134	-117	-132	-100	-123
GNB	LOVE 1121-2M	-168	-136	-129	-114	-122	-103	-120
GNB	LOVE 1121-7N	-162	-119	-109	-105	-110	-81	-100
GNB	MULLIGAN 822-24G	-163	-137	-127	-118	-121	-101	-118
GNB	NBU 1021-15I	-183	-163	-140	-110	-129	-93	-120
GNB	NBU 1021-25G	-177	-157	-138	-117	-131	-105	-125
GNB	NBU 1021-2O	-175	-132	-121	-105	-114	-90	-107
GNB	NBU 1021-30I	-167	-134	-130	-113	-123	-103	-123
GNB	NBU 1021-30N	-183	-152	-136	-118	-129	-107	-127
GNB	NBU 1022-09F4T	-162	-139	-129	-114	-124	-100	-119
GNB	NBU 1022-11F	-161	-129	-115	-97	-106	-74	-92
GNB	NBU 176	-162	-124					
GNB	NBU 20	-163	-142	-134	-95	-104	-84	-111
GNB	NBU 420	-165	-143	-127	-111	-123	-104	-121
GNB	NBU 424	-158	-127	-115	-107	-113	-95	-112
GNB	NBU 553-28E	-163	-136	-130	-98	-110	-91	-117
GNB	NBU 560-17E	-164	-138	-126	-97	-106	-76	-100
GNB	NBU 920-20L	-181	-132	-122	-116	-117	-101	-113
GNB	NBU 920-20P	-175	-134	-120	-107	-102	-96	-103
GNB	NBU 920-25P	-170	-135	-125	-102	-109	-106	-113
GNB	NBU 921-14L	-179	-142	-120	-111	-114	-85	-108
GNB	NBU 922-34D-3	-173	-140	-128	-117	-124	-104	-118
GNB	PAWNEE 3-181	-159	-129	-120	-115	-114	-100	-111
GNB	SOUTHMAN CANYON 923-31M	-171	-151	-133	-117	-126	-106	-124
GNB	WKRP 823-34A	-174	-142	-120	-119	-123	-109	-122

Mud gas data, Piceance Basin - bulk gas composition

well name	field	depths TVD	C1	C2	C3	iC4	nC4	iC5	nC5	fraction CO2	wetness
D	Grand Valley	5221	0.89	0.12	0.00	0.00	0.00	0.00	0.00	0.12	0.12
D	Grand Valley	5274	0.87	0.08	0.03	0.01	0.01	0.00	0.00	0.13	0.13
D	Grand Valley	5319	0.84	0.05	0.02					0.07	0.08
D	Grand Valley	5682	0.85	0.09	0.03	0.01	0.01	<0.01	<0.01	0.14	0.14
D	Grand Valley	5687	0.86	0.10	0.00	0.00	0.00	0.00	0.00	0.10	0.10
D	Grand Valley	5847	0.82	0.11	0.03	0.01	0.01	<0.01	<0.01	0.16	0.16
D	Grand Valley	5968	0.87	0.09	0.03	0.01	0.01	0.00	0.00	0.13	0.13
D	Grand Valley	6146	0.88	0.08	0.03	0.00	0.00	0.00	0.00	0.12	0.12
D	Grand Valley	6232	0.88	0.08	0.02					0.10	0.10
D	Grand Valley	6337	0.88	0.08	0.02	0.01	0.00	0.00	0.00	0.12	0.12
D	Grand Valley	6682	0.96	0.04	0.25	0.00	0.00	0.00	0.00	0.29	0.23
D	Grand Valley	6738	0.90	0.06	0.01					0.07	0.07
GGU 21B 33-691	**Mamm Creek**	5226	0.92	0.00	0.00	0.00	0.00	0.00	0.00	0.08	0.00
GGU 21B-33-691	**Mamm Creek**	6370	0.65	0.19	0.10	0.00	0.00	0.00	0.00	0.06	0.31
GGU 21B 33-691	**Mamm Creek**	6924	0.70	0.06	0.04	0.04	0.05	0.04	0.04	0.03	0.28
GGU 21B 33-691	**Mamm Creek**	7035	0.78	0.05	0.04	0.03	0.04	0.03	0.02	0.02	0.20
GGU 21B 33-691	**Mamm Creek**	7139	0.92	0.02	0.01	0.01	0.01	0.01	0.01	0.01	0.07
GGU 21B 33-691	**Mamm Creek**	7245	0.70	0.05	0.01	0.02	0.04	0.04	0.05	0.09	0.23
GGU 21B 33-691	**Mamm Creek**	7366	0.57	0.05	0.03	0.04	0.07	0.09	0.07	0.08	0.38
SPEC 41D-28-692	**Mamm Creek**	5608	0.90	0.00	0.00	0.00	0.00	0.00	0.00	0.10	0.00
SPEC 41D-28-692	**Mamm Creek**	5712	0.77	0.05	0.07	0.00	0.03	0.04	0.04	0.00	0.23
SPEC 42C-28-692	**Mamm Creek**	6530	0.94	0.02	0.01	0.00	0.01	0.01	0.00	0.01	0.05
SPEC 42C-28-692	**Mamm Creek**	6867	0.75	0.11	0.04	0.02	0.02	0.01	0.01	0.04	0.21
SPEC 42C-28-692	**Mamm Creek**	7036	0.71	0.11	0.04	0.02	0.03	0.02	0.01	0.06	0.25
R	Parachute	5661	0.75	0.01	0.06	0.02	0.01	0.01	<0.01	0.13	0.13
R	Parachute	5816	0.88	0.10	0.03	0.00	0.00	0.00	0.00		0.12
R	Parachute	5831	0.85	0.10	0.03	0.01	0.01	0.00	0.00		0.15
R	Parachute	5998	0.85	0.10	0.03	0.01	0.01	<0.01	<0.01	<0.01	0.15
R	Parachute	6103	0.94	0.06	0.00	0.00	0.00	0.00	0.00		0.06
R	Parachute	6245	0.95	0.04	0.01	0.00	0.00	0.00	0.00		0.05
R	Parachute	6336	0.95	0.05	0.00	0.00	0.00	0.00	0.00		0.05
R	Parachute	6372	0.82	0.11	0.03	0.01	0.01	<0.01	<0.01	0.01	0.16
R	Parachute	6513	0.97	0.03	0.01	0.00	0.00	0.00	0.00		0.03
R	Parachute	6613	0.93	0.01						0.06	0.01
R	Parachute	6713	0.95	0.04	0.01	0.00	0.00	0.00	0.00		0.05
R	Parachute	6939	0.96	0.01						0.03	0.01
R	Parachute	6939	0.96	0.03	0.01	0.00	0.00	0.00	0.00		0.04
R	Parachute	7038	0.79	0.14	0.03	0.01	0.01	0.01	<0.01	<0.01	0.20
R	Parachute	7150	0.90	0.07	0.03	0.00	0.00	0.00	0.00		0.10
R	Parachute	7195	0.92	0.07	0.02	0.00	0.00	0.00	0.00		0.08
R	Parachute	7251	0.92	0.03						0.05	0.03
R	Parachute	7354	0.95	0.05	0.00	0.00	0.00	0.00	0.00		0.05
R	Parachute	7417	0.91	0.08	<0.01	<0.01	<0.01			0.01	0.08

Note: See figure 4.2 for well locations.

Mud gas data, Piceance Basin - bulk gas composition

well name	field	depths TVD	C1	C2	C3	iC4	nC4	iC5	nC5	fraction CO2	wetness
R	Parachute	7520	0.99	0.01	0.00	0.00	0.00	0.00	0.00		0.01
R	Parachute	7628	0.98	0.02	0.00	0.00	0.00	0.00	0.00		0.02
R	Parachute	7718	0.97	0.01						0.01	0.01
K	Piceance	6578	1.00	0.00							0.00
K	Piceance	6578	1.00	0.00							0.00
K	Piceance	6688	0.96	0.04	0.05						0.09
K	Piceance	6728	0.95	0.05							0.05
K	Piceance	6788	0.97	0.03	0.00						0.03
K	Piceance	6789	0.97	0.03							0.03
K	Piceance	6789	0.97	0.03							0.03
K	Piceance	6883	0.97	0.03							0.03
K	Piceance	6887	0.98	0.02							0.02
K	Piceance	6958	0.98	0.03							0.03
K	Piceance	6978	0.98	0.02	0.00						0.02
K	Piceance	7050	0.98	0.02							0.02
K	Piceance	7108	0.99	0.01							0.01
K	Piceance	7228	1.00	0.00							0.00
K	Piceance	7228	1.00	0.00							0.00
BB	Rulison	6080	0.96	0.02						0.02	0.02
BB	Rulison	6355	0.81	0.06	0.01					0.12	0.08
BB	Rulison	6567	0.99							0.01	0.00
BB	Rulison	7162	0.88	0.06	0.02	0.01	<0.01			0.03	0.09
BB	Rulison	7402									
BB	Rulison	7463	0.86	0.09	0.03	0.01	0.01	<0.01		0.01	0.14
BB	Rulison	7678	0.88	0.07	0.02	0.01	<0.01	<0.01		0.01	0.10
BB	Rulison	8169	0.92	0.05	0.01	0.01				0.01	0.07
BB	Rulison	8343	0.96	0.02						0.02	0.02
FF	Rulison	5361	0.92							0.08	0.00
FF	Rulison	5461	0.86	0.09	0.04	0.00	0.00	0.00	0.00		0.14
FF	Rulison	5538	0.90	0.10	0.00	0.00	0.00	0.00	0.00		0.10
FF	Rulison	5709	0.85	0.09	0.03	0.01	0.01	<0.01	<0.01	0.01	0.14
FF	Rulison	5806	0.90	0.10	0.00	0.00	0.00	0.00	0.00		0.10
FF	Rulison	5923	1.00								0.00
FF	Rulison	6027	0.90	0.10	0.00	0.00	0.00	0.00	0.00		0.10
FF	Rulison	6182	0.87	0.10	0.04	0.00	0.00	0.00	0.00		0.13
FF	Rulison	6206	1.00	0.00	0.00	0.00	0.00	0.00	0.00		0.00
FF	Rulison	6279	0.85	0.08	0.01					0.06	0.10
FF	Rulison	6411	0.91	0.06	0.01	<0.01	<0.01	<0.01		0.01	0.07
FF	Rulison	6577	0.92	0.08	0.00	0.00	0.00	0.00	0.00		0.08
FF	Rulison	6696	0.94	0.06	0.00	0.00	0.00	0.00	0.00		0.06
FF	Rulison	6823	0.95	0.03						0.02	0.03
FF	Rulison	6944	0.81	0.10	0.06	0.02	0.01	0.00	0.00		0.19
FF	Rulison	7007	1.00	0.00	0.00	0.00	0.00	0.00	0.00		0.00
FF	Rulison	7110	0.91	0.07	0.01	<0.01	<0.01	<0.01	<0.01	<0.01	0.08

Note: See figure 4.2 for well locations.

Mud gas data, Piceance Basin - bulk gas composition

well name	field	depths TVD	C1	C2	C3	iC4	nC4	iC5	nC5	fraction CO2	wetness
FF	Rulison	7209	0.90	0.07	0.02	0.00	0.00	0.00	0.00		0.10
FF	Rulison	7301	0.95	0.04	0.01	0.00	0.00	0.00	0.00		0.05
FF	Rulison	7392	0.98	0.01	0.00	0.00	0.00	0.00	0.00		0.02
FF	Rulison	7489	0.96							0.04	0.00
FF	Rulison	7621	0.95	0.03	0.01	0.00	0.00	0.00	0.00		0.05
PP	Rulison	6968	0.77	0.13	0.05	0.02	0.01	0.01	<0.01	0.01	0.22
PP	Rulison	7087	0.83	0.12	0.05	0.00	0.00	0.00	0.00		0.17
PP	Rulison	7159	0.87	0.13	0.00	0.00	0.00	0.00	0.00		0.13
PP	Rulison	7178	0.78	0.13	0.05	0.01	0.01	0.01	<0.01	<0.01	0.22
PP	Rulison	7326	89.36	7.81	2.83	0.00	0.00	0.00	0.00		0.11
PP	Rulison	7541	90.01	7.64	2.35	0.00	0.00	0.00	0.00		0.10
PP	Rulison	7636	89.77	10.23	0.00	0.00	0.00	0.00	0.00		0.10
PP	Rulison	7696	85.73	11.28	3.00	0.00	0.00	0.00	0.00		0.14
PP	Rulison	7760	98.07	1.93	0.00	0.00	0.00	0.00	0.00		0.02
PP	Rulison	7774	0.89	0.08	0.01	0.01	<0.01	<0.01	<0.01	0.01	0.10
PP	Rulison	7850	92.29	7.71	0.00	0.00	0.00	0.00	0.00		0.08
PP	Rulison	7946	92.38	7.08	0.54	0.00	0.00	0.00	0.00		0.08
PP	Rulison	7993	100.00	0.00	0.00	0.00	0.00	0.00	0.00		0.00
PP	Rulison	8073	74.05	25.95	0.00	0.00	0.00	0.00	0.00		0.26
PP	Rulison	8305	83.78	12.12	4.10	0.00	0.00	0.00	0.00		0.16
JJ	Rulison	6481	0.97	0.02	0.01	0.00	0.00	0.00	0.00		0.03
JJ	Rulison	6495	0.93	0.06	0.01	0.01	<0.01	<0.01	<0.01	<0.01	0.08
JJ	Rulison	6585	0.91	0.06	0.02	0.01	0.01	0.00	0.00		0.09
JJ	Rulison	6716	0.89	0.09	0.02	0.00	0.00	0.00	0.00		0.11
JJ	Rulison	6788	0.62							0.38	0.00
DD	Rulison	4948	1.00	0.00							0.00
DD	Rulison	4948	1.00	0.00							0.00
DD	Rulison	5197	1.00	0.00							0.00
DD	Rulison	5197	1.00	0.00							0.00
DD	Rulison	5398	1.00	0.00							0.00
DD	Rulison	5398	0.94	0.06							0.06
DD	Rulison	5612	1.00	0.00							0.00
DD	Rulison	5612	1.00	0.00							0.00
II	Rulison	5457	0.76	0.15	0.10	0.00	0.00	0.00	0.00		0.24
II	Rulison	6569	1.00	0.00	0.00	0.00	0.00	0.00	0.00		0.00
II	Rulison	6571	0.71	0.16	0.13	0.00	0.00	0.00	0.00		0.29
II	Rulison	6827	0.88	0.09	0.03	0.00	0.00	0.00	0.00		0.12
II	Rulison	6925	0.92	0.08	0.00	0.00	0.00	0.00	0.00		0.08
II	Rulison	7027	0.85	0.11	0.04	0.00	0.00	0.00	0.00		0.15
II	Rulison	7275	1.00	0.00	0.00	0.00	0.00	0.00	0.00		0.00
II	Rulison	7372	0.94	0.06	0.00	0.00	0.00	0.00	0.00		0.06
II	Rulison	7469	0.88							0.12	0.00

Note: See figure 4.2 for well locations.

Mud gas data, Piceance Basin - carbon isotope composition

well name	field	depths TVD	13C C1	13C C2	13C C3	13C i-C4	13C n-C4	13C i-C4	13C n-C4	13C CO2
D	Grand Valley	5319	-40.5	-25.4	-21.9					-12.5
D	Grand Valley	5682	-40.4	-27.8	-25.4	-25.5	-24.4	-25.5	-23.8	-14.0
D	Grand Valley	5847	-38.4	-26.8	-23.3	-24.2	-22.8	-24.3	-23.3	-13.7
D	Grand Valley	6232	-38.9	-25.9	-24.2					-14.5
D	Grand Valley	6738	-38.8	-24.0	-20.8					-14.6
GGU 21B 33-691	**Mamm Creek**	5226	-48.5							-9.7
GGU 21B-33-691	**Mamm Creek**	6370	-42.6	-27.2	-23.7	-24.8	-22.9			-12.5
SPEC 41D-28-692	**Mamm Creek**	5608	-39.0							-13.6
SPEC 41D-28-692	**Mamm Creek**	5712	-36.1							-12.3
SPEC 42C-28-692	**Mamm Creek**	6530	-36.8							
SPEC 42C-28-692	**Mamm Creek**	6867	-41.5	-24.6	-21.5					-7.7
SPEC 42C-28-692	**Mamm Creek**	7036	-44.5	-25.9	-21.8					-10.5
R	Parachute	5661	-40.3	-27.4	-25.0	-25.7	-24.2	-25.4	-24.4	-15.0
R	Parachute	5998	-48.7	-27.6	-25.0	-25.3	-23.7	-24.9	-23.6	-25.8
R	Parachute	6372	-44.0	-26.8	-26.0	-24.0	-24.3	-24.9	-24.5	-25.7
R	Parachute	6613	-35.1	-21.7						-13.9
R	Parachute	6939	-37.9	-26.2						-12.8
R	Parachute	7038	-36.5	-25.3	-22.9	-24.1	-22.0	-23.8	-22.6	-22.2
R	Parachute	7251	-55.6	-31.7						-14.1
R	Parachute	7417	-44.5	-24.1	-20.9	-20.4	-21.0			-18.8
R	Parachute	7718	-52.2	-26.4						-14.4
K	Piceance	6578	-34.9							
K	Piceance	6789	-42.1	-25.5						
K	Piceance	7228	-41.1							
BB	Rulison	6080	-36.1	-25.2						-15.5
BB	Rulison	6355	-49.9	-30.3	-25.8					-14.4
BB	Rulison	6567	-11.5							-12.9
BB	Rulison	7162	-43.0	-28.7	-25.9	-26.5	-23.0			-13.8
BB	Rulison	7463	-34.1	-25.8	-23.3	-24.6	-23.2	-25.6		-12.4
BB	Rulison	7678	-40.5	-27.5	-23.7	-25.1	-22.9	-24.6		-14.3
BB	Rulison	8169	-36.1	-23.8	-21.8	-24.6				-10.7
BB	Rulison	8343	-41.7	-24.2						-6.9
FF	Rulison	5361	-26.5							-8.1
FF	Rulison	5709	-46.7	-29.9	-26.5	-26.3	-24.8	-26.3	-25.1	-10.0
FF	Rulison	5923	-13.5							

Note: See figure 4.2 for well locations.

Mud gas data, Piceance Basin - carbon isotope composition

well name	field	depths TVD	13C C1	13C C2	13C C3	13C i-C4	13C n-C4	13C i-C4	13C n-C4	13C CO2
FF	Rulison	6279	-43.5	-29.2	-25.8					-14.2
FF	Rulison	6411	-36.7	-29.4	-25.6	-26.2	-24.5	-26.6		-14.5
FF	Rulison	6823	-40.1	-26.0						-12.9
FF	Rulison	7110	-40.5		-21.3	-22.0	-21.1	-22.6	-21.7	-17.0
FF	Rulison	7489	-46.1							-14.3
PP	Rulison	6968	-39.4	-27.7	-25.2	-25.6	-24.2	-25.7	-23.8	-18.7
PP	Rulison	7178	-39.7	-28.0	-25.3	-26.5	-24.2	-26.0	-24.7	-13.4
PP	Rulison	7774	-40.5	-25.4	-21.9	-22.9	-21.4	-24.0	-23.1	-12.5
JJ	Rulison	6495	-48.2	-29.8	-26.8	-26.4	-24.9	-25.8	-24.4	-15.1
JJ	Rulison	6788	-48.4							-15.0
DD	Rulison	4948	-32.1							
DD	Rulison	5197	-28.4							
DD	Rulison	5398	-35.1							
DD	Rulison	5612	-28.4							
II	Rulison	7469	-38.0							-16.2

Note: See figure 4.2 for well locations.

Mud gas data, Piceance Basin - hydrogen isotope composition

well name	field	depths TVD	dD C1	dD C2	dD C3	dD i-C4	dD n-C4
D	Grand Valley	5319	-186				
D	Grand Valley	5682	-189	-155			
D	Grand Valley	5847	-182	-135	-131		
D	Grand Valley	6232	-189	-135			
D	Grand Valley	6738	-188				
GGU 21B-33-691	**Mamm Creek**	6370	**-210**				
GGU 21B 33-691	**Mamm Creek**	6924	**ND**	**-160**			
SPEC 41D-28-692	**Mamm Creek**	5608	**-210**				
SPEC 41D-28-692	**Mamm Creek**	5712	**-209**				
SPEC 42C-28-692	**Mamm Creek**	6530	**-192**				
SPEC 42C-28-692	**Mamm Creek**	6867	**-209**				
SPEC 42C-28-692	**Mamm Creek**	7036	**-213**				
R	Parachute	5661	-207	-228			
R	Parachute	5998	-176	-139	-125	-113	-101
R	Parachute	6372	-168	-137	-134	-109	-106
R	Parachute	6613	-178				
R	Parachute	6939	-184				
R	Parachute	7038	-166	-129	-123	-119	-122
R	Parachute	7251	-177	-127	-126		
R	Parachute	7417	-161	-124			
R	Parachute	7718	-170	-120			
K	Piceance	6578	-135				
K	Piceance	6789	-166				
K	Piceance	7228	-163				
BB	Rulison	6080	-195	-210			
BB	Rulison	6355	-198	-221			
BB	Rulison	7162	-187	-142			
BB	Rulison	7463	-188	-128			
BB	Rulison	7678	-169	-128	-151	-131	
BB	Rulison	8169	-180	-128			
BB	Rulison	8343	-149	-121			
JJ	Rulison	6495	-176	-147	-126	-117	-121
JJ	Rulison	6788	-198	-200			

Note: See figure 4.2 for well locations.

Mud gas data, Jonah Field - bulk gas composition

Area	Well	depth relative to top Lance	Sample Depth	fraction C1	fraction C2	fraction C3	fraction i-C4	fraction n-C4	fraction i-C5	fraction n-C5	CO2	wetness
Jonah	CAB 76-30	-2073	11417									
Jonah	CAB 76-30	-2196	11540	0.77	0.12	0.06	0.02	0.02				0.22
Jonah	CAB 76-30	-2203	11547	0.81	0.12	0.06	<.01	<.01				0.18
Jonah	JF 30-4	-2699	11473	0.66	0.13	0.11	0.03	0.03	0.01	0.01	0.02	
Jonah	JF 30-4	-2832	11606	0.63	0.13	0.13	0.06	0.05	0.00	0.00		0.37
Jonah	JF 30-4	-2946	11720	0.71	0.13	0.10	0.03	0.03	0.00	0.00		0.29
Jonah	JF 30-4	-2957	11731	0.79	0.10	0.06	0.02	0.01	0.01	0.01		0.21
Jonah	JF 30-4	-3057	11831	0.73	0.13	0.08	0.02	0.02	0.01	0.01	0.01	0.27
Jonah	JF 30-4	-3197	11971	0.84	0.10	0.06	0.00	0.00	0.00	0.00		0.16
Jonah	JF 38-4	-2064	10730	0.83	0.08	0.04	0.01	0.01	0.01	< 0.01	0.02	0.16
Jonah	JF 38-4	-2494	11160	0.60	0.14	0.11	0.04	0.03	0.01	< 0.01	0.08	0.35
Jonah	JF 38-4	-2630	11296	0.68	0.14	0.10	0.03	0.03	0.01	0.01		0.32
Jonah	JF 38-4	-2630	11296	0.85	0.06	0.02	0.01	0.01	<0.01	<0.01	0.05	0.11
Jonah	JF 38-4	-2634	11300	0.81	0.11	0.02	0.02	0.02	0.01	0.01		0.19
Jonah	JF 38-4	-2750	11416	0.66	0.15	0.10	0.03	0.02	0.01	< 0.01	0.03	0.32
Jonah	JF 38-4	-2882	11548	0.83	0.09	0.04	0.01	0.01	0.01	0.00		0.17
Jonah	JF 38-4	-3050	11716	0.84	0.09	0.04	0.01	0.01	0.01	0.00		0.16
Jonah	JF 38-4	-3062	11728	0.76	0.11	0.06	0.02	0.02	0.01	< 0.01	0.03	0.22
Jonah	JF 42-8	-220	8545	1.00	0.00							0.00
Jonah	JF 42-8	-459	8784	0.81	0.09	0.05	0.02	0.02	0.01	0.01		0.19
Jonah	JF 42-8	-515	8840	0.87	0.08	0.03	0.01	<0.01				0.12
Jonah	JF 42-8	-1020	9345	0.89	0.08	0.03						0.11
Jonah	JF 42-8	-1112	9437	0.86	0.09	0.03	0.01	0.01	0.00	0.00		0.14
Jonah	JF 42-8	-1182	9507	0.83	0.10	0.05	0.01	0.01				0.17
Jonah	JF 42-8	-1283	9608	0.82	0.10	0.04	0.01	0.01	0.01	0.00		0.18
Jonah	JF 42-8	-1357	9682	0.77	0.11	0.08	0.02	0.02	0.01	<0.01		0.24
Jonah	JF 42-8	-1867	10192	0.79	0.11	0.06	0.02	0.02				0.21
Jonah	JF 42-8	-2036	10361	0.79	0.11	0.05	0.02	0.01	0.01	0.00		0.21
Jonah	JF 42-8	-2086	10411	0.79	0.11	0.06	0.02	0.02	0.01	0.01		0.21
Jonah	JF 42-8	-2205	10530	0.85	0.08	0.04	0.01	0.01	0.00	0.00		0.15
Jonah	JF 42-8	-2415	10740	0.86	0.10	0.04	0.00	0.00	0.00	0.00		0.14
Jonah	JF 42-8	-2457	10782	0.87	0.13							0.13
Jonah	SHB 19-17	-1020	9946	0.83	0.07	0.04	0.02	0.01	0.02	0.01		0.17
Jonah	SHB 19-17	-1186.6	10112.6	0.89	0.07	0.03	0.01	0.01	0.00	0.00		0.11
Jonah	SHB 19-17	-1250	10176	0.74	0.07	0.08	0.01	0.01			0.08	0.20
Jonah	SHB 19-17	-1326	10252	0.91	0.06	0.02	0.00	0.00	0.00	0.00		0.09
Jonah	SHB 19-17	-1428	10354	0.89	0.06	0.02	0.01	0.01	0.01	0.01		0.11
Jonah	SHB 19-17	-1529	10455	0.88	0.07	0.03	0.01	0.01	< 0.01	< 0.01	0.01	0.11
Jonah	SHB 19-17	-1588	10514	0.91	0.06	0.02	0.00	0.00	0.00	0.00		0.09
Jonah	SHB 19-17	-1703	10629	0.99	0.01	0.00	0.00	0.00	0.00	0.00		0.01
Jonah	SHB 19-17	-1815	10741	0.99	0.00	0.00	0.00	0.00	0.00	0.00		0.01
Jonah	SHB 19-17	-1870	10796	0.88	0.06	0.02	0.01	0.01	0.01	0.01		0.12
Jonah	SHB 19-17	-2048	10974	0.93	0.02	0.01	0.01	0.01	< 0.01	< 0.01	0.02	0.05
Jonah	SHB 19-17	-2151	11077	0.88	0.08	0.04	0.00	0.00	0.00	0.00		0.12
Jonah	SHB 19-17	-2490	11416	0.86	0.09	0.05	0.00	0.00	0.00	0.00		0.14
Jonah	SHB 19-17	-2614	11540	0.85	0.07	0.03	0.01	0.01	0.01	0.01		0.15
Jonah	SHB 19-17	-2646	11572	0.80	0.09	0.06	0.02	0.02	0.01	< 0.01		0.19
Jonah	SHB 19-17	-2715	11641	0.79	0.10	0.06	0.02	0.02	0.01	0.00		0.21
Jonah	SHB 19-17	-2824	11750	0.78	0.10	0.06	0.02	0.02	0.01	0.00		0.22
Jonah	SHB 19-17	-2866	11792	0.67	0.14	0.08	0.02	0.02	0.01	< 0.01	0.05	0.29
Jonah	SHB 19-17	-2962	11888	0.78	0.11	0.06	0.01	0.01	0.01	0.01		0.22
Jonah	SHB 19-17	-3119	12045	0.77	0.10	0.06	0.02	0.01	0.01	< 0.01	0.04	0.20
Jonah	SHB 19-17	-3417	12343	0.74	0.13	0.08	0.02	0.02	0.01	0.01		0.26
Jonah	SHB 19-17	-3486	12412	0.77	0.12	0.06	0.02	0.02	0.01	0.00		0.23
Jonah	SHB 19-17	-3519	12445	0.80	0.09	0.04	0.01	0.01	< 0.01	< 0.01	0.03	0.16
Jonah	SHB 19-17	-3607	12533	0.83	0.09	0.04	0.01	0.01	0.02	0.01		0.17
Jonah	SHB 19-17	-3730	12656	0.85	0.08	0.04	0.01	0.01	0.00	0.00		0.15
Jonah	SHB 19-17	-3867	12793	0.75	0.12	0.07	0.02	0.02	0.02	0.01		0.25
Jonah	SHB 19-17	-3965	12891	0.79	0.10	0.05	0.01	0.01	< 0.01	< 0.01	0.03	0.18
Jonah	SHB 19-17	-4521	13447	0.75	0.09	0.07	0.02	0.02	0.01	< 0.01	0.03	0.22

Note: See figure 5.2 for well locations.

Mud gas data, Jonah Field - bulk gas composition

Area	Well	depth relative to top Lance	Sample Depth	fraction C1	fraction C2	fraction C3	fraction i-C4	fraction n-C4	fraction i-C5	fraction n-C5	CO2	wetness
Jonah	SHB 19-22	-3269	12195	0.86	0.08	0.03	< 0.01	< 0.01			0.03	0.11
Jonah	SHB 27-34	-2829	11528	0.85	0.09	0.05						0.14
Jonah	SHB 27-34	-2892	11591	0.91	0.09							0.09
Jonah	SHB 27-34	-2913	11612	0.90	0.10							0.10
Jonah	SHB 27-34	-3265	11964	0.88	0.08	0.03						0.11
Jonah	SHB 27-34	-3265	11964	0.83	0.10	0.05	0.02	0.02				0.19
Jonah	SHB 30-15	-2401	11677	1.00	0.00	0.00	0.00	0.00	0.00	0.00		0.00
Jonah	SHB 30-15	-2402	11678	0.83	0.10	0.04	0.01	0.01	0.01	0.00		0.17
Jonah	SHB 30-15	-2664	11940	0.81	0.11	0.04	0.01	0.01	0.01	0.00		0.19
Jonah	SHB 30-15	-2809	12085	0.88	0.07	0.03	0.01	0.01	0.00	0.00		0.12
Jonah	SHB 30-15	-2809.1	12085.1	0.86	0.07	0.03	0.01	0.01	0.01	0.01		0.14
Jonah	SHB 30-15	-3145	12421	0.86	0.08	0.03	0.01	0.01	0.00	0.00		0.14
Jonah	SHB 30-15	-3148	12424	0.80	0.11	0.05	0.01	0.01	0.01	0.00		0.20
Jonah	SHB 30-15	-3207	12483	0.86	0.08	0.03	0.01	0.01	0.00	0.00		0.14
Jonah	SHB 30-15	-3208	12484	0.85	0.08	0.03	0.01	0.01	0.01	0.01		0.15
Jonah	SHB 30-15	-3324	12600	0.86	0.07	0.03	0.01	0.01	0.01	0.00		0.14
Jonah	SHB 30-15	-3337	12613	0.80	0.08	0.04	0.01	0.01	< 0.01	< 0.01	0.06	0.15
Jonah	SHB 30-15	-3452	12728	0.84	0.08	0.04	0.01	0.01	0.01	0.01		0.16
Jonah	SHB 30-15	-3452.1	12728.1	0.83	0.08	0.04	0.01	0.01	0.01	0.01		0.17
Jonah	SHB 30-15	-3563.5	12839.5	0.85	0.08	0.03	0.01	0.01	<0.01	<.01	0.02	0.13
Jonah	SHB 30-15	-3566	12842	0.86	0.07	0.03	0.01	0.01	0.01	0.00		0.14
Jonah	SHB 30-15	-3567	12843	0.86	0.08	0.03	0.01	0.01	0.01	0.00		0.14
Jonah	SHB 30-20	-956	9542	0.97	0.03							0.03
Jonah	SHB 30-20	-1046	9632	0.92	0.05	0.02	0.00	0.00	0.00	0.00		0.08
Jonah	SHB 30-20	-1296	9882	0.91	0.07	0.03						0.10
Jonah	SHB 30-20	-2055	10641	0.91	0.07	0.03	0.01	0.01				0.12
Jonah	SHB 30-20	-2190	10776	0.84	0.09	0.04	0.01	0.01	0.01	0.00		0.16
Jonah	SHB 30-20	-2688	11274	0.87	0.09	0.04						0.13
Jonah	SHB 30-36	-149	9239	0.71	0.11	0.08	0.03	0.03	0.03	0.01		0.29
Jonah	SHB 30-36	-166	9256	1.00	0.00	0.00	0.00	0.00	0.00	0.00		0.00
Jonah	SHB 30-36	-174	9264	0.81	0.09	0.04	0.01	0.01			0.04	0.16
Jonah	SHB 30-36	-199	9289	0.89	0.08	0.03	0.00	0.00	0.00	0.00		0.11
Jonah	SHB 30-36	-283	9373	0.99	0.01	0.00	0.00	0.00	0.00	0.00		0.01
Jonah	SHB 30-36	-289	9379	0.86	0.08	0.03	0.01	0.01	0.01	0.01		0.14
Jonah	SHB 30-36	-361	9451	0.83	0.09	0.03	0.01	0.01			0.03	0.14
Jonah	SHB 30-36	-460	9550	0.58	0.14	0.14	0.05	0.05	0.02	0.01		0.42
Jonah	SHB 30-36	-548	9638	0.83	0.09	0.04	0.01	0.01	< 0.01	< 0.01	0.02	0.15
Jonah	SHB 30-36	-648	9738	0.75	0.12	0.07	0.02	0.02	0.01	0.00		0.25
Jonah	SHB 31-9	-521	9822	0.84	0.10	0.04	0.01	0.01	0.00	0.00		0.16
Jonah	SHB 31-9	-529	9830	0.92	0.03	0.01	0.01	<0.01	<0.01	<0.01	0.03	0.05
Jonah	SHB 31-9	-732	10033	0.83	0.09	0.04	0.01	0.02	0.01	0.01		0.17
Jonah	SHB 31-9	-770	10071	0.76	0.13	0.06	0.02	0.02	0.02	0.00		0.24
Jonah	SHB 31-9	-784.7	10085.7	0.76	0.10	0.05	0.02	0.03	0.02	0.02		0.24
Jonah	SHB 31-9	-1033	10334	0.83	0.10	0.04	0.01	0.01	0.01	0.00		0.17
Jonah	SHB 31-9	-1037	10338	0.83	0.10	0.04	0.01	0.01	0.01	0.00		0.17
Jonah	SHB 31-9	-1125	10426	0.86	0.09	0.03	0.01	0.01	0.00	0.00		0.14
Jonah	SHB 31-9	-1130	10431	0.88	0.07	0.02	0.01	0.01	<0.01	<0.01	0.02	0.11
Jonah	SHB 31-9	-1213	10514	0.86	0.09	0.03	0.01	0.01	0.00	0.00		0.14
Jonah	SHB 31-9	-1217	10518	0.76	0.12	0.06	0.02	0.02	0.01	0.01		0.24
Jonah	SHB 31-9	-1326	10627	0.82	0.07	0.03	0.02	0.02	0.02	0.02		0.18
Jonah	SHB 31-9	-1335	10636	0.87	0.06	0.02	0.01	0.01	<0.01	<0.01	0.03	0.10
Jonah	SHB 31-9	-1783	11084	0.88	0.09	0.02	0.01	0.01	0.00	0.00		0.12
Jonah	SHB 31-9	-1901	11202	0.87	0.09	0.03	0.01	0.01	0.00	0.00		0.13
Jonah	SHB 31-9	-1907	11208	0.89	0.07	0.01	0.01	0.00	0.01	0.01		0.11
Jonah	SHB 31-9	-1996	11297	0.83	0.10	0.04	0.01	0.01	0.00	0.00		0.17
Jonah	SHB 31-9	-2095	11396	0.95	0.03	0.02	0.00	0.00	0.00	0.00		0.05
Jonah	SHB 31-9	-2673	11974	0.86	0.09	0.03	0.01	0.01	0.00	0.00		0.14
Jonah	SHB 31-9	-2689	11990	0.86	0.09	0.05	0.00	0.00	0.00	0.00		0.14

Note: See figure 5.2 for well locations.

Mud gas data, Jonah Field - bulk gas composition

Area	Well	depth relative to top Lance	Sample Depth	fraction C1	fraction C2	fraction C3	fraction i-C4	fraction n-C4	fraction i-C5	fraction n-C5	CO2	wetness
Jonah	SHB 31-9	-3143	12444	0.79	0.08	0.03	0.01	0.01	<0.01	0.00	0.08	0.14
Jonah	SHB 31-9	-3274	12575	1.00	0.00	0.00	0.00	0.00	0.00	0.00		0.00
Jonah	SHB 31-9	-3396	12697	1.00	0.00	0.00	0.00	0.00	0.00	0.00		0.00
Jonah	SHB 31-9	-3404	12705	0.75	0.10	0.05	0.02	0.01	0.01	<0.01	0.06	0.20
Jonah	SHB 31-9	-3453	12754	1.00	0.00	0.00	0.00	0.00	0.00	0.00		0.00
Jonah	SHB 33-34	-1017	9838	1.00	0.00	0.00	0.00	0.00	0.00	0.00		0.00
Jonah	SHB 33-34	-1020	9841	0.85	0.08	0.03	0.01	0.01	<0.01	<0.01	0.02	0.13
Jonah	SHB 33-34	-1130	9951	0.93	0.07	0.00	0.00	0.00	0.00	0.00		0.07
Jonah	SHB 33-34	-1454	10275	0.84	0.09	0.04	0.01	0.01	0.01	0.01		0.16
Jonah	SHB 33-34	-1514	10335	0.85	0.07	0.03	0.01	0.01	<0.01	<0.01	0.03	0.12
Jonah	SHB 33-34	-1811	10632	1.00	0.00	0.00	0.00	0.00	0.00	0.00		0.00
Jonah	SHB 37-34	-137	8922	0.84	0.08	0.03	0.01	0.01	>0.01	>0.01	0.02	0.14
Jonah	SHB 37-34	-137	8922	0.82	0.10	0.05	0.01	0.01	0.00	0.00		0.18
Jonah	SHB 37-34	-258	9043	0.83	0.10	0.05	0.01	0.00	0.01	0.00		0.17
Jonah	SHB 37-34	-271	9056	0.65	0.13	0.10	0.04	0.03	0.01	0.01	0.02	0.34
Jonah	SHB 37-34	-414	9199	0.82	0.10	0.05	0.01	0.01	0.01	0.00		0.18
Jonah	SHB 37-34	-517	9302	0.73	0.12	0.08	0.02	0.02	0.01	>0.01	0.03	0.25
Jonah	SHB 37-34	-906	9691	0.84	0.09	0.04	0.01	0.01	0.01	0.00		0.16
Jonah	SHB 37-34	-1000	9785	0.83	0.08	0.04	0.01	0.01	0.02	0.01		0.17
Jonah	SHB 37-34	-1132	9917	0.84	0.09	0.04	0.01	0.01	0.00	0.00		0.16
Jonah	SHB 37-34	-1167	9952	0.84	0.08	0.04	0.01	0.01			0.02	0.14
Jonah	SHB 37-34	-1327	10112	0.83	0.09	0.04	0.01	0.01	0.01	0.01		0.17
Jonah	SHB 37-34	-1427	10212	0.86	0.08	0.03	0.01	0.01	0.01	0.00		0.14
Jonah	SHB 37-34	-1510	10295	0.86	0.08	0.03	0.01	0.01	0.01	0.00		0.14
Jonah	SHB 37-34	-1524	10309	0.90	0.05	0.02	0.01	0.01	>0.01	>0.01	0.01	0.09
Jonah	SHB 37-34	-1669	10454	0.88	0.07	0.03	0.01	0.01	0.00	0.00		0.12
Jonah	SHB 37-34	-1757	10542	0.86	0.08	0.04	0.01	0.01	0.00	0.00		0.14
Jonah	SHB 37-34	-1801	10586	0.82	0.09	0.05	0.01	0.01	0.01	0.00		0.18
Jonah	SHB 37-34	-1822	10607	0.79	0.09	0.05	0.02	0.01	0.01	>0.01	0.03	0.18
Jonah	SHB 37-34	-2072	10857	0.75	0.09	0.06	0.03	0.02	0.04	0.02		0.25
Jonah	SHB 37-34	-2111	10896	0.81	0.08	0.04	0.02	0.02	0.02	0.02		0.19
Jonah	SHB 37-34	-2242	11027	0.79	0.10	0.05	0.01	0.01	0.02	0.01		0.21
Jonah	SHB 37-34	-2340	11125	0.84	0.09	0.04	0.01	0.01	0.01	0.00		0.16
Jonah	SHB 37-34	-2433	11218	0.70	0.10	0.05	0.02	0.02	0.00	0.00	0.12	0.21
Jonah	SHB 37-34	-2660	11445	0.76	0.11	0.07	0.02	0.02	0.02	0.01		0.24
Jonah	SHB 37-34	-2767	11552	0.72	0.11	0.06	0.02	0.02	0.01	0.01	0.05	0.24
Jonah	SHB 37-34	-2881	11666	0.76	0.12	0.07	0.02	0.02	0.01	0.00		0.24
Jonah	SHB 37-34	-2996	11781	0.77	0.11	0.07	0.02	0.02	0.01	0.00		0.23
Jonah	SHB 37-34	-3037	11822	0.82	0.10	0.05	0.01	0.02	0.00	0.00		0.18
Jonah	SHB 37-34	-3051	11836	0.82	0.10	0.04	0.01	0.01	>0.01	>0.01	0.01	0.17
Jonah	SHB 37-34	-3157	11942	0.68	0.14	0.08	0.04	0.04	0.02	0.01		0.32
Jonah	SHB 37-34	-3185	11970	0.87	0.09	0.04	0.00	0.00	0.00	0.00		0.13
Jonah	SHB 37-34	-3310	12095	0.75	0.08	0.03	0.01	0.01			0.12	0.15
Jonah	SHB 37-34	-3446	12231	0.80	0.09	0.04	0.02	0.02	0.02	0.02		0.20
Jonah	SHB 42-27X	665	8145	0.81	0.11	0.05	0.01	0.01	0.00	0.00		0.19
Jonah	SHB 42-27X	663	8147	0.73	0.07	0.03	0.01	0.01	<0.01	<0.01	0.15	0.14
Jonah	SHB 42-27X	-303	9113	0.96	0.04	0.00	0.00	0.00	0.00	0.00		0.04
Jonah	SHB 42-27X	-303	9113	1.00	0.00	0.00	0.00	0.00	0.00	0.00		0.00
Jonah	SHB 42-27X	-583	9393	0.84	0.09	0.04	0.01	0.01	0.00	0.00		0.16
Jonah	SHB 42-27X	-967	9777	0.78	0.07	0.01					0.14	0.10
Jonah	SHB 42-27X	-1226	10036	1.00	0.00	0.00	0.00	0.00	0.00	0.00		0.00
Jonah	SHB 42-27X	-1529	10339	0.89	0.07	0.04	0.00	0.00	0.00	0.00		0.11
Jonah	SHB 42-27X	-2703	11513	0.76	0.06	0.04					0.14	0.12

Note: See figure 5.2 for well locations.

Mud gas data, Jonah Field - bulk gas composition

Area	Well	depth relative to top Lance	Sample Depth	fraction C1	fraction C2	fraction C3	fraction i-C4	fraction n-C4	fraction i-C5	fraction n-C5	CO2	wetness
Jonah	SHB 52-26	-370	9536	0.87	0.08	0.03	0.01	0.01	0.00	0.00		0.13
Jonah	SHB 52-26	-590	9756	0.87	0.07	0.03	0.01	0.01	0.01	0.01		0.13
Jonah	SHB 52-26	-726	9892	0.90	0.07	0.03	0.00	0.00	0.00	0.00		0.10
Jonah	SHB 52-26	-819	9985	0.76	0.17						0.07	0.18
Jonah	SHB 52-26	-882	10048	0.89	0.07	0.03	0.00	0.00	0.00	0.00		0.11
Jonah	SHB 52-26	-978	10144	0.73	0.09	0.05	0.01	0.01			0.11	0.18
Jonah	SHB 52-26	-1119	10285	0.91	0.07	0.02	0.00	0.00	0.00	0.00		0.09
Jonah	SHB 52-26	-1228	10394	0.77	0.10	0.05	0.02	0.01	0.01	>0.01	0.03	0.20
Jonah	SHB 52-26	-1337	10503	0.78	0.10	0.05	0.01	0.01	>0.01	>0.01	0.03	0.18
Jonah	SHB 52-26	-1464	10630	0.91	0.07	0.02	0.00	0.00	0.00	0.00		0.09
Jonah	SHB 73-28	-2247	10656	0.86	0.08	0.06	0.00	0.00	0.00	0.00		0.14
Jonah	SHB 73-28	-2571	10980	0.81	0.09	0.04	0.01	0.01	<0.01	<0.01	0.04	0.16
Jonah	SHB 73-28	-2665	11074	0.87	0.08	0.04	0.00	0.00	0.00	0.00		0.13
Jonah	SHB 73-28	-3053	11462	0.87	0.06	0.02	<0.01	<0.01	0.00	0.00	0.06	0.08
Jonah	SHB 73-28	-3061	11470	0.87	0.09	0.04	0.00	0.00	0.00	0.00		0.13
Jonah	SHB 73-28	-3152	11561	0.71	0.08	0.04	0.01	0.01	0.01	<0.01	0.14	0.17
Jonah	SHB 73-28	-3253	11662	1.00	0.00	0.00	0.00	0.00	0.00	0.00		0.00
Jonah	SHB 98-36	-2747	11887	1.00	0.00							0.00
Jonah	SHB 113-10	-263	9550	0.96	0.01	0.01	0.00	0.00	0.00	0.00	0.01	0.03
Jonah	SHB 113-10	-390	9677	0.92	0.03	0.01	0.01	0.01	0.01	0.00	0.01	0.07
Jonah	SHB 113-10	-508	9795	0.84	0.06	0.03	0.02	0.02	0.01	0.00	0.01	0.15
Jonah	SHB 113-10	-601	9888	0.80	0.08	0.03	0.03	0.03	0.01	0.01	0.01	0.19
Jonah	SHB 113-10	-631	9918	0.93	0.03	0.01	0.01	0.01	0.00	0.00	0.01	0.07
Jonah	SHB 113-10	-673	9960	0.75	0.07	0.03	0.03	0.03	0.04	0.04	0.02	0.24
Jonah	SHB 113-10	-794	10081	0.83	0.07	0.02	0.02	0.02	0.01	0.01	0.01	0.16
Jonah	SHB 113-10	-861	10148	0.84	0.06	0.02	0.02	0.02	0.01	0.01	0.01	0.15
Jonah	SHB 113-10	-1349	10636	0.86	0.06	0.02	0.02	0.02	0.01	0.01	0.00	0.14
Jonah	SHB 113-10	-1456	10743	0.90	0.04	0.01	0.01	0.01	0.00	0.00	0.02	0.08
Jonah	SHB 113-10	-1658	10945	0.86	0.04	0.01	0.01	0.01	0.01	0.02	0.02	0.12
Jonah	SHB 113-10	-1765	11052	0.87	0.06	0.02	0.02	0.02	0.01	0.00	0.00	0.12
Jonah	SHB 113-10	-1875	11162	0.88	0.05	0.02	0.02	0.01	0.01	0.00	0.00	0.11
Jonah	SHB 113-10	-1983	11270	1.00	0.00	0.00	0.00	0.00	0.00	0.00	0.00	0.00
Jonah	SHB 113-10	-2007	11294	0.89	0.05	0.02	0.01	0.01	0.01	0.01	0.01	0.10
Jonah	SHB 113-10	-2107	11394	0.91	0.04	0.01	0.01	0.01	0.00	0.00	0.01	0.08
Jonah	SHB 113-10	-2391	11678	0.87	0.05	0.02	0.02	0.01	0.01	0.00	0.01	0.12
Jonah	SHB 113-10	-2489	11776	0.73	0.07	0.03	0.03	0.03	0.02	0.02	0.06	0.23
Jonah	SHB 113-10	-3018	12305	0.79	0.07	0.04	0.04	0.03	0.01	0.01	0.01	0.21
Jonah	SHB 113-10	-3182	12469	0.98	0.01	0.00	0.00	0.00	0.00	0.00	0.00	0.02
Jonah	CAB 74-30 1	-1821	10953	0.79	0.08	0.04	0.03	0.03	0.01	0.01	0.01	0.20
Jonah	CAB 74-30 1	-2289	11421	0.89	0.04	0.02	0.02	0.01	0.01	0.00	0.01	0.10
Jonah	CAB 74-30 1	-2348	11480	0.74	0.09	0.05	0.05	0.04	0.02	0.01	0.01	0.25
Jonah	SHB 36-17	-2198	11023	0.68	0.08	0.05	0.05	0.05	0.03	0.03	0.02	0.30
Jonah	SHB 36-17	-2304	11129	0.80	0.05	0.03	0.03	0.03	0.01	0.01	0.03	0.17
Jonah	SHB 36-17	-2390	11215	0.92	0.02	0.01	0.01	0.01	0.01	0.00	0.01	0.06
Jonah	SHB 36-17	-2794	11619	0.67	0.06	0.03	0.03	0.04	0.02	0.02	0.13	0.24
Jonah	SHB 36-17	-2843	11668	0.78	0.07	0.03	0.02	0.02	0.01	0.01	0.06	0.17
Jonah	SHB 36-17	-2961	11786	0.74	0.08	0.05	0.04	0.04	0.01	0.01	0.03	0.24
Jonah	SHB 36-17	-3316	12141	0.96	0.00	0.00	0.00	0.00	0.00	0.00	0.04	0.00
Jonah	SHB 36-17	-3382	12207	0.82	0.08	0.03	0.02	0.02	0.01	0.00	0.02	0.16

Note: See figure 5.2 for well locations.

Mud gas data, Jonah Field - bulk gas composition

Area	Well	depth relative to top Lance	Sample Depth	fraction C1	fraction C2	fraction C3	fraction i-C4	fraction n-C4	fraction i-C5	fraction n-C5	CO2	wetness
Jonah	SHB 60-22	143	8765	0.83	0.06	0.02	0.02	0.02	0.01	0.01	0.03	0.14
Jonah	SHB 60-22	-202	9110	0.90	0.03	0.01	0.01	0.01	0.01	0.01	0.02	0.08
Jonah	SHB 60-22	-275	9183	0.82	0.06	0.02	0.02	0.02	0.01	0.01	0.04	0.15
Jonah	SHB 60-22	-465	9373	0.95	0.02	0.01	0.01	0.00	0.00	0.00	0.01	0.04
Jonah	SHB 60-22	-579	9487	0.85	0.05	0.02	0.02	0.02	0.01	0.01	0.02	0.13
Jonah	SHB 60-22	-726	9634	0.85	0.06	0.02	0.02	0.02	0.01	0.01	0.01	0.15
Jonah	SHB 60-22	-999	9907	0.85	0.06	0.02	0.02	0.02	0.01	0.01	0.01	0.14
Jonah	SHB 60-22	-1236	10144	0.89	0.04	0.02	0.01	0.01	0.01	0.01	0.01	0.10
Jonah	SHB 60-22	-1394	10302	0.85	0.06	0.03	0.02	0.02	0.01	0.01	0.01	0.14
Jonah	SHB 60-22	-1492	10400									
Jonah	SHB 60-22	-1680	10588	0.81	0.07	0.03	0.03	0.02	0.01	0.01	0.02	0.17
Jonah	SHB 60-22	-1837	10745	0.87	0.05	0.02	0.02	0.01	0.01	0.01	0.01	0.12
Jonah	SHB 60-22	-1944	10852	0.90	0.00	0.00	0.00	0.00	0.00	0.00	0.10	0.00
Jonah	SHB 60-22	-2137	11045	0.73	0.07	0.02	0.03	0.03	0.03	0.05	0.04	0.24
Jonah	SHB 60-22	-2221	11129	0.79	0.07	0.04	0.03	0.03	0.01	0.01	0.02	0.20
Jonah	SHB 60-22	-2449	11357	0.68	0.09	0.05	0.05	0.04	0.03	0.03	0.05	0.29
Jonah	SHB 60-22	-3102	12010	0.83	0.07	0.03	0.02	0.02	0.01	0.01	0.02	0.15
Jonah	SHB 60-22	-3296	12204	0.83	0.07	0.03	0.02	0.02	0.01	0.01	0.01	0.16
Jonah	SHB 60-22	-3485	12393	0.84	0.07	0.03	0.02	0.02	0.01	0.01	0.01	0.16
Jonah	SHB 60-22	-3594	12502	0.85	0.06	0.03	0.02	0.02	0.01	0.01	0.01	0.15
Jonah	SHB 60-22	-3906	12814	0.78	0.07	0.03	0.02	0.02	0.01	0.02	0.04	0.19
Jonah	SHB 60-22	-3983	12891	0.80	0.08	0.03	0.02	0.02	0.01	0.01	0.03	0.18
Jonah	SHB 60-22	-4019	12927	0.96	0.01	0.00	0.00	0.00	0.00	0.00	0.01	0.03
Jonah	JF 42-6	-520	8665	0.97	0.02	0.00	0.00	0.00	0.00	0.00	0.01	0.02
Jonah	JF 42-6	-698	8843	0.83	0.06	0.02	0.02	0.02	0.01	0.01	0.02	0.15
Jonah	JF 42-6	-844	8989	0.84	0.06	0.02	0.02	0.02	0.01	0.01	0.02	0.14
Jonah	JF 42-6	-955	9100	0.85	0.05	0.02	0.01	0.01	0.01	0.01	0.03	0.12
Jonah	JF 42-6	-1171	9316	0.86	0.03	0.01	0.01	0.02	0.02	0.02	0.03	0.11
Jonah	JF 42-6	-1358	9503	0.88	0.05	0.02	0.02	0.01	0.01	0.00	0.01	0.11
Jonah	JF 42-6	-1842	9987	0.79	0.08	0.03	0.02	0.02	0.01	0.01	0.03	0.18
Jonah	JF 42-6	-1966	10111	0.93	0.03	0.01	0.01	0.01	0.00	0.00	0.01	0.06
Jonah	JF 42-6	-2122	10267	0.85	0.06	0.03	0.02	0.02	0.01	0.01	0.01	0.14
Jonah	JF 42-6	-2371	10516	0.80	0.08	0.04	0.03	0.02	0.01	0.01	0.02	0.19
Jonah	JF 42-6	-2617	10762	0.73	0.08	0.04	0.04	0.03	0.02	0.02	0.05	0.24
Jonah	JF 42-6	-2786	10931	0.80	0.08	0.03	0.03	0.02	0.01	0.01	0.02	0.19
Jonah	JF 42-6	-2938	11083	0.67	0.09	0.03	0.03	0.04	0.02	0.02	0.09	0.26
Jonah	JF 42-6	-3337	11482	0.74	0.09	0.04	0.02	0.03	0.02	0.01	0.06	0.21

Note: See figure 5.2 for well locations.

Mud gas data, Jonah Field - carbon isotope composition

Area	Well	depth relative to top Lance	Sample Depth	13C C1	13C C2	13C C3	13C i-C4	13C n-C4	13C i-C5	13C n-C5	CO2
Jonah	CAB 76-30	-2073	11417	-35.8							
Jonah	CAB 76-30	-2196	11540	-38.6							
Jonah	CAB 76-30	-2203	11547	-37.7	-26.7	-24.7	-24.4				
Jonah	JF 30-4	-2699	11473	-41.6	-29.3	-26.6	-26.0	-25.5	-24.9	-24.8	-18.0
Jonah	JF 30-4	-3057	11831	-41.8	-28.5	-26.3	-25.8	-25.3	-25.0	-25.3	-17.7
Jonah	JF 38-4	-2064	10730	-32.2	-22.7	-22.6	-23.7	-23.5	-26.3	-25.5	-16.2
Jonah	JF 38-4	-2494	11160	-40.6	-28.0	-26.2	-25.9	-25.6	-25.8	-25.0	-17.5
Jonah	JF 38-4	-2630	11296	-36.5	-27.7	-27.4	-24.4	-25.6	-24.2	-24.9	-14.5
Jonah	JF 38-4	-2750	11416	-38.7	-27.5	-25.7	-25.2	-25.2	-24.9	-25.1	-17.5
Jonah	JF 38-4	-3062	11728	-33.7	-25.4	-25.2	-24.9	-25.0	-25.3	-24.8	-15.8
Jonah	JF 42-8	-220	8545	-33.4							
Jonah	JF 42-8	-515	8840	-37.2	-26.5	-25.1	-24.4	-24.4			
Jonah	JF 42-8	-1020	9345	-36.4	-26.2	-25.5					
Jonah	JF 42-8	-1182	9507	-38.0	-27.5	-25.8	-25.5	-25.3			
Jonah	JF 42-8	-1357	9682	-38.5	-27.4	-25.6	-25.3	-25.1	-24.8	-24.7	
Jonah	JF 42-8	-1867	10192	-39.8	-28.0	-26.3	-25.9	-25.5			
Jonah	JF 42-8	-2457	10782	-39.3	-27.9						
Jonah	SHB 19-17	-1250	10176	-39.3	-27.6	-28.1	-27.2	-26.2			-12.0
Jonah	SHB 19-17	-1529	10455	-35.3	-26.0	-25.4	-24.1	-24.6	-24.8	-24.0	-13.8
Jonah	SHB 19-17	-2048	10974	-35.6	-25.9	-26.0	-26.1	-24.5			-10.9
Jonah	SHB 19-17	-2646	11572	-38.8	-28.3	-26.6	-26.1	-25.7	-26.0	-25.0	-12.0
Jonah	SHB 19-17	-2866	11792	-4.4	-17.3	-21.5	-22.4	-22.4	-24.5	-22.6	-11.5
Jonah	SHB 19-17	-3119	12045	-37.8	-27.3	-26.1	-25.6	-25.2	-26.2	-25.3	13.3
Jonah	SHB 19-17	-3519	12445	-42.4	-30.1	-27.6	-26.2	-25.8	-25.7	-24.8	-13.0
Jonah	SHB 19-17	-3965	12891	-44.0	-29.8	-27.1	-26.8	-26.0	-26.9	-25.3	-13.7
Jonah	SHB 19-17	-4521	13447	-41.4	-24.4	-22.3	-22.7	-22.2	-23.2	-23.0	-13.8
Jonah	SHB 19-22	-3269	12195	-39.2	-26.6	-25.4		-24.4			
Jonah	SHB 27-34	-2829	11528	-41.4	-28.0	-25.6					
Jonah	SHB 27-34	-2892	11591	-43.8	-29.3						
Jonah	SHB 27-34	-2913	11612	-44.3	-29.6						
Jonah	SHB 27-34	-3265	11964	-40.8							
Jonah	SHB 27-34	-3265	11964	-40.5	-28.5	-26.1					
Jonah	SHB 30-15	-3337	12613	-37.8	-28.1	-27.1	-25.0	-26.2	-27.8	-23.9	-14.4
Jonah	SHB 30-15	-3563.5	12839.5	-37.8	-28.3	-26.2	-25.2	-25.4	-25.7	-25.3	-14.5
Jonah	SHB 30-20	-956	9542	-37.3	-29.4						
Jonah	SHB 30-20	-1296	9882	-42.0	-28.5	-26.6					
Jonah	SHB 30-20	-2055	10641	-33.5	-24.1	-24.6	-23.4	-24.2			
Jonah	SHB 30-20	-2688	11274	-40.0	-28.6	-26.7					
Jonah	SHB 30-36	-174	9264	-37.1	-25.1	-23.0	-23.3	-22.9			-13.7
Jonah	SHB 30-36	-361	9451	-38.0	-26.5	-24.1	-24.3	-23.2			-13.9
Jonah	SHB 30-36	-548	9638	-37.4	-26.1	-24.1	-24.2	-23.2	-23.9	-23.5	-13.5

Note: See figure 5.2 for well locations.

Mud gas data, Jonah Field - carbon isotope composition

Area	Well	depth relative to top Lance	Sample Depth	13C C1	13C C2	13C C3	13C i-C4	13C n-C4	13C i-C5	13C n-C5	CO2
Jonah	SHB 31-9	-529	9830	-36.0	-27.4	-25.7	-24.9	-25.6	-27.1	-23.9	-12.7
Jonah	SHB 31-9	-1130	10431	-32.6	-25.6	-25.2	-23.9	-24.9	-24.7	-23.7	-13.2
Jonah	SHB 31-9	-1335	10636	-34.1	-26.8	-26.2	-24.8	-25.9	-25.2	-23.7	-13.5
Jonah	SHB 31-9	-3143	12444	-37.0	-28.6	-26.7	-26.0	-26.5	-24.2		-14.9
Jonah	SHB 31-9	-3404	12705	-38.1	-28.4	-26.8	-26.2	-25.6	-26.9	-25.6	-14.5
Jonah	SHB 33-34	-1020	9841	-35.5	-27.1	-26.1	-25.2	-25.1	-24.8	-25.7	-13.0
Jonah	SHB 33-34	-1514	10335	-35.4	-27.1	-26.2	-25.0	-26.1	-26.0	-24.0	-14.1
Jonah	SHB 37-34	-137	8922	-36.7	-26.3	-24.3	-23.5	-23.4	-24.2	-22.5	-12.4
Jonah	SHB 37-34	-271	9056	-35.1	-23.9	-23.5	-23.9	-23.7	-23.9	-24.1	-12.8
Jonah	SHB 37-34	-517	9302	-39.5	-26.8	-25.7	-24.8	-25.0	-24.8	-24.3	-12.5
Jonah	SHB 37-34	-1167	9952	-40.4	-27.6	-25.9	-24.9	-24.6	-24.6	-24.1	-13.0
Jonah	SHB 37-34	-1524	10309	-41.4	-28.1	-26.4	-25.2	-25.5	-24.6	-24.8	-13.5
Jonah	SHB 37-34	-1822	10607	-42.3	-28.2	-26.4	-25.9	-25.8	-25.2	-24.8	-13.0
Jonah	SHB 37-34	-2433	11218	-42.4	-28.7	-26.8	-25.7	-25.8			-13.3
Jonah	SHB 37-34	-2767	11552	-42.4	-28.9	-26.8	-25.8	-26.0	-25.1	-25.3	-13.2
Jonah	SHB 37-34	-3051	11836	-42.7	-29.9	-26.5	-25.4	-25.5	-24.7	-25.4	-11.7
Jonah	SHB 37-34	-3310	12095	-42.1	-29.5	-27.0	-25.8	-26.1			-13.3
Jonah	SHB 42-27X	663	8147	-35.8	-25.8	-24.2	-24.4	-24.1	-24.7	-24.1	-14.7
Jonah	SHB 42-27X	-967	9777	-39.5	-27.6	-26.0					-13.6
Jonah	SHB 42-27X	-2703	11513	-41.9	-29.7	-27.9					-14.3
Jonah	SHB 52-26	-819	9985	-36.4	-25.3						-13.6
Jonah	SHB 52-26	-978	10144	-35.5	-18.7	-21.9	-22.3	-23.2			-13.8
Jonah	SHB 52-26	-1228	10394	-32.4	-24.7	-24.7	-24.8	-24.5	-24.7	-24.4	-13.2
Jonah	SHB 52-26	-1337	10503	-36.4	-27.3	-26.7	-26.3	-26.1	-25.6	-26.0	-12.2
Jonah	SHB 73-28	-2571	10980	-38.1	-28.4	-26.8	-25.7	-25.5	-27.4	-25.8	-13.8
Jonah	SHB 73-28	-3053	11462	-34.8	-24.5	-23.0	-23.9	-20.2			-13.3
Jonah	SHB 73-28	-3152	11561	-36.2	-26.4	-26.3	-25.0	-25.2	-28.2	-25.3	-14.0
Jonah	SHB 98-36	-2747	11887	-38.8							
Jonah	SHB 113-10	-263	9550	-35.2	-23.2						-10.8
Jonah	SHB 113-10	-390	9677	-36.3	-26.0	-24.4	-23.3	-23.5	-23.2	-22.8	-9.6
Jonah	SHB 113-10	-508	9795	-38.0	-26.7	-24.7	-23.6	-23.5	-22.8	-21.2	-10.8
Jonah	SHB 113-10	-601	9888	-35.8	-26.6	-24.8	-24.0	-23.7	-23.5	-23.1	-11.5
Jonah	SHB 113-10	-631	9918	-44.2	-25.3	-24.0	-21.8	-22.2	-21.9	-22.5	-10.8
Jonah	SHB 113-10	-673	9960	-37.1	-24.5	-23.0	-21.6	-22.1	-23.7	-24.7	-10.4
Jonah	SHB 113-10	-794	10081	-40.4	-24.3	-20.4					
Jonah	SHB 113-10	-861	10148	-37.3	-24.9	-22.8	-20.5	-22.2	-20.0	-21.5	-11.7
Jonah	SHB 113-10	-1349	10636	-35.7	-25.2	-24.0	-21.3	-22.4	-21.4	-20.9	
Jonah	SHB 113-10	-1456	10743	-42.7	-25.4	-22.7					
Jonah	SHB 113-10	-1658	10945	-48.1	-27.0	-24.8	-21.9	-22.4	-21.1	-21.6	-11.5
Jonah	SHB 113-10	-1765	11052	-35.5	-24.7	-23.5	-21.1	-22.1	-21.6	-20.7	-10.0
Jonah	SHB 113-10	-1875	11162	-43.6	-25.6	-23.5	-20.5	-21.8	-21.5	-21.7	-11.2
Jonah	SHB 113-10	-1983	11270	-33.0							
Jonah	SHB 113-10	-2007	11294	-38.7	-24.4	-21.5					
Jonah	SHB 113-10	-2107	11394	-39.4	-26.9	-24.5	-21.1	-22.6			-23.7
Jonah	SHB 113-10	-2391	11678	-41.5	-26.7	-24.9	-21.8	-21.8			-10.9
Jonah	SHB 113-10	-2489	11776	-39.0	-21.8						-11.5
Jonah	SHB 113-10	-3018	12305	-40.1	-25.7	-23.1	-22.0	-21.4	-21.0	-20.8	-6.6
Jonah	SHB 113-10	-3182	12469	-35.2	-23.2	-21.1					

Note: See figure 5.2 for well locations.

Mud gas data, Jonah Field - carbon isotope composition

Area	Well	depth relative to top Lance	Sample Depth	13C C1	13C C2	13C C3	13C i-C4	13C n-C4	13C i-C5	13C n-C5	CO2
Jonah	CAB 74-30 1	-1821	10953	-41.0	-25.1	-22.5	-21.0	-20.0	-21.1	-21.7	-11.5
Jonah	CAB 74-30 1	-2289	11421	-37.3	-26.7	-23.2	-21.3	-20.7			-9.6
Jonah	CAB 74-30 1	-2348	11480	-41.0	-27.9	-25.2	-23.8	-24.0	-22.0	-21.3	-10.3
Jonah	SHB 36-17	-2198	11023	-35.5	-22.1	-24.4	-23.4	-24.2	-22.9	-22.9	-10.4
Jonah	SHB 36-17	-2304	11129	-38.5	-26.8	-24.3	-22.4	-21.7	-22.4	-21.9	
Jonah	SHB 36-17	-2390	11215	-44.3	-24.7	-22.8	-21.0	-21.2			-12.3
Jonah	SHB 36-17	-2794	11619	-37.9	-22.7	-21.7	-21.1	-21.3	-22.7	-21.0	-13.2
Jonah	SHB 36-17	-2843	11668	-42.0	-25.5	-24.1	-21.1	-21.9	-20.3	-19.7	-13.5
Jonah	SHB 36-17	-2961	11786	-39.7	-28.0	-26.3	-23.9	-23.9	-22.6	-21.7	-14.9
Jonah	SHB 36-17	-3316	12141	-46.8							-13.5
Jonah	SHB 36-17	-3382	12207	-38.1	-26.6	-24.1	-21.7	-22.5	-21.4	-19.7	-13.5
Jonah	SHB 60-22	143	8765	-41.1	-23.5	-21.6	-20.7	-20.9			-9.5
Jonah	SHB 60-22	-202	9110	-31.1	-23.2	-21.1					-11.3
Jonah	SHB 60-22	-275	9183	-41.0	-23.3	-20.9					
Jonah	SHB 60-22	-465	9373	-38.8	-26.1	-23.0	-20.2	-20.3			-4.7
Jonah	SHB 60-22	-579	9487	-40.0	-23.7	-21.0		-18.0			-8.2
Jonah	SHB 60-22	-726	9634	-39.9	-23.5	-21.2	-20.2	-21.3	-21.4		-8.7
Jonah	SHB 60-22	-999	9907	-40.3	-23.2	-21.4	-19.0	-23.0			
Jonah	SHB 60-22	-1236	10144	-44.6	-22.5	-20.5		-19.1			-8.0
Jonah	SHB 60-22	-1394	10302	-39.4	-23.8	-21.5	-19.5	-18.9			-7.0
Jonah	SHB 60-22	-1492	10400	-31.6	-26.7						-9.4
Jonah	SHB 60-22	-1680	10588	-40.0	-22.6	-21.2	-19.1	-19.5			-8.4
Jonah	SHB 60-22	-1837	10745	-39.2	-23.6	-21.7	-18.9	-19.2	-20.5	-21.2	-11.6
Jonah	SHB 60-22	-1944	10852	-38.3							-10.6
Jonah	SHB 60-22	-2137	11045	-37.9	-21.6						
Jonah	SHB 60-22	-2221	11129	-43.7	-25.0	-23.0	-21.9	-21.5	-21.7	-20.9	-8.3
Jonah	SHB 60-22	-2449	11357	-41.6	-23.0	-21.5	-22.9	-20.8			-7.9
Jonah	SHB 60-22	-3102	12010	-41.3	-25.2	-23.8	-21.1	-20.6	-19.2	-20.0	-10.3
Jonah	SHB 60-22	-3296	12204	-39.6	-27.0	-22.7	-20.0	-20.5	-20.8		-9.6
Jonah	SHB 60-22	-3485	12393	-39.6	-27.3	-22.9	-20.8	-20.4	-20.4	-19.2	-9.2
Jonah	SHB 60-22	-3594	12502	-41.1	-25.9	-25.3	-21.3	-21.5			-9.0
Jonah	SHB 60-22	-3906	12814	-44.9	-29.1	-24.2	-20.9	-21.1			-10.5
Jonah	SHB 60-22	-3983	12891	-40.0	-25.7	-23.5	-20.7	-21.1	-19.8	-20.2	-11.5
Jonah	SHB 60-22	-4019	12927	-52.4	-26.7	-23.2	-20.0				-11.4
Jonah	JF 42-6	-520	8665	-44.4	-21.7	-19.9					-6.4
Jonah	JF 42-6	-698	8843	-40.5	-21.7	-19.8					-6.9
Jonah	JF 42-6	-844	8989	-42.6	-21.8	-20.1					-7.5
Jonah	JF 42-6	-955	9100	-46.8	-20.4	-20.5					-10.1
Jonah	JF 42-6	-1171	9316	-39.5	-23.0	-20.8					
Jonah	JF 42-6	-1358	9503								-10.0
Jonah	JF 42-6	-1842	9987	-32.0	-24.2	-21.0	-19.7	-18.4			-8.1
Jonah	JF 42-6	-1966	10111	-39.4	-26.5	-22.9	-20.9	-20.1			-6.9
Jonah	JF 42-6	-2122	10267	-43.4	-24.8	-21.7	-19.2	-19.2			-8.6
Jonah	JF 42-6	-2371	10516	-43.6	-23.4	-22.0					-6.7
Jonah	JF 42-6	-2617	10762	-44.9	-25.4	-24.2	-22.0				-8.2
Jonah	JF 42-6	-2786	10931	-51.7	-27.5	-26.2	-25.1	-25.3	-25.4	-24.2	-8.9
Jonah	JF 42-6	-2938	11083	-45.8	-25.2	-22.1	-22.1	-20.7			-8.2
Jonah	JF 42-6	-3337	11482	-40.1	-25.7	-23.1	-22.0	-21.4	-21.0	-20.8	-6.6

Note: See figure 5.2 for well locations.

Mud gas data, Jonah Field - hydrogen isotope composition

Area	Well	depth relative to top Lance	Sample Depth	dD C1	dD C2	dD C3	dD i-C4	dD n-C4	dD i-C5	dD n-C5
Jonah	JF 30-4	-2699	11473	-196	-177	-171	-149	-151		
Jonah	JF 30-4	-3057	11831	-200	-175	-183	-155	-156		
Jonah	JF 38-4	-2064	10730	-180	-160	-180	-168	-159		
Jonah	JF 38-4	-2630	11296	-189						
Jonah	JF 38-4	-2750	11416	-213	-180	-208	-169	-177		
Jonah	JF 38-4	-3062	11728	-203	-171	-205	-289	-180		
Jonah	JF 42-8	-220	8545	-147						-173
Jonah	JF 42-8	-515	8840	-199	-165					-164
Jonah	JF 42-8	-1020	9345	-192	-156					-156
Jonah	JF 42-8	-1182	9507	-194	-157	-196		-177		
Jonah	JF 42-8	-1357	9682	-188	-166	-172		-153		
Jonah	JF 42-8	-1867	10192	-193	-166	-177		-156		
Jonah	JF 42-8	-2415	10740							-157
Jonah	JF 42-8	-2457	10782	-210	-216					
Jonah	SHB 19-17	-1250	10176	-162						
Jonah	SHB 19-17	-1529	10455	-183						
Jonah	SHB 19-17	-2048	10974	-204						
Jonah	SHB 19-17	-2646	11572	-199	-177	-206	-167	-178		
Jonah	SHB 19-17	-2866	11792	-190						
Jonah	SHB 19-17	-3119	12045	-214						
Jonah	SHB 19-17	-3519	12445	-192	-169	-208				
Jonah	SHB 19-17	-3965	12891	-185	-151	-181				
Jonah	SHB 19-17	-4521	13447	-198	-158					
Jonah	SHB 30-15	-3337	12613	-202						
Jonah	SHB 30-15	-3563.5	12839.5	-179	-156					
Jonah	SHB 30-20	-956	9542	-200	-154					
Jonah	SHB 30-20	-1296	9882	-185						
Jonah	SHB 30-20	-2055	10641	-174	-156	-179		-144		
Jonah	SHB 30-20	-2688	11274	-188	-165	-183				
Jonah	SHB 30-36	-361	9451	-237						
Jonah	SHB 30-36	-548	9638	-244						
Jonah	SHB 31-9	-529	9830	-220						
Jonah	SHB 31-9	-1130	10431	-191						
Jonah	SHB 31-9	-1335	10636	-197						
Jonah	SHB 31-9	-3143	12444	-168						
Jonah	SHB 31-9	-3404	12705	-197						

Note: See figure 5.2 for well locations.

Mud gas data, Jonah Field - hydrogen isotope composition

Area	Well	depth relative to top Lance	Sample Depth	dD C1	dD C2	dD C3	dD i-C4	dD n-C4	dD i-C5	dD n-C5
Jonah	SHB 33-34	-1020	9841	-181						
Jonah	SHB 33-34	-1514	10335	-194						
Jonah	SHB 37-34	-137	8922	-220						
Jonah	SHB 37-34	-271	9056	-206	-163					
Jonah	SHB 37-34	-517	9302	-200						
Jonah	SHB 37-34	-1167	9952	-193	-159	-215				
Jonah	SHB 37-34	-1822	10607	-214	-226					
Jonah	SHB 37-34	-2433	11218	-202						
Jonah	SHB 37-34	-2767	11552	-192	-170	-193	-158	-159		
Jonah	SHB 37-34	-3051	11836	-179	-159	-186				
Jonah	SHB 37-34	-3310	12095	-212						
Jonah	SHB 42-27X	663	8147	-192						
Jonah	SHB 42-27X	-967	9777	-210						
Jonah	SHB 42-27X	-2703	11513	-217						
Jonah	SHB 52-26	-819	9985	-199						
Jonah	SHB 52-26	-978	10144	-207						
Jonah	SHB 52-26	-1228	10394	-205						
Jonah	SHB 52-26	-1337	10503	-206						
Jonah	SHB 73-28	-2571	10980	-181						
Jonah	SHB 73-28	-3053	11462	-192						
Jonah	SHB 98-36	-2747	11887	-208						
Jonah	SHB 113-10	-263	9550	ND						
Jonah	SHB 113-10	-390	9677	ND						
Jonah	SHB 113-10	-508	9795	-165						
Jonah	SHB 113-10	-601	9888	-190						
Jonah	SHB 113-10	-631	9918	-193						
Jonah	SHB 113-10	-673	9960	ND						
Jonah	SHB 113-10	-794	10081	-198						
Jonah	SHB 113-10	-861	10148	-205						
Jonah	SHB 113-10	-1349	10636	-194						
Jonah	SHB 113-10	-1456	10743	-201						
Jonah	SHB 113-10	-1658	10945	-178						
Jonah	SHB 113-10	-1765	11052	-193						
Jonah	SHB 113-10	-1875	11162	-187						
Jonah	SHB 113-10	-1983	11270	-203						
Jonah	SHB 113-10	-2007	11294	-206	-184					
Jonah	SHB 113-10	-2107	11394	-205						
Jonah	SHB 113-10	-2391	11678	-198						
Jonah	SHB 113-10	-2489	11776	-205						
Jonah	SHB 113-10	-3018	12305	ND						
Jonah	SHB 113-10	-3182	12469	-171	-180					
Jonah	CAB 74-30 1	-1821	10953	-197						
Jonah	CAB 74-30 1	-2289	11421	-207						
Jonah	CAB 74-30 1	-2348	11480	-206	-221					

Note: See figure 5.2 for well locations.

Mud gas data, Jonah Field - hydrogen isotope composition

Area	Well	depth relative to top Lance	Sample Depth	dD C1	dD C2	dD C3	dD i-C4	dD n-C4	dD i-C5	dD n-C5
Jonah	SHB 36-17	-2198	11023	-175	-82	-158				
Jonah	SHB 36-17	-2304	11129	-196	-191	-173	-154	-165	-145	-160
Jonah	SHB 36-17	-2390	11215	-222		-183	-158	-167	-147	-160
Jonah	SHB 36-17	-2794	11619	-219						
Jonah	SHB 36-17	-2843	11668	-203						
Jonah	SHB 36-17	-2961	11786	-173						
Jonah	SHB 36-17	-3316	12141	-169						
Jonah	SHB 36-17	-3382	12207	-189	-177					
Jonah	SHB 36-17	-3677	12502	-199	-175					
Jonah	SHB 36-17	-3867	12692	-200						
Jonah	SHB 60-22	143	8765	-196						
Jonah	SHB 60-22	-275	9183	-200						
Jonah	SHB 60-22	-465	9373	-192						
Jonah	SHB 60-22	-579	9487	-200						
Jonah	SHB 60-22	-726	9634	-199						
Jonah	SHB 60-22	-999	9907	-209	-182					
Jonah	SHB 60-22	-1236	10144	-213	-195					
Jonah	SHB 60-22	-1394	10302	-195						
Jonah	SHB 60-22	-1492	10400	-184						
Jonah	SHB 60-22	-1680	10588	-191						
Jonah	SHB 60-22	-1837	10745	-180						
Jonah	SHB 60-22	-1944	10852	-185						
Jonah	SHB 60-22	-2137	11045	-200						
Jonah	SHB 60-22	-2221	11129	-195	-190					
Jonah	SHB 60-22	-2449	11357	-170						
Jonah	SHB 60-22	-3102	12010	-189						
Jonah	SHB 60-22	-3296	12204	-202						
Jonah	SHB 60-22	-3485	12393	-174						
Jonah	SHB 60-22	-3594	12502	-195						
Jonah	SHB 60-22	-3906	12814	-176						
Jonah	SHB 60-22	-3983	12891	-208						
Jonah	JF 42-6	-520	8665	-194	-146					
Jonah	JF 42-6	-698	8843	-201						
Jonah	JF 42-6	-844	8989	-186						
Jonah	JF 42-6	-955	9100	-156						
Jonah	JF 42-6	-1171	9316	-191	-169					
Jonah	JF 42-6	-1358	9503	-204						
Jonah	JF 42-6	-1842	9987	-189						
Jonah	JF 42-6	-1966	10111	-197						
Jonah	JF 42-6	-2122	10267	-210						
Jonah	JF 42-6	-2371	10516	-198						
Jonah	JF 42-6	-2617	10762	-210	-106					
Jonah	JF 42-6	-2786	10931	-178						
Jonah	JF 42-6	-2938	11083	-209	-146					

Note: See figure 5.2 for well locations.

Mud gas data, Greater Natural Buttes Field - bulk gas composition

Area	Well	Sample Depth	fraction C1	fraction C2	fraction C3	fraction i-C4	fraction n-C4	fraction i-C5	fraction n-C5
GNB	NBU 921 2703AS	9171	0.74	0.12	0.08	0.00	0.01	0.00	0.00
GNB	NBU 921 2703AS	9209	0.74	0.13	0.07	0.02	0.02	0.01	0.01
GNB	NBU 921 2703 AS	9430	0.98	0.02	0.00	0.00	0.00	0.00	0.00
GNB	NBU 921 2703AS	9525	0.93	0.05	0.02	0.00	0.00	0.00	0.00
GNB	NBU 921 2703AS	9657	0.98	0.02	0.00	0.00	0.00	0.00	0.00
GNB	NBU 921 2703AS	10077	1.00	0.00	0.00	0.00	0.00	0.00	0.00
GNB	NBU 921 2703	10178	1.00	0.00	0.00	0.00	0.00	0.00	0.00
GNB	NBU 921 2703	10298	0.94	0.04	0.02	0.00	0.01	0.00	0.00
GNB	NBU 921 2703	10416	0.93	0.05	0.02	0.00	0.00	0.00	0.00
GNB	NBU 921 2703	10533	1.00	0.00	0.00	0.00	0.00	0.00	0.00
GNB	NBU 921 2703	10984	0.96	0.04	0.00	0.00	0.00	0.00	0.00
GNB	NBU 921 2703	11105	0.97	0.03	0.00	0.00	0.00	0.00	0.00
GNB	NBU 921 2703 AS	6754	1.00	0.00	0.00	0.00	0.00	0.00	0.00
GNB	NBU 921 2703 AS	7624	1.00	0.00	0.00	0.00	0.00	0.00	0.00
GNB	NBU 921 2703 AS	8077	0.92	0.05	0.02	0.01	0.01	0.00	0.00
GNB	NBU 921 2703 AS	8292	1.00	0.00	0.00	0.00	0.00	0.00	0.00
GNB	STATE 1021-32 O	3570	0.74	0.13	0.06	0.02	0.02	0.01	0.01
GNB	STATE 1021-32 O	3978	0.73	0.13	0.06	0.02	0.02	0.01	0.01
GNB	STATE 1021-32 O	5307	0.66	0.15	0.09	0.03	0.03	0.01	0.01
GNB	STATE 1021-32 O	5646	0.66	0.15	0.09	0.03	0.03	0.01	0.01
GNB	STATE 1021-32 O	5666	0.70	0.14	0.08	0.02	0.02	0.01	0.01
GNB	STATE 1021-32 O	5752	0.65	0.15	0.10	0.03	0.03	0.02	0.01
GNB	STATE 1021-32 O	5786	0.89	0.06	0.03	0.01	0.01	0.00	0.00
GNB	STATE 1021-32 O	5930	0.75	0.12	0.06	0.02	0.02	0.01	0.01
GNB	STATE 1021-32 O	5964	0.87	0.06	0.04	0.01	0.01	0.00	0.00
GNB	STATE 1021-32 O	7017	0.71	0.14	0.08	0.02	0.02	0.01	0.01
GNB	STATE 1021-32 O	7070	1.00	0.00	0.00	0.00	0.00	0.00	0.00
GNB	STATE 1021-32 O	7087	0.70	0.14	0.08	0.02	0.02	0.01	0.01
GNB	STATE 1021-32 O2	6505	0.83	0.09	0.04	0.01	0.01	0.01	0.01
GNB	STATE 1021-32 O2	6964	0.94	0.06	0.00	0.00	0.00	0.00	0.00
GNB	STATE 1021-32 O 2	7180	0.88	0.08	0.03	0.01	0.01	0.00	0.00
GNB	STATE 1021-32 O 2	7335	0.91	0.09	0.00	0.00	0.00	0.00	0.00
GNB	STATE 1021-32 O 2	7407	1.00	0.00	0.00	0.00	0.00	0.00	0.00
GNB	STATE 1021-32 O 2	7442	0.89	0.08	0.03	0.00	0.00	0.00	0.00
GNB	STATE 1021-32 O 2	7479	0.90	0.07	0.03	0.00	0.00	0.00	0.00
GNB	STATE 1021-32 O 2	7517	0.94	0.04	0.02	0.00	0.00	0.00	0.00
GNB	STATE 1021-32 O 2	7611	0.90	0.07	0.03	0.00	0.00	0.00	0.00
GNB	STATE 1021-32 O 2	7724	0.91	0.06	0.03	0.00	0.00	0.00	0.00
GNB	STATE 1021-32 O 2	7851	1.00	0.00	0.00	0.00	0.00	0.00	0.00
GNB	STATE 1021-32 O 2	7873	0.82	0.10	0.06	0.01	0.01	0.00	0.00
GNB	STATE 1021-32 O 2	7946	0.94	0.04	0.02	0.00	0.00	0.00	0.00
GNB	STATE 1021-32 O 2	8189	0.95	0.05	0.00	0.00	0.00	0.00	0.00
GNB	STATE 1021-32 O 2	8331	1.00	0.00	0.00	0.00	0.00	0.00	0.00
GNB	STATE 1021-32 O 2	8587	1.00	0.00	0.00	0.00	0.00	0.00	0.00
GNB	STATE 1021-32 O 2	8921	1.00	0.00	0.00	0.00	0.00	0.00	0.00

Note: See figure 6.1 for well locations.

Mud gas data, Greater Natural Buttes Field - carbon isotope composition

Area	Well	Sample Depth	13C C1	13C C2	13C C3	13C i-C4	13C n-C4	13C i-C5	13C n-C5	13C CO2
GNB	**NBU 921 2703AS**	**9171**	-38							
GNB	**NBU 921 2703AS**	**9209**	-37.7	-26.1	-24	-25.1	-23.8	-24.5	-24.6	
GNB	**NBU 921 2703 AS**	**9430**	-36.4	-27.1	-24.35	-24.8	-24.7	-23.4	-25.6	-10.1
GNB	**NBU 921 2703AS**	**9525**	-35.4	-26.9	-24.4	-25	-23.8	-23.6	-23.4	
GNB	**NBU 921 2703AS**	**9657**	-37.3	-26.7	-24.7	-25.7	-24.7	-24.6	-25.3	-12.9
GNB	**NBU 921 2703AS**	**10077**	-35.9	-25.1	-24.3	-23.6	-23.6	-23.9	-24.3	-10
GNB	**NBU 921 2703**	**10178**	-34.8	-25.4	-24.1	-24.9	-24.3	-24.1	-25	-11.6
GNB	**NBU 921 2703**	**10298**	-35.4	-28.3	-26.3	-26.9	-25.8	-25.8	-25.7	-8.3
GNB	**NBU 921 2703**	**10416**	-37.1	-26.9	-24.9	-24.1	-24.5	-25.7	-25.1	-10.3
GNB	**NBU 921 2703**	**10533**	-39.0	-27.6						-10.4
GNB	**NBU 921 2703**	**10984**	-39.7	-26.2	-23.2	-23.6	-22.2	-22.6	-20.7	-10.8
GNB	**NBU 921 2703**	**11105**	-35.3	-20.9	-14.5	-16.9	-15.1	-17.5	-16.7	-9.7
GNB	**NBU 921 2703 AS**	**6754**	-34.4	-22.6	-20	-18.5	-19.4	-20.3	-18	-2.7
GNB	**NBU 921 2703 AS**	**7624**	-40.4	-24.6	-24.1	-24.0	-23.4	-24.2	-23.5	-10.2
GNB	**NBU 921 2703 AS**	**8077**	-39.9	-24.3	-25	-21.7	-23.8	-23.5	-26.2	-5
GNB	**NBU 921 2703 AS**	**8292**	-38.8	-24.6	-23.2	-22.1	-22.6	-21.6	-22.9	-12.4
GNB	**STATE 1021-32 O**	**3570**	**-30.4**	**-23.2**	**-25.3**	**-23.5**	**-25.0**	**-23.3**	**-23.3**	**-9.1**
GNB	**STATE 1021-32 O**	**3978**	**-38.1**	**-27.8**	**-28.7**	**-27.9**	**-28.3**	**-25.2**	**-25.3**	**-9.7**
GNB	**STATE 1021-32 O**	**5307**	**-34.2**	**-21.6**	**-20.7**	**-20.6**	**-20.9**	**-21.7**	**-20.8**	
GNB	**STATE 1021-32 O**	**5646**	**-34.7**	**-28.4**	**-25.7**	**-26.1**	**-24.9**	**-25.2**	**-25.0**	**-6.6**
GNB	**STATE 1021-32 O**	**5666**	**-35.6**	**-25.1**	**-21.7**	**-21.8**	**-21.4**	**-21.8**	**-22.2**	**-9.7**
GNB	**STATE 1021-32 O**	**5752**	**-30.4**	**-25.4**	**-22.4**	**-23.4**	**-22.4**	**-23.8**	**-21.5**	**-9.7**
GNB	**STATE 1021-32 O**	**5786**	**-35.5**	**-27.9**	**-23.9**	**-24.1**	**-23.3**	**-24.2**	**-24.5**	
GNB	**STATE 1021-32 O**	**5930**	**-29.2**	**-24.1**	**-22.6**	**-23.0**	**-22.3**	**-23.3**	**-23.5**	
GNB	**STATE 1021-32 O**	**5964**	**-31.5**	**-23.7**	**-21.9**	**-23.6**	**-23.0**	**-22.4**	**-24.4**	
GNB	**STATE 1021-32 O**	**7017**	**-31.9**	**-29.0**	**-25.8**	**-25.9**	**-24.5**	**-25.0**	**-24.6**	**-10.7**
GNB	**STATE 1021-32 O**	**7070**	**-36.5**	**-28.6**	**-25.6**	**-26.2**	**-25.0**	**-25.0**	**-24.6**	**-8.5**
GNB	**STATE 1021-32 O**	**7087**	**-33.2**	**-28.2**	**-25.6**	**-25.2**	**-24.2**	**-24.5**	**-24.9**	**-3.2**
GNB	**STATE 1021-32 O2**	**6505**	**-29**	**-23**	**-22**	**-23**	**-23**	**-23**	**-24**	
GNB	**STATE 1021-32 O2**	**6964**	-39.3	-24	-21.8	-19.6	-23.3	-25	-26.3	-11.2
GNB	**STATE 1021-32 O 2**	**7180**	-31.1							-10.6
GNB	**STATE 1021-32 O 2**	**7335**	-40.9	-25	-23.1	-21.9	-22.8	-26.5	-26.9	-9.7
GNB	**STATE 1021-32 O 2**	**7407**	-34.8	-25.5	-23.9	-22.7	-23.2	-22	-23.3	-6.7
GNB	**STATE 1021-32 O 2**	**7442**	-42.1	-25.9	-23.2	-20.5	-23.9	-25.7	-26	-8.2
GNB	**STATE 1021-32 O 2**	**7479**	-37.8	-28.6	-26.2	-23.8	-23.3	-24.7	-22.9	-7.6
GNB	**STATE 1021-32 O 2**	**7517**	-40.9	-24.4	-25.1	-25.7	-24.7	-24.4	-23.4	-8.8
GNB	**STATE 1021-32 O 2**	**7611**	-44.5	-26.4	-26.6	-23.7	-25.2	-22.7	-24.4	-8.6
GNB	**STATE 1021-32 O 2**	**7724**	-45.7	-26.65	-26.7	-25.7	-26.2	-24.5	-24.8	-9.1
GNB	**STATE 1021-32 O 2**	**7851**	-40.9	-27.2	-25.7	-23	-23.7	-24.6	-24.7	-10
GNB	**STATE 1021-32 O 2**	**7873**	-46.5	-28.8	-27.1	-26.5	-25.8	-26.8	-25.1	
GNB	**STATE 1021-32 O 2**	**7946**	-37	-27.8	-26.5	-24.9	-24.7			-9.5
GNB	**STATE 1021-32 O 2**	**8189**	-37.3	-18.5	-18.8					-9.4
GNB	**STATE 1021-32 O 2**	**8331**	-30.6							-13.4
GNB	**STATE 1021-32 O 2**	**8587**	-48.4	-30.6	-28.4	-28	-28.4	-26.4	-25.7	-13.1
GNB	**STATE 1021-32 O 2**	**8921**	-32.1	-23.5	-25					-8.7

Note: See figure 6.1 for well locations.

Mud gas data, Greater Natural Buttes Field - hydrogen isotope composition

Area	Well	Sample Depth	dD C1	dD C2	dD C3
GNB	NBU 921 2703AS	9171	-180	-141	-133
GNB	NBU 921 2703AS	9209	-162		
GNB	NBU 921 2703 AS	9430	-160	-143	-126
GNB	NBU 921 2703AS	9525	-174		
GNB	NBU 921 2703AS	9657	-156		
GNB	NBU 921 2703AS	10077	-167	-133	
GNB	NBU 921 2703	10178	-178		
GNB	NBU 921 2703	10298	-178		
GNB	NBU 921 2703	10416	-181		
GNB	NBU 921 2703	10533	-183		
GNB	NBU 921 2703	10984	-153		
GNB	NBU 921 2703	11105	-163		
GNB	NBU 921 2703 AS	6754	-157	-129	
GNB	NBU 921 2703 AS	7624	-177		
GNB	NBU 921 2703 AS	8077	-193		
GNB	NBU 921 2703 AS	8292	-182	-150	
GNB	STATE 1021-32 O	3570	-186	-150	-163
GNB	STATE 1021-32 O	3978	-176	-156	
GNB	STATE 1021-32 O	5307	-174	-140	-152
GNB	STATE 1021-32 O	5646	-186	-132	-139
GNB	STATE 1021-32 O	5666	-161	-133	-122
GNB	STATE 1021-32 O	5752	-160	-123	-131
GNB	STATE 1021-32 O	5786	-157	-124	-129
GNB	STATE 1021-32 O	5930	-165	-131	-132
GNB	STATE 1021-32 O	5964	-161		
GNB	STATE 1021-32 O	7017	-164	-136	-130
GNB	STATE 1021-32 O	7070	-169		
GNB	STATE 1021-32 O	7087	-170	-133	-135
GNB	STATE 1021-32 O2	6505	-160		
GNB	STATE 1021-32 O2	6964	-193		
GNB	STATE 1021-32 O 2	7180	-174		
GNB	STATE 1021-32 O 2	7335	-185		
GNB	STATE 1021-32 O 2	7407	-199		
GNB	STATE 1021-32 O 2	7442	-182		
GNB	STATE 1021-32 O 2	7479	-205	-152	
GNB	STATE 1021-32 O 2	7517	-187		
GNB	STATE 1021-32 O 2	7611	-212		
GNB	STATE 1021-32 O 2	7724	-172		
GNB	STATE 1021-32 O 2	7851	-198		
GNB	STATE 1021-32 O 2	7873	-217	-186	-204
GNB	STATE 1021-32 O 2	7946	-198		
GNB	STATE 1021-32 O 2	8189	-200		
GNB	STATE 1021-32 O 2	8331	-216	-173	-158
GNB	STATE 1021-32 O 2	8587	-218	-274	-171
GNB	STATE 1021-32 O 2	8921	-170		

Note: See figure 6.1 for well locations.

Noble gas data, Piceance Basin fields, Jonah Field, Greater Natural Buttes Field

field	Sample Name	3He	error	%	4He	error	%	20Ne	error	%
Grand Valley	G	2.71E-13	8.80E-15	3.24E+00	8.85E-06	3.98E-08	4.49E-01	1.49E-09	5.47E-11	3.68E+00
Grand Valley	B	2.77E-13	1.12E-14	4.04E+00	1.19E-05	5.24E-08	4.41E-01	5.79E-09	9.62E-11	1.66E+00
Grand Valley	F	6.13E-13	2.17E-14	3.54E+00	1.18E-05	2.09E-08	1.77E-01	3.44E-09	9.08E-11	2.64E+00
Grand Valley	KK	3.51E-13	1.14E-14	3.24E+00	7.08E-06	1.72E-08	2.43E-01	5.22E-09	1.63E-10	3.11E+00
Grand Valley	S	2.49E-13	8.93E-15	3.59E+00	7.21E-06	1.44E-08	2.00E-01	2.72E-09	1.17E-10	4.29E+00
Grand Valley	EE	2.95E-13	1.19E-14	4.03E+00	7.55E-06	1.59E-08	2.11E-01	1.66E-09	6.45E-11	3.89E+00
Grand Valley	LL	3.24E-13	2.17E-14	6.70E+00	7.79E-06	1.89E-08	2.42E-01	1.34E-09	3.40E-11	2.53E+00
Grand Valley	T	2.74E-13	1.58E-14	5.75E+00	9.87E-06	1.74E-08	1.77E-01	1.55E-09	3.66E-11	2.37E+00
Parachute	O	3.29E-13	1.07E-14	3.24E+00	8.73E-06	1.39E-08	1.59E-01	1.93E-09	7.84E-11	4.07E+00
Parachute	M	3.58E-13	1.33E-14	3.71E+00	8.39E-06	1.30E-08	1.54E-01	5.90E-09	2.27E-10	3.84E+00
Parachute	P	3.47E-13	1.31E-14	3.76E+00	9.01E-06	1.30E-08	1.44E-01	2.27E-09	7.42E-11	3.26E+00
Parachute	A	3.25E-13	1.37E-14	4.23E+00	9.93E-06	1.83E-08	1.84E-01	1.46E-09	3.76E-11	2.57E+00
Parachute	L	3.64E-13	1.77E-14	4.87E+00	8.66E-06	1.41E-08	1.62E-01	1.89E-09	4.74E-11	2.51E+00
Parachute	I	3.11E-13	1.50E-14	4.83E+00	8.73E-06	1.57E-08	1.80E-01	1.65E-09	5.25E-11	3.17E+00
Parachute	N	3.89E-13	1.83E-14	4.71E+00	9.04E-06	1.58E-08	1.75E-01	1.75E-09	5.60E-11	3.21E+00
Parachute	Q	3.89E-13	1.46E-14	3.75E+00	9.31E-06	9.62E-09	1.03E-01	1.94E-09	5.35E-11	2.75E+00
Rulison	Z	2.67E-13	9.55E-15	3.58E+00	9.78E-06	6.51E-08	6.66E-01	2.83E-09	5.01E-11	1.77E+00
Rulison	GG	2.38E-13	8.92E-15	3.75E+00	1.01E-05	1.02E-07	1.01E+00	3.15E-09	5.67E-11	1.80E+00
Rulison	Y	2.56E-13	9.92E-15	3.87E+00	1.00E-05	1.01E-07	1.01E+00	4.89E-09	6.48E-11	1.33E+00
Rulison	EE	2.80E-13	1.15E-14	4.11E+00	1.07E-05	1.07E-07	1.00E+00	3.78E-09	7.86E-11	2.08E+00
Rulison	RR	4.79E-13	1.53E-14	3.20E+00	9.37E-06	1.58E-08	1.69E-01	3.38E-09	8.15E-11	2.41E+00
Rulison	CC	4.10E-13	1.34E-14	3.28E+00	9.76E-06	2.29E-08	2.34E-01	6.01E-09	2.21E-10	3.67E+00
Rulison	RR	4.47E-13	1.58E-14	3.54E+00	9.44E-06	1.40E-08	1.49E-01	1.94E-09	6.64E-11	3.42E+00
Rulison	HH	4.15E-13	1.39E-14	3.36E+00	1.30E-05	1.75E-08	1.35E-01	8.91E-09	1.09E-10	1.22E+00
Rulison	U	3.34E-13	1.07E-14	3.22E+00	1.00E-05	2.43E-08	2.43E-01	3.29E-09	5.44E-11	1.66E+00
Rulison	V	3.69E-13	1.32E-14	3.59E+00	8.65E-06	7.69E-09	8.90E-02	2.43E-09	7.72E-11	3.18E+00
Rulison	W	4.19E-13	1.78E-14	4.24E+00	9.38E-06	1.76E-08	1.87E-01	1.96E-09	6.63E-11	3.38E+00
Rulison	X	3.47E-13	1.04E-14	3.01E+00	9.51E-06	1.89E-08	1.98E-01	3.09E-09	1.09E-10	3.52E+00
Sample Name		**3He**	**error**	**%**	**4He**	**error**	**%**	**20Ne**	**error**	**%**
Jonah	Yellow Point 21-12V	3.18E-13	1.35E-14	4.24E+00	1.37E-05	2.94E-08	2.15E-01	5.56E-09	1.57E-10	2.83E+00
Jonah	Corona 67-30	2.87E-13	1.07E-14	3.71E+00	1.42E-05	3.21E-08	2.26E-01	6.55E-09	2.38E-10	3.63E+00
Jonah	Corona 79-19	3.05E-13	1.94E-14	6.36E+00	1.59E-05	2.99E-08	1.88E-01	6.57E-09	2.55E-10	3.88E+00
Jonah	SHB 41-29	2.48E-13	9.71E-15	3.92E+00	1.31E-05	2.48E-08	1.89E-01	4.36E-09	1.71E-10	3.93E+00
Jonah	Cabrito 17-25	2.83E-13	9.13E-15	3.23E+00	1.39E-05	3.48E-08	2.50E-01	6.49E-09	7.71E-11	1.19E+00
Jonah	SHB 53-17 #2	2.67E-13	9.72E-15	3.64E+00	1.43E-05	4.26E-08	2.98E-01	5.68E-09	1.84E-10	3.24E+00
Jonah	SHB 84-9	2.71E-13	1.15E-14	4.24E+00	1.52E-05	4.29E-08	2.82E-01	4.67E-09	1.48E-10	3.17E+00
Jonah	SHB 19-5	2.59E-13	1.14E-14	4.42E+00	1.19E-05	2.02E-08	1.70E-01	7.74E-09	2.99E-10	3.86E+00
Jonah	SHB 57-15 #2	2.27E-13	9.62E-15	4.24E+00	1.14E-05	2.16E-08	1.89E-01	4.40E-09	1.79E-10	4.07E+00
Jonah	SHB 53-20V	3.08E-13	2.07E-14	6.71E+00	1.44E-05	2.24E-08	1.56E-01	5.46E-09	9.32E-11	1.71E+00
Jonah	Corona SHP 16-18	2.53E-13	8.27E-15	3.27E+00	1.29E-05	2.04E-08	1.59E-01	3.76E-09	8.40E-11	2.24E+00
Jonah	Corona 61-31V	2.38E-13	7.99E-15	3.36E+00	1.23E-05	4.51E-08	3.67E-01	4.90E-09	1.23E-10	2.51E+00
Jonah	SHB 34-28	2.58E-13	1.49E-14	5.75E+00	1.12E-05	2.20E-08	1.97E-01	3.61E-09	7.85E-11	2.17E+00
Jonah	SOL 7-36	4.33E-13	1.84E-14	4.24E+00	1.92E-05	4.05E-08	2.11E-01	8.25E-09	2.36E-10	2.86E+00
field	**Sample Name**	3He	error	%	4He	error	%	20Ne	error	%
GNB	Mulligan 822-24G	1.39E-12	4.89E-14	3.51E+00	3.81E-05	8.44E-08	2.22E-01	3.85E-09	5.02E-11	1.31E+00
GNB	NBU 920-25P	6.98E-13	2.38E-14	3.41E+00	1.07E-05	3.58E-08	3.36E-01	2.72E-09	3.32E-11	1.22E+00
GNB	Love 1121-7N	8.44E-13	3.34E-14	3.96E+00	3.36E-05	8.20E-08	2.44E-01	3.85E-09	3.00E-11	7.81E-01
GNB	NBU 1021-20	6.90E-13	2.93E-14	4.24E+00	1.06E-05	3.74E-08	3.51E-01	5.45E-10	1.23E-11	2.25E+00
GNB	NBU 553-28E	6.36E-13	2.17E-14	3.41E+00	1.94E-05	3.12E-07	1.61E+00	1.59E-09	2.18E-11	1.37E+00
GNB	Hatch 923-14C	1.33E-12	5.63E-14	4.24E+00	3.18E-05	6.39E-08	2.01E-01	3.60E-09	2.06E-11	5.71E-01
GNB	NBU 20	4.76E-13	1.53E-14	3.22E+00	8.32E-06	5.83E-09	7.01E-02	1.51E-09	1.87E-11	1.24E+00
GNB	NBU 1022-11F	3.97E-13	1.45E-14	3.64E+00	1.45E-05	1.92E-08	1.33E-01	6.78E-09	5.13E-11	7.57E-01
GNB	NBU 921 14L	5.32E-13	1.60E-14	3.01E+00	1.66E-05	1.89E-08	1.14E-01	3.33E-09	3.15E-11	9.48E-01
GNB	BC 1122-5H	1.41E-12	4.29E-14	3.04E+00	2.44E-05	5.30E-08	2.17E-01	2.40E-08	1.80E-10	7.48E-01
GNB	NBU 922-34D-3	5.75E-13	1.73E-14	3.00E+00	1.10E-05	3.05E-08	2.76E-01	1.67E-07	1.10E-09	6.59E-01
GNB	Bonanza 1023-9J	8.65E-13	3.67E-14	4.24E+00	1.00E-05	3.50E-08	3.48E-01	1.90E-09	4.19E-11	2.20E+00
GNB	NBU 1021-30I	5.43E-13	2.30E-14	4.24E+00	1.31E-05	8.44E-08	6.44E-01	2.97E-09	2.97E-11	1.00E+00
GNB	NBU 920-20P	4.69E-13	1.61E-14	3.44E+00	1.32E-05	1.72E-07	1.30E+00	7.29E-09	1.13E-10	1.55E+00
GNB	NBU 420	6.64E-13	2.28E-14	3.44E+00	2.24E-05	2.92E-07	1.30E+00	6.53E-08	7.99E-10	1.22E+00

Note: See Figure 4.3, 5.3 and 6.2 for well locations.

Noble gas data, Piceance Basin fields, Jonah Field, Greater Natural Buttes Field

field	Sample Name	22Ne	error	%	21Ne	error	%	40Ar	error	%
Grand Valley	G	1.59E-10	8.44E-12	5.31E+00	6.07E-12	5.85E-13	9.64E+00	8.50E-06	5.61E-08	6.60E-01
Grand Valley	B	5.64E-10	1.21E-11	2.14E+00	2.18E-11	9.95E-13	4.56E+00	2.34E-05	1.09E-07	4.66E-01
Grand Valley	F	2.98E-10	1.62E-11	5.45E+00	1.27E-11	1.07E-12	8.41E+00	6.83E-06	4.35E-08	6.36E-01
Grand Valley	KK	4.92E-10	1.81E-11	3.68E+00	1.59E-11	1.04E-12	6.55E+00	1.25E-05	6.46E-08	5.17E-01
Grand Valley	S	2.32E-10	2.07E-11	8.91E+00	8.88E-12	9.27E-13	1.04E+01	7.89E-06	4.38E-08	5.55E-01
Grand Valley	EE	1.32E-10	5.62E-11	4.24E+01	5.22E-12	2.24E-12	4.28E+01	7.28E-06	4.12E-08	5.66E-01
Grand Valley	LL	1.42E-10	5.40E-12	3.81E+00	5.40E-12	4.48E-13	8.30E+00	9.06E-06	4.75E-08	5.24E-01
Grand Valley	T	1.53E-10	4.69E-12	3.06E+00	6.39E-12	4.49E-13	7.04E+00	9.92E-06	4.56E-08	4.59E-01
Parachute	O	1.62E-10	6.84E-12	4.22E+00	6.37E-12	4.65E-13	7.30E+00	7.54E-06	3.98E-08	5.27E-01
Parachute	M	5.58E-10	2.37E-11	4.25E+00	1.80E-11	1.16E-12	6.46E+00	1.05E-05	4.59E-08	4.37E-01
Parachute	P	1.68E-10	1.33E-11	7.95E+00	6.39E-12	6.22E-13	9.73E+00	8.51E-06	4.60E-08	5.41E-01
Parachute	A	1.49E-10	5.48E-12	3.67E+00	6.04E-12	4.29E-13	7.10E+00	8.40E-06	4.70E-08	5.60E-01
Parachute	L	1.55E-10	5.98E-12	3.85E+00	5.90E-12	4.46E-13	7.56E+00	7.41E-06	4.59E-08	6.19E-01
Parachute	I	1.44E-10	6.02E-12	4.18E+00	5.66E-12	4.16E-13	7.35E+00	7.79E-06	4.43E-08	5.69E-01
Parachute	N	1.41E-10	4.52E-12	3.20E+00	5.37E-12	3.30E-13	6.15E+00	7.84E-06	3.90E-08	4.98E-01
Parachute	Q	1.54E-10	5.47E-12	3.54E+00	6.04E-12	4.31E-13	7.14E+00	8.29E-06	3.89E-08	4.69E-01
Rulison	Z	2.55E-10	8.49E-12	3.32E+00	9.86E-12	7.40E-13	7.51E+00	8.75E-06	4.56E-08	5.22E-01
Rulison	GG	2.76E-10	8.82E-12	3.19E+00	1.12E-11	8.36E-13	7.47E+00	8.65E-06	3.93E-08	4.54E-01
Rulison	Y	4.63E-10	1.58E-11	3.41E+00	1.64E-11	1.41E-12	8.57E+00	8.16E-06	4.94E-08	6.05E-01
Rulison	EE	3.57E-10	8.80E-12	2.46E+00	1.36E-11	1.05E-12	7.75E+00	8.01E-06	5.34E-08	6.67E-01
Rulison	RR	2.72E-10	1.04E-11	3.81E+00	1.11E-11	9.09E-13	8.21E+00	7.18E-06	4.94E-08	6.89E-01
Rulison	CC	5.57E-10	2.46E-11	4.42E+00	1.84E-11	1.23E-12	6.67E+00	1.31E-05	7.98E-08	6.11E-01
Rulison	RR	1.52E-10	4.94E-12	3.25E+00	5.86E-12	3.42E-13	5.83E+00	6.81E-06	3.95E-08	5.80E-01
Rulison	HH	8.36E-10	1.31E-11	1.56E+00	2.79E-11	1.35E-12	4.84E+00	2.27E-05	1.87E-07	8.27E-01
Rulison	U	2.63E-10	1.17E-11	4.45E+00	9.00E-12	6.00E-13	6.67E+00	1.37E-05	6.94E-08	5.08E-01
Rulison	V	1.89E-10	7.11E-12	3.76E+00	6.87E-12	4.42E-13	6.43E+00	8.37E-06	5.11E-08	6.10E-01
Rulison	W	1.33E-10	6.17E-12	4.64E+00	5.28E-12	4.38E-13	8.30E+00	7.47E-06	4.78E-08	6.40E-01
Rulison	X	2.21E-10	1.09E-11	4.92E+00	7.93E-12	5.95E-13	7.50E+00	8.91E-06	5.05E-08	5.67E-01
Sample Name		**22Ne**	**error**	**%**	**21Ne**	**error**	**%**	**40Ar**	**error**	**%**
Jonah	Yellow Point 21-12V	5.09E-10	2.20E-11	4.32E+00	1.73E-11	1.05E-12	6.07E+00	1.55E-05	6.83E-08	4.42E-01
Jonah	Corona 67-30	6.09E-10	2.54E-11	4.17E+00	2.13E-11	1.14E-12	5.35E+00	1.68E-05	9.23E-08	5.49E-01
Jonah	Corona 79-19	6.07E-10	3.54E-11	5.83E+00	2.11E-11	1.42E-12	6.72E+00	1.75E-05	8.79E-08	5.02E-01
Jonah	SHB 41-29	3.85E-10	1.32E-11	3.43E+00	1.42E-11	8.32E-13	5.84E+00	1.31E-05	6.07E-08	4.64E-01
Jonah	Cabrito 17-25	5.83E-10	1.68E-11	2.88E+00	1.94E-11	1.07E-12	5.50E+00	1.94E-05	9.31E-08	4.81E-01
Jonah	SHB 53-17 #2	4.79E-10	2.17E-11	4.54E+00	1.74E-11	1.15E-12	6.64E+00	1.70E-05	8.97E-08	5.28E-01
Jonah	SHB 84-9	3.97E-10	1.35E-11	3.40E+00	1.44E-11	7.20E-13	5.00E+00	1.49E-05	6.56E-08	4.42E-01
Jonah	SHB 19-5	7.44E-10	2.84E-11	3.81E+00	2.52E-11	1.28E-12	5.09E+00	1.99E-05	1.12E-07	5.61E-01
Jonah	SHB 57-15 #2	3.97E-10	2.23E-11	5.63E+00	1.45E-11	9.88E-13	6.81E+00	1.23E-05	5.64E-08	4.60E-01
Jonah	SHB 53-20V	5.12E-10	1.79E-11	3.51E+00	1.85E-11	1.04E-12	5.62E+00	1.84E-05	9.64E-08	5.23E-01
Jonah	Corona SHP 16-18	3.39E-10	1.10E-11	3.25E+00	1.21E-11	5.44E-13	4.51E+00	1.34E-05	5.85E-08	4.35E-01
Jonah	Corona 61-31V	4.41E-10	1.96E-11	4.43E+00	1.57E-11	1.01E-12	6.45E+00	1.61E-05	7.10E-08	4.41E-01
Jonah	SHB 34-28	3.08E-10	1.39E-11	4.51E+00	1.09E-11	7.66E-13	7.04E+00	1.51E-05	6.74E-08	4.48E-01
Jonah	SOL 7-36	7.78E-10	2.53E-11	3.25E+00	2.71E-11	1.38E-12	5.10E+00	2.08E-05	1.13E-07	5.41E-01
field	**Sample Name**	22Ne	error	%	21Ne	error	%	40Ar	error	%
GNB	Mulligan 822-24G	3.50E-10	1.14E-11	3.26E+00	1.85E-11	6.63E-13	3.58E+00	2.54E-05	1.02E-07	4.03E-01
GNB	NBU 920-25P	2.63E-10	7.35E-12	2.79E+00	7.31E-12	3.90E-13	5.33E+00	1.49E-05	9.20E-08	6.17E-01
GNB	Love 1121-7N	3.69E-10	9.87E-12	2.67E+00	1.87E-11	5.58E-13	2.98E+00	1.91E-05	5.31E-08	2.78E-01
GNB	NBU 1021-20	4.75E-10	3.90E-12	8.20E-01	1.46E-11	2.90E-13	1.99E+00	NM	NM	NM
GNB	NBU 553-28E	1.62E-10	6.05E-12	3.74E+00	7.82E-12	3.11E-13	3.98E+00	1.07E-05	3.76E-08	3.52E-01
GNB	Hatch 923-14C	3.70E-10	1.30E-11	3.53E+00	1.68E-11	5.25E-13	3.13E+00	2.13E-05	1.36E-07	6.38E-01
GNB	NBU 20	1.43E-10	4.34E-12	3.03E+00	6.23E-12	2.35E-13	3.78E+00	8.64E-06	4.04E-08	4.67E-01
GNB	NBU 1022-11F	6.91E-10	2.41E-11	3.49E+00	2.77E-11	9.37E-13	3.39E+00	1.56E-05	5.30E-08	3.39E-01
GNB	NBU 921 14L	3.24E-10	1.20E-11	3.70E+00	1.28E-11	4.43E-13	3.46E+00	1.80E-05	5.77E-08	3.20E-01
GNB	BC 1122-5H	2.13E-09	2.88E-11	1.35E+00	7.65E-11	2.26E-12	2.95E+00	3.32E-05	1.19E-07	3.59E-01
GNB	NBU 922-34D-3	1.55E-08	5.63E-10	3.65E+00	4.40E-10	1.80E-11	4.09E+00	1.03E-04	2.98E-07	2.88E-01
GNB	Bonanza 1023-9J	1.74E-10	5.43E-12	3.12E+00	6.18E-12	2.50E-13	4.05E+00	9.83E-06	4.45E-08	4.52E-01
GNB	NBU 1021-30I	2.54E-10	9.84E-12	3.88E+00	9.25E-12	1.39E-13	1.50E+00	1.09E-05	4.63E-08	4.25E-01
GNB	NBU 920-20P	6.52E-10	1.80E-11	2.76E+00	2.06E-11	6.39E-13	3.11E+00	1.66E-05	1.12E-07	6.76E-01
GNB	NBU 420	6.38E-09	7.40E-11	1.16E+00	1.86E-10	5.01E-12	2.69E+00	4.48E-05	2.26E-07	5.05E-01

Note: See Figure 4.3, 5.3 and 6.2 for well locations.

Noble gas data, Piceance Basin fields, Jonah Field, Greater Natural Buttes Field

field	Sample Name	36Ar	Error	%	38Ar	error	%	84Kr	Error	%
Grand Valley	G	1.49E-08	1.48E-10	9.95E-01	2.70E-09	3.60E-11	1.34E+00	7.80E-10	9.44E-12	1.21E+00
Grand Valley	B	2.67E-08	2.17E-10	8.14E-01	4.87E-09	4.70E-11	9.66E-01	1.03E-09	3.62E-12	3.53E-01
Grand Valley	F	1.11E-08	7.79E-11	7.04E-01	1.96E-09	2.73E-11	1.39E+00	4.64E-10	4.70E-12	1.01E+00
Grand Valley	KK	3.70E-08	2.55E-10	6.91E-01	6.50E-09	5.78E-11	8.89E-01	8.87E-10	1.30E-11	1.47E+00
Grand Valley	S	1.76E-08	1.07E-10	6.13E-01	3.13E-09	1.79E-11	5.70E-01	8.20E-10	1.90E-11	2.31E+00
Grand Valley	EE	1.41E-08	1.08E-10	7.71E-01	2.53E-09	2.73E-11	1.08E+00	7.24E-10	1.60E-11	2.22E+00
Grand Valley	LL	2.34E-08	2.32E-10	9.90E-01	4.27E-09	4.47E-11	1.05E+00	6.84E-10	1.62E-11	2.37E+00
Grand Valley	T	1.56E-08	1.30E-10	8.30E-01	2.83E-09	3.87E-11	1.37E+00	7.81E-10	9.96E-12	1.28E+00
Parachute	O	1.47E-08	9.35E-11	6.37E-01	2.65E-09	2.33E-11	8.79E-01	7.46E-10	7.40E-12	9.93E-01
Parachute	M	2.52E-08	2.42E-10	9.61E-01	4.55E-09	2.99E-11	6.57E-01	1.10E-09	2.36E-11	2.14E+00
Parachute	P	1.71E-08	1.06E-10	6.24E-01	3.05E-09	2.81E-11	9.23E-01	8.72E-10	1.02E-11	1.17E+00
Parachute	A	1.48E-08	5.80E-11	3.93E-01	2.66E-09	3.61E-11	1.36E+00	7.41E-10	2.15E-11	2.91E+00
Parachute	L	1.50E-08	8.73E-11	5.82E-01	2.80E-09	7.15E-11	2.55E+00	7.36E-10	8.08E-12	1.10E+00
Parachute	I	1.52E-08	8.80E-11	5.78E-01	2.69E-09	2.59E-11	9.63E-01	7.64E-10	7.46E-12	9.76E-01
Parachute	N	1.53E-08	5.20E-11	3.40E-01	2.75E-09	3.27E-11	1.19E+00	7.91E-10	9.45E-12	1.20E+00
Parachute	Q	1.59E-08	7.79E-11	4.90E-01	2.83E-09	1.83E-11	6.47E-01	8.11E-10	9.61E-12	1.18E+00
Rulison	Z	1.66E-08	1.38E-10	8.33E-01	2.94E-09	3.33E-11	1.13E+00	8.75E-10	1.09E-11	1.25E+00
Rulison	GG	1.67E-08	1.73E-10	1.04E+00	3.06E-09	2.96E-11	9.67E-01	9.10E-10	4.19E-12	4.61E-01
Rulison	Y	1.74E-08	8.60E-11	4.94E-01	3.04E-09	6.38E-11	2.10E+00	8.53E-10	2.14E-12	2.51E-01
Rulison	EE	1.69E-08	1.24E-10	7.35E-01	3.02E-09	5.50E-11	1.82E+00	8.46E-10	3.11E-12	3.67E-01
Rulison	RR	1.40E-08	1.14E-10	8.10E-01	2.52E-09	3.09E-11	1.23E+00	6.05E-10	1.39E-11	2.31E+00
Rulison	CC	2.74E-08	1.57E-10	5.73E-01	4.88E-09	4.40E-11	9.01E-01	1.27E-09	2.86E-11	2.26E+00
Rulison	RR	1.29E-08	6.57E-11	5.10E-01	2.27E-09	2.63E-11	1.16E+00	5.74E-10	6.69E-12	1.17E+00
Rulison	HH	4.35E-08	2.16E-10	4.97E-01	7.87E-09	9.44E-11	1.20E+00	2.15E-09	3.36E-11	1.57E+00
Rulison	U	2.63E-08	1.36E-10	5.16E-01	4.73E-09	3.77E-11	7.98E-01	1.23E-09	1.73E-11	1.41E+00
Rulison	V	1.82E-08	9.55E-11	5.23E-01	3.30E-09	2.47E-11	7.49E-01	9.08E-10	3.96E-12	4.36E-01
Rulison	W	1.49E-08	7.26E-11	4.88E-01	2.60E-09	2.44E-11	9.42E-01	7.48E-10	1.11E-11	1.49E+00
Rulison	X	2.01E-08	1.11E-10	5.51E-01	3.62E-09	4.43E-11	1.22E+00	9.79E-10	1.12E-11	1.14E+00
Sample Name		**36Ar**	**Error**	**%**	**38Ar**	**error**	**%**	**84Kr**	**Error**	**%**
Jonah	Yellow Point 21-12V	2.83E-08	1.65E-10	5.83E-01	5.03E-09	2.61E-11	5.19E-01	1.46E-09	1.24E-11	8.50E-01
Jonah	Corona 67-30	3.08E-08	1.21E-10	3.93E-01	5.62E-09	7.11E-11	1.27E+00	1.48E-09	3.45E-11	2.33E+00
Jonah	Corona 79-19	3.01E-08	1.66E-10	5.50E-01	5.56E-09	8.13E-11	1.46E+00	1.52E-09	1.96E-11	1.29E+00
Jonah	SHB 41-29	2.47E-08	1.94E-10	7.87E-01	4.45E-09	2.15E-11	4.84E-01	1.37E-09	1.74E-11	1.27E+00
Jonah	Cabrito 17-25	3.79E-08	2.26E-10	5.95E-01	6.97E-09	6.63E-11	9.51E-01	1.87E-09	3.54E-11	1.89E+00
Jonah	SHB 53-17 #2	2.95E-08	1.29E-10	4.38E-01	5.35E-09	5.05E-11	9.45E-01	1.51E-09	2.24E-11	1.49E+00
Jonah	SHB 84-9	2.55E-08	2.47E-10	9.70E-01	4.58E-09	5.99E-11	1.31E+00	1.35E-09	1.40E-11	1.03E+00
Jonah	SHB 19-5	3.67E-08	2.67E-10	7.26E-01	6.65E-09	6.02E-11	9.06E-01	1.75E-09	2.99E-11	1.71E+00
Jonah	SHB 57-15 #2	2.37E-08	1.57E-10	6.63E-01	4.27E-09	3.69E-11	8.64E-01	1.26E-09	4.78E-12	3.78E-01
Jonah	SHB 53-20V	3.11E-08	4.38E-10	1.41E+00	5.64E-09	5.32E-11	9.43E-01	1.43E-09	2.68E-11	1.88E+00
Jonah	Corona SHP 16-18	2.32E-08	8.64E-11	3.72E-01	4.17E-09	4.70E-11	1.13E+00	1.17E-09	1.70E-11	1.45E+00
Jonah	Corona 61-31V	3.05E-08	2.30E-10	7.55E-01	5.50E-09	5.74E-11	1.04E+00	1.72E-09	1.27E-11	7.38E-01
Jonah	SHB 34-28	3.43E-08	2.51E-10	7.30E-01	6.19E-09	5.40E-11	8.72E-01	1.15E-09	1.03E-11	9.00E-01
Jonah	SOL 7-36	3.79E-08	2.02E-10	5.34E-01	6.76E-09	2.82E-11	4.18E-01	1.68E-09	2.85E-11	1.70E+00
field	**Sample Name**	36Ar	Error	%	38Ar	error	%	84KrC	Error	%
GNB	Mulligan 822-24G	2.97E-08	2.24E-10	7.54E-01	5.20E-09	1.77E-10	3.41E+00	1.27E-09	5.24E-11	4.14E+00
GNB	NBU 920-25P	2.43E-08	3.73E-10	1.54E+00	4.19E-09	1.93E-10	4.60E+00	1.16E-09	2.15E-11	1.86E+00
GNB	Love 1121-7N	2.69E-08	1.80E-10	6.70E-01	4.79E-09	4.29E-11	8.97E-01	1.25E-09	2.71E-11	2.16E+00
GNB	NBU 1021-20	NM	NM	NM	NM	NM	NM	NM	NM	NM
GNB	NBU 553-28E	1.68E-08	4.18E-10	2.48E+00	2.99E-09	1.05E-10	3.52E+00	7.70E-10	2.26E-11	2.94E+00
GNB	Hatch 923-14C	2.84E-08	7.00E-10	2.47E+00	4.93E-09	1.76E-10	3.58E+00	1.29E-09	3.23E-11	2.51E+00
GNB	NBU 20	1.43E-08	3.05E-10	2.13E+00	2.73E-09	1.05E-10	3.86E+00	6.96E-10	1.14E-11	1.63E+00
GNB	NBU 1022-11F	2.59E-08	4.90E-10	1.89E+00	4.74E-09	5.52E-11	1.16E+00	1.03E-09	2.34E-11	2.27E+00
GNB	NBU 921 14L	2.40E-08	2.49E-10	1.04E+00	4.43E-09	2.08E-10	4.70E+00	1.16E-09	1.01E-11	8.77E-01
GNB	BC 1122-5H	1.06E-07	1.21E-09	1.15E+00	1.95E-08	2.21E-10	1.13E+00	3.92E-09	3.95E-11	1.01E+00
GNB	NBU 922-34D-3	3.43E-07	2.98E-09	8.70E-01	6.25E-08	1.15E-09	1.84E+00	6.77E-09	5.94E-11	8.78E-01
GNB	Bonanza 1023-9J	1.77E-08	1.34E-10	7.58E-01	3.04E-09	6.61E-11	2.17E+00	1.01E-09	5.63E-11	5.58E+00
GNB	NBU 1021-30I	1.88E-08	1.27E-10	6.75E-01	3.30E-09	4.08E-11	1.24E+00	9.34E-10	5.33E-11	5.71E+00
GNB	NBU 920-20P	2.89E-08	2.58E-10	8.93E-01	5.24E-09	7.97E-11	1.52E+00	1.16E-09	1.72E-11	1.48E+00
GNB	NBU 420	1.39E-07	1.58E-09	1.14E+00	2.58E-08	3.06E-10	1.19E+00	3.19E-09	4.62E-11	1.45E+00

Note: See Figure 4.3, 5.3 and 6.2 for well locations.

Noble gas data, Piceance Basin fields, Jonah Field, Greater Natural Buttes Field

field	Sample Name	129XeC	Error	%	132XeC	error	%	134XeC	Error	%
GNB	Mulligan 822-24G	9.81E-11	5.43E-12	5.53E+00	1.01E-10	3.65E-12	3.63E+00	3.90E-11	1.02E-13	3.48E+00
GNB	NBU 920-25P	7.29E-11	5.11E-12	7.01E+00	7.33E-11	2.85E-12	3.89E+00	2.85E-11	9.29E-14	3.06E+00
GNB	Love 1121-7N	9.72E-11	4.08E-12	4.20E+00	9.77E-11	3.42E-12	3.50E+00	3.83E-11	7.14E-14	3.07E+00
GNB	NBU 1021-20	NM	NM	NM	NM	NM	NM	NM	NM	NM
GNB	NBU 553-28E	5.33E-11	3.35E-12	6.28E+00	5.32E-11	2.06E-12	3.88E+00	2.06E-11	6.09E-14	3.49E+00
GNB	Hatch 923-14C	9.57E-11	4.45E-12	4.66E+00	9.51E-11	3.22E-12	3.39E+00	3.65E-11	7.21E-14	3.19E+00
GNB	NBU 20	4.90E-11	3.34E-12	6.81E+00	4.77E-11	1.67E-12	3.50E+00	1.85E-11	5.58E-14	3.25E+00
GNB	NBU 1022-11F	7.08E-11	4.00E-12	5.65E+00	7.34E-11	2.58E-12	3.51E+00	2.81E-11	7.36E-14	3.49E+00
GNB	NBU 921 14L	8.33E-11	4.06E-12	4.88E+00	8.61E-11	2.72E-12	3.16E+00	3.28E-11	7.45E-14	3.87E+00
GNB	BC 1122-5H	2.26E-10	9.45E-12	4.18E+00	2.29E-10	8.41E-12	3.67E+00	8.87E-11	2.09E-13	4.85E+00
GNB	NBU 922-34D-3	1.50E-10	6.19E-12	4.13E+00	1.52E-10	5.26E-12	3.46E+00	5.93E-11	1.14E-13	4.38E+00
GNB	Bonanza 1023-9J	6.26E-11	4.49E-12	7.18E+00	6.46E-11	2.34E-12	3.63E+00	2.46E-11	7.85E-14	3.68E+00
GNB	NBU 1021-30I	5.84E-11	4.64E-12	7.94E+00	5.89E-11	1.77E-12	3.01E+00	2.21E-11	6.93E-14	3.36E+00
GNB	NBU 920-20P	7.54E-11	4.63E-12	6.14E+00	7.68E-11	2.58E-12	3.36E+00	3.00E-11	8.40E-14	3.66E+00
GNB	NBU 420	1.01E-10	5.13E-12	5.09E+00	1.02E-10	3.31E-12	3.24E+00	4.02E-11	7.68E-14	3.12E+00

Note: See Figure 4.3, 5.3 and 6.2 for well locations.

Noble gas ratios, Piceance Basin fields, Jonah Field, Greater Natural Buttes Field

field	Sample Name	3He/4He	error	%	3He/4He (R/	Error	%	1/4He	1/22Ne
Grand Valle	G	3.06E-08	1.00E-09	3.27E+00	2.19E-02	7.17E-04	3.27E+00	1.13E+05	6.30E+09
Grand Valle	B	2.34E-08	9.49E-10	4.06E+00	1.67E-02	6.78E-04	4.06E+00	8.42E+04	1.77E+09
Grand Valle	F	5.20E-08	1.84E-09	3.54E+00	3.71E-02	1.31E-03	3.54E+00	8.47E+04	3.36E+09
Grand Valle	KK	4.96E-08	1.61E-09	3.25E+00	3.54E-02	1.15E-03	3.25E+00	1.41E+05	2.03E+09
Grand Valle	S	3.46E-08	1.24E-09	3.59E+00	2.47E-02	8.87E-04	3.59E+00	1.39E+05	4.30E+09
Grand Valle	EE	3.91E-08	1.58E-09	4.04E+00	2.79E-02	1.13E-03	4.04E+00	1.32E+05	7.55E+09
Grand Valle	LL	4.16E-08	2.79E-09	6.70E+00	2.97E-02	1.99E-03	6.70E+00	1.28E+05	7.05E+09
Grand Valle	T	2.78E-08	1.60E-09	5.75E+00	1.99E-02	1.14E-03	5.75E+00	1.01E+05	6.53E+09
Parachute	O	3.77E-08	1.22E-09	3.25E+00	2.69E-02	8.75E-04	3.25E+00	1.15E+05	6.17E+09
Parachute	M	4.27E-08	1.58E-09	3.71E+00	3.05E-02	1.13E-03	3.71E+00	1.19E+05	1.79E+09
Parachute	P	3.85E-08	1.45E-09	3.76E+00	2.75E-02	1.04E-03	3.76E+00	1.11E+05	5.96E+09
Parachute	A	3.27E-08	1.39E-09	4.23E+00	2.34E-02	9.90E-04	4.23E+00	1.01E+05	6.70E+09
Parachute	L	4.20E-08	2.05E-09	4.87E+00	3.00E-02	1.46E-03	4.87E+00	1.15E+05	6.45E+09
Parachute	I	3.56E-08	1.72E-09	4.83E+00	2.55E-02	1.23E-03	4.83E+00	1.15E+05	6.93E+09
Parachute	N	4.30E-08	2.03E-09	4.72E+00	3.07E-02	1.45E-03	4.72E+00	1.11E+05	7.10E+09
Parachute	Q	4.18E-08	1.57E-09	3.75E+00	2.99E-02	1.12E-03	3.75E+00	1.07E+05	6.48E+09
Rulison	Z	2.73E-08	9.93E-10	3.64E+00	1.95E-02	7.09E-04	3.64E+00	1.02E+05	3.92E+09
Rulison	GG	2.35E-08	9.12E-10	3.88E+00	1.68E-02	6.52E-04	3.88E+00	9.88E+04	3.62E+09
Rulison	Y	2.56E-08	1.02E-09	4.00E+00	1.83E-02	7.32E-04	4.00E+00	9.99E+04	2.16E+09
Rulison	EE	2.63E-08	1.11E-09	4.23E+00	1.88E-02	7.95E-04	4.23E+00	9.38E+04	2.80E+09
Rulison	RR	5.11E-08	1.64E-09	3.20E+00	3.65E-02	1.17E-03	3.20E+00	1.07E+05	3.67E+09
Rulison	CC	4.20E-08	1.38E-09	3.29E+00	3.00E-02	9.87E-04	3.29E+00	1.02E+05	1.79E+09
Rulison	RR	4.73E-08	1.68E-09	3.54E+00	3.38E-02	1.20E-03	3.54E+00	1.06E+05	6.58E+09
Rulison	HH	3.19E-08	1.07E-09	3.37E+00	2.28E-02	7.66E-04	3.37E+00	7.69E+04	1.20E+09
Rulison	U	3.33E-08	1.08E-09	3.23E+00	2.38E-02	7.69E-04	3.23E+00	9.98E+04	3.80E+09
Rulison	V	4.27E-08	1.53E-09	3.59E+00	3.05E-02	1.09E-03	3.59E+00	1.16E+05	5.29E+09
Rulison	W	4.47E-08	1.90E-09	4.25E+00	3.19E-02	1.35E-03	4.25E+00	1.07E+05	7.53E+09
Rulison	X	3.65E-08	1.10E-09	3.01E+00	2.61E-02	7.86E-04	3.01E+00	1.05E+05	4.52E+09
Sample Name		**3He/4He**	**error**	**%**	**3He/4He (R/**	**Error**	**%**	**1/4He**	
Jonah	Yellow Point 21-12V	2.33E-08	9.88E-10	4.25E+00	1.66E-02	7.06E-04	4.25E+00	7.32E+04	1.97E+09
Jonah	Corona 67-30	2.02E-08	7.49E-10	3.71E+00	1.44E-02	5.35E-04	3.71E+00	7.02E+04	1.64E+09
Jonah	Corona 79-19	1.92E-08	1.22E-09	6.36E+00	1.37E-02	8.73E-04	6.36E+00	6.31E+04	1.65E+09
Jonah	SHB 41-29	1.89E-08	7.42E-10	3.93E+00	1.35E-02	5.30E-04	3.93E+00	7.63E+04	2.60E+09
Jonah	Cabrito 17-25	2.03E-08	6.58E-10	3.24E+00	1.45E-02	4.70E-04	3.24E+00	7.18E+04	1.71E+09
Jonah	SHB 53-17 #2	1.87E-08	6.83E-10	3.65E+00	1.34E-02	4.88E-04	3.65E+00	7.00E+04	2.09E+09
Jonah	SHB 84-9	1.78E-08	7.56E-10	4.25E+00	1.27E-02	5.40E-04	4.25E+00	6.57E+04	2.52E+09
Jonah	SHB 19-5	2.18E-08	9.65E-10	4.42E+00	1.56E-02	6.89E-04	4.42E+00	8.42E+04	1.34E+09
Jonah	SHB 57-15 #2	1.99E-08	8.44E-10	4.25E+00	1.42E-02	6.03E-04	4.25E+00	8.76E+04	2.52E+09
Jonah	SHB 53-20V	2.14E-08	1.44E-09	6.71E+00	1.53E-02	1.03E-03	6.71E+00	6.95E+04	1.95E+09
Jonah	Corona SHP 16-18	1.97E-08	6.44E-10	3.27E+00	1.41E-02	4.60E-04	3.27E+00	7.78E+04	2.95E+09
Jonah	Corona 61-31V	1.94E-08	6.55E-10	3.38E+00	1.39E-02	4.68E-04	3.38E+00	8.15E+04	2.27E+09
Jonah	SHB 34-28	2.31E-08	1.33E-09	5.75E+00	1.65E-02	9.49E-04	5.75E+00	8.94E+04	3.25E+09
Jonah	SOL 7-36	2.26E-08	9.60E-10	4.25E+00	1.62E-02	6.86E-04	4.25E+00	5.22E+04	1.29E+09
field	**Sample Name**	3He/4He	error	%	3He/4He (R/I	Error	%	1/4He	1/22Ne
GNB	Mulligan 822-24G	3.66E-08	1.29E-09	3.52E+00	2.61E-02	9.20E-04	3.52E+00	2.63E+04	2.86E+09
GNB	NBU 920-25P	6.55E-08	2.24E-09	3.43E+00	4.68E-02	1.60E-03	3.43E+00	9.37E+04	3.80E+09
GNB	Love 1121-7N	2.51E-08	9.97E-10	3.97E+00	1.79E-02	7.12E-04	3.97E+00	2.98E+04	2.71E+09
GNB	NBU 1021-20	6.48E-08	2.76E-09	4.26E+00	4.63E-02	1.97E-03	4.26E+00	9.39E+04	2.10E+09
GNB	NBU 553-28E	3.28E-08	1.24E-09	3.77E+00	2.35E-02	8.84E-04	3.77E+00	5.17E+04	6.19E+09
GNB	Hatch 923-14C	4.18E-08	1.77E-09	4.25E+00	2.98E-02	1.27E-03	4.25E+00	3.15E+04	2.70E+09
GNB	NBU 20	5.73E-08	1.84E-09	3.22E+00	4.09E-02	1.32E-03	3.22E+00	1.20E+05	6.99E+09
GNB	NBU 1022-11F	2.74E-08	9.97E-10	3.64E+00	1.96E-02	7.12E-04	3.64E+00	6.89E+04	1.45E+09
GNB	NBU 921 14L	3.21E-08	9.66E-10	3.01E+00	2.29E-02	6.90E-04	3.01E+00	6.02E+04	3.09E+09
GNB	BC 1122-5H	5.80E-08	1.77E-09	3.05E+00	4.14E-02	1.26E-03	3.05E+00	4.10E+04	4.68E+08
GNB	NBU 922-34D-3	5.21E-08	1.57E-09	3.01E+00	3.72E-02	1.12E-03	3.01E+00	9.07E+04	6.47E+07
GNB	Bonanza 1023-9J	8.62E-08	3.67E-09	4.26E+00	6.16E-02	2.62E-03	4.26E+00	9.97E+04	5.74E+09
GNB	NBU 1021-30I	4.14E-08	1.78E-09	4.29E+00	2.96E-02	1.27E-03	4.29E+00	7.63E+04	3.94E+09
GNB	NBU 920-20P	3.55E-08	1.30E-09	3.67E+00	2.53E-02	9.30E-04	3.67E+00	7.56E+04	1.53E+09
GNB	NBU 420	2.97E-08	1.09E-09	3.68E+00	2.12E-02	7.80E-04	3.68E+00	4.47E+04	1.57E+08

Note: See Figure 4.3, 5.3 and 6.2 for well locations.

Noble gas ratios, Piceance Basin fields, Jonah Field, Greater Natural Buttes Field

field	Sample Name	20Ne/22Ne	errorR/Ra	%	21Ne/22Ne	error	%	1/36Ar	40Ar/36Ar	error	%
Grand Valley	G	9.37E+00	6.05E-01	6.46E+00	3.82E-02	3.07E-03	8.04E+00	6.72E+07	5.71E+02	6.82E+00	1.19E+00
Grand Valley	B	1.03E+01	2.78E-01	2.71E+00	3.86E-02	1.56E-03	4.03E+00	3.74E+07	8.75E+02	8.21E+00	9.38E-01
Grand Valley	F	1.16E+01	7.00E-01	6.06E+00	4.27E-02	2.73E-03	6.40E+00	9.04E+07	6.18E+02	5.86E+00	9.49E-01
Grand Valley	KK	1.06E+01	5.12E-01	4.82E+00	3.23E-02	1.75E-03	5.42E+00	2.70E+07	3.38E+02	2.92E+00	8.63E-01
Grand Valley	S	1.17E+01	1.16E+00	9.89E+00	3.82E-02	2.07E-03	5.43E+00	5.70E+07	4.50E+02	3.72E+00	8.27E-01
Grand Valley	EE	1.25E+01	5.32E+00	4.26E+01	3.94E-02	2.24E-03	5.69E+00	7.11E+07	5.18E+02	4.95E+00	9.56E-01
Grand Valley	LL	9.46E+00	4.33E-01	4.57E+00	3.81E-02	2.81E-03	7.38E+00	4.27E+07	3.87E+02	4.33E+00	1.12E+00
Grand Valley	T	1.01E+01	3.91E-01	3.87E+00	4.17E-02	2.64E-03	6.33E+00	6.39E+07	6.34E+02	6.01E+00	9.48E-01
Parachute	O	1.19E+01	6.98E-01	5.86E+00	3.93E-02	2.34E-03	5.95E+00	6.82E+07	5.14E+02	4.25E+00	8.27E-01
Parachute	M	1.06E+01	6.06E-01	5.73E+00	3.22E-02	1.57E-03	4.87E+00	3.97E+07	4.16E+02	4.40E+00	1.06E+00
Parachute	P	1.36E+01	1.16E+00	8.59E+00	3.81E-02	2.14E-03	5.61E+00	5.86E+07	4.99E+02	4.12E+00	8.26E-01
Parachute	A	9.80E+00	4.39E-01	4.48E+00	4.05E-02	2.46E-03	6.08E+00	6.78E+07	5.69E+02	3.90E+00	6.84E-01
Parachute	L	1.22E+01	5.60E-01	4.60E+00	3.81E-02	2.47E-03	6.50E+00	6.67E+07	4.95E+02	4.21E+00	8.50E-01
Parachute	I	1.15E+01	6.01E-01	5.24E+00	3.92E-02	2.37E-03	6.05E+00	6.57E+07	5.12E+02	4.15E+00	8.12E-01
Parachute	N	1.24E+01	5.62E-01	4.53E+00	3.81E-02	2.00E-03	5.25E+00	6.54E+07	5.13E+02	3.09E+00	6.03E-01
Parachute	Q	1.26E+01	5.65E-01	4.49E+00	3.92E-02	2.43E-03	6.20E+00	6.29E+07	5.21E+02	3.53E+00	6.78E-01
Rulison	Z	1.11E+01	4.17E-01	3.77E+00	3.86E-02	2.60E-03	6.73E+00	6.04E+07	5.29E+02	5.20E+00	9.83E-01
Rulison	GG	1.14E+01	4.18E-01	3.67E+00	4.06E-02	2.74E-03	6.75E+00	6.00E+07	5.19E+02	5.89E+00	1.13E+00
Rulison	Y	1.06E+01	3.86E-01	3.65E+00	3.55E-02	2.79E-03	7.86E+00	5.74E+07	4.68E+02	3.66E+00	7.81E-01
Rulison	EE	1.06E+01	3.41E-01	3.22E+00	3.81E-02	2.80E-03	7.34E+00	5.91E+07	4.74E+02	4.70E+00	9.92E-01
Rulison	RR	1.24E+01	5.60E-01	4.51E+00	4.07E-02	2.95E-03	7.27E+00	7.14E+07	5.12E+02	5.45E+00	1.06E+00
Rulison	CC	1.08E+01	6.20E-01	5.75E+00	3.30E-02	1.65E-03	4.99E+00	3.65E+07	4.76E+02	3.99E+00	8.37E-01
Rulison	RR	1.28E+01	6.04E-01	4.72E+00	3.86E-02	1.87E-03	4.83E+00	7.77E+07	5.29E+02	4.09E+00	7.72E-01
Rulison	HH	1.07E+01	2.12E-01	1.98E+00	3.33E-02	1.53E-03	4.58E+00	2.30E+07	5.21E+02	5.03E+00	9.65E-01
Rulison	U	1.25E+01	5.92E-01	4.75E+00	3.42E-02	1.69E-03	4.96E+00	3.80E+07	5.18E+02	3.75E+00	7.24E-01
Rulison	V	1.28E+01	6.33E-01	4.93E+00	3.64E-02	1.90E-03	5.21E+00	5.48E+07	4.59E+02	3.69E+00	8.04E-01
Rulison	W	1.48E+01	8.48E-01	5.74E+00	3.98E-02	2.74E-03	6.88E+00	6.72E+07	5.02E+02	4.04E+00	8.05E-01
Rulison	X	1.40E+01	8.45E-01	6.05E+00	3.58E-02	2.03E-03	5.66E+00	4.98E+07	4.43E+02	3.51E+00	7.91E-01
Sample Name		**20Ne/22Ne**		**%**	**21Ne/22Ne**	**error**	**%**		**40Ar/36Ar**	**error**	**%**
Jonah	Yellow Point 21-12V	1.09E+01		5.17E+00	3.41E-02	1.45E-03	4.26E+00	3.54E+07	5.47E+02	4.00E+00	7.32E-01
Jonah	Corona 67-30	1.08E+01		5.53E+00	3.50E-02	1.17E-03	3.36E+00	3.25E+07	5.47E+02	3.69E+00	6.75E-01
Jonah	Corona 79-19	1.08E+01		7.00E+00	3.48E-02	1.17E-03	3.35E+00	3.32E+07	5.81E+02	4.33E+00	7.45E-01
Jonah	SHB 41-29	1.13E+01		5.21E+00	3.71E-02	1.75E-03	4.73E+00	4.06E+07	5.31E+02	4.85E+00	9.13E-01
Jonah	Cabrito 17-25	1.11E+01		3.11E+00	3.33E-02	1.56E-03	4.69E+00	2.64E+07	5.11E+02	3.91E+00	7.65E-01
Jonah	SHB 53-17 #2	1.19E+01		5.58E+00	3.63E-02	1.76E-03	4.84E+00	3.40E+07	5.77E+02	3.96E+00	6.86E-01
Jonah	SHB 84-9	1.18E+01		4.65E+00	3.63E-02	1.33E-03	3.66E+00	3.92E+07	5.82E+02	6.21E+00	1.07E+00
Jonah	SHB 19-5	1.04E+01		5.43E+00	3.38E-02	1.14E-03	3.38E+00	2.72E+07	5.43E+02	4.98E+00	9.17E-01
Jonah	SHB 57-15 #2	1.11E+01		6.95E+00	3.66E-02	1.40E-03	3.82E+00	4.22E+07	5.17E+02	4.17E+00	8.07E-01
Jonah	SHB 53-20V	1.07E+01		3.90E+00	3.61E-02	1.58E-03	4.39E+00	3.21E+07	5.91E+02	8.88E+00	1.50E+00
Jonah	Corona SHP 16-18	1.11E+01		3.95E+00	3.56E-02	1.11E-03	3.13E+00	4.30E+07	5.79E+02	3.31E+00	5.72E-01
Jonah	Corona 61-31V	1.11E+01		5.09E+00	3.57E-02	1.67E-03	4.68E+00	3.27E+07	5.27E+02	4.60E+00	8.74E-01
Jonah	SHB 34-28	1.17E+01		5.00E+00	3.54E-02	1.91E-03	5.41E+00	2.91E+07	4.39E+02	3.76E+00	8.56E-01
Jonah	SOL 7-36	1.06E+01		4.33E+00	3.48E-02	1.37E-03	3.93E+00	2.64E+07	5.49E+02	4.18E+00	7.60E-01
field	**Sample Name**	20Ne/22Ne		%	21Ne/22Ne	error	%		40Ar/36Ar	error	%
GNB	Mulligan 822-24G	1.10E+01		3.51E+00	5.30E-02	2.56E-03	4.84E+00	3.37E+07	8.56E+02	7.31E+00	8.55E-01
GNB	NBU 920-25P	1.03E+01		3.05E+00	2.78E-02	1.67E-03	6.02E+00	4.12E+07	6.14E+02	1.02E+01	1.66E+00
GNB	Love 1121-7N	1.04E+01		2.79E+00	5.07E-02	2.03E-03	4.01E+00	3.71E+07	7.09E+02	5.14E+00	7.25E-01
GNB	NBU 1021-20	1.15E+00		2.40E+00	3.07E-02	6.59E-04	2.15E+00	NM	NM	NM	NM
GNB	NBU 553-28E	9.84E+00		3.99E+00	4.84E-02	2.65E-03	5.47E+00	5.95E+07	6.36E+02	1.60E+01	2.51E+00
GNB	Hatch 923-14C	9.74E+00		3.57E+00	4.53E-02	2.14E-03	4.71E+00	3.53E+07	7.51E+02	1.91E+01	2.55E+00
GNB	NBU 20	1.05E+01		3.27E+00	4.35E-02	2.11E-03	4.84E+00	6.98E+07	6.03E+02	1.31E+01	2.18E+00
GNB	NBU 1022-11F	9.80E+00		3.57E+00	4.00E-02	1.94E-03	4.86E+00	3.85E+07	6.02E+02	1.16E+01	1.92E+00
GNB	NBU 921 14L	1.03E+01		3.82E+00	3.95E-02	2.00E-03	5.06E+00	4.16E+07	7.50E+02	8.14E+00	1.09E+00
GNB	BC 1122-5H	1.13E+01		1.54E+00	3.58E-02	1.16E-03	3.24E+00	9.46E+06	3.14E+02	3.77E+00	1.20E+00
GNB	NBU 922-34D-3	1.08E+01		3.70E+00	2.84E-02	1.56E-03	5.48E+00	2.91E+06	3.01E+02	2.76E+00	9.16E-01
GNB	Bonanza 1023-9J	1.09E+01		3.82E+00	3.55E-02	1.82E-03	5.11E+00	5.64E+07	5.54E+02	4.89E+00	8.82E-01
GNB	NBU 1021-30I	1.17E+01		4.01E+00	3.65E-02	1.52E-03	4.16E+00	5.31E+07	5.78E+02	4.61E+00	7.98E-01
GNB	NBU 920-20P	1.12E+01		3.17E+00	3.15E-02	1.31E-03	4.16E+00	3.46E+07	5.75E+02	6.44E+00	1.12E+00
GNB	NBU 420	1.02E+01		1.69E+00	2.91E-02	8.54E-04	2.93E+00	7.19E+06	3.22E+02	4.01E+00	1.24E+00

Note: See Figure 4.3, 5.3 and 6.2 for well locations.

Noble gas ratios, Piceance Basin fields, Jonah Field, Greater Natural Buttes Field

field	Sample Nar	38Ar/36Ar	Error	%	4He/36Ar	20 Ne/36Ar	84Kr/36Ar
Grand Valley	G	1.81E-01	3.02E-03	1.67E+00	5.95E+02	1.00E-01	5.24E-02
Grand Valley	B	1.82E-01	2.30E-03	1.26E+00	4.45E+02	2.17E-01	3.84E-02
Grand Valley	F	1.77E-01	2.76E-03	1.56E+00	1.07E+03	3.11E-01	4.20E-02
Grand Valley	KK	1.76E-01	1.98E-03	1.13E+00	1.92E+02	1.41E-01	2.40E-02
Grand Valley	S	1.79E-01	1.49E-03	8.37E-01	4.11E+02	1.55E-01	4.67E-02
Grand Valley	EE	1.80E-01	2.39E-03	1.33E+00	5.37E+02	1.18E-01	5.15E-02
Grand Valley	LL	1.82E-01	2.62E-03	1.44E+00	3.32E+02	5.73E-02	2.92E-02
Grand Valley	T	1.81E-01	2.89E-03	1.60E+00	6.31E+02	9.88E-02	4.99E-02
Parachute	O	1.81E-01	1.96E-03	1.09E+00	5.95E+02	1.31E-01	5.08E-02
Parachute	M	1.81E-01	2.11E-03	1.16E+00	3.33E+02	2.34E-01	4.36E-02
Parachute	P	1.79E-01	1.99E-03	1.11E+00	5.28E+02	1.33E-01	5.12E-02
Parachute	A	1.80E-01	2.55E-03	1.41E+00	6.73E+02	9.91E-02	5.03E-02
Parachute	L	1.87E-01	4.89E-03	2.62E+00	5.78E+02	1.26E-01	4.91E-02
Parachute	I	1.77E-01	1.98E-03	1.12E+00	5.73E+02	1.09E-01	5.02E-02
Parachute	N	1.80E-01	2.22E-03	1.24E+00	5.91E+02	1.14E-01	5.17E-02
Parachute	Q	1.78E-01	1.44E-03	8.11E-01	5.85E+02	1.22E-01	5.10E-02
Rulison	Z	1.78E-01	2.50E-03	1.41E+00	5.91E+02	1.71E-01	5.29E-02
Rulison	GG	1.84E-01	2.61E-03	1.42E+00	6.07E+02	1.89E-01	5.46E-02
Rulison	Y	1.75E-01	3.76E-03	2.16E+00	5.75E+02	2.81E-01	4.90E-02
Rulison	EE	1.79E-01	3.51E-03	1.96E+00	6.31E+02	2.23E-01	5.00E-02
Rulison	RR	1.80E-01	2.64E-03	1.47E+00	6.68E+02	2.41E-01	4.31E-02
Rulison	CC	1.78E-01	1.90E-03	1.07E+00	3.56E+02	2.19E-01	4.61E-02
Rulison	RR	1.77E-01	2.23E-03	1.26E+00	7.33E+02	1.51E-01	4.46E-02
Rulison	HH	1.81E-01	2.35E-03	1.30E+00	2.99E+02	2.05E-01	4.93E-02
Rulison	U	1.79E-01	1.71E-03	9.51E-01	3.80E+02	1.25E-01	4.68E-02
Rulison	V	1.81E-01	1.65E-03	9.14E-01	4.74E+02	1.33E-01	4.98E-02
Rulison	W	1.74E-01	1.85E-03	1.06E+00	6.30E+02	1.32E-01	5.03E-02
Rulison	X	1.80E-01	2.42E-03	1.34E+00	4.74E+02	1.54E-01	4.87E-02
Sample Name		**38Ar/36Ar**	**Error**	**%**	**4He/36Ar**	**20 Ne/36Ar**	**84Kr/36Ar**
Jonah	Yellow Point	1.78E-01	1.39E-03	7.81E-01	4.83E+02	1.96E-01	5.16E-02
Jonah	Corona 67-3	1.83E-01	2.42E-03	1.33E+00	4.63E+02	2.13E-01	4.81E-02
Jonah	Corona 79-1	1.85E-01	2.88E-03	1.56E+00	5.26E+02	2.18E-01	5.03E-02
Jonah	SHB 41-29	1.80E-01	1.67E-03	9.24E-01	5.32E+02	1.77E-01	5.56E-02
Jonah	Cabrito 17-2	1.84E-01	2.06E-03	1.12E+00	3.67E+02	1.71E-01	4.94E-02
Jonah	SHB 53-17 #	1.82E-01	1.89E-03	1.04E+00	4.85E+02	1.93E-01	5.12E-02
Jonah	SHB 84-9	1.80E-01	2.93E-03	1.63E+00	5.97E+02	1.83E-01	5.31E-02
Jonah	SHB 19-5	1.81E-01	2.10E-03	1.16E+00	3.23E+02	2.11E-01	4.77E-02
Jonah	SHB 57-15 #	1.80E-01	1.96E-03	1.09E+00	4.81E+02	1.85E-01	5.33E-02
Jonah	SHB 53-20V	1.81E-01	3.07E-03	1.69E+00	4.62E+02	1.75E-01	4.58E-02
Jonah	Corona SHP	1.80E-01	2.13E-03	1.19E+00	5.53E+02	1.62E-01	5.05E-02
Jonah	Corona 61-3	1.80E-01	2.32E-03	1.29E+00	4.02E+02	1.61E-01	5.62E-02
Jonah	SHB 34-28	1.80E-01	2.05E-03	1.14E+00	3.26E+02	1.05E-01	3.34E-02
Jonah	SOL 7-36	1.78E-01	1.21E-03	6.78E-01	5.06E+02	2.18E-01	4.44E-02
field	**Sample Nar**	38Ar/36Ar	Error	%			
GNB	Mulligan 822	1.75E-01	6.11E-03	3.49E+00	1.28E+03	1.29E-01	4.26E-02
GNB	NBU 920-25	1.73E-01	8.37E-03	4.85E+00	4.40E+02	1.12E-01	4.77E-02
GNB	Love 1121-7	1.78E-01	1.99E-03	1.12E+00	1.25E+03	1.43E-01	4.66E-02
GNB	NBU 1021-2	NM	NM	NM			
GNB	NBU 553-28	1.78E-01	7.67E-03	4.31E+00	1.15E+03	9.45E-02	4.58E-02
GNB	Hatch 923-1	1.74E-01	7.56E-03	4.35E+00	1.12E+03	1.27E-01	4.54E-02
GNB	NBU 20	1.90E-01	8.39E-03	4.41E+00	5.80E+02	1.05E-01	4.86E-02
GNB	NBU 1022-1	1.83E-01	4.06E-03	2.22E+00	5.59E+02	2.61E-01	3.97E-02
GNB	NBU 921 14	1.84E-01	8.87E-03	4.81E+00	6.91E+02	1.38E-01	4.81E-02
GNB	BC 1122-5H	1.85E-01	2.97E-03	1.61E+00	2.30E+02	2.27E-01	3.71E-02
GNB	NBU 922-34	1.82E-01	3.71E-03	2.04E+00	3.21E+01	4.86E-01	1.97E-02
GNB	Bonanza 10	1.71E-01	3.95E-03	2.30E+00	5.66E+02	1.07E-01	5.69E-02
GNB	NBU 1021-3	1.75E-01	2.47E-03	1.41E+00	6.96E+02	1.58E-01	4.96E-02
GNB	NBU 920-20	1.81E-01	3.20E-03	1.76E+00	4.58E+02	2.52E-01	4.03E-02
GNB	NBU 420	1.85E-01	3.04E-03	1.64E+00	1.61E+02	4.69E-01	2.29E-02

Note: See Figure 4.3, 5.3 and 6.2 for well locations.

Noble gas ratios, Piceance Basin fields, Jonah Field, Greater Natural Buttes Field

field	Sample Name	129Xe/132X	Error	%	134Xe/132X	Error	%
GNB	Mulligan 822-24G	9.75E-01	6.46E-02	6.62E+00	3.88E-01	1.41E-02	3.64E+00
GNB	NBU 920-25P	9.94E-01	7.97E-02	8.02E+00	3.89E-01	1.52E-02	3.90E+00
GNB	Love 1121-7N	9.94E-01	5.44E-02	5.47E+00	3.92E-01	1.37E-02	3.50E+00
GNB	NBU 1021-20	NM	NM	NM	NM	NM	NM
GNB	NBU 553-28E	1.00E+00	7.40E-02	7.38E+00	3.87E-01	1.51E-02	3.89E+00
GNB	Hatch 923-14C	1.01E+00	5.80E-02	5.76E+00	3.84E-01	1.30E-02	3.40E+00
GNB	NBU 20	1.03E+00	7.86E-02	7.66E+00	3.89E-01	1.37E-02	3.51E+00
GNB	NBU 1022-11F	9.65E-01	6.42E-02	6.65E+00	3.83E-01	1.35E-02	3.52E+00
GNB	NBU 921 14L	9.67E-01	5.63E-02	5.82E+00	3.81E-01	1.21E-02	3.17E+00
GNB	BC 1122-5H	9.87E-01	5.49E-02	5.56E+00	3.87E-01	1.42E-02	3.68E+00
GNB	NBU 922-34D-3	9.87E-01	5.32E-02	5.39E+00	3.91E-01	1.35E-02	3.47E+00
GNB	Bonanza 1023-9J	9.70E-01	7.80E-02	8.04E+00	3.81E-01	1.39E-02	3.64E+00
GNB	NBU 1021-30I	9.92E-01	8.43E-02	8.49E+00	3.75E-01	1.13E-02	3.03E+00
GNB	NBU 920-20P	9.81E-01	6.87E-02	7.00E+00	3.90E-01	1.31E-02	3.37E+00
GNB	NBU 420	9.86E-01	5.95E-02	6.04E+00	3.94E-01	1.28E-02	3.25E+00

Note: See Figure 4.3, 5.3 and 6.2 for well locations.